TECHNISCHE UNIVERSITÄT MÜNCHEN

TUM School of Life Sciences

Comparative analysis of meat-spoiling *Photobacterium* spp. and their response to modified atmospheres

Sandra Fuertes Pérez

Vollständiger Abdruck der von der TUM School of Life Sciences zur Erlangung des akademischen Grades einer

Doktorin der Naturwissenschaften (Dr. rer. nat.)

genehmigten Dissertation.

Vorsitzender:	Prof. Dr. Wilfried Schwab
Prüfer der Dissertation:	1. Prof. Dr. Rudi F. Vogel
	2. Prof. Dr. Lindsay Hall

Die Dissertation wurde am 02.02.2022 bei der Technischen Universität München eingereicht und durch die TUM School of Life Sciences am 01.04.2022 angenommen.

Table of content

1 Abstract

Due to the perishable nature of raw meat and meat products, the respective spoilage associated microbiota and the control of its growth are ongoing and constant fields of study. The determination of the “use by” date of the product requires constant update of knowledge with the objective of establishing more accurate shelf-life. That ensures that the product is neither discarded too early, which would increase the waste of the industry, nor that it ends up spoiled at the consumer causing returns and image losses, or even poses a health risk upon consumption if spoiled before the end of the shelf life. Common models to predict shelf life of modified atmosphere packaged (MAP) meats take into account the most prominent and common meat spoilers known, but there is a high lot-to-lot variation on the initial microbiota and not all species are cultivable by common control approaches. This is the case of photobacteria, a mostly marine-related group of bacteria that have been over recent years detected on raw meat and considered overlooked meat spoilers. This work delves into the study of *Photobacterium carnosum*, *P. phosphoreum* and to a lesser extent of *P. iliopiscarium* and their relevance to meat spoilage. During the study of their distribution, photobacteria have been found to be common on almost all types of cold-stored raw meats, regardless of the type of packaging or selling brand, and also on meat products, but undetected from other cold-stored products unrelated to meat or fish/seafood. The long incubation periods and partial selectivity of existing targeted isolation procedures are not quite feasible for routine control, screening of photobacteria or detection of the source of contamination on a processing plant. This study describes a novel culture-independent procedure based on the loop-mediated isothermal amplification (LAMP) technology. The method is aimed at the detection of photobacteria from raw meat and contaminated surfaces in two hours or less that would provide a primary screening tool with high sensitivity and specificity. Additionally, the study of marine- and meat-borne strains of the three species, both physiologically and at the genomic level revealed that they exhibit large intra- and inter-species diversity, also represented on the initial contamination of one single piece of meat, and are prone to frequent genetic exchange as a means to enrich their adapting capabilities. Overall, the results support a differentiation of characteristics and strategies followed to persist on a niche. *P. carnosum* appears as a species focused on diversification of carbon sources, with adaptation towards nutrient rich environments and the ability to use glycogen, which is a storage component in muscle and other animal tissues. The wider carbon utilization allows the species to compete in the environment despite its slower growth and lower capacity for stress resistance. *P. phosphoreum*, on the other hand, is able to compete via faster growth, stress resistance and antimicrobial activity. Its adaptation appears closer to

its previously reported marine environment, retaining bioluminescence for most strains, use of marine abundant compounds and higher amount of sodium-dependent transporters. The strategies of both appear effective, as they are found in high numbers on stored raw meat as a common occurrence. The species *P. iliopiscarium* is the only one that shows strain-specific environmental adaptations, with marine-borne strains retaining the use of marine-abundant carbohydrate utilization than *P. carnosum* strains. Additionally, the presence of photobacteria on packages with vacuum or modified atmospheres suggests a flexible metabolism that allows them to adapt towards the effects of the gases. However, the *in vitro* study of their growth and proteome under different modified atmospheres proves a different outcome for some of the gas combinations. The results suggest that deviations from air-like atmospheres incur in growth reduction, although limited thanks to the adaptive response of the species of photobacteria. The absence of oxygen tends to enhance the expression of anaerobic respiration, fermentative pathways and the counterbalance of resulting decrease in pH and release of carbon dioxide, regardless of the presence of environmental carbon dioxide. On the other hand, the presence of oxygen appears to trigger a response to oxidative stress that also responds to an increase in environmental oxygen concentration. Finally, the combination of carbon dioxide and oxygen results in a synergistic effect that enhances the oxidative stress and the effects of carbon dioxide towards the growth of photobacteria. When the combination includes high oxygen concentration (70%) and carbon dioxide, the mixture is able to override the stress response of photobacteria and inhibits their growth *in vitro*. This atmosphere appears as the only suited to control their sole presence, although the existence of concomitant bacteria is beneficial enough to still allow their proven development on meat *in situ* to high cell counts, leading to spoilage and a potential health risk upon consumption.

2 Zusammenfassung

Aufgrund der hohen Verderblichkeit von rohem Fleisch und Fleischprodukten ist die Untersuchung und Kontrolle ihrer Verderbs-Mikrobiota ein kontinuierliches Forschungsfeld. Das Verbrauchsdatum eines Produkts zu bestimmen erfordert eine ständige Wissensaktualisierung mit dem Ziel, die Haltbarkeit genauer festzulegen. Dies soll sicherstellen, dass das Produkt weder zu früh entsorgt wird, was die Menge an industriellem Abfall vergrößern würde, noch dass es zum Verkauf und der anschließenden Rückgabe verdorbener Produkte oder gar zu einem Gesundheitsrisiko für den Verbraucher wird. Gängige Modelle berücksichtigen nur die bekannten und häufigsten Fleischverderbsorganismen, und das obwohl das initiale Konsortium chargen-abhängig starke Variationen aufweist und bestimmte Arten nicht mit gängigen Methoden kultiviert werden können. Dies trifft auch auf Photobakterien zu, eine meist mit dem Meer assoziierte Bakteriengruppe, dessen Abundanz in den letzten Jahren auch auf rohem Fleisch nachgewiesen wurde und im Zusammenhang mit Fleischverderb bisher übersehen wurde. Diese Arbeit befasst sich mit der Untersuchung von *Photobacterium carnosum*-, *P. phosphoreum*- und in geringerem Umfang *P. Iliopiscarium* sowie ihrer Bedeutung für den Fleischverderb. Bei der Untersuchung ihrer Verbreitung wurde festgestellt, dass Photobakterien auf fast allen Arten von gekühlt gelagertem rohem Fleisch verbreitet sind, unabhängig von der Art der Verpackung oder der Marke, ebenso wie auf Fleischprodukten, jedoch nicht auf anderen kühl gelagerten Produkten ohne Bezug zu Fleisch. Die lange Inkubationszeit und die teilweise Selektivität bestehender Isolationsverfahren sind nicht praktikabel für die routinemäßige Kontrolle und das Screening von Photobakterien bzw. den Nachweis der Kontaminationsquelle in Verarbeitungsanlagen. Diese Studie beschreibt ein neuartiges kultivierungs-unabhängiges Verfahren, das auf der LAMP-Technologie (*Loop-Mediated Isothermal Amplification*) basiert und auf den Nachweis von Photobakterien von rohem Fleisch und kontaminierten Oberflächen in maximal zwei Stunden abzielt. Dieses Verfahren stellt ein elementares Screening-Tool mit hoher Empfindlichkeit und Spezifität dar. Darüber hinaus hat die Untersuchung von Stämmen mit marin- und Fleisch-assoziiertem Hintergrund aller drei Arten auf physiologischer- und genomischer Ebene ergeben, dass sie eine große intra- und interspezifische Diversität besitzen, die sich auch in der initialen Kontamination eines einzelnen Stücks Fleisch widerspiegelt. Die Stämme neigen zu einem häufigen genetischen Austausch, um ihre Anpassungsfähigkeiten an das jeweilige Habitat zu verbessern. Ingesamt unterstützen die Ergebnisse eine Differenzierung von Charakteristika und Streategien, die verfolgt werden, damit sich diese Organismen in einer Nische behaupten können. *P. carnosum* erscheint dabei als ein Spezies, die auf die Diversifizierung

der Nutzung unterschiedlicher Kohlenhydrate setzt, mit einer Anpassung an nährstoffreiche Habitate, die auch Glykogen enthalten können, das ein wichtiger Energiespeicher im Muskel und anderen tierischen Geweben ist. Die breitere Nutzung von Kohlenstoffquellen ermöglicht dieser Spezies eine gute Behauptung in einer Umgebung, obwohl sie langsamer wächst und eine geringere Stresstoleranz aufweist. Andererseits ist *P. phosphoreum* wettbewerbsstark durch sein schnelleres Wachstum, Stresstoleranz und antimikrobielle Aktivität. Seine Anpassung an Fleisch erscheint näher an seinen früher gefundenen Marinen Habitaten, was sich am Erhalt der Biolumineszenz in den meisten Stämmen zeigt, sowie an mehr Natrium-abhängigen Transportern und an der Nutzung von Substraten zeigt, die in marinen Habitaten vorherrschen. Beide Strategien erweisen sich als effektiv, wie sich an der hohen Zellzahl dieser Bakterien zeigt, die man in gelagertem Fleisch finden kann. Die Spezies *P. iliopiscarium* ist dier einzige, die stammspezifische Umweltanpassungen zeigt, und marine Isolate, die DMSO nutzen und flaggellare gencluster tragen umfasst, als auch Fleisch-Isolate, die ein Kohlenhydrat-Verwertungsmuster aufweisen, wie man es in *P. carnosum* Stämmen findet. Schließlich deutet das Vorkommen von Photobakterien in Verpackungen mit Vakuum- oder Schutzgasatmosphäre auf einen angepassten Stoffwechsel hin, der es ihnen ermöglicht, sich and die Auswirkungen der Gase anzupassen. Die Untersuchung von *in vitro* Wachstum und Proteom-Expression von Photobakterien unter verschiedenen Schutzgasatmosphären hat jedoch gezeigt, dass die Realität anders aussehen könnte als erwartet. Die Ergebnisse deuten darauf hin, dass Abweichungen von Luft-ähnlichen Gasgemischen zu reduziertem Wachstum führen, die aufgrund der adaptiven Anpassung der Photobakterien jedoch gemäßigt ausfallen. Anoxische Atmosphären erhöhen tendenziell die Expression von Enzmyen der anaeroben Atmung, des fermentativen Stoffwechsels und des Augleichs des auftretenden pH-Abfalls und der Abgabe von Kohlendioxid. Andererseits löst die Anwesenheit von Sauerstoff oxidativen Stress aus, der eine Antwort auf eine erhöhte Sauerstoffkonzentration in der Umgebung abbildet. Schließlich bewirkt die Kombination von Kohlendioxid und Sauerstoff einen synergistischen Effekt hinsichtlich der Erhöhung des oxidativen Stresses, mit der Folge der größten Hemmwirkung auf das Wachstum der Photobakterien. Obwohl dies in den meisten Fällen eine Anpassungsreaktion stimuliert, setzt die Kombination aus hoher Sauerstoffkonzentration und Kohlendioxid die Stressreaktion von Photobakterien außer Kraft und hemmt ihr Wachstum. Diese Schutzgasatmosphäre scheint am besten geeignet, um die alleinige Anwesenheit von Photobakterien zu kontrollieren. Allerdings scheint die Anwesenheit weiterer Bakterien bietet allerdings offensichtlich genug Schutz, um Photobakterien die Persistenz auf Fleisch zu ermöglichen, die schlussendlich zum Verderb sowie Gesundsheitsrisiken beim Verzehr führt.

3 Introduction

3.1 Relevance of meat spoilage for the industry

3.1.1 Meat demand

According to the report from the Food and Agriculture Organization of the United Nations (FAO), the industry of meat and meat products maintains a tendency to expand, increasing by 2.2% in 2021 compared to the previous year and with a total production of 345 million tons (FAO, 2021). However, it should not come as an unexpected piece of information, since global population keeps increasing. The food industry, and therefore also the meat industry, is predicted to have to expand further to be able to feed up to 9.6 billion people by the year 2050 (PRB, 2021).

The increase in production does not only require an expansion of infrastructure able to process the food, but also of the animal feed, dedicated land and livestock volume. The cost of expanding this industry to account for the massive increase of the world population might be just too high, and when production cannot meet demand, the cost of the product increases. Despite the existence of proposals for alternative foods (algae, insects, plant-based meat alternatives) or even cultured meats, (1) their mass production is still not ready and (2) the consumer acceptability of these products is still low compared to “biological” raw meat (Bryant and Barnett, 2020; Onwezen et al., 2021). Therefore, the traditional meat industry is still required and forced to increase production to meet demand expectations.

3.1.2 Waste in the meat industry

The increase and development of the meat industry is concomitant with an additional problem: food loss and food waste. It is the consequence of the expansion of the industry but at the same time an aspect that, if reduced, also significantly results in a reduction of the required expansion, since more food is available. According to the report by FAO, about 1.3 billion tons per year or one third of the total production of food destined for human consumption is lost or wasted, and about 12% of the meat and animal products end up not consumed (FAO, 2011; Thakur et al., 2020). In developed countries, half of the losses or waste of meat and meat products occur mostly either during the supply chain or at the hands of the consumers. Meat loss and waste in those conditions is mostly due to failure to meet quality standards or food safety concerns directly tied to the “best-before” dates (FAO, 2011). A reduction of meat (and in general food) waste and loss is still a relevant tool that might have a considerable impact on the efficiency of the industry where the limiting nature of resources does not allow for its expansion.

The shelf-life of a product is defined as the window of time a product retains its sensory, chemical, functional, physical and microbiological characteristics and remains safe under specific storage, manufacture and packaging conditions (Man, 2015). “Best before” date or “date of minimum durability of a food” is described as “*the date until which the food retains its specific properties when properly stored*” and does not pose a health risk, while the “use by” date is the term replacing the “best before” date “*on products which, from a microbiological point of view, are highly perishable and are therefore likely after a short period to constitute an immediate danger to human health*”, according to current legislation (Hazards et al., 2020). The latter is the information required on raw meat, defining its perishability and therefore the moment when not consumed meat becomes wasted food. Wrongly assigning proper consumption dates can have two outcomes: (1) the “use by” date is assigned later than the safe-window for its consumption, generating high-risk situations for the consumers health and safety, incurring in the possibility of hospitalization due to ingestion of spoiled meat, or (2) the date is assigned as an earlier date than required, and the product ends up being discarded despite maintaining its quality and safety, increasing waste, economic loss and meat consumption. However, the meat environment is complex due to its biochemistry and the microbiota that can be found on it is subjected to lot-to-lot variations that increase the difficulty of using models and predicting the exact spoilage process (Säde et al., 2017). Due to mentioned factors, assigning the shelf-life might not be a science as accurate as one may think.

Improving the establishment of the right shelf-life of meat and meat products requires deep understanding of the microbiology of meat, and how it affects its decay over time, as it is the microbial growth the main cause of the spoilage of meat, and therefore reduction of its self-life and increase of waste. Filling the knowledge gaps in meat science will contribute to a better control over the spoilage process of meat, and the establishment of exact safe consumption windows of time, reducing waste, monetary loss in the sector, and reducing the expansion of the production of meat to meet its demand.

3.2 The biochemistry of meat

Meat constitutes a complex system whose composition can strongly vary depending on the animal it comes from, the specific tissue or part of the body, the age of the animal and the conditions in which it has been kept (Cobos and Díaz, 2015). In general, the composition of meat can be summarized as 75% water, 19% protein, 3.5% of non-protein and soluble elements and 2.5% of lipids (López-Bote, 2017). The detailed composition of meat is displayed in Table 1.

Table 1. Chemical composition postmortem of muscle from typical adult livestock before any degradation has taken place. Adapted from López-Bote (2017).

Components				Wet %	Weight
Water					75.0
Protein					19.0
Lipid					2.50
	Neutral lipid, phospholipids, fatty acids, fat-soluble substance			2.50	
Carbohydrate					1.20
	Lactic acid		0.90		
	Glucose-6-phosphate		0.15		
	Glycogen		0.10		
	Glucose, traces of other glycolytic intermediates		0.05		
Soluble nonprotein substances					2.30
	Nitrogenous			1.65	
		Inosine monophosphate	0.30		
		Di- and tri-phosphopyridine nucleotides	0.10		
		Amino acids	0.35		
		Creatinine	0.55		
		Carnosine, anserine	0.35		
	Inorganic			0.65	
		Soluble phosphorous	0.20		
		Potassium	0.35		
		Sodium	0.05		
		Magnesium	0.02		
		Calcium, zinc, trace metals	0.03		
	Vitamins				

Proteins on meat are mainly divided into myofibrillar, sarcoplasmic and connective tissue proteins (Tornberg, 2005), in addition to endogenous enzymes (e.g. proteases, lipases, glycohydrolases, nucleotidases). Myofibrillar proteins are mainly represented by myosin, rich on glutamate, aspartate and dibasic amino acids (Lawrie and Ledward, 2006). The oxidation of myofibrillar proteins occurs as part of the post-mortem reactions, affecting proteins structure and functionality, water holding capacity, texture, flavor and nutritional value of the meat. This reaction is enhanced by presence of reactive oxygen species, oxidative enzymes, heme pigments, metals, lipid oxidation, acidification and chilling (Estevez, 2011). Sarcoplasmic proteins include several types but the most abundant is myoglobin, that gives the characteristic red color of meat and contains the prosthetic heme group. Red meat (beef,

pork, lamb) is formed by red fibers, with a high content of myoglobin, while white meat (chicken, turkey) is abundant in white fibers, with a low concentration of myoglobin (Cobos and Díaz, 2015). In low oxygen concentrations, the heme group in myoglobin turns into the pigment metmyoglobin, brown in color, that is usually associated with not-so-fresh meat (Cobos and Díaz, 2015). The connective tissue is mainly represented by collagen and elastin. Collagen is mainly formed by glycine, proline and hydroxyproline, while elastin contains mainly glycine and hydrophobic amino acids, with smaller amounts of proline and hydroxyproline (Cobos and Díaz, 2015).

Multiple endogenous enzymes on meat act upon its components, breaking them down and making them available to microorganisms. The activity of proteolytic enzymes increases during post-mortem modifications, softening the tissue and contributing to meat tenderness and releasing free amino acids (Warriss, 2010). Lipolytic enzymes act upon the meat lipids and release glycerol, fatty acids and phospholipids (Toldrá, 2012).

The type of meat also affects the lipid content (Warriss, 2010). The majority of lipids found on meat are represented by subcutaneous fat. On the other hand, the intramuscular lipids represent a much lower percentage of total fat, but their content is very variable, from 1 to 15% (Kauffman, 2012), also impacting the organoleptic characteristics of the meat. The lipid portion of meat is mainly formed by triglycerides (Wood et al., 2007), and in lower quantities diglycerides, monoglycerides, free fatty acids, fat-soluble vitamins, and cholesterol esters.

The carbohydrate portion, although small by itself, is mainly present in the form of glycogen, an α-D-glucose polysaccharide that acts as energy reservoir (Cobos and Díaz, 2015), that can vary up to 1.8% (Immonen and Puolanne, 2000; Immonen et al., 2000). The glycolysis that takes place post-mortem determines the availability of glucose and other glycolysis intermediates on the meat (Pösö and Puolanne, 2005). Additionally, available nucleotides can also result in the release of ribose by endogenous enzymes (Eskin and Shahidi, 2012). In the end, glucose and ribose, and to a lesser extent fructose and mannose, are the four main monosaccharides present on meat (Eskin and Shahidi, 2012; Koutsidis et al., 2008b; Lawrie and Ledward, 2006; Nychas et al., 2007).

Additionally, meat is a source of thiamine, riboflavin, niacin, vitamin B6 and vitamin B12, reaching concentrations of up to 10 mg/100g, minerals such as phosphorous, potassium, magnesium, iron, copper, zinc, selenium and in lower amounts calcium and sodium (Cobos and Díaz, 2015).

The conversion of muscle into meat occurs with a series of changes that include the progressive depletion of energy in the muscle, and the change of metabolism to anaerobic

lactic acid production, decreasing the pH to approximately 5.8 (Cobos and Díaz, 2015). Raw meat represents a substrate-rich environment with high water activity (0.99) (Lawrie and Ledward, 2006) able to support fast microbial growth (Feiner, 2006). In that context, microorganisms benefit from the release of free compounds that they can incorporate into their metabolism. Bacteria also contribute with their own degradation enzymes to the process, and release of products of their own metabolism that modify the characteristics of meat and contribute to their spoilage.

3.3 Meat spoilage

3.3.1 Rationale to delay spoilage

The spoilage stage of raw meat and meat products is not always an evident phenomenon. Its detection has a subjective component that heavily relies on the consumer's perception of changes on the meat, such as strong smell, loss of color or presence of slime. Despite the improvement and accuracy of the establishment of shelf-life of raw meat and meat products, the variables involved are too many and sometimes not possible to control. Several stages such as transportation or domestic storage are out of control of the manufacturer, and therefore introduce deviations in the period of time that meat remains fresh. Therefore spoilage prevention strategies are of critical importance in the production of meat and meat products.

The extension of the shelf-life of meat and meat products require the application of strategies for the reduction of the microbiological load that ultimately leads to spoilage of the food. Chilling and cold storage is one of the most effective methods for preservation of meat and meat products, as it inhibits growth of mesophilic bacteria or slows down their growth and metabolism. Meat is stored at 4 °C, as above temperatures enhance the growth of the meat microbiota, resulting in spoilage and shortening of the shelf-life (Koutsoumanis et al., 2006). Cold-storage is often paired with other technologies and types of packaging to increase effectiveness of microbiota reduction.

Vacuum packaging requires the removal of air from a package or film with low permeability for oxygen, sealing it hermetically afterwards (Smith et al., 1990). The presence of oxygen is responsible for the growth of aerobic bacteria, considered to be major contributors to the spoilage of meat, and the occurrence of oxidative reactions. Therefore removal of oxygen can help minimize those effects, although vacuum package is not suitable for all types of products due to their compression (Church and Parsons, 1995). Additionally, removal of oxygen can still promote growth of strictly anaerobic bacteria and in some cases such as in

beef, promote the formation of deoxymyoglobin that gives a purple-like coloration to the meat and reduces consumer acceptance (McMillin, 2008; Ščetar et al., 2010).

As a way to overcome some of the issues that vacuum package presents, another strategy is the use of modified atmospheres to reduce or inhibit a wider range of microbial growth while maintaining the organoleptic characteristics of the meat, a highly perishable product, and avoid compression of the product (Church and Parsons, 1995; Farber, 1991; McMillin et al., 1999). It is estimated that almost half (43%) of the freshly slaughtered meat in Europe is packed using said technique (Belcher, 2006; McMillin, 2008). The technique of modified atmosphere packaging (MAP) is defined as a change in the gas atmosphere surrounding a food product kept in a container that acts as gas-barrier (Young et al., 1988). Common gases utilized to prepare the gas mixtures include oxygen, carbon dioxide and nitrogen (Singh et al., 2011). Other gases, such as carbon monoxide, are only accepted in certain countries (United States and Norway) and only if applied in very low concentrations (Cornforth and Hunt, 2008; Djenane and Roncalés, 2018).

Typically, red meats are packaged with a mixture of 70 % oxygen and 30 % carbon dioxide, while white meats are most commonly packed under 70 % nitrogen and 30 % carbon dioxide (Eilert, 2005; McKee, 2007; Rossaint et al., 2015; Sante et al., 1994). Oxygen is used in packaging of red meat to keep its bright red color from deteriorating over time. It slows down the formation of metmyoglobin, responsible for giving red meat a brown-like color, and consequently losing the expected red coloration of fresh products (Luño et al., 1998; Mancini and Hunt, 2005; Taylor et al., 1990). Additionally, oxygen suppresses the growth of anaerobic bacteria and is reported to have inhibitory effects on aerobic bacteria when its concentration is high (Farber, 1991) by promoting the formation of reactive oxygen species and therefore oxidative stress that can lead to damage of lipids, proteins and DNA (Pan and Imlay, 2001). However, it has been reported that the use of high oxygen concentrations promotes the oxidation of lipids from the meat, and therefore the release of off-odors that might impact the acceptance (Jakobsen and Bertelsen, 2000; Jayasingh et al., 2002). Due to its inhibitory effects, the gas mixture of high oxygen and carbon dioxide is also used by some producers for packaging white meat (Meredith et al., 2014; Rossaint et al., 2015). The effects of carbon dioxide are mechanistically less clear than those of oxygen, although it is known to affect the adaptation, growth and division times of aerobic bacteria (Zhao et al., 1994) by influencing the pH, displacing the oxygen and therefore reducing its availability, structurally altering the membrane of bacteria and even interfering directly with their metabolism and function of several enzymes (Daniels et al., 1985). The last gas, nitrogen, is used due to its inert and tasteless nature to fill in the remaining percentage of the gas mixture and prevent

the collapse of the packages sometimes caused by adsorption of carbon dioxide by the meat (Church and Parsons, 1995).

3.3.2 Composition of the meat microbiota

Nychas et al. (2008) have defined the spoilage of meat as "an ecological phenomenon" that involves the modification of the substrates available on meat as a consequence of the growth of its microbiota during storage. The specific microbial presence established on the meat environment is highly dependent on several factors (e.g. intrinsic, processing, and extrinsic). Those factors ultimately define the type of spoilage microbiota on the meat, that will also influence the speed of spoilage and processes involved in it (Nychas et al., 2008). The microbiota that can be found on meat and derived products is highly diverse, since it originates from multiple sources (Doulgeraki et al., 2012; Gram et al., 2002; Jay et al., 2005; Nychas et al., 2007). Said microorganisms can originate from the animal itself, be present either in the intestinal tract or on the outside of the animal, or contaminants from the environment before, during or after slaughter (Koutsoumanis and Sofos, 2004). The percentage of microorganisms that are able to persist under specific selective conditions, become dominant, and ultimately lead to spoilage of the raw meat or meat products are called ephemeral or specific spoilage organisms (E/SSO) (Koutsoumanis and Nychas, 2000; Nychas et al., 2007). The microbiota of meat is commonly formed by a consortium of several species and a few that dominate it, while 42 different genera are listed as found on meat under different environmental conditions (Nychas et al., 2007).

The genus *Pseudomonas* has been often reported as dominant in the consortium responsible for spoilage of meat under aerobic conditions between the temperatures of -1 and 25 °C, and directly related to presence of slime and off-odors (Koutsoumanis et al., 2006; Stanbridge and Davies, 1998). According to Nychas et al. (2007), other species and genera can arise as dominant when modified atmospheres are used. *Brochothrix (B.) thermosphacta*, species of *Enterobacteriaceae* and lactic acid bacteria appear dominant under aerobic conditions when carbon dioxide is used as an inhibitory agent, while in vacuum packaged conditions, *Pseudomonas* spp., *B. thermosphacta* and *Shewanella putrefaciens* appear as the dominating ones. The presence of many of these bacteria manifests on the meat as slime, presence of sulphide odor, cabbage-like odor, production of greening compounds (e.g. H_2O_2, H_2S), or souring (Nychas et al., 2007; Skandamis and Nychas, 2002).

The divergence in the microbiota on meat reported over the years and the large number of species and genera listed enlightens the complexity of the process of meat spoilage, and the difficulties that arise when trying to evaluate the influence of the presence of a specific

species, and its contribution to the safety and quality of meat. The situation is aggravated by the gaps in knowledge considering the species that are yet unknown or undetected on meat, the limitations of the experimental approaches that often have to work with models, and overall the dynamics of how a specific microbiota reaches and develops on meat, and its direct correlation to its spoilage process.

3.4 *Photobacterium* as a marine genus and its relation to fish spoilage

3.4.1 Marine genus

Photobacterium (*P.*) was first described by (Beijerinck, 1889) as a bioluminescent genus of bacteria belonging to the *Vibrionaceae* family (*Proteobacteria*: *Gammaproteobacteria*), whose members are gram-negative bacteria, facultatively aerobic, with typically rod-shaped and with a requirement of sodium for growth. Since the first description of the genus, several new species have been described, and the genus now groups 37 species and 2 subspecies with a high degree of diversity (Parte et al., 2020), grouped in five different clades: Phosphoreum, Profundum, Damselae, Ganghwense and Leiognathi (Labella et al., 2018).

The genus is typically described as marine-related, with its members distributed in coastal, open-ocean and deep-sea environments and isolated from seawater, sediments, saline lake water and multiple parts of marine animals (Urbanczyk et al., 2010). Members of the genus have been found also displaying different life-styles, ranging from symbiotic, commensal, saprophytic or pathogenic relationships with marine animals, all providing a nutrient-rich environment, and transitioning to free-living in the sea water, a starvation-survival driven life-style (Morita, 1997).

The genus was initially described as comprised by bioluminescent bacteria. However, it is now known that it also includes non-bioluminescent species, and for some it is regarded as a strain-specific feature rather than a unified trait of the whole species (Urbanczyk et al., 2010). The bioluminescence trait is known to promote the establishment of symbiotic relationships with marine animals by colonizing their light organs, and also to facilitate attraction of phototactic animals that could serve as a potential niche for the bacteria or bait for the host. (Brodl et al., 2018; Nealson and Hastings, 1979; Tanet et al., 2019; Urbanczyk et al., 2010).

Multiple studies on photobacteria have been performed, focused on fish spoilage (Bjornsdottir-Butler et al., 2018; Bjornsdottir et al., 2009; Dalgaard et al., 1997), the study of the lux-rib operon (Urbanczyk et al., 2008; Urbanczyk et al., 2012), high pressure (Allen and Bartlett, 2000; Campanaro et al., 2005; Vezzi et al., 2005), salt tolerance (Wu et al., 2006), and pathogenicity (Balado et al., 2017; Matanza and Osorio, 2018). Reports and works

published on photobacteria are centered on the marine ecosystem, or report their presence as part of cross-contamination of lake or river waters, derived from the sea.

3.4.2 Fish spoilage

One of the most studied aspects of photobacteria is their contribution to fish and seafood spoilage. *P. phosphoreum* has been described as a common species present on marine fish and seafood, bioluminescent, and important contributor to the spoilage process of modified atmosphere, vacuum and air packed fish (Dalgaard et al., 1998; Gram and Huss, 1996; Reynisson et al., 2009). The species has been described as fish light-organ symbiont, highly resistant to CO_2, and able to reduce trimethylamine-oxide (TMAO) to trimethylamine (TMA), which is responsible for foul odors on the fish (Dalgaard, 1995; Dalgaard et al., 1997). TMAO is abundant on fish tissues, and levels of trimethylamine have been proposed as a measurement for bacterial deterioration on fish (Barrett and Kwan, 1985). In addition, the species has also been reported as a histamine producer on fish and seafood, leading upon consumption to scombroid fish poisoning in sensitive consumers, and therefore posing a health concern in the food industry (Bjornsdottir-Butler et al., 2018; Emborg et al., 2002; Jørgensen et al., 2000a; Lehane and Olley, 2000; Torido et al., 2012).

The species *P. iliopiscarium* has also been reported on fish, although reports are fewer and the involvement in the spoilage process has been less studied (Dunlap and Ast, 2005; Olofsson et al., 2007). It has, however, been reported the production of histamine by the species at low temperatures, with results revealing production of more than 500 ppm (Takahashi et al., 2015).

3.5 Photobacteria on meat

Despite the common classification of the genus *Photobacterium* as a marine-related genus, in the latest years species belonging to it have been found in association with raw meat. There have been reports of culture independent studies that detected presence of photobacteria from several meat sources that constitute the initial context for this work.

Nieminen et al. (2016) detected the presence of *Photobacterium* spp. and *Photobacterium phosphoreum* on pork samples by both culture dependent and independent studies. In said analysis, presence of the species was correlated to the concentration of acetoin, diacetyl and 3-methyl-1-butanol on meat, previously reported as indicator for sensory spoilage of meat (Argyri et al., 2011; Casaburi et al., 2015; Ercolini et al., 2006). Additionally, a metatranscriptomic study by Höll et al. (2019) also detected the presence of photobacteria on MAP packed skinless chicken breast. Results derived from said study predicted a similar metabolism of the species in presence of carbon dioxide both with high oxygen concentration

(70 %) and anoxically, as well as the production of biogenic amines such as tyramine, cadaverine, putrescine and agmatine. The study, on the other hand, failed to report on the presence of the histidine decarboxylase transcripts, despite several previous studies reporting on the production of histamine by *P. phosphoreum* (Bjornsdottir-Butler et al., 2018; Emborg et al., 2002; Jørgensen et al., 2000b). Additionally, *P. phosphoreum* was also predicted to convert pyruvate into ethanol, acetate, formate, lactate and acetoin, and utilize amino acids, lipids and carbohydrates as carbon sources.

Other culture independent studies also have reported presence of photobacteria on beef (Ercolini et al., 2010; Jaaskelainen et al., 2016; Pennacchia et al., 2011; Stellato et al., 2016), minced meat (Stoops et al., 2015), chicken (Dourou et al., 2021; Yu et al., 2019), pork (Bassey et al., 2021; Li et al., 2019; Stellato et al., 2016), minced pork (Cauchie et al., 2020; Koo et al., 2016), ostrich (Juszczuk-Kubiak et al., 2021) and donkey (Wei et al., 2021) and on samples of knives and surfaces from a butchery (Stellato et al., 2016). Additionally, photobacteria have been also detected on processed meats such as sausages or cooked ham (Bouju-Albert et al., 2018; Chen et al., 2020; Delhalle et al., 2016; Duthoo et al., 2021; Efenberger-Szmechtyk et al., 2021; Greppi et al., 2015; Pini et al., 2020; Poirier et al., 2020; Settanni et al., 2020; Wang et al., 2018).

Very few reports on the presence of photobacteria based on culture-dependent methods have been published. Apart from the study by Nieminen et al. (2016) that did identify several bioluminescent colonies, presence of a bioluminescent colony on pork had also been previously reported by Kuang et al. (2012) and identified as photobacteria.

Despite the wide study of the microbiota on meat, up to the point when previously mentioned studies were reported, the presence of photobacteria on meat was unknown. Works reporting presence of photobacteria often highlight the differences obtained between culture-dependent studies, where photobacteria are mostly undetected, and culture independent studies, that revealed even predominant presence of those species on meat. As psychrophilic and nutritionally fastidious bacteria, common culturing approaches for the total viable count (TVC) enumeration on meat tend to overlook photobacteria.

A selective isolation method specifically designed for the detection of photobacteria was reported by Hilgarth et al. (2018a), using incubation temperatures below the typical 30 - 37°C used in routine meat controls, that better suit the psychrophilic nature of most species of photobacteria. The method allowed the growth, detection and isolation of psychrophilic *Photobacterium* spp. on chicken breast, beef steaks and pork steaks packed either under modified atmosphere or air, up to 7 logCFU. The results also allowed the classification of photobacteria as pervasive constituents of the spoilage microbiota of meat due to their

widespread presence on different types of meat, capacity to grow to spoilage relevant numbers and both the predicted spoilage potential of these bacteria on meat, and the observed spoilage contribution on fish. Species detected included *P. phosphoreum*, *P. iliopiscarium*, and a new species, *P. carnosum*, described as the first *Photobacterium* species with a non-marine origin or isolation, and closest with the two species of photobacteria that share the meat niche (Hilgarth et al., 2018b). The new species has an even lower optimum growth temperature than the other two species detected on meat (10-15 °C vs. 15-25 °C) and is described as non-motile, non-bioluminescent, with similar sodium requirements (minimum of 0.5 % (w/v) NaCl) but lower salt tolerance (up to 4 % (w/v) NaCl), and able to show growth at the pH on meat (~5.8), also observed for *P. iliopiscarium* and *P. phosphoreum*.

The detection of photobacteria on meat in different locations across Europe and other continents, from different types of animals (e.g. chicken, beef, pork, minced meat) and packaging conditions (modified atmospheres with and without oxygen, vacuum, air), highlights that photobacteria should not be underestimated in their contribution to meat spoilage. Control over the shelf-life of meat and meat products will be incomplete without control over the population of photobacteria, and said control requires the study of their physiology and metabolic responses. However, it also refers to an improvement over the detection of their presence of meat since, despite abundant, they appear to be selective on the batches of meat colonized.

3.6 Detection and isolation

The studies performed up to this date reveal the relevance of photobacteria as part of the meat microbiota. Despite the reports of their presence in almost any sector of the meat industry and on multiple countries, not all packages of meat contain photobacteria (Cauchie et al., 2020; Duthoo et al., 2021; Hilgarth et al., 2018a; Stoops et al., 2015). Reliant, sensitive tools for the screening of meat, meat processing plants and butcheries are relevant to maintain control over their spread and source of contamination.

Thyssen and Ollevier (2015) describes that the isolation of *Photobacterium* species can be achieved by plating samples from marine environments or surface or intestinal contents of fish and other marine animals on blood agar, brain-heart infusion (BHI), tryptic soy agar (TSA), thiosulfate citrate bile sucrose agar (TCBS), and marine agar (MA), and that at least 1% (w/v) NaCl is required in the media. Mentioned approaches are not selective and rely on species of photobacteria being abundant and/or dominant in the marine ecosystem, bioluminescence of some of the species, and identification of the isolates after growth of a mixture of colonies on plates by performing physiological tests that differentiate species

(Budsberg et al., 2003; Reichelt and Baumann, 1973). However, Hilgarth et al. (2018a) already tested several media for the isolation of photobacteria from meat, and proved that without a selective agent and choice of proper growth conditions (low temperature), detection of photobacteria by culture-dependent methods was unlikely. The study also proved that identification of species by means of MALDI-TOF MS technology is possible, and simplifies the process. Still, culture-dependent methods require a heavy work-load and several days to obtain a positive result, needed for isolation but suboptimal for screening and detection.

Additionally, several studies make use of culture-independent studies (e.g. amplicon sequencing) for the detection of photobacteria in large batches of samples (Bouju-Albert et al., 2018; Pennacchia et al., 2011; Pini et al., 2020; Stoops et al., 2015). The technology is able to detect non-cultivated species that would be otherwise overlooked if growth conditions are not appropriate, but the discriminatory power is reduced since 16S gene sequence is almost 100% identical for close species of photobacteria (Hilgarth et al., 2018b; Sawabe et al., 2007) and the technology is expensive, and therefore not recommended for routine screening and control.

Dalgaard et al. (1996) developed a conductance based method for the detection of *P. phosphoreum* on fish by detection of reduction of TMAO, and Macé et al. (2013) developed a Real-Time PCR approach for the detection of the same species on fish. Both methods have proven to be able to detect the species of photobacteria on fish, but are untested on meat and meat products where photobacteria are not the predominant species. Both make use of specialized equipment and sample preparation. Additionally, the conductance method targets a reaction that is not prominent on meat since TMAO is not an abundant substance in it (Gram and Dalgaard, 2002).

4 Hypotheses

The shelf-life of raw meat is highly influenced by the microbiota present on its surface at the moment of packaging. Growth of spoilage bacteria originally present on it heavily reduces not only its organoleptic properties, but also its safety over time. The control over the growth of spoilage bacteria increases the shelf-life of the product, and the study of their behavior and dynamics helps establish the due-date more accurately, reducing the chances of the consumer discarding the product and the amount of waste. Photobacteria are nowadays regarded as common meat spoilers, yet they are still often overlooked and not much is known of their metabolism on that niche. The study of the meat-spoilage relevant species of the *Photobacterium* genus, therefore, fills a gap in meat science, which is required to further improve its preservation and quality. Molecular approaches should be developed, probed and exploited to detect, and monitor photobacteria in meat and other cold stored foods. Genomic and proteomic analyses should be employed to enable a reference to their natural habitats, and characterize their adaptation to the meat environment and response to different gases used in modified atmosphere packaging.

The working hypotheses of this study are divided into three chapters following postulates based on a common general objective.

Chapter 1: Detection of photobacteria

This section aimed at the development of a qualitative DNA-based detection method for the rapid detection of *Photobacterium* species on raw meat and associated surfaces to help investigate their origin and prevalence. The following postulates were probed:

- It is possible to develop a culture-independent method to rapidly confirm the presence/absence of photobacteria on raw meat and the processing environment in addition to the developed isolation method.
- LAMP technology provides the necessary traits for such a method: quick sample procedure, high fidelity, high specificity

These postulates were studied within the scope of the publication:

Fuertes-Perez, S., Hilgarth, M., Vogel, R.F., 2020. Development of a rapid detection method for *Photobacterium* spp. using Loop-mediated isothermal amplification (LAMP). Int J Food Microbiol 334. https://doi.org/10.1016/j.ijfoodmicro.2020.108805

Chapter 2: Characterization, diversity and comparative genomics of photobacteria isolated from marine and terrestrial sources

The aim of this section was to investigate the biodiversity of photobacteria on species level and below. Isolated strains of *P. carnosum*, *P. phosphoreum* and *P. iliopiscarium* should be identified and characterized based on physiological traits. In addition, comparative genomics should be utilized to further characterize divergence between species and strains and a putative correlation should be probed between their growth dynamics and predicted metabolism. The following postulates were probed:

- Photobacteria are abundant on different cold-stored food products
- *Photobacterium* diversity is dependent on the product
- The environmental niche of photobacteria is represented in the genome and phylogenetic relationships
- There is a clear delineation within the three species of photobacteria isolated from raw meat based on source of isolation, and contaminating strains present phenotypic and genotypic divergence, leading to environmentally driven adaptation, compared to those isolated from marine animals or seawater.
- The three species harbor high intra- and inter-species diversity within their genomes that explains differences on distribution and growth.

These postulates were studied within the scope of the publications:

Fuertes-Perez, S.*, Hauschild, P.*, Hilgarth, M., Vogel, R.F., 2019. Biodiversity of *Photobacterium* spp. isolated from meats. Front Microbiol 10, 2399. https://doi.org/10.3389/fmicb.2019.02399. *Shared first authorship for equal contribution.

Fuertes-Perez, S., Vogel, R.F., Hilgarth, M., 2021. Comparative genomics of *Photobacterium* species from terrestrial and marine habitats. Curr Res Microb Sci 2. https://doi.org/10.1016/j.crmicr.2021.100087.

Chapter 3: Proteomic adaptation of photobacteria towards different modified atmospheres

This section aimed to elucidate the adaptation of selected strains towards the modified atmospheres applied to packages of raw meat. To prove this, growth experiments should be conducted under modified atmospheres and a comparative proteomics study should be performed to characterize the influence of carbon dioxide, oxygen and their combination.

- Proteomic profiling can be used to study the adaptation of photobacteria to different conditions

- Photobacteria do not significantly change their metabolism based on the gas atmosphere.
- Commonly used gas mixtures are unable to reduce or inhibit the growth of *P. carnosum* and *P. phosphoreum* strains *in vitro*.

These postulates were studied within the scope of the publication:

Fuertes-Perez, S., Abele, M., Ludwig, C., Vogel, R.F., Hilgarth, M., 2022. Impact of modified atmospheres on growth and metabolism of meat-spoilage relevant *Photobacterium* spp. as predicted by comparative proteomics. Submitted manuscript.

5 Overall materials and methods

A summarized version of the overall materials and methods of all publications is included here.

The focus of this work is on the three species *Photobacterium carnosum*, *P. phosphoreum* and *P. iliopiscarium*. Members of said species isolated during this work are displayed in Table 2.

Table 2. List of self-isolated strains of the three species of photobacteria used in this study, including source and atmosphere of isolation, and the publication in which they were used.

Species	Strain	Source of isolation	Gas atmosphere	Section used
P. phosphoreum	TMW 2.2033	Chicken	MAP	1; 2; 3
	TMW 2.2034	Chicken	MAP	1; 2; 3
	TMW 2.2103	Beef	MAP	1; 2; 3; 4
	TMW 2.2125	Marinated turkey	Air	1; 2; 3
	TMW 2.2126	Marinated chicken	MAP	1; 2; 3
	TMW 2.2127	Marinated chicken	MAP	1; 2
	TMW 2.2128	Marinated chicken	MAP	1; 2
	TMW 2.2129	Marinated chicken	MAP	1; 2
	TMW 2.2130	Marinated chicken	MAP	1; 2; 3
	TMW 2.2131	Marinated chicken	MAP	1; 2
	TMW 2.2132	Marinated chicken	MAP	1; 2; 3
	TMW 2.2133	Marinated chicken	MAP	1; 2
	TMW 2.2134	Marinated chicken	MAP	1; 2; 3; 4
	TMW 2.2135	Marinated chicken	MAP	1; 2
	TMW 2.2136	Marinated chicken	MAP	1; 2
	TMW 2.2137	Marinated chicken	MAP	1; 2
	TMW 2.2138	Pork	Air	1; 2
	TMW 2.2139	Pork	Air	1; 2
	TMW 2.2140	Pork	Air	1; 2; 3
	TMW 2.2141	Marinated beef	MAP	1; 2
	TMW 2.2142	Marinated beef	MAP	1; 2; 3
	TMW 2.2143	Marinated beef	MAP	1; 2
	TMW 2.2144	Marinated beef	MAP	1; 2
	TMW 2.2145	Marinated beef	MAP	1; 2
P. carnosum	**TMW 2.2021^T / DMS 105454^T ***	Chicken	MAP	1; 2; 3; 4
	TMW 2.2022*	Chicken	MAP	1; 2
	TMW 2.2029*	Chicken	MAP	1; 2; 3
	TMW 2.2030*	Chicken	MAP	1; 2
	TMW 2.2097	Pork	MAP	1; 2; 3
	TMW 2.2098	Salmon	MAP	1; 2; 3
	TMW 2.2099	Salmon	MAP	1; 2
	TMW 2.2146	Chicken	MAP	1; 2
	TMW 2.2147	Chicken	MAP	1; 2; 3
	TMW 2.2148	Beef	Air	1; 2

	TMW 2.2149	Pork	MAP	1; 2; 3; 4
	TMW 2.2150	Chicken	Air	1; 2; 3
	TMW 2.2151	Marinated chicken	MAP	1; 2
	TMW 2.2152	Marinated chicken	MAP	1; 2
	TMW 2.2153	Marinated chicken	MAP	1; 2
	TMW 2.2154	Marinated chicken	MAP	1; 2
	TMW 2.2155	Marinated chicken	MAP	1; 2
	TMW 2.2156	Marinated chicken	MAP	1; 2
	TMW 2.2157	Marinated chicken	MAP	1; 2; 3
	TMW 2.2158	Marinated chicken	MAP	1; 2
	TMW 2.2159	Marinated chicken	MAP	1; 2
	TMW 2.2160	Marinated chicken	MAP	1; 2
	TMW 2.2161	Marinated chicken	MAP	1; 2
	TMW 2.2162	Marinated chicken	MAP	1; 2
	TMW 2.2163	Marinated chicken	MAP	1; 2; 3
	TMW 2.2164	Marinated chicken	MAP	1; 2
	TMW 2.2165	Marinated chicken	MAP	1; 2
	TMW 2.2166	Marinated chicken	MAP	1; 2
	TMW 2.2167	Marinated chicken	MAP	1; 2
	TMW 2.2168	Marinated chicken	MAP	1; 2
	TMW 2.2169	Marinated turkey	Air	1; 2; 3
	TMW 2.2186	Salmon	MAP	2; 3
	TMW 2.2187	Salmon	MAP	2; 3
	TMW 2.2188	Salmon	MAP	2; 3
	TMW 2.2189	Salmon	MAP	2; 3
	TMW 2.2190	Salmon	MAP	2; 3
	TMW 2.2035	Chicken	MAP	1; 2; 3
P. iliopiscarium	TMW 2.2172	Pork	MAP	1; 2
	TMW 2.2104	Pork	MAP	1; 2; 3

TMW = Lehrstuhl für Technische Mikrobiologie Weihenstephan, Technical University of Munich, Freising, GER.

DMS = Deutsche Sammlung von Mikroorganismen und Zellkulturen (DMSZ), Darmstadt, GER.

^{T} = marks the type strain of a species

1 = Development of a rapid detection method for *Photobacterium* spp. using Loop-mediated isothermal amplification (LAMP) (Section 6.1)

2 = Biodiversity of *Photobacterium* spp. isolated from meat (Section 6.2.1)

3 = Comparative genomics of *Photobacterium* species from terrestrial and marine habitats (Section 6.2.2)

4 = Impact of modified atmospheres on growth and metabolism of meat-spoilage relevant *Photobacterium* spp. as predicted by comparative proteomics (Section 6.3)

*Isolates obtained from previous work by Hilgarth et al. (2018b)

5.1 Isolation and detection of photobacteria

Isolation of photobacteria was performed as described by Hilgarth et al. (2018a), by homogenization of raw meat (or other types of food samples) in marine broth, plating the

resulting suspension on marine agar supplemented with 3g/L meat extract and 7 mg/L vancomycin, and incubating for 72h at 15 °C. Isolates were identified with MALDI-TOF MS by their low-molecular subproteome, and kept at -80 °C in glycerol solution for preservation until further use.

Routine cultivation of strains of photobacteria was performed aerobically in marine broth supplemented with 3 g/L meat extract at 15 °C for 48-72 h as described by Hilgarth et al. (2018a). A list of cultivation media and conditions is included in Table 3.

Table 3. Cultivation conditions for *Photobacterium* spp. during the present work.

Use	Media	Temperature	Incubation time	Atmosphere
Routine cultivation	Marine broth (supplemented 3 g/L meat extract, pH 7.6)	15 °C	48 - 72h	aerobic
Routine isolation	Marine agar (supplemented 3 g/L meat extract and 7 mg/L vancomycin, pH 7.6)	15 °C	72h	aerobic
Biodiversity growth analysis	Meat extract media (20 g/L meat extract, 20 g/L NaCl, pH 5.8)	4 °C	72h	aerobic
Proteomics pre-culture	Meat extract media (20 g/L meat extract, 20 g/L NaCl, pH 5.8)	15 °C	72h	aerobic/anaerobic
Gas influence	Meat simulation media (60 g/L meat extract, 0.5 % glycerol (w/v), 0.05 mM Tween 80, 2 µg/ml heminchloride, pH 5.8)	15 °C	48h	aerobic N_2 (100 %) O_2/N_2 (70/30%) N_2/CO_2 (70/30 %) $O_2/CO_2/N_2$ (21/30/49 %) O_2/CO_2 (70/30 %)

Loop-mediated isothermal amplification (LAMP) was the method chosen for the development of a rapid, culture-independent method for screening the presence and absence of photobacteria on raw meat and processing environment. The trimethylamine-N-oxide reductase (*tor*A) gene was chosen as the target for the primer design. Specificity was tested against species of photobacteria and species of common meat spoilers. Sensitivity of the reaction was tested by carrying out the detection approach of progressively smaller amounts of target DNA, while speed of the reaction and contribution of the primers was tested by monitoring in real time the progression of the LAMP assay. Several protocols for the fast processing of raw meat samples and DNA extraction were tested and optimized for utilization together with the LAMP assay. As a final step, the efficiency of the method was tested first on artificially contaminated samples of raw meat, and finally on naturally contaminated samples of pork, beef and chicken in a trial against the already optimized culture-dependent method for isolation of photobacteria (Figure 1).

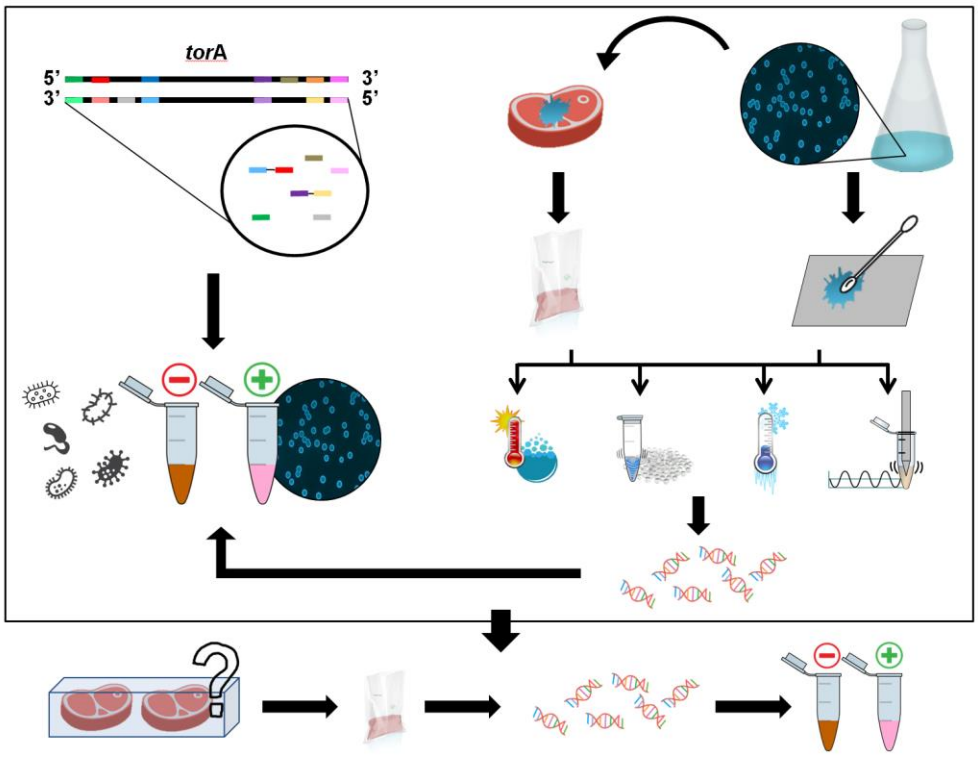

Figure 1. Graphical representation of protocol followed for the development of a LAMP-based approach for the detection of *Photobacterium* spp. on meat (Section 6.1)(Fuertes-Perez et al., 2020).

5.2 Characterization, diversity and comparative genomics of photobacteria isolated from marine and terrestrial sources

Several types of raw meat were probed for the presence of photobacteria using the aforementioned isolation method. Strain delineation was performed by genomic fingerprinting (RAPD)-PCR. The study of physiological diversity of photobacteria from meat was assessed by carrying out a diversity index analysis, experiments of growth dynamics on meat extract media, comparison of metabolic activities such as production of acid from multiple carbon sources (API 50CH), enzymatic activities (API ZYM), motility, bioluminescence and antibiotic resistance (Figure 2).

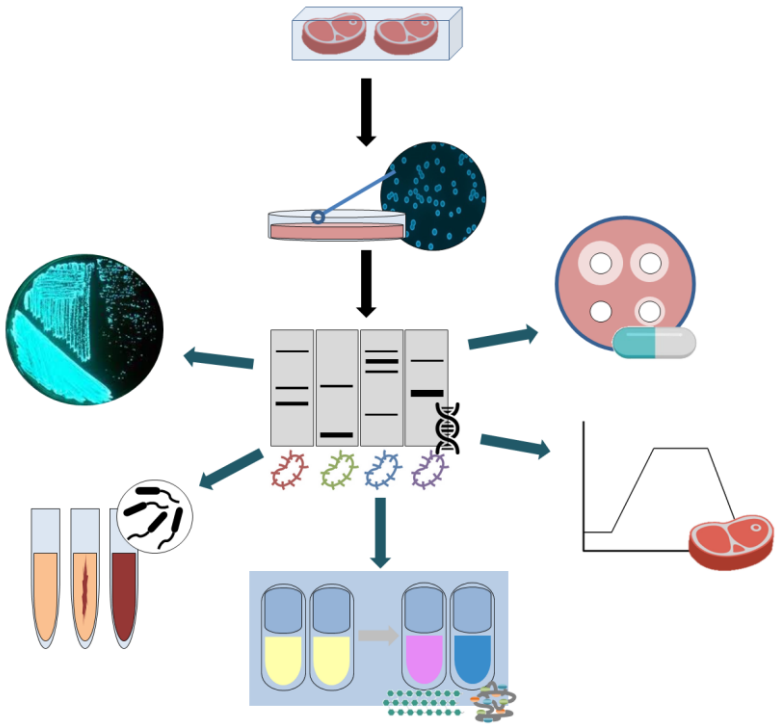

Figure 2. Graphical representation of protocol followed for the diversity analysis of strains of relevant species of photobacteria (Section 6.2.1)(Fuertes-Perez et al., 2019).

The study of the genomic features was performed on a total of 53 strains of photobacteria from both marine and terrestrial environments, with meat-borne strains being selected from those identified on the biodiversity analysis based on physiological characteristics. Genomes were either sequenced, from self-isolated strains, or obtained from NCBI database. Phylogenetic relationships were assessed by means of multilocus-sequence alignment (MLSA), *fur* gene, ANI values and codon usage. Additionally, we used online tools to search for plasmids with plasmidSPADES, phages with PHASTER, CRISPR-cas operons with CRISPR-finder, and secondary metabolites and bacteriocins clusters with BAGEL and antiSMASH. Finally, a targeted gene search allowed us to predict metabolic pathways, behavior and environmentally driven adaptations of the three species and their strains based on gene annotation (Figure 3).

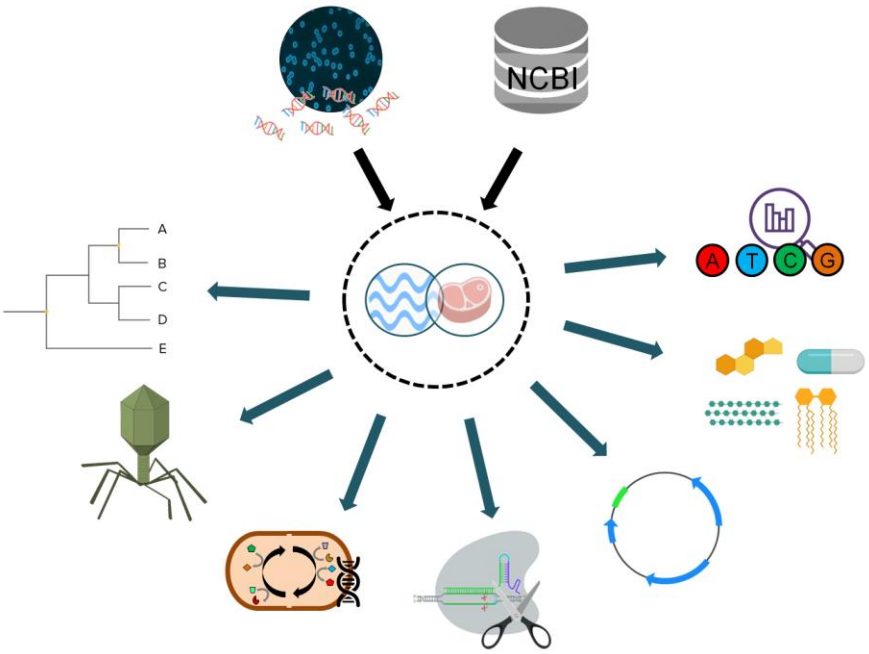

Figure 3. Graphical representation of protocol followed for the comparative genomics study of strains of *Photobacterium* spp. (Section 6.2.2)(Fuertes-Perez et al., 2021)

5.3 Proteomic adaptation of photobacteria towards different modified atmospheres

The effect of different gases on the growth and metabolism of photobacteria was assessed by performing and monitoring growth experiments on a meat simulation media at 15 °C under different atmospheres of two strains of both *P. phosphoreum* and *P. carnosum* species in triplicate. Gas atmospheres included: (a) air, (b) N_2, (c) O_2 (70%) / N_2 (30%), (d) N_2 (70%) / CO_2 (30%), (e) O_2 (21%) / CO_2 (30%) / N_2 (49%), (f) O_2 (70%) / CO_2 (30%). Growth parameters were obtained from the growth curves via RStudio software, and statistical analysis was carried out to identify significant differences. During exponential growth, samples were taken, processed, and analyzed by LC-MS/MS in order to obtain the proteome expression under each gas atmosphere. A comparative proteomics approach was performed via Perseus software in order to determine differentially expressed proteins between conditions, and therefore the effect of each individual gas: air, high oxygen (70%), anoxic conditions, carbon dioxide (30%), and the study of synergistic effects between carbon dioxide and oxygen (Figure 4).

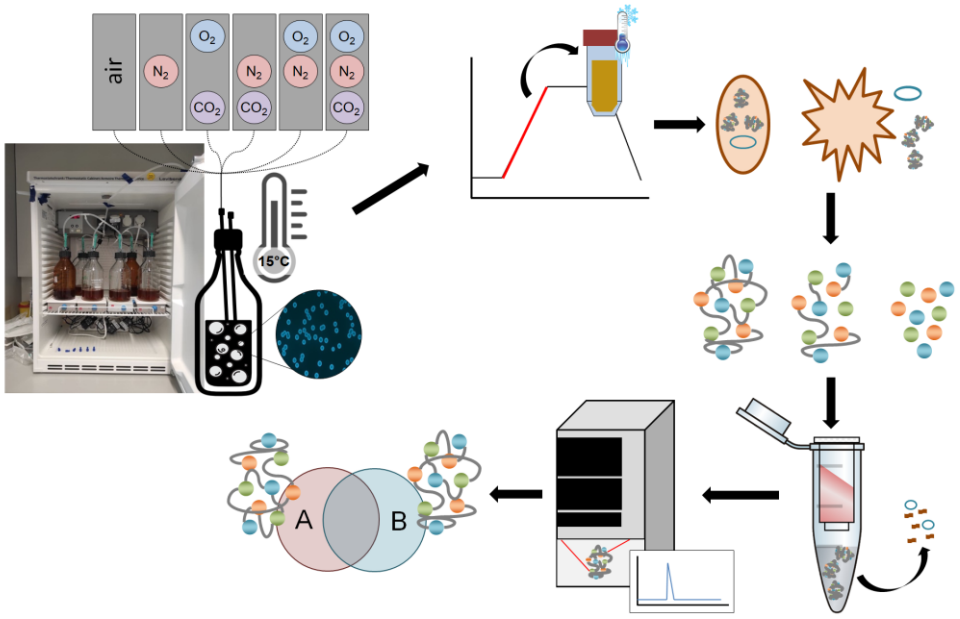

Figure 4. Graphical representation of protocol followed to study the influence of different gas atmospheres on the proteome of *Photobacterium* spp. (Section 6.3)(Fuertes-Perez et al., 2022)

6 Results (Publications)

6.1 Development of a rapid detection method for *Photobacterium* spp. using Loop-mediated isothermal amplification (LAMP)

The following work presents a novel LAMP-based methodology for detection of meat-spoilage relevant species of photobacteria, and an adapted procedure for quick processing of meat samples prior to performing the detection. The LAMP technology was chosen for its specificity, speed and the lack of dependency on specialized equipment. The six primers were designed to target the gene *tor*A, encoding the trimethylamine-N-oxide reductase enzyme, present in all *Photobacterium* species. The detection method was optimized based on primers performance and optimum temperature to give a positive/negative result in 1h, tested for specificity against multiple strains and species of photobacteria, and common meat spoilers, and for sensitivity, showing a detection limit close to culture-dependent methods. We additionally optimized the processing of the meat sample to be carried out in less than one hour, and tested the whole procedure on artificially contaminated samples. The final test consisted on comparing the detection of photobacteria with both the LAMP procedure and the adapted culture-dependent method on naturally contaminated samples of chicken, pork and beef. The LAMP methodology was able to give a positive result for one of the chicken samples in two hours, compared to the three days required for the alternative culture-dependent method, confirming additionally similar sensitivities. Although not quantitative, the present procedure could be a potent screening tool to control occurrence, distribution and entry route on the industry, but also as a screening tool for contaminated batches to pre-select for isolation.

Author contribution: Sandra Fuertes-Perez performed the experimental design and laboratory work concerning design of primers, testing and optimization of the methodology. In addition, she performed the data evaluation, wrote the first draft of the manuscript, created figures and tables, and participated in the reviewing process of the final text.

Publication agreement: The work presented in the next pages was published in the *International Journal of Food Microbiology* under subscription to Elsevier, current holder the publication rights. Under copyright policy of Elsevier, author rights authorize the authors of a publication to “Include in a thesis or dissertation (provided it is not published commercially)”.

International Journal of Food Microbiology 334 (2020) 108805

Contents lists available at ScienceDirect

International Journal of Food Microbiology

journal homepage: www.elsevier.com/locate/ijfoodmicro

Development of a rapid detection method for *Photobacterium* spp. using Loop-mediated isothermal amplification (LAMP)

Sandra Fuertes-Perez, Maik Hilgarth*, Rudi F. Vogel

Lehrstuhl Technische Mikrobiologie, Technische Universität München, 85354 Freising, Germany

ARTICLE INFO

Keywords:
Photobacterium carnosum
Photobacterium iliopiscarium
Photobacterium phosphoreum
Meat spoilage
Psychrophiles
Modified atmosphere packaging

ABSTRACT

While the abundance of photobacteria has previously been exclusively associated with marine environments and spoilage of seafood, several recent studies have demonstrated their status as pervasive constituents of the microbiota on packaged meats. Since their ubiquitous nature has been revealed, detection of their presence on meat, their entry route into meat processing environments and prevention of their growth is a novel emerging challenge for the food industry.

In this study, we have developed a highly sensitive and specific loop-mediated isothermal amplification (LAMP) assay for the detection of relevant species of photobacteria on foods, and tested its efficacy on meats. The gene encoding trimethylamine-N-oxide reductase (*tor*A) was chosen as the target for this assay. Designed primers based on the gene sequence proved their specificity by testing 67 isolates of 5 species of photobacteria (positive) as well as 63 strains of 16 species of other common meat spoilers (negative). The optimized assay takes 2 h including sample preparation and has a detection limit of only 10–11 copies (50 fg/reaction) of the average *Photobacterium* (*P.*) genome per reaction. Its applicability could be successfully demonstrated on naturally and artificially contaminated chicken, beef and pork samples and evaluated by comparison with a culture-dependent approach using selective media and MALDI-TOF MS for identification. The developed LAMP assay revealed presence of photobacteria on one naturally contaminated chicken sample stored at 4 °C long before (3 days) confirmation by the culture-dependent approach. This study demonstrates that the developed LAMP assay represents a reliable and sensitive method for rapid detection of photobacteria on meats. However, its specificity would allow the applicability of the methodology to be extended to other foods, e.g. fish and seafood where presence of photobacteria is directly linked to their shelf life. The method has no requirement for specialized equipment or specially trained personal allowing an easy implementation within the quality control of the food industry. Considering the lot-to-lot variations observed on meats regarding the presence of photobacteria and the impracticality of implementing quantitative methods within the routine control, the LAMP method can simplify and reduce the workload for detection of photobacteria on high sample numbers. Consequently, producers can identify batches/plants that need more stringent control, and are provided with a tool to determine the entry route of photobacteria into the processing and distribution chain of raw meats.

1. Introduction

Photobacterium (*P.*) is a genus of gram negative bacteria within the family of *Vibrionaceae* commonly associated with marine environments, usually found as free-living e.g. *P. angustum*, symbiotic e.g. *P. kishitanii* or even pathogenic relationships e.g. *P. damselae* in the sea and with marine animals (Labella et al., 2017; Urbanczyk et al., 2010). The genus includes known potent seafood spoilers *P. phosphoreum* (Ast and Dunlap, 2005; Dalgaard et al., 1997) and *P. iliopiscarium* (Takahashi et al., 2015), producers of biogenic amines and causatives of scombroid fish poisoning (Bjornsdottir-Butler et al., 2018; Emborg et al., 2002; Jorgensen et al., 2000; Lehane and Olley, 2000; Torido et al., 2012). However, novel recent studies have demonstrated their presence distant from marine environments. Photobacteria have been reported in amplicon sequencing studies on air and vacuum packaged beef (Pennacchia et al., 2011), modified atmosphere packaged (MAP) minced beef (Stoops et al., 2015), pork sausages (Bouju-Albert et al., 2018) and dry-fermented sausages (Pini et al., 2020). Additionally,

Abbreviations: LAMP, loop-mediated isothermal amplification; *P.*, *Photobacterium*; MALDI-TOF MS, matrix-assisted laser desorption/ionization-time of flight mass spectrometry

* Corresponding author.
E-mail addresses: sandra.fuertes-perez@tum.de (S. Fuertes-Perez), maik.hilgarth@tum.de (M. Hilgarth), rudi.vogel@wzw.tum.de (R.F. Vogel).

https://doi.org/10.1016/j.ijfoodmicro.2020.108805
Received 29 April 2020; Received in revised form 23 July 2020; Accepted 27 July 2020
Available online 06 August 2020

recent works have recovered multitude of isolates of *P. phosphoreum, P. iliopiscarium* and a novel species, *P. carnosum,* from pork (Hilgarth et al., 2018b; Nieminen et al., 2016), poultry, beef and turkey (Fuertes-Perez et al., 2019; Hilgarth et al., 2018b; Hilgarth et al., 2018c), including marinated meats. These studies have additionally revealed that photobacteria occur independently of the type of packaging used, i.e. air or protective packaging such as vacuum or modified atmospheres. A metatranscriptomic study on poultry meat by Höll et al. (2019) has also predicted the production of potent spoilage products e.g. biogenic amines, including putrescine, cadaverine, agmatine and tyramine. Their globally-spread occurrence on several types of meat and packaging conditions, and their ability to grow and reach relevant cell numbers of over 8 log CFU/g on meat ascertains these species as common meat spoilers (Fuertes-Perez et al., 2019).

Since common practices for reduction of spoilage microbiota e.g. change in the packaging atmosphere (Bingol and Ergun, 2011; Lorenzo and Gomez, 2012; McMillin, 2008) or use of marinades (Björkroth, 2005; Kargiotou et al., 2011) appear to not inhibit photobacterial growth, their presence becomes increasingly relevant for the food industry i.e. correct assignment of minimum shelf life, prevention of premature spoilage and identification of their entry route of contamination on meat in order to establish preventive measures. In addition to reports on their ability to produce biogenic amines, Dalgaard et al. (1998) have already proven that inhibition of photobacteria on fish has great impact on its shelf-life, emphasizing their role as spoilage microbiota. Therefore, prevention of the presence of *Photobacterium* species most likely has similar effects on meat shelf-life. In this context, a rapid and sensitive methodology for detection of photobacteria, easily transferable to on-site detection in the meat, fish and seafood industries, will function as a decision aid to determine in which batches of the raw material/packaged product, and in which sectors of a production plant more stringent control over presence of photobacteria is needed.

Available methodology for the specific isolation of photobacteria on meat so far is limited to a selective culture-dependent approach including identification by MALDI-TOF MS (Hilgarth et al., 2018b). This method, although reliable, requires 3 days to confirm the presence and enable enumeration of photobacteria, at which point the meat is already distributed and might be even past its shelf-life.

Culture-independent studies that include amplicon sequencing are additionally available for the detection of photobacteria as mentioned before (Bouju-Albert et al., 2018; Pennacchia et al., 2011; Pini et al., 2020; Stoops et al., 2015), but represent both time-consuming and expensive detection methods. Alternative methodology includes *P. phosphoreum* specific detection methods on fish products: a conductance based method (Dalgaard et al., 1996) and a PCR based detection method (Mace et al., 2013). Both methods, although specific, have not been optimized or tested on meat, and require specialized equipment and trained personal, which renders them impossible to be implemented as fast or routine (on-site) analysis in the food industry.

In contrast to these methods, loop-mediated isothermal amplification (LAMP) (Notomi et al., 2000) is a culture-independent assay that allows the in vitro amplification of specific DNA. Although similar to conventional PCR, the *Bst* DNA polymerase used in this assay is able to carry out the reaction at a constant temperature in 1 h due to its strand-displacement polymerase activity. It additionally allows direct evaluation of the results by including a method for detection of amplicons in the reaction mixture (e.g. turbidity determination, pH indicators). Both of these characteristics eliminate the need for specialized equipment (e.g. thermal cycles) or subsequent visualization by gel electrophoresis or sequencing.

The reaction requires addition of at least four primers: forward inner primer (FIP), backward inner primer (BIP), forward outer primer (F3) and backward outer primer (B3); with the possibility to include forward (LF) and backward (LB) loop primers that increase the speed, specificity and sensitivity of the reaction. Its mechanism is based on the formation of dumbbell-like DNA structures and conversion into stem-loop DNA by self-primed DNA synthesis. At the end of the reaction, several strands with varying number of repeats of the target sequence are formed, and thus products of different increasing size (Nagamine et al., 2002).

In summary, LAMP can function as a highly specific, sensitive, and fast assay, already being used on food for the detection of bacterial pathogens (e.g. *Listeria monocytogenes* on raw milk), detection of mycotoxin producers (e.g. *Aspergillus niger* Ochratoxin A producing strains) and food spoilage organisms (*Shewanella putrefaciens* on fish) (Niessen et al., 2013). The LAMP technology allows the detection of target sequences with no more requirements than a water bath and with direct visual evaluation after 1 hour reaction time.

Consequently, the aim of this study was to develop and optimize a qualitative LAMP approach for rapid detection of photobacterial species that are relevant to meat spoilage, but also present on fish and seafood, exhibiting high specificity and sensitivity. In addition, this study could confirm the applicability of the LAMP approach on meat samples to facilitate transfer and implementation within the food industry. As a fast and effortless screening method, it should reduce the workload as it enables an overview on lot-to-lot variations and a focus on contaminated samples, which only then should be tested with quantitative (elaborate) methods. Application of the methodology would act as a primary test and “decision aid” for producers to identify sectors, products and batches that require additional, more stringent control.

2. Materials and methods

2.1. Bacterial template DNA preparation

Bacteria used in this study are listed in Tables S1 and S2. Cultures of photobacteria were prepared in marine broth (MB, BD Difco) supplemented with 3 g/l meat extract, and incubated at 15 °C (10 °C for *Photobacterium profundum*) for 72 h. Common meat spoilers were grown in brain heart infusion (BHI, BD Difco) at 25 °C for 24 h.

DNA extraction was performed with E.Z.N.A. bacterial DNA extraction kit (OMEGA bio-tek, USA) using 3–5 ml of over-night cultures. Cells were centrifuged at 4000 × *g* for 10 min, and washed once with TE buffer (10 mM Tris, 1 mM EDTA, pH 8.0) before using the pellet for DNA extraction. The protocol was followed according to the manufacturer's instructions employing slight modifications to enhance extraction of the DNA. Incubation of the sample with lysozyme was prolonged to 1.5 h at 37 °C, followed by addition of glass beads and mixing on a vortexer for 5 min to lyse all cells. Incubation with RNase A was prolonged to 30 min at room temperature. After centrifugation of the empty columns for 2 min at maximum speed, the columns were left to dry at room temperature for 30 min. Finally, pre-heated (65 °C) elution buffer was added and incubated for 20 min at room temperature before centrifugation.

Concentration of bacterial DNA was determined in a NanoDrop 1000 spectrophotometer (Peqlab Biotechnologie GmbH, Erlangen, Germany), and adjusted to 10 ng/µl with sterile deionized water.

2.2. Loop-mediated isothermal amplification of DNA

Primers were designed with PrimerExplorer V5 software, based on the consensus sequence of the *tor*A gene from *Photobacterium carnosum* (TMW2.2021^{T} CIK00 00580, TMW2.2029 CIT27 02430), *Photobacterium phosphoreum* (TMW2.2033 MT385314, TMW2.2034 MT385315) and *Photobacterium iliopiscarium* (TMW2.2035 MT385313). Primer sequences are listed in Table 2.

The reaction mixture used for the LAMP amplification was adjusted for 25 µl total volume and 50 ng of total template DNA per reaction of purified DNA. Neutral red (2.5 mM, SERVA Electrophoresis GmbH, Heidelberg, Germany) was used as pH indicator to determine positive LAMP reactions, together with ammonium sulphate buffer (100 mM

Table 1
Composition of the reaction mixture for a total of 25 µl LAMP reaction volume.

	Volume per reaction (µl)	LAMP	Real-time LAMP
Buffer 10×	2.5	Ammonium sulphate buffer	MOPS buffer
Magnesium chloride ($MgCl_2$)	1		
Nucleotides (dNTPs)	3.5		
Primer mix	2.6		
Dye/pH indicator	1	Neutral red	V13-01184
Bst polymerase (8 U/µl)	1		
Water	8.4		
Template DNA	5		

ammonium sulphate, 100 mM potassium chloride, pH 8.7), magnesium chloride (200 mM), nucleotide mixture (10 mM each dNTP, ThermoFisher Scientific, Schwerte, Germany), primer mix (1.6 mM each FIP_torA and BIP_torA, 0.8 mM each LF_torA and LB_torA, and 0.2 mM each F3_torA and B3_torA) and *Bst* polymerase (8 U/µl, New England BioLabs GmbH, Frankfurt am Main, Germany). The water used was distilled, sterile filtered (0.2 µm filter, Sartorius Minisart, Goettingen, Germany) and UV treated (30 min). Sterile filter tips were used for pipetting to avoid contamination. The composition of the reaction mixture is shown in Table 1.

The LAMP reaction was tested from 50 °C to 70.5 °C to determine the optimum temperature using the same protocol described above both with and without loop primers included in the mixture. Positive reactions were indicated by a color change from yellow to pink.

The rest of the LAMP reactions were all performed for 1 h at 63 °C, chosen as optimum temperature as described later in the results (Section 3.1).

Sensitivity of the method was determined by applying the same protocol described above, and using as template serial dilutions of *Photobacterium carnosum* TMW2.2021^T purified DNA in water up to 10 fg/reaction.

Primer binding activity during LAMP reaction was determined with a real-time fluorescent reader (ESEQuant TS, Qiagen, Venlo, The Netherlands). V13-01184 DNA-intercalating dye (2.5 mM, Dyomics GmbH, Jena, Germany) was used instead of neutral red, together with MOPS buffer (200 mM MOPS (Gerbu Biotechnik GmbH, Heidelberg, Germany), 100 mM potassium chloride, 100 mM ammonium sulphate, pH 8.8) (Table 1). The protocol was performed according to Frisch and Niessen (2019).

Extracted purified DNA of *P. carnosum* TMW2.2021^T adjusted to 10 ng/µl was used as positive control for all LAMP assays, while sterile deionized water was used as negative control. Reactions were performed in triplicates.

2.3. Confirmation of the LAMP target

In order to confirm the target of the LAMP amplification after using *P. carnosum* TMW2.2021^T purified DNA as template, amplicons were electrophoretically separated, and the lowest molecular weight band observed in the gel was cut and purified using E.Z.N.A. gel extraction kit (OMEGA bio-tek, USA) according to instructions of the manufacturer. The concentration of the purified product was increased by a second amplification with primers F2_torA and B2_torA (Table 2) following the reaction mixture and thermoprotocol described in Tables S3 and S4 in order to enhance sequencing quality. Finally, secondary amplification product was subjected to Sanger sequencing using the same primers and the resulting sequences identified by using BLASTn.

2.4. Artificial contamination of meat samples

Fresh meat pieces (approximately 10 g, 20 cm^2) of MAP pork, chicken and beef were aseptically cut out and inoculated with 1 ml of a grown culture of *Photobacterium carnosum* TMW2.2021^T by dispensing it on top of the meat piece. Equally prepared samples of the three types of meat were instead inoculated with 1 ml of sterile media, serving as a negative control for the DNA extraction from meat. The meat samples were then treated as described in the following section (Section 2.5) for DNA extraction from meat samples and used to perform a LAMP reaction.

Table 2
List and sequence of primers used in this study. Degenerated bases were used according to IUPAC nomenclature: R (A or G), Y (C or T), W (A or T), M (C or A), K (T or G), S (G or C), D (A, G or T), B (C, G or T).

Primer	Sequence (5′–3′)
F3_torA	GGCARCAAGGRTTRGTYGA
B3_torA	GCCAAAAWGGGAATTTWTCMGAT
FIP_torA	TCCAGAAGGYGTWCCKARDCYATTA-ATTTMCMACWGAYCARACCT
BIP_torA	ATAGYCGTAAAATWGCBCGTTAT-GCCATGTGAWCGYTCTTC
LF_torA	CTCTAAAAGCMGCATGACTRACA
LB_torA	AACTAYSAGCATTGCCAAGGCC
F2_torA	ATTTMCMACWGAYCARACCT
B2_torA	GCCATGTGAWCGYTCTTC

2.5. Comparison DNA extraction methods from meat samples

Artificially contaminated meat pieces were used to evaluate four different DNA extraction methods (a-d), and additionally a fifth method (e) for surface sampling was tested. Meat samples were homogenized for 1 min with 5 ml of sterile deionized water (with 1% (v/v) Tween 20, 0.85% (w/v) NaCl). From the homogenized suspension, 2 ml were centrifuged (4000 ×*g*, 10 min), supernatant removed and pellet resuspended in 100 µl of TE buffer (pH 8.0). The suspension was subsequently treated according to four different methods for sample preparation: (a) mechanical disruption with glass beads, (b) sonication, (c) freeze/thaw and (d) boiling.

a. Glass beads (~25 mg, 0.1 mm ⌀, Sigma-Aldrich) were added to the suspension for mechanical disruption and cells were vortexed for 15 min at max speed to allow lysis of the cells. The suspension was afterwards centrifuged again (10,000 ×*g*, 10 min), and supernatant was carefully removed and directly used as template for LAMP reaction.
b. The suspension was sonicated for 10 min in a Sonorex Super ultrasonic bath (Bandelin, Berlin, Germany). Afterwards the sample was centrifuged at 10,000 ×*g* for 10 min, and the supernatant was carefully removed and directly used as template for LAMP reaction.
c. Three cycles of freezing/thawing were performed on the sample (Mozioglu et al., 2014). Each cycle consisted on freezing the sample for 5 min at −80 °C, followed by thawing for 10 min in a water bath at 60 °C. Afterwards, the sample was centrifuged at 5000 ×*g* for 10 min at room temperature. The supernatant was then used directly for LAMP assay.
d. The suspension was boiled at 95 °C for 20 min (Mozioglu et al., 2014), followed by brief vortexing and centrifugation at 12,500 ×*g* for 5 min and use of the supernatant directly for LAMP assay.
e. Surface sampling was tested by using a cotton swab on the surface of a petri dish previously wet with a grown culture of *P. carnosum* TMW2.2021T. The end of the cotton swab was then cut out and introduced in Eppendorf tubes containing 100 µl of TE buffer (pH 8.0). The suspension was vortexed for 1 min and sonicated for 10 min to allow disruption of the cells. The cotton swab was then removed and the remaining suspension was directly used for the LAMP assay.

In order to ensure optimum conditions for the LAMP reaction, the

pH of the samples obtained from methods a-e was determined before the LAMP assay, and adjusted when necessary to pH ~8.0 with 1–2 µl of potassium hydroxide (1 M).

2.6. Naturally contaminated meat samples

Fresh MAP chicken (5 samples), pork (3 samples) and beef (3 samples) meat was purchased in local supermarkets, transported on ice to the lab and used the same day of the purchase. Packages were open and the meat was cut in pieces of approximately 10 g and 20 cm^2 surface. For each sample and sampling point, two pieces were packed together and in contact: one for DNA extraction and LAMP reaction, and the other for conventional plating and CFU counting. The pieces were then repacked under high-oxygen modified atmosphere (70% O_2, 30% CO_2, Rotarius VG, Variovac PS SystemPack GmbH, Zarrentin, Germany) and stored at 4 °C. Meat was sampled at days 1, 2, 3, 4, 5 and 6 to determine and quantify the presence of photobacteria. At each time point, samples were taken for extraction of DNA from the meat according to the boiling method, as described in the previous section (Section 2.5), and simultaneously for selective cultivation-based detection method for photobacteria described by Hilgarth et al. (2018b). Samples were homogenized in 5 ml marine broth (3 g/l meat extract), plated on selective marine agar (MB, 3 g/l meat extract, 7 mg/l vancomycin, 1.6% (w/v) agar) and incubated at 15 °C for 72 h. Subsequently, CFU counts were determined and identified by their low-molecular sub-proteome with MALDI-TOF MS (Microflex LT spectrometer, Bruker Corporation, Billerica, MA, USA) using a direct transfer method.

3. Results

3.1. Parameter optimization and specificity of the LAMP based approach

LAMP primers were designed to target a region of approximately 200 bp in the *tor*A gene commonly present within the genus of *Photobacterium*. Fig. 1 shows the LAMP product of type strains of *Photobacterium* species relevant to meat spoilage, resulting in a typical ladder-like amplification pattern. The stringency of the primer was tested by sequencing of the amplicon and confirmed by BLASTn to specifically amplify the *tor*A sequence.

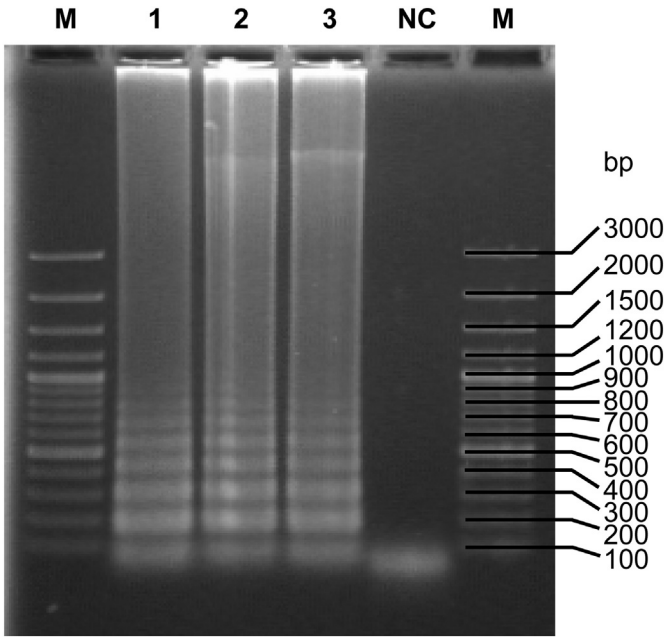

Fig. 1. LAMP amplification products visualized on an agarose gel. Lanes corresponds as follows: M, GeneRuler 100 bp Plus DNA ladder; 1, *Photobacterium carnosum* TMW2.2021^T; 2, *Photobacterium phosphoreum* DSM15556^T; 3, *Photobacterium iliopiscarium* DSM9896^T; NC, Negative control (sterile deionized water used instead of template DNA).

Determination of the optimal temperature and primer applicability was initially performed without addition of the loop primers, observing positive reactions from 57 °C to 63 °C. Subsequent reactions were therefore performed at 63 °C. Later tests with the addition of the loop primers confirmed that the amplification reaction still occurred above that temperature (Fig. 2). The assay shows a full color change (optimum) between 57 °C and 65.5 °C, while a weak color change was observed beyond this range. However, the optimum temperature of the *Bst* polymerase activity is specified to 60–65 °C and therefore, 63 °C was chosen as the optimum reaction temperature for the assay.

In regards to sensitivity, the LAMP assay was able to detect up to 50 fg/reaction (Fig. 3). According to the NCBI database and the available assemblies, out of the three relevant species used to design primers for this study, *P. carnosum* has the smallest genome with 3.97 Mbp, while *P. phosphoreum* has the greatest genome with 4.57 Mbp, being the average between the 3 type strains around 4.31 Mbp. Considering the sensitivity of the assay, the reaction would be able to detect from 11.7 to 10.1 genome copies in the reaction mixture, and an average of 10.7 copies.

The speed of the LAMP reaction was tested with either both loop primers, no loop primers, and the addition of only the forward or the backwards primer (Fig. 4). A lack of loop primers in the reaction leads to an amplification start at approx. 50 min. The maximum intensity of the signal was reached after 65 min, although tests using neutral red confirmed that a positive visual signal (change of color from yellow to pink) is already observed after 60 min. The addition of both loop primers resulted in a drastically reduced reaction time, with a starting amplification after only 10 min and finishing before 15 min of reaction have passed. Addition of only one of the loop primers to the mixture increases the reaction time to 20–25 min until completion, and both loop primers contribute similarly to the performance of the reaction. No signal corresponding to unspecific reactions was observed in the negative control.

The overall specificity of the reaction regarding members of the meat spoilage microbiome was performed by testing the extracted DNA of 63 strains of 16 species of common meat spoilers and of all available strains of *P. carnosum*, *P. phosphoreum* and *P. iliopiscarium* isolated from meat (63 strains) (Tables S1 and S2). Additionally, the type strains of *P. phosphoreum*, *P. iliopiscarium*, *P. kishitanii*, *P. angustum*, *P. profundum* and *P. leiognathi* isolated from marine environments were also included in the analysis. All strains of other meat spoiling genera resulted in a negative reaction, while all strains of *P. carnosum*, *P. iliopiscarium* and *P. phosphoreum* resulted in a positive reaction. Therefore, the specificity for detection of photobacteria could be demonstrated.

The type strains of *P. kishitanii* and *P. leiognathi* also resulted in a positive result, while *P. angustum* and *P. profundum* were negative.

In addition to the purified DNA of meat spoilers directly tested with LAMP, we identified members of the meat spoilage microbiome by MALDI-TOF MS on naturally contaminated meat samples that, when tested with our protocol, resulted in a negative reaction of the homogenized sample (Table S5), thus confirming that DNA of those species are not amplified by the described approach.

3.2. Optimization of the DNA extraction method from meat samples

Four different methods were tested for the preparation of meat samples and DNA extraction in triplicates with three relevant types of meat (poultry, beef, pork) to confirm their reproducibility in regards to purity of the DNA (Fig. 5). Quality of the resulting DNA was assessed by determination of 260/280 and 260/230 ratios that represent purity of the sample in regards to proteins, phenol and other contaminants in the case of the former, and carbohydrates, EDTA and phenol in the case of the latter, co-extracted with DNA. A 260/280 value of 1.8 is generally

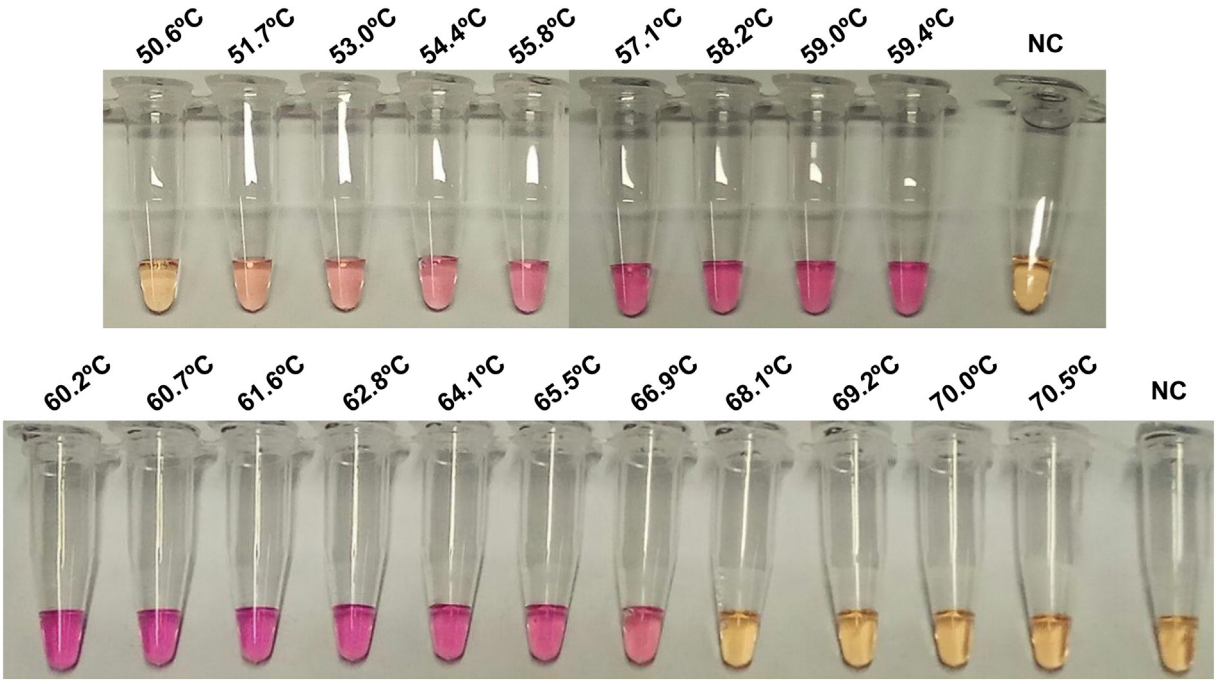

Fig. 2. Temperature gradient of LAMP assay with both loop primers using as template purified DNA of *P. carnosum* TMW2.2021^{T}. Temperatures are indicated for each tube. Yellow color corresponds to negative reaction, pink color corresponds to positive reaction. NC = negative control.

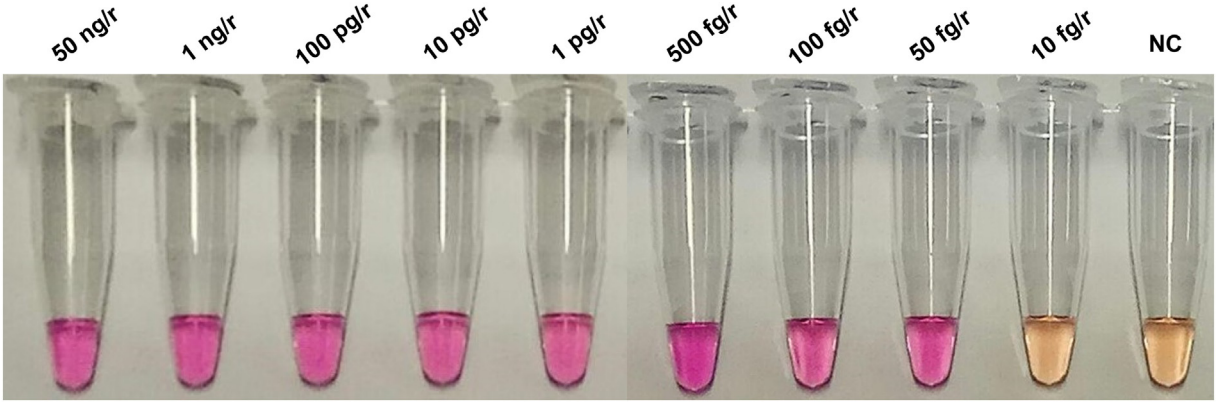

Fig. 3. Sensitivity test of LAMP assay using as template purified DNA of *P. carnosum* TMW2.2021^{T}. Yellow color corresponds to negative reaction, pink color corresponds to positive reaction. ng/r, nanogram of DNA per reaction; NC = negative control.

accepted as pure for DNA, while expected 260/230 values are commonly in the range of 2.0–2.2.

Mechanical disruption with glass beads and sonication were less suitable than boiling and freeze/thaw-cycling. DNA obtained from the former two methods had a lower purity in regards to protein contamination and other possible inhibitors, and a much higher variability (standard deviation) in terms of 260/230 ratio (DNA to carbohydrates, EDTA and phenol ratio). Method c (boiling) was the most suitable method in terms of removal of proteins, while maintaining also an acceptable 260/230 ratio. Concentration of the DNA obtained from the four methods ranged between 200 and 800 ng/μl, rather dependent on the sample than the method, i.e. there were no apparent differences.

Artificially contaminated samples of the three relevant types of meat were processed in triplicates with each of the methods and the resulting DNA suspension was tested with the LAMP assay. Only the samples obtained from the boiling protocol resulted in a positive reaction in all three replicas and three types of meat tested (Fig. 6). It was additionally observed that reaction mixtures with samples obtained from mechanical disruption (both with glass beads and sonication) contained solid particles in the reaction tube after incubation at 63 °C (pictures not shown).

The progression of the LAMP assay with artificially contaminated samples was visually evaluated after 30 min of incubation, and again after 60 min (pictures not shown). After 30 min several of the DNA samples from meat had not yet produced a positive result. However, upon incubating for an additional 30 min up to 1 h total reaction time, samples showed a complete change of color from yellow to pink.

None of the meat samples (chicken, beef and pork) used as negative control for each extraction method resulted in false positive reactions. Samples containing photobacteria were easily differentiated from those used as negative control after applying the boiling protocol.

Finally, in regards to surface sampling, the collection of the *Photobacterium* suspension with a cotton swab did result in positive reactions after 1 h incubation as expected.

3.3. Naturally contaminated meat samples

Chicken, pork and beef meat samples were tested for the presence of *Photobacterium* spp. by culture-dependent as well as the LAMP assay methods at several time points during the shelf-life of the meat. This

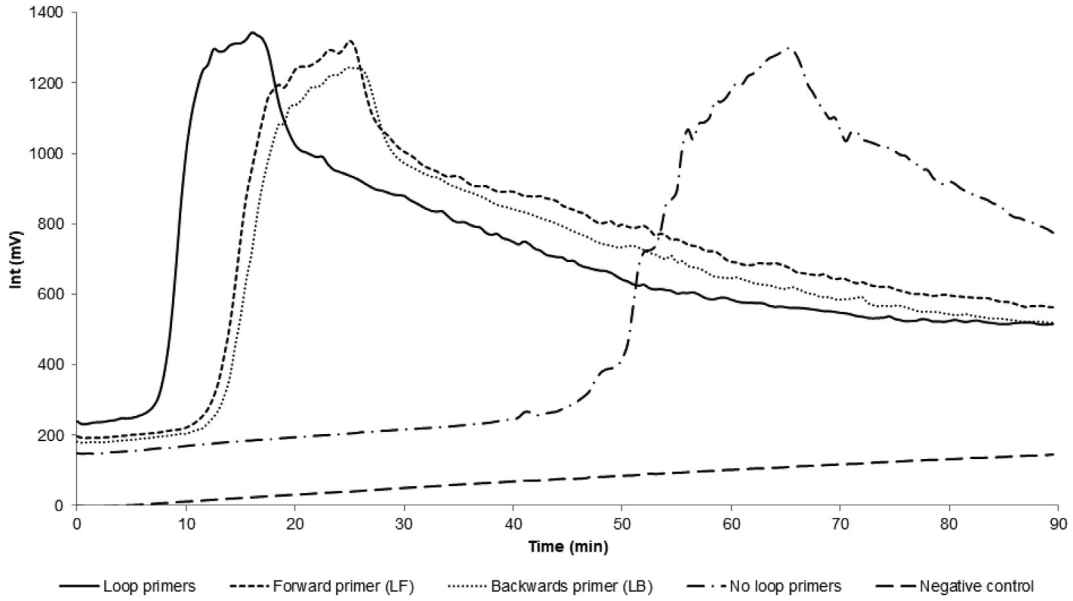

Fig. 4. Real time LAMP reaction with purified DNA of *P. carnosum* TMW2.2021[T]. The graph shows the signal intensity of the intercalating dye V13 at 63 ºC for 90 min during the amplification reaction.

test was performed with samples from at least three different batches.

No photobacteria were detected in any of the pork samples by any of the two approaches (table not included). In regards to the chicken, only one of the five samples checked resulted in a positive reaction at time point 2 (Fig. 7A). The culture-dependent method revealed the presence of 3.58 log CFU/g *P. carnosum* at said time point. Both the LAMP assay and culture-dependent approach were able to detect photobacteria in subsequent days, reaching 5.87 log CFU/g at the last time point (Table 3).

Photobacteria were additionally detected on selective agar plates at day 3 on one beef sample at a concentration of 0.93 log CFU/g (one single colony), while LAMP was still negative. On day 5, the same sample revealed a weakly positive LAMP reaction in one of the triplicates (Fig. 7B), but no photobacteria were recovered on agar plates (Table 4). At no other sampling point, presence of photobacteria was detected either on agar plates or LAMP reaction.

4. Discussion

Specific species of photobacteria (*P. phosphoreum*, *P. carnosum* and *P. iliopiscarium*) can be considered as common meat spoilers. Therefore, a method for their early, fast and sensitive detection (long before reaching a critical spoilage value of log 7 CFU/g) for convenient transfer into the industry can reduce the workload and facilitate the design of appropriate control strategies for photobacteria. We chose to develop a fast qualitative assay for the presence of photobacteria since even a suggested low initial contamination concentration will lead to high relevant cell numbers on meats, negatively impacting the quality and shelf life of the meat.

We chose to target the *tor*A gene of photobacteria, encoding for the trimethylamine-N-oxide reductase (TMAO reductase), involved in the reduction of trimethylamine N-oxide (TMAO) into trimethylamine (TMA) as part of the electron transport chain. The substrate for this enzyme is common on fish tissues, and its reduction is involved in the production of foul-smelling and fish spoilage (Timm and Jorgensen, 2002). Most species of photobacteria contain *tor*A, but it is only found in a few species of common meat spoilers (e.g. *Serratia liquefaciens*, *S. plymuthica*, *S. fonticola*, *Hafnia alvei, Escherichia coli*). Furthermore, high significant dissimilarity between *tor*A sequences of meat spoilers to the gene sequence found in photobacteria makes it a suitable target gene for specific detection. A previous study by Dalgaard et al. (1996) had already effectively targeted the enzyme TMAO reductase for the

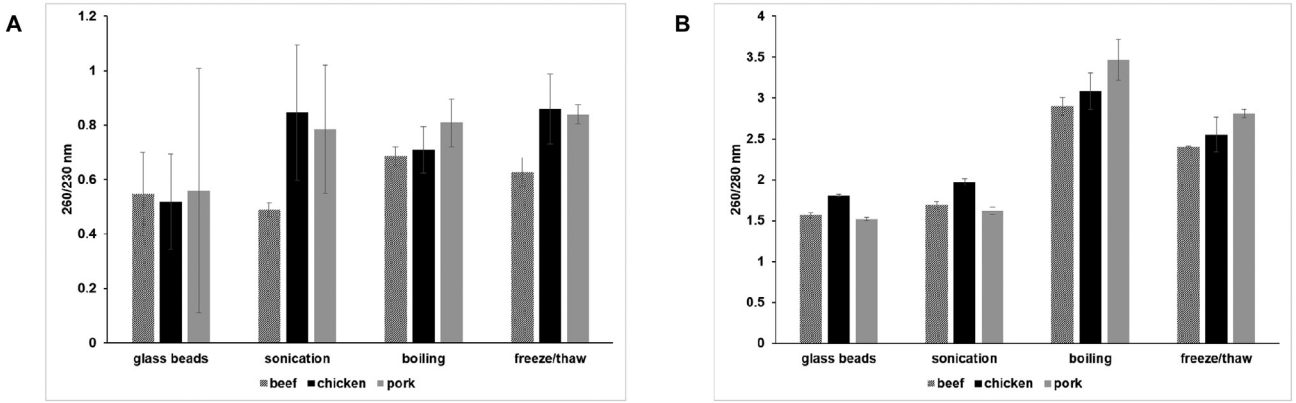

Fig. 5. Purity of the DNA extracted from beef, chicken and pork samples using the four methods described and tested (mechanical disruption with glass beads, cells disruption by sonication, boiling, and freeze/thaw cycles). Purity was measured with NanoDrop and results are shown in the form of A. 260/230 ratio that represents DNA purity in regards to carbohydrates, EDTA and phenol; and B. 260/280 ratio, that represents DNA purity in regards to proteins, phenol and other contaminants.

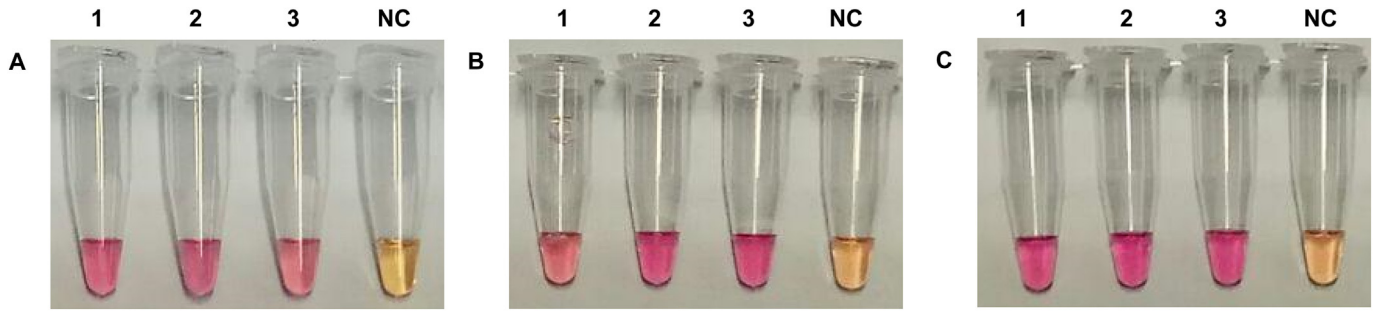

Fig. 6. Results of the LAMP performed with artificially contaminated samples of A. pork, B. chicken, and C. beef samples in triplicate, obtained with the boiling DNA extraction method. Numbers represent the three replicas of the experiment, and on the left side of each picture the negative control inoculated with sterile media (NC); Pink = positive reaction; yellow = negative reaction.

quantitative detection of *P. phosphoreum* on fish by establishing a conductance method to measure its reaction. Our developed LAMP assay represents a sophisticated method with high specificity, improved sensitivity and no dependency on dedicated equipment, reducing the time required to qualitatively assess the presence of photobacteria and allowing a broader detection i.e. the three main species relevant in meat spoilage: *P. phosphoreum*, *P. iliopiscarium* and *P. carnosum*.

4.1. Optimized LAMP parameters and reaction mixture

The LAMP assay has already been successfully applied in the food industry for the control of production of mycotoxins, and detection of pathogens and spoilage microbiota in different types of food, according to Niessen et al. (2013). Major considerations and variations in the LAMP protocol for different assays rely on the optimum parameters for the reaction, e.g. temperature, reaction time, and method for the detection of a positive amplification.

Neutral red was chosen in our assay as pH indicator for the visual confirmation of a positive reaction. The method has been successfully tested by Tanner et al. (2015) and implemented in later studies by Frisch and Niessen (2019) and Niessen et al. (2018). Neutral red changes its color from yellow to pink, as the release of protons during the amplification decreases the pH of the reactions mixture and requires only visual evaluation to confirm the results. The dye is simply added to the reaction mixture prior to incubation, eliminating the risk of post contamination by opening the tubes after reaction (Niessen et al., 2013).

Our results for the real-time LAMP assay demonstrated that it is possible to obtain a positive reaction after 15 min reaction time using purified and concentrated DNA. When using DNA from a meat sample extracted with our developed rapid and simple isolation protocol, a reaction time of 60 min is necessary to heavily decrease the occurrence of false negative results, due to a lower purity and concentration of the target DNA.

Table 3
Results of naturally contaminated chicken samples over the sampling period, for both LAMP assay and culture dependent method of detecting photobacteria.

Chicken	LAMP assay					Culture-dependent (log CFU/g photobacteria)				
Day	C1	C2	C3	C4	C5	C1	C2	C3	C4	C5
1	–	–	–	–	–	–	–	–	–	–
2	–	+	–	–	–	–	3.58	–	–	–
3	–	+	–	–	–	–	4.44	–	–	–
4	–	+	–	–	–	–	5.48	–	–	–
5	–	+	–	–	–	–	5.66	–	–	–
6	–	+	–	–	–	–	5.87	–	–	–

Table 4
Results of naturally contaminated beef samples over the sampling period, for both LAMP assay and culture dependent method of detecting photobacteria.

Beef	LAMP assay			Culture-dependent (log CFU/g photobacteria)		
Day	B1	B2	B3	B1	B2	B3
1	–	–	–	–	–	–
2	–	–	–	–	–	–
3	–	–	–	0.93	–	–
4	–	–	–	–	–	–
5	(+)[a]	–	–	–	–	–
6	–	–	–	–	–	–

[a] The reaction was weakly positive and only in one of the triplicates.

Although a difference was observed in the temperature range at which the LAMP reaction occurs when adding loop primers, 63 °C was the highest temperature yielding a positive result under both conditions and within the optimum temperature range for the *Bst* polymerase as recommended by the provider (60–65 °C).Therefore, 63 °C was chosen as optimum temperature for the LAMP assay.

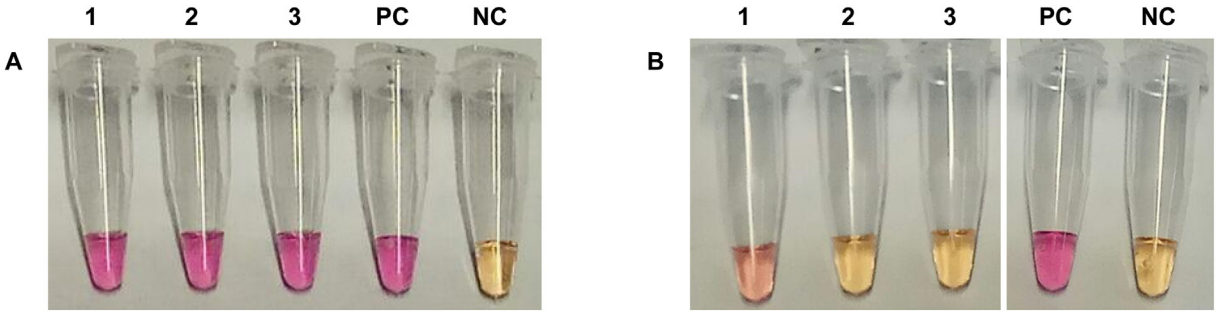

Fig. 7. Results of LAMP assay performed with naturally contaminated samples. A. Sample C2 on sampling day 2, 1-3 triplicates of the sample undiluted. B. Sample B1 on sampling day 5, 1-3 triplicates of the sample undiluted. NC = negative control (water), PC = positive control *P. carnosum* TMW2.2021^{T}. For interpretation: pink = positive reaction (weak pink = weak positive reaction), yellow = negative reaction.

4.2. Sample preparation for LAMP

Common DNA extraction kits usually require the use of columns and multiple specific reagents, increasing the cost of the methodology, and take long preparation time (several hours) to ensure a high quality of the purified DNA. Our protocol is very simplified, rapid, and avoids the use of enzymes, extraction steps with harmful chemicals, or expensive equipment and material. It only requires 1 h to process the samples and, although the purity is lower than obtained from commercial kits, the DNA sample produced has enough quality to ensure no interference with the progression of LAMP assay. In addition, the *Bst* polymerase used in the LAMP assay is less sensitive to the presence of inhibitors (Niessen et al., 2013).

The heat treatment from the boiling protocol, previously implemented by Ressmann et al. (2015) appears effective in the removal of DNases and enough possible LAMP inhibitors from the sample. The boiling protocol produced the DNA with better quality, and was the only one leading to positive results in all artificially contaminated samples. The reproducibility of the LAMP assay when using DNA obtained by each protocol was the critical decisive parameter and boiling was chosen as the optimal DNA extraction (method d) out of the five tested.

In case of the cotton swab method, it proved to be effective when sampling wet surfaces where cell concentration (and therefore possible inhibitors) was low. This would allow sampling of surfaces in the industry with only 10–15 min sample preparation, and simplify detection of the entry route or determination of the source of contamination (e.g. knives, conveyor belts, water, gloves).

4.3. Target affinity and specificity

Target affinity was validated by sequencing of the amplification product, confirming its identity as the *torA* gene and expected size of ~200 bp.

The developed LAMP assay showed great specificity enabling detection of all tested strains of the three relevant species: *P. phosphoreum*, *P. iliopiscarium* and *P. carnosum*, despite of their origin. We deliberately chose to design primers targeting all three major species on meat since their occurrence is concomitant on many products (Hilgarth et al., 2018b) and their spoilage contribution is suggested to be additive (Fuertes-Perez et al., 2019).

It is known that the major species described as spoilage microbiota on fish are *P. phosphoreum* and *P. iliopiscarium*, also responsible for reported cases of fish poisoning (Bjornsdottir-Butler et al., 2018; Dalgaard et al., 1998; Dalgaard et al., 2003; Emborg et al., 2002; Takahashi et al., 2015), and *P. carnosum* has additionally been recently reported on MAP salmon, although suggested as a cross-contamination event (Fuertes-Perez et al., 2019). Therefore, the applicable spectrum of the LAMP assay could also be extended to seafood products in order to rapidly identify contamination with potentially histamine producing strains and reduce health risks. Furthermore, *Photobacterium kishitanii* and *P. leiognathi*, both detected by our assay, have been described as symbiotic bacteria on marine animals (Ast et al., 2007; Urbanczyk et al., 2010). Our assay could therefore be applied also in environmental studies on photobacteria and their occurrence as symbiotic organisms in marine animals.

The specificity of the LAMP assay was assessed by testing purified and concentrated DNA of several species of prominent meat spoilers, including the following major spoilers widely distributed in at least two of the types of meat tested: *Lactococcus piscium*, *Leuconostoc gelidum* ssp. *gelidum*, *Carnobacterium* spp., *Serratia liquefaciens*, *Hafnia alvei*, *Pseudomonas* spp., and *Brochothrix thermosphacta* (Hilgarth et al., 2018a; Hilgarth et al., 2018d; Höll et al., 2016; Nieminen et al., 2016). All common spoilers produced desired negative results in our LAMP assay.

Other accessory meat spoilers include: *S. proteamaculans*, *Lactobacillus sakei*, *Yersinia enterocolitica*, *Rothia nasimurium*, *Rahnella* spp., *Pantoea agglomerans*, *Enterococcus faecalis*, *E. faecium* and *Buttiauxella* spp. (Höll et al., 2016; Remenant et al., 2015). These species also occurred on samples within our LAMP trial and were identified by MALDI-TOF (total of 55 species). The samples with no photobacteria present again yielded a desired negative LAMP result. These combined results confirm that the presence of other species of meat microbiota does not produce false positive results in our LAMP assay, demonstrating its high stringency for presence of photobacteria.

Some of the species tested or detected on naturally contaminated meat can additionally be found on fish and seafood, involved in their spoilage (e.g. *Pseudomonas* spp., *B. thermosphacta, Carnobacterium* spp.) (Mace et al., 2013; Remenant et al., 2015). The stringency of the specificity of the method emphasizes its transferability to fish and seafood in addition to raw meat.

4.4. Detection limit of the LAMP assay

The developed LAMP methodology is able to detect 10–11 copies (50 ft.) of the *Photobacterium* genome per reaction. Translated to the isolation protocol from meat, the LAMP assay would have a theoretical detection limit of ~1.62–1.74 log CFU/g of meat similar to the theoretical detection limit of a culture dependent approach (Hilgarth et al., 2018b). Therefore, the sensitivity of the LAMP assay allows the detection of photobacteria long before onset of spoilage or the end of the shelf-life, in 2 h, and offers a rapid and direct knowledge over presence of photobacteria. Even though it has a high sensitivity, the numbers of photobacteria on meat required to produce a positive reaction are high enough to ensure that non-significant numbers of dead cells do not result in a positive reaction. In addition, it is possible to enable semi-quantitative predication of the assay modifying the detection limit of the methodology/positive threshold value by simple dilution of the sample.

4.5. First LAMP trial on naturally contaminated samples

Photobacteria, although common on meat, and ubiquitous in terms of type of meat, type of packaging, and country of origin of the meat, are not present in all packages of meat. Previous studies have already reported differences in the abundance of photobacteria between different packages of the same meat and brand (Fuertes-Perez et al., 2019; Hilgarth et al., 2018b), and presence of photobacteria in about 50% of the packages checked (14/28 packages). The lot-to-lot variations, which has been demonstrated also for other meat spoilers (Sade et al., 2017), emphasizes the need for a non-time consuming methodology, allowing the screening of high amounts of samples with low requirements of time, equipment, reagents and personnel. Screening of high sample numbers allows producers to check each production and distribution plant to determine in which sectors photobacteria are of major concern and need more stringent measurements.

Therefore, we conducted a trial with our developed LAMP assay on several random samples of different types on meat (beef, poultry and pork). Out of 11 total samples tested, only one sample of poultry meat was consistently contaminated with over 3 log CFU/g numbers of photobacteria. The reduced presence in comparison to Hilgarth et al. (2018b) was probably a result of the small sample size in this study, confirming also that the presence of photobacteria on meat is up to date unpredictable and may be periodically fluctuating. Screening the same amount of samples with conventional culture-dependent approach would heavily increase work-load and time with no guarantee of detection. Photobacteria were also sporadically detected on a beef sample with both methods at different time-points. Results proved that presence of photobacteria was lower than the theoretical detection method for the culture-dependent approach, and therefore positive results by both methods were most likely a consequence of pure chance, explaining also the difference in the time point of detection. Vice-versa,

the fact that no isolates could be recovered in the sample with a weak positive result in the LAMP reaction suggests that the LAMP approach appears to be able to indicate the presence of photobacteria even below the detection limit of culture dependent approaches. However, this assumption should be confirmed in future applications.

Taken together, this study presents a novel rapid LAMP assay that would offer a reduction of workload, cost and an improvement of early detection of photobacteria on meat (and potentially also seafood and fish) in comparison to available culture-dependent and independent approaches. At the same time, it appears unlikely that routine control would be able to adopt an additional photobacteria-specific laborious cultural method to control these besides other meat spoilers. Hence, both culture-dependent and culture-independent methodologies e.g. PCR approach (Mace et al., 2013) represent valuable tools that should be used in a combined approach on those samples positive by LAMP assay to either recovery of isolates (the former) or quantification of photobacteria (both).

The developed LAMP reaction is rapid, highly specific as well as sensitive, and requires no dedicated equipment or training. The methodology has proven to be applicable on different types of meat, and demonstrated a good correlation compared to the tested selective cultivation-dependent approach. The simplicity of this method provides a possibility for easy transference of this assay to the on-site detection in the industry and its successful implementation would enable early qualitative confirmation of presence of photobacteria within the shelf-life of the meat, even prior to its distribution.

Since shelf life of fish and seafood products are directly linked to presence of photobacteria (Dalgaard et al., 1998) and given the fact that photobacteria produce the relevant spoilage compounds also on meat (Höll et al., 2019), photobacteria are suggested to have the similar impact on shelf life of meats. Giving their acknowledged status as potent spoilage bacteria and demonstrated lot-to-lot variations that can lead to shelf life fluctuations, improved detection is desirable to establish if further quantitative routine control of presence of photobacteria is needed within the industry.

Furthermore, the LAMP approach combined with surface sampling could enable producers to track their entry routes into the processing environment in order to establish preventive measures against this group.

Declaration of competing interest

The authors declare no conflict of interest.

Acknowledgements

Prof. Dr. Ludwig Niessen (TU Munich, Germany) provided insight on the LAMP methodology and advice on the performance of some protocols in the study.

Author contributions

Fuertes-Perez, Sandra: term, conceptualization, methodology, validation, formal analysis, investigation, resources, data curation, writing the original draft, writing (review and editing), visualization.

Hilgarth, Maik: definition, conceptualization, writing (review and editing), visualization, supervision, project administration.

Vogel, Rudi F.: writing (review and editing), project administration, funding acquisition.

Funding

This work was partially funded by the German Federal Ministry for Economic Affairs and Energy via the German Federation of Industrial Research Associations (AiF) and the Industry Association for Food Technology and Packaging (IVLV); project number AiF 20113N1.

Appendix A. Supplementary data

Supplementary data to this article can be found online at https://doi.org/10.1016/j.ijfoodmicro.2020.108805.

References

Ast, J.C., Dunlap, P.V., 2005. Phylogenetic resolution and habitat specificity of members of the *Photobacterium phosphoreum* species group. Environ. Microbiol. 7, 1641–1654.
Ast, J.C., Cleenwerck, I., Engelbeen, K., Urbanczyk, H., Thompson, F.L., De Vos, P., Dunlap, P.V., 2007. *Photobacterium kishitanii* sp. nov., a luminous marine bacterium symbiotic with deep-sea fishes. Int. J. Syst. Evol. Microbiol. 57, 2073–2078.
Bingol, E.B., Ergun, O., 2011. Effects of modified atmosphere packaging (MAP) on the microbiological quality and shelf life of ostrich meat. Meat Sci. 88, 774–785.
Björkroth, J., 2005. Microbiological ecology of marinated meat products. Meat Sci. 70, 477–480.
Bjornsdottir-Butler, K., Abraham, A., Harper, A., Dunlap, P.V., Benner Jr., R.A., 2018. Biogenic amine production by and phylogenetic analysis of 23 *Photobacterium* species. J. Food Prot. 81, 1264–1274.
Bouju-Albert, A., Pilet, M.F., Guillou, S., 2018. Influence of lactate and acetate removal on the microbiota of French fresh pork sausages. Food Microbiol. 76, 328–336.
Dalgaard, P., Mejlholm, O., Huss, H.H., 1996. Conductance method for quantitative determination of *Photobacterium phosphoreum* in fish products. J. Appl. Bacteriol. 81, 57–64.
Dalgaard, P., Manfio, G.P., Goodfellow, M., 1997. Classification of photobacteria associated with spoilage of fish products by numerical taxonomy and pyrolysis mass spectrometry. Zentralbl. Bakteriol 285, 157–168.
Dalgaard, P., Garcia Munoz, L., Mejlholm, O., 1998. Specific inhibition of *Photobacterium phosphoreum* extends the shelf life of modified-atmosphere-packed cod fillets. J. Food Prot. 61, 1191–1194.
Dalgaard, P., Mejlholm, O., Christiansen, T.J., Huss, H.H., 2003. Importance of *Photobacterium phosphoreum* in relation to spoilage of modified atmosphere-packed fish products. Lett. Appl. Microbiol. 24, 373–378.
Emborg, J., Laursen, B.G., Rathjen, T., Dalgaard, P., 2002. Microbial spoilage and formation of biogenic amines in fresh and thawed modified atmosphere-packed salmon (Salmo salar) at 2 degrees C. J. Appl. Microbiol. 92, 790–799.
Frisch, L.M., Niessen, L., 2019. Development and optimization of a group-specific loop-mediated isothermal amplification (LAMP) assay for the detection of patulin-producing *Penicillium* species. Int. J. Food Microbiol. 298, 20–30.
Fuertes-Perez, S., Hauschild, P., Hilgarth, M., Vogel, R.F., 2019. Biodiversity of *Photobacterium* spp. isolated from meats. Front. Microbiol. 10, 2399.
Hilgarth, M., Behr, J., Vogel, R.F., 2018a. Monitoring of spoilage-associated microbiota on modified atmosphere packaged beef and differentiation of psychrophilic and psychrotrophic strains. J. Appl. Microbiol. 124, 740–753.
Hilgarth, M., Fuertes-Perez, S., Ehrmann, M., Vogel, R.F., 2018b. An adapted isolation procedure reveals *Photobacterium* spp. as common spoilers on modified atmosphere packaged meats. Lett. Appl. Microbiol. 66, 262–267.
Hilgarth, M., Fuertes, S., Ehrmann, M., Vogel, R.F., 2018c. *Photobacterium carnosum* sp. nov., isolated from spoiled modified atmosphere packaged poultry meat. Syst. Appl. Microbiol. 41, 44–50.
Hilgarth, M., Nani, M., Vogel, R.F., 2018d. Assertiveness of meat-borne *Lactococcus piscium* strains and their potential for competitive exclusion of spoilage bacteria in situ and in vitro. J. Appl. Microbiol. 124, 1243–1253.
Höll, L., Behr, J., Vogel, R.F., 2016. Identification and growth dynamics of meat spoilage microorganisms in modified atmosphere packaged poultry meat by MALDI-TOF MS. Food Microbiol. 60, 84–91.
Höll, L., Hilgarth, M., Geissler, A.J., Behr, J., Vogel, R.F., 2019. Prediction of in situ metabolism of photobacteria in modified atmosphere packaged poultry meat using metatranscriptomic data. Microbiol. Res. 222, 52–59.
Jorgensen, L.V., Dalgaard, P., Huss, H.H., 2000. Multiple compound quality index for cold-smoked salmon (*Salmo salar*) developed by multivariate regression of biogenic amines and pH. J. Agric. Food Chem. 48, 2448–2453.
Kargiotou, C., Katsanidis, E., Rhoades, J., Kontominas, M., Koutsoumanis, K., 2011. Efficacies of soy sauce and wine base marinades for controlling spoilage of raw beef. Food Microbiol. 28, 158–163.
Labella, A.M., Arahal, D.R., Castro, D., Lemos, M.L., Borrego, J.J., 2017. Revisiting the genus *Photobacterium*: taxonomy, ecology and pathogenesis. Int. Microbiol. 20, 1–10.
Lehane, L., Olley, J., 2000. Histamine fish poisoning revisited. Int. J. Food Microbiol. 58, 1–37.
Lorenzo, J.M., Gomez, M., 2012. Shelf life of fresh foal meat under MAP, overwrap and vacuum packaging conditions. Meat Sci. 92, 610–618.
Mace, S., Mamlouk, K., Chipchakova, S., Prevost, H., Joffraud, J.J., Dalgaard, P., Pilet, M.F., Dousset, X., 2013. Development of a rapid real-time PCR method as a tool to quantify viable *Photobacterium phosphoreum* bacteria in salmon (*Salmo salar*) steaks. Appl. Environ. Microbiol. 79, 2612–2619.
McMillin, K.W., 2008. Where is MAP going? A review and future potential of modified atmosphere packaging for meat. Meat Sci. 80, 43–65.
Mozioglu, E., Akgoz, M., Tamerler, C., Kocagöz, Z.T., 2014. A simple guanidinium isothiocyanate method for bacterial genomic DNA isolation. Turk. J. Biol. 38, 125–129.
Nagamine, K., Hase, T., Notomi, T., 2002. Accelerated reaction by loop-mediated isothermal amplification using loop primers. Mol. Cell. Probes 16, 223–229.

Nieminen, T.T., Dalgaard, P., Björkroth, J., 2016. Volatile organic compounds and *Photobacterium phosphoreum* associated with spoilage of modified-atmosphere-packaged raw pork. Int. J. Food Microbiol. 218, 86–95.
Niessen, L., Luo, J., Denschlag, C., Vogel, R.F., 2013. The application of loop-mediated isothermal amplification (LAMP) in food testing for bacterial pathogens and fungal contaminants. Food Microbiol. 36, 191–206.
Niessen, L., Bechtner, J., Fodil, S., Taniwaki, M.H., Vogel, R.F., 2018. LAMP-based group specific detection of aflatoxin producers within *Aspergillus* section *Flavi* in food raw materials, spices, and dried fruit using neutral red for visible-light signal detection. Int. J. Food Microbiol. 266, 241–250.
Notomi, T., Okayama, H., Masubuchi, H., Yonekawa, T., Watanabe, K., Amino, N., Hase, T., 2000. Loop-mediated isothermal amplification of DNA. Nucleic Acids Res. 28, E63.
Pennacchia, C., Ercolini, D., Villani, F., 2011. Spoilage-related microbiota associated with chilled beef stored in air or vacuum pack. Food Microbiol. 28, 84–93.
Pini, F., Aquilani, C., Giovannetti, L., Viti, C., Pugliese, C., 2020. Characterization of the microbial community composition in Italian Cinta Senese sausages dry-fermented with natural extracts as alternatives to sodium nitrite. Food Microbiol. 89, 103417.
Remenant, B., Jaffrès, E., Dousset, X., Pilet, M.F., Zagorec, M., 2015. Bacterial spoilers of food: behavior, fitness and functional properties. Food Microbiol. 45, 45–53.
Ressmann, A.K., González García, E., Khlan, D., Gaertner, P., Mach, R.L., Krska, R., Brunner, K., Bica, K., 2015. Fast and efficient extraction of DNA from meat and meat derived products using aqueous ionic liquid buffer systems. New J. Chem. 39, 4994–5002.
Sade, E., Penttinen, K., Björkroth, J., Hultman, J., 2017. Exploring lot-to-lot variation in spoilage bacterial communities on commercial modified atmosphere packaged beef. Food Microbiol. 62, 147–152.
Stoops, J., Ruyters, S., Busschaert, P., Spaepen, R., Verreth, C., Claes, J., Lievens, B., Van Campenhout, L., 2015. Bacterial community dynamics during cold storage of minced meat packaged under modified atmosphere and supplemented with different preservatives. Food Microbiol. 48, 192–199.
Takahashi, H., Ogai, M., Miya, S., Kuda, T., Kimura, B., 2015. Effects of environmental factors on histamine production in the psychrophilic histamine-producing bacterium *Photobacterium iliopiscarium*. Food Control 52, 39–42.
Tanner, N.A., Zhang, Y., Evans Jr., T.C., 2015. Visual detection of isothermal nucleic acid amplification using pH-sensitive dyes. Biotechniques 58, 59–68.
Timm, M., Jorgensen, B.M., 2002. Simultaneous determination of ammonia, dimethylamine, trimethylamine and trimethylamine-n-oxide in fish extracts by capillary electrophoresis with indirect UV-detection. Food Chem. 76, 509–518.
Torido, Y., Takahashi, H., Kuda, T., Kimura, B., 2012. Analysis of the growth of histamine-producing bacteria and histamine accumulation in fish during storage at low temperatures. Food Control 26, 174–177.
Urbanczyk, H., Ast, J.C., Dunlap, P.V., 2010. Phylogeny, genomics, and symbiosis of *Photobacterium*. FEMS Microbiol. Rev. 35, 324–342.

International Journal of Food Microbiology 346 (2021) 109176

Contents lists available at ScienceDirect

International Journal of Food Microbiology

journal homepage: www.elsevier.com/locate/ijfoodmicro

Corrigendum

Corrigendum to "Development of a rapid detection method for *Photobacterium* spp. using Loop-mediated isothermal amplification (LAMP)" [Int. J. Food Microbiol. 334 (2020), 108805]

Sandra Fuertes-Perez, Maik Hilgarth *, Rudi F. Vogel

Lehrstuhl Technische Mikrobiologie, Technische Universität München, 85354 Freising, Germany

The authors regret ⟨to inform that an involuntary error was made in Material and methods Section 2.2 regarding the concentration of the primers used in the LAMP reaction mix. The concentration was erroneously stated as mM, whereas μM is correct. Therefore, we would like to correct as follows:

"[…] primer mix (15.38 μM of both FIP_torA and BIP_torA, 7.69 μM of both LF_torA and LB_torA, and 1.92 μM of both F3_torA and B3_torA in the premixed primer mix, respectively, for a final concentration in the LAMP reaction mix of 1.6 μM both FIP_torA and BIP_torA, 0.8 μM both LF_torA and LB_torA, and 0.2 μM both F3_torA and B3_torA, respectively.) […]"⟩.

The authors would like to apologise for any inconvenience caused.

Declaration of competing interest

The authors declare that they have no known competing financial interests or personal relationships that could have appeared to influence the work reported in this paper.

DOI of original article: https://doi.org/10.1016/j.ijfoodmicro.2020.108805.
* Corresponding author.
E-mail address: maik.hilgarth@tum.de (M. Hilgarth).

https://doi.org/10.1016/j.ijfoodmicro.2021.109176

Available online 5 April 2021

6.2 Characterization, diversity and comparative genomics of photobacteria isolated from marine and terrestrial sources

This chapter comprises two different publications that are to be discussed together.

6.2.1 Biodiversity of *Photobacterium* spp. isolated from meat

This study was performed in order to provide a comprehensive overview on the distribution of the relevant species on meat, and determine inter- and intra-species physiological characteristics. Multiple food samples from both industrial producers and local butcheries were purchased and screened for the presence of photobacteria by means of a culture-dependent approach. Their presence was common on poultry, beef and pork products, from all types of tested packed atmospheres and regardless of the use of marinades. Additionally, the species *P. carnosum* was for the first time reported on fish. Isolates found were identified as strains of *P. phosphoreum*, *P. carnosum* or *P. iliopiscarium*, and further characterized by study of their genomic fingerprinting, growth dynamics, metabolic activities and resistance to antibiotics. Both species and strains showed distinct characteristics that were, however, not linked to the type of meat from where the isolates were obtained. Results show that the diversity of the initial contamination on meat is already high by the time photobacteria reach it. The species *P. phosphoreum* showed improved growth parameters compared to the other two species, stronger alkalization of the media that could be linked to production of amines and wider and stronger resistance to antibiotics, although *P. carnosum* showed the widest carbohydrate utilization and acid production, suggesting a stronger capability to adapt to more than one niche. In addition, we observed that both *P. phosphoreum* and *P. iliopiscarium* meat-borne strains showed distinct characteristics that separate them from their fish-borne type strains, suggesting both species may have diverged into subpopulations as an adaptive response to different niche colonization. On the other hand, *P. carnosum* remains a homogeneous species whose presence on fish may have been due to cross-contamination rather than a common niche.

Author contributions: Sandra Fuertes-Perez performed the experimental design, the laboratory work with *P. carnosum* strains, data evaluation and figures and tables creation. She contributed to writing the original draft of the manuscript and further revisions.

frontiers in Microbiology

ORIGINAL RESEARCH
published: 18 October 2019
doi: 10.3389/fmicb.2019.02399

Biodiversity of *Photobacterium* spp. Isolated From Meats

Sandra Fuertes-Perez†, Philippa Hauschild†, Maik Hilgarth and Rudi F. Vogel*

Lehrstuhl Technische Mikrobiologie, Technische Universität München, Freising, Germany

Photobacteria are common psychrophilic bacteria found in marine environments. Recently, several studies revealed high numbers of *Photobacterium* (*P.*) spp. on packaged fresh meat. Their occurrence appears relevant for the spoilage of meat, since species of the genus are already known as potent fish spoilage organisms. Here we report on distribution, biodiversity, and specific traits of *P. carnosum* (n = 31), *P. phosphoreum* (n = 24), and *P. iliopiscarium* (n = 3) strains from different foods. Biodiversity was assessed by genomic fingerprinting, diversity index analysis, growth dynamics, comparison of metabolic activities, and antibiotic resistance. We observed a ubiquitous occurrence of the species on all common meats independent of packaging conditions and producer, suggesting contamination during an established processing or packaging step. Regarding biodiversity, the three species differed clearly in their growth properties and metabolic characteristics, with *P. phosphoreum* growing the fastest and showing the strongest alkalization of the media. On strain level we also recorded variations in enzymatic reactions, acid production, and antibiotic resistances not restricted to specific meat types. This depicts high biodiversity on species and strain level on each contaminated meat sample. Our analysis showed that meat-borne strains of *P. phosphoreum* and *P. iliopiscarium* clearly differ from their type strains from a marine habitat. Additionally, we report for the first time isolation of *P. carnosum* strains from packaged fish, which in contrast showed comparable phenotypic properties to meat-borne strains. This hints at different initial origins of *P. phosphoreum/P. iliopiscarium* (marine background) and *P. carnosum* (no demonstrated marine background) contaminations on fish and meat, respectively.

Keywords: *Photobacterium carnosum*, *Photobacterium phosphoreum*, *Photobacterium iliopiscarium*, meat spoilage, psychrophilic spoilers, modified atmosphere packaging

OPEN ACCESS

Edited by:
Gianluigi Mauriello, University of Naples Federico II, Italy

Reviewed by:
Elina Johanna Säde, University of Helsinki, Finland
Stefano Raimondi, University of Modena and Reggio Emilia, Italy

****Correspondence:***
Maik Hilgarth
maik.hilgarth@tum.de

† These authors have contributed equally to this work as joint first authors

Specialty section:
This article was submitted to Food Microbiology, a section of the journal Frontiers in Microbiology

Received: *24 June 2019*
Accepted: *03 October 2019*
Published: *18 October 2019*

Citation:
Fuertes-Perez S, Hauschild P, Hilgarth M and Vogel RF (2019) Biodiversity of Photobacterium spp. Isolated From Meats. Front. Microbiol. 10:2399. doi: 10.3389/fmicb.2019.02399

INTRODUCTION

Photobacteria are Gram-negative, facultatively aerobic members of the Vibrionaceae family and well known as marine-related species (Lo et al., 2014; Li et al., 2017; Wang et al., 2017). First described in 1889 (Beijerinck, 1889), the genus currently comprises 30 valid species, and 2 subspecies (Parte, 2018). Photobacteria occur free-living in seawater and sediments or in interaction with marine animals (Urbanczyk et al., 2011; Labella et al., 2017), e.g., the symbiosis of bioluminescent strains within the light organs of deep sea fish (Hendrie et al., 1970). However, photobacteria are also known as effective saprotrophs in marine habitats (Urbanczyk et al., 2011). In this context, certain species, i.e., *Photobacterium* (*P.*) *phosphoreum* and *P. iliopiscarium* constitute a

considerable problem in the food industry, representing potent spoilers of chilled fish and seafood products (Okuzumi et al., 1994; Dalgaard et al., 1997). The spoilage processes involve production of biogenic amines such as histamine (Okuzumi et al., 1994; Jorgensen et al., 2000; Emborg et al., 2002; Torido et al., 2012; Takahashi et al., 2015; Bjornsdottir-Butler et al., 2018) that can lead to scombroid fish poisoning (Lehane and Olley, 2000).

Previous studies based on culture-independent approaches have revealed presence of photobacteria gene sequences on pork (Nieminen et al., 2016), pork sausages (Bouju-Albert et al., 2018), beef (Pennacchia et al., 2011), and minced meat (Stoops et al., 2015; Nieminen et al., 2016). In only one of these studies very few isolates of *P. phosphoreum* were recovered (Nieminen et al., 2016) since common control methods rely on standard agars and cultivation at temperatures between 25 and 30°C, which do not allow isolation of fastidious and psychrophilic photobacteria. Highly frequent isolation was recently demonstrated by Hilgarth et al. (2018a) employing a novel, targeted selective isolation procedure for recovery of photobacteria from foods. *P. phosphoreum* and *P. iliopiscarium* were isolated from modified atmosphere packaged (MAP) poultry, pork, and beef (only *P. phosphoreum*) (Hilgarth et al., 2018a). *P. phosphoreum* was firstly described in 1878 (Cohn, 1878) and re-evaluated in 1889 (Beijerinck, 1889) as a luminous isolate from the sea. It is adapted to high-pressure (Labella et al., 2017), grows optimally at 15–20°C, and occurs frequently as predominant spoiler on fish products (Gram and Huss, 1996; Reynisson et al., 2009). *P. iliopiscarium* was described by Onarheim et al. (1994) as *Vibrio iliopiscarium* and later reassigned to *Photobacterium* by Urakawa et al. (1999). There are several studies reporting *P. iliopiscarium* isolates from marine fish (Dunlap and Ast, 2005; Olofsson et al., 2007; Thyssen and Ollevier, 2015; Hilgarth et al., 2018a) but only few that describe them as predominant (Olofsson et al., 2007). Just as *P. phosphoreum*, it prefers 15–20°C for growth (Onarheim et al., 1994; Hilgarth et al., 2018b). In addition, a new psychrophilic species, *P. carnosum*, was recently discovered on meat. It also prefers 10–15°C and was described as the first species of the genus that is unrelated to marine habitats (Hilgarth et al., 2018b). This new species was reported as the major representative of the *Photobacterium* genus on poultry and beef, while it was less abundant on pork.

Not only do these psychrophilic bacteria occur in high numbers on meat, but they also exhibit spoilage potential. A recent metatranscriptomic study has predicted its potential for production of several biogenic amines, such as putrescine, cadaverine, agmatine, tyramine, and gamma-amino-butyric acid as well as various other spoilage compounds that are known for other potent meat spoilers (Höll et al., 2019).

Until now, knowledge on the origin and biodiversity of *P. carnosum*, *P. phosphoreum*, and *P. iliopiscarium* on food products and especially meats is very limited. This study aimed at elucidation of their distribution and diversity in order to identify specific traits of the species and possible correlations between the source of isolation, genotypes, or physiotypes. For this, we surveyed and reviewed the occurrence of photobacteria on meat samples from local butchers and supermarkets. Selected isolates from different samples were then used to thoroughly study biodiversity.

MATERIALS AND METHODS

Isolation and Identification of Photobacteria

Isolation was carried out as described in the isolation protocol from Hilgarth et al. (2018a). Samples purchased and kept at 4°C were cut and homogenized in marine broth (DIFCO). Samples were plated on marine agar [marine broth, 1.6% agar-agar (w/v)] supplemented with 3 g/L meat extract and 7 mg/L vancomycin, and incubated at 15°C for 72 h. Composition of the base marine broth media includes: peptone 5 g/L, yeast extract 1 g/L, sodium chloride 19.45 g/L, ferric citrate 0.1 g/L, magnesium chloride 5.9 g/L, magnesium sulfate 3.24 g/L, calcium chloride 1.8 g/L, potassium chloride 0.55 g/L, sodium bicarbonate 0.16 g/L, potassium bromide 0.08 g/L, strontium chloride 34 mg/L, boric acid 22 mg/L, sodium silicate 4 mg/L, sodium fluoride 2.4 mg/L, ammonium nitrate 1.6 mg/L, and disodium phosphate 8 mg/L. Isolates were identified based on their low-molecular subproteome with MALDI-TOF MS on a Microflex LT Spectrometer (Bruker Corporation, Billerica, MA, United States) by direct transfer method and on-target extraction (Usbeck et al., 2013; Hilgarth et al., 2018a). An in-house database containing mass spectrometry profiles of various photobacteria species was established by sequencing of housekeeping genes in order to guarantee reliable identification. In total at least three packages per meat type were analyzed for abundance of photobacteria. Type strains *P. phosphoreum* DSM15556^T and *P. iliopiscarium* DSM9896^T, obtained from the German Strain Collection (DSMZ), were also part of the selected strains. Additionally, the type strain *P. carnosum* TMW2.2021^T and some already described strains of the species (TMW2.2022, TMW2.2029, and TMW2.2030) were included (Hilgarth et al., 2018b).

Genomic Fingerprinting

Randomly amplified polymorphic DNA (RAPD)-PCR fingerprinting was used to assess the number of different strains within all isolates and select them for subsequent characterization. RAPD-PCR was performed with the primer M13V (5′-GTT TTC CCA GTC ACG AC-3′) (Ehrmann et al., 2003). Bands were separated by electrophoresis in agarose gel (1.4% w/v, 150 V, 2.5 h). Lambda DNA/*Eco*RI plus *Hin*dIII Marker (Thermo Scientific, Hampshire, United Kingdom) was used as molecular weight marker and for normalization/standardization of the gel pattern for comparison. Similarities in fingerprint pattern were analyzed with Bionumerics V7.6.2 (Applied Maths, Sint-Martens-Latem, Belgium). Hierarchical clustering analysis was carried out by unweighted pair group method with arithmetic mean (UPGMA) method and Dice similarity coefficient with 1% tolerance. After the initial strain delineation by RAPD-PCR for all isolates, the RAPD approach was again performed twice for all strains of the three species to assess the reproducibility of the observed

patterns and ensure the fidelity of the clustering. Furthermore, the similarity of triplicates of all strains was compared to the triplicates of the closest related strain in order to further validate the strain delineation and distinctness.

Randomly amplified polymorphic DNA PCR protocol was additionally carried out with primer M14V (5′-CTG TCC AGT CAC GTC-3′) with all selected strains in order to confirm their distinctness and diversity within the species. Protocol and standardization was performed as described for M13V primer.

Diversity Index Analysis

Individual rarefaction analysis and calculation of diversity indices for evenness (Simpson, 1949), entropy (Shannon and Weaver, 1949), and richness (Chao, 1984) was performed using PAST software 3.25 (Hammer et al., 2001) with operational taxonomic units [OTUs (Schloss and Handelsman, 2005)] defined as distinct/unique RAPD genomic fingerprinting representing distinct genotypes on strain level. A p-value < 0.05 was defined as significantly different. Coverage (%) of genotypes was calculated using Good's coverage estimator as described by Good (1953) with the equation:

$$C = \left(1 - \frac{N_1}{n}\right) * 100, \quad (1)$$

with N_1 representing OTUs only found once (singletons) and n as the total number of individuals (strains).

Growth Analysis in Meat Simulation Medium

Growth curves were performed with all isolated strains of the three species of photobacteria used in this study, a total of 31 strains of *P. carnosum*, 24 strains of *P. phosphoreum*, and 3 strains of *P. iliopiscarium*, in addition to the marine type strains of *P. phosphoreum* (DSM15556^T) and *P. iliopiscarium* (DSM9896^T). Inoculum was prepared from an overnight culture in marine broth at 15°C, by centrifuging the cells (4000 × *g*, 10 min), washing them with NaCl 2% (w/v), and resuspending on meat-simulation media. Growth curves were started by inoculating meat-simulation media (20 g/L meat extract, 20 g/L NaCl, pH 5.8) in 50 mL Erlenmeyer flasks at an initial OD_{600} of 0.05. Cultures were incubated at 4°C with constant agitation, and samples were taken regularly for OD_{600} measurement. The pH of the culture was measured at maximum OD_{600}. Growth curves were adjusted to parametric models with RStudio v1.1.463 and grofit package v.1.1.1-1 (Kahm et al., 2010) to determine lag phase (lag), maximum growth rate (U), and maximum OD_{600}. Growth curves were performed in triplicates and data were further analyzed in IBM SPSS Statistics v23.0.0.0. Tests for normality (Shapiro–Wilk) and homogeneity of variances (Levene test) were carried out for each set of data. One-way ANOVA followed by HSD Tukey *post hoc* test determined significant differences between the strains of each species. Welch-ANOVA and Games-Howell *post hoc* tests were used in case of heterogeneity of variances. Significance level was determined by $p < 0.05$.

Motility Test

Motility for all strains was determined by the soft agar stab method. Meat-simulation media supplemented with 3 g/L agar was poured into tubes. Motility was measured based on the turbidity of the soft agar around the stabbing zone.

Bioluminescence of *P. phosphoreum* Strains

Bioluminescence in darkness was scored by visual comparison of the intensity on marine agar plates for all *P. phosphoreum* strains. Suspensions with the same OD_{600} were prepared for all strains, plated on marine agar plates, and incubated at 15°C for 72 h.

Antibiotic Resistance Test

Antibiotic resistance of all strains of the three species of photobacteria was assessed by disc diffusion assay. All discs were purchased from Oxoid (Thermo Scientific, Hampshire, United Kingdom).

Metabolic Characterization

Metabolic characterization was assessed for a representative group of all the strains of the three species of photobacteria. A total of 14 strains of *P. phosphoreum*, 16 strains of *P. carnosum*, and 3 strains of *P. iliopiscarium* were assessed for carbohydrate acid production and enzymatic activities. Production of acid from different carbon sources was assessed by the API 50CH test (bioMérieux, Marcy-l'Étoile, France). Several enzymatic activities were tested with the API ZYM test (bioMérieux, Marcy-l'Étoile, France) according to the instructions from the manufacturer. Both procedures were performed according to the methodology followed by Hilgarth et al. (2018b) and data for *P. carnosum* TMW2.2021/2.2022/2.2029/2.2030, *P. phosphoreum* DSM15556^T, and *P. iliopiscarium* DSM9896^T were taken from this study.

Hierarchical Cluster Analysis

Hierarchical cluster based on the results for physiological tests of selected strains was carried out by a Heatmapper tool[1] with average linkage criteria and Euclidean distance.

RESULTS

Occurrence of Photobacteria on Selected Food Products

Various food samples were obtained from local retailers and butchers and screened on the presence of photobacteria. We detected them on several meat types and on marine fish (**Table 1**), on MAP packaged, vacuum packaged, and air stored samples and also on marinated meats. The contaminated samples originated thereby from large supermarket chains as well as from small local shops. However, not all samples contained photobacteria, even if they originated from the same producer. We also found different species compositions that were dependent on the meat type. In

[1] www2.heatmapper.ca/expression/

TABLE 1 | Detection of *Photobacterium* spp. on different meats.

Packaging atmosphere	Meat type	Origin	Detected *Photobacterium* spp.	Relative abundance of *Photobacterium* spp. (%)	CFU photobacteria [log_{10}(CFU/g)]	CFU bacteria [log_{10}(CFU/g)]
Air	Chicken	Local butchery	*P. carnosum*	100	6.29	7.67
Air	Beef	Local butchery	*P. carnosum*	100	7.54	9.22
Air	Pork	Local butchery	*P. phosphoreum*	100	8.57	9.34
Air	Codfish	Local fish shop	*P. phosphoreum*	100	NA	NA
Air	Marinated turkey	Supermarket	*P. carnosum* *P. phosphoreum*	25 75	7.17	8.28
MAP	Marinated chicken	Supermarket	*P. carnosum* *P. phosphoreum*	96 4	4.54	4.63
MAP	Marinated beef	Supermarket	*P. phosphoreum*	100	8.76	9.66
MAP	Chicken*	Supermarket	*P. carnosum* *P. phosphoreum* *P. iliopiscarium*	71 27 2	6.56	6.57
MAP	Beef*	Supermarket	*P. carnosum* *P. phosphoreum*	90 9	3.55	4.19
MAP	Pork*	Supermarket	*P. carnosum* *P. phosphoreum* *P. iliopiscarium*	5 26 69	7.07	7.13
MAP	Salmon	Supermarket	*P. carnosum* *P. phosphoreum* *P. iliopiscarium* *Photobacterium* sp.	7 58 22 13	6.77	6.8
Vacuum	Beef	Supermarket	*P. carnosum* *Photobacterium* sp.	96 4	6.72	6.72
Vacuum	Pork	Supermarket	*P. carnosum* *Photobacterium* sp.	99 1	7.15	7.15

*Representative types of spoiled meat samples where photobacteria were detected, and the common distribution of photobacteria found on them. The meat samples were bought in different supermarkets and shops and then incubated at 4°C until they were expired. Its spoilage community on selective medium was then analyzed with MALDI-TOF MS. CFU was determined on the base of the selective media consisting on marine broth supplemented with 3 g/L meat extract and 7 mg/L vancomycin. *Information obtained from Hilgarth et al. (2018a) and appended for comparison. NA, quantification was not possible due to overgrow of bacteria on plates, but photobacteria were recovered by observing bioluminescent colonies.*

addition to our previously published data, we identified only two species – *P. carnosum* and *P. phosphoreum* – on beef and turkey. On chicken and pork, and additionally on salmon, we detected *P. carnosum*, *P. phosphoreum*, and *P. iliopiscarium* (**Table 1**). Besides different meats, we analyzed a variety of additional food products to determine the distribution of photobacteria in the food industry. We did not detect photobacteria in algae (dried and salad), ready-to-eat salad (MAP, 2 samples), and sprouts (MAP); raw milk (12 samples), mozzarella cheese (3 samples), and eggs (3 samples); scallops (defrosted), trout, shrimps (cooked, defrosted) and sea salt; and minced meat (beef and mixed, 5 samples), bacon (2 samples), cooked ham, raw ham, and dried meat (pork).

Genetic Differentiation

In total, we recovered 163 *P. carnosum*, 113 *P. phosphoreum*, and 3 *P. iliopiscarium* isolates from chicken, turkey, pork beef, and salmon (total $n = 279$). Based on differences in their RAPD pattern obtained with primer M13V, we were able to discriminate 31 strains of *P. carnosum*, 24 of *P. phosphoreum*, and 3 strains of *P. iliopiscarium* within all isolates for further investigations on biodiversity. Genotypic distinctness of the strains were further validated with a RAPD approach using primer M14V. Isolates of *P. phosphoreum* from MAP farmed salmon showed no distinct or unique genotypes and were therefore considered as redundant strains. However, we recovered two strains of *P. carnosum* from salmon that were not abundant on other meats. Additional detailed information regarding the sample of origin of every strain used in this study can be found in **Supplementary Table S1**.

Calculation of diversity indices (**Table 2**) and an individual rarefaction analysis (**Supplementary Figure S1**) were carried out for all strains of each species with OTUs based on distinct genomic fingerprinting patterns. The analysis demonstrated that biodiversity of *P. phosphoreum* and *P. carnosum* was completely or almost completely covered by the strains isolated in this study, respectively. This was indicated by saturated rarefaction curves, a high calculated coverage value (>99%, >96%) and an identical or very similar richness of the expressed Chao-1 value to the actual number of genotypes. Additionally, both species were not significantly different regarding their ecological evenness and entropy ($p > 0.05$). Regarding *P. iliopiscarium*, calculation of diversity indices and comparison to the other two species were not expedient since only three isolates with three different genotypes could be recovered.

Chromosomal RAPD fingerprints of the strains of the three species were subjected to hierarchical cluster analysis and could be affiliated to several separate groups (**Figure 1**). In rare cases, RAPD pattern was highly similar and had a 100% dice similarity

TABLE 2 | Diversity indices of photobacteria species using genotyping OTUs.

Species	*P. phosphoreum*	*P. carnosum*	*P. iliopiscarium*
Individuals (isolates)	113	163	3
OTUs (strains)	24	31	3
Simpson (evenness)	0.9526	0.9406	–
Shannon (entropy)	3.106	3.081	–
Chao-1 (richness)	24	34.75	–
Good's coverage estimator (%)	99.12	96.32	0

in one RAPD approach using primer M13V with selected isolates. However, in the other two RAPD-PCR approaches with primer M13V, they exhibited different patterns indicating highly similar, but different strains (**Supplementary Figure S2**). Furthermore, patterns obtained with additional primer M14V validated their distinctness (**Supplementary Figure S3**).

Additional analysis of triplicates of all strains confirmed that they cluster together and apart from triplicates of the closest related strains in each case, indicating that respective replicates of one strain were more similar to each other than to other strains. The cluster similarity (dice coefficient) of the triplicates of each strain was at least 3.7% (*P. phosphoreum*), 3.9% (*P. carnosum*), and 22.7% (*P. iliopiscarium*) different from the cluster similarity of triplicates of the respective closest related strain.

Both *P. phosphoreum* and *P. carnosum* strains separated in 10 groups with a threshold of 76 and 79.5% similarity, respectively. Compared to this, the three strains of *P. iliopiscarium* clustered with lower similarity (≤66.7%). Strains from the same meat type did not form coherent cluster, except of *P. phosphoreum* strains from pork and the *P. carnosum* strains from fish. We additionally performed a cluster analysis of all strains of the three species with both primers M13V and M14V (**Supplementary Figures S4**, **S5**). All strains from one species cluster together and apart from strains of the other two species thus validating our approach.

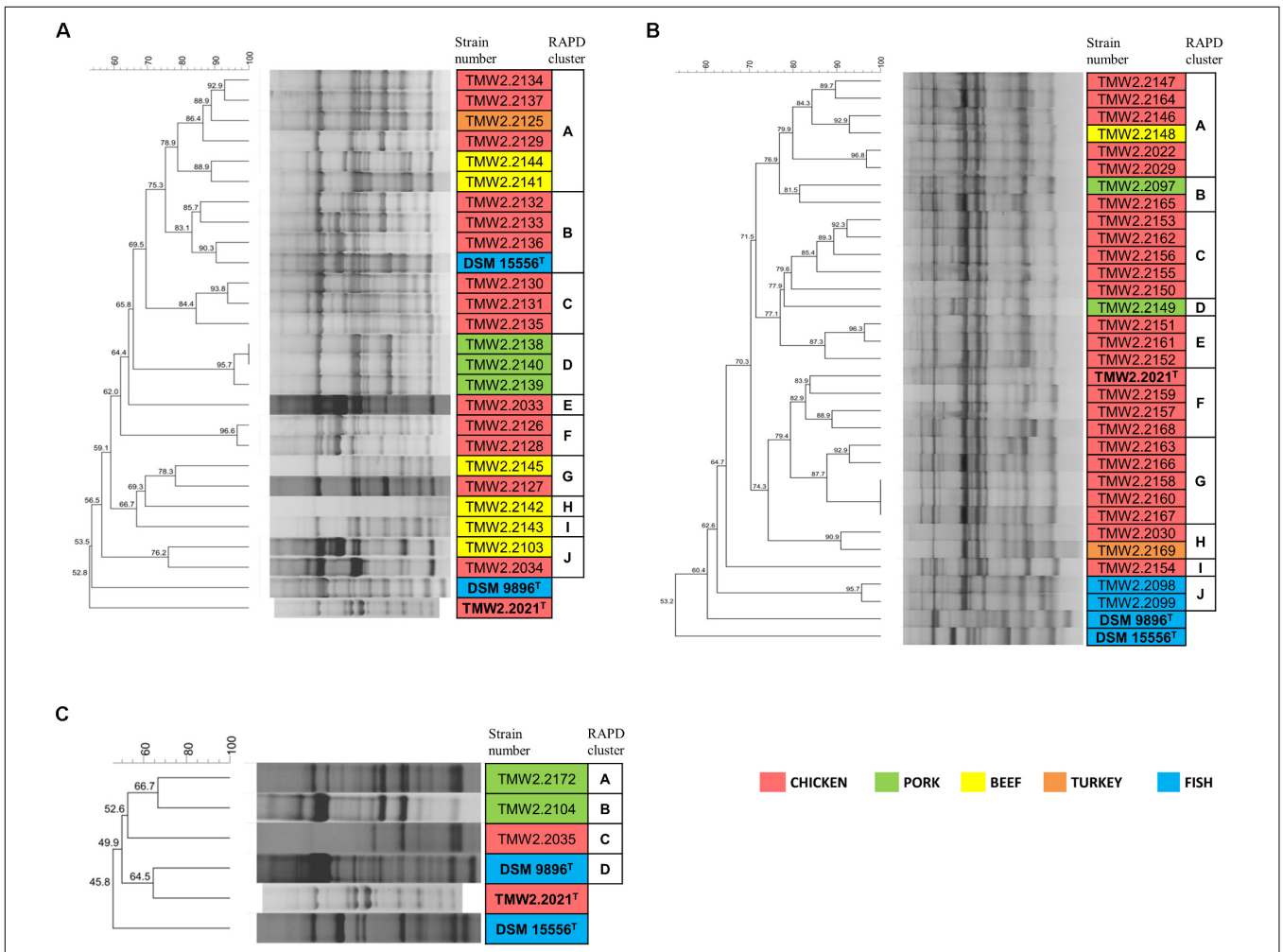

FIGURE 1 | RAPD-clustering of the selected strains. Hierarchical clustering was calculated with the unweighted pair group method with arithmetic mean (UPGMA), Dice similarity coefficient, and 1% tolerance. The similarity values are shown at the nodes of the tree. Different colors specify the isolation sources and bold letters the type strains. Further resolution of the most similar *P. phosphoreum* and *P. carnosum* strains RAPD-clustering is shown in **Supplementary Figure S2**.
(A) *P. phosphoreum*, type strain DSM 15556^T, **(B)** *P. carnosum*, type strain TMW2.2021^T, **(C)** *P. iliopiscarium*, type strain DSM 9896^T.

Physiological Differentiation

We furthermore performed physiotyping experiments to correlate the identified genome-based diversity in relation to phenotypic traits. For that, we monitored the maximum OD_{600}, maximum growth rate (U), and lag phase (lag) at 4°C in meat simulation medium at pH 5.8 to mimic cold storage of meats (**Table 3**). For both – lag phase and maximum growth rate – we could classify the strains in three statistically ($p < 0.05$) different groups within each of the species, and scores were assigned to each of them: short (3), medium (2), and long (0) lag phase and fast (3), medium (2), and slow (0) maximum growth rate. In the case of the pH, since its change is closely related to the production of spoilage substances like biogenic amines, the strains were classified in four groups as they decrease the pH (≤5.7, score 0), leave it unchanged (5.7–5.9, score 1), increase it up to 1 unit (5.9–6.8, score 2), or highly increase it (≥6.8, score 3). The behavior in the medium indicates highly diverse physiotypes that were independent of the isolation source (**Figure 2**).

Photobacterium phosphoreum strains reached the highest maximum OD_{600} (up to 4.99), had significantly higher growth rates than *P. carnosum* and *P. iliopiscarium* (p-values < 0.05), and tended to increase the pH to a considerable extent (up to pH 7.47). In contrast, *P. carnosum* strains grew up to comparatively low maximum OD_{600} (up to 1.7), had 10 times lower growth rates, and tended to decrease or keep the initial pH value. The only exception was strain TMW2.2169 that alkalized the medium to 7.08. The different influence of the species on the pH was statistically confirmed (p-values < 0.05); however, both species included strains that alkalized or acidified the medium at maximum OD_{600}. Regarding the lag phase, *P. carnosum* strains adapted to the media approximately half as fast as *P. phosphoreum* strains. Its average lag phase of 47–101 h was significantly longer than the one of both *P. phosphoreum* (21–55 h) and *P. iliopiscarium* (33–42 h, p-values < 0.05). The average lag phase of *P. iliopiscarium* was comparable to *P. phosphoreum* (p-value 0.767) whereas its maximum growth rate was comparable to *P. carnosum* (p-value 0.189). However, the tendency of *P. iliopiscarium* strains to increase the pH only slightly at its maximum OD_{600} (pH 6.32–6.56) was significantly different from the other two species (p-values < 0.05).

We observed no general correlation of the growth parameters with the RAPD fingerprint and the isolation source (**Figure 2**). Nevertheless, *P. phosphoreum* and *P. iliopiscarium* type strains from marine habitats were one of the slowest growing strains of each species, respectively.

Furthermore, *P. iliopiscarium* type strain and additional four *P. phosphoreum* strains from chicken (TMW2.2127, TMW2.2129, TMW2.2130, and TMW2.2134) showed motility after 3 days incubation. The rest of the strains, together with all strains from *P. carnosum*, were non-motile after 3 days. Bioluminescence was a frequent trait of the selected *P. phosphoreum* strains and several meat-borne strains exhibited much higher luminescence than the type strain. Only three *P. phosphoreum* strains from chicken (TMW2.2137, TMW2.2129, and TMW2.2134) did not show bioluminescence at all.

TABLE 3 | Growth parameters of *Photobacterium* spp. in meat-simulation media at 4°C.

Species	Maximum OD_{600}	Maximum growth rate	Lag phase (h)	pH
P. phosphoreum	3.10–4.99	0.168–0.468	21.17–55.08	5.62–7.47
P. iliopiscarium	1.38–2.05	0.033–0.144	32.76–41.83	6.32–6.56
P. carnosum	1.36–1.71	0.019–0.061	46.97–101.14	5.43–7.08

Summary of values obtained for the maximum OD_{600}, maximum growth rate (U), lag phase, and pH at maximum OD_{600} during growth of the three species of photobacteria in meat-simulation media at 4°C.

Resistance to Antibiotics

We recorded the tolerance of the strains for 15 antibiotics by measuring their inhibition zones (**Table 4** and **Figure 3**) to evaluate possible correlations between genotypes, isolation sources, and antibiotic resistances. In general, we observed high resistance in almost all strains to clindamycin, apramycin, penicillin G, and sulfonamides but sensitivity to chloramphenicol and norfloxacin. However, a few strains of *P. phosphoreum* exhibited resistance against chloramphenicol and norfloxacin (**Figure 3A** and **Supplementary Table S2**). In case of antibiotics with various extent of inhibition, the strains tended to be distributed to either low/high (*P. phosphoreum*) or low/medium/high resistance (*P. carnosum* and *P. iliopiscarium*). *P. carnosum* appeared to be the most sensitive species comprising the highest number of sensitive strains, especially regarding rifampicin, ampicillin, and tetracycline (**Supplementary Table S3** and **Figure 3B**). *P. iliopiscarium* strains appeared to be more similar to the *P. phosphoreum* group than to the *P. carnosum* group regarding resistance to antibiotics (**Figure 3C** and **Supplementary Table S4**). Within the species, we did not observe an explicit correlation of antibiotic resistance and isolation source or RAPD clustering. The same applied to the remarkable resistance of some *P. phosphoreum* strains for chloramphenicol and norfloxacin. Furthermore, the type strains revealed no clear differentiation compared to the other strains of the species.

Metabolic Properties of Representative Strains

Biochemical API 50CH and API ZYM tests were conducted with 20 strains of *P. carnosum*, 15 strains of *P. phosphoreum*, and 3 strains of *P. iliopiscarium* in order to study metabolic versatility (**Figure 4**). All three species produced acid from glucose, mannose, fructose, ribose, and *n*-acetylglucosamine. Additionally, they all responded positively in the tests for alkaline phosphatase, acid phosphatase, and leucine arylamidase. None of the strains produced acid from erythritol, D-arabinose, L-arabinose, D-xylose, L-xylose, D-adonitol, methyl-bD-xylopyranoside, L-sorbose, L-rhamnose, dulcitol, inositol, D-mannitol, D-sorbitol, methyl-α-D-mannopyranoside, amygdalin, arbutin, salicin, D-trehalose, inulin, D-melezitose, D-raffinose, xylitol, D-lyxose, D-tagatose, D-fucose, D-arabitol, and L-arabitol. None of the strains responded positively in the tests

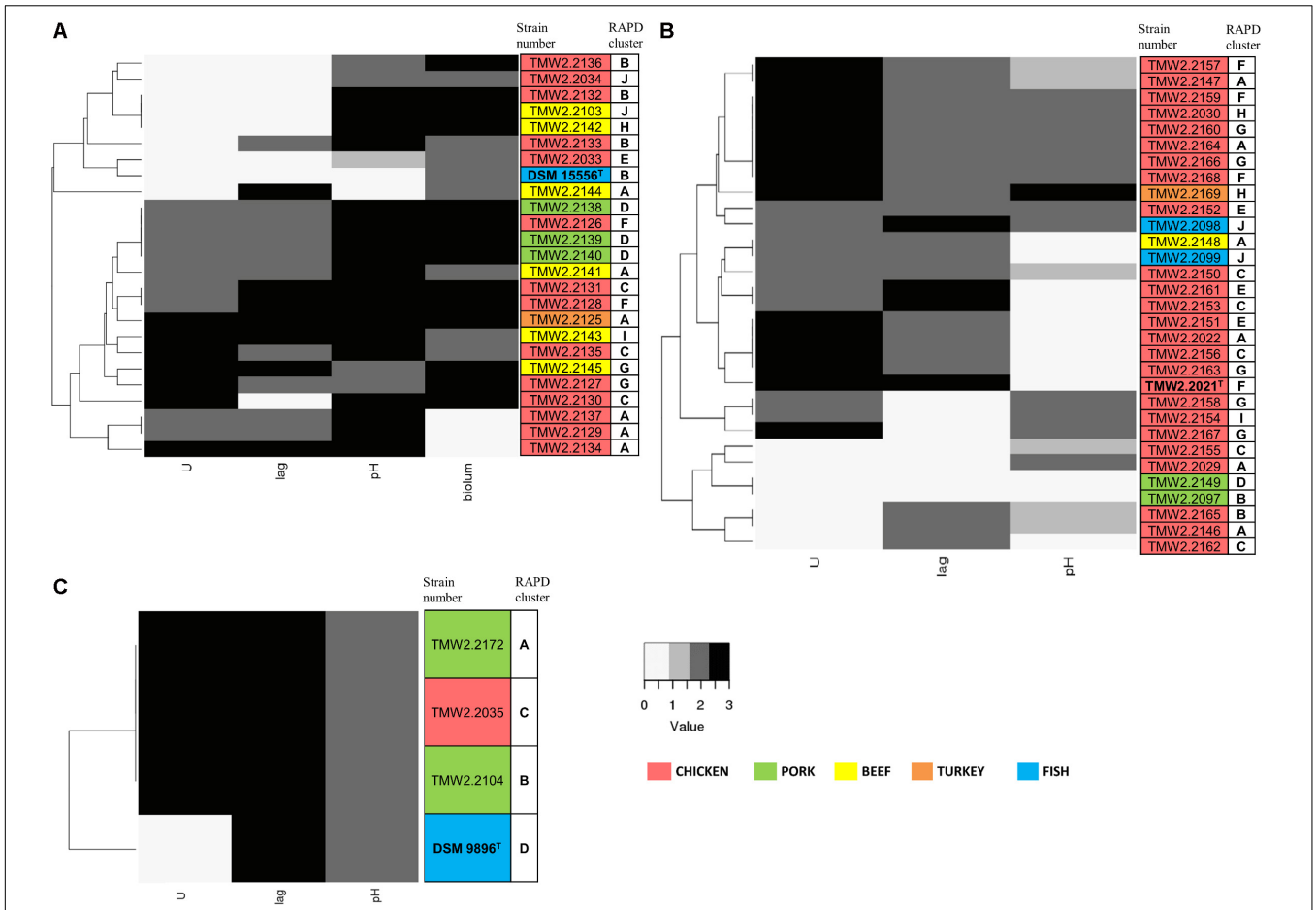

FIGURE 2 | Clustering of the strains by their growth rate (U), lag phase (lag), influence on pH, and bioluminescence (biolum, if existing). Growth rate and lag phase were determined in meat simulation medium at 4°C. Mean values were statistically grouped as low/medium/high and scored from 0 to 3. The highest score was given to the highest growth rates and lowest lag phases, respectively, and a score of 2 was given to medium values. The pH was measured when the cultures reached their highest OD_{600} and scored as follows: 0 – pH ≤5.7, 1 – pH 5.7–5.9, 2 – pH 5.9–6.8, 3 – pH >6.8. Bioluminescence of *P. phosphoreum* was evaluated manually on agar plates. The highest score was given to the strongest bioluminescence. The different isolation sources are displayed in colors and type strains are marked with bolt letters. **(A)** *P. phosphoreum*, type strain DSM 15556^T, **(B)** *P. carnosum*, type strain TMW2.2021, **(C)** *P. iliopiscarium*, type strain DSM 9896^T.

TABLE 4 | Range diameter of the inhibition zones (mm) as summary of all isolates per species.

Species	DA	NOR	NA	AMP	S3	W	P	S	APR	RD	CN	K	C	E	TE
P. carnosum	6	24–46	18–40	6–32	6–32	16–38	6–10	6–28	6–18	16–32	12–30	10–30	36–50	6–26	6–26
P. iliopiscarium	6	20–24	18–19	6–15	6	6–20	6–15	9–13	6–10	11–18	11–16	10–16	33–35	6–10	6–10
P. phosphoreum	6	14–34	8–25	6–12	6–22	6–26	6–12	6–18	6–11	9–22	7–23	6–22	6–38	7–25	6–21

A diameter of 6 mm was regarded as no inhibition at all. C, chloramphenicol 30 μg; NOR, norfloxacin 10 μg; S3, sulfonamides 300 μg; APR, apramycin 25 μg; P, penicillin G 5 μg; DA, clindamycin 2 μg; NA, nalidixic acid 30 μg; W, trimethoprim 5 μg; AMP, ampicillin 10 μg; S, streptomycin 25 μg; RD, rifampicin 5 μg; CN, gentamycin 10 μg; K, kanamycin 30 μg; E, erythromycin 15 μg; TE, tetracycline 30 μg.

for lipase C14, chymotrypsin, α-galactosidase, β-glucosidase, α-mannosidase, and α-fucosidase.

Still, we identified some traits that differed between the species (**Supplementary Table S5**). Several *P. carnosum* strains produced acid from methyl-α-D-glucopyranoside, cellobiose, saccharose, glycogen, gentiobiose, turanose, and L-fucose in contrast to *P. phosphoreum* and *P. iliopiscarium* strains. *P. carnosum* was additionally the only species with positive or weak positive reactions in the test for α-glucosidase but without acid production from potassium 5-ketogluconate. Strains of *P. phosphoreum* were the only ones being positive for cystine arylamidase and β-glucuronidase and also the only ones that did not produce acid from starch. In contrast, *P. iliopiscarium* strains did not show any unique spectrum of acid production from carbohydrates or enzymatic reactions within the tests. Overall, *P. carnosum* strains covered the broadest carbohydrate utilization spectrum and *P. phosphoreum* strains the most positive enzymatic reactions of all three species.

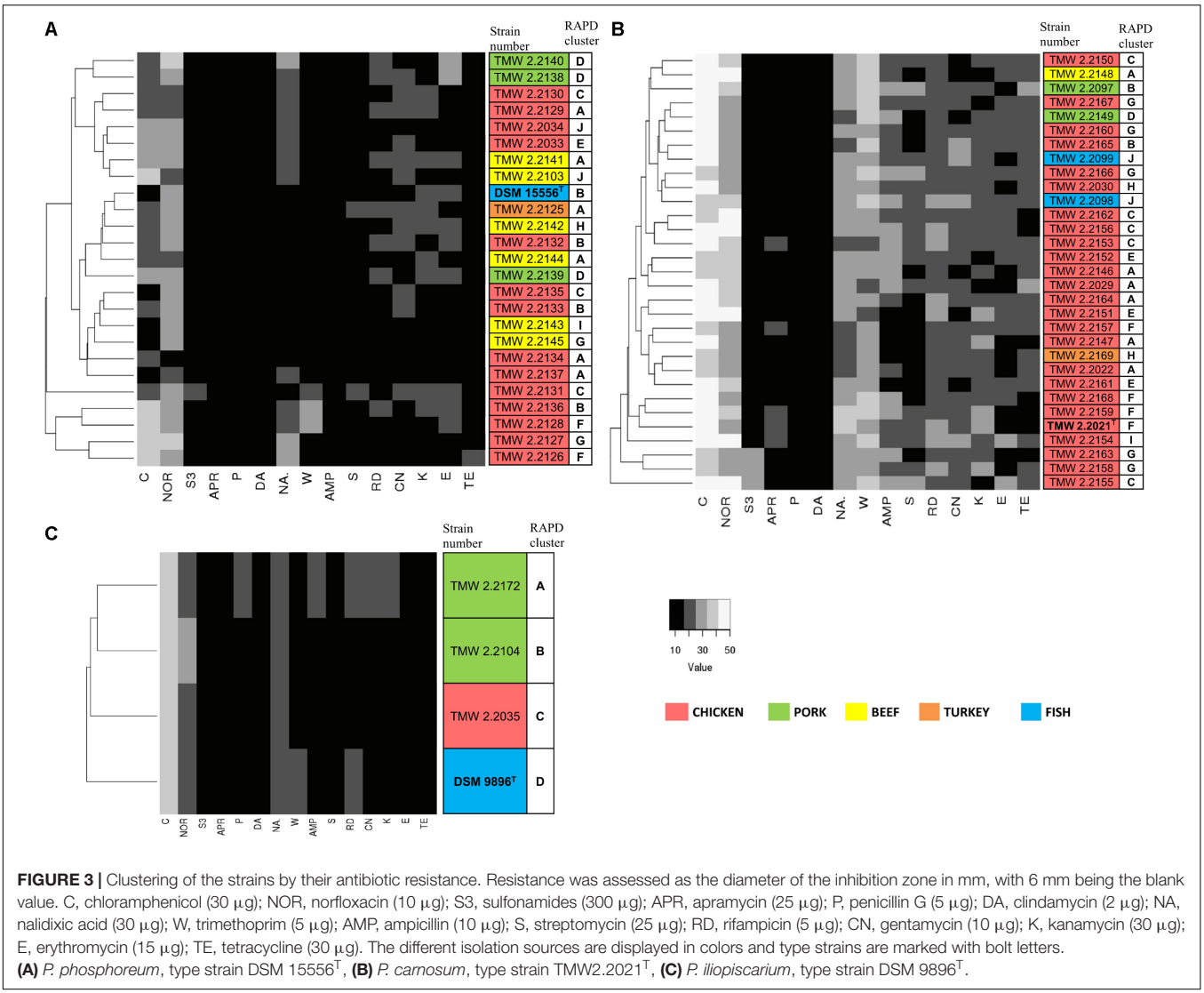

FIGURE 3 | Clustering of the strains by their antibiotic resistance. Resistance was assessed as the diameter of the inhibition zone in mm, with 6 mm being the blank value. C, chloramphenicol (30 μg); NOR, norfloxacin (10 μg); S3, sulfonamides (300 μg); APR, apramycin (25 μg); P, penicillin G (5 μg); DA, clindamycin (2 μg); NA, nalidixic acid (30 μg); W, trimethoprim (5 μg); AMP, ampicillin (10 μg); S, streptomycin (25 μg); RD, rifampicin (5 μg); CN, gentamycin (10 μg); K, kanamycin (30 μg); E, erythromycin (15 μg); TE, tetracycline (30 μg). The different isolation sources are displayed in colors and type strains are marked with bolt letters.
(A) *P. phosphoreum*, type strain DSM 15556^T, **(B)** *P. carnosum*, type strain TMW2.2021^T, **(C)** *P. iliopiscarium*, type strain DSM 9896^T.

Within the species, the differences of the marine type strains *P. phosphoreum* DSM15556^T and *P. iliopiscarium* DSM9896^T to the meat-borne strains were particularly notable. We observed three enzymatic tests that were negative in *P. phosphoreum* DSM15556^T but at least weakly positive in all the other *P. phosphoreum* strains (C4 esterase, C8 esterase–lipase, naphthol-AS-BI-phosphohydrolase; **Supplementary Table S5**). On the other hand, three carbohydrates were exclusively used by the type strain for acid production (glycerol, D-lactose, and D-melibiose). We saw also three reactions that were different for *P. iliopiscarium* DSM9896^T compared to meat-borne *P. iliopiscarium* strains (C8 esterase–lipase, valine arylamidase, and starch metabolism).

Furthermore, we identified a correlation of isolation source and metabolic properties that was depicted by the clustering of almost all *P. phosphoreum* strains from beef (**Figure 4A**). However, we could not identify clear differences of *P. carnosum* strains from meat and *P. carnosum* strains from fish (**Supplementary Table S5**). The test results of the *P. carnosum* type strain TMW2.2021^T were also not clearly different when compared to the other meat-borne strains. Nevertheless, both *P. carnosum* strains from salmon cluster together and both strains from pork cluster apart from the rest (**Figure 4B**). In each species we observed some reactions that were solely positive in single strains. *P. carnosum* TMW2.2163 was the only strain producing acid from saccharose, cellobiose, gentiobiose, turanose, and L-fucose (**Figure 4B**). *P. phosphoreum* TMW2.2130 was conspicuous by β-glucuronidase activity and *P. iliopiscarium* TMW2.2035 by acid production from potassium 2-ketogluconate (**Figures 4A,C**).

DISCUSSION

This is the first study that investigated biodiversity of meat-borne isolates of *Photobacterium* spp., isolated a wide variety of strains and explored strain- as well as species-specific traits. The data obtained from our study give further evidence that photobacteria,

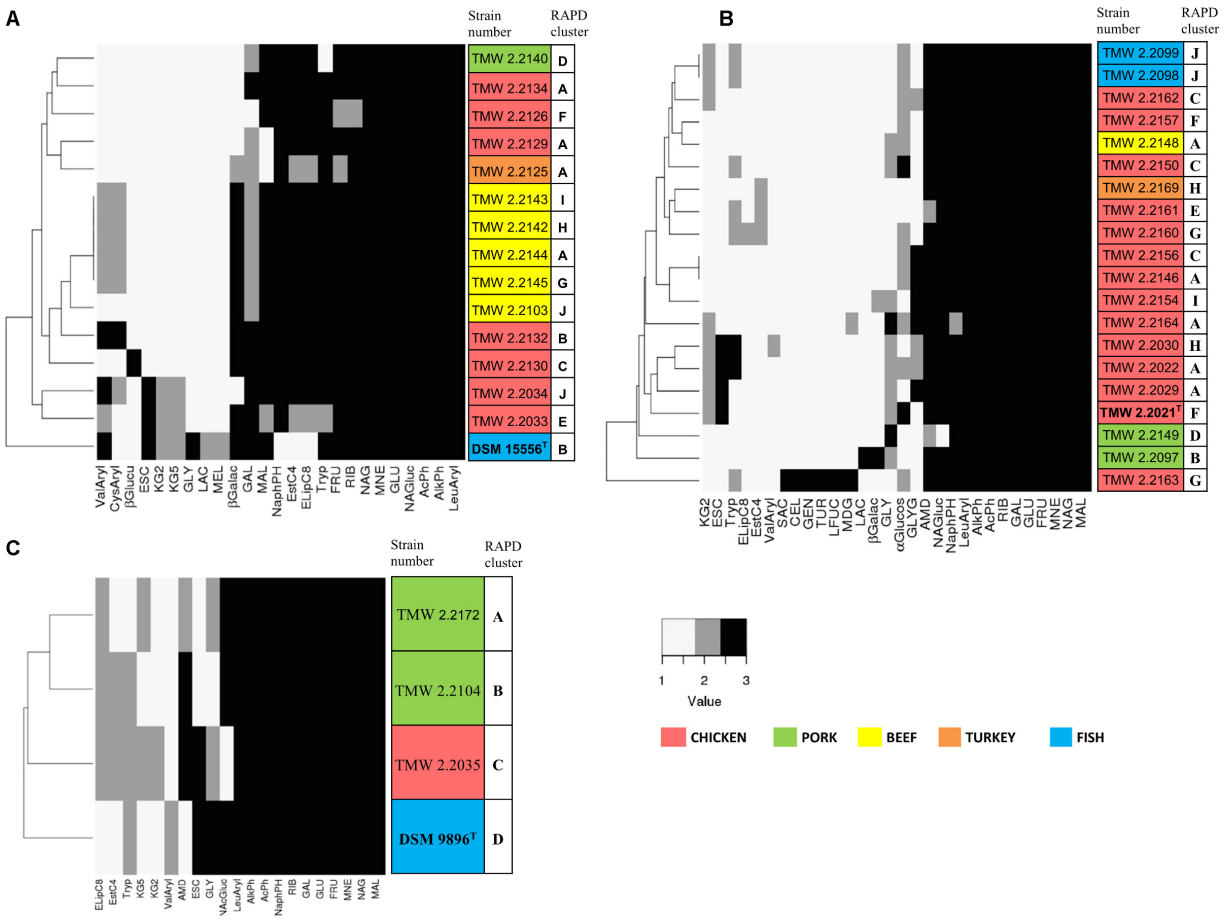

FIGURE 4 | Clustering of selected strains by metabolic properties based on API 50CH and API ZYM. The reactions prove acid production from single carbohydrates (API 50CH) and presence of selected enzymes (API ZYM). Each clustering shows only reactions that were positive at least in one isolate. Reactions were scored as 1 (negative reaction), 2 (weak positive reaction), and 3 (strong positive reaction). The different isolation sources are displayed in colors and type strains are marked with bolt letters. **(A)** *P. phosphoreum*, type strain DSM 15556^T, **(B)** *P. carnosum*, type strain TMW2.2021^T, **(C)** *P. iliopiscarium*, type strain DSM 9896^T. API50ch: GLY, glycerol; RIB, D-ribose; GAL, D-galactose; GLU, D-glucose; FRU, D-fructose; MNE, D-mannose; MDG, methyl-αD-glucopyranoside; NAG, *N*-acetylglucosamine; ESC, esculin; CEL, D-cellobiose; MAL, D-maltose; LAC, D-lactose; MEL, D-melibiose; SAC, D-saccharose; AMD, starch; GLYG, glycogen; GEN, gentiobiose; TUR, D-turanose; LFUC, L-fucose; KG2, potassium 2-ketogluconate; KG5, potassium 5-ketogluconate. APIzym: AlkPh, alkaline phosphatase; EstC4, esterase (C4); ELipC8, esterase lipase (C8); LeuAryl, leucine arylamidase; ValAryl, valine arylamidase; CysAryl, cystine arylamidase; Tryp, trypsin; AcPh, acid phosphatase; NaphPH, naphthol-AS-BI-phosphohydrolase; βGalac, β-galactosidase; βGlucu, β-glucuronidase; αGlucos, α-glucosidase; NAG, *N*-acetyl-β-glucosaminidase.

specifically *P. phosphoreum*, *P. carnosum*, and *P. iliopiscarium*, are widespread contaminants of different meats, as previously stated in Hilgarth et al. (2018a).

Distribution of *Photobacterium* spp. Contaminants

Recently, reports on the presence of photobacteria have emerged, mostly in culture-independent studies without actual isolation. All these reports were widespread over different countries, i.e., Germany (Hilgarth et al., 2018a), Belgium (Stoops et al., 2015), Italy (Pennacchia et al., 2011), Denmark (Nieminen et al., 2016), France (Bouju-Albert et al., 2018), and China (Li et al., 2019), demonstrating the global relevance of photobacteria to meat spoilage. Together with this, the data of our study confirm that contamination of meat with *Photobacterium* spp. is not sporadic, but rather a general issue associated with the meat industry. They also suggest that the contamination source might be similar in all types of meat, and therefore should be located in a common part of the slaughtering, processing, or packaging of the meat. This would also allow speculation on the presence of photobacteria associated with livestock, prior to the slaughtering process. However, given the psychrophilic nature of these organisms, and the inability of *P. carnosum* to grow at temperatures >20°C, or *P. phosphoreum* and *P. iliopiscarium* >25°C (Hilgarth et al., 2018b), it appears unlikely that these bacteria are autochthonous members of the animal gut-microbiome. Furthermore, we did not recover any photobacteria from other animal-derived products besides meat, nor from MAP packed-, protein- rich-, or sea-related vegetables. This suggests that, in relationship to food contamination and spoilage, photobacteria seem to only be able to reach detectable

numbers on meat (and fish). We also did not detect photobacteria on two types of seafood (scallops and shrimps). However, these products had been deep-frozen before sampling and it has been reported that deep-freezing reduces photobacteria below detection limits for culture-dependent methods (Emborg et al., 2002; Dalgaard et al., 2006).

Occurrence and Diversity of *Photobacterium* spp. on Packaged Meats

Calculated rarefaction and diversity indices revealed that the large quantity of isolates analyzed in this study reflects expected abundances. It therefore allows representative assessment of diversity within and between the species *P. carnosum* (31 strains from 163 isolates) and *P. phosphoreum* (24 strains from 113 isolates). The high evenness of *P. phosphoreum* and *P. carnosum* strains demonstrate the absence of dominant genotypes and suggest a rather general adaptation of the strains. However, even strains from the same meat sample showed clear genotypic and phenotypic variability, which suggests an initial contamination that is already considerably diverse. Furthermore, ecological entropy of both species was not significantly different meaning the same degree of overall biodiversity also on species level. Regarding *P. iliopiscarium*, the low number of recovered isolates (three isolates with three genotypes) suggests that there may be more diversity within the meat-borne strains than the ones recovered in this study.

We did not isolate any photobacteria from either minced beef- or mixed minced meat in this study. However, culture-independent reports of *Photobacterium* spp. (Pennacchia et al., 2011; Stoops et al., 2015) indicate that the genus can be present on minced meat, even if they do not grow to detectable numbers. It may be speculated that other meat spoilers dominate on minced meat and simply overgrow photobacteria due to shorter doubling time. Recently, presence of *Pseudomonas* spp. has been reported on MAP minced meat (Hilgarth et al., 2019) that might act as possible fast growing competitor of *Photobacterium* spp.

We also observed that not all samples of meat cuts are contaminated with photobacteria, even if they come from the same producer. This could indicate a low level of initial contamination and distribution by chance (Höll et al., 2019). A low initial contamination may also explain the different distribution of the three *Photobacterium* species on different meat types (Hilgarth et al., 2018a).

The growth of photobacteria appears also be independent of the packaging method since photobacteria occur independently of the employment of modified atmosphere, vacuum, or air packaging (Hilgarth et al., 2018a). This is supported by Höll et al. (2019) who predicted that there is little to no effect of the choice of atmosphere on the growth of photobacteria, based on similar gene expression under different MAP conditions. This suggests that the current modified atmosphere composition and vacuum packages, commonly used to extend the shelf-life and optimum qualities of meat and fish (McKee, 2007; McMillin, 2008; Bingol and Ergun, 2011; Lorenzo and Gomez, 2012; Rossaint et al., 2014), are insufficient to reduce spoilage-associated photobacteria on meat. Furthermore, the detection of photobacteria on marinated meats demonstrated that marinating – a process to introduce antimicrobials (Björkroth, 2005; Kargiotou et al., 2011) – will also not prevent photobacterial spoilage.

Adaptation to Food as an Ecological Niche

Results from the carbon metabolism and enzymatic activities, together with distribution of growth rates and lag phase, suggest that *P. carnosum* strains are more homogeneous with lower variability than *P. phosphoreum* and *P. iliopiscarium* strains. While it was possible to clearly differentiate the marine type strain of the two latter from the meat-borne strains, *P. carnosum* seems to share common traits for all the strains, independently of the source of isolation. Additionally, our results for the growth and metabolic traits indicate adaptation of *P. carnosum* to meat or other nutrient rich environments, as stated before by Hilgarth et al. (2018b). *P. carnosum* also lacks bioluminescence and motility, two common traits of symbiotic or free-living marine photobacteria. This supports missing adaptation of the species to sea-related environments. Still, for the first time, *P. carnosum*, a species described as terrestrial and unrelated to sea environments, was detected on MAP salmon. However, our data on missing subpopulations referring to respective environments support the hypothesis that the isolates from (freshwater) farmed salmon do not originate from a marine environment, but rather from a contamination later in the processing and packaging. The fact that *P. phosphoreum* isolates originating from the same MAP farmed salmon showed no distinct genotypes, i.e., were also found on meats, further supports that hypothesis. In contrast, *P. phosphoreum* and *P. iliopiscarium* appear to have different marine as well as meat-borne subpopulations with specific adaptations to the respective environment as demonstrated by the differences of the meat borne strains to their marine type strains.

Reactions for lipase C14, esterase C4, and esterase–lipase C8 were negative or at most weakly positive for almost all strains of the three species. Additionally, all of the *P. phosphoreum* meat-borne strains and some from *P. iliopiscarium* and *P. carnosum* were negative for glycerol. However, Höll et al. (2019) confirmed the expression of lipase and genes encoding for enzymes involved in lipid and glycerol utilization in photobacteria. This suggests that the lipase was not expressed in API medium or that this type of lipase do not lead to a positive reaction within the API ZYM test and that utilization of glycerol does not result in acidification of the medium. However, almost all strains of the three species showed positive reactions for the main monomeric carbohydrates found in meat, i.e., glucose, fructose, mannose, ribose (Aliani and Farmer, 2005a,b; Koutsidis et al., 2008a,b; Meinert et al., 2009a,b). Furthermore, the species *P. carnosum* shows a wider metabolic capability in terms of carbohydrate utilization than the other two species. Many of the carbohydrates used exclusively by *P. carnosum* are plant (e.g., starch, cellobiose, gentiobiose, turanose) or meat related (e.g., glycogen). Regarding growth on

meat-simulation media, we observed that the species has the lowest maximum growth rates and longer adaptation times in the meat-simulation media used in this study. However, it is found in some meat types in larger amounts and cell counts than any of the other two species. This suggests that *P. carnosum* is adapted to more complex media and has specific growth requirements that the other two species do not have.

Safety Concerning Aspects of *Photobacterium* Species

The observed variable alkalization or acidification of the growth medium with up to two pH values difference demonstrates the great variety of strain physiotypes. This might also be of relevance for the respective potential as meat spoiler since alkalization indicates production of biogenic amines and ammonia from amino acid metabolism. The ability of *P. phosphoreum* to produce histamine and other biogenic amines in fish has been previously reported (Jorgensen et al., 2000; Stoops et al., 2015; Nieminen et al., 2016). The increase of pH in the media up to 7.5 might be an indicator for the potential of some of our isolates, i.e., certain strains of *P. phosphoreum* to produce higher amounts of biogenic amines, which is also predicted in the transcriptomic analysis of Höll et al. (2019).

Another important safety aspect deals with bacterial resistance to antibiotics. Administration of antibiotics to poultry, swine, and calves in the agricultural industry is known as disease treatment and control (Nisha, 2008; Muaz et al., 2018) and therefore possibly linked to resistance of meat spoiling bacteria. However, we did not observe a clear pattern that would allow to link the source of isolation to the antibiotic resistances determined in this study. Our results suggest that the species have intrinsic resistance to clindamycin, apramycin, penicillin G, and sulfonamides. However, resistance to the other antibiotics occurs differentially on strain level. The fact that closely related strains with similar chromosomal fingerprints did not exhibit similar antibiotic resistances suggests that these resistances may be located on mobile genetic elements and therefore possibly be transferable. This transferability might also occur for chloramphenicol and norfloxacin resistance in *P. phosphoreum*, as only few of its strains show complete resistance to them in contrast to the common tendency of the three species. The suggested transferability of the resistance to chloramphenicol, being one of the drugs of last resort [DoLR (World-Health-Organization, 2001)], harbors potential health concerns.

CONCLUSION

This study demonstrates that, even though the initial contamination is likely to be low, photobacteria strains from meat display a great diversity with specific genotypic, phenotypic, and physiotypic traits. Due to previous association with solely marine environments and lack of optimized detection methods, biodiversity of meat-borne *P. phosphoreum*, *P. iliopiscarium*, and *P. carnosum* was hitherto unexplored. On the basis of our results, we can assume that their entry route as meat contaminants might occur during slaughtering, derived from the exterior of the animal or environment, but not from the gut – following colonization of general processing and packaging facilities. Divergence of the meat-borne and the marine type strains of *P. phosphoreum* and *P. iliopiscarium* on the one hand and homogeneity of *P. carnosum* strains on the other hand suggests different environmental adaptation and possibly also separate origin of contamination. Additionally, diversity of metabolic capabilities and antibiotic resistances appear to be widespread and mostly not linked to a specific isolation source. This reveals the presence of a highly variable and rich community of photobacteria on each meat that combines multiple physio- and genotypes with potential relevance to food safety worldwide.

DATA AVAILABILITY STATEMENT

All datasets generated for this study are included in the manuscript/**Supplementary Files**.

AUTHOR CONTRIBUTIONS

SF-P and PH performed the laboratory work and data evaluation, wrote the first draft of the manuscript, and designed the study. MH performed the diversity index analysis, helped to draft the study, and supervised the work of SF-P and PH. RV initiated the project and supervised the work of SF-P and PH. All authors read and approved the final manuscript.

FUNDING

This work was partially funded by the German Federal Ministry for Economic Affairs and Energy via the German Federation of Industrial Research Associations (AiF) and the Industry Association for Food Technology and Packaging (IVLV); project number AiF 20113N1.

SUPPLEMENTARY MATERIAL

The Supplementary Material for this article can be found online at: https://www.frontiersin.org/articles/10.3389/fmicb.2019.02399/full#supplementary-material

REFERENCES

Aliani, M., and Farmer, L. J. (2005a). Precursors of chicken flavor. I. Determination of some flavor precursors in chicken muscle. *J. Agric. Food Chem.* 53, 6067–6072. doi: 10.1021/jf050085t

Aliani, M., and Farmer, L. J. (2005b). Precursors of chicken flavor. II. Identification of key flavor precursors using sensory methods. *J. Agric. Food Chem.* 53, 6455–6462. doi: 10.1021/jf050087d

Beijerinck, M. W. (1889). Le photobacterium luminosum, bactérie lumineuse de la Mer du Nord. *Arch. Neerl. Sci. Exact. Nat.* 23, 401–427.

Bingol, E. B., and Ergun, O. (2011). Effects of modified atmosphere packaging (MAP) on the microbiological quality and shelf life of ostrich meat. *Meat Sci.* 88, 774–785. doi: 10.1016/j.meatsci.2011.03.013

Björkroth, J. (2005). Microbiological ecology of marinated meat products. *Meat Sci.* 70, 477–480. doi: 10.1016/j.meatsci.2004.07.018

Bjornsdottir-Butler, K., Abraham, A., Harper, A., Dunlap, P. V., and Benner, R. A. Jr. (2018). Biogenic amine production by and phylogenetic analysis of 23 photobacterium species. *J. Food Prot.* 81, 1264–1274. doi: 10.4315/0362-028X.JFP-18-022

Bouju-Albert, A., Pilet, M. F., and Guillou, S. (2018). Influence of lactate and acetate removal on the microbiota of french fresh pork sausages. *Food Microbiol.* 76, 328–336. doi: 10.1016/j.fm.2018.06.011

Chao, A. (1984). Nonparametric estimation of the number of classes in a population. *Scand. J. Statist.* 11, 265–270.

Cohn, F. (1878). *Lettter to J. Penn which Describes Micrococcus Phosphoreum, Versameling van Stucken Betreffende het Geneeskundig Staats Toerzich*, 126–130.

Dalgaard, P., Madsen, H. L., Samieian, N., and Emborg, J. (2006). Biogenic amine formation and microbial spoilage in chilled garfish (Belone belone belone)–effect of modified atmosphere packaging and previous frozen storage. *J. Appl. Microbiol.* 101, 80–95. doi: 10.1111/j.1365-2672.2006.02905.x doi: 10.1111/j.1365-2672.2006.02905.x

Dalgaard, P., Mejlholm, O., Christiansen, T. J., and Huss, H. H. (1997). Importance of *Photobacterium* phosphoreum in relation to spoilage of modified atmosphere-packed fish products. *Lett. Appl. Microbiol.* 24, 373–378. doi: 10.1046/j.1472-765X.1997.00152.x

Dunlap, P. V., and Ast, J. C. (2005). Genomic and phylogenetic characterization of luminous bacteria symbiotic with the deep-sea fish Chlorophthalmus albatrossis (*Aulopiformes*: *Chlorophthalmidae*). *Appl. Environ. Microbiol.* 71, 930–939. doi: 10.1128/AEM.71.2.930-939.2005

Ehrmann, M. A., Muller, M. R., and Vogel, R. F. (2003). Molecular analysis of sourdough reveals Lactobacillus mindensis sp. *nov*. *Int. J. Syst. Evol. Microbiol.* 53(Pt 1), 7–13. doi: 10.1099/ijs.0.02202-0

Emborg, J., Laursen, B. G., Rathjen, T., and Dalgaard, P. (2002). Microbial spoilage and formation of biogenic amines in fresh and thawed modified atmosphere-packed salmon (*Salmo salar*) at 2 degrees C. *J. Appl. Microbiol.* 92, 790–799. doi: 10.1046/j.1365-2672.2002.01588.x

Good, I. J. (1953). The population frequencies of species and the estimation of population parameters. *Biometrika* 40, 237–264. doi: 10.1093/biomet/40.3-4.237

Gram, L., and Huss, H. H. (1996). Microbiological spoilage of fish and fish products. *Int. J. Food Microbiol.* 33, 121–137. doi: 10.1016/0168-1605(96)01134-8

Hammer, O., Harper, D., and Ryan, P. (2001). PAST: paleontological statistics software package for education and data analysis. *Palaeontol. Electronica* 4, 9.

Hendrie, M. S., Hodgkiss, W., and Shewan, J. M. (1970). The identification, taxonomy and classification of luminous bacteria. *Microbiology* 64, 151–169. doi: 10.1099/00221287-64-2-151

Hilgarth, M., Fuertes-Perez, S., Ehrmann, M., and Vogel, R. F. (2018a). An adapted isolation procedure reveals Photobacterium spp. as common spoilers on modified atmosphere packaged meats. *Lett. Appl. Microbiol.* 66, 262–267. doi: 10.1111/lam.12860

Hilgarth, M., Fuertes, S., Ehrmann, M., and Vogel, R. F. (2018b). Photobacterium carnosum sp. nov., isolated from spoiled modified atmosphere packaged poultry meat. *Syst. Appl. Microbiol.* 41, 44–50. doi: 10.1016/j.syapm.2017.11.002

Hilgarth, M., Lehner, E. M., Behr, J., and Vogel, R. F. (2019). Diversity and anaerobic growth of Pseudomonas spp. isolated from modified atmosphere packaged minced beef. *J. Appl. Microbiol.* 127, 159–174. doi: 10.1111/jam.14249

Höll, L., Hilgarth, M., Geissler, A. J., Behr, J., and Vogel, R. F. (2019). Prediction of in situ metabolism of photobacteria in modified atmosphere packaged poultry meat using metatranscriptomic data. *Microbiol. Res.* 222, 52–59. doi: 10.1016/j.micres.2019.03.002

Jorgensen, L. V., Huss, H. H., and Dalgaard, P. (2000). The effect of biogenic amine production by single bacterial cultures and metabiosis on cold-smoked salmon. *J. Appl. Microbiol.* 89, 920–934. doi: 10.1046/j.1365-2672.2000.01196.x

Kahm, M., Hasenbrink, G., Lichtenberg-Fraté, H., Ludwig, J., and Kschischo, M. (2010). Grofit: fitting biological growth curves with R. *J. Statist. Softw.* 33, 1–12.

Kargiotou, C., Katsanidis, E., Rhoades, J., Kontominas, M., and Koutsoumanis, K. (2011). Efficacies of soy sauce and wine base marinades for controlling spoilage of raw beef. *Food Microbiol.* 28, 158–163. doi: 10.1016/j.fm.2010.09.013

Koutsidis, G., Elmore, J. S., Oruna-Concha, M. J., Campo, M. M., Wood, J. D., and Mottram, D. S. (2008a). Water-soluble precursors of beef flavour: I. Effect of diet and breed. *Meat Sci.* 79, 124–130. doi: 10.1016/j.meatsci.2007.08.008

Koutsidis, G., Elmore, J. S., Oruna-Concha, M. J., Campo, M. M., Wood, J. D., and Mottram, D. S. (2008b). Water-soluble precursors of beef flavour. Part II: effect of post-mortem conditioning. *Meat Sci.* 79, 270–277. doi: 10.1016/j.meatsci.2007.09.010

Labella, A. M., Arahal, D. R., Castro, D., Lemos, M. L., and Borrego, J. J. (2017). Revisiting the genus *Photobacterium*: taxonomy, ecology and pathogenesis. *Int. Microbiol.* 20, 1–10. doi: 10.2436/20.1501.01.280

Lehane, L., and Olley, J. (2000). Histamine fish poisoning revisited. *Int. J. Food Microbiol.* 58, 1–37. doi: 10.1016/s0168-1605(00)00296-8

Li, N., Zhang, Y., Wu, Q., Gu, Q., Chen, M., Zhang, Y., et al. (2019). High-throughput sequencing analysis of bacterial community composition and quality characteristics in refrigerated pork during storage. *Food Microbiol.* 83, 86–94. doi: 10.1016/j.fm.2019.04.013

Li, Y., Zhou, M., Wang, F., Wang, E. T., Du, Z., Wu, C., et al. (2017). *Photobacterium* proteolyticum sp. nov., a protease-producing bacterium isolated from ocean sediments of Laizhou Bay. *Int. J. Syst. Evol. Microbiol.* 67, 1835–1840. doi: 10.1099/ijsem.0.001873

Lo, N., Jin, H. M., and Jeon, C. O. (2014). *Photobacterium* aestuarii sp. nov., a marine bacterium isolated from a tidal flat. *Int. J. Syst. Evol. Microbiol.* 64(Pt 2), 625–630. doi: 10.1099/ijs.0.056861-0

Lorenzo, J. M., and Gomez, M. (2012). Shelf life of fresh foal meat under MAP, overwrap and vacuum packaging conditions. *Meat Sci.* 92, 610–618. doi: 10.1016/j.meatsci.2012.06.008

McKee, L. (2007). "Microbiological and sensory properties of fresh and frozen poultry," in *Handbook of Meat, Poultry and Seafood Quality*, eds M. Leo, and L. Nollet, (Hoboken, NJ: John Wiley & Sons), 87–498.

McMillin, K. W. (2008). Where is MAP Going? A review and future potential of modified atmosphere packaging for meat. *Meat Sci.* 80, 43–65. doi: 10.1016/j.meatsci.2008.05.028

Meinert, L., Schafer, A., Bjergegaard, C., Aaslyng, M. D., and Bredie, W. L. (2009a). Comparison of glucose, glucose 6-phosphate, ribose, and mannose as flavour precursors in pork; the effect of monosaccharide addition on flavour generation. *Meat Sci.* 81, 419–425. doi: 10.1016/j.meatsci.2008.08.018

Meinert, L., Tikk, K., Tikk, M., Brockhoff, P. B., Bredie, W. L., Bjergegaard, C., et al. (2009b). Flavour development in pork. Influence of flavour precursor concentrations in longissimus dorsi from pigs with different raw meat qualities. *Meat Sci.* 81, 255–262. doi: 10.1016/j.meatsci.2008.07.031

Muaz, K., Riaz, M., Akhtar, S., Park, S., and Ismail, A. (2018). Antibiotic residues in chicken meat: global prevalence, threats, and decontamination strategies: a review. *J. Food Prot.* 81, 619–627. doi: 10.4315/0362-028X.JFP-17-086

Nieminen, T. T., Dalgaard, P., and Bjorkroth, J. (2016). Volatile organic compounds and *Photobacterium* phosphoreum associated with spoilage of modified-atmosphere-packaged raw pork. *Int. J. Food Microbiol.* 218, 86–95. doi: 10.1016/j.ijfoodmicro.2015.11.003

Nisha, A. R. (2008). Antibiotic residues - A global health hazard. *Ve. World* 1, 375–377.

Okuzumi, M., Hiraishi, A., Kobayashi, T., and Fujii, T. (1994). Photobacterium histaminum sp. nov., a histamine-producing marine bacterium. *Int. J. Syst. Bacteriol.* 44, 631–636. doi: 10.1099/00207713-44-4-631

Olofsson, T. C., Ahrné, S., and Molin, G. (2007). The bacterial flora of vacuum-packed cold-smoked salmon stored at 7°C, identified by direct 16S rRNA gene analysis and pure culture technique. *J. Appl. Microbiol.* 103, 109–119. doi: 10.1111/j.1365-2672.2006.03216.x

Onarheim, A. M., Wiik, R., Burghardt, J., and Stackebrandt, E. (1994). Characterization and identification of two Vibrio species indigenous to the intestine of fish in cold sea water; description of *Vibrio* iliopiscarius sp. *nov*. *Syst. Appl. Microbiol.* 17, 370–379. doi: 10.1016/S0723-2020(11)80053-6

Parte, A. C. (2018). LPSN – List of Prokaryotic names with Standing in Nomenclature (bacterio.net), 20 years on. *Int. J. Syst. Evol. Microbiol.* 68, 1825–1829. doi: 10.1099/ijsem.0.002786

Pennacchia, C., Ercolini, D., and Villani, F. (2011). Spoilage-related microbiota associated with chilled beef stored in air or vacuum pack. *Food Microbiol.* 28, 84–93. doi: 10.1016/j.fm.2010.08.010

Reynisson, E., Lauzon, H. L., Magnusson, H., Jonsdottir, R., Olafsdottir, G., Marteinsson, V., et al. (2009). Bacterial composition and succession during storage of North-Atlantic cod (*Gadus* morhua) at superchilled temperatures. *BMC Microbiol.* 9:250. doi: 10.1186/1471-2180-9-250

Rossaint, S., Klausmann, S., and Kreyenschmidt, J. (2014). Effect of high-oxygen and oxygen-free modified atmosphere packaging on the spoilage process of poultry breast fillets. *Poult. Sci.* 94, 93–103. doi: 10.3382/ps/peu001

Schloss, P. D., and Handelsman, J. (2005). Introducing DOTUR, a computer program for defining operational taxonomic units and estimating species richness. *Appl. Environ. Microbiol.* 71, 1501–1506. doi: 10.1128/AEM.71.3.1501-1506.2005

Shannon, C., and Weaver, W. (1949). *The Mathematical Theory of Communication*. Urbana, IL: University of Illinois Press.

Simpson, E. H. (1949). Measurement of Diversity. *Nature* 163, 688–688. doi: 10.1038/163688a0

Stoops, J., Ruyters, S., Busschaert, P., Spaepen, R., Verreth, C., Claes, J., et al. (2015). Bacterial community dynamics during cold storage of minced meat packaged under modified atmosphere and supplemented with different preservatives. *Food Microbiol.* 48, 192–199. doi: 10.1016/j.fm.2014.12.012

Takahashi, H., Ogai, M., Miya, S., Kuda, T., and Kimura, B. (2015). Effects of environmental factors on histamine production in the psychrophilic histamine-producing bacterium Photobacterium iliopiscarium. *Food Control* 52, 39–42. doi: 10.1016/j.foodcont.2014.12.023

Thyssen, A., and Ollevier, F. (2015). "Photobacterium," in *Bergey's Manual of Systematics of Archaea and Bacteria*, eds W. B. Whitman, F. Rainey, P. Kämpfer, M. Trujillo, J. Chun, P. DeVos, et al. (Hoboken, NJ: Wiley), 1–11.

Torido, Y., Takahashi, H., Kuda, T., and Kimura, B. (2012). Analysis of the growth of histamine-producing bacteria and histamine accumulation in fish during storage at low temperatures. *Food Control* 26, 174–177. doi: 10.1016/j.foodcont.2012.01.009

Urakawa, H., Kita-Tsukamoto, K., and Ohwada, K. (1999). Reassessment of the taxonomic position of Vibrio iliopiscarius (Onarheim et al., 1994) and proposal for Photobacterium iliopiscarium comb. nov. *Int. J. Syst. Evol. Microbiol.* 49, 257–260. doi: 10.1099/00207713-49-1-257

Urbanczyk, H., Ast, J. C., and Dunlap, P. V. (2011). Phylogeny, genomics, and symbiosis of Photobacterium. *FEMS Microbiol. Rev.* 35, 324–342. doi: 10.1111/j.1574-6976.2010.00250.x

Usbeck, J. C., Kern, C. C., Vogel, R. F., and Behr, J. (2013). Optimization of experimental and modelling parameters for the differentiation of beverage spoiling yeasts by Matrix-Assisted-Laser-Desorption/Ionization-Time-of-Flight mass spectrometry (MALDI-TOF MS) in response to varying growth conditions. *Food Microbiol.* 36, 379–387. doi: 10.1016/j.fm.2013.07.004

Wang, X., Wang, Y., Yang, X., Sun, H., Li, B., and Zhang, X. H. (2017). Photobacterium alginatilyticum sp. nov., a marine bacterium isolated from bottom seawater. *Int. J. Syst. Evol. Microbiol.* 67, 1912–1917. doi: 10.1099/ijsem.0.001886

World-Health-Organization (2001). *WHO Model Prescribing Information - Drugs Used in Bacterial Infections*. Geneva: WHO.

Conflict of Interest: The authors declare that the research was conducted in the absence of any commercial or financial relationships that could be construed as a potential conflict of interest.

6.2.2 Comparative genomics of *Photobacterium* species from terrestrial and marine habitats

The biodiversity study performed on the three species of photobacteria relevant to meat spoilage revealed multiple differences between strains of the same species isolated from meat, and suggested a source-related divergence of strains of *P. phosphoreum* and *P. iliopiscarium*. The present work utilized a comparative genomics study to analyze in depth those differences on a larger set of marine-borne strains of the three species, and in order to establish differences between species that could explain their isolation frequency and distribution. Genomes of both marine-borne and meat-borne strains of each species were acquired and probed for distinct features. At the moment of this publication, new strains of *P. carnosum* had been isolated from MAP packed salmon, supposedly as a cross contamination from the processing environment, and were included in the analysis. All of them appear to be prone to the exchange of genetic material that might be used as a strategy to increase advantageous characteristics and increase survivability, and is also translated to the accumulation of secondary metabolites gene clusters. While similar in the scope of the whole genus, the three species harbor fundamental differences that might shape their interaction with the environment and concomitant microbiota. *P. carnosum* appears a cohesive species focused on diversification of carbon utilization, while its counterpart *P. phosphoreum*, represented by two subspecies, is suggested to utilize antimicrobial properties and stress adaptation to outgrow possible competitors and dominate in the microbial consortia. The third species *P. iliopiscarium*, the least abundant of the three, does show a significant divergence between those strains isolated from different sources, also represented by distribution of features such as the flagellar cluster, suggesting an environmentally driven adaptation of the species.

Author contribution: Sandra Fuertes-Perez performed the experimental design and laboratory work concerning DNA extraction prior to sequencing. In addition, she performed the phylogenetic and genome analysis, including use of online tools and gene search (main experiments and methodology). She performed the data evaluation, wrote the first draft of the manuscript, created figures and tables, and participated in the reviewing process of the final text.

Current Research in Microbial Sciences 2 (2021) 100087

Contents lists available at ScienceDirect

Current Research in Microbial Sciences

journal homepage: www.sciencedirect.com/journal/current-research-in-microbial-sciences

Comparative genomics of *Photobacterium* species from terrestrial and marine habitats

Sandra Fuertes-Perez, Rudi F. Vogel, Maik Hilgarth *

Lehrstuhl für Technische Mikrobiologie, Technische Universität München, Germany

ARTICLE INFO

Keywords:
Photobacterium
Genomics
Meat spoilage
Ecology
Adaptation
Metabolism

ABSTRACT

Photobacterium (*P.*) is a genus widely studied in regards to its association with and ubiquitous presence in marine environments. However, certain species (*P. phosphoreum, P. carnosum, P. iliopiscarium*) have been recently described to colonize and spoil raw meats without a marine link. We have studied 27 strains from meat as well as 26 strains from marine environments in order to probe for intraspecies marine/terrestrial subpopulations and identify distinct genomic features acquired by environmental adaptation. We have conducted phylogenetic analysis (MLSA, ANI, *fur*, codon usage), search of plasmids (plasmidSPADES), phages (PHASTER), CRISPR-cas operons (CRISPR-finder) and secondary metabolites gene clusters (antiSMASH, BAGEL), in addition to a targeted gene search for specific pathways (e.g. TCA cycle, pentose phosphate, respiratory chain) and elements relevant for growth, adaptation and competition (substrate utilization, motility, bioluminescence, sodium and iron transport). *P. carnosum* appears as a conserved single clade, with one isolate from MAP fish clustering apart that doesn't, however, show distinct features that could indicate different adaptation. The species harbors genes for a wide carbon source utilization (glycogen/starch, maltose, pullulan, fucose) for colonization of diverse niches in its genome. *P. phosphoreum* is represented by two different clades on the phylogenetic analyses not correlating to their origin or distribution of other features analyzed that can be divided into two novel subspecies based on genome-wide values. A more diverse antimicrobial activity (sactipeptides, microcins), production of secondary metabolites (siderophores and arylpolyenes), stress response and adaptation (bioluminescence, sodium transporters, catalase, high affinity for oxygen cytochrome cbb3 oxidase, DMSO reductase and proton translocating NADH dehydrogenase) is predicted compared to the other species. *P. iliopiscarium* was divided into two clades based on source of isolation correlating with phylogeny and distribution of several traits. The species shows traits common to the other two species, similar carbon utilization/transport gene conservation as *P. carnosum* for the meat-isolated strains, and predicted utilization of marine-common DMSO and flagellar cluster for the sea-isolated strains. Results additionally suggest that photobacteria are highly prone to horizontal acquisition/loss of genetic material and genetic transduction, and that it might be a strategy for increasing the frequency of strain- or species-specific features that offers a growth/competition advantage.

Introduction

Photobacterium has originally been a genus closely related to marine environments, with members ranging from fish and seafood spoilers (e.g. *P. phosphoreum* and *P. iliopiscarium*) (Ast and Dunlap, 2005; Dalgaard et al., 1997; Takahashi et al., 2015), pathogens (e.g. *P. damselae*), symbionts (e.g. *P. kishitanii*) and free-living bacteria (e.g. *P. angustum*) (Labella et al., 2017; Urbanczyk et al., 2010). Members of the genus are gram-negative, facultatively aerobic and mostly psychro- and halophilic, and motile (Urbanczyk et al., 2010).

In the food industry, the species *P. phosphoreum* and *P. iliopiscarium* are closely monitored on fish and seafood as they represent potent spoilers and a health risk. Both are reported as common and abundant fish spoilers (Dalgaard et al., 1998) responsible for the production of foul odors and biogenic amines, such as histamine (Bjornsdottir-Butler et al., 2018; Bjornsdottir et al., 2009; Emborg et al., 2002; Torido et al., 2012), whose presence leads to scombroid fish poisoning upon consumption (Lehane and Olley, 2000).

However, their presence is not exclusive of aquatic areas, as they have also been reported on raw meat. *P. phosphoreum, P. carnosum,*

* Corresponding author.
E-mail address: maik.hilgarth@tum.de (M. Hilgarth).

https://doi.org/10.1016/j.crmicr.2021.100087
Received 3 November 2021; Accepted 26 November 2021
Available online 28 November 2021

originally isolated from poultry meat (Hilgarth et al., 2018b), and to a lesser extent *P. iliopiscarium*, are considered as common meat spoilers due to their ubiquitous presence on meat, their ability to grow to relevant numbers, and their predicted potential to spoil it (Fuertes-Perez et al., 2019; Höll et al., 2019). These species have been reported on culture indepentent studies on air and vacuum packaged beef (Pennacchia et al., 2011), modified atmosphere packaged (MAP) minced beef (Stoops et al., 2015), pork sausages (Bouju-Albert et al., 2018) and dry-fermented sausages (Pini et al., 2020). Complementary to these studies, culture depent studies have also reported on both detection and isolation of *Photobacterium* species on poultry, beef, turkey and pork, independently of type of packaging atmosphere and marinate (Fuertes-Perez et al., 2019; Hilgarth et al., 2018a, 2018b; Nieminen et al., 2016). Further studies have established that despite their widespread presence on raw meat, in several countries and in high numbers, they are not in all packages of the same batch, and might even follow some seasonal pattern (Fuertes-Perez et al., 2019), making their detection and recovery a fastidious task, even with targeted isolation methods (Fuertes-Perez et al., 2020; Hilgarth et al., 2018a).

A previous study has revealed high diversity within these *Photobacterium* species, and suggested a correlation between the source of isolation and phenotypic characteristics (Fuertes-Perez et al., 2019). High diversity within the genus was also reported by a previous study on comparative genomics of marine photobacteria where 16 of the 28 available *Photobacterium* species were included, and the authors report the presence of traits that appear linked to the lifestyle of the species (Machado and Gram, 2017).

The metabolism of *P. phosphoreum* as a model species for photobacteria has been previously described by Höll et al. (2019) in a metatranscriptomics analysis from meat. Photobacteria on meat are predicted to have little regard for the atmosphere used for packaging. The study also reported versatility for these bacteria, predicted to use a variety of carbon sources such as common sugars (e.g. glucose, ribose), amino acids and lipids (e.g. glycerol) and produce spoilage products such as biogenic amines. However, differences on species and strain level could not be resolved in that study.

Studies have been published previously on the genomics of photobacteria, either on a limited number of strains of several species of the genus (Machado and Gram, 2017; Urbanczyk et al., 2010), focused on strains of a specific species (Roslan et al., 2020; Yu et al., 2019) or certain relevant traits such as piezophilic adaptation (Allen and Bartlett, 2000; Campanaro et al., 2005; Hauschild et al., 2020), salt adaptation (Wu et al., 2006), lux-rib operon (Urbanczyk et al., 2008, 2012) and motility (Eloe et al., 2008). Since *P. phosphoreum, P. iliopisicarum* and *P. carnosum* are the first species widely found in a completely aquatic-unrelated environment, this study aimed to explore the genomic diversity based on terrestrial versus aquatic isolates and between the species.

Materials and methods

DNA extraction and sequencing

In total, 27 strains of the species *Photobacterium phosphoreum* (10 strains), *P. iliopiscarium* (2 strains) and *P. carnosum* (13 strains) were inoculated in marine broth (MB) supplemented with 3 g/L meat extract, and grown overnight at 15 °C. From each of the grown cultures, 5 ml were used to perform a DNA extraction with the E.Z.N.A. Bacterial DNA kit (OMEGA, Bio-Rad) with modifications in the protocol according to Fuertes-Perez et al. (2020).

Whole genome sequencing was performed on the obtained high quality DNA with Illumina HiSeq technology by Eurofins (Germany). Assembly of the genomes was performed by SPAdes (Bankevich et al., 2012). The DNA sequences were annotated by NCBI under Bioproject ID PRJNA590348.

Additionally, all the available genomes (as of August 2021) in NCBI database of the three species were retrieved and added to this study. Table S1 shows the strain denomination, source and country of isolation, origin of the genome sequence and the WGS accession number of all isolates of *P. carnosum* (15 strains), *P. phosphoreum* (26 strains) and *P. iliopiscarium* (6 strains) used in this study.

Annotation and gene search

The annotation was performed by the NCBI Prokaryotic Genome Annotation Pipeline (PGAP) (Angiuoli et al., 2008) under the aforementioned Bioproject ID for those not yet uploaded. In order to increase the accuracy of the annotation, the genomes were additionally annotated with Rapid Annotation Subsystem Technology (RAST) server (Aziz et al., 2008), TIGR annotation (Ouyang et al., 2007) and the NCBI subcellular localization. The data obtained from different annotations was connected using PERSEUS (Tyanova et al., 2016), and used for the search of specific genes and metabolic pathways. Identities of the genes of interest were additionally manually curated using BLAST (https://blast.ncbi.nlm.nih.gov) (Altschul et al., 1990). Accession numbers for the genes searched in this study can be found in the table S2.

Extraction of the pan-, core- and accessory genome of each species was achieved with the BlAst Diagnostic Gene findEr (BADGE) (Behr et al., 2016), with default settings, but adjusting the "megablast percent identity cut" and "megablast within group qscov" to 95/0.95 for analysis within a species, and 85/0.85 for the analysis between species. Its output was used to obtain the graphic representation by species with Blast Ring Image Generator (BRIG) (Alikhan et al., 2011), using the annotated ORFs of the pan-genome of each species as reference.

General genome statistics

The shotgun whole genome sequences of the strains used in this study were analyzed with CMG biotools (Vesth et al., 2013). General statistics such as genome size, GC content and codon usage were obtained using the aforementioned tools. They were additionally used for the generation of pan- and core-genome graphs included in this study.

Phylogenetic analysis

Based on the annotation performed as detailed in the previous section, several housekeeping gene sequences were extracted to construct an MLSA based tree. Used genes include the DNA gyrase subunit B (*gyr*B), RNA polymerase sigma factor (*rpo*D), protein recombinase A (*rec*A), DNA-directed RNA polymerase subunit alpha (*rpo*A), cell division protein (*fts*Z) and cell-shape determining protein (*mre*B). The accession number of the housekeeping genes used are displayed in table S3. Alignments were performed by ClustalW (Thompson et al., 1994) and dendrograms constructed using the maximum likelihood algorithm (Felsenstein, 1981) and Tamura-Nei model (Tamura and Nei, 1993), using MEGA v7 software (Kumar et al., 2016) and tested with 1000 bootstrap replications. Additionally, we also constructed a phylogenetic tree based on the *fur* gene, with the maximum likelihood and Tamura-Nei model, and tested with 1000 bootstrap replications.

The software JSpecies (Richter and Rossello-Mora, 2009) was used to calculate the average nucleotide identity (ANI) of all the strains of each species, with pairwise genome comparison of the whole genome shotgun sequences by means of the ANIb algorithm (Goris et al., 2007).

The Genome-to-Genome Distance Calculator by DSMZ (Meier--Kolthoff et al., 2013, 2014) was used to determine and evaluate presence of possible subspecies within each of the three species of photobacteria included in this study.

Plasmid search

Plasmid presence was predicted for genomes of self-isolated strains with the plasmidSPAdes algorithm (Antipov et al., 2016). The sequences

were compared and annotation was extracted to determine if specific additional functions were granted by presence of said plasmids.

In addition, previously described *Photobacterium* plasmids were blasted against all the contigs of the strains included in this study using CLC Main Workbench (QIAGEN). Compared plasmids include: pPHDD1 (FN597600.2), pAQU1 (AB571865.1), pP99–018 (AB277723.1), pP91278 (AB277724.1), pPHDP60 (KC344732.1), pPHDP10 (DQ069059.1), pPHDP70 (KP100338.1), pP9014 (AB453229.1), pPH1 (AY789019.1), pPBPR1 (CR377818.1), and Gung47 (KC687076.1) from *P. gaetbulicola*, as previously performed for several species by Machado and Gram (2017).

Additional online tools

Secondary metabolites were identified by submitting the entire genomes to the online tool antiSMASH 5.0 (Blin et al., 2019; Medema et al., 2011), and the resulting sequences and clusters were compared to each other with BLAST.

In addition to antiSMASH, that also allows the detection of bacteriocin related gene clusters, the genomes were submitted to BAGEL4 (de Jong et al., 2006) in order to identify bacteriocins-related gene clusters and ribosomally synthesized and post-translationaly modified peptides (RiPPs).

PHASTER (Arndt et al., 2016; Zhou et al., 2011) was utilized to search and identify prophages in all the genomes included in this study. The resulting sequences were also compared using BLAST and grouped by similarity with a cuttoff of 70/70 identity/coverage percentage.

The contigs of each of the strains of the three species of photobacteria were analyzed with CRISPRFinder (Grissa et al., 2007). The direct repeats (DR) and protospacers of each of the CRISPR-Cas systems identified were compared using BLAST to each other and to the sequences of identified prophages. Identical spacers were grouped together in order to establish phylogenetic relationships between strains.

Results

Phylogenic and taxonomic analyses

We have used an MLSA based analysis of six housekeeping genes up to 4952 bp of total concatenated length (Fig. 1A) and the average nucleotide identity (ANI) (Fig. 1B), for comparison of the phylogenetic relationships.

One available genome of *P. iliopiscarium* (NCIMB 13355) and six of *P. phosphoreum* (JCM 21184, FS-2.3, FS-6.2, FS-6.3, GCSL-P60, GCSL-P64) were found to be clones of other available genomes in the database (>99.9% ANI similarity) and therefore removed from the analysis. Accession numbers for those genomes are also included in table S1.

Results for the MLSA and ANI values appear to be similar (pairwise ANI values comparison can be found in table S4). Both approaches show a clear differentiation of the three species. Whitin the *P. phosphoreum* and *P. iliopiscarium* species, there is a separation in two main cluster that remain constant through the analyses. Although not by source of isolation, strains AK-4, AK-5, AK-8, FS-6.1 and FS-3.2, all isolated from marine environment, from *P. phosphoreum* are consistently separated from the rest of the strains of the species with ANI values of ~95–96% to the rest of the strains, close to the species demarcation values. *In silico* DDH values obtained from the DMSZ genome-to-genome distance calculator lie between 68 and 76%, below the proposed threshold for delineation of a subspecies (<79%). Therefore, the five strains of *P. phosphoreum* forming an external cluster appear to constitute a new subspecies within the species of photobacteria.

In the case of *P. iliopiscarium*, however, the separation of strains TMW

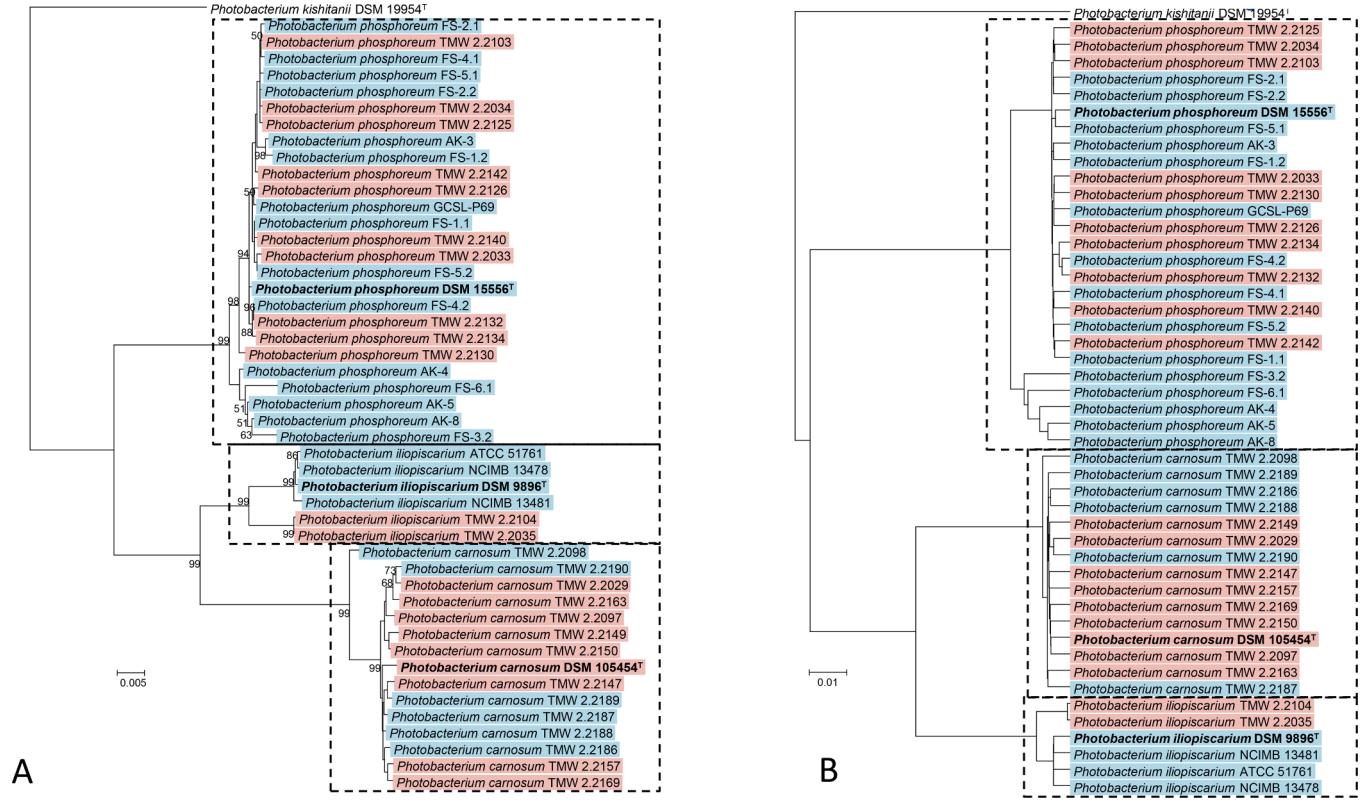

Fig. 1. A. MLSA phylogenetic tree (=4952 bp) based on the Maximum likelihood algorithm and Tamura-Nei model tested with 1000 bootstrap replications. Bootstrap values equal to or above 50 are shown. Concatenated genes include *gyr*B (=1209 bp), *rpo*D (=855 bp), *rec*A (=585 bp), *rpo*A (=927 bp), *fts*Z (=619 bp), *mre*B (=757 bp) in that order. B. ANI pairwise values based dendrogram. Both clusterings show differentiation by species marked by discontinuous line, and distinction between meat-isolated (red) and fish-isolated (blue) strains of each species. Type strains of each species are shown in bold letters and marked with a ^{T}.

2.2104 and TMW 2.2035 does correlate to the distinct source of isolation based on meat or fish/aquatic origin. Although no separation of isolates is observed in *P. carnosum*, one single salmon-isolated strain (TMW 2.2098) does cluster appart from the rest in both analysis.

We additionally tested the validity of the *fur* gene as identification marker for the three species of photobacteria (Figure S1), proposed by Machado and Gram (2015). The resulting phylogenetic tree is consistent with the clustering obtained from the MLSA and ANI values, supporting the subpopulations observed for *P. phosphoreum* and *P. iliopiscarium*, but not *P. carnosum* outlier strain.

Finally, we clustered the isolates based on codon usage (Figure S2). Differences in codon usage are low, and although delineation of species is conserved, clustering of strains is not supported by any of the other analysis. *P. phosphoreum* and *P. carnosum* show each two distinct clusters containing strains of mixed sources of isolation, while *P. iliopiscarium* shows one single strain isolated from meat (TMW 2.2035) as outlier.

Genome characteristics

We calculated an average genome size and GC content of 4.24 Mbp and 38.65%, 4.33 Mbp and 39.01%, 4.66 Mbp and 39.46% for *P. carnosum, P. iliopiscarium* and *P. phosphoreum* species, respectively. The representation of GC% content and genome size for all isolates is displayed in Figure S3.

Statistical analysis ($p < 0.05$) revealed significant variability between the GC content of the three species, and between the genome size of *P. phosphoreum* to the other two species. Additionally, we found significant differences between *P. phosphoreum* strains isolated from fish (4.58 Mbp and 39.53% GC), and those isolated from meat (4.79 Mbp and 39.35% GC), but not for the other two species.

The resulting pan-genome of the species varies between 12,699 annotated genes and 11.6 Mbp for *P. phosphoreum*, 6158 annotated genes and 5.7 Mbp from *P. iliopiscarium* and 8410 annotated genes and 7.7 Mbp from *P. carnosum*. The statistics for each of the genomes analyzed can be found in table S5.

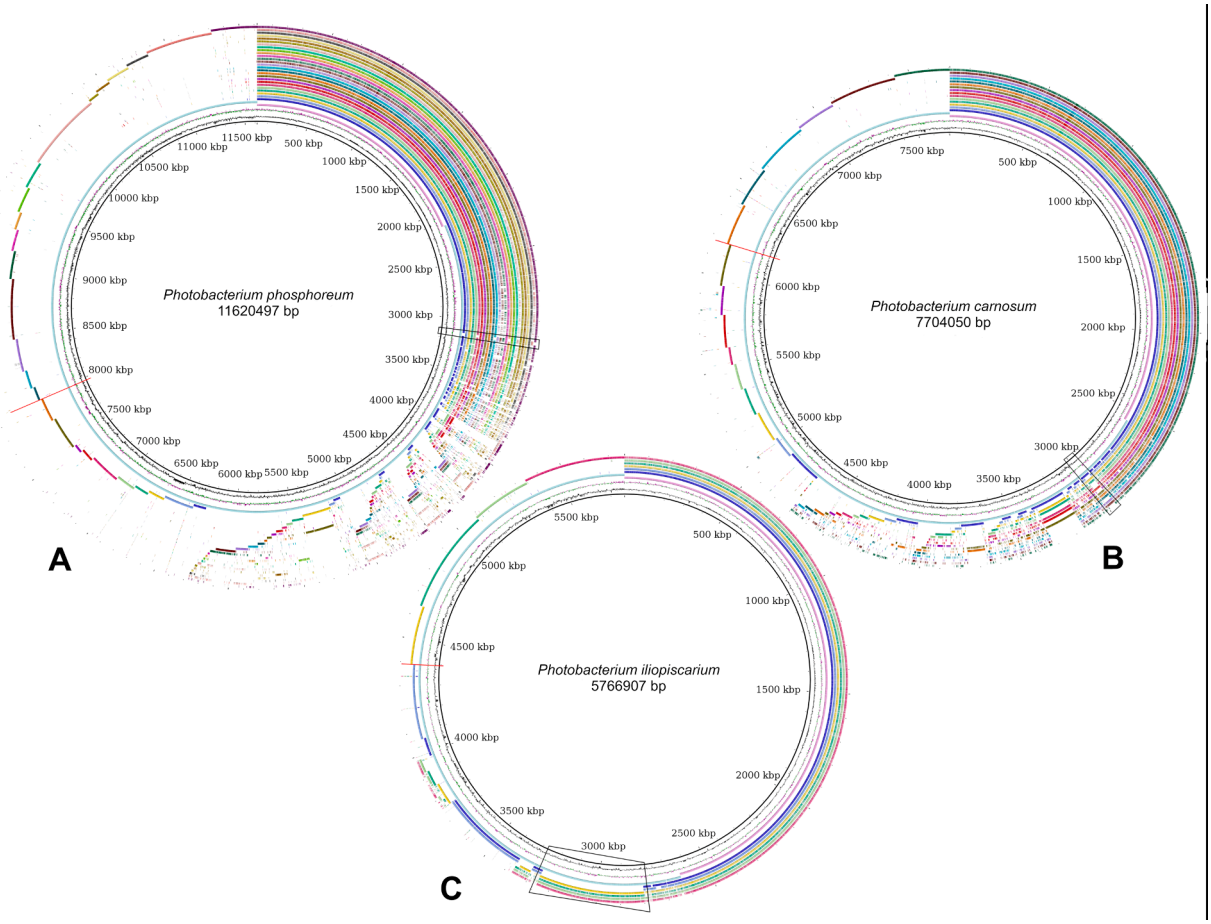

Fig. 2. Representation of the genomes of all strains of each species using the pan-genome of the species as reference, created with BRIG and using a cutoff of 90/90 identity/coverage. Inner pink line represents the core genome of the species, while the following blue line represents the accessory genome of each species. The genome of each strain is represented by a differently colored ring following the former two. **A** *P. phosphoreum*: core genome, accessory genome; and strains: TMW 2.2033; TMW 2.2034; TMW 2.2103; TMW 2.2125; TMW 2.2126; TMW 2.2130; TMW 2.2132; TMW 2.2134; TMW 2.2140; TMW 2.2142; **DSM 15556^T**; AK-3; AK-4; AK-5; AK-8; FS-1.1; FS-1.2; FS-2.1; FS-2.2; FS-3.2; FS-4.1; FS-4.2; FS-5.1; FS-5.2; FS-6.1; GCSL-P69. **B** *P. carnosum*: core genome, accessory genome; and strains: **DSM 105454^T**; TMW 2.2029; TMW 2.2097; TMW 2.2147; TMW 2.2149; TMW 2.2150; TMW 2.2157; TMW 2.2163; TMW 2.2169; TMW 2.2098; TMW 2.2186; TMW 2.2187; TMW 2.2188; TMW 2.2189; TMW 2.2190. **C** *P. iliopiscarium*: core genome, accessory genome; and strains: TMW 2.2035; TMW 2.2104; **DSM 9896^T**; ATCC 51761; NCIMB 13478; NCIMB 13481. The red line divides for each species the strain-specific genome of the meat-isolated (before the line) strains and the fish-isolated strains (after the line). The black box represents the cluster of genes extracted with known function.

Figure S4 and Fig. 2 show the variation of pan- and core-genome sizes with each new strain included in the analysis and the BRIG overlapping representation of the pan-, core- and accesory genome of each species, respectively. The size of the core-genome is stabilized at ~3 Mbp and already 2 to 3 strains appear enough to cover its diversity within each species.

Out of all the annotated genes of each species, 17.7% (2248 genes) in *P. phosphoreum*, 44.3% (2731 genes) in *P. iliopiscarium* and 32.0% (2694 genes) in *P. carnosum* represent the core genome of the species respectively. Between 30 and 50% of the total genes of a species are grouped within the strain-specific part of the accessory genome.

The annotation reveals that in each case the 33–48% of the total genes in the genome are only predicted proteins with no assigned or unknown function (Figure S5). These hypothetical proteins appear mainly distributed across the strain specific genome of each strain (47–57% of the total strain specific gene pool). The three species also accumulate multiple mobile elements (e.g. transposases) that can sum up to 2–3% of the total genome content.

BADGE and BRIG based untargeted gene search

Using the BRIG representation as reference, we identified clusters of genes only shared by a fraction of the strains of each species. The flagellar cluster was the main function present in those regions (black box in Fig. 2). Its distribution correlates to the source of isolation and phylogenetic analysis in the case of *P. iliopiscarium*, being only present in fish-borne strains. Presence of the flagellar cluster in the other two species is not tied to source of isolation or clades identified in the MLSA analysis, and it appears mostly random. All members of the proposed subspecies of *P. phosphoreum* contain the intact flagellar cluster.

We additionally found that fish/marine strains of *P. iliopiscarium* contain in their genome several genes belonging to a type IV secretion system (black box Fig. 2C), not present in any of the meat-borne strains. Remaining regions of group specific genes are mostly hypothetical proteins or mobile elements, but we identified no additional growth, survival or adaptation predicted advantages.

Targeted gene search

The summary of present/absent pathways and genes is displayed in Fig. 3 and table S6 and focused on the main differences between species and strains since overall metabolism of the three species has already been described by Hilgarth (2018).

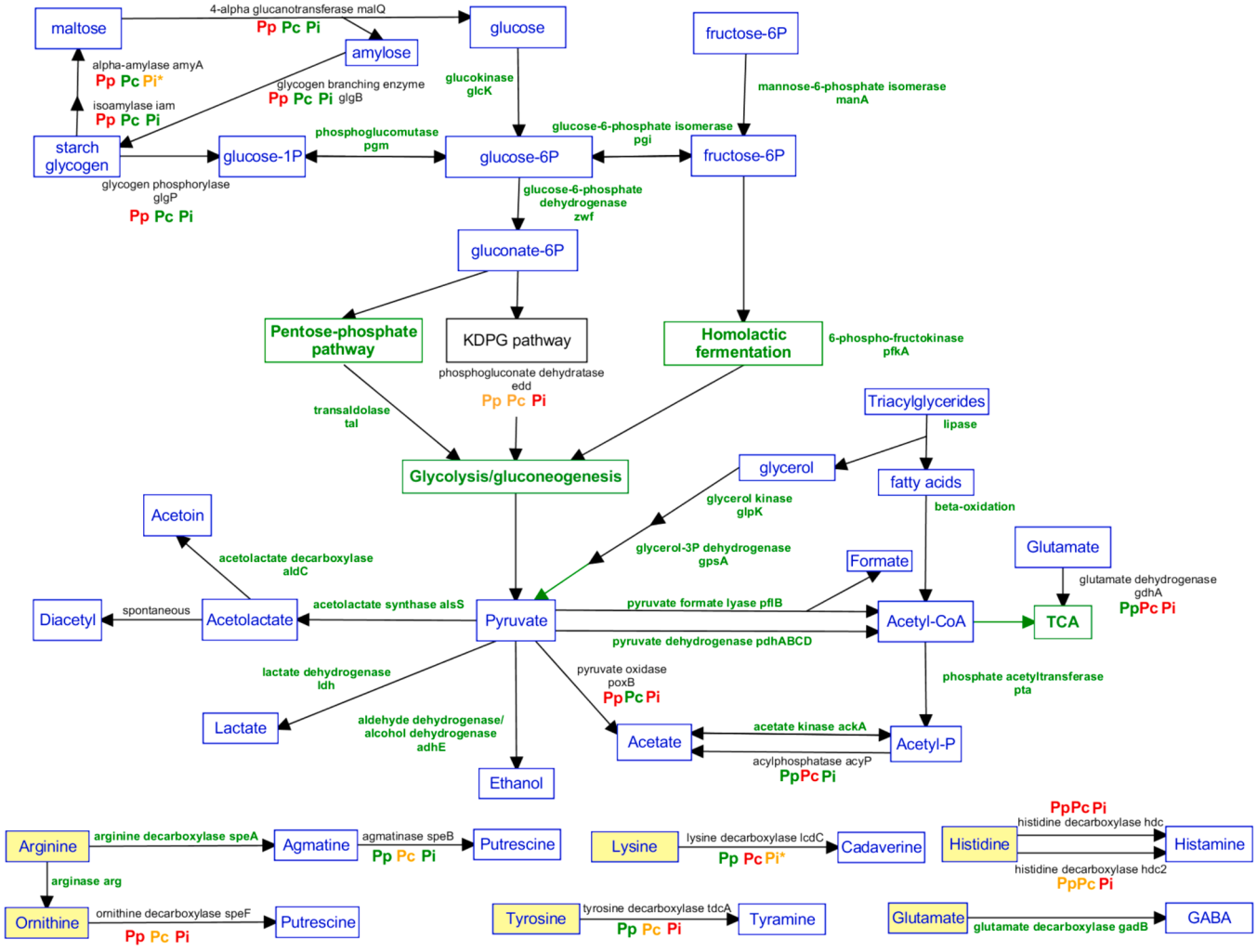

Fig. 3. Representation of pathways and genes present in the three species of photobacteria. Genes in green were found in all strains screened. Genes in black were found in only some of the isolates and have a color code for each species where: Pp = *P. phosphoreum*, Pi = *P. iliopiscarium*, Pc = *P. carnosum*; green=present in all strains of a species, red=absent in all strains of the species, orange=present in some strains of the species. An asterisk indicates that there is a source-of-isolation based distribution of the gene.

- **Carbohydrate metabolism**

All strains share the required set of genes for the glycolysis/gluconeogenesis, pentose phosphate pathway, and homolactic fermentation, but not the heterolactic due to missing xylulose-5-phosphate phosphoketolase gene (*xpk*A). The Entner-Doudoroff route is only complete in one *P. carnosum* strain (TMW 2.2186) and two *P. phosphoreum* strains (FS-5.1, FS-6.1), all marine, with only the phosphogluconate dehydratase gene (*ed*D) missing from the rest.

In addition to glucose and fructose, all strains are predicted to use ribose and mannose, although we could not find presence of specific transporters for the uptake of ribose, and the PTS mannose specific transporter (subunit A) is absent in some *P. carnosum* strains and meat-isolated *P. iliopiscarium* strains.

We found the ribonucleotide reductase subunits genes in all strains (*nrd*AB), needed for the conversion of nucleosides to deoxy-nucleosides. Its assembly subunit was found in all strains of *P. phosphoreum*, but only two fish-isolated strains of *P. carnosum* (TMW 2.2098, TMW 2.2186) and no *P. iliopiscarium*.

The degradation of glycogen and starch (glycogen phosphorylase *glg*P and glycogen debranching enzyme *glg*X), together with maltose/maltodextrin transport (*mal*F, *mal*G, *mal*K) is only predicted for *P. carnosum* and *P. iliopiscarium*. However, we found no enzymes for the synthesis of glycogen/starch. Subunit *mal*E of the maltose/maltodextrin transport and α-amylase coding gene were only found in *P. carnosum* and meat-isolated strains of *P. iliopiscarium*.

The α-galactosidase was ubiquitous in both species, but only randomly present in some strains of *P. phosphoreum*. The α-mannosidase was found also in all strains of *P. iliopiscarium*, random strains of *P. carnosum* and one single fish-borne strain of *P. phosphoreum*. We found a galctose/methyl-galactoside transporter randomly distributed in two of the species, but only meat-borne strains for *P. iliopiscarium*.

- **Pyruvate metabolism**

All screened strains are predicted producers of acetate, ethanol, lactate, formate, acetolactate (and ultimately acetoin). The enzyme pyruvate oxidase (*pox*B), responsible for the formation of acetate, carbon dioxide and hydrogen peroxide from pyruvate) was found in all strains of *P. carnosum* but none of the strains of the other two species, while the enzyme acylphosphatase (*acyl*P, acetyl-P to acetate) was only present in *P. phosphoreum* and *P. iliopiscarium*.

- **Tricarboxylic acid cycle (TCA)**

The complete set of genes for the TCA and the glyoxylate cycle are present in the genomes of all strains and species analyzed. Anaplerotic routes related genes initiated from amino acids are mostly present in the genomes of all strains, with the exception of the glutamate dehydrogenase (*gdh*A) to incorporate glutamate in the form of α-ketoglutarate into the TCA cycle, only present in all strains of *P. phosphoreum*.

- **Triacylglyceride metabolism**

Genes required for the cleavage of lipids, transport and degradation of glycerol and fatty acids (β-oxidation, both aerobic and anaerobic) are also equally present in all strains.

- **Amino acids**

Amino acid degrading genes are present in all strains, including the complete ADI pathway with production of ammonia and carbon dioxide (arginine deiminase *arc*A, ornithine transcarbamoylase *arc*B, carbamate kinase *arc*C), degradation of aspartate to iminosuccinate via aspartate oxidase (*nad*B) releasing hydrogen peroxide, conversion of serine to pyruvate via serine dehydratase (*sda*AB), conversion of aspartate and oxoglutarate to glutamate and pyruvate via aspartate aminotransferase (aspB) and oxaloacetate-decarboxylating malate dehydrogenase (*mdh*).

All strains of the three species contain a minimum of 2 and up to 7 loci of the arginine decarboxylase (*spe*A) coding gene, producing carbon dioxide and agmatine from arginine, and one loci of the glutamate decarboxylase (*gad*B), responsible for the production of gamma-aminoburyric acid (GABA). Further degradation of agmatine into putrescine and urea via agmatinase (*spe*B) is predicted in all strains except the one divergent fish-isolated *P. carnosum* strain TMW 2.2098. Conversion of arginine into ornithine and urea via arginase gene (*arg*) was predicted in all strains, but further conversion of ornithine into putrescine and carbon dioxide via ornithine decarboxylase (*spe*F) was exclusively predicted for two strains of *P. carnosum* (meat-isolated TMW 2.2029 and fish-isolated TMW 2.2189).

Decarboxylation of lysine to cadaverine (and carbon dioxide) via lysine decarboxylase (*lcd*C) was only predicted for *P. phosphoreum* strains, and fish-isolated *P. iliopiscarium* strains. Production of tyramine from tyrosine by the tyrosine decarboxylase (*tdc*A) was predicted for all *P. phosphoreum* strains and two meat-isolated *P. carnosum* strains (TMW 2.2147 and TMW 2.2157). We did not find the histidine decarboxylase gene (*hdc*) in any of the screened genomes. However, we detected a histidine-histamine antiporter and a proposed alternative histidine decarboxylase (*hdc*2) in one fish-isolated *P. carnosum* strain (TMW 2.2187), and 11 *P phosphoreum* strains (random distribution).

- **Respiration**

All strains are predicted to have a functional respiratory chain (Figure S6) and synthesize heme. All strains have two NADH dehydrogenase loci (*ndh*) and one copy of the sodium transporting NADH:ubiquinone reductase complex (*nqr*A-F). Only subunit *nuo*B from the proton transporting NADH:quinone oxidoreductase is present in all strains, and additionally all *P. phosphoreum* strains (except AK-8, FS-3.2, FS-6.1) contain an entire set of all its subunits (*nuo*A-N). All strains contained complete cytochrome c and bd oxidases (*cox*ABC, *cyd*ABX). Additionally, the cytochrome cbb3-type oxidase (*cco*NOP), was present in *P. phosphoreum* and *P. iliopiscarium* but missing in all strains of *P. carnosum*.

All strains are predicted to use fumarate (fumarate reductase, *frd*ABCD), trimethylamine-N-oxide (TMAO reductase, *tor*A, producing trimethyl–amine TMA), nitrate (nitrate reductase, *nap*AB), nitrite (nitrite reductase, producing ammonia, *nir*BD) and sulfate (sulfate denylyltransferase *cys*DN, adenylyl-sulfate kinase *cys*C, phosphoadenylyl-sulfate reductase *cys*H, assimilatory sulfite reductase *cys*JI, releasing H_2S) as alternative electron acceptors. Only marine-strains of *P. iliopiscarium* and randomly distributed strains of *P. phosphoreum* contain the DMSO reductase (*dms*ABC, producing dimethyl sulfide).

- **Environmental adaptation and stress response**

As previously studied by Hauschild et al. (2020), we have investigated the genomes of all strains for the presence of genes facilitating salt, pressure and oxidative stress response as well as life-style related traits such as motility, bioluminescence, sodium intake and iron accumulation.

Pressure response related genes are all present in all strains and species with the exception of porin-like protein *omp*L, randomly distributed in *P. carnosum* and *P. phosphoreum*, and only present in meat-isolated *P. iliopiscarium* strains. Salt response relevant genes were found in all strains with the exception of outer membrane proteins *omp*W/*omp*V and porin *omp*C/*omp*F, absent in all genomes. All strains have the superoxide dismutase (2 copies, also hydrogen peroxide producing) and catalase/peroxidase enzymes genes against oxidative stress. Additionally, all *P. phosphoreum* strains and *P. iliopiscarium* NCIMB 13481 contain an additional copy of the superoxide dismutase and catalase in their genome.

The flagellar gene cluster is complete only in randomly distributed strains of *P. carnosum* and *P. phosphoreum*, and only in marine-isolated strains of *P. iliopiscarium*. *P. phosphoreum* is the only species containing the entire lux-rib operon (all strains).

We searched for all sodium and sodium-dependent transporters's genes available. Their abundance only differed at the species level, with *P. phosphoreum* having 4–5 more loci on average. No differences were observed based on source of isolation/clades. The same applies to iron transports and unspecific stress proteins (cold-, heat-, phage-shock proteins and universal stress proteins).

Reintjes et al. (2019) utilize in their work laminarin, xylan, chondroitin sulfate, arabinogalactan, fucoidan and pullulan as common substrates in marine habitats and/or substrates whose hydrolyzing enzymes are widely distributed on marine bacteria. We found genes for the hydrolysis of arabinogalactan (beta-galactosidase) in all strains. Additionally we found xylose transporters exclusive for *P. phosphoreum* strains, and an endoxylanase ubiquitous for said species, randomly distributed in *P. carnosum*, and tied to marine-isolated *P. iliopiscarium* strains. The hydrolysis of pullulan, on the other hand, is exclusive and common in *P. iliopiscarium* and *P. carnosum*, but absent in *P. phosphoreum*. Although all strains checked contained an L-fucose symporter, only *P. carnosum* meat-borne strain TMW 2.2163 has the rest of the enzymes needed to utilize fucose, and therefore fucoidan.

- **Plasmids and Virulence Genes**

We found no match in any of the strains for the virulence genes identified in *P. damselae* phospholipase-D damselysin gene (*dly*) and the pore-forming toxin gene (*hlyA*), or the common plasmids identified in the genus *Photobacterium*.

PlasmidSPAdes identified 35 contigs that conform circular DNA segments in 15 of the 27 screened strains, distributed in the three species of photobacteria. Many of the predicted plasmids had a low coding density. Associated functions refer to conjugation proteins, mobile elements, secretion systems and toxin/antitoxin systems, and do not appear to offer any evolutionary or physiological advantage to their respective strains.

Secondary metabolism and additional features

Results for the identified features of each strain are summarized in Fig. 4.

- **Prophages and CRISPR**

PHASTER identified 32 intact phages in 26 strains of the three species. Two of them, in the genome of *P. carnosum* TMW 2.2098 and

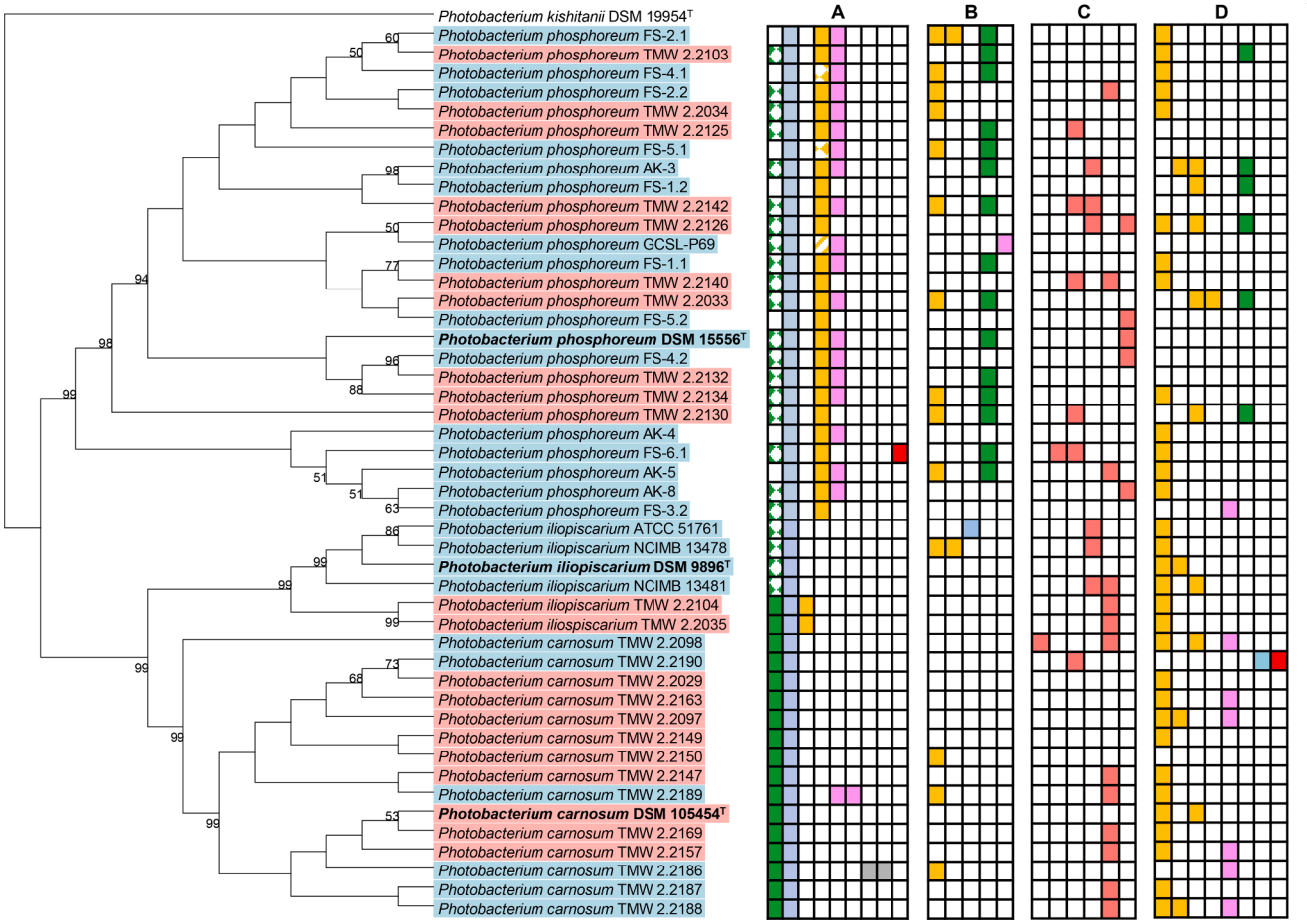

Fig. 4. Summary figure of results from online tools search. The tree is based on the MLSA phylogenetic tree. Type strains of each species are marked in bold and with a T. Source of isolation of each strain is marked by a color code: red for meat, blue for fish. Results for each online tool is displayed in a different grid, marked with different colors for the different types of metabolites, and separated in different colors for a different identity fo the same type of metabolite. Additionally, different patterns in the same column indicate that, despire being the same cluster, they differ in the organization of the genes. **A** Identified secondary metabolites with antiSMASH: betalactones (■), bacteriocins (■), arylpolyenes (■), siderophores (■), butyrolactones (■), type III polyketide synthase (■). **B** Identified bacteriocins with BAGEL: sactipeptides (■), colicin (■), microcin (■), penisin II (■). **C** Intact bacteriophages are displayed in different columns for different sequences (■). **D** CRISPR-cas clusters are displayed in different colors for different types of cas genes, and grouped in columns by gene architecture and direct repeat sequence: type I-F (■), type I-C (■), type I-D (■), type I-E (■), type III-D (■).

P. phosphoreum FS-6.1 respectively are unique, while the rest of them are repetitions of 4 unknown phages, only one of them species specific (*P. phosphoreum*). Three of the common phages appear to code for endolysins, required for the lytic cycle.

We additionally queried the genomes for presence of CRISPR-Cas systems, that appeared frequent among the species of photobacteria. Type I-F appears to be the most common but we also found evidence of type I-C and type I-D in some of the strains from both *P. carnosum* and *P. phosphoreum*, and genes identified as type III-D or type I-E in *P. carnosum* TMW 2.2190.

Protospacers and direct repeats were specific for each type of cas-operon and ranging from 4 to 64 in numbers. Some sequences are duplicated in the same strain or are present in more than one strain with random distribution, but most are unique.

The unique prophage of *P. carnosum* strain TMW 2.2098 was identical to unique protospacers of *P. phosphoreum* strains TMW 2.2034, TMW 2.2103, TMW 2.2140 and *P. carnosum* TMW 2.2163. The unique prophage from *P. phosphoreum* FS-6.1 strain, was identical to two unique protospacers of *P. phosphoreum* AK-4 strain. Since protospacers can offer an overview on previous phage attacks, and considering these events were only observed for two unique phages, it is possible they represent tools for competition even against other species/strains of photobacteria.

- **Secondary metabolites**

We identified with antiSMASH the presence of beta-lactone producing gene clusters, uniquitous for *P. carnosum* and *P. iliopiscarium,* and random in *P. phosphoreum*, with two different architectures.

One bacteriocin production gene cluster detected via antiSMASH was identical in all screened strains. However, BAGEL predicted bacteriocin production only in random strains of the three species. *P. phosphoreum* (10), *P. carnosum* (3) and *P. iliopiscarium* (1) strains are predicted to produce sactipeptides (one or two types). *P. phosphoreum* is also predicted to produce microcin (15 strains). Additionally, one *P. phosphoreum* strain (GCSL-P69) and one *P. iliopiscarium* strain (ATCC 51761) are predicted to be penisin II and colicin producers, respectively.

Production of arylpolyenes was predicted on all strains of *P. phosphoreum*. In addition, the two meat-isolated strains of *P. iliopiscarium* have been predicted to also produce one type of arylpolyene, different from that present on *P. phosphoreum* strains. The distribution of a siderophore-production cluster was observed in most strains of *P. phosphoreum* with a random distribution and one single salmon-isolated strain of *P. carnosum*, TMW 2.2189, also predicted to produce a second type of siderophore. Production of butyrolactones was only predicted in a different fish-isolated strain of *P. carnosum* (TMW 2.2186), and production of type III polyketide synthase (T3PKS) was reserved to a single marine-related *P. phosphoreum* strain (FS-6.1). These last traits appear as only specific for unique strains.

Discussion

Phylogeny and taxonomy

16S rRNA gene sequences have limited discriminatory power, and the group comprising *P. phosphoreum, P. iliopiscarium, P. carnosum* and *P. kishitanii* share identical 16S rRNA gene sequences (Hilgarth et al., 2018b; Sawabe et al., 2007). A previous study on the *Vibrionaceae* family proposes the use of the ferric uptake regulator (*fur*) as identification marker (Machado and Gram, 2015). We found that *fur* could be effectively used for clustering of the three species we analyzed, and results were consistent with other analysis. However, it appears to lose discriminatory power between strains of a single species and we conclude for that purpose that the use of several concatenated sequences (MLSA) or alternative genes would still offer a more realistic representation of phylogenetic relationships.

Phylogeny based on ANIb values and MLSA suggest that *P. carnosum* species constitutes one single clade whose strains, with the exception of strain TMW 2.2098 form MAP salmon, which appears to be a cross contamination from processing, are closely related to each other. On the other hand, *P. phosphoreum* and *P. iliopiscarium* both appear to split into two clades, environmentally-driven based on the source of isolation in the case of the latter. This distribution of the three species in either one or two conserved clades/subgroups is in agreement with previous work by (Fuertes-Perez et al., 2019) on their phenotypic characterization. Based on ANIb values (95–6%) and in silico DDH values (<79%), the two different clades within *P. phosphoreum* constitute two subspecies, which should be proposed in a future taxonomic publication.

Genome variability

Machado and Gram (2017) reported a genome size and GC content of 4.2 - 6.4 Mbp and 38.7 - 50.9% respectively for 16 of the 35 species of photobacteria used in their work, including *P. phosphoreum* and *P. iliopiscarium*. This findings are in accordance to the results of our analysis for the three species. According to (Musto et al., 2004, 2005, 2006), the GC content of the genome has a direct correlation to the optimum growth temperature of the species. The significant differences on the GC content of the genomes of all three of the species are in accordance with the higher optimum temperatures at which *P. phosphoreum* and *P. iliopiscarium* are able to grow (15 - 25 °C, ~39% GC) in comparison to *P. carnosum* (10 – 15 °C, ~38% GC) (Hilgarth et al., 2018b).

The pan-genome of the three species includes a large repertoire of accessory genes, many of which occur in only a single isolate, suggesting that these organisms are prone to horizonal gene transfer. The low variability in codon usage between strains and species suggests that acquired genes might come from bacteria with similar GC% content, maybe even other photobacteria. Despite an enrichment of these regions in elements devoid of known function, the high genome variability and exchange observed in photobacteria might be an advantageous strategy to acquisition of new capabilities for adaptation, stress response, competition and new niche colonization.

Distribution of multiple features on photobacteria appear not linked to isolation source or phylogenetic grouping (e.g. flagellar cluster for *P. carnosum* and *P. phosphoreum*, KDPG pathway, amino acid decarboxylases, bacteriophages, CRISPR-cas systems, bacteriocins and siderophores), as pointed out before by Machado and Gram (2017) in an analysis of 16 *Photobacterium* species (35 strains, including 2 marine-strains of both *P. iliopiscarium* and *P. phosphoreum*, but none of *P. carnosum*, and no terrestrial strains of any species).

The number of transposases suggests that these species might be prone to transposon-mediated exchange of genes, although less than their high-pressure adapted counterpart *P. profundum* (Aziz et al., 2010; Machado and Gram, 2017). Additionally, the high amount of protospacers per strain found in each CRISPR-cas locus, described as the prokariotic defense mechanism against external attacks (Pourcel et al., 2005) and the common presence of bacteriophages in their genome suggests that these species of photobacteria are also prone to phage infections.

Adaptation and competitiveness

The results suggest different levels of environmental adaptation not only at the species level, as is the case of *P. carnosum*, but also based on observed phylogenetic clades in the case of *P. iliopiscarium*.

- **Substrate utilization**

Utilization of a variety of carbohydrates appears to be the most diversified section of the genome of the photobacteria. Predicted utilization of common sugars (e.g. ribose, glucose, fructose and mannose) is

consistent with results of acid production from different substrates reported by Fuertes-Perez et al. (2019). These four substrates constitute the main components of the carbohydrates present on meat (Eskin and Shahidi, 2012; Koutsidis et al., 2008; Lawrie and Ledward, 2006; Nychas et al., 2007). However, glucose, fructose and mannose are also highly abundant in fish (Tarr, 1966) and therefore their utilization does not necessarily represent an environmental adaptation, but rather a statement of their ability to grow on both meat and fish.

Both *P. carnosum* and *P. iliopiscariu*m have the glycogen phosphorylase (*glg*P) and glycogen debranching enzyme genes, and only *P. carnosum* and meat-borne strains of *P. iliopiscarium* have the α-amylase gene, that breaks down alpha-linked polyssacharides such as glycogen and starch. Glycogen can be found both on meat and fish, but while it can be highly abundant in muscle meat, up to 1.8% (Immonen and Puolanne, 2000; Immonen et al., 2000; Ninios et al., 2014; Pethick et al., 1995; Trowbridge and Francis, 1910) even after 3 weeks (Koutsidis et al., 2008), it is reported to fluctuate in the 40 – 200 mg/100 g range in fish (Guillaume et al., 2001; Tarr, 1966). Since this gene is also present in other marine photobacteria such as *P. kishitanii* (PSV18756.1), *P. damselae* (TMX76883.1), *P. lutimaris* (PSU35927.1), *P. proteolyticum* (OLQ70040.1) it is unlikely that this is an acquired environmental advantage, but rather loss of the genes on *P. phosphoreum* in adaptation to more parasitic/symbiontic behavior as established by Henrissat et al. (2002). On the other hand, availability of additional substrates would allow *P. carnosum* and *P. iliopiscarium*, slower growers (Fuertes-Perez et al., 2019), to be more competitive in the meat environment.

We found in addition that photobacteria are able to degrade other polyssacharides that were previously reported as common in marine environments (Reintjes et al., 2019). While predicted degradation of pullulan and maltose import appears *P. carnosum* and *P. iliopiscarium* specific (and more so the meat-born strains of the latter), xylose degradation and transport is predicted as more common for *P. phosphoreum* and fish-strains of *P. iliopiscarium*. Additionally, one single strain of *P. carnosum* (TMW 2.2163) has the genes required for the degradation of L-fucose and fucoidan, and is able to express them according to results of acid production from carbohydrates reported by Fuertes-Perez et al., 2019. The strain-specificity to these genes suggests that they were acquired horizontally, although all strains appear to contain one L-fucose:proton symporter. Fucose is mostly present in plants and algae, and also in mammals as part of different types of glycans (Becker and Lowe, 2003), but there are no reports of its significant presence on either raw fish or meat. The three cases might represent and advantage in other niches not meat or fish related, but rather plant based (marine or terrestrial), supporting the idea that photobacteria might be more widespread that known. Yet, *P. iliopiscarium* strains display substrate preferences based on strain origin and clade distribution, with meat-borne strains closer to *P. carnosum* (sugar transports, α-amylase), while fish-borne strains are closer to *P. phosphoreum* (xylose utilization). Xylanases also appear to have quite a relevance in the industry (e.g. paper industry) (Qeshmi et al., 2020).

In addition to the glycolysis and pentose phosphate pathway, we could also find one fish-borne strain of *P. carnosum* and two fish-borne strains of *P. phosphoreum* with both key enzymes for the alternative Entner-Doudoroff pathway. Flamholz et al. (2013) suggests advantage in using this alternative pathway by utilizing far fewer enzymes as a trade-off with the lower energy yield, and it additionally allows the utilization of gluconate as energy source (Vegge et al., 2016).

- **Respiration**

All isolates are predicted to carry out aerobic and anerobic respiration. The sodium-translocating NADH:quinone oxidoreductase found in all strains, an analog to Complex I of the respiratory chain that pumps Na+ instead of *H*+ (Verkhovsky and Bogachev, 2010), is consistent with the sodium requirement of the three photobacterium species (Fuertes--Perez et al., 2019; Hauschild et al., 2020; Hilgarth et al., 2018a, 2018b). However, presence of high-oxygen affinity cytochrome cbb3-type oxidase (Pitcher and Watmough, 2004) in *P. phosphoreum* and *P. iliopiscarium*, and the full copy of the proton-translocating Complex I (*nuo*A-N) only present in *P. phosphoreum* strains might offer advantages in low anoxic/microaerobic and low sodium environments, respectively. The three *P. phosphoreum* strains missing the proton-transporting complex might indicate that the sodium-translocating analog is still the commonly used by these species of photobacteria.

The three species have a variety of reductases aimed at utilization of several alternative electron acceptors during anaerobic respiration. Nitrate and trimethylamine-N-oxide (TMAO) are examples of compounds they can use, but while abundant on marine environments and fish (Koike and Hattori, 1978; Yancey et al., 1982), are scarce on meat (Cho et al., 2017; Iammarino and Di Taranto, 2012). DMSO reductase is another example only prevalent in *P. phosphoreum* and fish-borne *P. iliopiscarium* strains, and an additional link of said isolates to a marine environment (Lee et al., 1999).

Siderophores are iron-chelating molecules that allow their producers an efficient way of recovering iron for respiration and redox reactions from environments with low availability (Comi, 2017; Gram et al., 2002). We observed an enrichment of siderophore producing gene clusters in *P. phosphoreum* that might suggest an advantage in low-iron availability, or high competitive microbiota environments such as meat.

- **Antimicrobial activity**

P. phosphoreum shows more predicted diversity of bacteriocin production than the other two species, although all isolates are predicted to produce at least one type of bacteriocin. Out of the four different types of bacteriocins predicted on photobacteria, microcin (only in *P. phosphoreum*) appears to be commonly produced by *Enterobacteriaceae* against other bacteria including those belonging to the same family, such as *E. coli* (Baquero et al., 2019). Colicins, one of the most studied group of bacteriocins, are usually produced by gram-negative bacteria and thoroughly studied in strains of *E. coli* (Micenkova et al., 2019) as effective agent against other strains of the same species. Finally, penisin was described first as a novel lantibiotic, product of *Paenibacillus ehimensis*, able to kill methicillin-resistant *Staphylococcus aureus* (Baindara et al., 2016). Both colicin and penisin II synthesis clusters are unique to one strain, most likely acquired by horizontal exchange. Results suggest that *P. phosphoreum* might compensate for the narrower carbon utilization of the species by producing bacteriocins against a wider selection of competitors in the same niche.

Some predicted bacteriocins might have additional external value. Sactipeptides, microcins and penisin appear valuable in the pharmaceutical industry as starting point for development of new antibiotics (Baindara et al., 2016; Himes, 2017; Severinov and Nair, 2012).

The type IV secretion system appears only on the marine-isolated strains of *P. iliopiscarium*. This type of secretion systems are mainly known for their involvement in bacterial conjugation, and their presence would contribute to the horizontal gene tansfer higher frequency (Wallden et al., 2010), but they also provide means for manipulation and removal of competing bacteria by secretion of macromolecules into other cells (Sgro et al., 2019).

- **Marine habitat-specific features**

Gene loci involved in bioluminescence, high pressure, osmotolerance have directly been linked to marine-adapted bacteria in other works (Brodl et al., 2018; Campanaro et al., 2005; Hauschild et al., 2020), although Moran et al. (2007) proposed that cultured marine bacteria and non-marine related bacteria mainly differed only in their sodium-based transport systems. These features appear as either species-specific features (bioluminescence) or as loci duplications with a higher copy frequency in *P. phosphoreum* (sodium-dependent transporters, stress and oxidative stress response) not linked to the source of

isolation. *P. phosphoreum* appears, therefore, better adapted to marine environments, and better suited for stress-responding, giving it advantage despite a narrower carbon source utilization.

The flagellar cluster has a random distribution except for *P. iliopiscarium*, correlating to source of isolation and phylogeny. Its expression, however, might require specific circumstances, as previous studies did not detect motility on strains with the complete set of genes (Fuertes-Perez et al., 2019). Motility has been defined as critical in the survival as free-living bacteria in marine-environments (Eloe et al., 2008) and therefore the absence of the flagellar cluster is likely due to loss of the genes in adaptation to the meat/fish environment where motility is not required.

- **Food safety and spoilage**

All strains of photobacteria have spoilage potential on meat and are predicted producers of H_2O_2 from pyruvate (*pox, P. carnosum*), aspartate and arginine (both highly abundant on meat (Holló et al., 2001) resulting in greening of the meat. All strains are predicted producers of acetate and lactate from pyruvate and/or acetyl-CoA contributing to a lowering of the pH and sour odors (Gram et al., 2002). In addition, all strains are predicted producers of putrescine from arginine (except one *P. carnosum* strain), with cases in some strains of tyramine (from tyrosine), cadaverine (from lysine) and putrescine (from ornithine) producers. Finally, more relevant on fish spoilage, all of them are predicted to produce trimethylamine from TMAO, more relevant in fish and responsible for foul-odors (Gram and Dalgaard, 2002).

Although *P. phosphoreum* and *P. iliopiscarium* have been largely described as histamine producers on fish (Bjornsdottir-Butler et al., 2018; Bjornsdottir et al., 2009; Kanki et al., 2004), and the histamine production of several fish-isolated strains previously measured (López Caballero et al., 2002; Morii and Kasama, 2004; Torido et al., 2012; Wang et al., 2020), we did not detect presence of the *hdc* gene in any of the screened isolates, also reported by Machado and Gram, 2017. Measured production of histamine in some of the isolates included in this study (AK-3, AK-8, FS-1.1, FS-1.2, FS-2.1, FS-4.2), reported by Bjornsdottir-Butler et al., 2018, might be due to the presence of an alternative histidine decarboxylase gene (*hdc*2) recently identified by Bjornsdottir-Butler et al., 2020. Detection of the *hdc*2 gene in one *P. carnosum* and 11 *P phosphoreum* strains suggests production of histamine and therefore health risk by their presence on meat. Regarding available *P. phosphoreum* sequences of the *hdc* gene, identification of the respective isolates was mostly performed by physiological tests (e.g. bioluminescence) and 16S rRNA sequences (BAE94284.1, BAE94283.1, BAC45246.1, AAO65983.1) (Kanki et al., 2004), insufficient criteria to differentiate close *Photobacterium* species (e.g. *P. kishitanii* and *P. phosphoreum*) (Ast and Dunlap, 2005; Machado and Gram, 2015; Sawabe et al., 2007). Results suggest that previous reports on presence of the *hdc* locus on *P. phosphoreum* were either due to misidentification of the isolates, or to its strain-specific nature (i.e. not common to the entire species, only to some strains).

Conclusion

This study reports high genomic diversity present within the three species of photobacteria known to be relevant in meat and seafood spoilage. Central pathways involving the most common carbon sources e.g. glycolysis, gluconeogenesis, pentose phosphate pathway, beta-oxidation of lipids, TCA and glyoxylate cycle, the majority of anaplerotic routes and amino acid metabolism, are generally conserved in all strains and species. However, there are differences in multiple metabolic routes between or within the species (e.g. pyruvate oxidase, KDPG pathway, respiration), utilization of less common carbon sources (e.g. maltose, glycogen), production of metabolites (e.g. biogenic amines), adaptative features (e.g. stress response) and antimicrobial activity (e.g. bacteriocins). The proposed high frequency of genetic exchange in photobacteria suggests itself as an advantageous strategy, despite accumulation of elements devoid of function, aimed at diversification and acquisition of beneficial characteristics.

P. carnosum strains form a single clade species with one divergent strain from MAP salmon that does not, however, show distinct traits or predicted adaptation to a different niche indicating cross-contamination within processing/packaging. The species appears mostly focused on diversification of carbon sources available for energy production and adapted to nutrient rich environments from meat, fish or even plant origin. On the other hand, *P. phosphoreum*, as results suggest, is represented by two clades, which appear to represent two novel subspecies within. However, this differentiation is not clearly reflected by predicted metabolic divergence or isolation origin. In contrast to *P. carnosum*, this species has a wider diversity of antimicrobial activity, predicted stronger response to stress and low availability of resources (e.g. iron, oxygen and sodium) and adaptation to more than one life-style (e.g. symbiontic), better fit to eliminate or outgrow possible competitors. Finally, *P. iliopiscarium* is divided into two clades, fish- and meat-borne, which show several examples of an evolutionary adaptative response. Meat-borne strains appear more similar to *P. carnosum* and retain similar carbon utilization and transport oriented genes, while fish-isolated strains retain the utilization of marine-common compounds (e.g. DMSO) and motility directed to a free-lifestyle.

CRediT authorship contribution statement

Sandra Fuertes-Perez: Conceptualization, Data curation, Formal analysis, Investigation, Methodology, Validation, Visualization, Writing – original draft. **Rudi F. Vogel:** Project administration, Funding acquisition, Conceptualization, Supervision, Writing – review & editing. **Maik Hilgarth:** Project administration, Funding acquisition, Conceptualization, Supervision, Resources, Writing – review & editing.

Declaration of Competing Interest

The authors declare that they have no known competing financial interests or personal relationships that could have appeared to influence the work reported in this paper.

Funding

Part of this work was funded by the German Federal Ministry for Economic Affairs and Energy via the German Federation of Industrial Research Associations (AiF) and the Industry Association for Food Technology and Packaging (IVLV); project number AiF 20113N1.

Supplementary materials

Supplementary material associated with this article can be found, in the online version, at doi:10.1016/j.crmicr.2021.100087.

References

Alikhan, N.F., Petty, N.K., Ben Zakour, N.L., Beatson, S.A., 2011. BLAST Ring Image Generator (BRIG): simple prokaryote genome comparisons. BMC Genomics 12, 402.
Allen, E.E., Bartlett, D.H., 2000. FabF is required for piezoregulation of cis-vaccenic acid levels and piezophilic growth of the deep-Sea bacterium Photobacterium profundum strain SS9. J. Bacteriol. 182, 1264–1271.
Altschul, S.F., Gish, W., Miller, W., Myers, E.W., Lipman, D.J., 1990. Basic local alignment search tool. J. Mol. Biol. 215, 403–410.
Angiuoli, S.V., Gussman, A., Klimke, W., Cochrane, G., Field, D., Garrity, G., Kodira, C.D., Kyrpides, N., Madupu, R., Markowitz, V., Tatusova, T., Thomson, N., White, O., 2008. Toward an online repository of Standard Operating Procedures (SOPs) for (meta)genomic annotation. OMICS 12, 137–141.
Antipov, D., Hartwick, N., Shen, M., Raiko, M., Lapidus, A., Pevzner, P.A., 2016. plasmidSPAdes: assembling plasmids from whole genome sequencing data. Bioinformatics 32, 3380–3387.
Arndt, D., Grant, J.R., Marcu, A., Sajed, T., Pon, A., Liang, Y., Wishart, D.S., 2016. PHASTER: a better, faster version of the PHAST phage search tool. Nucleic. Acids. Res. 44, W16–W21.

Ast, J.C., Dunlap, P.V., 2005. Phylogenetic resolution and habitat specificity of members of the Photobacterium phosphoreum species group. Environ. Microbiol. 7, 1641–1654.
Aziz, R.K., Bartels, D., Best, A.A., DeJongh, M., Disz, T., Edwards, R.A., Formsma, K., Gerdes, S., Glass, E.M., Kubal, M., Meyer, F., Olsen, G.J., Olson, R., Osterman, A.L., Overbeek, R.A., McNeil, L.K., Paarmann, D., Paczian, T., Parrello, B., Pusch, G.D., Reich, C., Stevens, R., Vassieva, O., Vonstein, V., Wilke, A., Zagnitko, O., 2008. The RAST Server: rapid annotations using subsystems technology. BMC Genomics 9, 75.
Aziz, R.K., Breitbart, M., Edwards, R.A., 2010. Transposases are the most abundant, most ubiquitous genes in nature. Nucleic. Acids. Res. 38, 4207–4217.
Baindara, P., Chaudhry, V., Mittal, G., Liao, L.M., Matos, C.O., Khatri, N., Franco, O.L., Patil, P.B., Korpole, S., 2016. Characterization of the Antimicrobial Peptide Penisin, a Class Ia Novel Lantibiotic from Paenibacillus sp. Strain A3. Antimicrob. Agents Chemother. 60, 580–591.
Bankevich, A., Nurk, S., Antipov, D., Gurevich, A.A., Dvorkin, M., Kulikov, A.S., Lesin, V. M., Nikolenko, S.I., Pham, S., Prjibelski, A.D., Pyshkin, A.V., Sirotkin, A.V., Vyahhi, N., Tesler, G., Alekseyev, M.A., Pevzner, P.A., 2012. SPAdes: a new genome assembly algorithm and its applications to single-cell sequencing. J. Comput. Biol. 19, 455–477.
Baquero, F., Lanza, V.F., Baquero, M.R., Del Campo, R., Bravo-Vazquez, D.A., 2019. Microcins in enterobacteriaceae: peptide antimicrobials in the eco-active intestinal chemosphere. Front. Microbiol. 10, 2261.
Becker, D.J., Lowe, J.B., 2003. Fucose: biosynthesis and biological function in mammals. Glycobiology 13, 41R–53R.
Behr, J., Geissler, A.J., Schmid, J., Zehe, A., Vogel, R.F., 2016. The identification of novel diagnostic marker genes for the detection of beer spoiling pediococcus damnosus strains using the blast diagnostic gene findEr. PLoS ONE 11.
Bjornsdottir-Butler, K., Abraham, A., Harper, A., Dunlap, P.V., Benner Jr., R.A., 2018. Biogenic amine production by and phylogenetic analysis of 23 photobacterium species. J. Food Prot. 81, 1264–1274.
Bjornsdottir-Butler, K., May, S., Hayes, M., Abraham, A., Benner Jr., R.A., 2020. Characterization of a novel enzyme from Photobacterium phosphoreum with histidine decarboxylase activity. Int. J. Food Microbiol. 334, 108815.
Bjornsdottir, K., Bolton, G.E., McClellan-Green, P.D., Jaykus, L.A., Green, D.P., 2009. Detection of gram-negative histamine-producing bacteria in fish: a comparative study. J. Food Prot. 72, 1987–1991.
Blin, K., Shaw, S., Steinke, K., Villebro, R., Ziemert, N., Lee, S.Y., Medema, M.H., Weber, T., 2019. antiSMASH 5.0: updates to the secondary metabolite genome mining pipeline. Nucleic. Acids. Res. 47, W81–W87.
Bouju-Albert, A., Pilet, M.F., Guillou, S., 2018. Influence of lactate and acetate removal on the microbiota of French fresh pork sausages. Food Microbiol. 76, 328–336.
Brodl, E., Winkler, A., Macheroux, P., 2018. Molecular Mechanisms of Bacterial Bioluminescence. Comput. Struct. Biotechnol. J. 16, 551–564.
Campanaro, S., Vezzi, A., Vitulo, N., Lauro, F.M., D'Angelo, M., Simonato, F., Cestaro, A., Malacrida, G., Bertoloni, G., Valle, G., Bartlett, D.H., 2005. Laterally transferred elements and high pressure adaptation in Photobacterium profundum strains. BMC Genomics 6, 122.
Cho, C.E., Taesuwan, S., Malysheva, O.V., Bender, E., Tulchinsky, N.F., Yan, J., Sutter, J. L., Caudill, M.A., 2017. Trimethylamine-N-oxide (TMAO) response to animal source foods varies among healthy young men and is influenced by their gut microbiota composition: a randomized controlled trial. Mol. Nutr. Food Res. 61.
Comi, G., 2017. Chapter 8 - spoilage of meat and fish. In: Bevilacqua, A., Corbo, M.R., Sinigaglia, M. (Eds.), The Microbiological Quality of Food. Woodhead Publishing, pp. 179–210.
Dalgaard, P., Garcia Munoz, L., Mejlholm, O., 1998. Specific inhibition of Photobacterium phosphoreum extends the shelf life of modified-atmosphere-packed cod fillets. J. Food Prot. 61, 1191–1194.
Dalgaard, P., Manfio, G.P., Goodfellow, M., 1997. Classification of photobacteria associated with spoilage of fish products by numerical taxonomy and pyrolysis mass spectrometry. Zentralbl. Bakteriol. 285, 157–168.
de Jong, A., van Hijum, S.A., Bijlsma, J.J., Kok, J., Kuipers, O.P., 2006. BAGEL: a web-based bacteriocin genome mining tool. Nucleic. Acids. Res. 34, W273–W279.
Eloe, E.A., Lauro, F.M., Vogel, R.F., Bartlett, D.H., 2008. The deep-sea bacterium Photobacterium profundum SS9 utilizes separate flagellar systems for swimming and swarming under high-pressure conditions. Appl. Environ. Microbiol. 74, 6298–6305.
Emborg, J., Laursen, B.G., Rathjen, T., Dalgaard, P., 2002. Microbial spoilage and formation of biogenic amines in fresh and thawed modified atmosphere-packed salmon (Salmo salar) at 2 °C. J. Appl. Microbiol. 92, 790–799.
Eskin, N.A.M., Shahidi, F., 2012. Biochemistry of Foods, 3rd Ed. Elsevier, London.
Felsenstein, J., 1981. Evolutionary trees from DNA sequences: a maximum likelihood approach. J. Mol. Evol. 17, 368–376.
Flamholz, A., Noor, E., Bar-Even, A., Liebermeister, W., Milo, R., 2013. Glycolytic strategy as a tradeoff between energy yield and protein cost. Proc. Natl. Acad. Sci. U. S. A. 110, 10039–10044.
Fuertes-Perez, S., Hauschild, P., Hilgarth, M., Vogel, R.F., 2019. Biodiversity of *Photobacterium* spp. isolated from meats. Front. Microbiol.
Fuertes-Perez, S., Hilgarth, M., Vogel, R.F., 2020. Development of a rapid detection method for Photobacterium spp. using Loop-mediated isothermal amplification (LAMP). Int. J. Food Microbiol. 334.
Goris, J., Konstantinidis, K.T., Klappenbach, J.A., Coenye, T., Vandamme, P., Tiedje, J. M., 2007. DNA-DNA hybridization values and their relationship to whole-genome sequence similarities. Int. J. Syst. Evol. Microbiol. 57, 81–91.
Gram, L., Dalgaard, P., 2002. Fish spoilage bacteria – problems and solutions. Curr. Opin. Biotechnol. 13, 262–266.
Gram, L., Ravn, L., Rasch, M., Bruhn, J.B., Christensen, A.B., Givskov, M., 2002. Food spoilage—interactions between food spoilage bacteria. Int. J. Food Microbiol. 78, 79–97.
Grissa, I., Vergnaud, G., Pourcel, C., 2007. CRISPRFinder: a web tool to identify clustered regularly interspaced short palindromic repeats. Nucleic. Acids. Res. 35, W52–W57.
Guillaume, J., Kaushik, S., Bergot, P., Metailler, R., 2001. Nutrition and Feeding of Fish and Crustaceans, 1st Ed. Springer Publishing House, London.
Hauschild, P., Hilgarth, M., Vogel, R.F., 2020. Hydrostatic pressure- and halotolerance of Photobacterium phosphoreum and P. carnosum isolated from spoiled meat and salmon. Food Microbiol., 103679
Henrissat, B., Deleury, E., Coutinho, P.M., 2002. Glycogen metabolism loss: a common marker of parasitic behaviour in bacteria? Trends Genet. 18, 437–440.
Hilgarth, M., 2018. Spoilage-Associated Psychrotrophic and Psychrophilic Microbiota on Modified Atmosphere Packaged Beef. Lehrstuhl für Technische Mikrobiologie. Technische Universität München, Freising.
Hilgarth, M., Fuertes-Perez, S., Ehrmann, M., Vogel, R.F., 2018a. An adapted isolation procedure reveals Photobacterium spp. as common spoilers on modified atmosphere packaged meats. Lett. Appl. Microbiol. 66, 262–267.
Hilgarth, M., Fuertes, S., Ehrmann, M., Vogel, R.F., 2018b. Photobacterium carnosum sp. nov., isolated from spoiled modified atmosphere packaged poultry meat. Syst. Appl. Microbiol. 41, 44–50.
Himes, P., 2017. Studies toward understanding the biosynthesis of sactipeptides and the creation of peptide natural product libraries through mrna display, eshelman school of pharmacy. Division of Chemical Biology and Medicinal Chemistry.
Höll, L., Hilgarth, M., Geissler, A.J., Behr, J., Vogel, R.F., 2019. Prediction of in situ metabolism of photobacteria in modified atmosphere packaged poultry meat using metatranscriptomic data. Microbiol. Res. 222, 52–59.
Holló, G., Tözsér, J., Hol, I., Csapó, J., Szücs, E., 2001. Effect of breed, live weight on the fatty acid, amino acid content and on the biological value of beef. Acta Alimentaria 30, 313–322.
Iammarino, M., Di Taranto, A., 2012. Nitrite and nitrate in fresh meats: a contribution to the estimation of admissible maximum limits to introduce in directive 95/2/EC. Int. J. Food Sci. Technol. 47, 1852–1858.
Immonen, K., Puolanne, E., 2000. Variation of residual glycogen-glucose concentration at ultimate pH values below 5.75. Meat Sci. 55, 279–283.
Immonen, K., Ruusunen, M., Hissa, K., Puolanne, E., 2000. Bovine muscle glycogen concentration in relation to finishing diet, slaughter and ultimate pH. Meat Sci. 55, 25–31.
Kanki, M., Yoda, T., Ishibashi, M., Tsukamoto, T., 2004. Photobacterium phosphoreum caused a histamine fish poisoning incident. Int. J. Food Microbiol. 92, 79–87.
Koike, I., Hattori, A., 1978. Denitrification and ammonia formation in anaerobic coastal sediments. Appl. Environ. Microbiol. 35, 278–282.
Koutsidis, G., Elmore, J.S., Oruna-Concha, M.J., Campo, M.M., Wood, J.D., Mottram, D. S., 2008. Water-soluble precursors of beef flavour. Part II: effect of post-mortem conditioning. Meat Sci. 79, 270–277.
Kumar, S., Stecher, G., Tamura, K., 2016. MEGA7: molecular evolutionary genetics analysis version 7.0 for bigger datasets. Mol. Biol. Evol. 33, 1870–1874.
Labella, A.M., Arahal, D.R., Castro, D., Lemos, M.L., Borrego, J.J., 2017. Revisiting the genus Photobacterium: taxonomy, ecology and pathogenesis. Int. Microbiol. 20, 1–10.
Lawrie, R.A., Ledward, D.A., 2006. Lawrie's Meat Science, 7th Ed. Woodhead Publishing Limited, Cambridge.
Lee, P.A., de Mora, S.J., Levasseur, M., 1999. A review of dimethylsulfoxide in aquatic environments. Atmosphere-Ocean 37, 439–456.
Lehane, L., Olley, J., 2000. Histamine fish poisoning revisited. Int. J. Food Microbiol. 58, 1–37.
López Caballero, M.E., Álvarez, M.D., Sánchez Fernández, J.A., Moral, A., 2002. Photobacterium phosphoreum isolated as a luminescent colony from spoiled fish, cultured in model system under controlled atmospheres. Eur. Food Res. Technol. 215, 390–395.
Machado, H., Gram, L., 2015. The fur gene as a new phylogenetic marker for Vibrionaceae species identification. Appl. Environ. Microbiol. 81, 2745–2752.
Machado, H., Gram, L., 2017. Comparative genomics reveals high genomic diversity in the genus photobacterium. Front. Microbiol. 8, 1204.
Medema, M.H., Blin, K., Cimermancic, P., de Jager, V., Zakrzewski, P., Fischbach, M.A., Weber, T., Takano, E., Breitling, R., 2011. antiSMASH: rapid identification, annotation and analysis of secondary metabolite biosynthesis gene clusters in bacterial and fungal genome sequences. Nucleic. Acids. Res. 39, W339–W346.
Meier-Kolthoff, J.P., Auch, A.F., Klenk, H.P., Goker, M., 2013. Genome sequence-based species delimitation with confidence intervals and improved distance functions. BMC Bioinformatics 14, 60.
Meier-Kolthoff, J.P., Hahnke, R.L., Petersen, J., Scheuner, C., Michael, V., Fiebig, A., Rohde, C., Rohde, M., Fartmann, B., Goodwin, L.A., Chertkov, O., Reddy, T., Pati, A., Ivanova, N.N., Markowitz, V., Kyrpides, N.C., Woyke, T., Goker, M., Klenk, H.P., 2014. Complete genome sequence of DSM 30083(T), the type strain (U5/41(T)) of Escherichia coli, and a proposal for delineating subspecies in microbial taxonomy. Stand Genomic Sci. 9, 2.
Micenkova, L., Bosak, J., Kucera, J., Hrala, M., Dolejsova, T., Sedo, O., Linke, D., Fiser, R., Smajs, D., 2019. Colicin Z, a structurally and functionally novel colicin type that selectively kills enteroinvasive Escherichia coli and Shigella strains. Sci. Rep. 9, 11127.
Moran, M.A., Belas, R., Schell, M.A., Gonzalez, J.M., Sun, F., Sun, S., Binder, B.J., Edmonds, J., Ye, W., Orcutt, B., Howard, E.C., Meile, C., Palefsky, W., Goesmann, A., Ren, Q., Paulsen, I., Ulrich, L.E., Thompson, L.S., Saunders, E., Buchan, A., 2007. Ecological genomics of marine Roseobacters. Appl. Environ. Microbiol. 73, 4559–4569.

Morii, H., Kasama, K., 2004. Activity of two histidine decarboxylases from Photobacterium phosphoreum at different temperatures, pHs, and NaCl concentrations. J. Food Prot. 67, 1736–1742.
Musto, H., Naya, H., Zavala, A., Romero, H., Alvarez-Valin, F., Bernardi, G., 2004. Correlations between genomic GC levels and optimal growth temperatures in prokaryotes. FEBS Lett. 573, 73–77.
Musto, H., Naya, H., Zavala, A., Romero, H., Alvarez-Valin, F., Bernardi, G., 2005. The correlation between genomic G+C and optimal growth temperature of prokaryotes is robust: a reply to Marashi and Ghalanbor. Biochem. Biophys. Res. Commun. 330, 357–360.
Musto, H., Naya, H., Zavala, A., Romero, H., Alvarez-Valin, F., Bernardi, G., 2006. Genomic GC level, optimal growth temperature, and genome size in prokaryotes. Biochem. Biophys. Res. Commun. 347, 1–3.
Nieminen, T.T., Dalgaard, P., Bjorkroth, J., 2016. Volatile organic compounds and Photobacterium phosphoreum associated with spoilage of modified-atmosphere-packaged raw pork. Int. J. Food Microbiol. 218, 86–95.
Ninios, T., Lundén, J., Korkeala, H., Fredriksson-Ahomaa, M., 2014. Meat Inspection and Control in the Slaughterhouse, 1st Ed. John Wiley & Sons, New York.
Nychas, G.-.J., Marshall, D.L., Sofos, J., 2007. Meat, poultry, and seafood. Food Microbiol. 105–140.
Ouyang, S., Zhu, W., Hamilton, J., Lin, H., Campbell, M., Childs, K., Thibaud-Nissen, F., Malek, R.L., Lee, Y., Zheng, L., Orvis, J., Haas, B., Wortman, J., Buell, C.R., 2007. The TIGR rice genome annotation resource: improvements and new features. Nucleic. Acids. Res. 35, D883–D887.
Pennacchia, C., Ercolini, D., Villani, F., 2011. Spoilage-related microbiota associated with chilled beef stored in air or vacuum pack. Food Microbiol. 28, 84–93.
Pethick, D., Rowe, J., Tudor, G., 1995. Glycogen metabolism and meat quality.
Pini, F., Aquilani, C., Giovannetti, L., Viti, C., Pugliese, C., 2020. Characterization of the microbial community composition in Italian Cinta Senese sausages dry-fermented with natural extracts as alternatives to sodium nitrite. Food Microbiol. 89, 103417.
Pitcher, R.S., Watmough, N.J., 2004. The bacterial cytochrome cbb3 oxidases. Biochim. Biophys. Acta 1655, 388–399.
Pourcel, C., Salvignol, G., Vergnaud, G., 2005. CRISPR elements in Yersinia pestis acquire new repeats by preferential uptake of bacteriophage DNA, and provide additional tools for evolutionary studies. Microbiology (Reading) 151, 653–663.
Qeshmi, F.I., Homaei, A., Fernandes, P., Hemmati, R., Dijkstra, B.W., Khajeh, K., 2020. Xylanases from marine microorganisms: a brief overview on scope, sources, features and potential applications. Biochim Biophys Acta Proteins Proteom 1868, 140312.
Reintjes, G., Arnosti, C., Fuchs, B., Amann, R., 2019. Selfish, sharing and scavenging bacteria in the Atlantic Ocean: a biogeographical study of bacterial substrate utilisation. ISME J 13, 1119–1132.
Richter, M., Rossello-Mora, R., 2009. Shifting the genomic gold standard for the prokaryotic species definition. Proc. Natl. Acad. Sci. U. S. A. 106, 19126–19131.
Roslan, N.N., Ngalimat, M.S., Leow, A.T.C., Oslan, S.N., Baharum, S.N., Sabri, S., 2020. Genomic and phenomic analysis of a marine bacterium, Photobacterium marinum J15. Microbiol. Res. 233, 126410.
Sawabe, T., Kita-Tsukamoto, K., Thompson, F.L., 2007. Inferring the evolutionary history of vibrios by means of multilocus sequence analysis. J. Bacteriol. 189, 7932–7936.
Severinov, K., Nair, S.K., 2012. Microcin C: biosynthesis and mechanisms of bacterial resistance. Future Microbiol. 7, 281–289.
Sgro, G.G., Oka, G.U., Souza, D.P., Cenens, W., Bayer-Santos, E., Matsuyama, B.Y., Bueno, N.F., Dos Santos, T.R., Alvarez-Martinez, C.E., Salinas, R.K., Farah, C.S., 2019. Bacteria-killing type IV secretion systems. Front Microbiol. 10, 1078.
Stoops, J., Ruyters, S., Busschaert, P., Spaepen, R., Verreth, C., Claes, J., Lievens, B., Van Campenhout, L., 2015. Bacterial community dynamics during cold storage of minced meat packaged under modified atmosphere and supplemented with different preservatives. Food Microbiol. 48, 192–199.
Takahashi, H., Ogai, M., Miya, S., Kuda, T., Kimura, B., 2015. Effects of environmental factors on histamine production in the psychrophilic histamine-producing bacterium Photobacterium iliopiscarium. Food Control 52, 39–42.
Tamura, K., Nei, M., 1993. Estimation of the number of nucleotide substitutions in the control region of mitochondrial DNA in humans and chimpanzees. Mol. Biol. Evol. 10, 512–526.
Tarr, H.L.A., 1966. Post-mortem changes in glycogen, nucleotides, sugar phosphates, and sugars in fish muscles–a review. J. Food Sci. 31, 846–854.
Thompson, J.D., Higgins, D.G., Gibson, T.J., 1994. CLUSTAL W: improving the sensitivity of progressive multiple sequence alignment through sequence weighting, position-specific gap penalties and weight matrix choice. Nucleic. Acids. Res. 22, 4673–4680.
Torido, Y., Takahashi, H., Kuda, T., Kimura, B., 2012. Analysis of the growth of histamine-producing bacteria and histamine accumulation in fish during storage at low temperatures. Food Control 26, 174–177.
Trowbridge, P.F., Francis, C.K., 1910. The glycogen content of beef flesh. J. Ind. Eng. Chem. 2, 215–216.
Tyanova, S., Temu, T., Sinitcyn, P., Carlson, A., Hein, M.Y., Geiger, T., Mann, M., Cox, J., 2016. The Perseus computational platform for comprehensive analysis of (prote) omics data. Nat. Methods 13, 731–740.
Urbanczyk, H., Ast, J.C., Dunlap, P.V., 2010. Phylogeny, genomics, and symbiosis of Photobacterium. FEMS Microbiol. Rev. 35, 324–342.
Urbanczyk, H., Ast, J.C., Kaeding, A.J., Oliver, J.D., Dunlap, P.V., 2008. Phylogenetic analysis of the incidence of lux gene horizontal transfer in Vibrionaceae. J. Bacteriol. 190, 3494–3504.
Urbanczyk, H., Furukawa, T., Yamamoto, Y., Dunlap, P.V., 2012. Natural replacement of vertically inherited lux-rib genes of Photobacterium aquimaris by horizontally acquired homologues. Environ. Microbiol. Rep. 4, 412–416.
Vegge, C.S., Jansen van Rensburg, M.J., Rasmussen, J.J., Maiden, M.C., Johnsen, L.G., Danielsen, M., MacIntyre, S., Ingmer, H., Kelly, D.J., 2016. Glucose metabolism via the entner-doudoroff pathway in campylobacter: a rare trait that enhances survival and promotes biofilm formation in some isolates. Front. Microbiol. 7, 1877.
Verkhovsky, M.I., Bogachev, A.V., 2010. Sodium-translocating NADH:quinone oxidoreductase as a redox-driven ion pump. Biochim. Biophys. Acta 1797, 738–746.
Vesth, T., Lagesen, K., Acar, Ö., Ussery, D., 2013. CMG-biotools, a free workbench for basic comparative microbial genomics. PLoS ONE 8.
Wallden, K., Rivera-Calzada, A., Waksman, G., 2010. Type IV secretion systems: versatility and diversity in function. Cell. Microbiol. 12, 1203–1212.
Wang, D., Yamaki, S., Kawai, Y., Yamazaki, K., 2020. Histamine production behaviors of a psychrotolerant histamine-producer, morganella psychrotolerans, in various environmental conditions. Curr. Microbiol. 77, 460–467.
Wu, L., Lin, X., Wang, F., Ye, D., Xiao, X., Wang, S., Peng, X., 2006. OmpW and OmpV are required for NaCl regulation in Photobacterium damsela. J. Proteome Res. 5, 2250–2257.
Yancey, P.H., Clark, M.E., Hand, S.C., Bowlus, R.D., Somero, G.N., 1982. Living with water stress: evolution of osmolyte systems. ScienceScience 217, 1214–1222.
Yu, Y., Zhang, Z., Wang, Y., Liao, M., Rong, X., Li, B., Wang, K., Chen, J., Zhang, H., 2019. Complete genome sequence of photobacterium damselae Subsp. damselae Strain SSPD1601 isolated from deep-sea cage-cultured sebastes schlegelii with septic skin Ulcer. Int. J. Genom. 2019, 4242653.
Zhou, Y., Liang, Y., Lynch, K.H., Dennis, J.J., Wishart, D.S., 2011. PHAST: a fast phage search tool. Nucleic. Acids. Res. 39, W347–W352.

6.3 Impact of modified atmospheres on growth and metabolism of meat-spoilage relevant *Photobacterium* spp. as predicted by comparative proteomics

Submitted manuscript

Previous studies had reported the presence of photobacteria on raw meat packaged under modified atmosphere, and the prediction of invariable metabolism of the bacteria when subjected to different gas mixtures. The study of the impact of the different gases on the proteome of the most relevant species of photobacteria on meat spoilage was intended to confirm the effectiveness of the packaging strategies in reducing their number. By studying the growth and proteome of photobacteria under different gas mixtures, we could confirm that the presence/absence of oxygen and carbon dioxide do impact the ability to grow on meat. We have observed the growth reduction effects of increased oxygen concentration, most likely due to oxidative stress, and carbon dioxide, that appears to enhance the effects of oxygen when present, or otherwise is likely induce osmotic stress. And what is more, we have observed an inhibitory effect of the combination of carbon dioxide and oxygen in high concentrations due to saturation of the stress response that challenges the distribution so far observed on packages of raw meat packed under said atmosphere. Therefore, the study proves that photobacteria should be inhibited by modified atmospheres using high oxygen concentration. However, the presence of concomitant bacteria and the meat surface conditions appear to have a protective effect and explain their persistence in high cell numbers on food ultimately leading to its spoilage.

Author contribution: Sandra Fuertes-Perez performed the experimental design, main experiments and methodology, preparation of the samples and analysis of the elsewhere generated proteomics raw data. In addition, she performed the data evaluation, wrote the first draft of the manuscript, created figures and tables, and participated in the reviewing process of the final text.

Impact of modified atmospheres on growth and metabolism of meat-spoilage relevant *Photobacterium* spp. as predicted by comparative proteomics

Fuertes-Pérez, S[1]., Abele, M.[2], Ludwig, C. [2], Vogel, R.F. [1], Hilgarth, M. [1,*]

[1]Lehrstuhl für Technische Mikrobiologie, Technische Universität München, Germany

[2]Bayerisches Zentrum für Biomolekulare Massenspektrometrie (BayBioMS), Technische Universität München, Germany

*corresponding author:

Dr. Maik Hilgarth,

maik.hilgarth@tum.de

Other authors:

sandra.fuertes-perez@tum.de

miriam.abele@tum.de

tina.ludwig@tum.de

rudi.vogel@wzw.tum.de

Keywords: *Photobacterium*, meat, spoilage, MAP, proteomics.

1. Abstract

Modified atmosphere packaging (MAP) is a common strategy to selectively prevent the growth of certain species of meat spoiling bacteria. While studies on the effectiveness of MAP are still scarce on a putative control over the population of photobacteria detected as meat spoilers, they could develop means to enhance safety and quality of raw meat. This study aimed to determine the impact on photobacteria of two modified atmospheres: high oxygen MAP (70% O_2, 30% CO_2, red and white meats), and oxygen-free MAP (70% N_2, 30% CO_2, also white meats and seafood). We have conducted growth experiments of the two main species found on meat, *Photobacterium carnosum (P.)* and *P. phosphoreum,* on a meat simulation media under different gas mixtures of nitrogen, oxygen and carbon dioxide representing air-, high oxygen- and vacuum-like conditions with and without carbon dioxide present. Growth was monitored based on optical density, and samples were taken during exponential growth for a comparative proteomic analysis that allowed the determination of the effects of the different gases and their synergy. Growth under air atmosphere appears optimal particularly for *P. carnosum*. Observed enhancement affected energy metabolism, respiration, oxygen consuming reactions, and a predicted preference for lipids as carbon source. However, all the other atmospheres show some degree of growth reduction. An increase in oxygen concentration leads to an increase in enzymes counteracting oxidative stress for both species, and enhancement of heme utilization and iron-sulfur cluster assembly proteins for *P. phosphoreum*. Absence of oxygen appears to switch the metabolism towards fermentative pathways, where either ribose (*P. phosphoreum)*, or glycogen (*P. carnosum)* appear to be the preferred substrates. Additionally, it promotes the use of alternative electron donors/acceptors, mainly formate and nitrate/nitrite. Stress response is manifested as enhanced expression of enzymes able to produce ammonia (e.g. carbonic anhydrase, hydroxylamine reductase) and regulate osmotic stress. Our results suggest that photobacteria do not sense the environmental levels of carbon dioxide but rather adapt to their own anaerobic metabolism. The regulation in presence of carbon dioxide is limited and strain-specific under anaerobic conditions. However, when oxygen at air-like concentration is present together with carbon dioxide the oxidative stress appears enhanced compared to air conditions (very low carbon dioxide), explained if both gases have a synergistic effect. This is further supported by the increase in oxygen concentration in presence of carbon dioxide. The atmosphere is able to fully inhibit *P. carnosum*, heavily reduce *P. phosphoreum* growth *in vitro* and trigger diversification of energy production with higher energetic cost, highlighting the importance of concomitant bacteria for their growth on raw meat under said atmosphere.

2. Introduction

Modified atmosphere packaging (MAP) employs an exchange of the natural atmospheric gas mixture that surrounds a product for a different composition of gases, aimed at prolongation of the shelf life a product (McMillin et al., 1999). This method has been used to control the growth of the initial microbiota of raw meat for several years, and consequently their deteriorating effects (McMillin, 2008; Yam et al., 2005). The meat industry commonly uses oxygen (O_2), nitrogen (N_2) and carbon dioxide (CO_2) on modified atmospheres (Singh et al., 2011), to inhibit bacterial growth on red meat (O_2 (70%) / CO_2 (30%)), and white meat (O_2 or N_2 (70%) / CO_2 (30%)) while maintaining the organoleptic characteristics of raw meat and avoid consumer rejection (Eilert, 2005; McKee, 2007; Rossaint et al., 2015; Sante et al., 1994). Inhibition or reduction of growth of diverse spoilage microorganisms benefits the extension of the shelf-life of raw meat and therefore reduces the production of waste derived from the industry.

High oxygen concentration is used to maintain the bright red color of fresh meat (Luño et al., 1998; Taylor et al., 1990), retard the formation of brown and undesirable metmyoglobin (Mancini and Hunt, 2005) and inhibit strictly anaerobic and microaerobic bacteria (Farber, 1991). It favors formation of superoxide radicals that induce oxidative stress on bacteria (Pan and Imlay, 2001). However, it also promotes oxidation of lipids on meat and generation of off-odors (Jakobsen and Bertelsen, 2000; Jayasingh et al., 2002). Additional carbon dioxide is used to directly inhibit the growth of aerobic bacteria on fresh meat (Zhao et al., 1994). It is suggested to act by displacing available oxygen, influence on the pH, inducing structural alteration of the cell membrane, or interfere with the metabolism of the bacteria (Daniels et al., 1985).

Photobacteria are typically marine-related bacteria found as symbionts and pathogens of sea animals, in seawater suspension, and spoilers of seafood and fish (Ast and Dunlap, 2005; Dalgaard et al., 1997; Labella et al., 2017; Takahashi et al., 2015; Urbanczyk et al., 2010). Some species of the genus *Photobacterium* (*P.*), however, have been found to also colonize and spoil raw meat. Species *P. phosphoreum* and *P. carnosum,* have been reported as relevant microbiota on raw chicken and turkey (Fuertes-Perez et al., 2019), pork (Nieminen et al., 2016), beef (Pennacchia et al., 2011), sausages (Bouju-Albert et al., 2018; Pini et al., 2020) and minced meat (Stoops et al., 2015) (including marinated meat), under multiple gas atmospheres such as air, vacuum and MAP (high oxygen and oxygen-absent) (Fuertes-Perez et al., 2019; Hilgarth et al., 2018a; Hilgarth et al., 2018b).

Previous research based on metatranscriptomic data of naturally contaminated meat reported little regulation in response to carbon dioxide and, therefore, predicted that the

metabolism of photobacteria was not differentially affected by the use of modified atmospheres with or without oxygen in combination with carbon dioxide (Höll et al., 2019). Other reports, however, which quantified photobacteria directly on artificially contaminated meat revealed that combination of high oxygen and carbon dioxide is, indeed, able to reduce and almost inhibit their growth (Hauschild et al., 2021).

Cell enumeration provides an overall idea of the response of bacteria to a specific environmental condition, but the underlying mechanisms of adaptation that these bacteria utilize remain unknown. It is, therefore, necessary to target the qualitative and quantitative measurement of expressed genes, proteins and consumed or produced metabolites for said purpose. “Omic” technologies have already been used to unveil the regulation behind the behavior and metabolism of other meat spoiling bacteria (Kolbeck et al., 2020; Orihuel et al., 2018; Quintieri et al., 2018; Wang et al., 2018), leaving still a gap of knowledge for *Photobacterium* spp., and the response of specific strains, on meat.

We have monitored the growth of photobacteria *in vitro* under different gas mixtures and followed a comparative proteomics approach in order to determine the direct influence of oxygen and carbon dioxide and their concentration. This study aimed to elucidate the molecular regulations that allow photobacteria to grow and adapt to the packaging conditions using modified atmospheres, as well as determining the overall metabolic mechanisms these bacteria use to grow on raw meat. The use of proteomics, able to depict the enzymatic machinery of the cell, the predictions should allow a closer understanding of their metabolism than previous transcriptomic studies, and therefore provide novel insights.

3. Materials and methods

Bacterial strains and pre-culture

Strains of both species were selected as representative isolates from raw meat. Two strains per species were chosen in order to cover their previously reported high intra-species variability (Fuertes-Perez et al., 2019; Fuertes-Perez et al., 2021). *P. carnosum* TMW 2.2021^{T} (DSM 105454^{T}) is the described type strain of the species (Hilgarth et al., 2018b), isolated from MAP raw chicken meat. Strain TMW 2.2149 was previously isolated from MAP pork (Fuertes-Perez et al., 2019). *P. phosphoreum* strains TMW 2.2103 and TMW 2.2134 were isolated from MAP beef and poultry meat, respectively (Fuertes-Perez et al., 2019).

Strains were inoculated in a pre-culture of meat-extract media according to Fuertes-Perez et al. (2019), prepared with 20 g/L meat extract, 20 g/L NaCl, pH 5.8) from the same glycerol stock every time. Pre-cultures were incubated at 15 ºC overnight in Erlenmeyer flasks for aerobic growth conditions, or in gas tight Schott bottles for anaerobic conditions. Cells from

the pre-culture were harvested, washed once with 0.85 % NaCl (w/v) solution and re-suspended again in the same solution for further inoculation of the cultures.

Growth under different gas atmospheres

Growth of the selected strains was tested on gas tight locked glass bottles, filled with 0.4 L of Meat-Simulation-Media (MSM) media prepared according to Kolbeck et al. (2019). MSM contains 6 % meat extract (w/v) (Merck, Darmstadt, Germany) as the minimum amount at which growth was observed, 0.5 % glycerol (w/v) (Gerbu Biotechnik GmbH, Heidelberg, Germany) and 0.05 mM Tween80 (Gerbu Biotechnik GmbH, Heidelberg, Germany). Additionally, the media contains 2 µg/ml heminchloride (Roth, Karlsruhe, Germany) dissolved in dimethylsulfoxide (99.8 %) (Roth, Karlsruhe, Germany) added after autoclaving the media. The pH of the media was adjusted to 5.8 with 100 % lactic acid.

Bacteria were inoculated at a start optical density of 0.1 at 600 nm. The growth was monitored by optical density measurement for 48 h or until the stationary phase was reached, with constant gas flow, stirring at 120 rpm and at 15 ºC. Gas mixtures utilized and pumped into the bottles during growth were: (a) air, (b) N_2 (100%), (c) O_2/N_2, (70/30 %) (d) N_2/CO_2 (70/30 %), (e) $O_2/CO_2/N_2$ (21/30/49 %), (f) O_2/CO_2 (70/30 %). Samples for proteomic analysis were collected by centrifugation (4000 xg, 5 min, 4 °C) of 100 ml of culture during exponential growth, when calculated amount of cells was above log 7 CFU ml^{-1}. Cells were washed twice with 0.85 % NaCl solution, snap-frozen with liquid nitrogen, and stored at -80 °C. During the whole sampling process, samples were kept on ice. All experiments were performed in triplicate for each gas atmosphere and each strain.

Growth parameters and statistical analysis

Optical density measurements obtained for the triplicates of each experiment were used as input for the open source software RStudio (v. 3.3.0) together with the CRAN package grofit (v. 1.1.1-1) to obtain lag-phase (ʎ), maximum optical density (OD_{max}) and maximum growth rate (μ_{max}) of the bacteria. Parameters for the analysis were kept as default. Differences between the mean values of each parameter were analyzed with IBM SPSS Statistics v. 28.0 software (IBM Corp., Armonk, NY) by performing one-way analysis of variance (ANOVA) between the gas atmospheres used for each strain, followed by a post-hoc Tukey test with a confidence interval set at 95 % ($p < 0.05$).

Preparation of samples for proteomic analysis

Preparation of samples for proteomics analysis was performed with an in-solution sample processing protocol. Shortly, cells were resuspended in 8M urea lysis buffer and mechanically disrupted with glass beads on a vortex for 10 min at 4 °C. The protein concentration was determined by the BCA method according to manufacturer’s instructions.

A total of 20 µg of protein per sample were reduced (10 mM DTT for 30 mins at 30 °C) and carbamidomethylated (55 mM CAA for 30 mins at room temperature in darkness). Digestion of the proteins was carried out by adding trypsin at a 1/100 enzyme/protein ratio (w/w) for 1 h and afterwards by adding another 1/100 enzyme/protein ratio overnight at 37 °C.

After digest, stage tip purification was performed. Therefore, the pH of the samples was measured (pH<3) with pH strips (MColorpHast, Merck, GER). The in-house build C18 tips using 3 disks (3M) were equilibrated consecutively with 250 µl 100% ACN, 250 ul elution solution (40% ACN, 0.1% FA) and 250 µl washing solution (2% ACN, 0.1% FA) at 1500 g. Every sample was loaded on the column (5 min at 500 g) and the sample was three times desalted with washing buffer (2% ACN, 0.1% FA) for 2 min at 1500 g. Finally, peptides were eluted with two times 50 µl elution solution (40% ACN, 0.1% FA) for 2 min at 500g. The solvent of all samples was completely subtracted in a centrifugal evaporator (Centrivap Cold Trap -50, Labconco, US), freshly suspended before MS measurement in washing solution (2% ACN, 0.1% FA) and ~0,1 µg of digest were injected into the mass spectrometer per measurement.

LC-MS/MS analysis and data generation

LC-MS/MS measurements were carried out on an Ultimate 3000 RSLCnano system coupled to a Q-Exactive HF-X mass spectrometer (Thermo Fisher Scientific). Full proteome analyses were performed by delivering 0.1 µg of peptides to a trap column (self-packed, ReproSil-pur C18-AQ, 5 mm, Dr. Maisch, 20 mm x 75 mm) at a flow rate of 5 µL/min (HPLC grade water with 0.1% formic acid). Peptides were transferred to an analytical column (ReproSil Gold C18- AQ, 3 mm, Dr. Maisch, 450 mm 75 mm, self-packed) after 10 min of loading, and separated with a 50 min linear gradient that ranged from 4 to 32% of solvent B (0.1% formic acid in acetonitrile and 5% (v/v) DMSO) at 300 nL/min flow rate. Both nanoLC solvents contained 5% DMSO to boost MS intensity (solvent A = 0.1% formic acid in HPLC grade water and 5% (v/v) DMSO) (Hahne et al., 2013). The Q-Exactive HF-X mass spectrometer was set in data dependent acquisition (DDA) and positive ionization mode during operation. MS1 spectra (360–1300 m/z) were recorded at a resolution of 60,000 using a maximum injection time (maxIT) of 45 ms and an automatic gain control (AGC) target value of 3e6. In case of the full proteome analyses, up to 18 peptide precursors were selected for fragmentation. Precursors with charge state 2 to 6 were the only ones selected and dynamic exclusion of 25 sec was enabled. Higher energy collision induced dissociation (HCD) and normalized collision energy (NCE) of 26% were used for peptide fragmentation. The precursor isolation window width was set to 1.3 m/z. MS2 Resolution was 15.000 with an AGC target value of 1e5 and maximum injection time (maxIT) of 25 ms (full proteome).

Identification and quantification of proteins using MaxQuant

The software MaxQuant (version 1.6.3.4) with its built-in search engine Andromeda (Cox et al., 2011; Tyanova et al., 2016a) was used to perform peptide identification and quantification. MS2 spectra were searched against the NCBI proteome database of *P. carnosum* TMW 2.2021^T (NPIB01), TMW 2.2149 (WMDL01), and *P. phosphoreum* TMW 2.2103 (WMCZ01), TMW 2.2134 (WMCU01), supplemented with common contaminants (built-in option in MaxQuant). Trypsin/P was specified as proteolytic enzyme. Precursor tolerance was set to 4.5 ppm, and fragment ion tolerance to 20 ppm. Results were adjusted to 1% false discovery rate (FDR) on peptide spectrum match (PSM) level and protein level by a target-decoy approach that uses reversed protein sequences. It was established a minimal peptide length of seven amino acids and the “match-between-run” function was disabled. Carbamidomethylated cysteine was set as fixed modification and oxidation of methionine and N-terminal protein acetylation as variable modifications. The proteins differentially regulated between two growth conditions were evaluated using the label-free quantification algorithm provided by MaxQuant (LFQ)(Cox et al., 2014). Intensity based absolute quantification (iBAQ) (Schwanhäusser et al., 2011) was carried out to evaluate the expression of proteins within the same sample.

Statistical analysis of proteomic data and interpretation of results

Data processing was performed using the Perseus software (Tyanova et al., 2016b). The workflow included filtering out proteins only identified by site, reverse or from potential contaminants and performing a $\log_2$ transformation of the values. We considered only proteins that were detected in at least two out of three replicates in each gas condition. For differential protein analysis we performed Welch t-tests between each pair of gas conditions. Proteins that met the requirements of q-value < 0.05 and log2 fold change > 2 were considered differentially expressed. Functional annotation of the proteins was obtained from the databases NCBI, Rapid Annotation Subsystem Technology (RAST) server (Aziz et al., 2008), TIGR annotation (Ouyang et al., 2007) and the Kyoto Encyclopedia of Genes and Genomes (KEGG); and manually curated using BLAST.

We performed six different comparisons between conditions to identify the effects of: oxygen (21 %) (**I.** air_vs_N_2); high oxygen (70 %) (**II.** O_2/N_2_vs_N_2, **III.** Air_vs_O_2/N_2); carbon dioxide (30 %) under anoxic conditions (**IV.** N_2_vs_N_2/CO_2); carbon dioxide under oxic conditions (**V.** N_2/CO_2_vs_O_2/CO_2/N_2, **VI.** O_2/CO_2/N_2_vs_O_2/CO_2).

4. Results and discussion

Overview

Growth experiments were performed under different gas mixtures in order to determine the direct effects on the growth behaviour of the four strains of photobacteria, and on each of the growth parameters (μ_{max}, OD_{max}, lag-phase). All strains were able to grow under five of the six atmospheres tested in this study (air, N_2, N_2/CO_2 O_2/N_2, $O_2/CO_2/N_2$). No growth was observed for *P. carnosum* strains under high oxygen MAP (O_2/CO_2) and therefore only the effects of carbon dioxide under anaerobic or air-like oxygen-concentration conditions were analyzed. Table S1 and figure 1 contain a summary and representation of growth parameters (μ_{max}, OD_{max}, lag-phase) for each strain and gas atmosphere. Additionally, figure S1 includes the growth curves for all strains and conditions.

Growth parameters observed were mostly consistent with results reported by Fuertes-Perez et al. (2019) under air-like conditions: *P. phosphoreum* strains represent the fast grower with shorter lag-phase and higher maximum growth rates and optical density reached. The lag-phase observed under air conditions ranged from 14 to 21h, and 2 to 6h for *P. carnosum* and *P. phosphoreum* strains, respectively. This is considerably faster than previously observed adaption times by Fuertes-Perez et al. (2019) that reached even 101h lag-phase. This could be due to the lower inoculation optical density of said study and the lower incubation temperatures that slow down the metabolism of bacteria. We observed a gradual pattern of reduction for both maximum growth rate and maximum optical density when deviating from air-like conditions in the order: Increased oxygen concentration (mildest reduction), removal oxygen, introduction of carbon dioxide, and combination high oxygen concentration and carbon dioxide (strongest reduction).

Previous works reported on their distribution as meat contaminants in all types of packaging (vacuum, MAP, air) (Fuertes-Perez et al., 2019), and previous work by (Höll et al., 2019) reported similar transcript expression and metabolism when comparing MAP conditions with and without oxygen. However, the results from growth experiments and the amount of differentially expressed proteins between conditions suggest significant effects of both oxygen and carbon dioxide (and their concentration) on the behavior of the two species of photobacteria. Our results are also supported by a growth competition experiment by Hauschild et al. (2021), where MAP atmosphere also showed inhibitory effects on the growth of *P. phosphoreum* and *P. carnosum*. The same study also reported improvement in growth of *P. carnosum* in presence of other meat spoilers, suggesting observed growth of the species under modified atmospheres with high oxygen might be dependent on concomitant bacteria.

Proteomics analysis were carried out for each strain and growth condition in order to establish a correlation between observed growth dynamics and adaptive proteome regulation. To visualize the high quality of the proteomics data set, and the excellent reproducibility of the different gas atmosphere experiments, we performed an unsupervised hierarchical clustering analysis of all samples (Figures S2 and S3). All replicates of one gas experiment clustered tightly together. Samples from oxic and anoxic conditions separated maximally in the clustering analysis, demonstrating that the highest impact on the cellular proteome of both species arose from the change of aerobic to anaerobic metabolism.

The number of total detected and quantified proteins out of those coded in the genome of each strain was 2222 (54.7 %), 2164 (61.8 %) for *P. carnosum* strains TMW 2.2021^{T} and TMW 2.2149, respectively, and 2303 (54.3 %), 2418 (60.8 %) for *P. phosphoreum* strains TMW 2.2103 and TMW 2.2134 respectively.

The effect of each gas on the proteome was determined by comparing differentially expressed proteins between conditions, shown on Table 1 for clarification. All proteins differentially expressed between conditions for each of the strains of photobacteria are displayed in Table S2. We found that between 17 and 119 protein groups for *P. carnosum*, and 9 and 126 protein groups for *P. phosphoreum* were differentially expressed, including up- as well as downregulated proteins as indicated in Table 1.

In Table 2 we summarized the overall impact of each gas atmosphere used for meat packaging on growth and proteomic regulation. A summary of the affected pathways/reactions observed as a response to each gas is displayed in Table 3.

Expression of the respiratory chain

According to a comparative genomics study on photobacteria reported by Fuertes-Perez et al. (2021), all strains analyzed encode a complete respiratory chain in their genomes. Figure 2 contains an entire summary of genes present in the genomes of each strain, as well as a summary of expression. Complexes shared by all four strains include two NADH dehydrogenase (*ndh*), one sodium transporting NADH:ubiquinone reductase complex (*nqr*A-F), succinate dehydrogenase complex, cytochrome c oxidase (*cox*ABC), cytochrome bc complex (*qcr*ABC), cytochrome bd oxidase (*cyd*ABX), and at least two copies of the ATP-synthase proton pump. Photobacteria were also predicted to use multiple alternative electron acceptors such as fumarate, trimethylamine-N-oxide, nitrate, nitrite and sulphate. Additionally, only *P. phosphoreum* strains contained a proton translocating NADH:quinone oxidoreductase complex (*nuo*A-N) and a cytochrome cbb3-type oxidase (*cco*NOP).

Some of the respiratory enzymes were not detected in the proteomic data of this study. Cytochrome c oxidase (*cox*ABC, *cyo*A-E, *cco*NOP), cytochrome bc complex (*qcr*ABC) and

cytochrome b were absent in all strains under all conditions. Specific subunits of come other complexes were also missing, including *nqr*D, *nuo*HJKLMN, *cyd*BX, F0F1 ATP synthase subunit AC and succinate dehydrogenase subunit CD. We found constitutive expression of non-electrogenic NADH dehydrogenase (*ndh*), proton-translocating NADH-dehydrogenase complex subunits *nuo*EFG, Na^+ translocating NADH-dehydrogenase complex subunits *nqr*ACF, cytochrome bd oxidase subunit *cyd*A, succinate dehydrogenase complex subunits AB and ATP synthase subunits B and α-ε. The expression of an additional NADH dehydrogenase complex by *P. phosphoreum*, which is known to be proton dependent rather than sodium dependent, might influence the efficiency of the respiratory chain and explain to some extent the faster growth of the species aerobically in comparison to *P. carnosum*, previously also reported by Fuertes-Perez et al. (2019).

Many of the enzymes that were not detected by proteomics in this study were integral membrane proteins (IMPs). IMPs are notoriously challenging proteins for proteomics analyses due to their low solubility when they contain amphipathic structures as well as their low expression levels (Jeffery, 2016; Vit and Petrak, 2017; Whitelegge, 2013). Difficulties in membrane-bound protein extraction is supported by the fact that expressed complex subunits are in most cases peripheral, such as ATP synthase subunits α-ε (Jonckheere et al., 2012) and NADH-dehydrogenase sub-units *nuo*EFG (Falk-Krzesinski and Wolfe, 1998).

A transcriptomics based study on photobacteria reported identified transcripts of genes belonging to the respiratory chain that we could not detect in the proteomics data of this study, which further strengthens the hypothesis that those proteins are expressed but that the proteomic analysis was unable to detect them (Hauschild et al., 2022).

In summary, our data suggest that photobacteria constitutively express a complete functional respiratory chain. As predicted before by Fuertes-Perez et al. (2021), they use both the non-electrogenic and sodium-translocating version of Complex I, which is in agreement with the sodium requirement of these bacteria (Hilgarth et al., 2018a; Hilgarth et al., 2018b), while *P. phosphoreum* additionally also expressed the proton-translocating version. We only have evidence of expression of cytochrome bd oxidase complex. However, it is able to catalyze by itself the complete reduction of oxygen to water and bypass both complex II and III of the respiratory chain (not detected but present in the genome), coupling the generated proton motive force to the ATP synthesis by the ATP synthase complex (Giuffre et al., 2014), therefore still functioning as a complete respiratory chain.

Regulation towards presence of oxygen in air-like condition

The effect of the presence of oxygen (air-like conditions) was determined by growth experiments and the comparison of air_vs_N_2 conditions (Table 1). The growth of three of

the four strains of photobacteria was positively influenced by the presence of oxygen (21%), with statistically significant (p-value < 0.05) increase of μ_{max} and OD_{max} up to 3 (TMW 2.2021^T) and 4 times (TMW 2.2103) respectively. Strain TMW 2.2149 showed low growth values in all conditions and displayed improvement of only the OD_{max}. *P. carnosum* shows a stronger regulatory response to presence/absence of oxygen than *P. phosphoreum*.

Direct adaptation to aerobic conditions are observed in *P. carnosum* by upregulation of respiratory chain enzymes succinate dehydrogenase (TMW 2.2021^T), cytochrome bd oxidase (TMW 2.2149), and one copy of the ATP-synthase proton pump. Additionally, we detected a slight increase of expression of enzymes with oxidoreductase activity in presence of oxygen for both species to maintain the redox balance of the metabolic machinery with enhanced activity. *P. carnosum* increased expression of enzymes of the pyruvate oxidation (TMW 2.2021^T), TCA cycle and production of lipoic acid under oxic conditions (Figure 3), essential as a cofactor for mitochondrial metabolism (including pyruvate dehydrogenase reaction) (Solmonson and DeBerardinis, 2018), and serves as an antioxidant reacting with reactive oxygen species (Packer et al., 1995). The upregulation of these pathways represents the higher energetic yield under this atmosphere and observed enhanced growth of all strains.

The increased expression of oxygen consuming acetolactate synthase enzyme in *P. carnosum* strains under oxic conditions is also interpreted as an adaptive mechanism of the bacteria to the environmental gas atmosphere. In addition, the biosynthesis of valine, leucine and isoleucine is upregulated under oxic conditions for *P. carnosum* (Figure 3). These three amino acids also represent three of the five most common amino acids in the proteome of the species (Fuertes-Perez et al., 2021), and the synthesis of their enhancement can be interpreted as a sign of increase of metabolic activity derived by the optimum growth conditions.

Despite constitutive expression of enzymes superoxide dismutase and catalase/peroxidase in all strains, *P. carnosum* TMW 2.2021^T expressed anti-oxidative stress enzymes already with 21 % oxygen. Concomitantly, alkyl hydroperoxide reductase, primary scavenger of hydrogen peroxide in *Escherichia coli* (Seaver and Imlay, 2001) had a higher expression than in anaerobic conditions for the same strain. The lack of enhancement in the expression of the same enzymes on the other strain of *P. carnosum*, TMW 2.2149, might explain the lack of improved growth (μ_{max}) under air-like conditions observed the strain. Unlike *P. phosphoreum*, showing no differential regulation, results suggest a higher sensitivity, and therefore earlier response, of *P. carnosum* to stress. This was also supported by previously predicted higher sensitivity to oxidative stress (Fuertes-Perez et al., 2021), and the

demonstrated sensitivity to other types of stress such as high pressure, temperature and salt concentration (Hauschild et al., 2020; Hilgarth et al., 2018b).

Fatty acid oxidation complex subunits had an enhanced expression under aerobic conditions: *fad*J, *fad*B for *P. carnosum* TMW 2.2149 and *fad*I for *P. phosphoreum* TMW 2.2103 and TMW 2.2134). This suggests enhanced utilization of lipids as preferential carbon sources under oxic conditions. Under conditions of "unlimited" oxygen, photobacteria might preferentially perform β-oxidation of lipids, since the ATP yield is higher, and the consumption of oxygen is unhindered (Leverve et al., 2007). As a consequence, photobacteria will contribute to the rancidity during meat spoilage (Mozuraityte et al., 2016) and provide free fatty acids by lipase activity also for other bacteria leading to accelerated spoilage.

Regulation towards increased oxygen concentration

The effects of high oxygen concentration (70%) could be observed by comparison of growth experiments and the differentially expressed proteins between conditions: I. O_2/N_2_vs_N_2 and air_vs_O_2/N_2 (Table 1). *P. carnosum* strains show significantly lower μ_{max} and OD_{max} values with a higher oxygen availability compared to low oxygen or anoxic conditions. *P. phosphoreum* displays preference for low oxygen concentrations in all three parameters, but the parameters μ_{max} and OD_{max} show significantly higher values under high oxygen conditions compared to anaerobic growth, of more than 2 times the value. This might be a result of already suggested higher sensitivity of *P. carnosum* to oxidative stress (Fuertes-Perez et al., 2021) and *P. phosphoreum* being able to cope better with it.

Proteins affected by high levels of oxygen were similar to those observed in air-like conditions, and in many cases even more enhanced by the increase in oxygen concentration. The effect of the presence of oxygen is comparable regardless of concentration of oxygen on the respiratory chain and pyruvate oxidation for *P. carnosum*, and on the oxidoreductase activity and fatty acid oxidation for both species. Additionally, *P. carnosum* strain TMW 2.2149 showed enhanced glycerol utilization (glycerol kinase *glp*K) with increased oxygen concentration (Figure 3).

Iron uptake was upregulated for *P. carnosum* strains under high oxygen conditions for its utilization in heme- and iron-sulfur biosynthesis, required for aerobic respiration (Paul et al., 2017). On the other hand, heme utilization protein *hut*Z and heme carrier protein *hut*X had a higher expression for *P. phosphoreum* strains, both part of an operon that binds heme and was suggested to act either as storage for said molecule, or to facilitate its traffic from the membrane to proteins (Wyckoff et al., 2004). Finally, we found an increase of expression in iron-sulfur cluster assembly proteins for *P. phosphoreum* strains, cofactors required for

several essential pathways such as respiration, carbon metabolism, and protection from oxidizing agents (Mendel et al., 2020).

Additionally we detected an increase in the response to oxidative stress in both species as an upregulation of several preventive enzymes such as: alkyl hydroperoxide reductase, DNA starvation/stationary phase protection protein (linked to protection against multiple types of stress including oxidative (Karas et al., 2015)), thiol peroxidase (prevents membrane lipid oxidation (Cha et al., 2004), superoxide dismutase, catalase, peroxidase and thioredoxin (antioxidant activity (Koharyova and Kolarova, 2008)). *P. phosphoreum* strain TMW 2.2103 also showed upregulation of the histidine biosynthesis pathway (Figure 3), with reported antioxidant and reactive oxygen species scavenger activities (Wade and Tucker, 1998).

Despite the higher availability of oxygen, growth appears hindered in all cases, proving that the increase in oxygen concentration does have an inhibitory effect to some extent in photobacteria, most likely derived from the increase in oxidative stress. However, growth was still observed. We conclude that high oxygen alone is not able to inhibit photobacteria or prevent their growth to spoilage relevant levels.

Regulation towards anaerobic conditions

Comparisons previously analyzed in order to reveal effect of oxic conditions (air_vs_N_2 and O_2/N_2_vs_N_2) were also the base to determine the effects of growth in absence of oxygen. The lack of oxygen appears to have a general detrimental impact on the growth of photobacteria compared to air-like conditions particularly on the maximum OD_{600} reached, with the aforementioned exception of *P. carnosum* strain TMW 2.2149 and its μ_{max}. We found that *P. phosphoreum* does enhance the expression of proteins of the respiratory chain under anoxic conditions, which could suggest a compensatory adaptation of the species to the absence of oxygen and therefore deviation from the higher energetic yield of aerobic respiration. However, it is important to note that the media (as the meat system) used does not contain alternative electron acceptors such as TMAO, nitrate or sulfate, predicted to be used by photobacteria (Fuertes-Perez et al., 2021). Therefore, their absence is likely to contribute to the observed growth reduction due to lacking respiratory activity. This idea is supported by Hilgarth et al. (2018b), which reported similar growth of photobacteria under anaerobic and air conditions on marine agar containing nitrate (Hilgarth et al., 2018b).

There is an upregulation of one gene copy of the ATP-synthase proton pump for *P. phosphoreum* strains (also observed for *P. carnosum* TMW 2.2021T), while the other copy was upregulated only for *P. carnosum* under oxic conditions. Gene duplication in this case appears to respond to an environmental adaptive strategy, with one copy serving as the main

proton pump in optimal oxic conditions, and the other as a compensatory copy under anoxic atmospheres.

There is an enhanced expression of enzymes involved in the use of alternative electron acceptors/donors in both species, but stronger in *P. carnosum* strains, many of which also show constitutive expression on all conditions. We detected upregulation in some of the strains of trimethylamine-N oxide reductase, fumarate reductase and nitrite reductase, in addition to formate dehydrogenase (Figure 4). In particular nitrite reductase, formate dehydrogenase and hydroxylamine reductase had a higher expression than the rest on the four strains analyzed. Formate is used by bacteria as alternative electron donor and coupled to the reduction of electron acceptors such as fumarate or nitrate (Ferry, 1990). In addition, cytochrome c (*nap*C/*nir*T) family protein was also only expressed under anoxic conditions for strain TMW 2.2021^{T}, previously reported as mediator during anaerobic respiration with nitrate or nitrite using formate as electron donor (Simon et al., 2000). Results suggest that despite using more than one type of electron acceptor, which could also lower the energy output of the anaerobic respiration, nitrate/nitrite and formate might be the preferred redox couple. Nitrite and nitrate are both compounds commonly used in meat preservation even in the European Union, but mostly on cured meats rather than raw unprocessed, and it natural availability on meat is low (Ferysiuk and Wójciak, 2020). However, they are common in water, and their use might be a remaining conserved feature from the common lifestyle of photobacteria as marine bacteria.

Both species show higher expression of enzymes involved in the use of carbohydrates under anoxic conditions, resulting from the lack of oxygen and alternative electron acceptors (no respiration), and the switch to fermentative/sugars utilization pathways. Still, both species also appear to have different preferences for the carbohydrate itself. *P. carnosum* strains heavily increase expression of glycogen and maltose degradation/transport pathways (Figure 4). *P. phosphoreum* strains, on the other hand, due to lack of glycogen and maltose utilization enzymes, regulated mainly the ribose metabolism. Glycogen, ribose and even maltose can be found commonly on raw meat with average values of 1.87 g/kg, 0.5-1 mmol/kg and 0.02-0.2 mmol/kg respectively (Koutsidis et al., 2008a, b). The ability of *P. carnosum* to metabolize the three sugars, in contrast to *P. phosphoreum*, only able to utilize ribose, had already been reported (Fuertes-Perez et al., 2021), together with the production of acid from their utilization (Fuertes-Perez et al., 2019).

In addition to the utilization of carbohydrates we also observed an increase in activity of unspecific peptidases/proteases on both species. The lack of alternative electron acceptors present in the media hinders the anaerobic respiration, reducing the energetic yield, and in

turn it might enhance the diversification of carbon sources in order to increase the total energy output.

We observed enhanced expression of a battery of enzymes involved in pH balance and alkalization, that might represent a response to acidification of the media during carbohydrate fermentation as previously reported by (Fuertes-Perez et al., 2019). The carbonic anhydrase (only *P. carnosum* strains) helps maintaining pH homeostasis by interconverting CO_2 and acid (Occhipinti and Boron, 2019). Both the nitrite reductase and hydroxylamine reductase from nitrogen metabolism have increased expression on both species, able to produce ammonia from nitrite or hydroxylamine to increase the pH (Figure 4). To a lesser extent we observed increase in expression of choline trimethylamine-lyase (*cut*C) in one strain (TMW 2.2021^T) of *P. carnosum* able to deaminate choline into trimethylamine (TMA). Choline can be found on raw meat at average levels of 0.7 mg/g (Lewis et al., 2015), and TMA is one of the main spoilage products generated by photobacteria on fish (Dalgaard, 1995). We also observed enhanced expression of anaerobic glycerol-3-phosphate dehydrogenase on *P. phosphoreum* strains and *P. carnosum* strain TMW 2.2021^T that catalyzes the production and accumulation of glycerol and helps maintain osmoregulation during osmotic stress conditions (Albertyn et al., 1994).

Impact of carbon dioxide under anaerobic conditions

The comparison of anoxic conditions with and without addition of carbon dioxide (N_2_vs_N_2/CO_2) allows the determination of the direct effect of carbon dioxide alone on analyzed photobacteria. In terms of growth it appears to negatively impact the growth of photobacteria by significantly decreasing the μ_{max} and the OD_{max} of all strains in comparison to the rest of conditions (except O_2/CO_2).

Most pathways appear unaffected under anoxic conditions when comparing presence and absence of carbon dioxide. No common strategy to the strains of each species was identified to counteract the presence of carbon dioxide that was specific to high environmental levels of carbon dioxide rather than a response to anaerobic metabolism. We only observed strain-specific regulations of single enzymes, such as an increase of trimethylamine-N-oxide reductase (*tor*A) enzyme in *P. carnosum* TMW 2.2149, producing trimethylamine and contributing to alkalization. *P. carnosum* TMW 2.2021T strain showed higher regulation of cellular stress proteins. In addition, *P. phosphoreum* strains TMW 2.2103 and TMW 2.2134 also showed higher expression of the glutathione-S-transferase and bifunctional glutathionylspermidine amidase/synthase enzymes (involved in redox sensing and protein S-thiolation (Pai et al., 2011)), respectively, in presence of carbon dioxide.

In conclusion, photobacteria do not show a common adaptation to environmental presence of carbon dioxide alone, but the the adaptation to CO_2 is rather strain-specific. This might be due to already present mechanisms against changes of pH or disruption of the membrane due to carbon dioxide/acidification under anoxic conditions, when their metabolism switches to fermentative pathways. We suggest that photobacteria do adapt to carbon dioxide/acidification as a response to their own metabolism and presence/absence of oxygen, rather than sensing the environmental levels of carbon dioxide. Consequently, the higher concentration of the gas might increase the adverse effect on the bacteria and, since no adaptation to increased stress is performed to counteract the detrimental effect of CO_2, the growth is negatively affected.

Proposed synergistic effect of oxygen and carbon dioxide

The effects of combined carbon dioxide and oxygen at air-like conditions were determined by the comparison N_2/CO_2_vs_$O_2/CO_2/N_2$, and considering the effects of aerobic vs. anaerobic conditions without presence of carbon dioxide. Presence of air-like oxygen concentration when carbon dioxide is present appears to benefit growth (μ_{max} and OD_{max}) of all strains when compared to the sole presence of carbon dioxide anaerobically. However, it is only statistically significant for *P. carnosum* strains: μ_{max} of TMW 2.2149 and OD_{max} for both strains.

When oxygen is introduced again the gas mixture in presence of carbon dioxide, similar regulations are observed as when carbon dioxide was absent (air vs N_2). There is an enhanced expression of oxidoreductase activity, transport of iron and other metals that might be required for the synthesis of cofactors, pyruvate oxidation, synthesis of lipoic acid, TCA cycle and fatty acid degradation for *P. carnosum* strains, and enhanced expression of heme utilization proteins, oxidoreductase activity, iron transport, assembly of iron-sulfur clusters for *P. phosphoreum*. Additionally, we observed an increase in oxidative stress and cellular stress proteins on *P. phosphoreum* strains and *P. carnosum* TMW 2.2149 strain. The induction of oxidative stress response was absent from most strains when the oxygen concentration was still 21%, but it appears enhanced when the comparison is made in presence of carbon dioxide. These results might suggest a synergistic effect between carbon dioxide and oxygen that emulates the effects of high oxygen concentrations even at low oxygen percentages (21%) when carbon dioxide is present. The enhanced effect of the lower oxygen concentration might be tied to the suggested disruptive mechanism of action of carbon dioxide over the cell membrane (Daniels et al., 1985), allowing a faster diffusion of oxygen into the cell, thereby emulating the effects of the higher oxygen concentration.

We also observed a reduction of expression of acid-counteracting reactions as a response to aerobic growth, even in presence of carbon dioxide, supporting the idea that photobacteria

do not sense the environmental levels of carbon dioxide. The enzyme hydroxylamine reductase had a lower expression in presence of oxygen for *P. carnosum* strains, and so did the enzyme carbonic anhydrase for *P. carnosum* strain TMW 2.2021^{T}. The lysine decarboxylase, with lower expression levels for *P. phosphoreum* strains in presence of oxygen, catalyzes the proton-dependent decarboxylation of L-lysine to produce the polyamine cadaverine. It also plays a role in pH homeostasis by consuming protons and neutralizing the acidic by-products of carbohydrate fermentation (Moreau, 2007). The enzyme glutamate decarboxylase, also with a lower expression for *P. phosphoreum* strains, is reported as one of the most efficient methods for growth under acidic conditions via production of γ-aminobutyrate (GABA) for *Lysteria monocytogenes* (Cotter et al., 2005).

Regarding other decarboxylase, we observed constitutive expression of the amino acid decarboxylases present in the genome of the four strains, whose activity leads to the production of biogenic amines. Enzymes arginine decarboxylase (L-arginine to agmatine and CO_2), agmatinase (agmatine to putrescine and urea) and glutamate decarboxylase (L-glutamate to GABA and CO_2) were expressed constitutively for all four strains. Additionally, both *P. phosphoreum* strains constitutively expressed tyrosine decarboxylase (L-tyrosine to tyramine and CO_2) and lysine decarboxylase (L-lysine to cadaverine and CO_2). Results revealed that regardless of the atmosphere used, photobacteria are able to produce a wide range of biogenic amines and contaminate the raw meat upon growth, as previously predicted by transcriptomics analysis before (Höll et al., 2019).

Impact of high oxygen and carbon dioxide

The effects of the increase in oxygen concentration (up to 70%) compared to air-like conditions in presence of carbon dioxide were studied by the comparison $O_2/CO_2/N_2$_vs_O_2CO_2, and considering the effects of increased oxygen concentration alone. The increase in oxygen concentration when carbon dioxide is present significantly impacts the growth of photobacteria by fully inhibiting *P. carnosum* and decreasing the growth rate and maximum OD of both *P. phosphoreum* strains.

Response to oxidative stress between high and low oxygen in presence of carbon dioxide was the same, contrary to observed results between the same conditions in absence of carbon dioxide. These results again support the idea of a synergistic effect of carbon dioxide and oxygen, and that the response of photobacteria to said stress already reaches its peak with low oxygen concentrations rather than with 70%.

The increase of oxygen concentration in the gas mixture induces higher expression of multiple proteins on both strains of *P. phosphoreum* when compared to the low oxygen mixture. The response of both strains appears to be the enhancement of expression of most

pathways and reactions in the cells, including the respiratory chain, oxidoreductase activity, alternative electron acceptors and donors, pyruvate metabolism, TCA cycle, glyoxylate cycle, fatty acid degradation, and amino acids metabolism. The response observed in both strains suggests that the combination of high oxygen and carbon dioxide in the gas mixture is enough to override the stress response of the bacteria. While it is not possible to determine the specific response of *P. carnosum* due to its lack of growth, we suggest that *P. phosphoreum* enters a state where survival is prioritized, expressing the entire metabolic machinery as a "panic" reaction and trading off the energy required to maintain such a large enzymatic range for the diversification of energy production. The observed growth parameters also suggest that this trade-off might allow the photobacteria to survive under high stress conditions, but growth is severely hindered due to an energetic yield being either very low or null.

We observed, however, that proteins related to the heme utilization and iron-sulfur cluster assembly were significantly less expressed in conditions with high oxygen and carbon dioxide compared to low oxygen and carbon dioxide, contrary to observed between the two conditions in absence of carbon dioxide, which might be an indication that photobacteria are not able to efficiently use oxygen in this gas mixture despite its higher percentage, and therefore do not fully benefit from the higher yield of aerobic metabolism.

Despite previous reports supporting the reduced growth of photobacteria under modified atmosphere packaged raw meat (Hauschild et al., 2021), it is still a common niche from which these species are isolated (Fuertes-Perez et al., 2019) in high cell numbers of $>10^8$ log CFU/g. While we deliberately chose to study specific strains alone *in vitro* in this study without any interference or bias by a consortium or variations of substrates, differences in observed growth might be due to presence of other species of meat spoilers or differences in the model used for growth compared to naturally-contaminated raw meat. Spoilage species can have an influence by consumption of oxygen and reduction of part of the stress induced as it is the case of *B. thermosphacta* (Kolbeck et al., 2019), or commensal relationships with photobacteria (Hauschild et al., 2021; Hauschild et al., 2022). Additionally, the model used in this study, due to the limitations in proteomic sample collection, requires planktonic growth with constant shaking reducing the formation of protective strategies such as biofilms that modify diffusion of gases to the cells (Flemming, 1993).

5. Author Contributions

SF-P: conceptualization, data curation, formal analysis, investigation, methodology, validation, visualization, visualization, writing- original draft.

MA: mass spectrometric analysis, quality control, validation, writing-editing and review

CL: proteomic conceptualization, quality control, supervision, writing-editing and review

MH: project administration, funding acquisition, conceptualization, supervision, writing-editing and review

RFV: project administration, funding acquisition, conceptualization, supervision, resources, writing- editing and review

6. Conflict of Interest

No conflict of interest is declared by the authors.

7. Funding

Part of this work was funded by the Federal Ministry for Economic Affairs and Climate Action (BMWK) via the German Federation of Industrial Research Associations (AiF) and the Industry Association for Food Technology and Packaging (IVLV); project number AiF 20113N1. CL and MA were supported by EPIC-XS, project number 823839, funded by the Horizon 2020 program of the European Union.

8. Data availability

Proteomics raw data, MaxQuant search results and the used protein sequence databases have been deposited with the ProteomeXchange Consortium via the PRIDE partner repository (https://www.ebi.ac.uk/pride/) and can be accessed using the data set identifier PXD031343 (reviewer account username: reviewer_pxd031343@ebi.ac.uk, password: yfqFhUM0).

9. Tables

Table 1. Effects studied and direct comparisons between conditions performed to study them. The total number of proteins differentially regulated between conditions with the requirements of q-value < 0.05 and log2 fold change > 2 are stated for each comparison and each strain. For each value, in green the number of proteins with a higher expression under the first condition, while in red the number of proteins with a higher expression under the second condition. N.A. = lack of proteomic data due to complete growth inhibition of the strain.

Effect to study	Comparison of conditions	*P. carnosum*		*P. phosphoreum*	
		TMW 2.2021^T	TMW 2.2149	TMW 2.2103	TMW 2.2134
Effect of atmospheric O2 concentration (20%/0%)	air_vs_N_2	78 (27/51)	86 (49/37)	37 (16/21)	56 (28/28)
Effect of high oxygen concentration (70%/0%)	O_2/N_2_vs_N_2	119 (59/60)	111 (73/38)	94 (45/49)	91 (40/51)
Effect of high oxygen concentration (70%/20%)	air_vs_O_2/N_2	28 (11/17)	43 (19/24)	9 (2/7)	22 (8/14)
Effect of carbon dioxide under anoxic conditions	N_2_vs_N_2/CO_2	28 (20/8)	17 (4/13)	48 (32/16)	43 (30/13)
Effect of oxygen concomitant of CO_2 presence (20%/0% O_2; high O_2 MAP)	N_2/CO_2_vs_O_2/CO_2/N_2	83 (36/47)	68 (47/21)	126 (76/50)	104 (50/54)
Effect of elevated oxygen concomitant of CO_2 presence (70%/20%; high O_2 MAP)	O_2/CO_2/N_2_vs_O_2/CO_2	N.A.	N.A.	126 (21/105)	114 (15/99)

Table 2. Summary of the predicted effect of the packaging atmosphere on the growth of photobacteria. Impact of each gas atmosphere on the growth and proteome of each strain is displayed (- no effect, + moderate effect, ++ strong effect, +++ very strong effect, N.A. no data available. Expected inhibition of growth of photobacteria on meat packages under each atmosphere is included.

		Vacuum			MAP (no oxygen): white meat			MAP (high oxygen, 70%): red meat		
		Growth	Proteome	Expected inhibition	Growth	Proteome	Expected inhibition	Growth	Proteome	Expected inhibition
P. carnosum	TMW 2.2021^T	+	++	No	+	+	No	N.A.	N.A.	Yes
	TMW 2.2149	+	++	No	+	+	No	N.A.	N.A.	Yes
P. phosphoreum	TMW 2.2103	+	+	No	+	+	No	++	++	Yes
	TMW 2.2134	+	+	No	+	+	No	++	++	Yes

Growth on air (21% oxygen) is used as the optimum and baseline for the growth comparison with other growth conditions. Effect on the growth is evaluated based on observed reduction: "*no effect*" indicates no significant difference to optimum conditions, "*moderate effect*" indicates reduction on the growth parameters but still observed growth, "*strong effect*" indicates great reduction of growth parameters. Effect on the proteome was evaluated based on the amount of differentially regulated proteins.

647 **Table 3.** Summary of observed pathways/reactions affected as a consequence of the different gases
648 and concentrations for both species of photobacteria. Strain-specific regulations are marked with an
649 asterisk and the strain that showed the regulation specified between brackets. Pathway assignation
650 was performed manually.

	P. carnosum	*P. phosphoreum*
Oxygen (21%)	Respiratory chain Oxidoreductase activity Pyruvate metabolism *(TMW 2.2021^T) TCA cycle Synthesis lipoic acid Oxygen consuming reactions Synthesis of valine, leucine, isoleucine Oxidative stress *(TMW 2.2021^T) Degradation of fatty acids *(TMW 2.2149)	Oxidoreductase activity Degradation of fatty acids
Oxygen (70%)	Oxidative stress Iron uptake	Oxidative stress Heme utilization/transport Iron-sulfur cluster assembly Histidine biosynthesis *(TMW 2.2103)
Vacuum (N_2)	Respiratory chain *(TMW 2.2021^T) Alternative electron acceptors/donors Carbohydrate utilization Peptidases/proteases pH homeostasis Osmoregulation *(TMW 2.2021^T)	Respiratory chain Alternative electron acceptors/donors Carbohydrate utilization Peptidases/proteases pH homeostasis Osmoregulation
Carbon dioxide	pH homeostasis *(TMW 2.2149) Cellular stress *(TMW 2.2021^T)	Redox sensing *(TMW 2.2103) Protein S-thiolation *(TMW 2.2134)
Carbon dioxide + Oxygen (21%)	Oxidative stress *(TMW 2.2149) Cellular stress *(TMW 2.2149) pH homeostasis	Oxidative stress Cellular stress pH homeostasis
Carbon dioxide + Oxygen (70%)		Respiratory chain Oxidoreductase activity Alternative electron acceptors/donors Pyruvate metabolism TCA cycle Glyoxylate cycle Fatty acid degradation Amino acids metabolism Heme utilization/transport Iron-sulfur cluster assembly

651

10. Figures

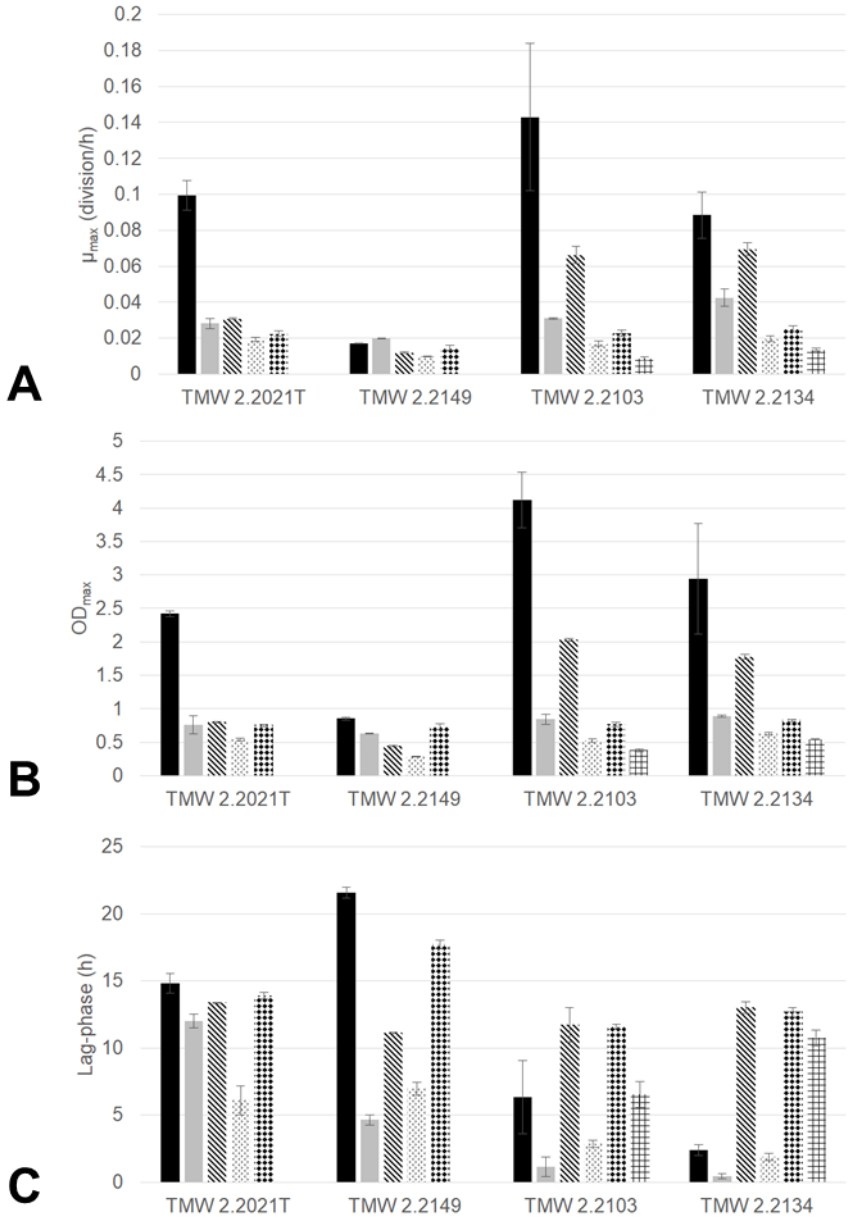

Figure 1. Growth parameters **A**. maximum growth rate (μ_{max}, division/h), **B**. OD_{max}, **C**. lag-phase (h) of *P. carnosum* TMW 2.2021^T, TMW 2.2149 and *P. phosphoreum* TMW 2.2103, TMW 2.2134 under different gas mixtures: ■ air, ▒ N_2, ▨ O_2/N_2, ▩ N_2/CO_2, ▩ $O_2/CO_2/N_2$, ▩ O_2/CO_2.

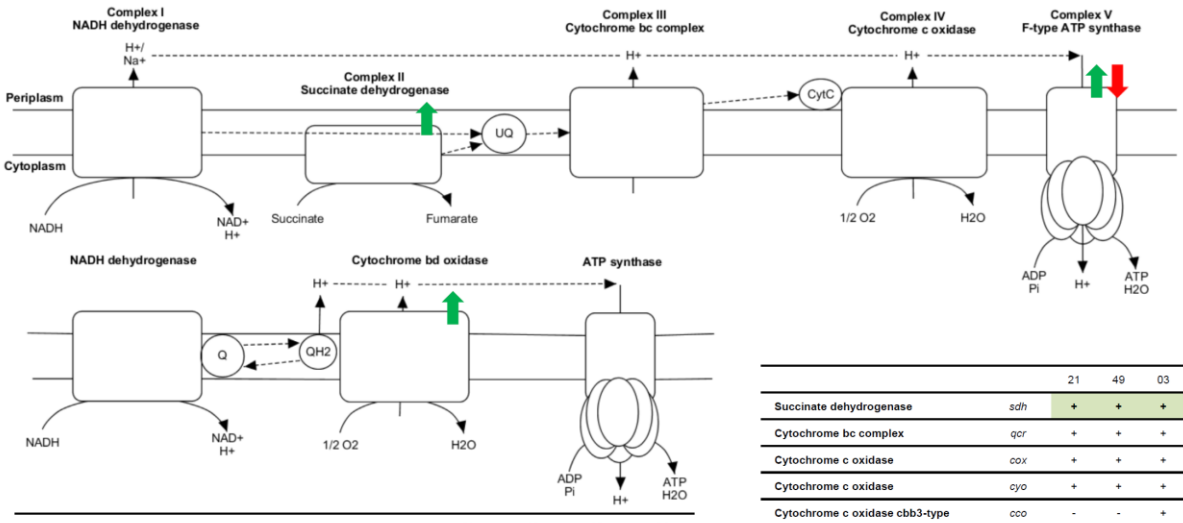

		21	49	03	34
NADH dehydrogenase	*ndh*	+	+	+	+
NADH dehydrogenase (H+)	*nuo*A	-	-	+	+
	*nuo*B	+	+	+	+
	*nuo*C	-	-	+	+
	*nuo*D	-	-	+	+
	*nuo*E-G	-	-	+	+
	*nuo*H	-	-	+	+
	*nuo*I	-	-	+	+
	*nuo*J-N	-	-	+	+
NADH dehydrogenase (Na+)	*nqr*A-C	+	+	+	+
	*nqr*D	+	+	+	+
	*nqr*E	+	+	+	+
	*nqr*F	+	+	+	+
Cytochrome bd oxidase	*cyd*A	+	+	+	+
	*cyd*B	+	+	+	+
	*cyd*X	+	+	+	+

		21	49	03	34
Succinate dehydrogenase	*sdh*	+	+	+	+
Cytochrome bc complex	*qcr*	+	+	+	+
Cytochrome c oxidase	*cox*	+	+	+	+
Cytochrome c oxidase	*cyo*	+	+	+	+
Cytochrome c oxidase cbb3-type	*cco*	-	-	+	+
F-type ATP synthase	A	+	+	+	+
	B	+	+	+	+
	C	+	+	+	+
	α-ε	+	+	+	+
Heme biosynthesis		+	+	+	+

Alternative electron acceptors/donors		21	49	03	34
Fumarate reductase	*frd*	+	+	+	+
TMAO reductase	*torA*	+	+	+	+
Nitrate reductase	*nap*	+	+	+	+
Nitrite reductase		+	+	+	+
Hydroxylamine reductase		+	+	+	+
Formate dehydrogenase		+	+	+	+
NiFe hydrogenase		+	+	+	+
Sulphate adenylyltransferase	Cys	+	+	+	+
Assimilatory sulfite reductase		+	+	+	+
Dimethyl sulfoxide reductase		-	-	+	+

Figure 2. Representation of the functional respiratory chain according to enzymes coded in the genome of photobacteria. Colored arrows represent the regulation points when comparing oxic and anoxic conditions observed: green= higher expression under aerobic conditions, compared to anaerobic, red= higher expression under anaerobic conditions. The tables include a summary of proteins involved in the respiratory chain for each strain: 21= *P. carnosum* TMW 2.2021^{T}, 49= *P. carnosum* TMW 2.2149, 03= *P. phosphoreum* TMW 2.2103, 34=*P. phosphoreum* TMW 2.2134. - = the gene is not present in the genome of the strain, + (blank) = the gene is present in the genome of the strain but no data for its expression was found in the proteome, + (orange) = the gene is present in the genome of the strain and expression data was found in some of the conditions analyzed, + (green) = the gene is present in the genome of the strain and expression data was found in all conditions analyzed.

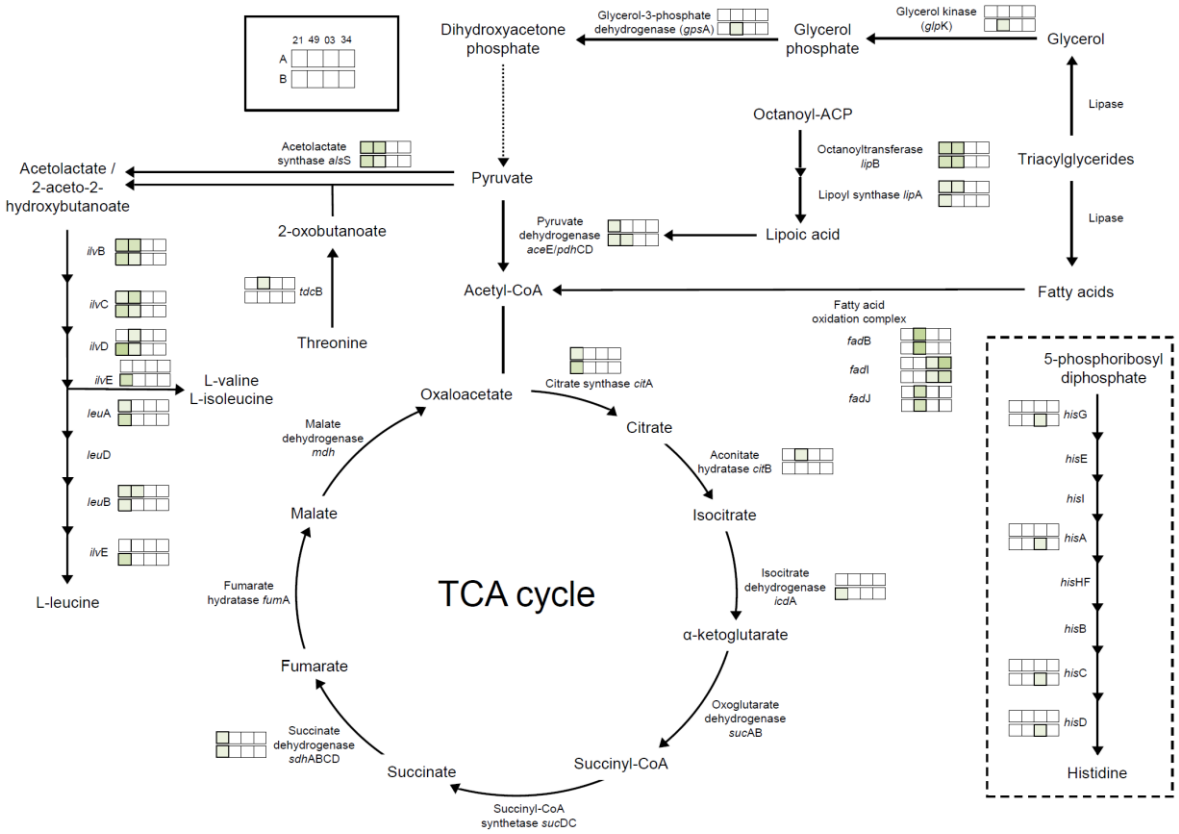

672

673 **Figure 3.** Regulation of enzymes observed under aerobic conditions. The colored boxes
674 display the observed regulation for each strain. Each row of the colored boxes corresponds
675 to one comparison: A. air_vs_N_2, B. O_2N_2_vs_N_2. Each column of the colored boxes
676 corresponds to one strain: *P. carnosum* 21=TMW 2.2021^T, 49=TMW 2.2149, *P.*
677 *phosphoreum* 03=TMW 2.2103, 34=TMW 2.2134. Color code is represented by ☐ 2 $\log_2$
678 (diff.), ☐ 3 $\log_2$ (diff.), ☐ 4 $\log_2$ (diff.), ☐ 5 $\log_2$ (diff.), ☐ 6 $\log_2$ (diff.), ☐ 7 $\log_2$ (diff.), ☐ 8 $\log_2$
679 (diff.).

680

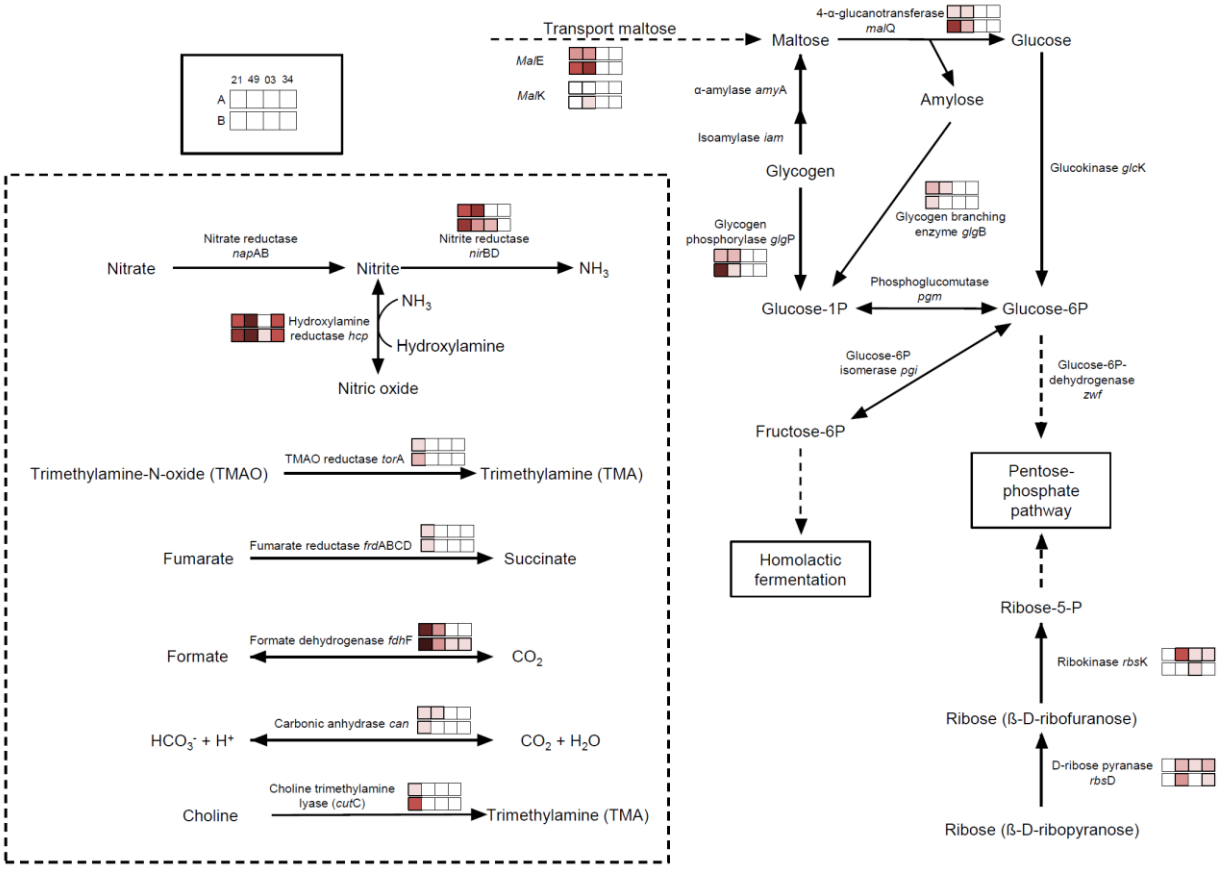

681

682 **Figure 4.** Regulation of enzymes observed under anaerobic conditions. The colored boxes
683 display the observed regulation for each strain. Each row of the colored boxes corresponds
684 to one comparison: A. air_vs_N_2, B. O_2N_2_vs_N_2. Each column of the colored boxes
685 corresponds to one strain: *P. carnosum* 21=TMW 2.2021^T, 49=TMW 2.2149, *P.*
686 *phosphoreum* 03=TMW 2.2103, 34=TMW 2.2134. Color code is represented by ☐ -2 $\log_2$
687 (diff.), ☐ -3 $\log_2$ (diff.), ☐ -4 $\log_2$ (diff.), ☐ -5 $\log_2$ (diff.), ☐ -6 $\log_2$ (diff.), ☐ -7 $\log_2$ (diff.), ☐ -8
688 $\log_2$ (diff.).

11. References

Albertyn, J., Hohmann, S., Thevelein, J.M., Prior, B.A., 1994. GPD1, which encodes glycerol-3-phosphate dehydrogenase, is essential for growth under osmotic stress in *Saccharomyces cerevisiae*, and its expression is regulated by the high-osmolarity glycerol response pathway. Mol Cell Biol 14, 4135-4144.

Ast, J.C., Dunlap, P.V., 2005. Phylogenetic resolution and habitat specificity of members of the *Photobacterium phosphoreum* species group. Environ Microbiol 7, 1641-1654.

Aziz, R.K., Bartels, D., Best, A.A., DeJongh, M., Disz, T., Edwards, R.A., Formsma, K., Gerdes, S., Glass, E.M., Kubal, M., Meyer, F., Olsen, G.J., Olson, R., Osterman, A.L., Overbeek, R.A., McNeil, L.K., Paarmann, D., Paczian, T., Parrello, B., Pusch, G.D., Reich, C., Stevens, R., Vassieva, O., Vonstein, V., Wilke, A., Zagnitko, O., 2008. The RAST Server: rapid annotations using subsystems technology. BMC Genomics 9, 75.

Bouju-Albert, A., Pilet, M.F., Guillou, S., 2018. Influence of lactate and acetate removal on the microbiota of French fresh pork sausages. Food Microbiol 76, 328-336.

Cha, M.K., Kim, W.C., Lim, C.J., Kim, K., Kim, I.H., 2004. *Escherichia coli* periplasmic thiol peroxidase acts as lipid hydroperoxide peroxidase and the principal antioxidative function during anaerobic growth. J Biol Chem 279, 8769-8778.

Cotter, P.D., Ryan, S., Gahan, C.G., Hill, C., 2005. Presence of GadD1 glutamate decarboxylase in selected *Listeria monocytogenes* strains is associated with an ability to grow at low pH. Appl Environ Microbiol 71, 2832-2839.

Cox, J., Hein, M.Y., Luber, C.A., Paron, I., Nagaraj, N., Mann, M., 2014. Accurate proteome-wide label-free quantification by delayed normalization and maximal peptide ratio extraction, termed MaxLFQ. Mol Cell Proteomics 13, 2513-2526.

Cox, J., Neuhauser, N., Michalski, A., Scheltema, R.A., Olsen, J.V., Mann, M., 2011. Andromeda: a peptide search engine integrated into the MaxQuant environment. J Proteome Res 10, 1794-1805.

Dalgaard, P., 1995. Qualitative and quantitative characterization of spoilage bacteria from packed fish. Int J Food Microbiol 26, 319-333.

Dalgaard, P., Manfio, G.P., Goodfellow, M., 1997. Classification of photobacteria associated with spoilage of fish products by numerical taxonomy and pyrolysis mass spectrometry. Zentralbl Bakteriol 285, 157-168.

Daniels, J.A., Krishnamurthi, R., Rizvi, S.S.H., 1985. A review of effects of carbon dioxide on microbial growth and food quality. J Food Prot 48, 532-537.

Eilert, S.J., 2005. New packaging technologies for the 21st century. Meat Sci 71, 122-127.

Falk-Krzesinski, H.J., Wolfe, A.J., 1998. Genetic analysis of the *nuo* locus, which encodes the proton-translocating NADH dehydrogenase in *Escherichia coli*. J Bacteriol 180, 1174-1184.

Farber, J.M., 1991. Microbiological aspects of modified-atmosphere packaging technology - a review (1). J Food Prot 54, 58-70.

Ferry, J.G., 1990. Formate dehydrogenase. FEMS Microbiol Rev 7, 377-382.

Ferysiuk, K., Wójciak, K.M., 2020. Reduction of nitrite in meat products through the application of various plant-based ingredients. Antioxidants (Basel, Switzerland) 9, 711.

Flemming, H.-C., 1993. Biofilms and environmental protection. Water Sci Technol 27, 1-10.

Fuertes-Perez, S., Hauschild, P., Hilgarth, M., Vogel, R.F., 2019. Biodiversity of *Photobacterium* spp. isolated from meats. Front Microbiol.

Fuertes-Perez, S., Vogel, R.F., Hilgarth, M., 2021. Comparative genomics of *Photobacterium* species from terrestrial and marine habitats. CRMICR 2, 100087.

Giuffre, A., Borisov, V.B., Arese, M., Sarti, P., Forte, E., 2014. Cytochrome bd oxidase and bacterial tolerance to oxidative and nitrosative stress. Biochim Biophys Acta 1837, 1178-1187.

Hahne, H., Pachl, F., Ruprecht, B., Maier, S.K., Klaeger, S., Helm, D., Médard, G., Wilm, M., Lemeer, S., Kuster, B., 2013. DMSO enhances electrospray response, boosting sensitivity of proteomic experiments. Nat Methods 10, 989-991.

Hauschild, P., Hilgarth, M., Vogel, R.F., 2020. Hydrostatic pressure- and halotolerance of *Photobacterium phosphoreum* and *P. carnosum* isolated from spoiled meat and salmon. Food Microbiol, 103679.

Hauschild, P., Vogel, R.F., Hilgarth, M., 2021. Influence of the packaging atmosphere and presence of co-contaminants on the growth of photobacteria on chicken meat. Int J Food Microbiol 351, 109264.

Hauschild, P., Vogel, R.F., Hilgarth, M., 2022. Transcriptomic analysis of the response of *Photobacterium phosphoreum* and *Photobacterium carnosum* to co-contaminants on chicken meat. Submitted manuscript.

Hilgarth, M., Fuertes-Perez, S., Ehrmann, M., Vogel, R.F., 2018a. An adapted isolation procedure reveals *Photobacterium* spp. as common spoilers on modified atmosphere packaged meats. Lett Appl Microbiol 66, 262-267.

Hilgarth, M., Fuertes, S., Ehrmann, M., Vogel, R.F., 2018b. *Photobacterium carnosum* sp. nov., isolated from spoiled modified atmosphere packaged poultry meat. Syst Appl Microbiol 41, 44-50.

Höll, L., Hilgarth, M., Geissler, A.J., Behr, J., Vogel, R.F., 2019. Prediction of *in situ* metabolism of photobacteria in modified atmosphere packaged poultry meat using metatranscriptomic data. Microbiol Res 222, 52-59.

Jakobsen, M., Bertelsen, G., 2000. Colour stability and lipid oxidation of fresh beef. Development of a response surface model for predicting the effects of temperature, storage time, and modified atmosphere composition. Meat Sci 54, 49-57.

763 Jayasingh, P., Cornforth, D.P., Brennand, C.P., Carpenter, C.E., Whittier, D.R., 2002.
764 Sensory evaluation of ground beef stored in high-oxygen modified atmosphere packaging. J
765 Food Sci 67, 3493-3496.
766 Jeffery, C.J., 2016. Expression, solubilization, and purification of bacterial membrane
767 proteins. Curr Protoc Protein Sci 83, 29 15 21-29 15 15.
768 Jonckheere, A.I., Smeitink, J.A., Rodenburg, R.J., 2012. Mitochondrial ATP synthase:
769 architecture, function and pathology. J Inherit Metab Dis 35, 211-225.
770 Karas, V.O., Westerlaken, I., Meyer, A.S., 2015. The DNA-binding protein from starved cells
771 (*Dps*) utilizes dual functions to defend cells against multiple stresses. J Bacteriol 197, 3206-
772 3215.
773 Koharyova, M., Kolarova, M., 2008. Oxidative stress and thioredoxin system. Gen Physiol
774 Biophys 27, 71-84.
775 Kolbeck, S., Ludwig, C., Meng, C., Hilgarth, M., Vogel, R.F., 2020. Comparative proteomics
776 of meat spoilage bacteria predicts drivers for their coexistence on modified atmosphere
777 packaged meat. Front Microbiol 11, 209.
778 Kolbeck, S., Reetz, L., Hilgarth, M., Vogel, R.F., 2019. Quantitative oxygen consumption and
779 respiratory activity of meat spoiling bacteria upon high oxygen modified atmosphere. Front
780 Microbiol 10, 2398.
781 Koutsidis, G., Elmore, J.S., Oruna-Concha, M.J., Campo, M.M., Wood, J.D., Mottram, D.S.,
782 2008a. Water-soluble precursors of beef flavour. Part II: Effect of post-mortem conditioning.
783 Meat Sci 79, 270-277.
784 Koutsidis, G., Elmore, J.S., Oruna-Concha, M.J., Campo, M.M., Wood, J.D., Mottram, D.S.,
785 2008b. Water-soluble precursors of beef flavour: I. Effect of diet and breed. Meat Sci 79,
786 124-130.
787 Labella, A.M., Arahal, D.R., Castro, D., Lemos, M.L., Borrego, J.J., 2017. Revisiting the
788 genus *Photobacterium*: taxonomy, ecology and pathogenesis. Int Microbiol 20, 1-10.
789 Leverve, X., Batandier, C., Fontaine, E., 2007. Choosing the right substrate. Novartis Found
790 Symp 280, 108-121; discussion 121-107, 160-104.
791 Lewis, E.D., Zhao, Y.Y., Richard, C., Bruce, H.L., Jacobs, R.L., Field, C.J., Curtis, J.M.,
792 2015. Measurement of the abundance of choline and the distribution of choline-containing
793 moieties in meat. Int J Food Sci Nutr 66, 743-748.
794 Luño, M., Beltrán, J.A., Roncalés, P., 1998. Shelf-life extension and colour stabilisation of
795 beef packaged in a low O_2 atmosphere containing CO: Loin steaks and ground meat. Meat
796 Sci 48, 75-84.
797 Mancini, R.A., Hunt, M.C., 2005. Current research in meat color. Meat Sci 71, 100-121.
798 McKee, L., 2007. Microbiological and sensory properties of fresh and frozen pork products,
799 pp. 395-404.

McMillin, K.W., 2008. Where is MAP going? A review and future potential of modified atmosphere packaging for meat. Meat Sci 80, 43-65.
McMillin, K.W., Huang, N.Y., Ho, C.P., Smith, B.S., 1999. Quality and shelf-life of meat in case-ready modified atmosphere packaging, in: Xiong, Y.L., Chi-Tang, H., Shahidi, F. (Eds.), Quality Attributes of Muscle Foods. Springer US, Boston, MA, pp. 73-93.
Mendel, R.R., Hercher, T.W., Zupok, A., Hasnat, M.A., Leimkühler, S., 2020. The requirement of inorganic Fe-S clusters for the biosynthesis of the organometallic molybdenum cofactor. Inorganics 8, 43.
Moreau, P.L., 2007. The lysine decarboxylase *Cad*A protects *Escherichia coli* starved of phosphate against fermentation acids. J Bacteriol 189, 2249-2261.
Mozuraityte, R., Kristinova, V., Rustad, T., 2016. Oxidation of Food Components, in: Caballero, B., Finglas, P.M., Toldrá, F. (Eds.), Encyclopedia of Food and Health. Academic Press, Oxford, pp. 186-190.
Nieminen, T.T., Dalgaard, P., Bjorkroth, J., 2016. Volatile organic compounds and *Photobacterium phosphoreum* associated with spoilage of modified-atmosphere-packaged raw pork. Int J Food Microbiol 218, 86-95.
Occhipinti, R., Boron, W.F., 2019. Role of carbonic anhydrases and inhibitors in acid-base physiology: insights from mathematical modeling. Int J Mol Sci 20.
Orihuel, A., Teran, L., Renaut, J., Vignolo, G.M., De Almeida, A.M., Saavedra, M.L., Fadda, S., 2018. Differential proteomic analysis of lactic acid bacteria-*Escherichia coli* O157:H7 interaction and its contribution to bioprotection strategies in meat. Front Microbiol 9, 1083.
Ouyang, S., Zhu, W., Hamilton, J., Lin, H., Campbell, M., Childs, K., Thibaud-Nissen, F., Malek, R.L., Lee, Y., Zheng, L., Orvis, J., Haas, B., Wortman, J., Buell, C.R., 2007. The TIGR Rice Genome Annotation Resource: improvements and new features. Nucleic Acids Res 35, D883-887.
Packer, L., Witt, E.H., Tritschler, H.J., 1995. Alpha-lipoic acid as a biological antioxidant. Free Radic Biol Med 19, 227-250.
Pai, C.-H., Wu, H.-J., Lin, C.-H., Wang, A.H.-J., 2011. Structure and mechanism of *Escherichia coli* glutathionylspermidine amidase belonging to the family of cysteine; histidine-dependent amidohydrolases/peptidases. Protein Sci 20, 557-566.
Pan, N., Imlay, J.A., 2001. How does oxygen inhibit central metabolism in the obligate anaerobe Bacteroides thetaiotaomicron. Mol Microbiol 39, 1562-1571.
Paul, B.T., Manz, D.H., Torti, F.M., Torti, S.V., 2017. Mitochondria and iron: current questions. Expert Rev Hematol 10, 65-79.
Pennacchia, C., Ercolini, D., Villani, F., 2011. Spoilage-related microbiota associated with chilled beef stored in air or vacuum pack. Food Microbiol 28, 84-93.

836 Pini, F., Aquilani, C., Giovannetti, L., Viti, C., Pugliese, C., 2020. Characterization of the
837 microbial community composition in Italian Cinta Senese sausages dry-fermented with
838 natural extracts as alternatives to sodium nitrite. Food Microbiol 89, 103417.
839 Quintieri, L., Giribaldi, M., Giuffrida, M.G., Creanza, T.M., Ancona, N., Cavallarin, L., De
840 Angelis, M., Caputo, L., 2018. Proteome response of *Staphylococcus xylosus* DSM 20266T
841 to anaerobiosis and nitrite exposure. Front Microbiol 9, 2275.
842 Rossaint, S., Klausmann, S., Kreyenschmidt, J., 2015. Effect of high-oxygen and oxygen-free
843 modified atmosphere packaging on the spoilage process of poultry breast fillets. Poult Sci 94,
844 96-103.
845 Sante, V., Renerre, M., Lacourt, A., 1994. Effect of modified atmosphere packaging on color
846 stability and on microbiology of turkey breast meat. J Food Qual 17, 177-195.
847 Schwanhäusser, B., Busse, D., Li, N., Dittmar, G., Schuchhardt, J., Wolf, J., Chen, W.,
848 Selbach, M., 2011. Global quantification of mammalian gene expression control. Nature 473,
849 337-342.
850 Seaver, L.C., Imlay, J.A., 2001. Alkyl hydroperoxide reductase is the primary scavenger of
851 endogenous hydrogen peroxide in *Escherichia coli*. J Bacteriol 183, 7173-7181.
852 Simon, J., Gross, R., Einsle, O., Kroneck, P.M., Kröger, A., Klimmek, O., 2000. A *Nap*C/*Nir*T-
853 type cytochrome c (*Nrf*H) is the mediator between the quinone pool and the cytochrome c
854 nitrite reductase of *Wolinella succinogenes*. Mol Microbiol 35, 686-696.
855 Singh, P., Wani, A.A., Saengerlaub, S., Langowski, H.C., 2011. Understanding critical factors
856 for the quality and shelf-life of MAP fresh meat: a review. Crit Rev Food Sci Nutr 51, 146-
857 177.
858 Solmonson, A., DeBerardinis, R.J., 2018. Lipoic acid metabolism and mitochondrial redox
859 regulation. J Biol Chem 293, 7522-7530.
860 Stoops, J., Ruyters, S., Busschaert, P., Spaepen, R., Verreth, C., Claes, J., Lievens, B., Van
861 Campenhout, L., 2015. Bacterial community dynamics during cold storage of minced meat
862 packaged under modified atmosphere and supplemented with different preservatives. Food
863 Microbiol 48, 192-199.
864 Takahashi, H., Ogai, M., Miya, S., Kuda, T., Kimura, B., 2015. Effects of environmental
865 factors on histamine production in the psychrophilic histamine-producing bacterium
866 *Photobacterium iliopiscarium*. Food Control 52, 39-42.
867 Taylor, A.A., Down, N.F., Shaw, B.G., 1990. A comparison of modified atmosphere and
868 vacuum skin packing for the storage of red meats. Int J Food Sci Technol 25, 98-109.
869 Tyanova, S., Temu, T., Cox, J., 2016a. The MaxQuant computational platform for mass
870 spectrometry-based shotgun proteomics. Nat Protoc 11, 2301-2319.

Tyanova, S., Temu, T., Sinitcyn, P., Carlson, A., Hein, M.Y., Geiger, T., Mann, M., Cox, J., 2016b. The Perseus computational platform for comprehensive analysis of (prote)omics data. Nat Methods 13, 731-740.

Urbanczyk, H., Ast, J.C., Dunlap, P.V., 2010. Phylogeny, genomics, and symbiosis of *Photobacterium*. FEMS Microbiol Rev 35, 324-342.

Vit, O., Petrak, J., 2017. Integral membrane proteins in proteomics. How to break open the black box? J Proteomics 153, 8-20.

Wade, A.M., Tucker, H.N., 1998. Antioxidant characteristics of L-histidine. J Nutr Biochem 9, 308-315.

Wang, G., Ma, F., Chen, X., Han, Y., Wang, H., Xu, X., Zhou, G., 2018. Transcriptome analysis of the global response of *Pseudomonas fragi* NMC25 to modified atmosphere packaging stress. Front Microbiol 9, 1277.

Whitelegge, J.P., 2013. Integral membrane proteins and bilayer proteomics. Anal Chem 85, 2558-2568.

Wyckoff, E.E., Schmitt, M., Wilks, A., Payne, S.M., 2004. *Hut*Z is required for efficient heme utilization in *Vibrio cholerae*. J Bacteriol 186, 4142-4151.

Yam, K.L., Takhistov, P.T., Miltz, J., 2005. Intelligent packaging: concepts and applications. J Food Sci 70, R1-R10.

Zhao, Y., Wells, J.H., McMillin, K.W., 1994. Applications of dynamic modified atmosphere packaging systems for fresh red meats: Review3. J Muscle Foods 5, 299-328.

7 Discussion

This thesis was dedicated to the study of meat spoilage relevant species of photobacteria. Techniques were developed and/or improved for their control and detection, and a comprehensive overview is provided upon the study of the genomic and physiological diversity of the species. Also, the influence of gas atmospheres used in food packaging is demonstrated on their proteome, which predicts their adaptive mechanisms and metabolism. The following theses, which are derived from this work and initial working hypotheses, are discussed in this section:

(1) Detection of photobacteria and their entry route as contaminants benefits from culture-independent approaches
(2) Photobacteria are abundant and widespread on cold-stored raw meat but heavily suffer from lot-to-lot variations
(3) The diversity on meat samples within the species is high both at the physiological and genomic level
(4) *Photobacterium* spp. show some but limited signs of environmentally driven adaptations
(5) The species have fundamental differences that might mark their behavior, growth and interactions on a niche
(6) Modified atmospheres are able to affect the growth and proteomic expression of photobacteria

7.1 Detection of photobacteria and their entry route as contaminants benefits from culture-independent approaches

As common marine microbiota, fish spoilers and pathogens, photobacteria have been previously studied and multiple species have been isolated from marine or sea-related sources. Detection and isolation methods often rely on their dominant presence of photobacteria on marine habitats, or their bioluminescent properties to identify their colonies on agar plates, therefore not requiring targeted isolation procedures, but rather media that cover the nutritional requirements such as marine broth (MB) (Thyssen and Ollevier, 2015). On meat, however, photobacteria are not commonly reported as dominant, although still abundant (Hilgarth et al., 2018a; Höll et al., 2019). Hilgarth et al. (2018a) already reported that failing to increase the selectivity of the media used by the addition of vancomycin greatly reduced the chances of detecting photobacteria on chicken. The reason behind it being that photobacteria are overgrown by other concomitant bacteria such as *B. thermosphacta*, even when media specifically reported for the isolation of *Photobacterium* species were used (e.g.

marine broth, TCBS). Selectivity plays a much more important role in detection and isolation of photobacteria from additional sources other than those tied to the marine environment.

The selective procedure for isolation of photobacteria described by Hilgarth et al. (2018a) is effective and allows their detection even when meat spoilage is still not advanced. However, despite the reduction of the microbial load able to grow and the increase in sensitivity in regards to photobacteria, other species and genera are still simultaneously isolated. Vancomycin is a glycopeptide antibiotic particularly effective against staphylococci, streptococci and the vast majority of gram-positive bacteria (Wilhelm, 1991), that inhibits growth of major spoilers *B. thermosphacta*, *Carnobacterium* spp. and *Lactococcus piscium* strains among others, but not of *Pseudomonas* spp. (Hilgarth et al., 2018a). The genus *Pseudomonas* has proven in culture-dependent studies to be the other major type of bacteria isolated together with *Photobacterium* spp. on the selective media, and specially under air conditions even in higher numbers, followed in some samples by *Serratia* spp. that are also not inhibited by the selective media (Hilgarth et al., 2018a). An optimization of the media by reduction of additional concomitant bacteria that are not inhibited by the primary antibiotic in the media would allow an increase in the sensitivity when species of the *Pseudomonas* or *Serratia* genus, among other, might outgrow photobacteria.

However, performed tests that aimed at the optimization of the selectivity of the media yielded unsatisfactory results. Strategies tested during the extension of this project (unpublished results) included the use of additional antibiotics or inhibitory substances on the media, enrichment of the samples in liquid culture and at 15 °C for the optimum growth of relevant species of photobacteria (Hilgarth et al., 2018a; Hilgarth et al., 2018b), and the evaluation of growth conditions between relevant species of photobacteria and *Pseudomonas* spp. such as increase in salt concentration of the media. However, tests proved that either *Pseudomonas* spp. growth was not inhibited, or when some reduction was achieved, it simultaneously affected the recovery of *Photobacterium* isolates, therefore reducing the sensitivity of the methodology, and possibly leading to an underestimation of the population of photobacteria on the sample. The described methodology already reaches a compromise between sensitivity and selectivity, and therefore improvements in the detection were focused on alternative or complementary methodology.

The value of the culture-dependent method is unquestionable, as it provides both detection and isolation of photobacteria from meat. However, the workload can easily become too heavy depending on the number of samples for processing, the minimum amount of time required to determine the presence/absence of photobacteria is 48-72h, and the fast identification of *Photobacterium* species requires specialized equipment (MALDI-TOF MS)

and a constructed in-house database of bacteria. Additionally, the lot-to-lot variation of their presence does not guarantee their detection/isolation.

During the period of time in which this thesis was developed a chicken slaughter plant and a pork and beef meat processing plant were visited and screened by the culture-dependent selective approach for the presence of *Photobacterium* spp. Results (unpublished) from samples did reveal the presence of photobacteria on packed meat obtained at the end, but not along the processing chain, questioning if the application of culture-dependent methods to sample large areas such as industrial production buildings is suboptimal due to the large area to cover and workload. Although other studies employing 16S sequencing analysis managed to report presence of *Photobacterium* spp. on samples where photobacteria have not been detected with culture-dependent methods, such as processed meats (Bouju-Albert et al., 2018; Pennacchia et al., 2011; Pini et al., 2020; Stoops et al., 2015) or from knives and cutting board from a butchery (Stellato et al., 2016), the technique is rather expensive to be used as a routine control or screening method, and often relies on third parties that will not provide results before 24h.

The development of a targeted detection method that does not rely on cultivation removes the requirement for cells to be in a cultivable state, reduces heavy workload and production of waste derived from dilutions, plating and identification and reduces the time before results by eliminating cell growth periods. Additionally, by choosing as base methodology the loop-mediated isothermal amplification (LAMP) we guarantee the improved specificity and sensitivity by the increase of the number of primers, in addition to a decrease in the reaction time, proven to be reduced to 1h for our LAMP assay and a total of 2h including preparation of the meat or surface sample, before a positive or negative result can be achieved (Fuertes-Perez et al., 2020). By comparison, available methodologies for the detection of photobacteria on food samples, not relying on cultivation, take 12 to 50h in the case of a conductance method developed by Dalgaard et al. (1996), and 6h in the case of an already existing real-time PCR-based procedure for detection of photobacteria on fish developed by Macé et al. (2013). While these methods are still optimal for quantification of photobacteria on fish samples, they have not been tested on meat where other spoilers might be a concern, and might not be optimal as a screening method in the industry due to the lower sensitivity, 3 log CFU/g vs. 1.62-1.74 log CFU/g of the LAMP assay, and the requirement for specialized equipment (e.g. real-time PCR thermocycler, Malthus 2000 microbiological analyzer, DNA extraction kits), in contrast to the utilization of a simple water bath with temperature control in the case of the LAMP assay.

Both the conductance-based method and our LAMP assay focus on the presence of the trimethylamine-N-oxide reductase (*tor*A) gene on all strains/species of photobacteria, which was additionally confirmed for the relevant species *P. phosphoreum*, *P. carnosum* and *P. iliopiscarium*, and meat-borne strains (Fuertes-Perez et al., 2021). However, the measurement in change of conductance of the cells requires the media to contain TMAO, and the cells to actively reduce it for them to be detected (Dalgaard et al., 1996). In addition to photobacteria not generally being the dominant genus/species, TMAO is not an abundant substance on meat (Gram and Dalgaard, 2002), and its reduction might not be an accurate representation of the photobacteria population. In contrast, the LAMP assay only requires the cells to be present to detect their genetic material.

Regarding the evaluation of results, the aim of the method was to provide an easy to implement, fast, reliable and sensitive way of detecting photobacteria, not only for laboratory studies, but also as a routine control in the meat industry that would not heavily increase the workload when performed in parallel with existing quality/safety controls. Therefore we favored a visual evaluation method based on a pH indicator previously tested by Tanner et al. (2015) rather than other tested methods such as turbidity, difficult to see or evaluate visually or requiring a turbidity measuring instrument (Mori et al., 2004; Mori et al., 2001), or intercalating dyes that require UV illumination (Goto et al., 2009). Evaluation of a positive reaction of the developed LAMP assay does not require prior training and, although it does not offer a quantification of the concentration of photobacteria on the sample, it can be approximated by means of serial dilutions and the detection limit of the assay.

Trials on both artificially and naturally contaminated samples with the developed methodology prove the efficacy of the method in detecting photobacteria on chicken, pork and beef before the advancement of spoilage, at the same time point that culture-dependent methods would be able to detect them, but obtaining a positive result in 2h rather than three days. The trials also demonstrate that the methodology can be carried out to sample contaminated surfaces, and its characteristics make it easy to implement within the industry and for basic research. The simplicity and quick reaction of the method is a valuable tool for the following cases:

- Identification of the source of contamination or entrance route of photobacteria in butcheries, slaughters and production plants that require coverage of large areas.
- Routine screening and safety control of the batches of meat in slaughters and production plants.
- Preliminary screening of meat and meat products prior to carrying out other approaches with heavier workload, more expensive, or with a high expense of

consumables and production of waste, given the lot-to-lot variation in the presence of photobacteria on meat.

- Screening hitherto unknown sources that might contain photobacteria for basic research.

7.2 Photobacteria are abundant and widespread on cold-stored raw meat but heavily suffer from lot-to-lot variations

The reports prior to this present work expose the presence of photobacteria from several meat related sources. The distribution is widespread on multiple sectors of the meat industry including raw meat, processed meat and even cooked meat and various types of packaging. The contribution of photobacteria to meat spoilage represents an issue not only in Germany, but in great part of Europe and China, highlighting their global relevance. Table 4 contains a collection of the reports on photobacteria from meat-related sources and data that help to understand the ubiquity of photobacteria. The results from this work do not only confirm the presence and isolation of species *P. phosphoreum*, *P. carnosum* and *P. iliopiscarium* by culture-dependent methods from chicken, pork and beef in high numbers and from modified atmosphere packages, but additionally report their isolation from turkey meat, from air and vacuum packages, from a local butchery, and for the first time from products with marinades, often used for control of spoilage of raw meat (Kargiotou et al., 2011; Lytou et al., 2017).

The majority of contaminated products were reportedly stored at low temperatures between 0 and 10 °C, with exceptions raising them up to 19 °C (Greppi et al., 2015), but still falling within the range of temperatures at which the three main relevant species, *P. phosphoreum*, *P. carnosum* and *P. iliopiscarium,* are able to grow (Hilgarth et al., 2018b). We could not find signs of presence of photobacteria in any of the screened cooked or processed meat products or minced meat, despite culture-independent reports providing evidence of the contrary (Cauchie et al., 2020; Duthoo et al., 2021; Koo et al., 2016; Stoops et al., 2015). However, contamination of minced meat, processed and cooked products were all reported by means of culture-independent studies based on amplicon sequencing that is unable to differentiate between death cells, viable cells, or even cells in a non-cultivable state (Cangelosi and Meschke, 2014; Li et al., 2017).

The multiple reports of the detection of photobacteria (Table 4) and their detection on already cooked or processed products suggest that the origin or the contamination is environmental. In addition, Stellato et al. (2016) reported on the detection of photobacteria on knives, surfaces and the hands of an operator from butcheries. The main source of the contamination might be, therefore, tied to a common issue or bacterial reservoir on the processing/slaughtering plants, also suggested before by Rouger et al. (2017) for the general

spoilage community. This reservoir would be derived from a common resource (such as water baths or the cooling system) that would be responsible for fluctuating contamination on meat, and re-contamination of cooked products, considering that the species of photobacteria found on meat are unable to withstand temperatures above 25-30 °C (Hilgarth et al., 2018b).

Another phenomenon that appears to affect the distribution of photobacteria on meat is the lot-to-lot variation. Figure 5 (unpublished results) shows the distribution of bacteria isolated from raw meat where photobacteria were detected, either modified atmosphere packaged or from a local butchery (unpackaged) using the selective approach described by Hilgarth et al. (2018a). While the TVC and total photobacteria counts are much higher in the unpackaged samples, photobacteria appear overgrown by concomitant bacteria such as *Pseudomonas* spp. In contrast, modified atmospheres appear to have a selective effect and allow photobacteria to be dominant on the isolation media. The samples from pork are the only ones where *P. iliopiscarium* is reported in high numbers, although samples shown on the figure represent the only instances of detection of the species on meat samples during the length of this work. *P. carnosum* is mainly reported on chicken and beef, and *P. phosphoreum* present on pork and to a lesser extent on chicken and beef.

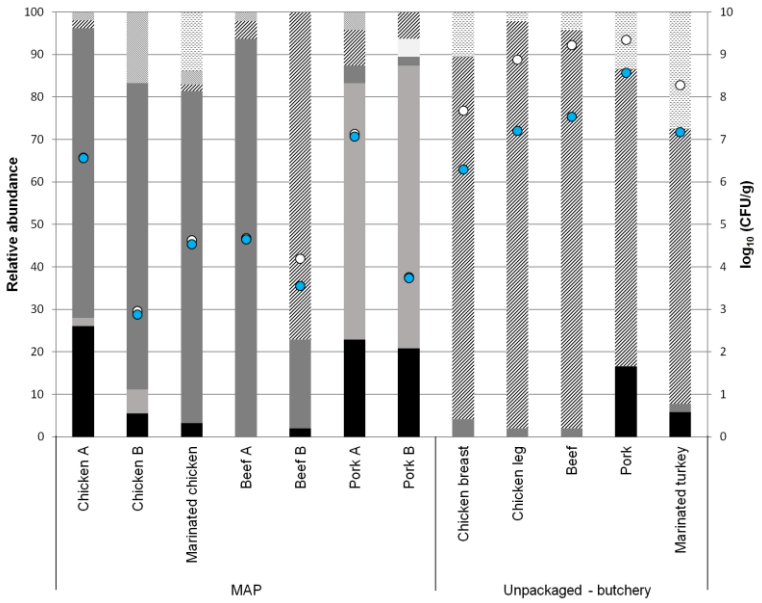

Figure 5. Distribution of detected microbiota on different meat samples, purchased in local supermarkets or butcheries using the selective isolation procedure described by Hilgarth et al. (2018a). The type of sample is described in the x-axis together with the type of atmosphere the sample was packaged in. The y-axis includes on the left the relative abundance of the different species (bars), and the right y-axis contains the $\log_{10}$ (CFU/g) of total bacteria on the sample (○) and the $\log_{10}$ (CFU/g) of total photobacteria (●). *P. phosphoreum* (■), *P. iliopiscarium* (■), *P. carnosum* (■), *Photobacterium* sp. (□), *Pseudomonas* spp. (▨), others (▩), non-reliable identification (▩).

Figure 6 (unpublished results) shows the distribution of the microbiota on samples of beef, chicken and pork packaged under modified atmospheres from the same distribution brand and supermarket over a year. The figure shows a higher prevalence of photobacteria on chicken and beef, especially of *P. carnosum* (followed by *P. phosphoreum*) and absence of *P. iliopiscarium*. In addition, the distribution of contaminated samples fluctuates over the months too. The variations between batches of meat is a known occurrence reported for other meat spoilers (Säde et al., 2017), but also for photobacteria by both culture-dependent and culture-independent studies (Cauchie et al., 2020; Duthoo et al., 2021; Fuertes-Perez et al., 2019; Hilgarth et al., 2018a; Stoops et al., 2015). As a consequence, detection might fluctuate and the isolation or sequencing procedures might not reveal the presence of photobacteria on certain batches of meat. The presence of photobacteria experiences heavy variations in numbers and species present based on type of meat, packaging conditions, and even over the length of the year, hindering the task of delineating accurately their distribution.

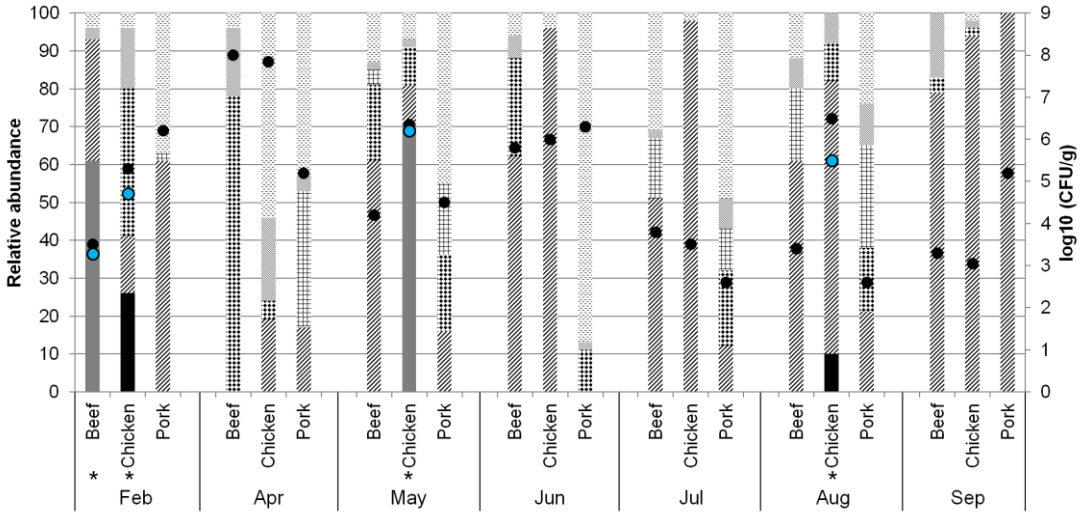

Figure 6. Distribution of detected microbiota with selective isolation procedure described by Hilgarth et al. (2018a) on beef, chicken and pork pieces of meat MAP packed from the same distribution brand along several months of the year (x-axis). The left y-axis shows the relative abundance of each species (bars), while the right y-axis shows the $\log_{10}$ (CFU/g) of bacteria detected: black dots (●) TVC, blue dots (●) total *Photobacterium* spp. viable counts. *P. phosphoreum* (■), *P. carnosum* (■), *Pseudomonas* spp. (▨), *Serratia* spp. (▦), *Candida sake* (▦), others (▩), non-reliable identification (▩). The asterisk (*) on the x-axis marks the samples contaminated with photobacteria for clarity.

According to description by Thyssen and Ollevier (2015), *Photobacterium* species are facultative anaerobic, chemoorganotrophic and with a requirement for sodium ions (optimum 160-280 mM Na^+). It is reported that most species do not have specific organic requirements and are able to grow on minimal medium based on seawater inorganic content, D-glucose and NH_4Cl. Strains of *P. phosphoreum* are reported to require L-methionine alone or combined with other amino acids (Reichelt and Baumann, 1973; Ruby et al., 1980). The

methionine content is higher in proteins of animal origin when compared to those of other origins such as plants (Elango, 2020). Additionally, the sodium concentration on meat appears not enough to cover the growth requirements of photobacteria (<1 mg/g meat). However, it has already been reported that the requirement for sodium might be unspecific and mostly osmotic, and that replacement of part of the sodium requirement can be achieved by other salts such as potassium, much more abundant (Pratt, 1963).

Reports of photobacteria outside the marine and meat processing environments are so far missing, and screening of alternative niches such as dairy and dairy-related products or vegetables yielded negative results (Fuertes-Perez et al., 2019), suggesting that presence of photobacteria is limited to marine niches, fish and seafood, and cold-stored meat and meat products.

Table 4. Summary of detected reports of photobacteria on meat and meat products, indicating when available the source of isolation and temperature of storage, the country were the product was produced, atmosphere in which photobacteria were found, and the methodology (culture-dependent or independent) that revealed their presence.

Source	Atmosphere	Country	Detection	Publication
Beef (1 ° C)	Vacuum	Italy	16S sequencing	(Ercolini et al., 2010)
Beef (chilled)	Air, vacuum	Italy	16S sequencing	(Pennacchia et al., 2011)
Commercial pork (4 °C)	N.A. (air)	China	Cultured	(Kuang et al., 2012)
Salami (14-19 °C)	Air	Italy	16S sequencing	(Greppi et al., 2015)
Minced beef (4 °C)	MAP (O_2/CO_2)	Belgium	16S sequencing	(Stoops et al., 2015)
Beef (6 °C)	Vacuum, MAP (O_2/CO_2)	Finland	16S sequencing	(Jaaskelainen et al., 2016)
Minced pork (4 °C)	N.A. (air)	Korea	16S sequencing	(Koo et al., 2016)
Beef Pork Knife butchery Chopping board butchery Operators hand butchery	N.A. (air)	Italy	16S sequencing	(Stellato et al., 2016)
Steak tartare (4-8 °C)	N.A. (food wrap)	Belgium	16S sequencing	(Delhalle et al., 2016)
Pork (4 °C)	MAP (O_2/CO_2)	Denmark	Cultured 16S sequencing	(Nieminen et al., 2016)
Pork sausages (4-8 °C)	MAP (O_2/CO_2)	France	16S sequencing	(Bouju-Albert et al., 2018)
Pork, beef, chicken (4 °C)	MAP (O_2/CO_2)	Germany	Cultured	(Hilgarth et al., 2018a)
Pork dry-cured sausage	N.A.	China	16S sequencing	(Wang et al., 2018)
Chicken breast (4 °C)	MAP (O_2/CO_2)(N_2/CO_2)	Germany	16S sequencing	(Höll et al., 2019)
Chicken carcass	Air	Belgium	16S sequencing	(Yu et al., 2019)
Pork (4 °C)	N.A.	China	16S sequencing	(Li et al., 2019)
Chicken Beef Pork Marinated turkey Marinated chicken Marinated beef (4 °C)	Air, MAP (O_2/CO_2), Vacuum	Germany	Cultured	(Fuertes-Perez et al., 2019)
Minced pork	Film wrap, MAP	Belgium	16S sequencing	(Cauchie et al., 2020)

	(O_2/CO_2)			
Roasted duck (4 °C)	MAP (N_2/CO_2)	China	16S sequencing	(Chen et al., 2020)
Dry-fermented sausages	N.A. (air)	Italy	16S sequencing	(Pini et al., 2020)
Poultry sausages Pork sausages (4-8 °C)	Air, MAP	France	16S sequencing	(Poirier et al., 2020)
Horse salami Beef salami Pork salami (13 °C)	N.A. (air)	Italy	16S sequencing	(Settanni et al., 2020)
Chicken Beef (4 °C)	Air, MAP (O_2/CO_2)	Germany	Cultured LAMP	(Fuertes-Perez et al., 2020)
Pork loins (-2 °C)	MAP (N_2/CO_2)	China	16S sequencing	(Bassey et al., 2021)
Chicken (0 – 10 °C)	Film wrap	Greece	16S sequencing	(Dourou et al., 2021)
Smoked pork sausage (4 °C)	MAP (N_2/CO_2)	Poland	16S sequencing	(Efenberger-Szmechtyk et al., 2021)
Ostrich meat (4 °C)	Vacuum	Poland	16S sequencing	(Juszczuk-Kubiak et al., 2021)
Donkey meat (4 °C)	Film wrap	China	16S sequencing	(Wei et al., 2021)
Cooked ham Cooked chicken products (7-8 °C)	MAP (N_2/CO_2)	Belgium	16S sequencing	(Duthoo et al., 2021)

7.3 The diversity on meat samples within the species is high both at the physiological and genomic level

The three species of photobacteria whose study is the focus of this thesis display a high level of diversity at multiple levels, highlighting that maybe their relatively recently discovered involvement on meat spoilage should not have been a surprise at all. These bacteria show variations not only in their distribution on samples, but also on their physiological and genotypic characteristics, both at inter- and intra-species levels, that suggests a constant drive for adaptation and persistence.

The use of amplicon sequencing and other culture-independent studies allows the detection of photobacteria, but in most cases it is reported as detection of the genus rather than the individual species (Pennacchia et al., 2011; Stoops et al., 2015) due to the low discriminatory power of the 16S gene in closely related species (Sawabe et al., 2007). Therefore the species distribution and diversity on a batch of samples is hard to elucidate. Studies that report the direct isolation of photobacteria from meat-related sources represent a much more accurate source to determine how diverse the population of photobacteria is. Their presence on multiple types of meat is unquestionable, but not equivalent. Photobacteria appear to have a certain preference for the type of meat they colonize, with uneven distributions based on animal and type of package. On culture-dependent based studies, *P. carnosum* and *P. phosphoreum* appear the most common species, with *P. carnosum* being the most abundant

on chicken and beef, and *P. phosphoreum* on pork, and in particular those pieces MAP packed (Fuertes-Perez et al., 2019; Hilgarth et al., 2018a)(Figure 5). On the other hand, *P. iliopiscarium* detection has been much lower and mostly correlated to the sampling of pork pieces (Fuertes-Perez et al., 2019). However, instances of *P. phosphoreum* present in high numbers on chicken also exist (Figures 5 and 6), weakening the tendency. Although *P. carnosum* tends to be overall the most abundant species found on meat, both species can be found either alone or together, increasing the diversity of the population of bacteria on the same sample. Despite the slight differences in e.g. fatty acid composition between the three types of meat (Bohrer, 2017; Pereira and Vicente, 2013), it appears that both species are able to reach high relevant numbers on the three types of meat. Therefore, it could also be speculated that species distribution is dependent on the concomitant bacteria on the meat, the in-house population of photobacteria at the slaughter, and the specific strains involved that might be more or less competitive.

The uneven distribution is not only observed in regards to the species present on one type of meat or sample, but also to the diversity within each of the species. The diversity of the contaminant bacterial community on a piece of meat is dependent on the animal, the slaughtering procedure, the post-slaughtering processing, storage temperature, packaging atmosphere, the use of marinades and other additives and the sanitizing treatments applied (Rouger et al., 2017), establishing diversity differences between the types of meat screened. Once the initial contamination is established, the diversity is reduced with the increase of the total bacterial load (Chaillou et al., 2015; Höll et al., 2016). The study of the distribution of strains at advanced storage times suggested that at the moment of contamination of the meat during the production chain, the initial contamination can already be quite diverse, with more than 15 different strains on one single piece of meat remaining at the moment of sampling (Fuertes-Perez et al., 2019).

Although the species might display preferences for the meat of specific animals they colonize, the strains isolated are not exclusive of said types. As mentioned before, it is speculated that the origin of the contamination on meat can be found along the processing/slaughtering chain. The bacterial reservoir might promote the differentiation into new strains rather than an origin in the gut of the animal. The absence of a strain/type of meat specificity was additionally proven by the lack of correlation between the source of isolation of a strain and the results of the physiological tests or similarity clusters applied to them, except when considering differences between marine-borne and meat-borne isolates (Fuertes-Perez et al., 2019; Fuertes-Perez et al., 2021).

The strains of the three species, however, do accumulate a certain degree of variability and diverse features that differentiate them from each other and enrich the adaptability of the three species. The comparative genomics study on the three species of photobacteria shows signs of frequent events of genomic acquisition/loss of genes via horizontal exchange that result in large segments of their genome being strictly strain-specific (Fuertes-Perez et al., 2021). The genomes of the three species tend to accumulate transposases and other mobile elements. In addition, the presence of bacteriophage and plasmid sequences integrated in the genome together with the analysis of CRISPR-cas clusters, regarded as the bacterial immune system (Makarova et al., 2015), suggest frequency of infections from external DNA (Attar, 2015; Makarova et al., 2015). The transposable, bacteriophage and conjugative elements have been previously suggested as main mechanisms behind the evolutionary path within the family *Vibrionaceae* (Gu et al., 2009; Lilburn et al., 2010; Reen et al., 2006; Urbanczyk et al., 2010; Vitulo et al., 2007).

The low variability in characteristics such as the GC% content or the usage of codons in their genome would suggest that the acquired segments must come from bacteria with similar characteristics, and maybe even other concomitant members of the genus. There was also a much higher abundance of elements devoid of annotated function in those predicted horizontally transferred segments, than those that truly offered an adaptive advantage. In said scenario, the higher the diversity of species and strains of bacteria (and photobacteria) on the same sample the more likely the occurrence of horizontal gene transfer and the more likely to acquire advantageous and adaptive characteristics.

Events of horizontal transfer have already been discussed in the context of photobacteria for several of their features such as the *lux-rib* operon, chitin pathway or the deoxyribodipyrimidine photolyase (Hunt et al., 2008; Lauro et al., 2014; Urbanczyk et al., 2008). Machado and Gram (2017) also did a study on the *Photobacterium* genus reporting high incidence of acquired features, and the randomness of their distribution. Said random distribution was also present when studying several strains of the same species (*P. phosphoreum*, *P. carnosum* and *P. iliopiscarium*). Physiological tests and genomic analysis provided evidence of this phenomenon for the utilization of uncommon carbohydrates (e.g. L-fucose, *P. carnosum*)), resistance to antibiotics (e.g. chloramphenicol, *P. phosphoreum*), acidification of the media, predicted biogenic amine production (e.g. histamine, putrescine, cadaverine), flagellar cluster and motility, distribution of pathways (e.g. KDPG pathway), and predicted production of bacteriocins and siderophores (Fuertes-Perez et al., 2019; Fuertes-Perez et al., 2021).

Finally, the apparently frequent acquisition of new features by the three species of photobacteria raises not only concern, but also possibilities. On one hand, it means that strains of the species could continuously adapt and become harder to control or raise their spoilage potential. On the other, it opens up possibilities for the pharmaceutical and similar industries, already explored for the genus in the discovery of new drugs (Machado et al., 2015; Machado et al., 2014; Nielsen et al., 2014; Wietz et al., 2010), since the biosynthetic clusters tied to the production of secondary metabolites are, according to Khaldi et al. (2008), mostly acquired by HGT. Photobacteria already show signs of acquired production of secondary metabolites, some of which might be interesting for the pharmaceutical and similar industries (e.g. sactipeptides, microcins, penisin) to develop new antibiotics (Baindara et al., 2016; Himes, 2017; Severinov and Nair, 2012).

7.4 *Photobacterium* spp. show some but limited signs of environmentally driven adaptations

Meat-borne strains of the three species of photobacteria do not show signs of divergence from each other based on their respective source of isolation, and it appears that the structural and composition differences of the animals are not enough to stimulate an adaptive response to each of them. However, photobacteria were originally described as marine bacteria, with different types of lifestyle, and it is possible that the colonization of a new niche such as meat has been accompanied by adaptations driven by the change in environment.

A variable degree of adaption to different niches was observed for the three species. Features such as bioluminescence, osmotolerance and resistance to osmotic stress, or the tolerance and adaptation to high pressure are some of the features commonly attributed to marine bacteria (Brodl et al., 2018; Campanaro et al., 2005; Hauschild et al., 2020). Bioluminescence is a feature mainly observed in the ocean, either for the self-gain of the organism to attract animals that serve as niche, or as the result of a symbiotic relationship between a bioluminescent bacteria and animals (Widder, 2010). *P. phosphoreum* is the only of the three species studied that has retained the entire *lux-rib* operon in their genome, and that is able to display bioluminescence when in culture. However, it has also shown that the feature is strain-dependent, as the species contains at least three strains (meat-borne) with no visible bioluminescence (Fuertes-Perez et al., 2019; Fuertes-Perez et al., 2021). Moran et al. (2007) differentiates marine and non-marine bacteria by the amount of sodium transports and sodium-based transport systems, of which *P. phosphoreum* strains have a higher number encoded in their genome (Fuertes-Perez et al., 2021). The three species appear capable of osmoregulation and to withstand the effects of high pressure, common in the deep sea, based on predictions derived from their genetic machinery. However, a study by

Hauschild et al. (2020) tested the resistance of species *P. carnosum* and *P. phosphoreum* and reported on a higher general resistance of the latter to both types of stress. This is not the first instance of photobacteria not expressing their genetic machinery, as it was also observed for the motility in all strains of *P. carnosum* despite an approximate half of the strains containing the full flagellar cluster in their genome (Fuertes-Perez et al., 2019; Fuertes-Perez et al., 2021). Finally, the three species retain their ability to utilize trimethylamine-N-oxide (TMAO) and nitrate/nitrite as alternative electron acceptors in the respiratory chain, both compounds abundant on fish or marine environments but rather scarce on meat (Cho et al., 2017; Iammarino and Di Taranto, 2012; Koike and Hattori, 1978; Yancey et al., 1982). The data suggest that *P. phosphoreum* retains the most adaptations to marine-environments, which define its primary niche.

On the other hand, the loss of several of the mentioned features by *P. carnosum* such as bioluminescence, reduction of sodium transporters, reduced high pressure and osmotolerance could be signs of the contrary. This species does not show clear signs of divergence on strains isolated from different sources, therefore indicating that the isolates from MAP salmon are cross contaminants and that this species appears as homogeneous for terrestrial environments. The entire species has also lost the ability to utilize DMSO, an abundant compound in the marine-environment (Lee et al., 1999), as alternative electron acceptor in the respiratory chain. However, the species contains a wider variety of genes dedicated to the utilization of several different carbohydrates as carbon sources, also confirmed by acid production (Fuertes-Perez et al., 2019; Fuertes-Perez et al., 2021), as a suggested adaptation to nutrient rich (terrestrial) environments such as meat, previously proposed by Hilgarth et al. (2018b) or plant-based. Carbohydrates usage by *P. carnosum* includes the use of glycogen, a primary carbon source on raw meat (Immonen and Puolanne, 2000; Immonen et al., 2000; Koutsidis et al., 2008b; Ninios et al., 2014; Pethick et al., 1995; Trowbridge and Francis, 1910), but rather scarce on fish (Guillaume et al., 2001; Tarr, 1966). In contrast, *P. phosphoreum* appears to have lost the ability to use glycogen. Henrissat et al. (2002) proposes that the loss of the ability to synthesize and degrade glycogen on bacteria might be associated to favoring a life-style rather parasitic or symbiotic, such as the one observed between the latter species and marine animals (Beijerinck, 1889; Hendrie et al., 1970).

The existence of subpopulations within photobacteria has been suggested. The species *P. carnosum* and *P. phosphoreum* show certain signs of environmentally driven adaption of the whole species, but do not offer evidences of clear differentiation between those strains isolated from a marine or meat-related environment from a genetic point of view, although

the latter does provide evidence of a different undescribed sub-species by genome-sequence identity. However, *P. iliopiscarium* exhibits clear delineation of strains correlated to the source of isolation that was both tested by physiological and genomic features, and corroborated by phylogenetic clustering (Fuertes-Perez et al., 2019; Fuertes-Perez et al., 2021). Said adaptions are similar to those observed for the other two species, but they appear to have driven the strains of a single species in opposite evolutionary directions. Fish-borne strains of the species retain the flagellar cluster and the ability to utilize DMSO as alternative electron acceptor. Meat-borne strains, on the other hand, display a similar pattern of carbohydrate utilization and transport as *P. carnosum* (Fuertes-Perez et al., 2019; Fuertes-Perez et al., 2021).

7.5 The species have fundamental differences that might mark their behavior, growth and interactions on a niche

Due to the phylogenetic proximity of the three species of photobacteria, a great part of their metabolic properties are shared and common. A surface-level overview of their metabolism might suggest that overall all of them behave similarly when growing on meat, with complete pathways in all three species for glycolysis/gluconeogenesis, pentose phosphate pathway, homolactic fermentation, TCA and glyoxylate cycle, pyruvate oxidation, and amino acid, fatty acid and glycerol degradation (Fuertes-Perez et al., 2021; Höll et al., 2019). However, the predictions based on their genome, observed proteome expression and growth experiments reveal differences on the species that suggest different strategies when dealing with their environment.

Despite the similar detection and isolation rates of both *P. carnosum* and *P. phosphoreum* on meat, the results show great differences in growth on a meat-model system. *P. carnosum* displayed much lower growth rates, maximum optical densities and longer adaption times before growth was observed than *P. phosphoreum* (Fuertes-Perez et al., 2022; Fuertes-Perez et al., 2019), while *P. iliopiscarium*, with much lower incidence on meat, showed comparable adaption times to *P. phosphoreum,* but growth rates comparable to *P. carnosum*.

The three species are predicted to be able to respire both aerobically and anaerobically via the use of multiple different electron acceptors, and be able to ferment in the absence of a better alternative (Fuertes-Perez et al., 2021). The ability to grow under multiple atmospheres was also previously reported and can be derived from their presence in multiple types of modified atmosphere packed meat (Table 4). However, it is still clear that air-like conditions remain the optimum for their growth when compared to other atmospheres (Fuertes-Perez et al., 2022; Hauschild et al., 2021).

Under air-like conditions it appears that *P. carnosum* tends to differentially regulate several mechanisms for the efficient use of oxygen in the media, including an enhancement of the respiratory chain and energy metabolism. This is in contrast to the much lower regulation observed on *P. phosphoreum* under the same conditions that relies on the base-line expression of the same proteins rather than an enhancement (Fuertes-Perez et al., 2022). The difference in response might also mark the adaption times observed for the two species, with *P. carnosum* requiring longer times to modify the expression of the enzymes and adapt them to the environmental conditions.

They all contain a common sodium-translocating NADH dehydrogenase as the first complex in the respiratory chain that reflects their sodium requirement in the media (Thyssen and Ollevier, 2015), predicted to be the preferential type of NADH dehydrogenase during respiration based on the proteome profile detected (Fuertes-Perez et al., 2022), rather than the more common proton-translocating NADH-dehydrogenase only present in the genomes of most *P. phosphoreum* strains, but absent from the proteomic data (Fuertes-Perez et al., 2021). Still, the existence of an alternative complex and an additional cytochrome cbb3-type oxidase with high oxygen affinity (Pitcher and Watmough, 2004) in both *P. phosphoreum* and *P. iliopiscarium* might confer them advantage and increase the efficiency of oxygen utilization. The study by Hauschild et al. (2022) did confirm the presence of transcripts of those complexes, and therefore they could act as a complementary working complex for the respiratory chain. The predicted higher potential of *P. phosphoreum* to produce siderophores to capture environmental iron, used in redox reactions and respiration (Comi, 2017; Gram et al., 2002), might increase the competitive potential of the species above the other two.

All three species were predicted to utilize glucose, fructose, glucose and mannose (Fuertes-Perez et al., 2021), the main carbohydrates present on meat (Aliani and Farmer, 2005a, b; Koutsidis et al., 2008a, b; Meinert et al., 2009a; Meinert et al., 2009b), and the prediction was confirmed by acid production (Fuertes-Perez et al., 2019). Therefore, based on carbon utilization, the three species are equipped to grow both on the meat and on the fish, where glucose, fructose and mannose are highly abundant (Tarr, 1966). While the use of glucose appears to be constitutive, the species show preferences on carbohydrate utilization during anaerobic fermentation. *P. carnosum*, is predicted to preferentially use glycogen (although still predicted to use ribose) as compared to *P. phosphoreum*, which is unable to use it, and is predicted to preferentially use ribose (Fuertes-Perez et al., 2022). *P. carnosum* might gain an advantage given the abundance of the glycogen on meat, of up to 1.8% of the meat weight (Immonen and Puolanne, 2000; Immonen et al., 2000; Ninios et al., 2014; Pethick et al., 1995; Trowbridge and Francis, 1910). Additionally, the wider diversification of carbon

sources observed for *P. carnosum* and *P. iliopiscarium*, even from sources other than meat (e.g. plant-based carbohydrates), would help counterbalance their slower growth rates, being able to still switch and consume other energy sources as other faster bacteria deplete them. While carbohydrates tend to be a major carbon source for many bacteria, observations also revealed that, under optimum air-like conditions, photobacteria might utilize fatty acids as primary source of energy (Fuertes-Perez et al., 2022) given the higher total ATP yield (Leverve et al., 2007). Finally, as mentioned before, the three species are predicted to degrade amino acids as energy source. All strains are predicted to be able to carry out most of the anaplerotic routes involved in the incorporation of amino acids into the TCA cycle, with the exception of glutamate dehydrogenase (*gdh*A), only present in *P. phosphoreum* strains (glutamate to α-ketoglutarate) (Fuertes-Perez et al., 2021). However, an enhancement of the utilization of proteins as carbon sources was not observed, except for a slight increase in expression of unspecific peptidades/proteases under anaerobic conditions (Fuertes-Perez et al., 2022). Hauschild et al. (2022) reported on a preferred use of fatty acids and proteins as energy source when photobacteria are growing on meat with concomitant bacteria. Moreover, given the reported requirement of *P. phosphoreum* for L-methionine, it is likely that photobacteria constitutively utilize amino acids as energy source, but might not be under all circumstances the preferred substrate.

All strains considered in the study from the three species shared the capability to modify the surrounding environment to a certain extent. Several of the derived products from the metabolism of proteins and the ß-oxidation of lipids translate into foul-odors that the consumer can perceive and correlate to spoilage (Flores, 2017; Jakobsen and Bertelsen, 2000; Jayasingh et al., 2002). The production of greening on meat derived from the release of hydrogen peroxide from different sources (pyruvate or amino acids), production of sour odors and modification of the pH by production of compounds such as acetate, lactate, ammonia or trimethylamine are predicted for all strains (Fuertes-Perez et al., 2021; Gram and Dalgaard, 2002; Gram et al., 2002). However, *in vitro* measurements of pH variations on a meat model show that *P. phosphoreum* has a higher tendency to alkalize the media than the other two species, while the tendency of *P. carnosum* is to decrease or maintain it (Fuertes-Perez et al., 2019). It has been suggested that the influence over the pH might also have a correlation to the production of biogenic amines by photobacteria, although to a different extent for the species. In that context, *P. phosphoreum* might be the main producer of biogenic amines, given also previous reports of the high release of histamine to the media by the species (López Caballero et al., 2002; Morii and Kasama, 2004; Torido et al., 2012; Wang and LaPointe, 2020). The production of biogenic amines, such as putrescine from arginine (all strains) and ornithine (strain-specific), gamma-aminobutyric acid (GABA) from

glutamate (all strains), cadaverine from lysine (strain-specific), and tyramine from tyrosine (strain-specific), was predicted for the species from their genome (Fuertes-Perez et al., 2021; Höll et al., 2019). Furthermore, the expression of present amino acid decarboxylases in the proteome of strains TMW 2.2021^{T}, TMW 2.2149 (*P. carnosum*) and TMW 2.2103 and TMW 2.2134 (*P. phosphoreum*) appeared constitutive, confirming that use of amino acids is independent on the growing conditions and constant for photobacteria, and predicted constitutive production of at least agmatine, putrescine, GABA, tyramine and cadaverine (Fuertes-Perez et al., 2022). Finally, although Höll et al. (2019) and Machado and Gram (2017) reported on the absence of known homologs to the histidine decarboxylase gene on *P. phosphoreum*, an alternative histidine decarboxylase (*hdc*2) described by Bjornsdottir-Butler et al. (2020) was found as strain-specific in *P. phosphoreum* and *P. carnosum* strains. Said version of the enzyme might be responsible for the multiple reports on the production of histamine by *P. phosphoreum* (López Caballero et al., 2002; Morii and Kasama, 2004; Torido et al., 2012; Wang et al., 2020), although its distribution is strain-specific rather than a common trait for the whole species.

In regards to the relationships established with other concomitant bacteria in the media, the wider predicted bacteriocin production observed for *P. phosphoreum* against other bacteria (e.g. microcin (Baquero et al., 2019)) suggests that the strategy followed by the species is focused on elimination of possible competitors in the environment rather than diversification of energy sources. This might also be the case for those *P. iliopiscarium* marine-borne strains containing type IV secretion system, involved in conjugation events but also on secretion of macromolecules into other cells and removal of competitors (Sgro et al., 2019; Wallden et al., 2010).

Predictions derived from the genome of the species revealed a general similar capacity to respond to sources of stress such as high pressure or osmotic unbalance. However, an study by Hauschild et al. (2020) proved that *P. carnosum* had a higher sensitivity to both. Response to oxidative stress was predicted to be slightly enhanced for *P. phosphoreum* and *P. iliopiscarium* species via the duplication of genes superoxide dismutase and catalase (Fuertes-Perez et al., 2021). The difference in sensitivity between *P. phosphoreum* and *P. carnosum* was confirmed later by the response to oxidative stress displayed by the species when growing under oxic conditions. *P. carnosum* already displayed signs of oxidative stress even under air-like conditions, whereas *P. phosphoreum* required high-oxygen concentrations to show any response to it (Fuertes-Perez et al., 2022), and proving that gene duplication might have an adaptive function behind on photobacteria.

Differences in stress-response were additionally observed in regards to antibiotic resistance and growth requirements. *P. carnosum* showed the greatest and widest sensitivity to tested antibiotics (Fuertes-Perez et al., 2019), and the narrowest growth conditions of temperature, salt concentration and pH of the three species, reported by Hilgarth et al. (2018b). Overall, *P. carnosum* displays the strongest sensitivity to external stress of the three species. Still, the species is able to adapt and, as the proteomics results reveal, accordingly modify the expression of its proteome in response to most stress-sources (Fuertes-Perez et al., 2022). Additionally, a study by Hauschild et al. (2021) revealed that *P. carnosum* might benefit from the presence of other concomitant bacteria under certain atmosphere-induced sub-optimal conditions and improve its survivability.

Overall, the data obtained sustain the perception of *P. carnosum* as bacteria with slower growth due to lower stress-resistance capabilities, lower respiratory efficiency, and longer adaption times derived from more extensive proteomic regulation under optimum growth conditions. The species, however, is suggested to focus its strategy on diversification on the use of energy sources and optimization of their utilization depending on the colonized niche. On the other hand, *P. phosphoreum*, better at resisting to environmental stress, limits its regulatory response under optimum conditions due to higher base-line efficiency in order to grow faster, and focuses its strategy on removal of possible competitors. *P. iliopiscarium* appears to share strategies of both previously mentioned species, but be able to master none, and remain relegated to a minor presence than the other two both in the meat system and in the marine environment.

7.6 Modified atmospheres are able to affect the growth and proteome of photobacteria

Modified atmospheres are a common method used for extending the shelf-life of meat and meat products and limit the growth of spoilage microbiota (Church and Parsons, 1995; Farber, 1991; McMillin, 2008; McMillin et al., 1999). The technology relies on the negative effects that carbon dioxide, high concentrations of oxygen, or the lack of oxygen might have on the growth of bacteria. Their effects have been tested on multiple species of spoilers with different outcomes, since the tolerance or development of adaptive strategies varies greatly, from complete inhibition of the bacteria, to the total lack of effect on them (Erichsen and Molin, 1981; Kolbeck et al., 2020; Rossaint et al., 2015).

Table 4 displayed in section 7.2 presents the multiple studies where the presence of photobacteria has been reported on meat and meat products, and it includes packaging under all types of modified atmospheres (N_2 70% / CO_2 30%, O_2 70% / CO_2 30 % and vacuum packaging) (Bassey et al., 2021; Chen et al., 2020; Fuertes-Perez et al., 2019).

Evidences point towards the absence of an inhibitory effect of the modified atmospheres on photobacteria and their ability to grow regardless of the packaging conditions (modified atmospheres with and without oxygen) as it was previously suggested by Höll et al. (2019), which constitutes itself a problem due to the spoilage potential of the three species reported on meat (Fuertes-Perez et al., 2019; Fuertes-Perez et al., 2021; Hilgarth et al., 2018a) and fish (Dalgaard et al., 1997; Emborg et al., 2002; Jørgensen et al., 2000a).

However, evidences from this work point towards the existence of an influence of each of the gases and their concentrations on the metabolism of the two dominant spoiling species: *P. phosphoreum* and *P. carnosum* (Fuertes-Perez et al., 2022). While the overall effect of the gases on the proteome regulation is similar for both species, the extent to which each of them affects their growth diverges, as a consequence of the different adapting capabilities of the two species to a surrounding gas atmosphere that deviates from optimum air-like conditions. Despite both species possessing and constitutively expressing the proper genetic machinery to counteract most types of stress that could be induced by the gases, such as oxidative stress, changes in the pH, or disruption of the osmotic balance, *P. phosphoreum* appears in all cases better suited to withstand negative environmental conditions (Fuertes-Perez et al., 2022; Fuertes-Perez et al., 2021; Hauschild et al., 2020; Hilgarth et al., 2018b).

The use of vacuum, carbon dioxide alone or the use of high oxygen concentrations would pose a problem for the meat industry, since they do not appear enough to truly hinder the growth of photobacteria, but rather only limit it, as it was also reported by Hauschild et al. (2021). Photobacteria do show signs of adaptation to those atmospheres that allow them to, although not optimally, reach high cell numbers (Fuertes-Perez et al., 2022).

We have observed that the use of atmospheres without oxygen, regardless of the presence of carbon dioxide, is predicted to enhance the metabolic machinery dedicated to fermentative pathways and anaerobic respiration (Fuertes-Perez et al., 2022). Despite the demonstrated growth of photobacteria in the absence of oxygen (Hilgarth et al., 2018b), they are present but scarce on vacuum packages, and the growth experiments proved some degree of reduction compared to optimum conditions (Fuertes-Perez et al., 2022). The lack of alternative electron acceptors in the meat environment that causes hindering of the anaerobic respiration might be the cause for the growth reduction observed under anoxic conditions, supported by the enhancement of the use of nitrite as alternative electron acceptor under anoxic conditions. In addition, as a response to the acidification of the media predicted by the utilization of carbohydrates, the bacteria appear to activate alkalization routes tied to the production of ammonia and amines such as trimethylamine (TMA), a spoilage product (Dalgaard, 1995), from choline, present on meat (Lewis et al., 2015).

Despite the constitutive expression of several decarboxylases responsible for the production of biogenic amines, it appears that their expression is reduced in conditions where oxygen is present despite the presence of carbon dioxide in the gas mixture (Fuertes-Perez et al., 2022). In this sense, the use of the modified atmosphere that contains 70% N_2 and 30% CO_2, mostly used in the European Union for the packaging of chicken (the most common source of isolation of photobacteria) (Fuertes-Perez et al., 2019; Hilgarth et al., 2018a; Hilgarth et al., 2018b), would be ineffective and even possibly counterproductive to some extent. It is predicted that photobacteria are unable to properly sense the environmental levels of carbon dioxide, rather adapting to their own anaerobic metabolism when in absence of oxygen. Despite some predicted negative effects of the gas among those attributed to it, such as disruption of the membrane or alteration of the pH (Daniels et al., 1985), it is not, by itself, an effective measure against the growth of photobacteria. These findings were similarly reported by Hauschild et al. (2021), that observed some, but insufficient, growth reduction on both species by the presence of carbon dioxide with, however, similar capabilities to adapt and tolerate its presence with and without other bacteria present.

A similar situation can be described for the use alone of high oxygen concentrations, reported to have negative effects on the growth of some species of photobacteria, such as *P. phosphoreum,* when used in concentrations either too high or too low (Nealson, 1978). Despite evident signs of oxidative stress induced on both species (Fuertes-Perez et al., 2022), it appears to be the least severe of the negative effects induced on the growth of *Photobacterium* spp. The bacteria benefit from the large battery of oxygen radicals' counteracting enzymes (Fuertes-Perez et al., 2021), and the enhanced expression of several of them (Fuertes-Perez et al., 2022), to limit the growth reduction suffered.

However, the combined use of carbon dioxide and high concentration of oxygen tell a different story. While there are several evidences of photobacteria present on meat packed under said atmosphere (Table 4), photobacteria appear unable to cope with the combined and synergistic effect of both gases (Fuertes-Perez et al., 2022), also reported by Hansen et al. (2021) on cod fillets and Hauschild et al. (2021) on raw meat. As it was mentioned before, the use of carbon dioxide alone is insufficient to hinder enough the growth of photobacteria, but effective enough in combination with 70% oxygen.

Previously reported effects of the gases include the presence of oxygen enhancing the sensitivity to other types of stress on bacteria (Amanatidou, 2001), such as the one exerted by carbon dioxide, or even the reduction of the activity of the respiratory chain in presence of carbon dioxide previously reported for *Pseudomonas* spp. (Gill and Tan, 1980). However, the bacteria show signs of suffering a stronger oxidative stress when carbon dioxide and oxygen

are present together (Fuertes-Perez et al., 2022) also reported by Hauschild et al. (2022). The effect could be attributed to the cell membrane disruptive mechanism attributed to carbon dioxide allowing a faster diffusion of oxygen inside the cell and emulating the effects of a higher concentration of the gas.

In summary, both species of photobacteria do suffer the effects of the variation on the surrounding atmosphere, and experience some reduction on their ability to grow when compared to optimum air-like conditions. In most cases, those effects are limited and insufficient to inhibit or control the population of photobacteria on meat, and therefore slow down their spoilage process. The use of combined carbon dioxide and high oxygen concentration, on the other hand, appears effective against growth of the species. However, the reports of photobacteria on raw meat packaged under modified atmospheres using high oxygen concentrations are multiple (Table 4) and provide evidence of growth over the storage period of the sample (Bassey et al., 2021; Fuertes-Perez et al., 2020). It has been reported that the presence of concomitant bacteria such as *B. thermosphacta* or *Pseudomonas* spp. can play an enhancing effect on the growth of *Photobacterium* spp. under high stress conditions (Hauschild et al., 2021; Hauschild et al., 2022), or alleviate part of the stress by consumption of oxygen (Kolbeck et al., 2019). In addition, the lack of constant agitation and existence of a solid surface within the real meat system (rather than the liquid model used in this work) allows the possibility to form protective structures such as biofilms that confer resistance to environmental conditions (Møretrø and Langsrud, 2017). Said reasons might represent the difference between effects observed *in vitro*, and their persistence in high, relevant cell numbers on the meat packages regardless of the atmosphere used.

8 Conclusion

The present work offers insight into a comparative analysis of meat-spoilage relevant species of photobacteria: *P. carnosum*, *P. phosphoreum* and *P. iliopiscarium.* The development of a new simple and fast detection method enables new measures of control over the source of contamination, but also allows the further understanding of the full extent of the distribution of photobacteria on the food industry. The study of their physiological and genetic characteristics, and the intrinsic diversity displayed within each species represents a step forward in broadening the knowledge of these bacteria. Said knowledge allows the answering of questions regarding the origin of the contamination on meat, the adaption to each niche, or the fundamental differences between them that shape their persistence, dominance and influence on the meat system. Furthermore, comparative analyses allow us to understand that current methodologies for the control of bacteria on meat might not be sufficient when applied to the real meat system i.e. dissection and re-assembly of the system/consortium remains an ongoing challenge.

9 Acknowledgements

Too many names should fill this section, and too little is the space I can dedicate to it, for I do not wish to bore the reader with names of people they don't know, and certainly my thanks will be warmer given in person. But I would like to dedicate some well-deserved words to those without whom I would not be writing this text.

First and foremost to Rudi, the reason I could spend these past years doing my PhD, the person that offered me this opportunity, and somebody that has demonstrated each day that is willing to fight for his students and for each of them getting the title of Doctor. And to Maik, with whom I have spent more hours than I can recall seated in front of the data, looking for solutions to each puzzle, keeping in mind the reward of a promised home-made warm delicious meal for each closed chapter. To both of you, thank you, and thank you again for reading to the end of my texts despite the awfully long sentences I so much love to write.

To my colleagues and specially my office-mates, because we have seen each other in the good, and in the bad, gone together through cries, through laughs, but best of all through candy-throwing parties. And to Sandra, who, if I was informed correctly, had already reserved a place for me in the -80 °C freezer before I even set foot on Freising, most certainly an honor, and who will always be the orchid lady.

And yes, I guess I'll have to include her… my partner in crime, the other photo-lady, the garden-elf, as I believe (and she would agree) the term gnome is more fitting for me than her. I don't think going through another Doom Day will be the same ever again, but I will keep the trophy of our survival as safe as Sam kept Frodo for three full movies. You were the Jean to my Locke these years, and I feel I might have ended inside a barrel filled with disgusting liquid if I didn't have a hand to help me when needed.

To my friends in the distance and not so distant: you know who you are, and my sentimentalism won't be a weapon against me I give willingly. Special mention to my favorite drama queen because, well, what is the world without drama but a dull and boring place? While I write these paragraphs and I remember the good memories, I can truly say: journey before destination, but also: why accept being a stick, when you could become fire?.

To Oscar, for what we have, and for what we are, a matter better discussed away from public ears (or eyes).

Por ultimo a mi familia, que por fin recibirá una respuesta a la pregunta "¿cuando terminas la tesis?". Y en especial a mis padres, porque soy quien soy gracias a ellos, asi que bien podría poner sus nombres como autores del texto.

10 Publications, presentations, collaborations and funding

10.1 Publications

Fuertes, S., Laca, A., Oulego, P., Paredes, B., Rendueles, M. and Díaz, M. (2017). Development and characterization of egg yolk and egg yolk fractions edible films. Food Hydrocolloids, 70, pp.229-239.

https://doi.org/10.1016/j.foodhyd.2017.04.007

Hilgarth, M., **Fuertes, S.**, Ehrmann, M., Vogel, R.F., 2018. *Photobacterium carnosum* sp. nov., isolated from spoiled modified atmosphere packaged poultry meat. Syst Appl Microbiol 41, 44-50

https://doi.org/10.1016/j.syapm.2017.11.002

Hilgarth, M., **Fuertes Perez, S.**, Ehrmann, M. and Vogel, R. (2018). An adapted isolation procedure reveals *Photobacterium* spp. as common spoilers on modified atmosphere packaged meats. Letters in Applied Microbiology, 66(4), pp.262-267.

https://doi.org/10.1111/lam.12860

Fuertes-Perez, S., Hauschild, P., Hilgarth, M., Vogel, R.F., 2019. Biodiversity of *Photobacterium* spp. isolated from meats. Front Microbiol 10, 2399.

https://doi.org/10.3389/fmicb.2019.02399

Fuertes-Perez, S., Hilgarth, M., Vogel, R.F., 2020. Development of a rapid detection method for *Photobacterium* spp. using Loop-mediated isothermal amplification (LAMP). Int J Food Microbiol 334.

https://doi.org/10.1016/j.ijfoodmicro.2020.108805

Erratum in: 10.1016/j.ijfoodmicro.2021.109176

Fuertes-Perez, S., Vogel, R.F., Hilgarth, M., 2021. Comparative genomics of *Photobacterium* species from terrestrial and marine habitats. Curr Res Microb Sci 2.

https://doi.org/10.1016/j.crmicr.2021.100087

Fuertes-Perez, S., Abele, M., Ludwig, C., Vogel, R.F., Hilgarth, M., 2022. Impact of modified atmospheres on growth and metabolism of meat-spoilage relevant *Photobacterium* spp. as predicted by comparative proteomics. Submitted manuscript.

10.2 Presentations at academic symposia

Fuertes-Perez, S., 2019. *Photobacterium carnosum*: a novel underestimated psychrophilic meat spoiler. Poster presentation. Microbial Diversity Conference, Italian Society of Food, Agricultural and Environmental Microbiology (SIMTREA). Presented the 25.09.2019 in Catania, Italy.

Fuertes-Perez, S., 2019. Biodiversity of *Photobacterium* spp. isolated from meats. Poster presentation. Innovations in Food Packaging, Shelf Life and Food Safety Conference, Fraunhofer Institute for Process Engineering and Packaing IVV. Presented the 08.10.2019 in Erding, Germany.

10.3 Oral presentations at meetings of the steering committee (AiF 20113N)

Fuertes-Perez, S., Hilgarth, M., Vogel, R.F. 2018. Origin and control of photobacteria in meat spoilage. Oral presentation as an annual project update meeting of the AiF steering committee. Dated 29.11.2018, Freising, Germany.

Fuertes-Perez, S., Hilgarth, M., Vogel, R.F. 2019. Biodiversity and detection of photobacteria on meat. Oral presentation as an annual project update meeting of the AiF steering committee. Dated 28.11.2019, Freising, Germany.

Fuertes-Perez, S., Hilgarth, M., Vogel, R.F. 2020. Comparative genomics of *Photobacterium* spp. relevant on meat spoilage. Oral presentation as an annual project update meeting of the AiF steering committee. Dated 26.11.2020, Freising, Germany.

Fuertes-Perez, S., Hilgarth, M., Vogel, R.F. 2021. Growth and comparative proteomics of photobacteria under modified atmospheres. Oral presentation as an annual project update meeting of the AiF steering committee. Dated 20.07.2021, Freising, Germany.

10.4 Collaboration

Mass spectrometry measurements for the comparative proteomics study (Section 6.3) were performed by the Bayerisches Zentrum für Biomolekulare MassenSpektrometrie (BayBioMS, Freising, Germany).

11 Funding

The work of this thesis was part of the project “Kontrolle psychrophiler Photobackterien beim Fleischverderb” (“Control of psychrophilic photobacteria on meat spoilage”), funded by the Federal Ministry for Economic Affairs and Climate Action (BMWK) via the German Federation of Industrial Research Associations (AiF) and the Industry Association for Food Technology and Packaging (IVLV) under the project number AiF 20113N1.

12 List of abbreviations

°C	Celsius degree
ANI	Average Nucleotide Identity
B.	Brochothrix
BHI	Brain-Heart Infusion
CFU	Colony Forming Unit
DMSO	Dimethylsulfoxid
DMSZ	Deutsche Sammlung von Mikroorganismen und Zellkulturen
E/SSO	Ephemeral or Specific Spoilage Organisms
FAO	Food and Agriculture Organization of the United Nations
g	Gram
GABA	γ-aminobutyric acid
h	Hour
HGT	Horizontal Gene Transfer
KDPG pathway	2-dehydro-3-deoxy-phosphogluconate Pathway or Entner-Doudoroff route
L	Litre
LAMP	Loop-Mediated Isothermal Amplification
LC-MS/MS	Liquid Chromatography with Tandem Mass Spectrometry
MA	Marine Agar
MALDI-TOF MS	Matrix-assisted Lasser Desorption/ionization Time-of-flight Mass Spectrometry
MAP	Modified Atmosphere Packaging
MB	Marine Broth
mg	Miligram
ml	Mililitre
MLSA	Multilocus Sequence Alignment
mM	Milimolar
P.	Photobacterium
PCR	Polymerase Chain Reaction
ppm	Parts Per Million
RAPD	Random Amplified Polymorphic DNA
spp./sp.	Species (several/one)
TCA cycle	Tricarboxylic acid cycle
TCBS	Thiosulfate Citrate Bile Sucrose
TMA	Trimethylamine
TMAO	Trimethylamine-N-Oxide
TMW	Lehrstuhl für Technische Mikrobiologie
TSA	Tryptic Soy Agar
TVC	Total Viable Count
UV	Ultraviolet
w/v	Weight per Volume
µg	Microgram

14 References

Aliani, M., Farmer, L.J., 2005a. Precursors of chicken flavor. I. Determination of some flavor precursors in chicken muscle. J Agric Food Chem 53, 6067-6072.

Aliani, M., Farmer, L.J., 2005b. Precursors of chicken flavor. II. Identification of key flavor precursors using sensory methods. J Agric Food Chem 53, 6455-6462.

Allen, E.E., Bartlett, D.H., 2000. *Fab*F is required for piezoregulation of cis-vaccenic acid levels and piezophilic growth of the deep-sea bacterium *Photobacterium profundum* strain SS9. J Bacteriol 182, 1264-1271.

Amanatidou, A., 2001. High oxygen as an additional factor in food preservation, S.l.

Argyri, A.A., Doulgeraki, A.I., Blana, V.A., Panagou, E.Z., Nychas, G.J., 2011. Potential of a simple HPLC-based approach for the identification of the spoilage status of minced beef stored at various temperatures and packaging systems. Int J Food Microbiol 150, 25-33.

Attar, N., 2015. How CRISPR captures spacer invaders. Nat Rev Microbiol 13, 738-739.

Baindara, P., Chaudhry, V., Mittal, G., Liao, L.M., Matos, C.O., Khatri, N., Franco, O.L., Patil, P.B., Korpole, S., 2016. Characterization of the antimicrobial peptide penisin, a class Ia novel lantibiotic from *Paenibacillus* sp. strain A3. Antimicrob Agents Chemother 60, 580-591.

Balado, M., Benzekri, H., Labella, A.M., Claros, M.G., Manchado, M., Borrego, J.J., Osorio, C.R., Lemos, M.L., 2017. Genomic analysis of the marine fish pathogen *Photobacterium damselae* subsp. *piscicida*: insertion sequences proliferation is associated with chromosomal reorganisations and rampant gene decay. Infect Genet Evol 54, 221-229.

Baquero, F., Lanza, V.F., Baquero, M.R., Del Campo, R., Bravo-Vazquez, D.A., 2019. Microcins in *Enterobacteriaceae*: peptide antimicrobials in the eco-active intestinal chemosphere. Front Microbiol 10, 2261.

Barrett, E., Kwan, H., 1985. Bacterial reduction of trimethylamine oxide. Annu Rev Microbiol 39, 131-149.

Bassey, A.P., Chen, Y., Zhu, Z., Odeyemi, O.A., Gao, T., Olusola, O.O., Ye, K., Li, C., Zhou, G., 2021. Evaluation of spoilage indexes and bacterial community dynamics of modified atmosphere packaged super-chilled pork loins. Food Control 130, 108383.

Beijerinck, M.W., 1889. Le Photobacterium luminosum. Bactérie luminosum de la Mer Nord. Arch Néerl Sci 23, 401-427.

Belcher, J.N., 2006. Industrial packaging developments for the global meat market. Meat Sci 74, 143-148.

Bjornsdottir-Butler, K., Abraham, A., Harper, A., Dunlap, P.V., Benner, R.A., Jr., 2018. Biogenic amine production by and phylogenetic analysis of 23 *Photobacterium* species. J Food Prot 81, 1264-1274.

Bjornsdottir-Butler, K., May, S., Hayes, M., Abraham, A., Benner, R.A., Jr., 2020. Characterization of a novel enzyme from *Photobacterium phosphoreum* with histidine decarboxylase activity. Int J Food Microbiol 334, 108815.

Bjornsdottir, K., Bolton, G.E., McClellan-Green, P.D., Jaykus, L.A., Green, D.P., 2009. Detection of gram-negative histamine-producing bacteria in fish: a comparative study. J Food Prot 72, 1987-1991.

Bohrer, B.M., 2017. Review: nutrient density and nutritional value of meat products and non-meat foods high in protein. Trends Food Sci Technol 65, 103-112.

Bouju-Albert, A., Pilet, M.F., Guillou, S., 2018. Influence of lactate and acetate removal on the microbiota of French fresh pork sausages. Food Microbiol 76, 328-336.

Brodl, E., Winkler, A., Macheroux, P., 2018. Molecular mechanisms of bacterial bioluminescence. Comput Struct Biotechnol J 16, 551-564.

Bryant, C., Barnett, J., 2020. Consumer acceptance of cultured meat: an updated review (2018–2020). Appl Sci 10.

Budsberg, K.J., Wimpee, C.F., Braddock, J.F., 2003. Isolation and identification of *Photobacterium phosphoreum* from an unexpected niche: migrating salmon. Appl Environ Microbiol 69, 6938-6942.

Campanaro, S., Vezzi, A., Vitulo, N., Lauro, F.M., D'Angelo, M., Simonato, F., Cestaro, A., Malacrida, G., Bertoloni, G., Valle, G., Bartlett, D.H., 2005. Laterally transferred elements and high pressure adaptation in *Photobacterium profundum* strains. BMC Genomics 6, 122.

Cangelosi, G.A., Meschke, J.S., 2014. Dead or alive: molecular assessment of microbial viability. Appl Environ Microbiol 80, 5884-5891.

Casaburi, A., Piombino, P., Nychas, G.J., Villani, F., Ercolini, D., 2015. Bacterial populations and the volatilome associated to meat spoilage. Food Microbiol 45, 83-102.

Cauchie, E., Delhalle, L., Taminiau, B., Tahiri, A., Korsak, N., Burteau, S., Fall, P.A., Farnir, F., Baré, G., Daube, G., 2020. Assessment of spoilage bacterial communities in food wrap

and modified atmospheres-packed minced pork meat samples by 16S rDNA metagenetic analysis. Front Microbiol 10.

Chaillou, S., Chaulot-Talmon, A., Caekebeke, H., Cardinal, M., Christieans, S., Denis, C., Desmonts, M.H., Dousset, X., Feurer, C., Hamon, E., Joffraud, J.J., La Carbona, S., Leroi, F., Leroy, S., Lorre, S., Macé, S., Pilet, M.F., Prévost, H., Rivollier, M., Roux, D., Talon, R., Zagorec, M., Champomier-Vergès, M.C., 2015. Origin and ecological selection of core and food-specific bacterial communities associated with meat and seafood spoilage. ISME J 9, 1105-1118.

Chen, X., Zhao, J., Zhu, L., Luo, X., Mao, Y., Hopkins, D.L., Zhang, Y., Dong, P., 2020. Effect of modified atmosphere packaging on shelf life and bacterial community of roast duck meat. Food Research International 137, 109645.

Cho, C.E., Taesuwan, S., Malysheva, O.V., Bender, E., Tulchinsky, N.F., Yan, J., Sutter, J.L., Caudill, M.A., 2017. Trimethylamine-N-oxide (TMAO) response to animal source foods varies among healthy young men and is influenced by their gut microbiota composition: a randomized controlled trial. Mol Nutr Food Res 61.

Church, I.J., Parsons, A.L., 1995. Modified atmosphere packaging technology: a review. J Sci Food Agric 67, 143-152.

Cobos, Á., Díaz, O., 2015. Chemical composition of meat and meat products, in: Cheung, P.C.K., Mehta, B.M. (Eds.), Handbook of Food Chemistry. Springer Berlin Heidelberg, Berlin, Heidelberg, pp. 471-510.

Comi, G., 2017. Spoilage of Meat and Fish, in: Bevilacqua, A., Corbo, M.R., Sinigaglia, M. (Eds.), The Microbiological Quality of Food. Woodhead Publishing, pp. 179-210.

Cornforth, D.P., Hunt, M.C., 2008. Low-oxygen packaging of fresh meat with carbon monoxide: meat quality, microbiology, and safety. NFS Faculty Publications.

Dalgaard, P., 1995. Qualitative and quantitative characterization of spoilage bacteria from packed fish. Int J Food Microbiol 26, 319-333.

Dalgaard, P., Garcia Munoz, L., Mejlholm, O., 1998. Specific inhibition of *Photobacterium phosphoreum* extends the shelf life of modified-atmosphere-packed cod fillets. J Food Prot 61, 1191-1194.

Dalgaard, P., Manfio, G.P., Goodfellow, M., 1997. Classification of photobacteria associated with spoilage of fish products by numerical taxonomy and pyrolysis mass spectrometry. Zentralbl Bakteriol 285, 157-168.

Dalgaard, P., Mejlholm, O., Huss, H.H., 1996. Conductance method for quantitative determination of *Photobacterium phosphoreum* in fish products. J Appl Microbiol 81, 57-64.

Daniels, J.A., Krishnamurthi, R., Rizvi, S.S.H., 1985. A review of effects of carbon dioxide on microbial growth and food quality. J Food Prot 48, 532-537.

Delhalle, L., Korsak, N., Taminiau, B., Nezer, C., Burteau, S., Delcenserie, V., Poullet, J.B., Daube, G., 2016. Exploring the bacterial diversity of Belgian steak tartare using metagenetics and quantitative real-time PCR analysis. J Food Prot 79, 220-229.

Djenane, D., Roncalés, P., 2018. Carbon monoxide in meat and fish packaging: advantages and limits. Foods 7, 12.

Doulgeraki, A.I., Ercolini, D., Villani, F., Nychas, G.J., 2012. Spoilage microbiota associated to the storage of raw meat in different conditions. Int J Food Microbiol 157, 130-141.

Dourou, D., Spyrelli, E.D., Doulgeraki, A.I., Argyri, A.A., Grounta, A., Nychas, G.-J.E., Chorianopoulos, N.G., Tassou, C.C., 2021. Microbiota of chicken breast and thigh fillets stored under different refrigeration temperatures assessed by next-generation sequencing. Foods 10, 765.

Dunlap, P.V., Ast, J.C., 2005. Genomic and phylogenetic characterization of luminous bacteria symbiotic with the deep-sea fish *Chlorophthalmus albatrossis* (Aulopiformes: *Chlorophthalmidae*). Appl Environ Microbiol 71, 930-939.

Duthoo, E., Rasschaert, G., Leroy, F., Weckx, S., Heyndrickx, M., De Reu, K., 2021. The microbiota of modified-atmosphere-packaged cooked charcuterie products throughout their shelf-life period, as revealed by a complementary combination of culture-dependent and culture-independent analysis. Microorganisms 9, 1223.

Efenberger-Szmechtyk, M., Gałązka-Czarnecka, I., Otlewska, A., Czyżowska, A., Nowak, A., 2021. *Aronia melanocarpa* (Michx.) Elliot, *Chaenomeles superba* Lindl. and *Cornus mas* L. leaf extracts as natural preservatives for pork meat products. Molecules 26, 3009.

Eilert, S.J., 2005. New packaging technologies for the 21st century. Meat Sci 71, 122-127.

Elango, R., 2020. Methionine nutrition and metabolism: insights from animal studies to inform human nutrition. J Nutr 150, 2518S-2523S.

Emborg, J., Laursen, B.G., Rathjen, T., Dalgaard, P., 2002. Microbial spoilage and formation of biogenic amines in fresh and thawed modified atmosphere-packed salmon (*Salmo salar*) at 2 degrees C. J Appl Microbiol 92, 790-799.

Ercolini, D., Ferrocino, I., La Storia, A., Mauriello, G., Gigli, S., Masi, P., Villani, F., 2010. Development of spoilage microbiota in beef stored in nisin activated packaging. Food Microbiol 27, 137-143.

Ercolini, D., Russo, F., Torrieri, E., Masi, P., Villani, F., 2006. Changes in the spoilage-related microbiota of beef during refrigerated storage under different packaging conditions. Appl Environ Microbiol 72, 4663-4671.

Erichsen, I., Molin, G., 1981. Microbial flora of normal and high pH beef stored at 4 C in different gas environments. J Food Prot 44, 866-869.

Eskin, N.A.M., Shahidi, F., 2012. Biochemistry of foods, 3rd ed. Elsevier, London.

Estevez, M., 2011. Protein carbonyls in meat systems: a review. Meat Sci 89, 259-279.

FAO, 2011. Global food losses and food waste - extent, causes and prevention., Rome, Italy.

FAO, 2021. Food Outlook - Biannual report on global food markets. FAO, Rome, Italy.

Farber, J.M., 1991. Microbiological aspects of modified-atmosphere packaging technology - a review. J Food Prot 54, 58-70.

Feiner, G., 2006. The protein and fat content of meat, Meat products handbook. Practical science and technology. Woodhead Publishing Limited, Cambridge, England, pp. p.1-32.

Flores, M., 2017. The eating quality of meat: III — flavor, Lawrie´ s Meat Science. Elsevier, pp. 383-417.

Fuertes-Perez, S., Abele, M., Ludwig, C., Vogel, R.F., Hilgarth, M., 2022. Impact of modified atmospheres on growth and metabolism of meat-spoilage relevant *Photobacterium* spp. as predicted by comparative proteomics. Submitted manuscript.

Fuertes-Perez, S., Hauschild, P., Hilgarth, M., Vogel, R.F., 2019. Biodiversity of *Photobacterium* spp. isolated from meats. Front Microbiol 10.

Fuertes-Perez, S., Hilgarth, M., Vogel, R.F., 2020. Development of a rapid detection method for *Photobacterium* spp. using loop-mediated isothermal amplification (LAMP). Int J Food Microbiol 334.

Fuertes-Perez, S., Vogel, R.F., Hilgarth, M., 2021. Comparative genomics of *Photobacterium* species from terrestrial and marine habitats. CRMICR 2.

Gill, C.O., Tan, K.H., 1980. Effect of carbon dioxide on growth of meat spoilage bacteria. Appl Environ Microbiol 39, 317-319.

Goto, M., Honda, E., Ogura, A., Nomoto, A., Hanaki, K.-I., 2009. Colorimetric detection of loop-mediated isothermal amplification reaction by using hydroxy naphthol blue. BioTechniques 46, 167-172.

Gram, L., Dalgaard, P., 2002. Fish spoilage bacteria – problems and solutions. Curr Opin Biotechnol 13, 262-266.

Gram, L., Huss, H.H., 1996. Microbiological spoilage of fish and fish products. Int J Food Microbiol 33, 121-137.

Gram, L., Ravn, L., Rasch, M., Bruhn, J.B., Christensen, A.B., Givskov, M., 2002. Food spoilage - interactions between food spoilage bacteria. Int J Food Microbiol 78, 79-97.

Greppi, A., Ferrocino, I., La Storia, A., Rantsiou, K., Ercolini, D., Cocolin, L., 2015. Monitoring of the microbiota of fermented sausages by culture independent rRNA-based approaches. Int J Food Microbiol 212, 67-75.

Gu, J., Neary, J., Cai, H., Moshfeghian, A., Rodriguez, S.A., Lilburn, T.G., Wang, Y., 2009. Genomic and systems evolution in *Vibrionaceae* species. BMC Genomics 10 Suppl 1, S11.

Guillaume, J., Kaushik, S., Bergot, P., Metailler, R., 2001. Nutrition and feeding of fish and crustaceans, 1st ed. Springer Publishing House, London.

Hansen, A.Å., Langsrud, S., Berget, I., Gaarder, M.Ø., Moen, B., 2021. High oxygen packaging of atlantic cod fillets inhibits known spoilage organisms, but sensory quality is not improved due to the growth of *Carnobacterium/Carnobacteriaceae*. Foods 10, 1754.

Hauschild, P., Hilgarth, M., Vogel, R.F., 2020. Hydrostatic pressure- and halotolerance of *Photobacterium phosphoreum* and *P. carnosum* isolated from spoiled meat and salmon. Food Microbiol, 103679.

Hauschild, P., Vogel, R.F., Hilgarth, M., 2021. Influence of the packaging atmosphere and presence of co-contaminants on the growth of photobacteria on chicken meat. Int J Food Microbiol 351, 109264.

Hauschild, P., Vogel, R.F., Hilgarth, M., 2022. Transcriptomic analysis of the response of *Photobacterium phosphoreum* and *Photobacterium carnosum* to co-contaminants on chicken meat. Submitted manuscript.

Hazards, E.P.o.B., Koutsoumanis, K., Allende, A., Alvarez-Ordonez, A., Bolton, D., Bover-Cid, S., Chemaly, M., Davies, R., De Cesare, A., Herman, L., Nauta, M., Peixe, L., Ru, G., Simmons, M., Skandamis, P., Suffredini, E., Jacxsens, L., Skjerdal, T., Da Silva Felicio, M.T., Hempen, M., Messens, W., Lindqvist, R., 2020. Guidance on date marking and related food information: part 1 (date marking). EFSA J 18, e06306.

Hendrie, M.S., Hodgkiss, W., Shewan, J.M., 1970. The identification, taxonomy and classification of luminous bacteria. Microbiology 64, 151-169.

Henrissat, B., Deleury, E., Coutinho, P.M., 2002. Glycogen metabolism loss: a common marker of parasitic behaviour in bacteria? Trends Genet 18, 437-440.

Hilgarth, M., Fuertes-Perez, S., Ehrmann, M., Vogel, R.F., 2018a. An adapted isolation procedure reveals *Photobacterium* spp. as common spoilers on modified atmosphere packaged meats. Lett Appl Microbiol 66, 262-267.

Hilgarth, M., Fuertes, S., Ehrmann, M., Vogel, R.F., 2018b. *Photobacterium carnosum* sp. nov., isolated from spoiled modified atmosphere packaged poultry meat. Syst Appl Microbiol 41, 44-50.

Himes, P., 2017. Studies toward understanding the biosynthesis of sactipeptides and the creation of peptide natural product libraries through mRNA display, Eshelman School of Pharmacy, Division of Chemical Biology and Medicinal Chemistry.

Höll, L., Behr, J., Vogel, R.F., 2016. Identification and growth dynamics of meat spoilage microorganisms in modified atmosphere packaged poultry meat by MALDI-TOF MS. Food Microbiol 60, 84-91.

Höll, L., Hilgarth, M., Geissler, A.J., Behr, J., Vogel, R.F., 2019. Prediction of *in situ* metabolism of photobacteria in modified atmosphere packaged poultry meat using metatranscriptomic data. Microbiol Res 222, 52-59.

Hunt, D.E., Gevers, D., Vahora, N.M., Polz, M.F., 2008. Conservation of the chitin utilization pathway in the *Vibrionaceae*. Appl Environ Microbiol 74, 44-51.

Iammarino, M., Di Taranto, A., 2012. Nitrite and nitrate in fresh meats: a contribution to the estimation of admissible maximum limits to introduce in directive 95/2/EC. Int J Food Sci Technol 47, 1852-1858.

Immonen, K., Puolanne, E., 2000. Variation of residual glycogen-glucose concentration at ultimate pH values below 5.75. Meat Sci 55, 279-283.

Immonen, K., Ruusunen, M., Hissa, K., Puolanne, E., 2000. Bovine muscle glycogen concentration in relation to finishing diet, slaughter and ultimate pH. Meat Sci 55, 25-31.

Jaaskelainen, E., Hultman, J., Parshintsev, J., Riekkola, M.L., Bjorkroth, J., 2016. Development of spoilage bacterial community and volatile compounds in chilled beef under vacuum or high oxygen atmospheres. Int J Food Microbiol 223, 25-32.

Jakobsen, M., Bertelsen, G., 2000. Colour stability and lipid oxidation of fresh beef. Development of a response surface model for predicting the effects of temperature, storage time, and modified atmosphere composition. Meat Sci 54, 49-57.

Jay, J.M., Loessner, M.J., Golden, D.A., 2005. Modern food microbiology, 7th ed. Springer, Boston, MA.

Jayasingh, P., Cornforth, D.P., Brennand, C.P., Carpenter, C.E., Whittier, D.R., 2002. Sensory evaluation of ground beef stored in high-oxygen modified atmosphere packaging. J Food Sci 67, 3493-3496.

Jørgensen, L.V., Dalgaard, P., Huss, H.H., 2000a. Multiple compound quality index for cold-smoked salmon (*Salmo salar)* developed by multivariate regression of biogenic amines and pH. J Agric Food Chem 48, 2448-2453.

Jørgensen, L.V., Huss, H.H., Dalgaard, P., 2000b. The effect of biogenic amine production by single bacterial cultures and metabiosis on cold-smoked salmon. J Appl Microbiol 89, 920-934.

Juszczuk-Kubiak, E., Dekowska, A., Sokołowska, B., Połaska, M., Lendzion, K., 2021. Evaluation of the spoilage-related bacterial profiles of vacuum-packaged chilled ostrich meat by next-generation DNA sequencing approach. Processes 9, 803.

Kargiotou, C., Katsanidis, E., Rhoades, J., Kontominas, M., Koutsoumanis, K., 2011. Efficacies of soy sauce and wine base marinades for controlling spoilage of raw beef. Food Microbiol 28, 158-163.

Kauffman, R.G., 2012. Meat Composition, Handbook of Meat and Meat Processing. CRC Press.

Khaldi, N., Collemare, J., Lebrun, M.-H., Wolfe, K.H., 2008. Evidence for horizontal transfer of a secondary metabolite gene cluster between fungi. Genome Biol 9, R18.

Koike, I., Hattori, A., 1978. Denitrification and ammonia formation in anaerobic coastal sediments. Appl Environ Microbiol 35, 278-282.

Kolbeck, S., Ludwig, C., Meng, C., Hilgarth, M., Vogel, R.F., 2020. Comparative proteomics of meat spoilage bacteria predicts drivers for their coexistence on modified atmosphere packaged meat. Front Microbiol 11, 209.

Kolbeck, S., Reetz, L., Hilgarth, M., Vogel, R.F., 2019. Quantitative oxygen consumption and respiratory activity of meat spoiling bacteria upon high oxygen modified atmosphere. Front Microbiol 10, 2398.

Koo, O.K., Baker, C.A., Kim, H.J., Park, S.H., Ricke, S.C., 2016. Metagenomic assessment of the microbial diversity in ground pork products from markets in the North Central Region of South Korea. J Environ Sci Health B 51, 622-627.

Koutsidis, G., Elmore, J.S., Oruna-Concha, M.J., Campo, M.M., Wood, J.D., Mottram, D.S., 2008a. Water-soluble precursors of beef flavour. Part I. Effect of diet and breed. Meat Sci 79, 124-130.

Koutsidis, G., Elmore, J.S., Oruna-Concha, M.J., Campo, M.M., Wood, J.D., Mottram, D.S., 2008b. Water-soluble precursors of beef flavour. Part II. Effect of post-mortem conditioning. Meat Sci 79, 270-277.

Koutsoumanis, K., Nychas, G.J., 2000. Application of a systematic experimental procedure to develop a microbial model for rapid fish shelf life predictions. Int J Food Microbiol 60, 171-184.

Koutsoumanis, K., Stamatiou, A., Skandamis, P., Nychas, G.J., 2006. Development of a microbial model for the combined effect of temperature and pH on spoilage of ground meat, and validation of the model under dynamic temperature conditions. Appl Environ Microbiol 72, 124-134.

Koutsoumanis, K.P., Sofos, J.N., 2004. Microbial contamination of carcasses and cuts., in: Jensens, W.K. (Ed.), Encyclopedia of Meat Sciences. Elsevier Academic Press, Amsterdam, pp. 727-737.

Kuang, G., Xiao, A., Chen, Q., Chen, X., Zhang, D., Wang, H., Sun, Z., 2012. Characterization of PB-CS01, a novel *Photobacterium* strain isolated from commercial pork. J Anim Vet Adv 11, 4292-4296.

Labella, A.M., Castro, M.D., Manchado, M., Borrego, J.J., 2018. Description of new and amended clades of the genus *Photobacterium*. Microorganisms 6.

Lauro, F.M., Eloe-Fadrosh, E.A., Richter, T.K., Vitulo, N., Ferriera, S., Johnson, J.H., Bartlett, D.H., 2014. Ecotype diversity and conversion in *Photobacterium profundum* strains. PLOS ONE 9, e96953.

Lawrie, R.A., Ledward, D.A., 2006. Lawrie's meat science, 7th ed. Woodhead Publishing Limited, Cambridge.

Lee, P.A., de Mora, S.J., Levasseur, M., 1999. A review of dimethylsulfoxide in aquatic environments. Atmos - Ocean 37, 439-456.

Lehane, L., Olley, J., 2000. Histamine fish poisoning revisited. Int J Food Microbiol 58, 1-37.

Leverve, X., Batandier, C., Fontaine, E., 2007. Choosing the right substrate. Novartis Found Symp 280, 108-121; discussion 121-107, 160-104.

Lewis, E.D., Zhao, Y.-Y., Richard, C., Bruce, H.L., Jacobs, R.L., Field, C.J., Curtis, J.M., 2015. Measurement of the abundance of choline and the distribution of choline-containing moieties in meat. Int J Food Sci Nutr 66, 743-748.

Li, N., Zhang, Y., Wu, Q., Gu, Q., Chen, M., Zhang, Y., Sun, X., Zhang, J., 2019. High-throughput sequencing analysis of bacterial community composition and quality characteristics in refrigerated pork during storage. Food Microbiol 83, 86-94.

Li, R., Tun, H.M., Jahan, M., Zhang, Z., Kumar, A., Dilantha Fernando, W.G., Farenhorst, A., Khafipour, E., 2017. Comparison of DNA-, PMA-, and RNA-based 16S rRNA Illumina sequencing for detection of live bacteria in water. Sci Rep 7, 5752-5752.

Lilburn, T.G., Gu, J., Cai, H., Wang, Y., 2010. Comparative genomics of the family *Vibrionaceae* reveals the wide distribution of genes encoding virulence-associated proteins. BMC Genomics 11, 369.

López-Bote, C., 2017. Chemical and Biochemical Constitution of Muscle, in: Toldra, F. (Ed.), Lawrie´s meat science, 8th ed. Woodhead Publishing, pp. 99-158.

López Caballero, M.E., Álvarez, M.D., Sánchez Fernández, J.A., Moral, A., 2002. *Photobacterium phosphoreum* isolated as a luminescent colony from spoiled fish, cultured in model system under controlled atmospheres. Eur. Food Res. Technol. 215, 390-395.

Luño, M., Beltrán, J.A., Roncalés, P., 1998. Shelf-life extension and colour stabilisation of beef packaged in a low O_2 atmosphere containing CO: Loin steaks and ground meat. Meat Sci 48, 75-84.

Lytou, A.E., Panagou, E.Z., Nychas, G.E., 2017. Effect of different marinating conditions on the evolution of spoilage microbiota and metabolomic profile of chicken breast fillets. Food Microbiol 66, 141-149.

Macé, S., Mamlouk, K., Chipchakova, S., Prévost, H., Joffraud, J.-J., Dalgaard, P., Pilet, M.-F., Dousset, X., 2013. Development of a rapid real-time PCR method as a tool to quantify viable *Photobacterium phosphoreum* bacteria in salmon (*Salmo salar*) steaks. Appl Environ Microbiol 79, 2612-2619.

Machado, H., Giubergia, S., Mateiu, R.V., Gram, L., 2015. *Photobacterium galatheae* sp. *nov*., a bioactive bacterium isolated from a mussel in the Solomon Sea. Int J Syst Evol Microbiol 65, 4503-4507.

Machado, H., Gram, L., 2017. Comparative genomics reveals high genomic diversity in the genus *Photobacterium*. Front Microbiol 8, 1204.

Machado, H., Månsson, M., Gram, L., 2014. Draft genome sequence of *Photobacterium halotolerans* S2753, producer of bioactive secondary metabolites. Genome Announc 2, e00535-00514.

Makarova, K.S., Wolf, Y.I., Alkhnbashi, O.S., Costa, F., Shah, S.A., Saunders, S.J., Barrangou, R., Brouns, S.J.J., Charpentier, E., Haft, D.H., Horvath, P., Moineau, S., Mojica, F.J.M., Terns, R.M., Terns, M.P., White, M.F., Yakunin, A.F., Garrett, R.A., van der Oost, J., Backofen, R., Koonin, E.V., 2015. An updated evolutionary classification of CRISPR–Cas systems. Nat Rev Microbiol 13, 722-736.

Man, D., 2015. Shelf life. John Wiley & Sons, Inc., West Sussex, England.

Mancini, R.A., Hunt, M.C., 2005. Current research in meat color. Meat Sci 71, 100-121.

Matanza, X.M., Osorio, C.R., 2018. Transcriptome changes in response to temperature in the fish pathogen *Photobacterium damselae* subsp. *damselae*: clues to understand the emergence of disease outbreaks at increased seawater temperatures. PLOS ONE 13, e0210118.

McKee, L., 2007. Microbiological and sensory properties of fresh and frozen pork products, Handbook of meat, poultry and seafood quality, pp. 395-404.

McMillin, K.W., 2008. Where is MAP going? A review and future potential of modified atmosphere packaging for meat. Meat Sci 80, 43-65.

McMillin, K.W., Huang, N.Y., Ho, C.P., Smith, B.S., 1999. Quality and shelf-life of meat in case-ready modified atmosphere packaging, in: Xiong, Y.L., Chi-Tang, H., Shahidi, F. (Eds.), Quality Attributes of Muscle Foods. Springer US, Boston, MA, pp. 73-93.

Meinert, L., Schäfer, A., Bjergegaard, C., Aaslyng, M.D., Bredie, W.L.P., 2009a. Comparison of glucose, glucose 6-phosphate, ribose, and mannose as flavour precursors in pork; the effect of monosaccharide addition on flavour generation. Meat Sci 81, 419-425.

Meinert, L., Tikk, K., Tikk, M., Brockhoff, P.B., Bredie, W.L.P., Bjergegaard, C., Aaslyng, M.D., 2009b. Flavour development in pork. Influence of flavour precursor concentrations in longissimus dorsi from pigs with different raw meat qualities. Meat Sci 81, 255-262.

Meredith, H., Valdramidis, V., Rotabakk, B.T., Sivertsvik, M., McDowell, D., Bolton, D.J., 2014. Effect of different modified atmospheric packaging (MAP) gaseous combinations on *Campylobacter* and the shelf-life of chilled poultry fillets. Food Microbiol 44, 196-203.

Moran, M.A., Belas, R., Schell, M.A., Gonzalez, J.M., Sun, F., Sun, S., Binder, B.J., Edmonds, J., Ye, W., Orcutt, B., Howard, E.C., Meile, C., Palefsky, W., Goesmann, A., Ren, Q., Paulsen, I., Ulrich, L.E., Thompson, L.S., Saunders, E., Buchan, A., 2007. Ecological genomics of marine Roseobacters. Appl Environ Microbiol 73, 4559-4569.

Møretrø, T., Langsrud, S., 2017. Residential bacteria on surfaces in the food industry and their implications for food safety and quality. Compr Rev Food Sci Food Saf 16, 1022-1041.

Mori, Y., Kitao, M., Tomita, N., Notomi, T., 2004. Real-time turbidimetry of LAMP reaction for quantifying template DNA. J Biochem Biophys Methods 59, 145-157.

Mori, Y., Nagamine, K., Tomita, N., Notomi, T., 2001. Detection of loop-mediated isothermal amplification reaction by turbidity derived from magnesium pyrophosphate formation. Biochem Biophys Res Commun 289, 150-154.

Morii, H., Kasama, K., 2004. Activity of two histidine decarboxylases from *Photobacterium phosphoreum* at different temperatures, pHs, and NaCl concentrations. J Food Prot 67, 1736-1742.

Morita, R.Y., 1997. Bacteria in oligotrophic environments: starvation-survival lifestyle. New York (N.Y.) : Chapman and Hall.

Nealson, K.H., 1978. Isolation, identification, and manipulation of luminous bacteria, Methods in Enzymology. Academic Press, pp. 153-166.

Nealson, K.H., Hastings, J.W., 1979. Bacterial bioluminescence: its control and ecological significance. Microbiol Rev 43, 496-518.

Nielsen, A., Månsson, M., Bojer, M.S., Gram, L., Larsen, T.O., Novick, R.P., Frees, D., Frøkiær, H., Ingmer, H., 2014. Solonamide B inhibits quorum sensing and reduces *Staphylococcus aureus* mediated killing of human neutrophils. PLOS ONE 9, e84992.

Nieminen, T.T., Dalgaard, P., Björkroth, J., 2016. Volatile organic compounds and *Photobacterium phosphoreum* associated with spoilage of modified-atmosphere-packaged raw pork. Int J Food Microbiol 218, 86-95.

Ninios, T., Lundén, J., Korkeala, H., Fredriksson-Ahomaa, M., 2014. Meat inspection and control in the slaughterhouse, 1st ed. John Wiley & Sons, New York.

Nychas, G.-J., Marshall, D.L., Sofos, J., 2007. Meat, poultry, and seafood. Food Microbiology: Fundamentals and Frontiers, 105-140.

Nychas, G.-J.E., Skandamis, P.N., Tassou, C.C., Koutsoumanis, K.P., 2008. Meat spoilage during distribution. Meat Sci 78, 77-89.

Olofsson, T.C., Ahrné, S., Molin, G., 2007. The bacterial flora of vacuum-packed cold-smoked salmon stored at 7 degrees C, identified by direct 16S rRNA gene analysis and pure culture technique. J Appl Microbiol 103, 109-119.

Onwezen, M.C., Bouwman, E.P., Reinders, M.J., Dagevos, H., 2021. A systematic review on consumer acceptance of alternative proteins: pulses, algae, insects, plant-based meat alternatives, and cultured meat. Appetite 159, 105058.

Pan, N., Imlay, J.A., 2001. How does oxygen inhibit central metabolism in the obligate anaerobe *Bacteroides thetaiotaomicron*. Mol Microbiol 39, 1562-1571.

Parte, A.C., Sarda Carbasse, J., Meier-Kolthoff, J.P., Reimer, L.C., Goker, M., 2020. List of prokaryotic names with standing in nomenclature (LPSN) moves to the DSMZ. Int J Syst Evol Microbiol 70, 5607-5612.

Pennacchia, C., Ercolini, D., Villani, F., 2011. Spoilage-related microbiota associated with chilled beef stored in air or vacuum pack. Food Microbiol 28, 84-93.

Pereira, P.M., Vicente, A.F., 2013. Meat nutritional composition and nutritive role in the human diet. Meat Sci 93, 586-592.

Pethick, D., Rowe, J., Tudor, G., 1995. Glycogen metabolism and meat quality.

Pini, F., Aquilani, C., Giovannetti, L., Viti, C., Pugliese, C., 2020. Characterization of the microbial community composition in Italian Cinta Senese sausages dry-fermented with natural extracts as alternatives to sodium nitrite. Food Microbiol 89, 103417.

Pitcher, R.S., Watmough, N.J., 2004. The bacterial cytochrome cbb3 oxidases. Biochim Biophys Acta 1655, 388-399.

Poirier, S., Luong, N.-D.M., Anthoine, V., Guillou, S., Membré, J.-M., Moriceau, N., Rezé, S., Zagorec, M., Feurer, C., Frémaux, B., Jeuge, S., Robieu, E., Champomier-Vergès, M., Coeuret, G., Cauchie, E., Daube, G., Korsak, N., Coroller, L., Desriac, N., Desmonts, M.-H., Gohier, R., Werner, D., Loux, V., Rué, O., Dohollou, M.-H., Defosse, T., Chaillou, S., 2020. Large-scale multivariate dataset on the characterization of microbiota diversity, microbial growth dynamics, metabolic spoilage volatilome and sensorial profiles of two industrially produced meat products subjected to changes in lactate concentration and packaging atmosphere. Data Br 30, 105453.

Pösö, A.R., Puolanne, E., 2005. Carbohydrate metabolism in meat animals. Meat Sci 70, 423-434.

Pratt, D., 1963. Specificity of the solute requirement by marine bacteria on primary isolation from sea-water. Nature 199, 1308-1308.

PRB, 2021. 2021 World Population Data Sheet. PRB.

Reen, F.J., Almagro-Moreno, S., Ussery, D., Boyd, E.F., 2006. The genomic code: inferring *Vibrionaceae* niche specialization. Nat Rev Microbiol 4, 697-704.

Reichelt, J.L., Baumann, P., 1973. Taxonomy of the marine, luminous bacteria. Arch Mikrobiol 94, 283-330.

Reynisson, E., Lauzon, H.L., Magnússon, H., Jónsdóttir, R., Ólafsdóttir, G., Marteinsson, V., Hreggviðsson, G.Ó., 2009. Bacterial composition and succession during storage of North-Atlantic cod (*Gadus morhua*) at superchilled temperatures. BMC Microbiol 9, 250.

Rossaint, S., Klausmann, S., Kreyenschmidt, J., 2015. Effect of high-oxygen and oxygen-free modified atmosphere packaging on the spoilage process of poultry breast fillets. Poult Sci 94, 96-103.

Rouger, A., Tresse, O., Zagorec, M., 2017. Bacterial contaminants of poultry meat: sources, species, and dynamics. Microorganisms 5, 50.

Ruby, E., Greenberg, E., Hastings, J., 1980. Planktonic marine luminous bacteria: species distribution in the water column. Appl Environ Microbiol 39, 302-306.

Säde, E., Penttinen, K., Björkroth, J., Hultman, J., 2017. Exploring lot-to-lot variation in spoilage bacterial communities on commercial modified atmosphere packaged beef. Food Microbiol 62, 147-152.

Sante, V., Renerre, M., Lacourt, A., 1994. Effect of modified atmosphere packaging on color stability and on microbiology of turkey breast meat. J Food Qual 17, 177-195.

Sawabe, T., Kita-Tsukamoto, K., Thompson, F.L., 2007. Inferring the evolutionary history of vibrios by means of multilocus sequence analysis. J Bacteriol 189, 7932-7936.

Ščetar, M., Kurek, M., Galić, K., 2010. Trends in meat and meat products packaging-a review. Croat J Food Sci Technol 2, 32-48.

Settanni, L., Barbaccia, P., Bonanno, A., Ponte, M., Di Gerlando, R., Franciosi, E., Di Grigoli, A., Gaglio, R., 2020. Evolution of indigenous starter microorganisms and physicochemical parameters in spontaneously fermented beef, horse, wild boar and pork salamis produced under controlled conditions. Food Microbiol 87, 103385.

Severinov, K., Nair, S.K., 2012. Microcin C: biosynthesis and mechanisms of bacterial resistance. Future Microbiol 7, 281-289.

Sgro, G.G., Oka, G.U., Souza, D.P., Cenens, W., Bayer-Santos, E., Matsuyama, B.Y., Bueno, N.F., Dos Santos, T.R., Alvarez-Martinez, C.E., Salinas, R.K., Farah, C.S., 2019. Bacteria-killing type IV secretion systems. Front Microbiol 10, 1078.

Singh, P., Wani, A.A., Saengerlaub, S., Langowski, H.C., 2011. Understanding critical factors for the quality and shelf-life of MAP fresh meat: a review. Crit Rev Food Sci Nutr 51, 146-177.

Skandamis, P.N., Nychas, G.J., 2002. Preservation of fresh meat with active and modified atmosphere packaging conditions. Int J Food Microbiol 79, 35-45.

Smith, J., Ramaswamy, H., Simpson, B., 1990. Developments in food packaging technology. Part II. Storage aspects. Trends Food Sci Technol Nov, 111-118.

Stanbridge, L.H., Davies, A.R., 1998. Microbiology of chill-stored meat, Microbiology of meat and poultry. Blackie Academic & Professional, London, UK, pp. 174-219.

Stellato, G., Storia, A.L., Filippis, F.D., Borriello, G., Villani, F., Ercolini, D., Elkins, C.A., 2016. Overlap of spoilage-associated microbiota between meat and the meat processing environment in small-scale and large-scale retail distributions. Appl Environ Microbiol 82, 4045-4054.

Stoops, J., Ruyters, S., Busschaert, P., Spaepen, R., Verreth, C., Claes, J., Lievens, B., Van Campenhout, L., 2015. Bacterial community dynamics during cold storage of minced meat packaged under modified atmosphere and supplemented with different preservatives. Food Microbiol 48, 192-199.

Takahashi, H., Ogai, M., Miya, S., Kuda, T., Kimura, B., 2015. Effects of environmental factors on histamine production in the psychrophilic histamine-producing bacterium *Photobacterium iliopiscarium*. Food Control 52, 39-42.

Tanet, L., Tamburini, C., Baumas, C., Garel, M., Simon, G., Casalot, L., 2019. Bacterial bioluminescence: light emission in *Photobacterium phosphoreum* is not under quorum-sensing control. Front Microbiol 10.

Tanner, N.A., Zhang, Y., Evans, T.C., 2015. Visual detection of isothermal nucleic acid amplification using pH-sensitive dyes. BioTechniques 58, 59-68.

Tarr, H.L.A., 1966. Post-mortem changes in glycogen, nucleotides, sugar phosphates, and sugars in fish muscles - a review. J Food Sci 31, 846-854.

Taylor, A.A., Down, N.F., Shaw, B.G., 1990. A comparison of modified atmosphere and vacuum skin packing for the storage of red meats. Int J Food Sci Technol 25, 98-109.

Thakur, M., Modi, V.K., Khedkar, R., Singh, K., 2020. Sustainable food waste management - concepts and innovations, 1 ed. Springer, Singapore.

Thyssen, A., Ollevier, F., 2015. *Photobacterium*.

Toldrá, F., 2012. Biochemistry of processing meat and poultry., in: Hui, Y.H. (Ed.), Food biochemistry and food processing, 2nd ed. Blackwell Publishing, Iowa, USA, p. p. 315.

Torido, Y., Takahashi, H., Kuda, T., Kimura, B., 2012. Analysis of the growth of histamine-producing bacteria and histamine accumulation in fish during storage at low temperatures. Food Control 26, 174-177.

Tornberg, E., 2005. Effects of heat on meat proteins - implications on structure and quality of meat products. Meat Sci 70, 493-508.

Trowbridge, P.F., Francis, C.K., 1910. The glycogen content of beef flesh. J Ind Eng Chem 2, 215-216.

Urbanczyk, H., Ast, J.C., Dunlap, P.V., 2010. Phylogeny, genomics, and symbiosis of *Photobacterium*. FEMS Microbiol Rev 35, 324-342.

Urbanczyk, H., Ast, J.C., Kaeding, A.J., Oliver, J.D., Dunlap, P.V., 2008. Phylogenetic analysis of the incidence of *lux* gene horizontal transfer in *Vibrionaceae*. J Bacteriol 190, 3494-3504.

Urbanczyk, H., Furukawa, T., Yamamoto, Y., Dunlap, P.V., 2012. Natural replacement of vertically inherited *lux-rib* genes of *Photobacterium aquimaris* by horizontally acquired homologues. Environ Microbiol Rep 4, 412-416.

Vezzi, A., Campanaro, S., D'Angelo, M., Simonato, F., Vitulo, N., Lauro, F.M., Cestaro, A., Malacrida, G., Simionati, B., Cannata, N., Romualdi, C., Bartlett, D.H., Valle, G., 2005. Life at depth: *Photobacterium profundum* genome sequence and expression analysis. Science 307, 1459-1461.

Vitulo, N., Vezzi, A., Romualdi, C., Campanaro, S., Valle, G., 2007. A global gene evolution analysis on *Vibrionaceae* family using phylogenetic profile. BMC Bioinform 8, S23.

Wallden, K., Rivera-Calzada, A., Waksman, G., 2010. Type IV secretion systems: versatility and diversity in function. Cell Microbiol 12, 1203-1212.

Wang, D., Yamaki, S., Kawai, Y., Yamazaki, K., 2020. Histamine production behaviors of a psychrotolerant histamine-producer, *Morganella psychrotolerans*, in various environmental conditions. Curr Microbiol 77, 460-467.

Wang, X., Zhang, Y., Ren, H., Zhan, Y., 2018. Comparison of bacterial diversity profiles and microbial safety assessment of salami, Chinese dry-cured sausage and Chinese smoked-cured sausage by high-throughput sequencing. LWT 90, 108-115.

Wang, Y., LaPointe, G., 2020. Arabinogalactan utilization by *Bifidobacterium longum* subsp. *longum* NCC 2705 and *Bacteroides caccae* ATCC 43185 in monoculture and coculture. Microorganisms 8.

Warriss, P.D., 2010. Meat science: an introductory text.

Wei, Z., Chu, R., Li, L., Zhang, J., Zhang, H., Pan, X., Dong, Y., Liu, G., 2021. Study on microbial community succession and protein hydrolysis of donkey meat during refrigerated storage based on Illumina NOVA sequencing technology. Food science of animal resources 41, 701-714.

Widder, E.A., 2010. Bioluminescence in the ocean: origins of biological, chemical, and ecological diversity. Science 328, 704-708.

Wietz, M., Mansson, M., Gotfredsen, C.H., Larsen, T.O., Gram, L., 2010. Antibacterial compounds from marine *Vibrionaceae* isolated on a global expedition. Mar Drugs 8, 2946-2960.

Wilhelm, M.P., 1991. Vancomycin. Mayo Clin Proc 66, 1165-1170.

Wood, J.D., Enser, M., Richardson, R.I., Whittington, F.M., 2007. Fatty acids in meat and meat products, in: Chow, C.K. (Ed.), Fatty acids in foods and their health implications, 3rd ed. CRC Press.

Wu, L., Lin, X., Wang, F., Ye, D., Xiao, X., Wang, S., Peng, X., 2006. *Omp*W and *Omp*V are required for NaCl regulation in *Photobacterium damselae*. J Proteome Res 5, 2250-2257.

Yancey, P.H., Clark, M.E., Hand, S.C., Bowlus, R.D., Somero, G.N., 1982. Living with water stress: evolution of osmolyte systems. Science 217, 1214-1222.

Young, L.L., Reviere, R.D., Cole, A.B., 1988. Fresh red meats: a place to apply modified atmospheres. Food Technol (USA) 42, 65-69.

Yu, Z., Peruzy, M.F., Dumolin, C., Joossens, M., Houf, K., 2019. Assessment of food microbiological indicators applied on poultry carcasses by culture combined MALDI-TOF MS identification and 16S rRNA amplicon sequencing. Food Microbiol 82, 53-61.

Zhao, Y., Wells, J.H., McMillin, K.W., 1994. Applications of dynamic modified atmosphere packaging systems for fresh red meats: review. J Muscle Foods 5, 299-328.

15 Appendix

15.1 Supplementary files to publication 1

Table S1. Species and strains of *Photobacterium* spp. tested with LAMP reaction, with purified DNA (50 ng/reaction). (+) positive reaction, (-) negative reaction.

Species	Source of isolation	Packaging	Strain	LAMP reaction
Photobacterium carnosum	Chicken	MAP[a]	TMW2.2021[T, b] DSM 105454[T, c]	+
Photobacterium carnosum	Chicken	MAP	TMW2.2022	+
Photobacterium carnosum	Chicken	MAP	TMW2.2029	+
Photobacterium carnosum	Chicken	MAP	TMW2.2030	+
Photobacterium carnosum	Pork	MAP	TMW2.2097	+
Photobacterium carnosum	Salmon	MAP	TMW2.2098	+
Photobacterium carnosum	Salmon	MAP	TMW2.2099	+
Photobacterium carnosum	Chicken	MAP	TMW2.2146	+
Photobacterium carnosum	Chicken	MAP	TMW2.2147	+
Photobacterium carnosum	Beef	Air	TMW2.2148	+
Photobacterium carnosum	Pork	MAP	TMW2.2149	+
Photobacterium carnosum	Chicken	Air	TMW2.2150	+
Photobacterium carnosum	Chicken	MAP	TMW2.2151	+
Photobacterium carnosum	Chicken	MAP	TMW2.2152	+
Photobacterium carnosum	Chicken	MAP	TMW2.2153	+

Species	Source of isolation	Packaging	Strain	LAMP reaction
Photobacterium carnosum	Chicken	MAP	TMW2.2154	+
Photobacterium carnosum	Chicken	MAP	TMW2.2155	+
Photobacterium carnosum	Chicken	MAP	TMW2.2156	+
Photobacterium carnosum	Chicken	MAP	TMW2.2157	+
Photobacterium carnosum	Chicken	MAP	TMW2.2158	+
Photobacterium carnosum	Chicken	MAP	TMW2.2159	+
Photobacterium carnosum	Chicken	MAP	TMW2.2160	+
Photobacterium carnosum	Chicken	MAP	TMW2.2161	+
Photobacterium carnosum	Chicken	MAP	TMW2.2162	+
Photobacterium carnosum	Chicken	MAP	TMW2.2163	+
Photobacterium carnosum	Chicken	MAP	TMW2.2164	+
Photobacterium carnosum	Chicken	MAP	TMW2.2165	+
Photobacterium carnosum	Chicken	MAP	TMW2.2166	+
Photobacterium carnosum	Chicken	MAP	TMW2.2167	+
Photobacterium carnosum	Chicken	MAP	TMW2.2168	+
Photobacterium carnosum	Turkey	Air	TMW2.2169	+
Photobacterium carnosum	Fish	MAP	TMW2.2186	+
Photobacterium carnosum	Fish	MAP	TMW2.2187	+
Photobacterium carnosum	Fish	MAP	TMW2.2188	+

Species	Source of isolation	Packaging	Strain	LAMP reaction
Photobacterium carnosum	Fish	MAP	TMW2.2189	+
Photobacterium carnosum	Fish	MAP	TMW2.2190	+
Photobacterium phosphoreum	Fish	-	DSM 15556^{T}	+
Photobacterium phosphoreum	Chicken	MAP	TMW2.2033	+
Photobacterium phosphoreum	Chicken	MAP	TMW2.2034	+
Photobacterium phosphoreum	Beef	MAP	TMW2.2103	+
Photobacterium phosphoreum	Turkey	Air	TMW2.2125	+
Photobacterium phosphoreum	Chicken	MAP	TMW2.2126	+
Photobacterium phosphoreum	Chicken	MAP	TMW2.2127	+
Photobacterium phosphoreum	Chicken	MAP	TMW2.2128	+
Photobacterium phosphoreum	Chicken	MAP	TMW2.2129	+
Photobacterium phosphoreum	Chicken	MAP	TMW2.2130	+
Photobacterium phosphoreum	Chicken	MAP	TMW2.2131	+
Photobacterium phosphoreum	Chicken	MAP	TMW2.2132	+
Photobacterium phosphoreum	Chicken	MAP	TMW2.2133	+
Photobacterium phosphoreum	Chicken	MAP	TMW2.2134	+
Photobacterium phosphoreum	Chicken	MAP	TMW2.2135	+
Photobacterium phosphoreum	Chicken	MAP	TMW2.2136	+
Photobacterium phosphoreum	Chicken	MAP	TMW2.2137	+

Species	Source of isolation	Packaging	Strain	LAMP reaction
Photobacterium phosphoreum	Pork	Air	TMW2.2138	+
Photobacterium phosphoreum	Pork	Air	TMW2.2139	+
Photobacterium phosphoreum	Pork	Air	TMW2.2140	+
Photobacterium phosphoreum	Beef	MAP	TMW2.2141	+
Photobacterium phosphoreum	Beef	MAP	TMW2.2142	+
Photobacterium phosphoreum	Beef	MAP	TMW2.2143	+
Photobacterium phosphoreum	Beef	MAP	TMW2.2144	+
Photobacterium phosphoreum	Beef	MAP	TMW2.2145	+
Photobacterium iliopiscarium	Fish	-	DSM 9896^{T}	+
Photobacterium iliopiscarium	Chicken	MAP	TMW2.2035	+
Photobacterium iliopiscarium	Pork	MAP	TMW2.2104	+
Photobacterium iliopiscarium	Pork	MAP	TMW2.2172	+
Photobacterium angustum	Seawater	-	DSM 19184^{T}	-
Photobacterium kishitanii	Fish	-	DSM 19954^{T}	+
Photobacterium profundum	Deep-sea sediment	-	DSM 21095^{T}	-
Photobacterium leiognathi	Fish	-	DSM 21260^{T}	+

[T] marks the type strain of each species.

[a] MAP = Modified Atmosphere Packaged

[b] TMW = Lehrstuhl für Technische Mikrobiologie Weihenstephan, Technical University of Munich, Freising, GER.

[c] DSM = Deutsche Sammlung von Mikroorganismen und Zellkulturen (DMSZ), Darmstadt, GER.

Table S2. Species and strains of common meat spoilers tested with LAMP reaction, with purified DNA (50 ng/reaction). (+) positive reaction, (-) negative reaction.

Species	Source of isolation	Packaging	Strain	LAMP reaction
Brochothrix thermosphacta	Beef	MAP[a]	TMW2.2101[b]	-
Brochothrix thermosphacta	Pork	MAP	TMW2.1872	-
Brochothrix thermosphacta	Turkey	MAP	TMW2.1873	-
Brochothrix thermosphacta	Chicken	MAP	TMW2.1874	-
Carnobacterium divergens	Beef	MAP	TMW2.1907	-
Carnobacterium divergens	Chicken	MAP	TMW2.1577	-
Carnobacterium divergens	Chicken	MAP	TMW2.1868	-
Carnobacterium divergens	Turkey	MAP	TMW2.1869	-
Carnobacterium divergens	Chicken	MAP	TMW2.1870	-
Carnobacterium divergens	Beef	MAP	TMW2.1871	-
Carnobacterium maltaromaticum	Chicken	MAP	TMW2.1581	-
Carnobacterium maltaromaticum	Chicken	MAP	TMW2.1867	-
Carnobacterium maltaromaticum	Raw milk	-	TMW2.1624 DSM 20342[T, c]	-
Carnobacterium maltaromaticum	Chicken	MAP	TMW2.1582	-
Carnobacterium maltaromaticum	Chicken	MAP	TMW2.1583	-
Serratia liquefaciens	Milk	-	TMW2.1625 DSM 4487[T]	-

Species	Source of isolation	Packaging	Strain	LAMP reaction
Serratia liquefaciens	Beef	MAP	TMW2.1905	-
Serratia proteamaculans	-	-	TMW2.491	-
Lactococcus carnosus	Beef	MAP	TMW2.1612^{T}	-
Lactococcus carnosus	Beef	MAP	TMW2.1613	-
Lactococcus paracarnosus	Beef	MAP	TMW2.1615^{T}	-
Lactococcus paracarnosus	Beef	MAP	TMW2.1614	-
Lactotoccus piscium	Pork	MAP	TMW2.2178	-
Lactococcus piscium	Beef	MAP	TMW2.1902	-
Lactococcus piscium	Beef	MAP	TMW2.1903	-
Lactococcus piscium	Beef	MAP	TMW2.1894	-
Lactococcus piscium	Beef	MAP	TMW2.1895	-
Lactococcus piscium	Beef	MAP	TMW2.1896	-
Lactococcus piscium	Beef	MAP	TMW2.1897	-
Lactococcus piscium	Beef	MAP	TMW2.1898	-
Lactococcus piscium	Beef	MAP	TMW2.1899	-
Lactococcus piscium	Beef	MAP	TMW2.1893	-
Lactococcus piscium	Beef	MAP	TMW2.1900	-
Lactococcus piscium	Chicken	MAP	TMW2.2176	-
Lactococcus piscium	Pork	MAP	TMW2.2177	-

Species	Source of isolation	Packaging	Strain	LAMP reaction
Leuconostoc gelidum subsp. *gelidum*	Beef	MAP	TMW2.1618	-
Leuconostoc gelidum subsp. *gelidum*	Beef	MAP	TMW2.1620	-
Leuconostoc gelidum subsp. *gelidum*	Chicken	MAP	TMW2.2191	-
Leuconostoc gelidum subsp. *gasicomitatum*	Beef	MAP	TMW2.1616	-
Leuconostoc gelidum subsp. *gasicomitatum*	Beef	MAP	TMW2.1617	-
Leuconostoc gelidum subsp. *gasicomitatum*	Beef	MAP	TMW2.1619	-
Leuconostoc gelidum subsp. *gasicomitatum*	Chicken	MAP	TMW2.1507	-
Hafnia alvei	-	-	TMW2.1622 DSM 30163^{T}	-
Hafnia alvei	Chicken	MAP	TMW2.1857	-
Hafnia alvei	Chicken	MAP	TMW2.1858	-
Hafnia alvei	Chicken	MAP	TMW2.1859	-
Hafnia alvei	Chicken	MAP	TMW2.1860	-
Hafnia alvei	Beef	MAP	TMW2.1904	-
Pseudomonas weihenstephanensis	Beef	MAP	TMW2.1728	-
Pseudomonas weihenstephanensis	Beef	MAP	TMW2.2077	-
Pseudomonas weihenstephanensis	Beef	MAP	TMW2.2078	-

Species	Source of isolation	Packaging	Strain	LAMP reaction
Pseudomonas lundensis	Beef	MAP	TMW2.2076	-
Pseudomonas lundensis	Beef	-	TMW2.1623 DSM 6252^{T}	-
Pseudomonas versuta	Beef	MAP	TMW2.2083	-
Pseudomonas meridiana	Beef	MAP	TMW2.2086	-
Pseudomonas fragi	Beef	MAP	TMW2.2082	-
Pseudomonas fragi	Beef	MAP	TMW2.2080	-
Pseudomonas fragi	Chicken	MAP	TMW2.1634	-
Pseudomonas simiae	Beef	MAP	TMW2.2085	-
Pseudomonas sp.	Beef	MAP	TMW2.2087	-
Pseudomonas sp.	Beef	MAP	TMW2.2089	-
Pseudomonas sp.	Beef	MAP	TMW2.2090	-
Pseudomonas sp.	Beef	MAP	TMW2.2091	-

^{T} marks the type strain of each species.

[a] MAP = Modified Atmosphere Packaged

[b] TMW = Lehrstuhl für Technische Mikrobiologie Weihenstephan, Technical University of Munich, Freising, GER.

[c] DSM = Deutsche Sammlung von Mikroorganismen und Zellkulturen (DMSZ), Darmstadt, GER.

Table S3. Reaction mixture of secondary amplification performed with the product of the LAMP assay with primers F2/B2.

Reagent	Volume per 50 µl reaction (µl)
DEPC dH2O	42.25
10x buffer w/ MgCl2	5
dNTPs (10 mM each)	1
Forward primer (100 µm)	0.25
Reverse primer (100 µm)	0.25
Taq polymerase (5 U/µl)	0.25
Template	1

Table S4. Thermoprotocol of secondary PCR amplification of the product from the LAMP assay with primers F2/B2.

Step	Conditions
Initial denaturation	94 ºC / 5’
Denaturation	95 ºC / 45‘’
Annealing	52 ºC / 90‘’
Extension	72 ºC / 2‘
Cycles	X34
Final extension	72 ºC / 5’

Table S5. Species identified on meat by culture-dependent MALDI-TOF MS. Species occurred in samples that resulted in a negative LAMP reaction, thus not being amplified by designed primers. The species were identified by picking colonies on the selective media and analyzing them with MALDI-TOF MS as detailed in the materials and methods (2.6).

Detected species on meat
Acinetobacter guillouiae
Acinetobacter johnsonii
Acinetobacter sp.
Arthrobacter psychrolactophilus
Arthrobacter spp.
Brenneria alni
Brochothrix thermosphacta
Buttiauxella gaviniae
Candida spp.
Candida zeylanoides
Carnobacterium divergens
Carnobacterium maltaromaticum
Chryseobacterium scophthalmum
Enterococcus durans
Enterococcus faecalis
Enterococcus faecium
Enterococcus hirae
Escherichia coli

Detected species on meat
Ewingella Americana
Hafnia alvei
Kocuria carniphila
Lactobacillus sakei
Lactobacillus spp.
Lactococcus garvieae
Lactococcus piscium
Leuconostoc gelidum ssp. gasicomitatum
Leuconostoc gelidum ssp. gelidum
Leuconostoc mesenteroides
Macrococcus caseolyticus
Microbacterium foliorum
Microbacterium liquefaciens
Microbacterium maritypicum
Pantoea agglomerans
Proteus vulgaris
Pseudoclavibacer helvolus
Pseudomonas spp.
Rahnella aquatilis

Detected species on meat
Rothia nasimurium
Serratia fonticola
Serratia liquefaciens
Serratia plymuthica
Serratia proteamaculans
Serratia spp.
Shewanella baltica
Shewanella sp.
Staphylococcus aureus
Staphylococcus condiment
Staphylococcus equorum
Staphylococcus saprophyticus
Staphylococcus spp.
Staphylococcus warneri
Stenotrophomonas maltophilia
Yarrowia lipolytica
Yersinia enterocolitica ssp enterocolitica
Yersinia spp.

15.2 Supplementary files to publication 2

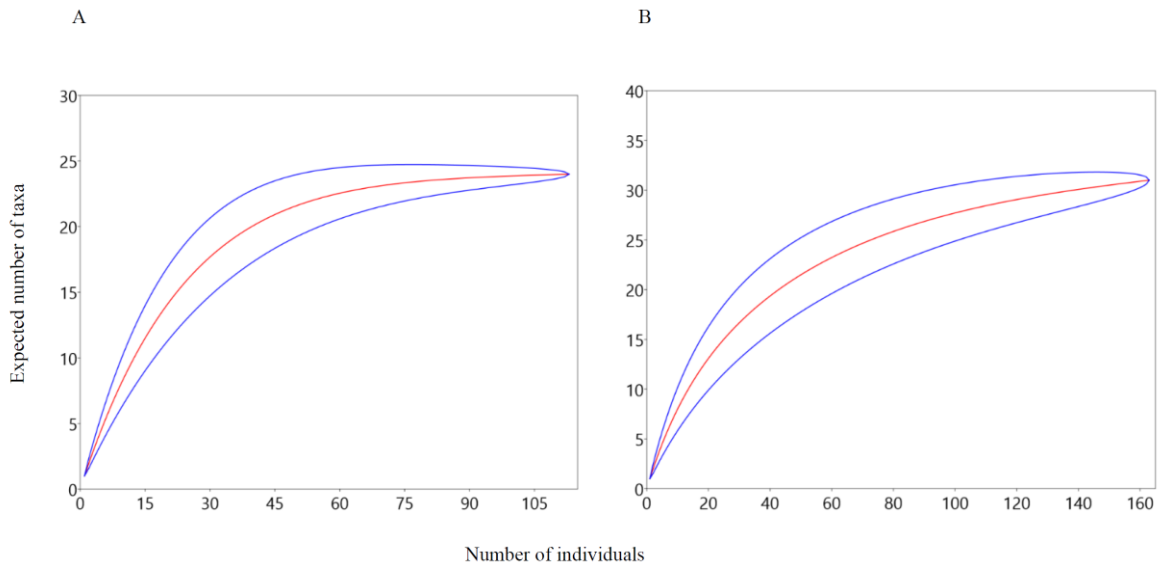

Figure S1. Rarefaction analysis visualization of A *P. phosphoreum* and B *P. carnosum*. Blue line shows 95 confidence interval.

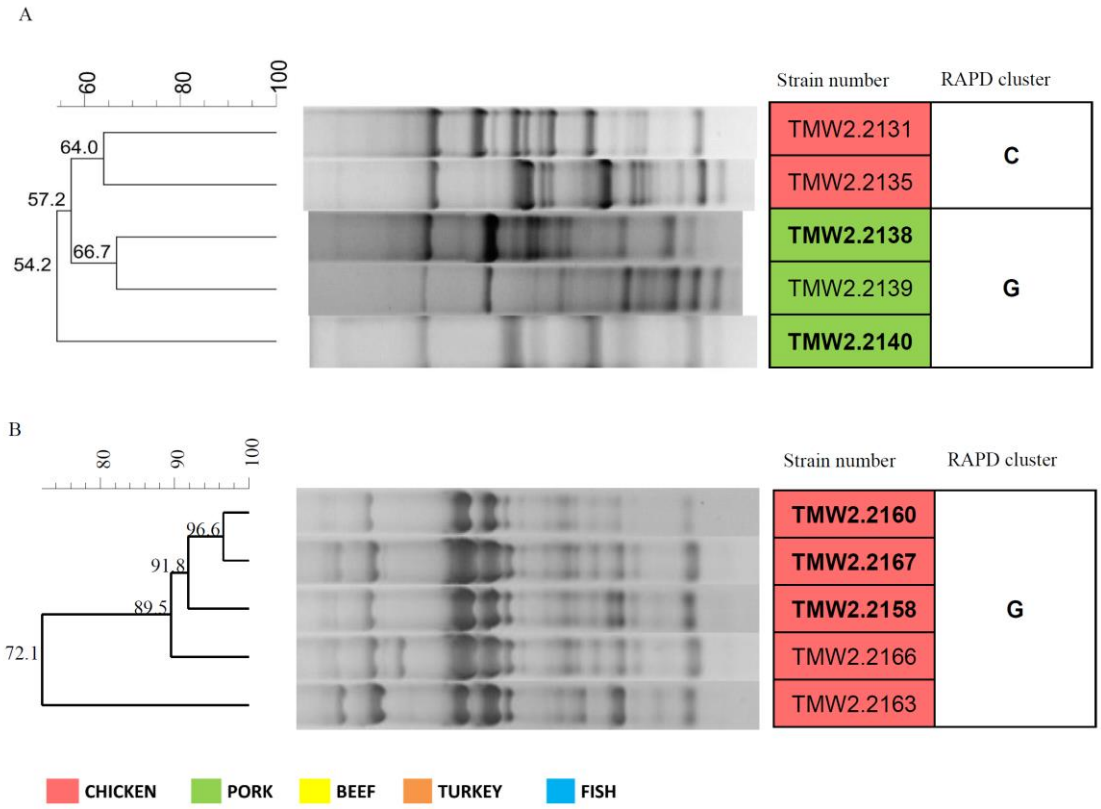

Figure S2. RAPD-clustering of the most similar strains of *P. phosphoreum* and *P carnosum* used for the preliminary strain selection. Hierarchical clustering was calculated with the unweighted pair group method with arithmetic mean (UPGMA), Dice similarity coefficient and 1% tolerance. The RAPD-clustering of all selected isolates in the manuscript (see Fig. 1) shows high similarity of strains TMW 2.2138 TMW 2.2140 from *P. phosphoreum* and strains TMW 2.2160, TMW 2.2167, TMW 2.2158 from *P. carnosum* respectively. However, initial comparison of all recovered isolates showed clear differences of the mentioned strains from **A** *P. phosphoreum* and **B** *P. carnosum.* Therefore, isolates were kept for the further study.

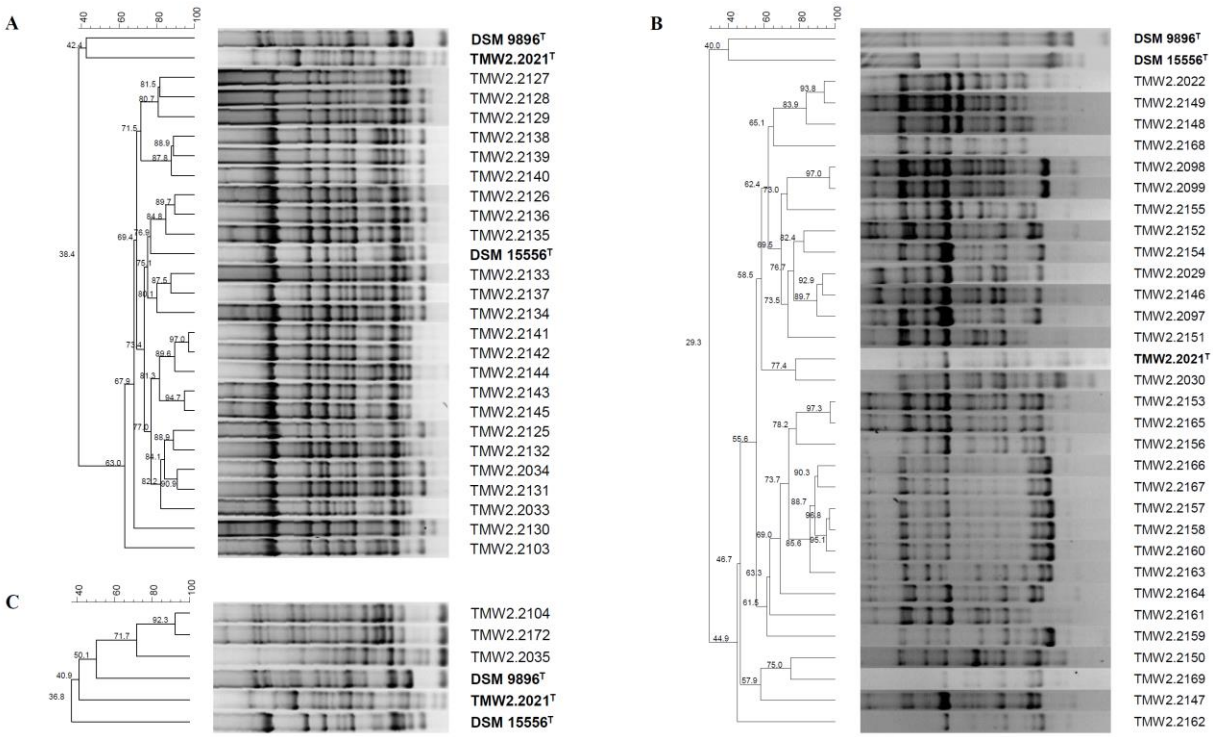

Figure S3. RAPD-clustering of the selected strains with additional primer M14V. Strain differentiation based on primer M13V was confirmed with additional primer M14V. Hierarchical clustering was calculated with the unweighted pair group method with arithmetic mean (UPGMA), Dice similarity coefficient and 1% tolerance. The similarity values are shown at the nodes of the tree. **A** *P. phosphoreum* type strain DSM 15556**T** **B** *P. carnosum* type strain TMW 2.2021^{T} **C** *P. iliopiscarium* type strain DSM 9896^{T}.

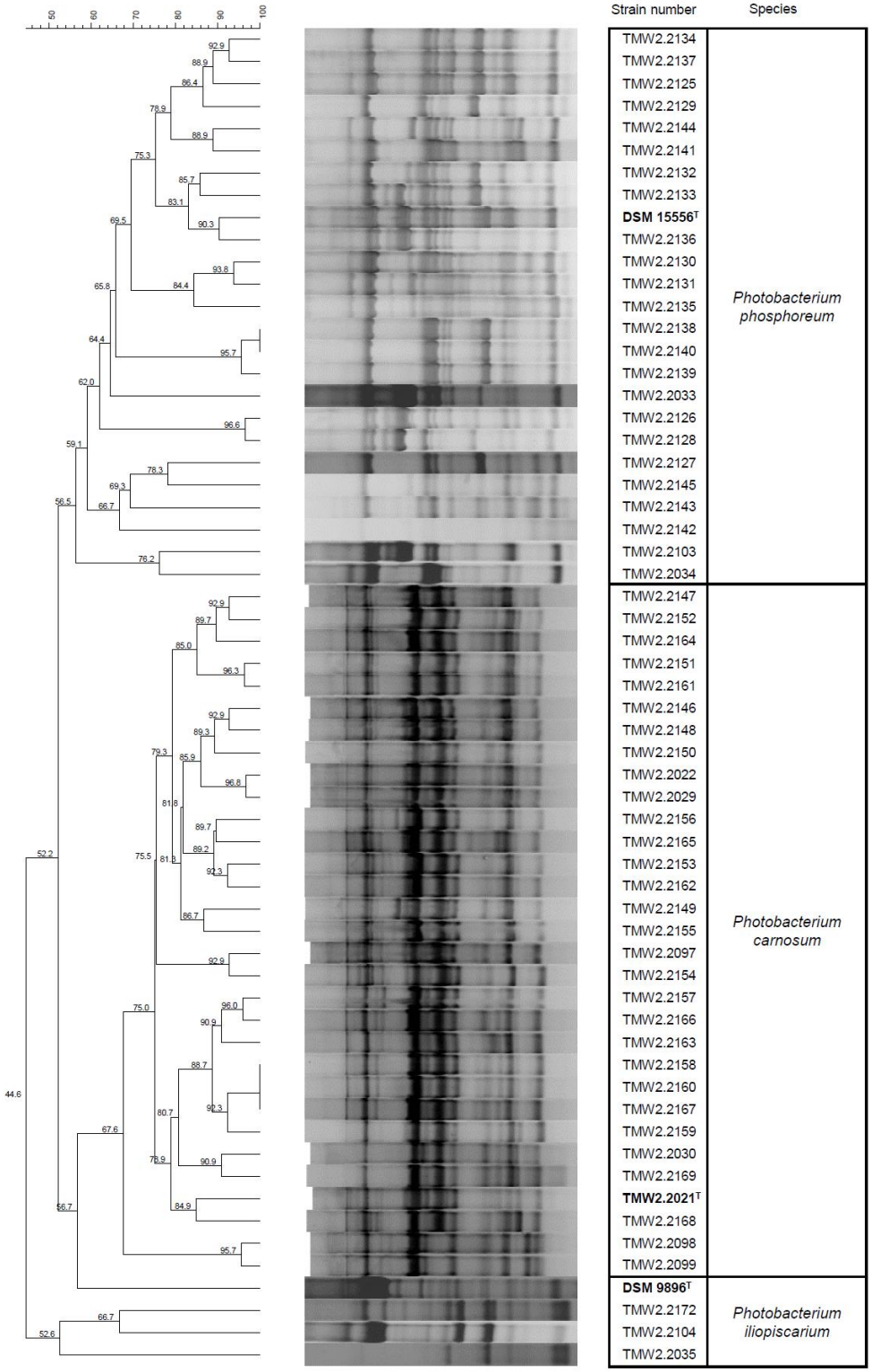

Figure S4. RAPD-clustering of all the selected strains of the three species of photobacteria together. Hierarchical clustering was calculated with the unweighted pair group method with arithmetic mean (UPGMA), Dice similarity coefficient and 1% tolerance. Similarity values are shown at the nodes of the tree. All strains of one species cluster together and apart from the strains belonging to another species.

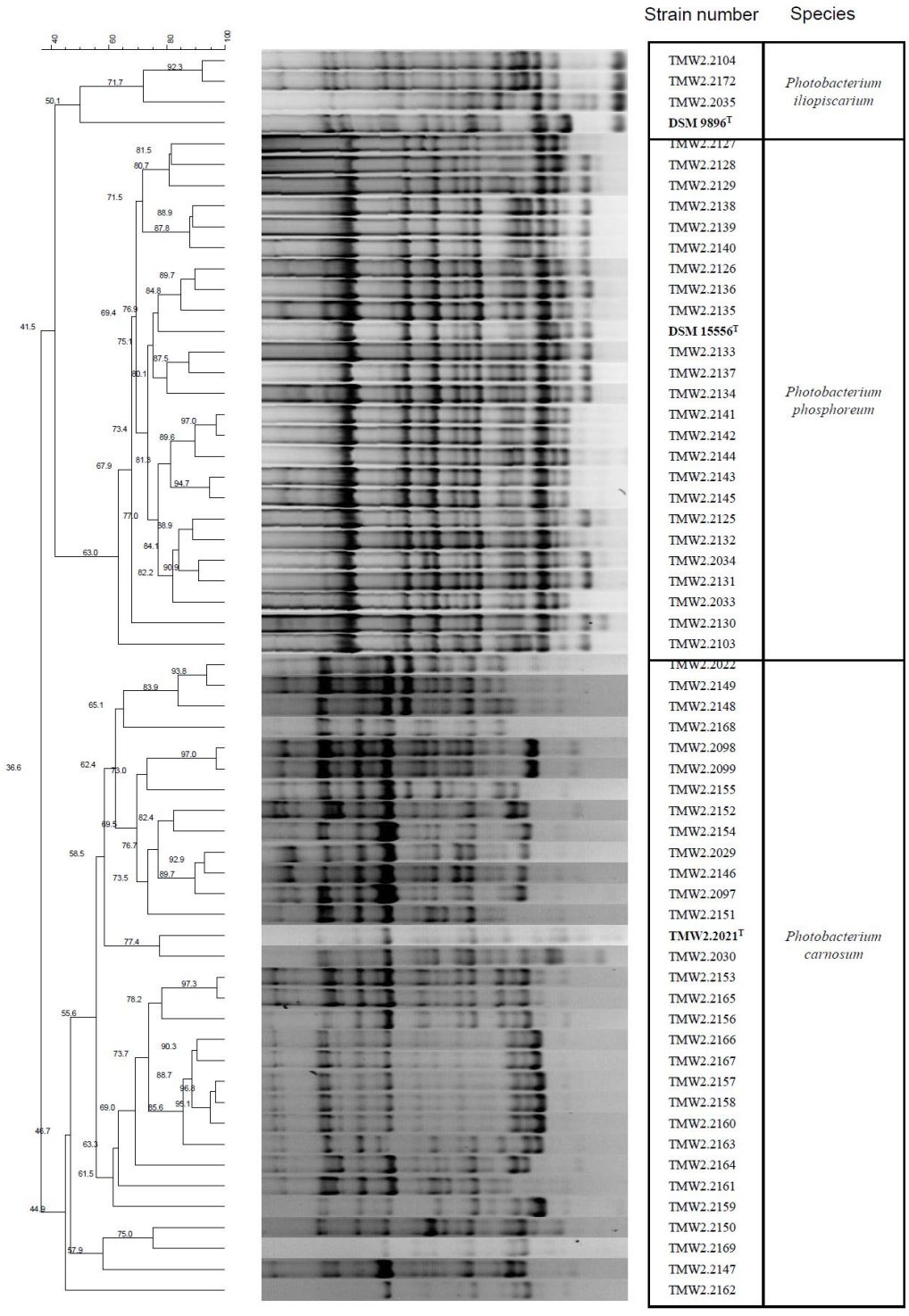

Figure S5. RAPD-clustering of the selected strains of all three species with additional primer M14V. Species differentiation based on primer M13V was confirmed with additional primer M14V. Hierarchical clustering was calculated with the unweighted pair group method with arithmetic mean (UPGMA), Dice similarity coefficient and 1% tolerance. The similarity values are shown at the nodes of the tree. Selected strains of all three species were included *P. phosphoreum* type strain DSM 15556^T, *P. carnosum* type strain TMW 2.2021^T, *P. iliopiscarium* type strain DSM 9896^T.

Table S1. Strains origin. Origin by type of packaging, type of meat, and sample, of the strains included in the study. The number of isolates screened refers to the number of isolates from that species that were recovered from the sample, and compared by RAPD PCR approach. The number of strains refers to the amount of strains obtained from the recovered isolates.

Package	Meat type	Contaminated/ Sampled	Sample	*P. carnosum* isolates screened	*P. carnosum* strains	TMW	*P. phosphoreum* isolates screened	*P. phosphoreum* strains	TMW	*P. iliopiscarium* isolates screened	*P. iliopiscarium* strains	TMW
MAP	Chicken*	5/15	1	-	-	-	4	2	TMW2.2033 TMW2.2034	1	1	TMW2.2035
			2	21	2	TMW2.2021** TMW2.2022** TMW2.2030** TMW2.2146 TMW2.2147	-	-	-	-	-	-
			3			TMW2.2029**	-	-	-	-	-	-
MAP	Beef*	2/2	1	-	-	-	2	1	TMW2.2103	-	-	-
MAP	Pork*	2/9	1	7	2	TMW2.2097 TMW2.2149	-	-	-	1	1	TMW2.2104
			2	-	-	-	-	-	-	1	1	TMW2.2172
MAP	Marinated chicken	2/3	1	99	15	TMW2.2151 TMW2.2152 TMW2.2153 TMW2.2155 TMW2.2156 TMW2.2157 TMW2.2158 TMW2.2159 TMW2.2160 TMW2.2161 TMW2.2162 TMW2.2163 TMW2.2164 TMW2.2165 TMW2.2166	26	12	TMW2.2134 TMW2.2137 TMW2.2129 TMW2.2132 TMW2.2133 TMW2.2136 TMW2.2130 TMW2.2131 TMW2.2135 TMW2.2127 TMW2.2126 TMW2.2128	-	-	-
			2	27	3	TMW2.2167 TMW2.2168 TMW2.2154	-	-	-	-	-	-
MAP	Marinated beef	1/3	1	-	-	-	35	5	TMW2.2144 TMW2.2141 TMW2.2145 TMW2.2142 TMW2.2143	-	-	-
MAP	Salmon	6/6	1	3	1	TMW2.2099	27	-	-	-	-	-
			2	1	1	TMW2.2098	10	-	-	-	-	-
Air	Chicken	1/4	1	3	1	TMW2.2150	-	-	-	-	-	-
Air	Beef	1/3	1	1	1	TMW2.2148	-	-	-	-	-	-
Air	Pork	1/3	1	-	-	-	7	3	TMW2.2138 TMW2.2139 TMW2.2140	-	-	-
Air	Marinated turkey	1/3	1	1	1	TMW2.2169	2	1	TMW2.2125	-	-	-

*Samples marked belong to the previous study by Hilgarth *et al.*, 2018a.

**Marked strains were obtained from the previous work by Hilgarth *et al.*, 2018b, from the *P. carnosum* sp. nov. species description.

Table S2. Antibiotic inhibition zone of *P. phosphoreum*. Diameter values in mm of the inhibition zone observed for every antibiotic and each of the selected isolates of *P. phosphoreum*. The diameter of the antibiotic discs was measured as 6 mm, and therefore values of 6 in the table represent no inhibition zone observed.

Strain	Clindamycin DA 2 µg	Norfloxacin NOR 10 µg	Nalidixic acid NA 30 µg	Ampicillin AMP 10 µg	Sulphonamides S3 300 µg	Trimetoprim W 5 µg	Penicillin G P 5 µg	Streptomycin S 25 µg	Apramycin APR 15 µg	Rifampicin RD 5 µg	Gentamycin CN 10 µg	Kanamycin K 30 µg	Chloramphenicol C 30 µg	Erythromycin E 15 µg	Tetracyclin TE 30 µg
TMW 2.2103	6	22	19	6	6	6	6	10	6	13	15	14	35	13	6
TMW 2.2033	6	25	20	6	6	6	6	11	8	12	15	14	31	10	7
TMW 2.2034	6	25	20	6	6	6	6	10	6	11	14	13	27	8	6
TMW 2.2126	6	32	25	8	6	6	6	7	6	14	7	6	36	11	21
TMW 2.2127	6	34	25	6	6	6	6	10	6	13	8	6	38	11	6
TMW 2.2128	6	25	22	6	6	25	6	8	6	12	10	7	36	17	6
TMW 2.2138	6	25	20	11	6	6	6	13	11	18	16	14	20	24	6
TMW 2.2139	6	32	9	12	6	6	12	12	9	15	14	16	25	21	6
TMW 2.2140	6	33	25	11	6	6	10	11	10	17	10	12	20	25	6
TMW 2.2125	6	30	10	6	6	6	6	16	11	15	17	20	16	14	6
DSM 15556^T	6	29	9	6	6	6	6	12	10	13	13	20	13	15	6
TMW 2.2141	6	26	20	6	6	6	6	12	6	16	18	16	30	15	6
TMW 2.2142	6	25	10	6	6	6	6	12	10	12	23	20	15	17	6
TMW 2.2143	6	24	8	6	6	6	6	13	6	11	11	9	12	8	6
TMW 2.2144	6	21	9	6	6	6	6	10	10	14	14	22	18	11	6
TMW 2.2145	6	28	8	6	6	6	6	9	11	12	10	6	6	9	6
TMW 2.2129	6	21	20	6	6	6	6	14	8	15	18	15	23	12	6
TMW 2.2130	6	22	20	10	6	6	6	12	6	13	15	15	17	8	6
TMW 2.2131	6	31	8	6	22	23	6	18	11	10	19	20	16	15	6
TMW 2.2132	6	25	9	6	6	6	6	9	10	16	16	14	17	17	6
TMW 2.2133	6	26	8	6	6	6	6	8	6	13	15	11	15	10	6
TMW 2.2134	6	14	11	8	6	6	6	12	9	9	12	6	16	8	6
TMW 2.2135	6	26	8	9	6	6	6	6	10	11	17	13	13	7	6
TMW 2.2136	6	28	18	6	9	26	6	14	10	22	14	18	37	22	6
TMW 2.2137	6	21	18	6	6	6	6	6	9	12	12	11	6	8	6

Table S3. Antibiotic inhibition zone of *P. carnosum*. Diameter values in mm of the inhibition zone observed for every antibiotic and each of the selected isolates of *P. carnosum*. The diameter of the antibiotic discs was measured as 6 mm, and therefore values of 6 in the table represent no inhibition zone observed.

Strain	Clindamycin DA 2 µg	Norfloxacin NOR 10 µg	Nalidixic acid NA 30 µg	Ampicillin AMP 10 µg	Sulphonamides S3 300 µg	Trimetoprim W 5 µg	Penicillin G P 5 µg	Streptomycin S 25 µg	Apramycin APR 15 µg	Rifampicin RD 5 µg	Gentamycin CN 10 µg	Kanamycin K 30 µg	Chloramphenicol C 30 µg	Erythromycin E 15 µg	Tetracyclin TE 30 µg
TMW 2.2021^T	6	26	40	20	6	28	6	20	16	26	20	30	46	12	12
TMW 2.2022	6	32	18	18	6	28	6	14	6	16	20	18	38	14	18
TMW 2.2029	6	36	28	32	6	16	10	20	6	22	22	14	46	8	26
TMW 2.2030	6	32	24	20	6	32	6	22	12	20	20	20	44	10	18
TMW 2.2098	6	36	26	24	6	36	6	22	6	24	24	16	40	16	22
TMW 2.2099	6	32	28	18	6	30	6	16	10	22	26	20	42	14	20
TMW 2.2097	6	38	28	24	6	36	6	28	6	20	20	18	50	12	24
TMW 2.2146	6	36	26	28	6	26	10	14	6	20	12	18	40	6	20
TMW 2.2147	6	28	22	10	6	24	6	14	10	20	16	28	42	6	14
TMW 2.2148	6	44	24	20	6	38	6	14	6	20	12	12	44	20	20
TMW 2.2149	6	32	22	26	6	36	6	12	6	18	14	16	44	18	20
TMW 2.2150	6	40	30	18	6	34	6	18	6	16	14	18	48	16	22
TMW 2.2151	6	44	26	6	6	20	6	12	6	24	12	24	44	18	16
TMW 2.2152	6	36	26	30	6	24	6	16	6	22	16	10	40	20	16
TMW 2.2153	6	40	22	24	6	22	6	22	16	26	18	22	44	16	18
TMW 2.2154	6	44	28	22	6	34	6	18	16	30	30	20	50	26	22
TMW 2.2155	6	46	30	24	32	38	6	24	6	18	18	14	48	24	20
TMW 2.2156	6	42	24	26	6	30	6	20	6	24	18	16	42	16	6
TMW 2.2157	6	24	20	6	6	28	6	14	16	22	18	20	36	16	18
TMW 2.2158	6	26	24	22	30	24	6	16	14	24	18	24	40	14	20
TMW 2.2159	6	40	38	26	6	38	6	22	18	18	22	24	50	14	6
TMW 2.2160	6	24	26	20	6	32	6	12	10	22	20	16	42	16	20
TMW 2.2161	6	38	24	6	6	32	6	12	6	20	12	16	42	22	18
TMW 2.2162	6	44	24	22	6	32	6	20	12	22	18	20	40	16	12
TMW 2.2163	6	26	26	24	26	32	6	14	6	16	18	16	38	14	6
TMW 2.2164	6	36	26	16	6	24	6	6	6	32	16	16	42	22	18
TMW 2.2165	6	32	22	20	6	36	6	12	12	18	26	20	42	16	18
TMW 2.2166	6	32	26	24	6	34	6	24	12	20	16	18	38	18	18
TMW 2.2167	6	30	26	22	6	34	6	16	6	22	18	14	44	20	20
TMW 2.2168	6	28	28	28	6	36	6	14	12	20	18	16	48	16	6
TMW 2.2169	6	32	22	6	6	26	6	14	6	18	18	16	40	14	18

Table S4. Antibiotic inhibition zone of *P iliopiscarium*. Diameter values in mm of the inhibition zone observed for every antibiotic and each of the selected isolates of *P. iliopiscarium*. The diameter of the antibiotic discs was measured as 6 mm, and therefore values of 6 in the table represent no inhibition zone observed.

Strain	Clindamycin DA 2 µg	Norfloxacin NOR 10 µg	Nalidixic acid NA 30 µg	Ampicillin AMP 10 µg	Sulphonamides S3 300 µg	Trimetoprim W 5 µg	Penicillin G P 5 µg	Streptomycin S 25 µg	Apramycin APR 15 µg	Rifampicin RD 5 µg	Gentamycin CN 10 µg	Kanamycin K 30 µg	Chloramphenicol C 30 µg	Erythromycin E 15 µg	Tetracyclin TE 30 µg
DSM 9896^T	6	20	18	9	6	20	6	10	6	15	12	13	34	6	10
TMW 2.2035	6	20	18	6	6	6	6	9	6	11	12	10	33	10	6
TMW 2.2104	6	24	19	14	6	6	6	9	10	14	11	11	35	6	8
TMW 2.2172	6	20	19	15	6	6	15	13	9	18	16	16	33	10	6

Table S5. Comparison of positive metabolic reactions in API50ch and APIzym between type strain and the rest of isolates of the species. Summary of the positive reactions found in the selected *Photobacterium* strains. For each species, the table shows the results recorded for the type strain, and the results observed in at least one of the other strains of the species. Marked in light red are the differences observed between each of the type strains and the rest of the strains. In the case of *P. phosphoreum* and *P. iliopiscarium*, it additionally represents the differences between the sea-related type strain and the meat-related strains. Positive reactions are marked with a "+" sign, negative reactions are marked with a "-" sign, while weakly positive reactions are marked with a "w".

Reaction	*P. phosphoreum*		*P. carnosum*		*P. iliopiscarium*	
	DSM 15556^T	Species	TMW 2.2021^T	Species	DSM 9896^T	Species
Alkaline phosphatase	+	+	+	+	+	+
Esterase (C 4)	-	+/w	-	w/-	-	w/-
Esterase Lipase (C 8)	-	+/w	-	w/-	-	w
Leucine arylamidase	+	+	+	+	+	+
Valine arylamidase	+	+/w/-	-	w/-	w	-
Cystine arylamidase	-	+/w/-	-	-	-	-
Trypsin	+	+/w/-	-	+/w/-	w	w/-
Acid phosphatase	+	+	+	+	+	+
Naphthol-AS-BI-phosphohydrolase	-	+	+	+/w	+	+
β-galactosidase	+	+/w/-	-	+/w/-	-	-
β-glucuronidase	-	+/-	-	-	-	-
α-glucosidase	-	-	+	+/w/-	-	-
N-acetyl-β-glucosaminidase	+	+	+	+/-	+	+/-
Glycerol	+	-	w	+/w/-	+	w/-
D-ribose	+	+/w	+	+	+	+
D-galactose	+	+/w/-	+	+	+	+
D-glucose	+	+	+	+	+	+
D-fructose	+	+/w	+	+	+	+
D-mannose	+	+	+	+	+	+
Methyl-αD-glucopyranoside	-	-	-	+/w/-	-	-
N-acetylglucosamine	+	+	+	+	+	+
Esculin	+	+/-	+	+/-	+	+/-
D-cellobiose	-	-	-	+/-	-	-
D-maltose	+	+/w/-	+	+	+	+
D-lactose	w	-	-	+/-	-	-
D-melibiose	w	-	-	-	-	-
D-saccharose	-	-	-	+/-	-	-
Starch	-	-	+	+/w	-	+/w
Glycogen	-	-	-	+/w/-	-	-
Gentiobiose	-	-	-	+/-	-	-
D-turanose	-	-	-	+/-	-	-
L-fucose	-	-	-	+/-	-	-
Potassium 2-ketogluconate	w	w/-	w	w/-	-	w/-
Potassium 5-ketogluconate	w	w/-	-	-	-	w/-

15.3 Supplementary files to publication 3

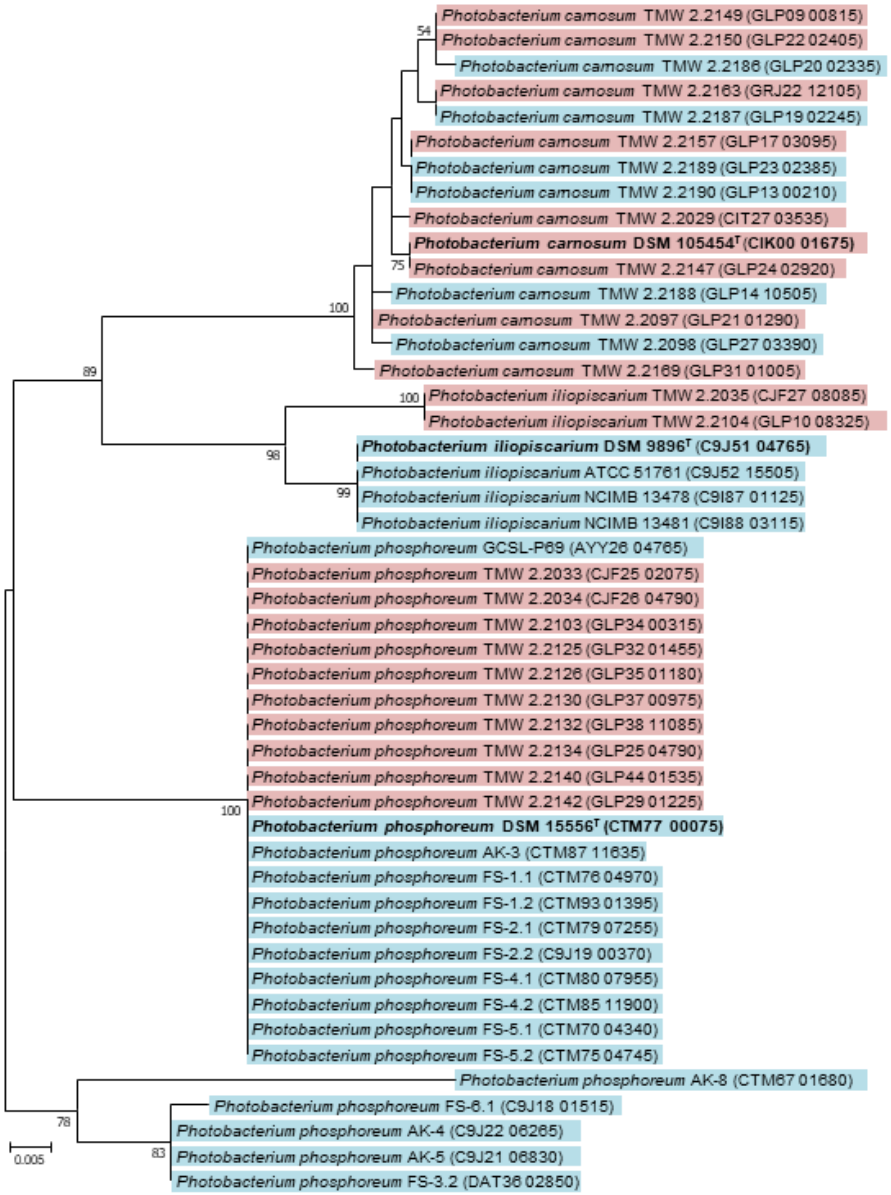

Figure S1. Phylogenetic tree based on the fur gene, created with the maximum likelihood algorithm, Tamura-Nei model and tested with 1000 bootstrap replications. Bootstrap values equal to or above 50 are shown. Clustering shows differentiation by species marked by discontinuous line, and distinction between meat-isolated (red) and fish-isolated (blue) strains of each species. Type strains of each species are shown in bold letters.

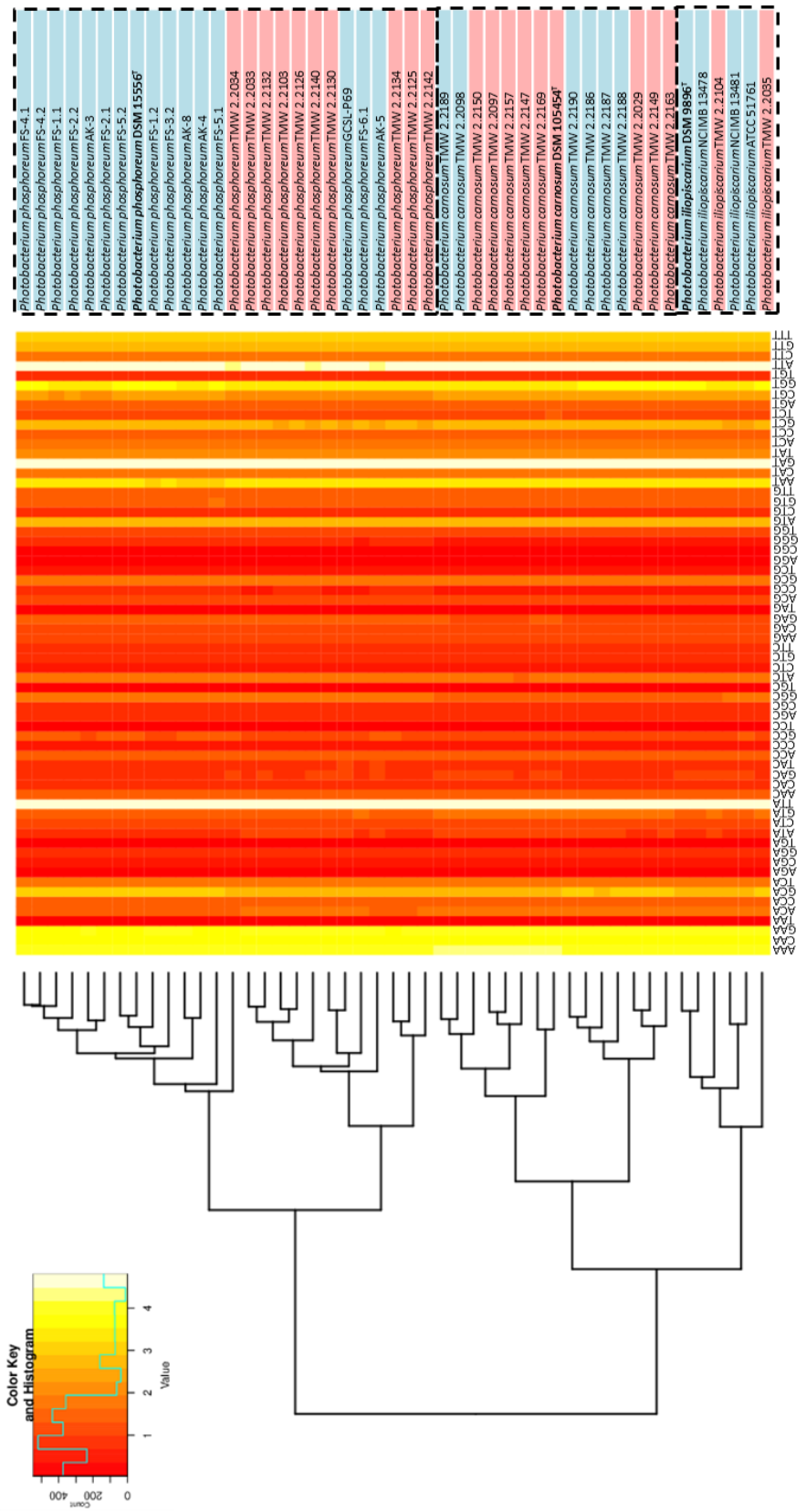

Figure S2. Codon usage-based dendrogram, showing abundance of each codon (red to white) in the genome of each strain of the three species. Discontinuous line separates strains of each species. Type strains of each species are marked in bold letters and with a T. Source of isolation of each strain is signaled with background color: red for meat, and blue for fish.

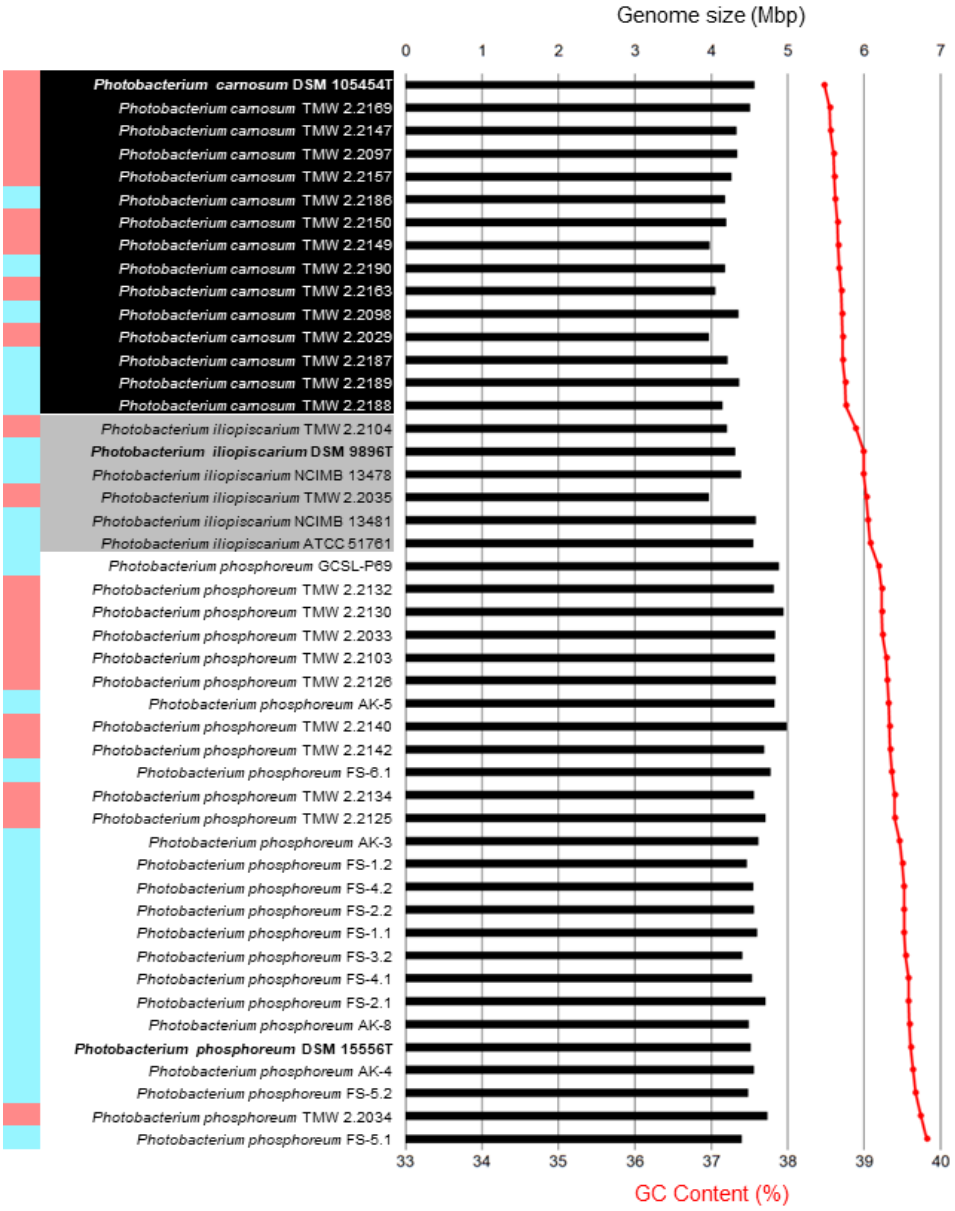

Figure S3. Genome size and GC % content of the genomes studied. Species are differentiated by grey-scale background: *P. carnosum* in black, *P. iliopiscarium* in grey and *P. phosphoreum* in white. Source of isolation (meat in red, fish in blue) is specified with a colored bar on the left of the strain designation. Genome size is displayed as horizontal bars in Mbp, while the GC content is displayed by red dots as percentage.

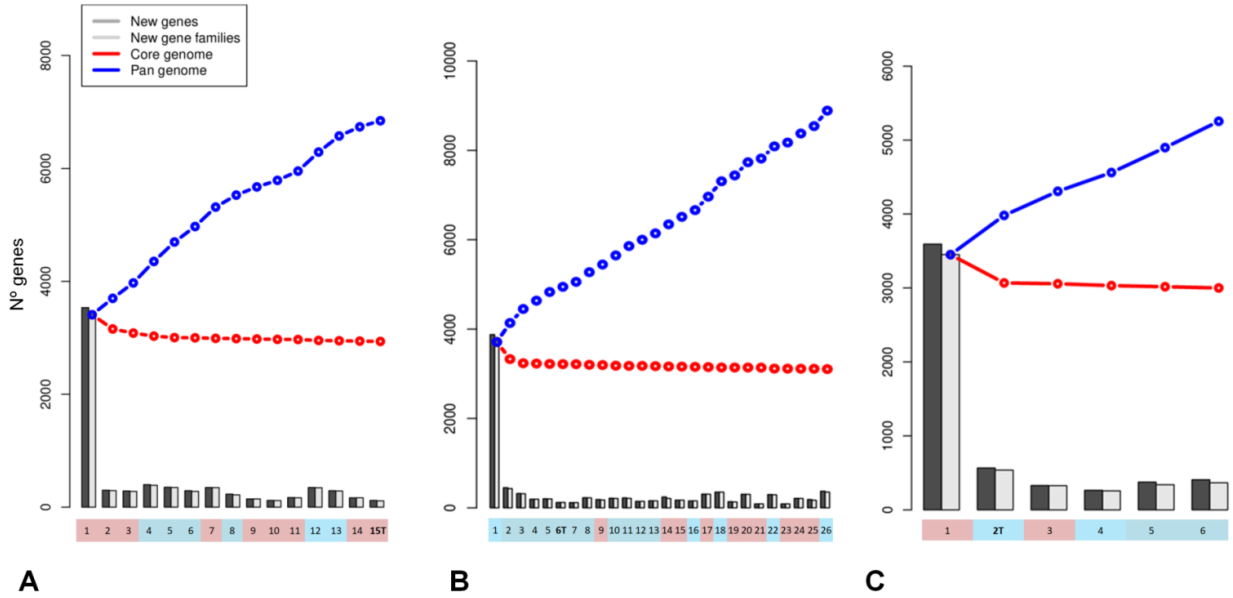

Figure S4. Pan- (blue line) and core- (red line) genome representation of each species. Calculation was performed by protein sequence BLAST, and the parameters set at 50/50 identity/coverage cutoff. Proteins matching were grouped as the same family, and those present in all genomes were considered part of the core-genome of the species. A *P. carnosum,* strains: 1. TMW 2.2029, 2. TMW 2.2149, 3. TMW 2.2163, 4. TMW 2.2188, 5. TMW 2.2190, 6. TMW 2.2186, 7. TMW 2.2150, 8. TMW 2.2187, 9. TMW 2.2157, 10. TMW 2.2147, 11. TMW 2 2097, 12. TMW 2.2098, 13. TMW 2.2189, 14. TMW 2.2169, 15. DSM 105454T. B *P. phosphoreum*, strains: 1. FS-3.2, 2. FS-5.1, 3. FS-1.2, 4. FS-4.1, 5. FS-5.2, 6. DSM 15556T, 7. FS-4.2, 8. AK-4, 9. TMW 2.2134, 10. AK-8, 11. FS-2.2, 12. FS-1.1, 13. AK-3, 14. TMW 2.2125, 15. TMW 2.2142, 16. FS-2.1, 17. TMW 2.2034, 18. FS-6.1, 19. TMW 2.2033, 20. TMW 2.2103, 21. TMW 2.2132, 22. GCSL-P69, 23. TMW 2.2126, 24. TMW 2.2130, 25. TMW 2.2140, 26. AK-5. C *P. iliopiscarium*, strains: 1. TMW 2.2035, 2. DSM 9896T, 3. TMW 2.2104, 4. NCIMB 13478, 5. NCIMB 13481, 6. ATCC 51761. The source of isolation is marked below the bars with color-code (meat in red, fish in blue).

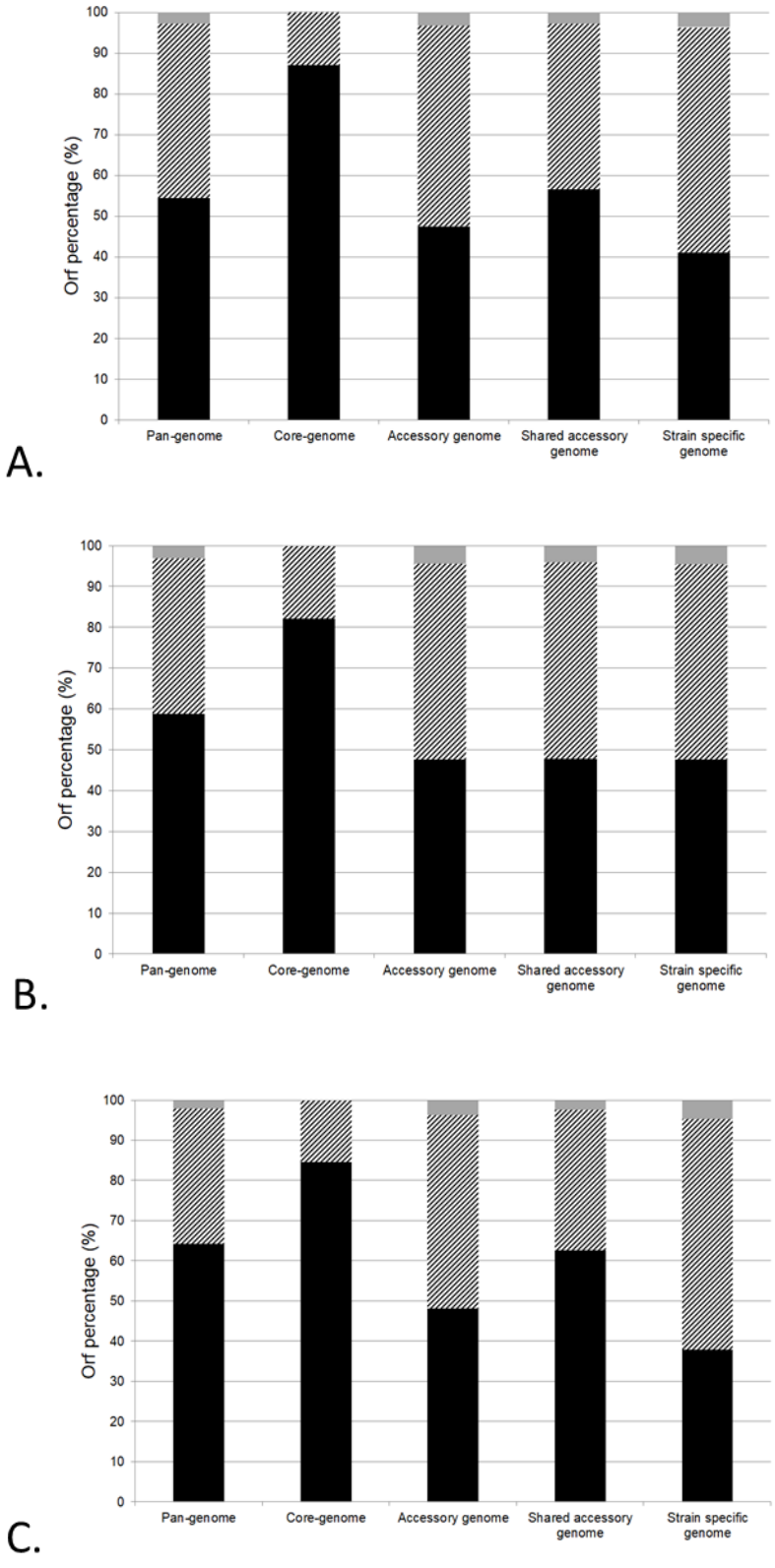

Figure S5. Distribution of ■ annotated genes/proteins, ▩ hypothetical proteins, ■ transposases/mobile elements in the entire genome of each of the species, and within the core-, accessory- and strain-specific part of the genome. A *P. phosphoreum*, B *P. carnosum*, C *P. iliopiscarium*.

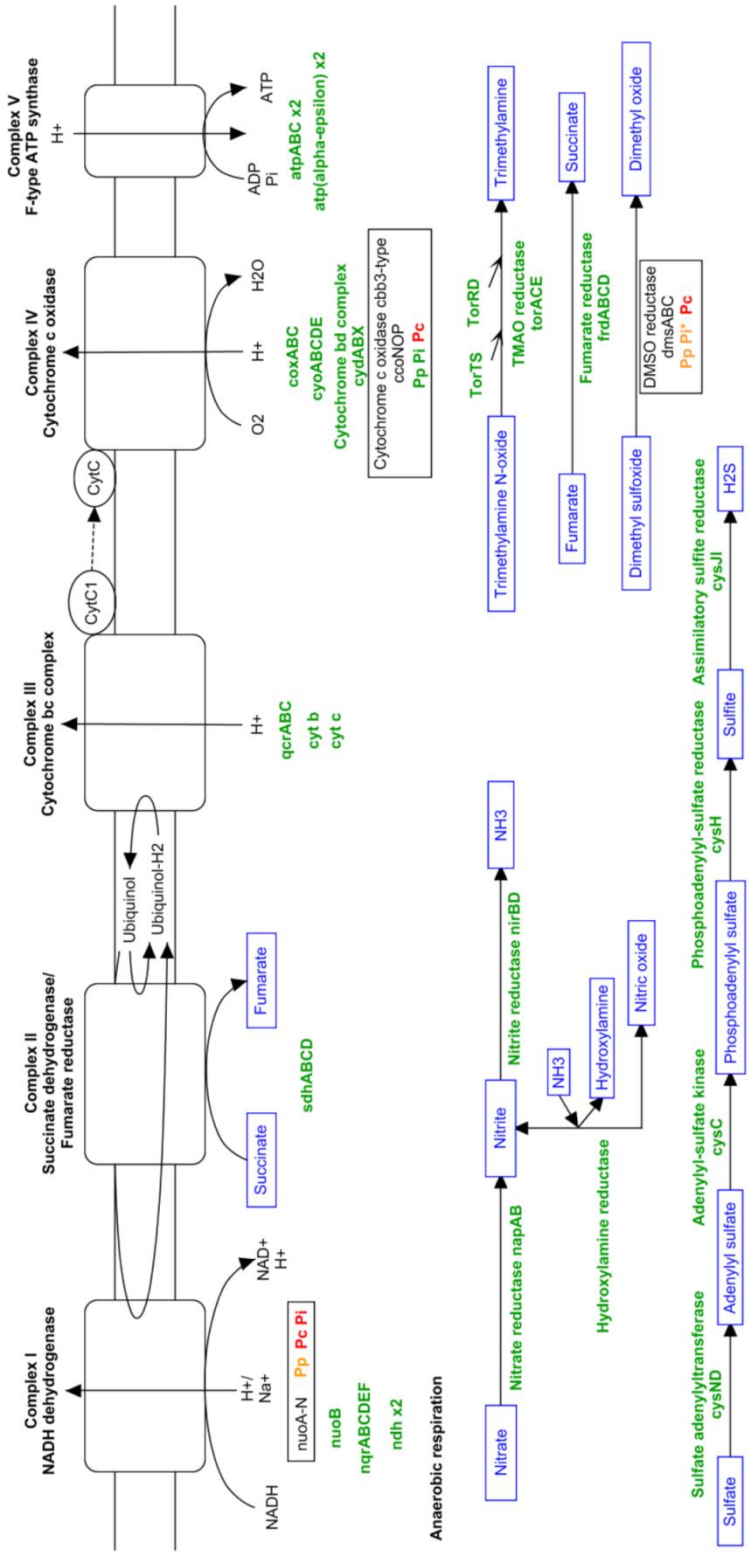

Figure S6. Respiratory chain of photobacteria. Genes in green were found in all strains screened. Genes in black were found in only some of the isolates and have a color code below for each species where: Pp = *P. phosphoreum*, Pi = *P. iliopiscarium*, Pc = *P. carnosum*; green=present in all strains of a species, red=absent in all strains of the species, orange=present in some strains of the species. An asterisk indicates that there is a source-of-isolation based distribution of the gene.

Table S1. All strains of photobacteria used in this study together with the source and country of isolation, source of the genome sequence and accession numbers. Additionally, the table includes at the end other strains that were available at the NCBI database but were identified as clones of other strains already included in the study. Type strains of each species are marked in bold letters and with a ^{T}.

Strain	Source of isolation	Geographic isolation	Source	WGS	
***Photobacterium carnosum* DSM 105454^{T}**	MAP chicken	Germany	Self-isolated	NPIB01	
Photobacterium carnosum TMW2.2029	MAP chicken	Germany	Self-isolated	NPMQ01	
Photobacterium carnosum TMW2.2097	MAP pork	Germany	Self-isolated	WMDP01	
Photobacterium carnosum TMW2.2098	MAP salmon	Germany	Self-isolated	WMDO01	
Photobacterium carnosum TMW2.2147	MAP chicken	Germany	Self-isolated	WMDN01	
Photobacterium carnosum TMW2.2149	MAP pork	Germany	Self-isolated	WMDL01	
Photobacterium carnosum TMW2.2150	Air chicken	Germany	Self-isolated	WMDK01	
Photobacterium carnosum TMW2.2157	MAP marinated chicken	Germany	Self-isolated	WMDI01	
Photobacterium carnosum TMW2.2163	MAP marinated chicken	Germany	Self-isolated	WUAU01	
Photobacterium carnosum TMW2.2169	Air marinated turkey	Germany	Self-isolated	WMDF01	
Photobacterium carnosum TMW2.2186	MAP salmon	Germany	Self-isolated	WMDE01	
Photobacterium carnosum TMW2.2187	MAP salmon	Germany	Self-isolated	WMDD01	
Photobacterium carnosum TMW2.2188	MAP salmon	Germany	Self-isolated	WMDC01	
Photobacterium carnosum TMW2.2189	MAP salmon	Germany	Self-isolated	WMDB01	
Photobacterium carnosum TMW2.2190	MAP salmon	Germany	Self-isolated	WMDA01	
***Photobacterium iliopiscarium* DSM 9896^{T}**	Herring pyloric ceca	Norway	NCBI database	PYOO01	
Photobacterium iliopiscarium ATCC 51761	Salmon (*Salmo salar*) pyloric ceca	Norway	NCBI database	PYOP01	
Photobacterium iliopiscarium NCIMB 13478	Spoiled cod fillet	Denmark	NCBI database	PYLX01	
Photobacterium iliopiscarium NCIMB 13481	Spoiled cod fillet	Denmark	NCBI database	PYLW01	
Photobacterium iliopiscarium TMW2.2104	MAP pork	Germany	Self-isolated	WMCN01	
Photobacterium iliospiscarium TMW2.2035	MAP chicken	Germany	Self-isolated	NQLV01	
***Photobacterium phosphoreum* DSM 15556^{T}**	Marine fish skin	Netherlands	NCBI database	PYOH01	
Photobacterium phosphoreum AK-3	Skin king salmon	USA:AK	NCBI database	PYND01	
Photobacterium phosphoreum AK-4	Skin Halibut	USA:AK	NCBI database	PYNC01	
Photobacterium phosphoreum AK-5	Intestine, *Oncorhynchus kisutch* (silver salmon)	USA:AK	NCBI database	PYNB01	
Photobacterium phosphoreum AK-8	Partially smoked flesh, *Oncorhynchus kisutch*	USA:AK	NCBI database	PYNA01	
Photobacterium phosphoreum FS-1.1	Skin milkfish	USA:MA	NCBI database	PYMZ01	
Photobacterium phosphoreum FS-1.2	Skin milkfish	USA:MA	NCBI database	PYMY01	
Photobacterium phosphoreum FS-2.1	Salmon	USA:CA	NCBI database	PYMX01	
Photobacterium phosphoreum FS-2.2	Salmon	USA:CA	NCBI database	PYMW01	
Photobacterium phosphoreum FS-3.2	Skin cod	USA:AK	NCBI database	PYMU01	
Photobacterium phosphoreum FS-4.1	Skin salmon	USA:CA	NCBI database	PYMT01	

Strain	**Source of isolation**	**Geographic isolation**	**Source**	**WGS**	
Photobacterium phosphoreum FS-4.2	Skin salmon	USA:CA	NCBI database	PYMS01	
Photobacterium phosphoreum FS-5.1	Skin haddock	N.A.	NCBI database	PYMR01	
Photobacterium phosphoreum FS-5.2	Skin haddock	N.A.	NCBI database	PYMQ01	
Photobacterium phosphoreum FS-6.1	Skin salmon	N.A.	NCBI database	PYMP01	
Photobacterium phosphoreum GCSL-P69	Skin cod	USA:AK	NCBI database	LZFG01	
Photobacterium phosphoreum TMW2.2033	MAP chicken	Germany	Self-isolated	NQLT01	
Photobacterium phosphoreum TMW2.2034	MAP chicken	Germany	Self-isolated	NQLU01	
Photobacterium phosphoreum TMW2.2103	MAP beef	Germany	Self-isolated	WMCZ01	
Photobacterium phosphoreum TMW2.2125	Air turkey	Germany	Self-isolated	WMCY01	
Photobacterium phosphoreum TMW2.2126	MAP marinated chicken	Germany	Self-isolated	WMCX01	
Photobacterium phosphoreum TMW2.2130	MAP marinated chicken	Germany	Self-isolated	WMCW01	
Photobacterium phosphoreum TMW2.2132	MAP marinated chicken	Germany	Self-isolated	WMCV01	
Photobacterium phosphoreum TMW2.2134	MAP marinated chicken	Germany	Self-isolated	WMCU01	
Photobacterium phosphoreum TMW2.2140	Air pork	Germany	Self-isolated	WMCS01	
Photobacterium phosphoreum TMW2.2142	MAP marinated beef	Germany	Self-isolated	WMCR01	
Photobacterium kishitanii DSM 19954^T	Light organi *Physiculus japonicus*	Japan	NCBI database	PYON01	
Clones	**Source of isolation**	**Geographic isolation**	**Source**	**WGS**	**Clone to**
Photobacterium iliopiscarium NCIMB 13355	Intestine, Herring	Norway	NCBI database	PYLU01	***Photobacterium iliopiscarium* DSM 9896^T**
Photobacterium phosphoreum JCM 21184	Marine fish skin	N.A.	NCBI database	MSCQ01	***Photobacterium phosphoreum* DSM 15556^T**
Photobacterium phosphoreum FS-2.3	Salmon	USA:CA	NCBI database	PYMV01	*Photobacterium phosphoreum* FS-2.1
Photobacterium phosphoreum FS-6.2	Skin salmon	N.A.	NCBI database	PYMO01	*Photobacterium phosphoreum* FS-6.1
Photobacterium phosphoreum FS-6.3	Skin salmon	N.A.	NCBI database	PYMN01	*Photobacterium phosphoreum* FS-6.1
Photobacterium phosphoreum GCSL-P60	King salmon	USA:AK	NCBI database	LZFE01	*Photobacterium phosphoreum* AK-3
Photobacterium phosphoreum GCSL-P64	Skin milkfish	USA:MA	NCBI database	LZFF01	*Photobacterium phosphoreum* FS-1.1

Figure S2. Accession numbers for all genes searched during the targeted gene search of the strains analyzed in this study from *P. phosphoreum*, *P. carnosum* and *P. iliopiscarium* species.

	P. carnosum														
	TMW 2.2021T	TMW 2.2029	TMW 2.2097	TMW 2.2147	TMW 2.2149	TMW 2.2150	TMW 2.2157	TMW 2.2163	TMW 2.2169	TMW 2.2098	TMW 2.2186	TMW 2.2187	TMW 2.2188	TMW 2.2189	TMW 2.2190
Pentose phosphate pathway															
6-phosphogluconolactonase (dev B)	CIK00_16850	CIT27_15305	GLP21_13380	GLP24_16320	GLP09_14870	GLP22_15710	GLP17_12540	GRJ22_13730	GLP31_05535	GLP27_18185	GLP20_16520	GLP19_07365	GLP14_14275	GLP23_13950	GLP13_18170
Phosphogluconate dehydrogenase (gnt Z)	CIK00_16855	CIT27_15300	GLP21_13385	GLP24_16325	GLP09_14875	GLP22_15715	GLP17_12535	GRJ22_13725	GLP31_05540	GLP27_18180	GLP20_16515	GLP19_07370	GLP14_14270	GLP23_13955	GLP13_18175
ribulose-5-phosphate 3-epimerase (RibuloseP<->XyluloseP) (rp e)	CIK00_06320	CIT27_11125	GLP21_07770	GLP24_09460	GLP09_04395	GLP22_09300	GLP17_08600	GRJ22_11350	GLP31_08695	GLP27_07955	GLP20_07425	GLP19_13485	GLP14_05455	GLP23_06615	GLP13_08000
Ribose 5-phosphate Isomerase (RiboseP <-> RibuloseP) (rpi A)	CIK00_17885	CIT27_14275	GLP21_05965	GLP24_15280	GLP09_11030	GLP22_13340	GLP17_11485	GRJ22_15080	GLP31_14490	GLP27_11230	GLP20_13685	GLP19_16135	GLP14_11290	GLP23_14320	GLP13_12285
Transketolase (*tkt* A)	CIK00_16330	CIT27_06105	GLP21_05570	GLP24_18930	GLP09_16680	GLP22_00140	GLP17_05415	GRJ22_00820	GLP31_08040	GLP27_01960	GLP20_05265	GLP19_01645	GLP14_02830	GLP23_07510	GLP13_16875
Transaldolase (*ta l*)	CIK00_16325	CIT27_06110	GLP21_05575	GLP24_18925	GLP09_16685	GLP22_00135	GLP17_05420	GRJ22_00815	GLP31_08045	GLP27_01965	GLP20_05260	GLP19_01640	GLP14_02835	GLP23_07515	GLP13_16870
Gluconeogenese															
Phoshoenolyruvate carboxylase (pyc) / PEPcase (ppc)	CIK00_06410	CIT27_11035	GLP21_07680	GLP24_09550	GLP09_04305	GLP22_09210	GLP17_08690	GRJ22_11260	GLP31_08785	GLP27_07865	GLP20_07335	GLP19_13395	GLP14_05365	GLP23_06705	GLP13_07910
Pyruvate carboxylase (pyc)															
phosphoenolpyruvate carboxykinase (pckA)	CIK00_14600	CIT27_13705	GLP21_15015	GLP24_14245	GLP09_11795	GLP22_12850	GLP17_16635	GRJ22_14505	GLP31_14980	GLP27_12165	GLP20_13125	GLP19_14860	GLP14_10810	GLP23_12570	GLP13_13670
PEP synthase (pps A)	CIK00_00060	CIT27_01905	GLP21_15440	GLP24_07465	GLP09_02445	GLP22_04020	GLP17_13155	GRJ22_05755	GLP31_02625	GLP27_05055	GLP20_02930	GLP19_09745	GLP14_15605	GLP23_18700	GLP13_02025
phosphoenolpyruvate utilizing protein	CIK00_00060	CIT27_01905	GLP21_15440	GLP24_07465	GLP09_02445	GLP22_04020	GLP17_13155	GRJ22_05755	GLP31_02625	GLP27_05055	GLP20_02930	GLP19_09745	GLP14_15605	GLP23_18700	GLP13_02025
malate dehydrogenase (oxaloacetate-decarboxylating)	CIK00_12535	CIT27_13035	GLP21_13105	GLP24_13125	GLP09_08665	GLP22_11080	GLP17_11065	GRJ22_13050	GLP31_12135	GLP27_10630	GLP20_12590	GLP19_14325	GLP14_08490	GLP23_09730	GLP13_13335
Aspartate/tyrosine/aromatic aminotransferase	CIK00_04000	CIT27_15900	GLP21_14465	GLP24_17005	GLP09_11945	GLP22_07795	GLP17_17565	GRJ22_16730	GLP31_16115	GLP27_16805	GLP20_05070	GLP19_10925	GLP14_02095	GLP23_16175	GLP13_05285
	CIK00_00510	CIT27_02360	GLP21_02460	GLP24_07025	GLP09_01985	GLP22_03575	GLP17_06610	GRJ22_08245	GLP31_02175	GLP27_04610	GLP20_03395	GLP19_03415	GLP14_00960	GLP23_10825	GLP13_01380
Aspartate oxidase	CIK00_17805	CIT27_14195	GLP21_05885	GLP24_15360	GLP09_10950	GLP22_13420	GLP17_11405	GRJ22_15000	GLP31_14410	GLP27_11310	GLP20_13605	GLP19_16055	GLP14_11370	GLP23_14400	GLP13_12205
Fructose-1,6-bisphosphatase (fdp)	CIK00_06480	CIT27_10965	GLP21_07610	GLP24_09620	GLP09_04235	GLP22_09140	GLP17_08760	GRJ22_11190	GLP31_08855	GLP27_07795	GLP20_07265	GLP19_13325	GLP14_05295	GLP23_06775	GLP13_07840
	CIK00_12515	CIT27_13055	GLP21_13125	GLP24_13145	GLP09_08645	GLP22_11100	GLP17_11085	GRJ22_13030	GLP31_12115	GLP27_10610	GLP20_12610	GLP19_14305	GLP14_08470	GLP23_09710	GLP13_13355
glucose-6-phosphatase (phosphatase PAP2 family) (g6pc)															
phosphatase PAP2 family	CIK00_09970	CIT27_01385	GLP21_09430	GLP24_12345	GLP09_10290	GLP22_05675	GLP17_09465	GRJ22_05235	GLP31_06060	GLP27_09755	GLP20_10140	GLP19_09225	GLP14_07105	GLP23_09355	GLP13_09255
Glycolysis															
glucokinase (*glc* K) putative / sugar kinase / ROK family sugar kinase	CIK00_04150	CIT27_08040	GLP21_14625	GLP24_08475	GLP09_12085	GLP22_07645	GLP17_07665	GRJ22_17945	GLP31_16280	GLP27_18840	GLP20_04925	GLP19_10750	GLP14_01940	GLP23_18085	GLP13_05130
					GLP09_08530	GLP22_01070		GRJ22_01735				GLP19_06660		GLP23_17795	
								GRJ22_18320							GLP13_03390
phosphoglucomutase (pgm)	CIK00_01655	CIT27_03515	GLP21_01310	GLP24_02940	GLP09_00835	GLP22_02425	GLP17_03075	GRJ22_12085	GLP31_01025	GLP27_03410	GLP20_02355	GLP19_02265	GLP14_10485	GLP23_02405	GLP13_00230
	CIK00_05715	CIT27_07695	GLP21_14265	GLP24_10440	GLP09_06480	GLP22_01935	GLP17_02320	GRJ22_02615	GLP31_11080	GLP27_00305	GLP20_10650	GLP19_05800	GLP14_03380	GLP23_11185	GLP13_03070
Glucose-6-phosphate isomerase (pgi)	CIK00_18350	CIT27_16090	GLP21_17110	GLP24_17510	GLP09_15540	GLP22_16695	GLP17_15135	GRJ22_17255	GLP31_16975	GLP27_15870	GLP20_15205	GLP19_16865	GLP14_16275	GLP23_15515	GLP13_16465
mannose-6-P isomerase (man A)	CIK00_13205	CIT27_04110	GLP21_03850	GLP24_19715 + GLP24_19720	GLP09_02860	GLP22_19005 + GLP22_19010		GRJ22_14010	GLP31_13840	GLP27_19405	GLP20_01290	GLP19_04190	GLP14_08065	GLP23_00230	GLP13_06215
glyceraldehyde phosphate dehydrogenase	CIK00_09410	CIT27_04585	GLP21_03405	GLP24_06025	GLP09_03370	GLP22_06185	GLP17_00395	GRJ22_06175	GLP31_12635	GLP27_09190	GLP20_00870	GLP19_04670	GLP14_09570	GLP23_00700	GLP13_05715
phosphoglycerate kinase	CIK00_17910	CIT27_14300	GLP21_05990	GLP24_15255	GLP09_11055	GLP22_13315	GLP17_11510	GRJ22_15105	GLP31_14515	GLP27_11205	GLP20_13710	GLP19_16160	GLP14_11265	GLP23_14295	GLP13_12310
phosphoglycerate mutase / phosphoglycerate mutase (2,3-diphosphoglycerate-independent)	CIK00_06545	CIT27_10900	GLP21_07540	GLP24_09685	GLP09_04170	GLP22_09075	GLP17_08825	GRJ22_11125	GLP31_08925	GLP27_07730	GLP20_07200	GLP19_13260	GLP14_05230	GLP23_06840	GLP13_07770
2,3-diphosphoglycerate-dependent phosphoglycerate mutase															
enolase	CIK00_17720	CIT27_14110	GLP21_05800	GLP24_15445	GLP09_10865	GLP22_13505	GLP17_11320	GRJ22_14915	GLP31_14325	GLP27_11395	GLP20_13520	GLP19_15970	GLP14_11455	GLP23_14485	GLP13_12120
pyruvate kinase	CIK00_00860	CIT27_02710	GLP21_02110	GLP24_06680	GLP09_01640	GLP22_03225	GLP17_06265	GRJ22_08590	GLP31_01825	GLP27_04265	GLP20_03740	GLP19_03065	GLP14_00615	GLP23_10190	GLP13_01035
	CIK00_12700	CIT27_12870	GLP21_12945	GLP24_12965	GLP09_08825	GLP22_10920	GLP17_10905	GRJ22_13210	GLP31_12295	GLP27_10790	GLP20_12430	GLP19_14485	GLP14_08650	GLP23_09890	GLP13_13175
glucose -> pyruvate Homolactic fermentation															
6-phosphofructokinase (pfk A)	CIK00_06500	CIT27_10945	GLP21_07585	GLP24_09640	GLP09_04215	GLP22_09120	GLP17_08780	GRJ22_11170	GLP31_08880	GLP27_07775	GLP20_07245	GLP19_13305	GLP14_05275	GLP23_06795	GLP13_07815
fructose-1,6-bisphosphate aldolase (fba A)	CIK00_17905	CIT27_14295	GLP21_05985	GLP24_15260	GLP09_11050	GLP22_13320	GLP17_11505	GRJ22_15100	GLP31_14510	GLP27_11210	GLP20_13705	GLP19_16155	GLP14_11270	GLP23_14300	GLP13_12305
glucose -> pyruvate Heterolactic fermentation															
phosphoketolase (xpk A)															
glucose-6-phosphate dehydrogenase (zwf)	CIK00_16845	CIT27_15310	GLP21_13375	GLP24_16315	GLP09_14865	GLP22_15705	GLP17_12545	GRJ22_13735	GLP31_05530	GLP27_18190	GLP20_16525	GLP19_07360	GLP14_14280	GLP23_13945	GLP13_18165
KDPG weg															
phosphogluconate dehydratase (ed d)											GLP20_17760				
KDPG aldolase (ed a)	CIK00_13585	CIT27_06895	GLP21_04735	GLP24_11030	GLP09_08535	GLP22_01075	GLP17_01470	GRJ22_01740	GLP31_07000	GLP27_01075	GLP20_08530	GLP19_06655	GLP14_14680	GLP23_17800	GLP13_02270
glucose-6-phosphate dehydrogenase (1.1.1.49/1.1.1.363)	CIK00_16845	CIT27_15310	GLP21_13375	GLP24_16315	GLP09_14865	GLP22_15705	GLP17_12545	GRJ22_13735	GLP31_05530	GLP27_18190	GLP20_16525	GLP19_07360	GLP14_14280	GLP23_13945	GLP13_18165
6-phosphogluconolactonase 3.1.1.31	CIK00_16850	CIT27_15305	GLP21_13380	GLP24_16320	GLP09_14870	GLP22_15710	GLP17_12540	GRJ22_13730	GLP31_05535	GLP27_18185	GLP20_16520	GLP19_07365	GLP14_14275	GLP23_13950	GLP13_18170
Ribose											GLP20_17765			GLP23_14590	GLP13_03395
D-ribose pyranase / Ribopyranase (*rbs* D) (ribopyranose -> ribofuranose)	CIK00_13550	CIT27_06860	GLP21_04770	GLP24_10995	GLP09_08475	GLP22_01015	GLP17_01435	GRJ22_01680	GLP31_07030	GLP27_01110	GLP20_08495	GLP19_06715	GLP14_14645	GLP23_19150	GLP13_02235
Ribokinase (*rbs* K)	CIK00_13570	CIT27_06880	GLP21_04750	GLP24_11015	GLP09_08495	GLP22_01035	GLP17_01455	GRJ22_01700	GLP31_07015	GLP27_01090	GLP20_08515	GLP19_06695	GLP14_14665	GLP23_19130	GLP13_02255
	CIK00_13555	CIT27_06865	GLP21_04765	GLP24_11000	GLP09_08480	GLP22_01020	GLP17_01440	GRJ22_01685		GLP27_01105	GLP20_08500	GLP19_06710	GLP14_14650	GLP23_19145	GLP13_02240
Ribose Transporter (ribose uptake protein) *rbs* U															
Putative deoxyribose-specific ABC transporter (*nup* A oder *yng* F)															
Ribose-5-phosphate isomerase (RpiA)	CIK00_17885	CIT27_14275	GLP21_05965	GLP24_15280	GLP09_11030	GLP22_13340	GLP17_11485	GRJ22_15080	GLP31_14490	GLP27_11230	GLP20_13685	GLP19_16135	GLP14_11290	GLP23_14320	GLP13_12285
Ribulose-phosphate 3-epimerase (Rpe)	CIK00_06320	CIT27_11125	GLP21_07770	GLP24_09460	GLP09_04395	GLP22_09300	GLP17_08600	GRJ22_11350	GLP31_08695	GLP27_07955	GLP20_07425	GLP19_13485	GLP14_05455	GLP23_06615	GLP13_08000
Xylulose-5-phosphate phosphoketolase (Xpk)															
ribose-5-phosphate pyrophosphokinase	CIK00_20390	CIT27_03750	GLP21_04225	GLP24_18650	GLP09_17205	GLP22_14920	GLP17_18180	GRJ22_16360	GLP31_19820	GLP27_14890	GLP20_17860	GLP19_18460	GLP14_08430	GLP23_18345	GLP13_15560
Nucleoside															
Nucleoside-diphosphate Kinase	CIK00_18940	CIT27_16610	GLP21_00145	GLP24_16110	GLP09_12535	GLP22_13695	GLP17_15565	GRJ22_07320	GLP31_15175	GLP27_16410	GLP20_15670	GLP19_11740	GLP14_14180	GLP23_12945	GLP13_16205
inosine-uridine nucleoside ribohydrolase (*iun* H)															
ribonucleoside nucleosidase (unspecific, RihC)	CIK00_04035	CIT27_15920	GLP21_14505	GLP24_16970	GLP09_11970	GLP22_07770	GLP17_17525	GRJ22_16705	GLP31_16155	GLP27_16835	GLP20_05045	GLP19_10890	GLP14_02070	GLP23_16150	GLP13_05265
purine (deoxy)nucleoside phosphorylase (RibP/Pur) (deoD)	CIK00_07190	CIT27_10275	GLP21_11195	GLP24_09095	GLP09_05555	GLP22_15175	GLP17_07930	GRJ22_10155	GLP31_07735	GLP27_07070	GLP20_06515	GLP19_12535	GLP14_04585	GLP23_04625	GLP13_08235

	P. carnosum													
	TMW 2.2021T	**TMW 2.2029**	**TMW 2.2097**	**TMW 2.2147**	**TMW 2.2149**	**TMW 2.2150**	**TMW 2.2157**	**TMW 2.2163**	**TMW 2.2169**	**TMW 2.2098**	**TMW 2.2186**	**TMW 2.2187**	**TMW 2.2188**	**TMW 2.2189**	**TMW 2.2190**
pyrimidine (deoxy)nucleoside phosphorylase (RibP/Pur) (deoA)	CIK00_07200	CIT27_10265	GLP21_11185	GLP24_09085	GLP09_05565	GLP22_15185	GLP17_07940	GRJ22_10165	GLP31_07725	GLP27_07060	GLP20_06505	GLP19_12525	GLP14_04575	GLP23_04615	GLP13_08245
purine/pyrimidine nucleosidase (Rib/Pur)															
ribose 1,5-phosphopentomutase (deoB)	CIK00_07195	CIT27_10270	GLP21_11190	GLP24_09090	GLP09_05560	GLP22_15180	GLP17_07935	GRJ22_10160	GLP31_07730	GLP27_07065	GLP20_06510	GLP19_12530	GLP14_04580	GLP23_04620	GLP13_08240
Nucleoside to Deoxynucleoside															
Ribonucleotide reductase alpha/assembly/beta															
nrd A	CIK00_01015	CIT27_02865	GLP21_01955	GLP24_18905	GLP09_01485	GLP22_03070	GLP17_06110	GRJ22_08745	GLP31_01670	GLP27_04110	GLP20_03895	GLP19_02910	GLP14_00460	GLP23_10345	GLP13_00880
nrdB	CIK00_01020	CIT27_02870	GLP21_01950	GLP24_18900	GLP09_01480	GLP22_03065	GLP17_06105	GRJ22_08750	GLP31_01665	GLP27_04105	GLP20_03900	GLP19_02905	GLP14_00455	GLP23_10350	GLP13_00875
nrdI										GLP27_17505	GLP20_16165				
DeoxyRibose from DNA															
Deoxyribose-phosphate aldolase (deoC)	CIK00_07205	CIT27_10260	GLP21_11180	GLP24_09080	GLP09_05570	GLP22_15190	GLP17_07945	GRJ22_10170	GLP31_07720	GLP27_07055	GLP20_06500	GLP19_12520	GLP14_04570	GLP23_04610	GLP13_08250
Ribose from free NTP/RNA															
to PP Pathway / Hetero															
Sugar transporters															
galactose/methyl galactoside ABC transporter ATP-binding protein MglA	CIK00_04630		GLP21_10240	GLP24_08100	GLP09_13535			GRJ22_03275			GLP20_04525		GLP14_01560		GLP13_04765
galactoside ABC transporter permease MglC	CIK00_04635		GLP21_10235	GLP24_08095	GLP09_13540			GRJ22_03280			GLP20_04520		GLP14_01555		GLP13_04760
methyl-galactoside ABC transporter substrate-binding protein MglB	CIK00_04625		GLP21_10245	GLP24_08105	GLP09_13530			GRJ22_03270			GLP20_04530		GLP14_01565		GLP13_04770
maltose/maltodextrin ABC transporter substrate-binding protein MalE	CIK00_11945	CIT27_09180	GLP21_11915	GLP24_00555	GLP09_07545	GLP22_08515	GLP17_04550	GRJ22_04255	GLP31_03195	GLP27_05225	GLP20_09185	GLP19_00290	GLP14_05900	GLP23_08710	GLP13_03735
		CIT27_09165		GLP24_00570			GLP17_04565		GLP31_03210				GLP14_05915		GLP13_03720
maltose ABC transporter permease MalF	CIK00_11950	CIT27_09185	GLP21_11910	GLP24_00550	GLP09_07540	GLP22_08520	GLP17_04545	GRJ22_04250	GLP31_03190	GLP27_05230	GLP20_09190	GLP19_00285	GLP14_05895	GLP23_08715	GLP13_03740
maltose ABC transporter permease MalG	CIK00_11955	CIT27_09190	GLP21_11905	GLP24_00545	GLP09_07535	GLP22_08525	GLP17_04540	GRJ22_04245	GLP31_03185	GLP27_05235	GLP20_09195	GLP19_00280	GLP14_05890	GLP23_08720	GLP13_03745
maltose/maltodextrin ABC transporter ATP-binding protein MalK	CIK00_18225	CIT27_09175	GLP21_11920	GLP24_00560	GLP09_07550	GLP22_08510	GLP17_04555	GRJ22_04260	GLP31_03200	GLP27_05220	GLP20_09180	GLP19_00295	GLP14_05905	GLP23_08705	GLP13_03730
PTS lactose/cellobiose transporter subunit IIA		CIT27_05825				GLP22_00510		GRJ22_01170	GLP31_18895	GLP27_01660	GLP20_05575	GLP19_01935	GLP14_02515		GLP13_15160
PTS cellobiose transporter subunit IIC		CIT27_05830				GLP22_00505		GRJ22_01165	GLP31_18890	GLP27_01665	GLP20_05570	GLP19_01930	GLP14_02520		GLP13_15165
PTS_system,_cellobiose-specific_IIB_component_(EC_2.7.1.205)		CIT27_05835				GLP22_00500		GRJ22_01160	GLP31_18885	GLP27_01670	GLP20_05565	GLP19_01925	GLP14_02525		GLP13_15170
PTS mannose transporter subunit IIA					GLP09_14195	GLP22_00320		GRJ22_01035				GLP19_01795		GLP23_17870	
PTS mannose transporter subunit IIB	CIK00_11620	CIT27_05140	GLP21_02855	GLP24_05465	GLP09_09450	GLP22_06745	GLP17_00955	GRJ22_06715	GLP31_04990	GLP27_10270	GLP20_00330	GLP19_05225	GLP14_07595	GLP23_01240	GLP13_12660
Sugars															
6-phospho-beta-glucosidase		CIT27_05820				GLP22_00515		GRJ22_01175	GLP31_18900	GLP27_01655	GLP20_05580	GLP19_01940	GLP14_02510		GLP13_15155
alpha-galactosidase	CIK00_18170	CIT27_09115	GLP21_11975	GLP24_00620	GLP09_07605	GLP22_08455	GLP17_04615	GRJ22_04315	GLP31_03260	GLP27_05165	GLP20_09125	GLP19_00350	GLP14_05965	GLP23_08650	GLP13_03670
			GLP21_08200												
beta-galactosidase			GLP21_08195												
beta-galactosidase subunit beta	CIK00_11185	CIT27_00170	GLP21_08860	GLP24_03890	GLP09_15085	GLP22_04400	GLP17_10240	GRJ22_09720	GLP31_04625	GLP27_11785	GLP20_11140	GLP19_07785	GLP14_11805	GLP23_05820	GLP13_10255
beta-galactosidase subunit alpha	CIK00_11190	CIT27_00175	GLP21_08855	GLP24_03895	GLP09_15090	GLP22_04405	GLP17_10245	GRJ22_09715	GLP31_04620	GLP27_11790	GLP20_11145	GLP19_07790	GLP14_11800	GLP23_05825	GLP13_10260
alpha-glucosidase	CIK00_12020	CIT27_09255	GLP21_11840	GLP24_00480	GLP09_07470	GLP22_08590	GLP17_04475	GRJ22_04180	GLP31_03120	GLP27_05300	GLP20_09260	GLP19_00215	GLP14_05825	GLP23_08785	GLP13_03810
	CIK00_16490					GLP22_00390		GRJ22_01105				GLP19_01870			GLP13_17040
beta-mannosidase	CIK00_12895	CIT27_12680	GLP21_12750	GLP24_12770	GLP09_09020	GLP22_10725	GLP17_10710	GRJ22_13405	GLP31_12490	GLP27_10985	GLP20_12235	GLP19_14685	GLP14_08845	GLP23_10085	GLP13_12985
	CIK00_19605	CIT27_05655	GLP21_05095	GLP24_13590	GLP09_08155	GLP22_00690	GLP17_14395	GRJ22_01345	GLP31_14070	GLP27_01475	GLP20_05790	GLP19_07025	GLP14_02345	GLP23_11645	GLP13_15000
alpha-mannosidase	CIK00_19460		GLP21_05015							GLP27_01355				GLP23_11520	
	CIK00_19465		GLP21_05010							GLP27_01350				GLP23_11515	
		CIT27_03045						GRJ22_08925		GLP27_03860			GLP14_00285		GLP13_00700
									GLP31_14105						
									GLP31_14110						
Glycogen															
Glycogen phosphorylase (*glg* P)	CIK00_18180	CIT27_09125	GLP21_11965	GLP24_00610	GLP09_07595	GLP22_08465	GLP17_04605	GRJ22_04305	GLP31_03250	GLP27_05175	GLP20_09135	GLP19_00340	GLP14_05955	GLP23_08660	GLP13_03680
UTP-glucose-1-phosphate uridylyltransferase (gta B)	CIK00_08525	CIT27_11330	GLP21_06840	GLP24_11555	GLP09_07335	GLP22_10050	GLP17_13700	GRJ22_12385	GLP31_10770	GLP27_08290	GLP20_07760	GLP19_13680	GLP14_06305	GLP23_08005	GLP13_09500
	CIK00_13355	CIT27_04290	GLP21_03700	GLP24_06330 + GLP24_18135	GLP09_02995		GLP17_16925		GLP31_13690	GLP27_18400	GLP20_01160	GLP19_04370	GLP14_07940	GLP23_00385	GLP13_06010
Glycogen synthase (*glg* A)															
starch synthase (GT5)															
glucoamylase (GH15)															
Glycogen biosynthesis protein (Glg D)															
1,4-alpha-glucan branching enzyme	CIK00_18190	CIT27_09135	GLP21_11955	GLP24_00600	GLP09_07585	GLP22_08475	GLP17_04595	GRJ22_04295	GLP31_03240	GLP27_05185	GLP20_09145	GLP19_00330	GLP14_05945	GLP23_08670	GLP13_03690
glycogen debranching enzyme (GH13)	CIK00_18200	CIT27_09145	GLP21_11945	GLP24_00590	GLP09_07575	GLP22_08485	GLP17_04585	GRJ22_04285	GLP31_03230	GLP27_05195	GLP20_09155	GLP19_00320	GLP14_05935	GLP23_08680	GLP13_03700
	CIK00_18220	CIT27_09170	GLP21_11925	GLP24_00565	GLP09_07555	GLP22_08505	GLP17_04560	GRJ22_04265	GLP31_03205	GLP27_05215	GLP20_09175	GLP19_00300	GLP14_05910	GLP23_08700	GLP13_03725
alpha-amylase (GH13)	CIK00_18165	CIT27_09110	GLP21_11980	GLP24_00625	GLP09_07610	GLP22_08450	GLP17_04620	GRJ22_04320	GLP31_03265	GLP27_05160	GLP20_09120	GLP19_00355	GLP14_05970	GLP23_08645	GLP13_03665
	CIK00_18215	CIT27_09160	GLP21_11930	GLP24_00575	GLP09_07560	GLP22_08500	GLP17_04570	GRJ22_04270	GLP31_03215	GLP27_05210	GLP20_09170	GLP19_00305	GLP14_05920	GLP23_08695	GLP13_03715
		CIT27_09330			GLP09_05470		GLP17_07845								GLP13_03880
4-alpha-glucanotransferase (GH13)	CIK00_18185	CIT27_09130	GLP21_11960	GLP24_00605	GLP09_07590	GLP22_08470	GLP17_04600	GRJ22_04300	GLP31_03245	GLP27_05180	GLP20_09140	GLP19_00335	GLP14_05950	GLP23_08665	GLP13_03685
alpha-glucosidase (GH13)	CIK00_12020	CIT27_09255	GLP21_11840	GLP24_00480	GLP09_07470	GLP22_08590	GLP17_04475	GRJ22_04180	GLP31_03120	GLP27_05300	GLP20_09260	GLP19_00215	GLP14_05825	GLP23_08785	GLP13_03810
	CIK00_16490					GLP22_00390		GRJ22_01105				GLP19_01870			GLP13_17040
Pullulanase -type alpha-1,6-glucosidase	CIK00_18160	CIT27_09105	GLP21_11985	GLP24_00630	GLP09_07615	GLP22_08445	GLP17_04625	GRJ22_04325	GLP31_03270	GLP27_05155	GLP20_09115	GLP19_00360	GLP14_05975	GLP23_08640	GLP13_03660
Pyruvate fates															
Pyruvate dehydrogenase complex (cluster)															
Pyruvate dehydrogenase alpha E1 (acetoin-oxidoreductase) pdhA / aceE (homodimeric)	CIK00_08990	CIT27_11795	GLP21_06370	GLP24_12015	GLP09_06870	GLP22_09580	GLP17_12970	GRJ22_12845	GLP31_10265	GLP27_08785	GLP20_08255	GLP19_14150	GLP14_06775	GLP23_08475	GLP13_09965

	P. carnosum														
	TMW 2.2021T	**TMW 2.2029**	**TMW 2.2097**	**TMW 2.2147**	**TMW 2.2149**	**TMW 2.2150**	**TMW 2.2157**	**TMW 2.2163**	**TMW 2.2169**	**TMW 2.2098**	**TMW 2.2186**	**TMW 2.2187**	**TMW 2.2188**	**TMW 2.2189**	**TMW 2.2190**
Pyruvate dehydrogenase beta E1 (oxo-isovaleriate dehydrogenase) pdhB															
Dihydrolipoamide acetyltransferase E2 pdhC	CIK00_08995	CIT27_11800	GLP21_06365	GLP24_12020	GLP09_06865	GLP22_09575	GLP17_12975	GRJ22_12850	GLP31_10260	GLP27_08790	GLP20_08260	GLP19_14155	GLP14_06780	GLP23_08480	GLP13_09970
Dihydrolipoyl-Dehydrogenase E3 pdhD	CIK00_09000	CIT27_11805	GLP21_06360	GLP24_12025	GLP09_06860	GLP22_09570	GLP17_12980	GRJ22_12855	GLP31_10255	GLP27_08795	GLP20_08265	GLP19_14160	GLP14_06785	GLP23_08485	GLP13_09975
Lactate++															
L-lactate dehydrogenase (ldh)															
D-lactate dehydrogenase (ldh)															
D-lactate dehydrogenase / 2-hydroxyacid dehydrogenase	CIK00_11665	CIT27_05185	GLP21_02810	GLP24_05420	GLP09_09405	GLP22_06790	GLP17_01000	GRJ22_06760	GLP31_05035	GLP27_10315	GLP20_00285	GLP19_05270	GLP14_07640	GLP23_01285	GLP13_12705
lactate dehydrogenase	CIK00_10805	CIT27_06150	GLP21_05590	GLP24_01880	GLP09_16705	GLP22_00115	GLP17_05440	GRJ22_00800	GLP31_08070	GLP27_01995	GLP20_05240	GLP19_01620	GLP14_02860	GLP23_07535	GLP13_17065
2-hydroxyacid dehydrogenase	CIK00_11665	CIT27_05185	GLP21_02810	GLP24_05420	GLP09_09405	GLP22_06790	GLP17_01000	GRJ22_06760	GLP31_05035	GLP27_10315	GLP20_00285	GLP19_05270	GLP14_07640	GLP23_01285	GLP13_12705
Acetate															
Phosphotransacetylase pta	CIK00_13060	CIT27_03970	GLP21_04000	GLP24_17720	GLP09_02730	GLP22_14705	GLP17_14675	GRJ22_16565	GLP31_17660	GLP27_15095	GLP20_15910	GLP19_04055	GLP14_08210	GLP23_00095	GLP13_15340
Pyruvate oxidase poxB	CIK00_07965	CIT27_00970	GLP21_09010	GLP24_04940	GLP09_15210	GLP22_05260	GLP17_15470	GRJ22_04820	GLP31_05645	GLP27_15535	GLP20_15055	GLP19_08815	GLP14_12790	GLP23_15375	GLP13_10880
Acetatekinase ackA	CIK00_13065	CIT27_03975	GLP21_03995	GLP24_17715	GLP09_02735	GLP22_14700	GLP17_14670	GRJ22_16570	GLP31_17655	GLP27_15100	GLP20_15915	GLP19_04060	GLP14_08205	GLP23_00100	GLP13_15335
Acylphosphatase (acyP)															
Ethanol															
Acetaldehyde dehydrogenase / Alcohol dehydrogenase adhE	CIK00_01380	CIT27_03240	GLP21_01585	GLP24_03215	GLP09_01110	GLP22_02700	GLP17_02800	GRJ22_11810	GLP31_01300	GLP27_03685	GLP20_02630	GLP19_02540	GLP14_00090	GLP23_02680	GLP13_00505
Ethanol/Acetate															
Pyruvate formate lyase (allerdings O2 sensitive) pflB	CIK00_13125	CIT27_04035	GLP21_03930	GLP24_17645	GLP09_02795	GLP22_14630	GLP17_14605	GRJ22_16630	GLP31_17600	GLP27_19705	GLP20_15985	GLP19_04120	GLP14_08140	GLP23_00160	GLP13_15275
Formate efflux transporter / formate-nitrite transporter focA	CIK00_13130	CIT27_04040	GLP21_03925	GLP24_17640	GLP09_02800	GLP22_14625	GLP17_14600	GRJ22_16635	GLP31_17595	GLP27_19710	GLP20_15990	GLP19_04125	GLP14_08135	GLP23_00165	GLP13_15270
acetaldehyde dehydrogenase	CIK00_04230					GLP22_07585									
alcohol dehydrogenase	CIK00_04240					GLP22_07575									
iron containing alcohol dehydrogenase	CIK00_10390	CIT27_06580	GLP21_13645	GLP24_01465	GLP09_11195	GLP22_12430	GLP17_05870	GRJ22_00360	GLP31_08490	GLP27_02425	GLP20_12690	GLP19_01165	GLP14_15050	GLP23_02855	GLP13_07105
	CIK00_19440	CIT27_05550	GLP21_05035	GLP24_18255	GLP09_08220	GLP22_00755	GLP17_14455	GRJ22_01420	GLP31_14140	GLP27_01375	GLP20_05850	GLP19_06965	GLP14_02290	GLP23_11540 + GLP23_12280	GLP13_18125
alcohol dehydrogenase AdhP															
Formate															
Formate acetyltransferase (PFL)	CIK00_13125	CIT27_04035	GLP21_03930	GLP24_17645	GLP09_02795	GLP22_14630	GLP17_14605	GRJ22_16630	GLP31_17600	GLP27_19705	GLP20_15985	GLP19_04120	GLP14_08140	GLP23_00160	GLP13_15275
formate dehydrogenase (fdh)															
fdhABCE															
A	CIK00_19980	CIT27_17415	GLP21_18405	GLP24_15880	GLP09_12300	GLP22_13930	GLP17_17670	GRJ22_07080	GLP31_15395	GLP27_18770	GLP20_17435	GLP19_11975	GLP14_13955	GLP23_12725	GLP13_18015
B	CIK00_19985	CIT27_17410	GLP21_18410	GLP24_15875	GLP09_12295	GLP22_13935	GLP17_17665	GRJ22_07075	GLP31_15400	GLP27_18775	GLP20_17430	GLP19_11980	GLP14_13950	GLP23_12720	GLP13_18020
C	CIK00_19990	CIT27_17405	GLP21_18415	GLP24_15870	GLP09_12290	GLP22_13940	GLP17_17660	GRJ22_07070	GLP31_15405	GLP27_18780	GLP20_17425	GLP19_11985	GLP14_13945	GLP23_12715	GLP13_18025
E	CIK00_19995	CIT27_17400	GLP21_18420	GLP24_15865	GLP09_12285	GLP22_13945	GLP17_17655	GRJ22_07065	GLP31_15410	GLP27_18785	GLP20_17420	GLP19_11990	GLP14_13940	GLP23_12710	GLP13_18030
Acetolactate															
Acetolactate synthase (alsS)	CIK00_10875	CIT27_17260	GLP21_13470	GLP24_03570	GLP09_17545	GLP22_17270	GLP17_18455	GRJ22_13635	GLP31_18570	GLP27_17700	GLP20_16680	GLP19_07455	GLP14_17365	GLP23_16895	GLP13_17730
Diacetyl															
spontaneous from acetolactate															
Acetoin															
Acetolactate decarboxylase aldC	CIK00_10870	CIT27_17255	GLP21_13465	GLP24_03565	GLP09_17550	GLP22_17265	GLP17_18450	GRJ22_13640	GLP31_18575	GLP27_17695	GLP20_16675	GLP19_07450	GLP14_17360	GLP23_16890	GLP13_17725
Butane-2,3-diol															
Diacetyl reductase (Acetoin reductase) budC / butA / bdhA															
Reoxidizing NADH (O_2)															
NADH oxidase putative!	CIK00_00715	CIT27_02565	GLP21_02255	GLP24_06825	GLP09_01785	GLP22_03370	GLP17_06410	GRJ22_08445	GLP31_01970	GLP27_04405	GLP20_03595	GLP19_03210	GLP14_00760	GLP23_10620	GLP13_01180
	CIK00_17990	CIT27_08950	GLP21_18250	GLP24_00785	GLP09_07780	GLP22_08290	GLP17_04800	GRJ22_04490	GLP31_03425	GLP27_13355	GLP20_11700	GLP19_00505	GLP14_06130	GLP23_03660	GLP13_06455
Na+ transporting NADH:ubiquinone oxidorreductase nqrF: NADH:ubiquinone oxidoreductase, Na(+)-translocating, F subunit	CIK00_02500	CIT27_12440	GLP21_00405	GLP24_02065	GLP09_00180	GLP22_11930	GLP17_03925	GRJ22_07585	GLP31_00180	GLP27_02550	GLP20_01510	GLP19_11485	GLP14_12505	GLP23_01560	GLP13_11715
NADH:ubiquinone reductase (Na(+)-transporting) subunit E	CIK00_02505	CIT27_12445	GLP21_00400	GLP24_02060	GLP09_00175	GLP22_11925	GLP17_03930	GRJ22_07580	GLP31_00175	GLP27_02545	GLP20_01505	GLP19_11490	GLP14_12500	GLP23_01555	GLP13_11720
NADH:ubiquinone reductase (Na(+)-transporting) subunit D	CIK00_02510	CIT27_12450	GLP21_00395	GLP24_02055	GLP09_00170	GLP22_11920	GLP17_03935	GRJ22_07575	GLP31_00170	GLP27_02540	GLP20_01500	GLP19_11495	GLP14_12495	GLP23_01550	GLP13_11725
Na(+)-translocating NADH-quinone reductase subunit C	CIK00_02515	CIT27_12455	GLP21_00390	GLP24_02050	GLP09_00165	GLP22_11915	GLP17_03940	GRJ22_07570	GLP31_00165	GLP27_02535	GLP20_01495	GLP19_11500	GLP14_12490	GLP23_01545	GLP13_11730
Na(+)-translocating NADH-quinone reductase subunit A + nqrB: NADH:ubiquinone oxidoreductase, Na(+)-translocating, B subunit	CIK00_02520	CIT27_12460					GLP17_03945					GLP19_11505			GLP13_11735
Na(+)-translocating NADH-quinone reductase subunit A			GLP21_00380	GLP24_02040	GLP09_00155	GLP22_11905		GRJ22_07560	GLP31_00155	GLP27_02525	GLP20_01485		GLP14_12480	GLP23_01535	
NADH:ubiquinone reductase (Na(+)-transporting) subunit B			GLP21_00385	GLP24_02045	GLP09_00160	GLP22_11910		GRJ22_07565	GLP31_00160	GLP27_02530	GLP20_01490		GLP14_12485	GLP23_01540	
NDH_I_M: proton-translocating NADH-quinone oxidoreductase, chain M	CIK00_10540	CIT27_06425	GLP21_13800	GLP24_01615	GLP09_11350	GLP22_12580	GLP17_05715	GRJ22_00515	GLP31_08340	GLP27_02270	GLP20_12840	GLP19_01335	GLP14_14900	GLP23_07815	GLP13_07255
(Na+)-NQR maturation NqrM	CIK00_02490	CIT27_12430	GLP21_00415	GLP24_02075	GLP09_00190	GLP22_11940	GLP17_03915	GRJ22_07595	GLP31_00190	GLP27_02560	GLP20_01520	GLP19_11475	GLP14_12515	GLP23_01570	GLP13_11705
Glycerol															
lipase	CIK00_08405	CIT27_00495	GLP21_08550	GLP24_04220	GLP09_04965	GLP22_04720	GLP17_10555	GRJ22_09410	GLP31_04295	GLP27_17350	GLP20_11450	GLP19_08105	GLP14_12050	GLP23_06130	GLP13_10580
putative esterase/lipase	CIK00_08405	CIT27_00495	GLP21_08550	GLP24_04220	TMW22148_GLP 11_07495	GLP22_04720	GLP17_10555	GRJ22_09410	GLP31_04295	GLP27_17350	GLP20_11450	GLP19_08105	GLP14_12050	GLP23_06130	GLP13_10580
Glycerol uptake facilitator protein (glpF) putative	CIK00_06470	CIT27_10975	GLP21_07620	GLP24_09610	GLP09_04245	GLP22_09150	GLP17_08750	GRJ22_11200	GLP31_08845	GLP27_07805	GLP20_07275	GLP19_13335	GLP14_05305	GLP23_06765	GLP13_07850
Dehydrogenation pathway															

	P. carnosum														
	TMW 2.2021T	**TMW 2.2029**	**TMW 2.2097**	**TMW 2.2147**	**TMW 2.2149**	**TMW 2.2150**	**TMW 2.2157**	**TMW 2.2163**	**TMW 2.2169**	**TMW 2.2098**	**TMW 2.2186**	**TMW 2.2187**	**TMW 2.2188**	**TMW 2.2189**	**TMW 2.2190**
glycerol dehydrogenase	CIK00_07235	CIT27_10230	GLP21_11150	GLP24_09050	GLP09_05600	GLP22_10585	GLP17_07975	GRJ22_10200	GLP31_07690	GLP27_07025	GLP20_06470	GLP19_12490	GLP14_04540	GLP23_04580	GLP13_08280
phosphoenolpyruvate-protein phosphotransferase (E/Ptsi)	CIK00_02355	CIT27_12295	GLP21_00550	GLP24_02210	GLP09_00325	GLP22_12075	GLP17_03780	GRJ22_07730	GLP31_00325	GLP27_02695	GLP20_01655	GLP19_11340	GLP14_12650	GLP23_01705	GLP13_11570
phosphocarrier protein (HPr)	CIK00_02350	CIT27_12290	GLP21_00555	GLP24_02215	GLP09_00330	GLP22_12080	GLP17_03775	GRJ22_07735	GLP31_00330	GLP27_02700	GLP20_01660	GLP19_11335	GLP14_12655	GLP23_01710	GLP13_11565
	CIK00_08680	CIT27_11485	GLP21_06680	GLP24_11705	GLP09_07180	GLP22_09890	GLP17_13540	GRJ22_12535	GLP31_10605	GLP27_08445	GLP20_07915	GLP19_13840	GLP14_06465	GLP23_08160	GLP13_09655
Phosphorylation pathway															
glycerol kinase (glpK)	CIK00_06475	CIT27_10970	GLP21_07615	GLP24_09615	GLP09_04240	GLP22_09145	GLP17_08755	GRJ22_11195	GLP31_08850	GLP27_07800	GLP20_07270	GLP19_13330	GLP14_05300	GLP23_06770	GLP13_07845
	CIK00_16590	CIT27_05840	GLP21_05275	GLP24_13415	GLP09_14025	GLP22_00495	GLP17_05120	GRJ22_01155	GLP31_18880	GLP27_01675	GLP20_05560	GLP19_01920	GLP14_02530	GLP23_19385	GLP13_15175
alpha-glycerophosphate oxidase (glpO) / glycerol-3-phosphate oxidase (aerobic)															
Glycerol-3-phosphate dehydrogenase (gpsA / glpD)	CIK00_06850	CIT27_10595	GLP21_07235	GLP24_09990	GLP09_03865	GLP22_08770	GLP17_09130	GRJ22_10820	GLP31_09215	GLP27_07420	GLP20_06895	GLP19_12955	GLP14_04925	GLP23_07145	GLP13_07465
NAD(P)H-dependent glycerol-3-phosphate dehydrogenase (gpsA / glpD)	CIK00_06530	CIT27_10915	GLP21_07555	GLP24_09670	GLP09_04185	GLP22_09090	GLP17_08810	GRJ22_11140	GLP31_08910	GLP27_07745	GLP20_07215	GLP19_13275	GLP14_05245	GLP23_06825	GLP13_07785
anaerobic glycerol-3-phosphate dehydrogenase subunit B	CIK00_16720	CIT27_15435	GLP21_13250	GLP24_16185	GLP09_14740	GLP22_15575	GLP17_12670	GRJ22_13865	GLP31_05400	GLP27_18035	GLP20_17385	GLP19_07230	GLP14_14405	GLP23_13820	GLP13_17910
anaerobic glycerol-3-phosphate dehydrogenase subunit C	CIK00_16715	CIT27_15440	GLP21_13245	GLP24_16180	GLP09_14735	GLP22_15570	GLP17_12675	GRJ22_13870	GLP31_05395	GLP27_18040	GLP20_17380	GLP19_07225	GLP14_14410	GLP23_13815	GLP13_17905
anaerobic glycerol-3-phosphate dehydrogenase subunit A	CIK00_16725	CIT27_15430	GLP21_13255	GLP24_16190	GLP09_14745	GLP22_15580	GLP17_12665	GRJ22_13860	GLP31_05405	GLP27_18030	GLP20_17390	GLP19_07235	GLP14_14400	GLP23_13825	GLP13_17915
Fatty acid beta-oxidation															
Aerobic															
long-chain fatty acid transporter fadL	CIK00_08400	CIT27_00500	GLP21_08545	GLP24_04225	GLP09_04970	GLP22_04725	GLP17_10560	GRJ22_09405	GLP31_04290	GLP27_17355	GLP20_11455	GLP19_08110	GLP14_12055	GLP23_06135	GLP13_10585
long-chain fatty acid CoA ligase fadD	CIK00_01510	CIT27_03370	GLP21_01455	GLP24_03085	GLP09_00980	GLP22_02570	GLP17_02930	GRJ22_11940	GLP31_01170	GLP27_03555	GLP20_02500	GLP19_02410	GLP14_10340	GLP23_02550	GLP13_00375
acyl-CoA dehydrogenase fadE	CIK00_00840	CIT27_02690	GLP21_02130	GLP24_06700	GLP09_01660	GLP22_03245	GLP17_06285	GRJ22_08570	GLP31_01845	GLP27_04285	GLP20_03720	GLP19_03085	GLP14_00635	GLP23_10170	GLP13_01055
	CIK00_18565	CIT27_16275	GLP21_17455	GLP24_17170	GLP09_15705	GLP22_16530	GLP17_14805	GRJ22_16880	GLP31_17305	GLP27_16035	GLP20_15540	GLP19_17290	GLP14_16865	GLP23_15680	GLP13_16630
3-hydroxyacyl-CoA dehydrogenase fadB	CIK00_16295	CIT27_15225	GLP21_16965	GLP24_16915	GLP09_12960	GLP22_16020	GLP17_14300	GRJ22_15640	GLP31_16840	GLP27_14855	GLP20_14245	GLP19_15845	GLP14_13900	GLP23_13730	GLP13_14550
acetyl-CoA acyltransferase fadA	CIK00_16290	CIT27_15220	GLP21_16960	GLP24_16910	GLP09_12965	GLP22_16015	GLP17_14295	GRJ22_15645	GLP31_16835	GLP27_14850	GLP20_14240	GLP19_15840	GLP14_13895	GLP23_13725	GLP13_14555
Anaerobic															
long-chain fatty acid CoA ligase put. fadK	CIK00_12680	CIT27_12890	GLP21_12965	GLP24_12985	GLP09_08805	GLP22_10940	GLP17_10925	GRJ22_13190	GLP31_12275	GLP27_10770	GLP20_12450	GLP19_14465	GLP14_08630	GLP23_09870	GLP13_13195
3-hydroxyacyl-CoA dehydrogenase fadJ	CIK00_01935	CIT27_12090	GLP21_00970	GLP24_02660	GLP09_00555	GLP22_12305	GLP17_03355	GRJ22_07920	GLP31_00745	GLP27_03115	GLP20_02075	GLP19_11150	GLP14_10165	GLP23_02125	GLP13_11380
acetyl-CoA acyltransferase fadI	CIK00_01940	CIT27_12095	GLP21_00965	GLP24_02655	GLP09_00550	GLP22_12300	GLP17_03360	GRJ22_07915	GLP31_00740	GLP27_03110	GLP20_02070	GLP19_11155	GLP14_10160	GLP23_02120	GLP13_11385
Complete Tricarboxylic acid cycle (TCA cycle)															
Citrate Synthase (citA)	CIK00_01635	CIT27_03495	GLP21_01330	GLP24_02960	GLP09_00855	GLP22_02445	GLP17_03055	GRJ22_12065	GLP31_01045	GLP27_03430	GLP20_02375	GLP19_02285	GLP14_10465	GLP23_02425	GLP13_00250
Aconitate hydratase (cit B)	CIK00_09010	CIT27_11815	GLP21_06350	GLP24_12035	GLP09_06850	GLP22_09560	GLP17_12990	GRJ22_12865	GLP31_10245	GLP27_08805	GLP20_08275	GLP19_14165	GLP14_06795	GLP23_08495	GLP13_09980
Isocitrate Dehydrogenase (icd A)	CIK00_09680	CIT27_04850	GLP21_03135	GLP24_05755	GLP09_03640	GLP22_06455	GLP17_00665	GRJ22_06445	GLP31_12905	GLP27_09470	GLP20_00600	GLP19_04940	GLP14_16040	GLP23_00970	GLP13_05445
Oxoglutarate dehydrogenase (suc AB)	CIK00_01605	CIT27_03465	GLP21_01360	GLP24_02990	GLP09_00885	GLP22_02475	GLP17_03025	GRJ22_12035	GLP31_01075	GLP27_03460	GLP20_02405	GLP19_02315	GLP14_10435	GLP23_02455	GLP13_00280
	CIK00_01610	CIT27_03470	GLP21_01355	GLP24_02985	GLP09_00880	GLP22_02470	GLP17_03030	GRJ22_12040	GLP31_01070	GLP27_03455	GLP20_02400	GLP19_02310	GLP14_10440	GLP23_02450	GLP13_00275
Succinyl-CoA-Synthetase (suc CD)	CIK00_01595	CIT27_03455	GLP21_01370	GLP24_03000	GLP09_00895	GLP22_02485	GLP17_03015	GRJ22_12025	GLP31_01085	GLP27_03470	GLP20_02415	GLP19_02325	GLP14_10425	GLP23_02465	GLP13_00290
	CIK00_01600	CIT27_03460	GLP21_01365	GLP24_02995	GLP09_00890	GLP22_02480	GLP17_03020	GRJ22_12030	GLP31_01080	GLP27_03465	GLP20_02410	GLP19_02320	GLP14_10430	GLP23_02460	GLP13_00285
Succinate dehydrogenase (complex II) (sdh ABCD)	CIK00_01615	CIT27_03475	GLP21_01350	GLP24_02980	GLP09_00875	GLP22_02465	GLP17_03035	GRJ22_12045	GLP31_01065	GLP27_03450	GLP20_02395	GLP19_02305	GLP14_10445	GLP23_02445	GLP13_00270
	CIK00_01620	CIT27_03480	GLP21_01345	GLP24_02975	GLP09_00870	GLP22_02460	GLP17_03040	GRJ22_12050	GLP31_01060	GLP27_03445	GLP20_02390	GLP19_02300	GLP14_10450	GLP23_02440	GLP13_00265
	CIK00_01625	CIT27_03485	GLP21_01340	GLP24_02970	GLP09_00865	GLP22_02455	GLP17_03045	GRJ22_12055	GLP31_01055	GLP27_03440	GLP20_02385	GLP19_02295	GLP14_10455	GLP23_02435	GLP13_00260
	CIK00_01630	CIT27_03490	GLP21_01335	GLP24_02965	GLP09_00860	GLP22_02450	GLP17_03050	GRJ22_12060	GLP31_01050	GLP27_03435	GLP20_02380	GLP19_02290	GLP14_10460	GLP23_02430	GLP13_00255
Fumarate hydratase (Fumarase) (fum A)	CIK00_00770	CIT27_02620	GLP21_02200	GLP24_06770	GLP09_01730	GLP22_03315	GLP17_06355	GRJ22_08500	GLP31_01915	GLP27_04350	GLP20_03650	GLP19_03155	GLP14_00705	GLP23_10565	GLP13_01125
Malate dehydrogenase (md h)	CIK00_12535	CIT27_13035	GLP21_13105	GLP24_13125	GLP09_08665	GLP22_11080	GLP17_11065	GRJ22_13050	GLP31_12135	GLP27_10630	GLP20_12590	GLP19_14325	GLP14_08490	GLP23_09730	GLP13_13335
Phosphoenolpyruvate carboxylase	CIK00_06410	CIT27_11035	GLP21_07680	GLP24_09550	GLP09_04305	GLP22_09210	GLP17_08690	GRJ22_11260	GLP31_08785	GLP27_07865	GLP20_07335	GLP19_13395	GLP14_05365	GLP23_06705	GLP13_07910
Glyoxylate cycle															
isocitrate lyase	CIK00_18845	CIT27_16705	GLP21_00050	GLP24_16015	GLP09_12440	GLP22_13790	GLP17_15660	GRJ22_07225	GLP31_15270	GLP27_16315	GLP20_15765	GLP19_11835	GLP14_14085	GLP23_12850	GLP13_16300
malate synthase	CIK00_18840	CIT27_16710	GLP21_00045	GLP24_16010	GLP09_12435	GLP22_13795	GLP17_15665	GRJ22_07220	GLP31_15275	GLP27_16310	GLP20_15770	GLP19_11840	GLP14_14080	GLP23_12845	GLP13_16305
AMINO ACIDS															
Arginine deiminase (arcA)	CIK00_12880	CIT27_12690	GLP21_12765	GLP24_12785	GLP09_09005	GLP22_10740	GLP17_10725	GRJ22_13390	GLP31_12475	GLP27_10970	GLP20_12250	GLP19_14670	GLP14_08830	GLP23_10070	GLP13_12995
									GLP31_07815	GLP27_07155	GLP20_06595				
ornithine carbamoyl transferase Ornithine transcarbmoylase (arcB)	CIK00_12870	CIT27_12700	GLP21_12775	GLP24_12795	GLP09_08995	GLP22_10750	GLP17_10735	GRJ22_13380	GLP31_12465	GLP27_10960	GLP20_12260	GLP19_14660	GLP14_08820	GLP23_10060	GLP13_13005
									GLP31_07825	GLP27_07165	GLP20_06605				
carbamate kinase (arcC)	CIK00_12875	CIT27_12695	GLP21_12770	GLP24_12790	GLP09_09000	GLP22_10745	GLP17_10730	GRJ22_13385	GLP31_12470	GLP27_10965	GLP20_12255	GLP19_14665	GLP14_08825	GLP23_10065	GLP13_13000
									GLP31_07820	GLP27_07160	GLP20_06600				
									GLP31_10305	GLP27_08745	GLP20_08215				
Arginase (arg)	CIK00_13605	CIT27_06915	GLP21_04715	GLP24_11050	GLP09_08560	GLP22_01100	GLP17_01490	GRJ22_01765	GLP31_06980	GLP27_01055	GLP20_08550	GLP19_06630	GLP14_14700	GLP23_14610	GLP13_02290
Malate dehydrogenase (md h)	CIK00_12535	CIT27_13035	GLP21_13105	GLP24_13125	GLP09_08665	GLP22_11080	GLP17_11065	GRJ22_13050	GLP31_12135	GLP27_10630	GLP20_12590	GLP19_14325	GLP14_08490	GLP23_09730	GLP13_13335
Aminotransferasen															
Aspartate Aminofransferase (Glu/OA) aspB	CIK00_06300	CIT27_11145	GLP21_07790	GLP24_09440	GLP09_04415	GLP22_09320	GLP17_08580	GRJ22_11370	GLP31_08675	GLP27_07975	GLP20_07445	GLP19_13505	GLP14_05475	GLP23_06595	GLP13_08020
Glutamate Dehydrogenase (aKG/NADH2) gdhA															
Serine dehydratase (rev.) (Pyr/NH3) sdaAB	CIK00_00790	CIT27_02640	GLP21_02180	GLP24_06750	GLP09_01710	GLP22_03295	GLP17_06335	GRJ22_08520	GLP31_01895	GLP27_04330	GLP20_03670	GLP19_03135	GLP14_00685	GLP23_10545	GLP13_01105
Aromatic amino acid aminotransferase (Tyr,Phe,His) (Glu) tyrB	CIK00_04000	CIT27_15900	GLP21_14465	GLP24_17005	GLP09_11945	GLP22_07795	GLP17_17565	GRJ22_16730	GLP31_16115	GLP27_16805	GLP20_05070	GLP19_10925	GLP14_02095	GLP23_16175	GLP13_05285
	CIK00_00510	CIT27_02360	GLP21_02460	GLP24_07025	GLP09_01985	GLP22_03575	GLP17_06610	GRJ22_08245	GLP31_02175	GLP27_04610	GLP20_03395	GLP19_03415	GLP14_00960	GLP23_10825	GLP13_01380
Branched-chain amino acid aminotransferase (Leu,Ile,Val) (Glu) ilvE	CIK00_16060	CIT27_14990	GLP21_16730	GLP24_16680	GLP09_13195	GLP22_15785	GLP17_14065	GRJ22_15875	GLP31_16605	GLP27_14625	GLP20_14010	GLP19_15610	GLP14_13665	GLP23_13495	GLP13_14785
Alanine dehydrogenase (ald)	CIK00_11110	CIT27_00095	GLP21_08935	GLP24_03820	GLP09_15010	GLP22_04325	GLP17_10165	GRJ22_09795	GLP31_04700	GLP27_11710	GLP20_11065	GLP19_07710	GLP14_11875	GLP23_05745	GLP13_10180
Alanine aminotransferase															
aspartate ammonia-lyase (aspA)	CIK00_17140	CIT27_15690	GLP21_16050	GLP24_15665	GLP09_14440	GLP22_16990	GLP17_15730	GRJ22_16240	GLP31_16500	GLP27_16630	GLP20_14660	GLP19_16570/GLP19_18510	GLP14_15845	GLP23_14095	GLP13_15930
aspartate oxidase (nadB)	CIK00_17805	CIT27_14195	GLP21_05885	GLP24_15360	GLP09_10950	GLP22_13420	GLP17_11405	GRJ22_15000	GLP31_14410	GLP27_11310	GLP20_13605	GLP19_16055	GLP14_11370	GLP23_14400	GLP13_12205
Biogenic amines production															

	P. carnosum														
	TMW 2.2021T	**TMW 2.2029**	**TMW 2.2097**	**TMW 2.2147**	**TMW 2.2149**	**TMW 2.2150**	**TMW 2.2157**	**TMW 2.2163**	**TMW 2.2169**	**TMW 2.2098**	**TMW 2.2186**	**TMW 2.2187**	**TMW 2.2188**	**TMW 2.2189**	**TMW 2.2190**
histidine-histamine antiporter (aminoacid permease)												GLP19_11900			
histidine decarboxylase hdcA															
histidine decarboxylase 2 hdc2 Bjornsdottir-Butler et al.												GLP19_11895			
arginine decarboxylase speA	CIK00_01030	CIT27_02880	GLP21_01940	GLP24_18890	GLP09_01470	GLP22_03055	GLP17_06095	GRJ22_08760	GLP31_01655	GLP27_04095	GLP20_03910	GLP19_02895	GLP14_00445	GLP23_10360	GLP13_00865
	CIK00_16465	CIT27_05970	GLP21_05400	GLP24_13290	GLP09_14150	GLP22_00365	GLP17_05245	GRJ22_01080	GLP31_07905	GLP27_20080	GLP20_05435	GLP19_01845	GLP14_02660	GLP23_07375	GLP13_17015
	CIK00_19235	CIT27_17225 + CIT27_18220		GLP24_19660	GLP09_17845		GLP17_19310	GRJ22_18395	GLP31_20580	GLP27_20000	GLP20_18960		GLP14_18745		GLP13_19245
	CIK00_20945	CIT27_18200	GLP21_07090					GRJ22_18425							
	CIK00_21050	CIT27_18215													
tyrosine decarboxylase tdcA				GLP24_17045			GLP17_17600								
ornithine decarboxylase speF		CIT27_17635													GLP13_19070
lysine decarboxylase lcdC															
agmatinase speB	CIK00_16470	CIT27_05965	GLP21_05395	GLP24_13295	GLP09_14145	GLP22_00370	GLP17_05240	GRJ22_01085	GLP31_07900		GLP20_05440	GLP19_01850	GLP14_02655	GLP23_07370	GLP13_17020
bifunctional glutathionylspermidine amidase/synthase	CIK00_08335	CIT27_00565	GLP21_08480	GLP24_04290	GLP09_05035	GLP22_04790	GLP17_10625	GRJ22_09340	GLP31_04225	GLP27_17420	GLP20_11520	GLP19_08175	GLP14_12120	GLP23_06200	GLP13_10650
glutamate decarboxylase gadB	CIK00_15595	CIT27_14510	GLP21_15500	GLP24_14865	GLP09_12625	GLP22_14295	GLP17_12170	GRJ22_15300	GLP31_15440	GLP27_14180	GLP20_17695	GLP19_15470	GLP14_13530	GLP23_13050	GLP13_14520
Electron donors															
NiFe hydrogenase															
hyd ABCDE	CIK00_11405	CIT27_00405	GLP21_08640	GLP24_04110	GLP09_04815	GLP22_04630	GLP17_10465	GRJ22_09500	GLP31_04395	GLP27_12005	GLP20_11360	GLP19_08015	GLP14_11580	GLP23_06040	GLP13_10490
	CIK00_11410	CIT27_00410	GLP21_08635	GLP24_04115	GLP09_04820	GLP22_04635	GLP17_10470	GRJ22_09495	GLP31_04390	GLP27_12010	GLP20_11365	GLP19_08020	GLP14_11575	GLP23_06045	GLP13_10495
	CIK00_11415	CIT27_00415	GLP21_08630	GLP24_04120	GLP09_04825	GLP22_04640	GLP17_10475	GRJ22_09490	GLP31_04385	GLP27_12015	GLP20_11370	GLP19_08025	GLP14_11570	GLP23_06050	GLP13_10500
	CIK00_11420	CIT27_00420	GLP21_08625	GLP24_04125	GLP09_04830	GLP22_04645	GLP17_10480	GRJ22_09485	GLP31_04380	GLP27_12020	GLP20_11375	GLP19_08030	GLP14_11565	GLP23_06055	GLP13_10505
	CIK00_11425	CIT27_00425	GLP21_08620	GLP24_04130	GLP09_04835	GLP22_04650	GLP17_10485	GRJ22_09480	GLP31_04375	GLP27_12025	GLP20_11380	GLP19_08035	GLP14_11560	GLP23_06060	GLP13_10510
Alternative electron receptors															
Fumarate reductase															
frdABCD	CIK00_17205	CIT27_15755	GLP21_16110	GLP24_15575	GLP09_14375	GLP22_18125	GLP17_18755	GRJ22_16305	GLP31_16560	GLP27_16695	GLP20_14600	GLP19_16505	GLP14_15910	GLP23_14030	GLP13_15865
	CIK00_17200	CIT27_15750	GLP21_16105	GLP24_15580	GLP09_14380	GLP22_18120	GLP17_18750	GRJ22_16300	GLP31_16555	GLP27_16690	GLP20_14605	GLP19_16510	GLP14_15905	GLP23_14035	GLP13_15870
	CIK00_17195	CIT27_15745	GLP21_16100	GLP24_15585	GLP09_14385	GLP22_18115	GLP17_18745	GRJ22_16295	GLP31_16550	GLP27_16685	GLP20_14610	GLP19_16515	GLP14_15900	GLP23_14040	GLP13_15875
	CIK00_17190	CIT27_15740	GLP21_16095	GLP24_15590	GLP09_14390	GLP22_18110	GLP17_18740	GRJ22_16290	GLP31_16545	GLP27_16680	GLP20_14615	GLP19_16520	GLP14_15895	GLP23_14045	GLP13_15880
TMAO reductase	CIK00_08435	CIT27_00465	GLP21_08580	GLP24_04190	GLP09_04935	GLP22_04690	GLP17_10525	GRJ22_09440	GLP31_04325	GLP27_17320	GLP20_11420	GLP19_08075	GLP14_12020	GLP23_06100	GLP13_10550
tor A															
Nitrate reductase	CIK00_02395	CIT27_12335	GLP21_00510	GLP24_02170	GLP09_00285	GLP22_12035	GLP17_03820	GRJ22_07690	GLP31_00285	TMW22099_HPQ 32_02470	GLP20_01615	GLP19_11380	GLP14_12610	GLP23_01665	GLP13_11610
nap AB	CIK00_02400	CIT27_12340	GLP21_00505	GLP24_02165	GLP09_00280	GLP22_12030	GLP17_03825	GRJ22_07685	GLP31_00280	TMW22099_HPQ 32_02475	GLP20_01610	GLP19_11385	GLP14_12605	GLP23_01660	GLP13_11615
	CIK00_02405	CIT27_12345	GLP21_00500	GLP24_02160	GLP09_00275	GLP22_12025	GLP17_03830	GRJ22_07680	GLP31_00275	TMW22099_HPQ 32_02480	GLP20_01605	GLP19_11390	GLP14_12600	GLP23_01655	GLP13_11620
	CIK00_02410	CIT27_12350	GLP21_00495	GLP24_02155	GLP09_00270	GLP22_12020	GLP17_03835	GRJ22_07675	GLP31_00270	TMW22099_HPQ 32_02485	GLP20_01600	GLP19_11395	GLP14_12595	GLP23_01650	GLP13_11625
hydroxylamine reductase	CIK00_10740	CIT27_06220	GLP21_05660	GLP24_01820	GLP09_16775	GLP22_00045	GLP17_05510	GRJ22_00730	GLP31_08135	GLP27_02065	GLP20_05175	GLP19_01550	GLP14_02925	GLP23_07605	GLP13_17135
Mannose-6-P isomerase	CIK00_13205	CIT27_04110	GLP21_03850		GLP09_02860			GRJ22_14010	GLP31_13840	TMW22099_HPQ 32_20090	GLP20_01290	GLP19_04190	GLP14_08065	GLP23_00230	GLP13_06215
manA				GLP24_19715/GLP24_19720		GLP22_19005/GLP22_19010									
nitrite reductase small subunit	CIK00_10975	CIT27_17360	GLP21_13570	GLP24_03670	GLP09_17360	GLP22_17370	GLP17_10015	GRJ22_13535	GLP31_18470	GLP27_17800	GLP20_16780	GLP19_07555	GLP14_17465	GLP23_16995	GLP13_17830
nitrite reductase large subunit	CIK00_10980	CIT27_17365	GLP21_13575	GLP24_03675	GLP09_17365	GLP22_17375	GLP17_10020	GRJ22_13530	GLP31_18465	GLP27_17805	GLP20_16785	GLP19_07560	GLP14_17470	GLP23_17000	GLP13_17835
sulphate adenylyltransferase cysD	CIK00_18255	CIT27_16185	GLP21_17205	GLP24_17415	GLP09_15635	GLP22_16600	GLP17_15230	GRJ22_17350	GLP31_17070	GLP27_15965	GLP20_15300	GLP19_16960	GLP14_16180	GLP23_15610	GLP13_16370
sulphate adenylyltransferase cysN	CIK00_18250	CIT27_16190	GLP21_17210	GLP24_17410	GLP09_15640	GLP22_16595	GLP17_15235	GRJ22_17355	GLP31_17075	GLP27_15970	GLP20_15305	GLP19_16965	GLP14_16175	GLP23_15615	GLP13_16365
assimilatory sulfite reductase	CIK00_18305	CIT27_16135	GLP21_17155	GLP24_17465	GLP09_15585	GLP22_16650	GLP17_15180	GRJ22_17300	GLP31_17020	GLP27_15915	GLP20_15250	GLP19_16910	GLP14_16230	GLP23_15560	GLP13_16420
dimethyl sulfoxide reductase subunit A															
dimethylsulfoxide reductase, chain B															
dimethyl sulfoxide reductase anchor subunit															
Respiration															
NADH dehydrogenase (non-electrogenic)															
ndh	CIK00_10855	CIT27_17240	GLP21_13450	GLP24_03550	GLP09_17565	GLP22_17250	GLP17_18435	GRJ22_13655	GLP31_18590	GLP27_17680	GLP20_16660	GLP19_07435	GLP14_17345	GLP23_16875	GLP13_17710
	CIK00_00715	CIT27_02565	GLP21_02255	GLP24_06825	GLP09_01785	GLP22_03370	GLP17_06410	GRJ22_08445	GLP31_01970	GLP27_04405	GLP20_03595	GLP19_03210	GLP14_00760	GLP23_10620	GLP13_01180
NADH-quinone oxidoreductase subunit A															
NADH-quinone oxidoreductase subunit B															

	P. carnosum														
	TMW 2.2021T	TMW 2.2029	TMW 2.2097	TMW 2.2147	TMW 2.2149	TMW 2.2150	TMW 2.2157	TMW 2.2163	TMW 2.2169	TMW 2.2098	TMW 2.2186	TMW 2.2187	TMW 2.2188	TMW 2.2189	TMW 2.2190
NADH dehydrogenase (quinone) subunit D NADH-quinone oxidoreductase subunit NuoE NADH-quinone oxidoreductase subunit NuoF NADH dehydrogenase (quinone) subunit G NADH-quinone oxidoreductase subunit NuoH NADH-quinone oxidoreductase subunit NuoI NADH-quinone oxidoreductase subunit J NADH-quinone oxidoreductase subunit NuoK NADH-quinone oxidoreductase subunit L NADH-quinone oxidoreductase subunit M NADH-quinone oxidoreductase subunit N															
NADH-quinone oxidoreductase subunit NuoB	CIK00_10520	CIT27_06445	GLP21_13780	GLP24_01595	GLP09_11330	GLP22_12560	GLP17_05735	GRJ22_00495	GLP31_08360	GLP27_02290	GLP20_12820	GLP19_01315	GLP14_14920	GLP23_07835	GLP13_07235
(Na+)-NQR maturation NqrM	CIK00_02490	CIT27_12430	GLP21_00415	GLP24_02075	GLP09_00190	GLP22_11940	GLP17_03915	GRJ22_07595	GLP31_00190	GLP27_02560	GLP20_01520	GLP19_11475	GLP14_12515	GLP23_01570	GLP13_11705
nqrF: NADH:ubiquinone oxidoreductase, Na(+)-translocating, F subunit	CIK00_02500	CIT27_12440	GLP21_00405	GLP24_02065	GLP09_00180	GLP22_11930	GLP17_03925	GRJ22_07585	GLP31_00180	GLP27_02550	GLP20_01510	GLP19_11485	GLP14_12505	GLP23_01560	GLP13_11715
NADH:ubiquinone reductase (Na(+)-transporting) subunit E	CIK00_02505	CIT27_12445	GLP21_00400	GLP24_02060	GLP09_00175	GLP22_11925	GLP17_03930	GRJ22_07580	GLP31_00175	GLP27_02545	GLP20_01505	GLP19_11490	GLP14_12500	GLP23_01555	GLP13_11720
NADH:ubiquinone reductase (Na(+)-transporting) subunit D	CIK00_02510	CIT27_12450	GLP21_00395	GLP24_02055	GLP09_00170	GLP22_11920	GLP17_03935	GRJ22_07575	GLP31_00170	GLP27_02540	GLP20_01500	GLP19_11495	GLP14_12495	GLP23_01550	GLP13_11725
Na(+)-translocating NADH-quinone reductase subunit C	CIK00_02515	CIT27_12455	GLP21_00390	GLP24_02050	GLP09_00165	GLP22_11915	GLP17_03940	GRJ22_07570	GLP31_00165	GLP27_02535	GLP20_01495	GLP19_11500	GLP14_12490	GLP23_01545	GLP13_11730
Na(+)-translocating NADH-quinone reductase subunit A + nqrB: NADH:ubiquinone oxidoreductase, Na(+)-translocating, B subunit	CIK00_02520	CIT27_12460					GLP17_03945					GLP19_11505			GLP13_11735
Na(+)-translocating NADH-quinone reductase subunit A			GLP21_00380	GLP24_02040	GLP09_00155	GLP22_11905		GRJ22_07560	GLP31_00155	GLP27_02525	GLP20_01485		GLP14_12480	GLP23_01535	
NADH:ubiquinone reductase (Na(+)-transporting) subunit B			GLP21_00385	GLP24_02045	GLP09_00160	GLP22_11910		GRJ22_07565	GLP31_00160	GLP27_02530	GLP20_01490		GLP14_12485	GLP23_01540	
NDH_I_M: proton-translocating NADH-quinone oxidoreductase, chain M	CIK00_10540	CIT27_06425	GLP21_13800	GLP24_01615	GLP09_11350	GLP22_12580	GLP17_05715	GRJ22_00515	GLP31_08340	GLP27_02270	GLP20_12840	GLP19_01335	GLP14_14900	GLP23_07815	GLP13_07255
Menaquinone synthese (8 steps) (Vitamin K)															
1,4-dihydroxy-2-naphthoate prenyltransferase (*men* A)	CIK00_06460	CIT27_10985	GLP21_07630	GLP24_09600	GLP09_04255	GLP22_09160	GLP17_08740	GRJ22_11210	GLP31_08835	GLP27_07815	GLP20_07285	GLP19_13345	GLP14_05315	GLP23_06755	GLP13_07860
Isochorismate synthase (menF)	CIK00_09290	CIT27_04465	GLP21_03525	GLP24_06150	GLP09_03245	GLP22_06065	GLP17_00270	GRJ22_06055 GRJ22_06055	GLP31_13515	GLP27_09070	GLP20_00990	GLP19_04545	GLP14_09690 GLP14_09690	GLP23_00580	GLP13_05835
2-succinyl-5-enolpyruvyl-6-hydroxy-3- cyclohexene-1-carboxylic-acid synthase (menD)	CIK00_09295	CIT27_04470	GLP21_03520	GLP24_06145	GLP09_03250	GLP22_06070	GLP17_00275	GRJ22_06060	GLP31_13510	GLP27_09075	GLP20_00985	GLP19_04550	GLP14_09685	GLP23_00585	GLP13_05830
2-succinyl-6-hydroxy-2, 4-cyclohexadiene-1-carboxylate synthase (menH)	CIK00_09300	CIT27_04475	GLP21_03515	GLP24_06140	GLP09_03255	GLP22_06075	GLP17_00280	GRJ22_06065	GLP31_13505	GLP27_09080	GLP20_00980	GLP19_04555	GLP14_09680	GLP23_00590	GLP13_05825
o-succinylbenzoate synthase (menC)	CIK00_09305	CIT27_04480	GLP21_03510	GLP24_06135	GLP09_03260	GLP22_06080	GLP17_00285	GRJ22_06070	GLP31_13500	GLP27_09085	GLP20_00975	GLP19_04560	GLP14_09675	GLP23_00595	GLP13_05820
2-methoxy-6-polyprenyl-1,4-benzoquinol methylase (ubiE)	CIK00_14350	CIT27_13960	GLP21_14765	GLP24_14495	GLP09_11545	GLP22_13100	GLP17_16285	GRJ22_14755	GLP31_14730	GLP27_12415	GLP20_13375	GLP19_15110	GLP14_11060	GLP23_12320	GLP13_13420
O-succinylbenzoate-CoA ligase (menE)	CIK00_09310	CIT27_04485	GLP21_03505	GLP24_06130	GLP09_03265	GLP22_06085	GLP17_00290	GRJ22_06075	GLP31_13495	GLP27_09090	GLP20_00970	GLP19_04565	GLP14_09670	GLP23_00600	GLP13_05815
1,4-dihydroxy-2-naphthoyl-CoA synthase (menB)	CIK00_10080	CIT27_01500	GLP21_09540	GLP24_12460	GLP09_10405	GLP22_05785	GLP17_09580	GRJ22_05350	GLP31_06170	GLP27_09865	GLP20_10030	GLP19_09340	GLP14_07215	GLP23_09465	GLP13_09140
cytochrome c oxidase															
Subunit I CoxA	CIK00_06815	CIT27_10630	GLP21_07270	GLP24_09955	GLP09_03900	GLP22_08805	GLP17_09095	GRJ22_10855	GLP31_09180	GLP27_07455	GLP20_06930	GLP19_12990	GLP14_04960	GLP23_07110	GLP13_07500
Subunit II CoxB	CIK00_06820	CIT27_10625	GLP21_07265	GLP24_09960	GLP09_03895	GLP22_08800	GLP17_09100	GRJ22_10850	GLP31_09185	GLP27_07450	GLP20_06925	GLP19_12985	GLP14_04955	GLP23_07115	GLP13_07495
Subunit III CoxC	CIK00_06805	CIT27_10640	GLP21_07280	GLP24_09945	GLP09_03910	GLP22_08815	GLP17_09085	GRJ22_10865	GLP31_09170	GLP27_07465	GLP20_06940	GLP19_13000	GLP14_04970	GLP23_07100	GLP13_07510
cytochrome c oxidase assembly protein Cox1	CIK00_06810	CIT27_10635	GLP21_07275	GLP24_09950	GLP09_03905	GLP22_08810	GLP17_09090	GRJ22_10860	GLP31_09175	GLP27_07460	GLP20_06935	GLP19_12995	GLP14_04965	GLP23_07105	GLP13_07505
cytochrome oxidase	CIK00_06790	CIT27_10655	GLP21_07295	GLP24_09930	GLP09_03925	GLP22_08830	GLP17_09070	GRJ22_10880	GLP31_09155	GLP27_07480	GLP20_06955	GLP19_13015	GLP14_04985	GLP23_07085	GLP13_07525
cytochrome o ubiquinol oxidase subunit IV cyoD	CIK00_11985	CIT27_09220	GLP21_11875	GLP24_00515	GLP09_07505	GLP22_08555	GLP17_04510	GRJ22_04215	GLP31_03155	GLP27_05265	GLP20_09225	GLP19_00250	GLP14_05860	GLP23_08750	GLP13_03775
cytochrome o ubiquinol oxidase subunit III cyoC	CIK00_11990	CIT27_09225	GLP21_11870	GLP24_00510	GLP09_07500	GLP22_08560	GLP17_04505	GRJ22_04210	GLP31_03150	GLP27_05270	GLP20_09230	GLP19_00245	GLP14_05855	GLP23_08755	GLP13_03780
cytochrome o ubiquinol oxidase subunit I cyoB	CIK00_11995	CIT27_09230	GLP21_11865	GLP24_00505	GLP09_07495	GLP22_08565	GLP17_04500	GRJ22_04205	GLP31_03145	GLP27_05275	GLP20_09235	GLP19_00240	GLP14_05850	GLP23_08760	GLP13_03785
CyoA: ubiquinol oxidase, subunit II	CIK00_12000	CIT27_09235	GLP21_11860	GLP24_00500	GLP09_07490	GLP22_08570	GLP17_04495	GRJ22_04200	GLP31_03140	GLP27_05280	GLP20_09240	GLP19_00235	GLP14_05845	GLP23_08765	GLP13_03790
cyoE_ctaB: protoheme IX farnesyltransferase	CIK00_11980	CIT27_09215	GLP21_11880	GLP24_00520	GLP09_07510	GLP22_08550	GLP17_04515	GRJ22_04220	GLP31_03160	GLP27_05260	GLP20_09220	GLP19_00255	GLP14_05865	GLP23_08745	GLP13_03770
	CIK00_06780	CIT27_10665	GLP21_07305	GLP24_09920	GLP09_03935	GLP22_08840	GLP17_09060	GRJ22_10890	GLP31_09145	GLP27_07490	GLP20_06965	GLP19_13025	GLP14_04995	GLP23_07075	GLP13_07535
cytochrome-c oxidase, cbb3-type subunit I ccoN cytochrome-c oxidase, cbb3-type subunit II ccoO cytochrome-c oxidase, cbb3-type subunit III ccoP cbb3-type cytochrome oxidase assembly protein CcoS CcoQ															
cytochrome bd oxidase															
Subunit I *cyd* A	CIK00_01320	CIT27_03180	GLP21_01645	GLP24_03275	GLP09_01170	GLP22_02760	GLP17_02740	GRJ22_11750	GLP31_01360	GLP27_03745	GLP20_02690	GLP19_02600	GLP14_00150	GLP23_02740	GLP13_00565
Subunit II *cyd* B	CIK00_01315	CIT27_03175	GLP21_01650	GLP24_03280	GLP09_01175	GLP22_02765	GLP17_02735	GRJ22_11745	GLP31_01365	GLP27_03750	GLP20_02695	GLP19_02605	GLP14_00155	GLP23_02745	GLP13_00570
subunit cydX	CIK00_01310	CIT27_03170	GLP21_01655	GLP24_03285	GLP09_01180	GLP22_02770	GLP17_02730	GRJ22_11740	GLP31_01370	GLP27_03755	GLP20_02700	GLP19_02610	GLP14_00160	GLP23_02750	GLP13_00575
NADH:ubiquinone oxidoreductase (ndh)															
	CIK00_00715	CIT27_02565	GLP21_02255	GLP24_06825	GLP09_01785	GLP22_03370	GLP17_06410	GRJ22_08445	GLP31_01970	GLP27_04405	GLP20_03595	GLP19_03210	GLP14_00760	GLP23_10620	GLP13_01180
Succinate dehydrogenase (complex II)															
sdhABCD	CIK00_01615	CIT27_03475	GLP21_01350	GLP24_02980	GLP09_00875	GLP22_02465	GLP17_03035	GRJ22_12045	GLP31_01065	GLP27_03450	GLP20_02395	GLP19_02305	GLP14_10445	GLP23_02445	GLP13_00270
	CIK00_01620	CIT27_03480	GLP21_01345	GLP24_02975	GLP09_00870	GLP22_02460	GLP17_03040	GRJ22_12050	GLP31_01060	GLP27_03445	GLP20_02390	GLP19_02300	GLP14_10450	GLP23_02440	GLP13_00265
	CIK00_01625	CIT27_03485	GLP21_01340	GLP24_02970	GLP09_00865	GLP22_02455	GLP17_03045	GRJ22_12055	GLP31_01055	GLP27_03440	GLP20_02385	GLP19_02295	GLP14_10455	GLP23_02435	GLP13_00260
	CIK00_01630	CIT27_03490	GLP21_01335	GLP24_02965	GLP09_00860	GLP22_02450	GLP17_03050	GRJ22_12060	GLP31_01050	GLP27_03435	GLP20_02380	GLP19_02290	GLP14_10460	GLP23_02430	GLP13_00255
cytochrome C															

	P. carnosum														
	TMW 2.2021T	**TMW 2.2029**	**TMW 2.2097**	**TMW 2.2147**	**TMW 2.2149**	**TMW 2.2150**	**TMW 2.2157**	**TMW 2.2163**	**TMW 2.2169**	**TMW 2.2098**	**TMW 2.2186**	**TMW 2.2187**	**TMW 2.2188**	**TMW 2.2189**	**TMW 2.2190**
cytochrome b	CIK00_08800	CIT27_11605	GLP21_06560	GLP24_11825	GLP09_07060	GLP22_09770	GLP17_12780	GRJ22_12655	GLP31_10485	GLP27_08565	GLP20_08035	GLP19_13960	GLP14_06585	GLP23_08280	GLP13_09775
cytochrome c	CIK00_02390	CIT27_12330	GLP21_00515	GLP24_02175	GLP09_00290	GLP22_12040	GLP17_03815	GRJ22_07695	GLP31_00290	GLP27_02660	GLP20_01620	GLP19_11375	GLP14_12615	GLP23_01670	GLP13_11605
Cytochrome c															
cytochrome c4	CIK00_14520	CIT27_13790	GLP21_14935	GLP24_14325	GLP09_11715	GLP22_12930	GLP17_16715	GRJ22_14585	GLP31_14900	GLP27_12245	GLP20_13205	GLP19_14940	GLP14_10890	GLP23_12490	GLP13_13590
cytochrome C554	CIK00_04100	CIT27_07985	GLP21_14575	GLP24_08530	GLP09_12030	GLP22_07700	GLP17_07720	GRJ22_17890	GLP31_16225	GLP27_18890	GLP20_04975	GLP19_10805	GLP14_01995	GLP23_18135	GLP13_05185
cytochrome bc complex bzw. cytochrom-c-reductase(Fe-S, b, c1)															
qcrA/qcrb/qcrC															
	CIK00_08795	CIT27_11600	GLP21_06565	GLP24_11820	GLP09_07065	GLP22_09775	GLP17_12775	GRJ22_12650	GLP31_10490	GLP27_08560	GLP20_08030	GLP19_13955	GLP14_06580	GLP23_08275	GLP13_09770
	CIK00_08800	CIT27_11605	GLP21_06560	GLP24_11825	GLP09_07060	GLP22_09770	GLP17_12780	GRJ22_12655	GLP31_10485	GLP27_08565	GLP20_08035	GLP19_13960	GLP14_06585	GLP23_08280	GLP13_09775
	CIK00_08805	CIT27_11610	GLP21_06555	GLP24_11830	GLP09_07055	GLP22_09765	GLP17_12785	GRJ22_12660	GLP31_10480	GLP27_08570	GLP20_08040	GLP19_13965	GLP14_06590	GLP23_08285	GLP13_09780
Fumarate reductase															
frdABCD															
	CIK00_17205	CIT27_15755	GLP21_16110	GLP24_15575	GLP09_14375	GLP22_18125	GLP17_18755	GRJ22_16305	GLP31_16560	GLP27_16695	GLP20_14600	GLP19_16505	GLP14_15910	GLP23_14030	GLP13_15865
	CIK00_17200	CIT27_15750	GLP21_16105	GLP24_15580	GLP09_14380	GLP22_18120	GLP17_18750	GRJ22_16300	GLP31_16555	GLP27_16690	GLP20_14605	GLP19_16510	GLP14_15905	GLP23_14035	GLP13_15870
	CIK00_17195	CIT27_15745	GLP21_16100	GLP24_15585	GLP09_14385	GLP22_18115	GLP17_18745	GRJ22_16295	GLP31_16550	GLP27_16685	GLP20_14610	GLP19_16515	GLP14_15900	GLP23_14040	GLP13_15875
	CIK00_17190	CIT27_15740	GLP21_16095	GLP24_15590	GLP09_14390	GLP22_18110	GLP17_18740	GRJ22_16290	GLP31_16545	GLP27_16680	GLP20_14615	GLP19_16520	GLP14_15895	GLP23_14045	GLP13_15880
Formate dehydrogenase															
fdhABCE															
A	CIK00_19980	CIT27_17415	GLP21_18405	GLP24_15880	GLP09_12300	GLP22_13930	GLP17_17670	GRJ22_07080	GLP31_15395	GLP27_18770	GLP20_17435	GLP19_11975	GLP14_13955	GLP23_12725	GLP13_18015
B	CIK00_19985	CIT27_17410	GLP21_18410	GLP24_15875	GLP09_12295	GLP22_13935	GLP17_17665	GRJ22_07075	GLP31_15400	GLP27_18775	GLP20_17430	GLP19_11980	GLP14_13950	GLP23_12720	GLP13_18020
C	CIK00_19990	CIT27_17405	GLP21_18415	GLP24_15870	GLP09_12290	GLP22_13940	GLP17_17660	GRJ22_07070	GLP31_15405	GLP27_18780	GLP20_17425	GLP19_11985	GLP14_13945	GLP23_12715	GLP13_18025
E	CIK00_19995	CIT27_17400	GLP21_18420	GLP24_15865	GLP09_12285	GLP22_13945	GLP17_17655	GRJ22_07065	GLP31_15410	GLP27_18785	GLP20_17420	GLP19_11990	GLP14_13940	GLP23_12710	GLP13_18030
Quinone Q-8 biosynthesis															
Chorismate pyruvate lyase (ubiC)	CIK00_06840	CIT27_10605	GLP21_07245	GLP24_09980	GLP09_03875	GLP22_08780	GLP17_09120	GRJ22_10830	GLP31_09205	GLP27_07430	GLP20_06905	GLP19_12965	GLP14_04935	GLP23_07135	GLP13_07475
4-hydroxybenzoate octaprenyltransferase (ubiA)	CIK00_06835	CIT27_10610	GLP21_07250	GLP24_09975	GLP09_03880	GLP22_08785	GLP17_09115	GRJ22_10835	GLP31_09200	GLP27_07435	GLP20_06910	GLP19_12970	GLP14_04940	GLP23_07130	GLP13_07480
3-octaprenyl-4-hydroxybenzoate carboxy-lyase (ubiD)	CIK00_19170	CIT27_17160	GLP21_07025	GLP24_17950	GLP09_15965	GLP22_17170	GLP17_16460	GRJ22_17790	GLP31_17915	GLP27_16940	GLP20_16325	GLP19_17570	GLP14_16970	GLP23_16040	GLP13_17345
2-octaprenylphenol 6-hydroxylase (ubiB)	CIK00_14360	CIT27_13950	GLP21_14775	GLP24_14485	GLP09_11555	GLP22_13090	GLP17_16275	GRJ22_14745	GLP31_14740	GLP27_12405	GLP20_13365	GLP19_15100	GLP14_11050	GLP23_12330	GLP13_13430
3-demethylubiquinol 3-O-methyltransferase (ubiG)	CIK00_01010	CIT27_02860	GLP21_01960	GLP24_18910	GLP09_01490	GLP22_03075	GLP17_06115	GRJ22_08740	GLP31_01675	GLP27_04115	GLP20_03890	GLP19_02915	GLP14_00465	GLP23_10340	GLP13_00885
2-octaprenyl-6-methoxyphenyl hydroxylase (ubiH)	CIK00_17860	CIT27_14250	GLP21_05940	GLP24_15305	GLP09_11005	GLP22_13365	GLP17_11460	GRJ22_15055	GLP31_14465	GLP27_11255	GLP20_13660	GLP19_16110	GLP14_11315	GLP23_14345	GLP13_12260
2-methoxy-6-octaprenyl-1,4-benzoquinol methylase (ubiE)	CIK00_14350	CIT27_13960	GLP21_14765	GLP24_14495	GLP09_11545	GLP22_13100	GLP17_16285	GRJ22_14755	GLP31_14730	GLP27_12415	GLP20_13375	GLP19_15110	GLP14_11060	GLP23_12320	GLP13_13420
2-octaprenyl-3-methyl-6-methoxy-1,4-benzoquinol hydroxylase (ubiF)	CIK00_14525	CIT27_13785	GLP21_14940	GLP24_14320	GLP09_11720	GLP22_12925	GLP17_16710	GRJ22_14580	GLP31_14905	GLP27_12240	GLP20_13200	GLP19_14935	GLP14_10885	GLP23_12495	GLP13_13595
ubiCADBGHEF															
F0F1-ATP synthase															
F0F1 ATP synthase subunit A	CIK00_13470	CIT27_06780	GLP21_04850	GLP24_10915	GLP09_08395	GLP22_00935	GLP17_01355	GRJ22_01600	GLP31_07110	GLP27_01190	GLP20_08415	GLP19_06795	GLP14_14565	GLP23_17675	GLP13_02155
ATP synthase F0 subunit B	CIK00_13480	CIT27_06790	GLP21_04840	GLP24_10925	GLP09_08405	GLP22_00945	GLP17_01365	GRJ22_01610	GLP31_07100	GLP27_01180	GLP20_08425	GLP19_06785	GLP14_14575	GLP23_17665	GLP13_02165
F0F1 ATP synthase subunit C	CIK00_13475	CIT27_06785	GLP21_04845	GLP24_10920	GLP09_08400	GLP22_00940	GLP17_01360	GRJ22_01605	GLP31_07105	GLP27_01185	GLP20_08420	GLP19_06790	GLP14_14570	GLP23_17670	GLP13_02160
F0F1 ATP synthase subunit alpha	CIK00_13490	CIT27_06800	GLP21_04830	GLP24_10935	GLP09_08415	GLP22_00955	GLP17_01375	GRJ22_01620	GLP31_07090	GLP27_01170	GLP20_08435	GLP19_06775	GLP14_14585	GLP23_17655	GLP13_02175
F0F1 ATP synthase subunit beta	CIK00_13500	CIT27_06810	GLP21_04820	GLP24_10945	GLP09_08425	GLP22_00965	GLP17_01385	GRJ22_01630	GLP31_07080	GLP27_01160	GLP20_08445	GLP19_06765	GLP14_14595	GLP23_17645	GLP13_02185
F0F1 ATP synthase subunit gamma	CIK00_13495	CIT27_06805	GLP21_04825	GLP24_10940	GLP09_08420	GLP22_00960	GLP17_01380	GRJ22_01625	GLP31_07085	GLP27_01165	GLP20_08440	GLP19_06770	GLP14_14590	GLP23_17650	GLP13_02180
F0F1 ATP synthase subunit delta	CIK00_13485	CIT27_06795	GLP21_04835	GLP24_10930	GLP09_08410	GLP22_00950	GLP17_01370	GRJ22_01615	GLP31_07095	GLP27_01175	GLP20_08430	GLP19_06780	GLP14_14580	GLP23_17660	GLP13_02170
F0F1 ATP synthase subunit epsilon	CIK00_13505	CIT27_06815	GLP21_04815	GLP24_10950	GLP09_08430	GLP22_00970	GLP17_01390	GRJ22_01635	GLP31_07075	GLP27_01155	GLP20_08450	GLP19_06760	GLP14_14600	GLP23_17640	GLP13_02190
F0F1 ATP synthase subunit A	CIK00_16130	CIT27_15060	GLP21_16800	GLP24_16750	GLP09_13125	GLP22_15855	GLP17_14135	GRJ22_15805	GLP31_16675	GLP27_14695	GLP20_14080	GLP19_15680	GLP14_13735	GLP23_13565	GLP13_14715
ATP synthase F0 subunit B	CIK00_16120	CIT27_15050	GLP21_16790	GLP24_16740	GLP09_13135	GLP22_15845	GLP17_14125	GRJ22_15815	GLP31_16665	GLP27_14685	GLP20_14070	GLP19_15670	GLP14_13725	GLP23_13555	GLP13_14725
F0F1 ATP synthase subunit C	CIK00_16125	CIT27_15055	GLP21_16795	GLP24_16745	GLP09_13130	GLP22_15850	GLP17_14130	GRJ22_15810	GLP31_16670	GLP27_14690	GLP20_14075	GLP19_15675	GLP14_13730	GLP23_13560	GLP13_14720
F0F1 ATP synthase subunit alpha	CIK00_16110	CIT27_15040	GLP21_16780	GLP24_16730	GLP09_13145	GLP22_15835	GLP17_14115	GRJ22_15825	GLP31_16655	GLP27_14675	GLP20_14060	GLP19_15660	GLP14_13715	GLP23_13545	GLP13_14735
F0F1 ATP synthase subunit beta	CIK00_16100	CIT27_15030	GLP21_16770	GLP24_16720	GLP09_13155	GLP22_15825	GLP17_14105	GRJ22_15835	GLP31_16645	GLP27_14665	GLP20_14050	GLP19_15650	GLP14_13705	GLP23_13535	GLP13_14745
F0F1 ATP synthase subunit gamma	CIK00_16105	CIT27_15035	GLP21_16775	GLP24_16725	GLP09_13150	GLP22_15830	GLP17_14110	GRJ22_15830	GLP31_16650	GLP27_14670	GLP20_14055	GLP19_15655	GLP14_13710	GLP23_13540	GLP13_14740
F0F1 ATP synthase subunit delta	CIK00_16115	CIT27_15045	GLP21_16785	GLP24_16735	GLP09_13140	GLP22_15840	GLP17_14120	GRJ22_15820	GLP31_16660	GLP27_14680	GLP20_14065	GLP19_15665	GLP14_13720	GLP23_13550	GLP13_14730
F0F1 ATP synthase subunit epsilon	CIK00_16095	CIT27_15025	GLP21_16765	GLP24_16715	GLP09_13160	GLP22_15820	GLP17_14100	GRJ22_15840	GLP31_16640	GLP27_14660	GLP20_14045	GLP19_15645	GLP14_13700	GLP23_13530	GLP13_14750
ATP F0F1 synthase subunit I	CIK00_16135	CIT27_15065	GLP21_16805	GLP24_16755	GLP09_13120	GLP22_15860	GLP17_14140	GRJ22_15800	GLP31_16680	GLP27_14700	GLP20_14085	GLP19_15685	GLP14_13740	GLP23_13570	GLP13_14710
Heme biosynthesis															
Glutamyl−tRNA reductase (hemA	CIK00_20405	CIT27_03765	GLP21_04210	GLP24_18665	GLP09_17220	GLP22_14905	GLP17_18195	GRJ22_16375	GLP31_19805	GLP27_14905	GLP20_17875	GLP19_18445	GLP14_08415	GLP23_18330	GLP13_15545
glutamate-1-semialdehyde-2,1-aminomutase (hemL)	CIK00_07640	CIT27_09825	GLP21_10740	GLP24_08640	GLP09_06010	GLP22_10175	GLP17_08380	GRJ22_10610	GLP31_07285	GLP27_06615	GLP20_06060	GLP19_12080	GLP14_04130	GLP23_04170	GLP13_08690
aminolevulinic acid dehydratase (hemB)	CIK00_05635	CIT27_07615	GLP21_14345		GLP09_06400	GLP22_01855	GLP17_02240	GRJ22_02535					GLP14_03460		GLP13_02990
	CIK00_14385	CIT27_13925	GLP21_14800	GLP24_14460	GLP09_11580	GLP22_13065	GLP17_16250	GRJ22_14720	GLP31_14765	GLP27_12380	GLP20_13340	GLP19_15075	GLP14_11025	GLP23_12355	GLP13_13455
Hydroxymethylbilane synthase (hemC)	CIK00_14420	CIT27_13890	GLP21_14835	GLP24_14425	GLP09_11615	GLP22_13030	GLP17_16215	GRJ22_14685	GLP31_14800	GLP27_12345	GLP20_13305	GLP19_15040	GLP14_10990	GLP23_12390	GLP13_13490
Uroporphyrinogen-III synthase (hemD)	CIK00_14415	CIT27_13895	GLP21_14830	GLP24_14430	GLP09_11610	GLP22_13035	GLP17_16220	GRJ22_14690	GLP31_14795	GLP27_12350	GLP20_13310	GLP19_15045	GLP14_10995	GLP23_12385	GLP13_13485
Uroporphyrinogen decarboxylase (hemE)	CIK00_17010	CIT27_15565	GLP21_15920	GLP24_15790	GLP09_14565	GLP22_16865	GLP17_15855	GRJ22_16115	GLP31_16375	GLP27_16500	GLP20_14785	GLP19_16695	GLP14_15720	GLP23_14225	GLP13_16055
Coproporphyrinogen III oxidase (oxygen independent) (hemN)	CIK00_14535	CIT27_13775	GLP21_14950	GLP24_14310	GLP09_11730	GLP22_12915	GLP17_16700	GRJ22_14570	GLP31_14915	GLP27_12230	GLP20_13190	GLP19_14925	GLP14_10875	GLP23_12505	GLP13_13605
Coproporphyrinogen III oxidase (oxygen independent) (hemN)	CIK00_14540	CIT27_13770	GLP21_14955	GLP24_14305	GLP09_11735	GLP22_12910	GLP17_16695	GRJ22_14565	GLP31_14920	GLP27_12225	GLP20_13185	GLP19_14920	GLP14_10870	GLP23_12510	GLP13_13610
Coproporphyrinogen III oxidase (oxygen dependent)	CIK00_15950	CIT27_14880	GLP21_19070	GLP24_18830	GLP09_13305	GLP22_18355	GLP17_18365	GRJ22_15985	GLP31_19945	GLP27_14515	GLP20_13900	GLP19_15500	GLP14_13555	GLP23_13385	GLP13_14895
menaquinone-dependent protoporphyrinogen IX dehydrogenase	CIK00_16310	CIT27_15240	GLP21_16980	GLP24_16930	GLP09_12945	GLP22_16035	GLP17_14315	GRJ22_15625	GLP31_16855	GLP27_14870	GLP20_14260	GLP19_15860	GLP14_13915	GLP23_13745	GLP13_14535
Ferrochelatase (hemH)	CIK00_01720	CIT27_03580	GLP21_01245	GLP24_02875	GLP09_00770	GLP22_02360	GLP17_03140	GRJ22_12150	GLP31_00960	GLP27_03345	GLP20_02290	GLP19_02200	GLP14_10550	GLP23_02340	GLP13_00165
Virulence															
VOC family virulence protein	CIK00_01850	CIT27_03705	GLP21_01115	GLP24_02745	GLP09_00640	GLP22_02230	GLP17_03270	GRJ22_12280	GLP31_00830	GLP27_03205	GLP20_02160	GLP19_02065	GLP14_10675	GLP23_02210	GLP13_00030
virulence factor BrkB family protein	CIK00_14580	CIT27_13725	GLP21_14995	GLP24_14265	GLP09_11775	GLP22_12870	GLP17_16655	GRJ22_14525	GLP31_14960	GLP27_12185	GLP20_13145	GLP19_14880	GLP14_10830	GLP23_12550	GLP13_13650
virulence protein															
virulence associated protein															
H2O2 related enzymes															
Production															
pyruvate oxidase (Pox)	CIK00_07965	CIT27_00970	GLP21_09010	GLP24_04940	GLP09_15210	GLP22_05260	GLP17_15470	GRJ22_04820	GLP31_05645	GLP27_15535	GLP20_15055	GLP19_08815	GLP14_12790	GLP23_15375	GLP13_10880
superoxide dismutase (Sod)	CIK00_09520	CIT27_04695	GLP21_03295	GLP24_05915	GLP09_03480	GLP22_06295	GLP17_00505	GRJ22_06285	GLP31_12745	GLP27_09310	GLP20_00760	GLP19_04780	GLP14_09460	GLP23_00810	GLP13_05605
	CIK00_04555	CIT27_08395	GLP21_10310	GLP24_08175	GLP09_13470	GLP22_07250	GLP17_07325	GRJ22_03205	GLP31_09860	GLP27_06265	GLP20_04600	GLP19_10435	GLP14_01625	GLP23_05245	GLP13_04835

	P. carnosum														
	TMW 2.2021T	TMW 2.2029	TMW 2.2097	TMW 2.2147	TMW 2.2149	TMW 2.2150	TMW 2.2157	TMW 2.2163	TMW 2.2169	TMW 2.2098	TMW 2.2186	TMW 2.2187	TMW 2.2188	TMW 2.2189	TMW 2.2190
H2O2 scavenging enzymes															
catalase															
catalase/peroxidase	CIK00_10715	CIT27_06245	GLP21_05685	GLP24_01795	GLP09_16800	GLP22_00020	GLP17_05535	GRJ22_00705	GLP31_08160	GLP27_02100	GLP20_05150	GLP19_01525	GLP14_02950	GLP23_07630	GLP13_17160
Pressure response															
TMAO reductase system sensor histidine kinase/response regulator TorS	CIK00_11775	CIT27_05305	GLP21_02705	GLP24_05315	GLP09_09300	GLP22_06895	GLP17_01105	GRJ22_06865	GLP31_05140	GLP27_10420	GLP20_00180	GLP19_05375	GLP14_07760	GLP23_17015	GLP13_12825
Molecular chaperone Dnak	CIK00_05940	CIT27_07920	GLP21_14040	GLP24_10215	GLP09_06705	GLP22_02165	GLP17_02550	GRJ22_02840	GLP31_11310	GLP27_00080	GLP20_10880	GLP19_05570	GLP14_03150	GLP23_11415	GLP13_03300
	CIK00_07030	CIT27_10415	GLP21_11335	GLP24_09280	GLP09_16360	GLP22_14965	GLP17_07780	GRJ22_09950	GLP31_20150	GLP27_07250	GLP20_06725	GLP19_12785	GLP14_04755	GLP23_04845	GLP13_18595
Molecular chaperone DnaJ	CIK00_05935	CIT27_07915	GLP21_14045	GLP24_10220	GLP09_06700	GLP22_02160	GLP17_02545	GRJ22_02835	GLP31_11305	GLP27_00085	GLP20_10875	GLP19_05575	GLP14_03155	GLP23_11410	GLP13_03295
	CIK00_07025	CIT27_10420	GLP21_11340	GLP24_09285	GLP09_16355	GLP22_14960	GLP17_07775	GRJ22_09945	GLP31_20145	GLP27_07255	GLP20_06730	GLP19_12790	GLP14_04760	GLP23_04850	GLP13_18600
Molecular chaperone GroEL	CIK00_17160	CIT27_15710	GLP21_16070	GLP24_15645	GLP09_14420	GLP22_17010	GLP17_15710	GRJ22_16260	GLP31_16520	GLP27_16650	GLP20_14640	GLP19_16550	GLP14_15865	GLP23_14075	GLP13_15910
	CIK00_17165	CIT27_15715	GLP21_16075	GLP24_15615	GLP09_14415	GLP22_18090	GLP17_18715	GRJ22_16265	GLP31_16525	GLP27_16655	GLP20_14635	GLP19_16545	GLP14_15870	GLP23_14070	GLP13_15905
Co-chaperone GroES	CIK00_17155	CIT27_15705	GLP21_16065	GLP24_15650	GLP09_14425	GLP22_17005	GLP17_15715	GRJ22_16255	GLP31_16515	GLP27_16645	GLP20_14645	GLP19_16555	GLP14_15860	GLP23_14080	GLP13_15915
Outer membrane protein OmpH	CIK00_15835	CIT27_14765	GLP21_15730	GLP24_15095	GLP09_12855	GLP22_14525	GLP17_12400	GRJ22_15530	GLP31_15670	GLP27_14410	GLP20_16880	GLP19_15240	GLP14_13300	GLP23_13280	GLP13_14290
Porin-like protein OmpL	CIK00_07350									GLP27_06910	GLP20_06355		GLP14_04425		
Transcription activator system ToxR	CIK00_01735	CIT27_03595	GLP21_01230	GLP24_02860	GLP09_00755	GLP22_02345	GLP17_03155	GRJ22_12165	GLP31_00945	GLP27_03330	GLP20_02275	GLP19_02185	GLP14_10565	GLP23_02325	GLP13_00150
ToxS	CIK00_01740	CIT27_03600	GLP21_01225	GLP24_02855	GLP09_00750	GLP22_02340	GLP17_03160	GRJ22_12170	GLP31_00940	GLP27_03325	GLP20_02270	GLP19_02180	GLP14_10570	GLP23_02320	GLP13_00145
RNA polymerase sigma factor RpoE	CIK00_17800	CIT27_14190	GLP21_05880	GLP24_15365	GLP09_10945	GLP22_13425	GLP17_11400	GRJ22_14995	GLP31_14405	GLP27_11315	GLP20_13600	GLP19_16050	GLP14_11375	GLP23_14405	GLP13_12200
Anti-sigma E factor RseA	CIK00_17795	CIT27_14185	GLP21_05875	GLP24_15370	GLP09_10940	GLP22_13430	GLP17_11395	GRJ22_14990	GLP31_14400	GLP27_11320	GLP20_13595	GLP19_16045	GLP14_11380	GLP23_14410	GLP13_12195
Sigma-E factor regulatory protein RseB	CIK00_17790	CIT27_14180	GLP21_05870	GLP24_15375	GLP09_10935	GLP22_13435	GLP17_11390	GRJ22_14985	GLP31_14395	GLP27_11325	GLP20_13590	GLP19_16040	GLP14_11385	GLP23_14415	GLP13_12190
Transcriptional regulator RseC	CIK00_17785	CIT27_14175	GLP21_05865	GLP24_15380	GLP09_10930	GLP22_13440	GLP17_11385	GRJ22_14980	GLP31_14390	GLP27_11330	GLP20_13585	GLP19_16035	GLP14_11390	GLP23_14420	GLP13_12185
Exodeoxyribonuclease V subunit alpha, RecD	CIK00_15650	CIT27_14580	GLP21_15555	GLP24_14920	GLP09_12680	GLP22_14350	GLP17_12225	GRJ22_15355	GLP31_15495	GLP27_14235	GLP20_17640	GLP19_15415	GLP14_13475	GLP23_13105	GLP13_14465
Salt Response															
Outer membrane protein OmpW															
Major outer membrane protein OmpV															
RNA polymerase sigma factor RpoS	CIK00_05230	CIT27_07195	GLP21_04340	GLP24_11390	GLP09_13910	GLP22_01440	GLP17_01830	GRJ22_02115	GLP31_06600	GLP27_00775	GLP20_08925	GLP19_06290	GLP14_03855	GLP23_14900	GLP13_02570
	CIK00_17680	CIT27_14070	GLP21_05760	GLP24_15485	GLP09_10825	GLP22_13545	GLP17_11280	GRJ22_14875	GLP31_14285	GLP27_11435	GLP20_13480	GLP19_15930	GLP14_11495	GLP23_14525	GLP13_12080
Two-component system response regulator OmpR	CIK00_06735	CIT27_10710	GLP21_07350	GLP24_09875	GLP09_03980	GLP22_08885	GLP17_09015	GRJ22_10935	GLP31_09100	GLP27_07535	GLP20_07010	GLP19_13070	GLP14_05040	GLP23_07030	GLP13_07580
Two-component system sensor histidine kinase EnvZ	CIK00_06730	CIT27_10715	GLP21_07355	GLP24_09870	GLP09_03985	GLP22_08890	GLP17_09010	GRJ22_10940	GLP31_09095	GLP27_07540	GLP20_07015	GLP19_13075	GLP14_05045	GLP23_07025	GLP13_07585
Porin OmpC/OmpF															
Sodium transporters															
sodium:alanine symporter family protein	CIK00_00135	CIT27_01980	GLP21_15365	GLP24_07390	GLP09_02370	GLP22_03945	GLP17_13230	GRJ22_05830	GLP31_02550	GLP27_04980	GLP20_03005	GLP19_09820	GLP14_17135	GLP23_14960	GLP13_01950
	CIK00_07515	CIT27_09950	GLP21_10870	GLP24_08770	GLP09_05880	GLP22_10305	GLP17_08255	GRJ22_10480	GLP31_07410	GLP27_06745	GLP20_06190	GLP19_12210	GLP14_04260	GLP23_04300	GLP13_08560
sodium:alanine (sodium:glycine) symporter family protein	CIK00_00185	CIT27_02030	GLP21_15315	GLP24_07340	GLP09_02320	GLP22_03895	GLP17_13280	GRJ22_05880	GLP31_02500	GLP27_04930	GLP20_03055	GLP19_03935	GLP14_17185	GLP23_15010	GLP13_01900
sodium:proton antiporter	CIK00_16570	CIT27_05860	GLP21_05295	GLP24_13395	GLP09_14045	GLP22_00475	GLP17_05140	GRJ22_01135	GLP31_18860	GLP27_01695	GLP20_05540	GLP19_01900	GLP14_02550	GLP23_19405	GLP13_15195
	CIK00_08495	CIT27_11300	GLP21_06870	GLP24_11525	GLP09_07365	GLP22_10080	GLP17_13730	GRJ22_12355	GLP31_10800	GLP27_08260	GLP20_07730	GLP19_13650	GLP14_06275	GLP23_07975	GLP13_09470
	CIK00_09375	CIT27_04550	GLP21_03440	GLP24_06060	GLP09_03335	GLP22_06150	GLP17_00360	GRJ22_06140	GLP31_12600	GLP27_09155	GLP20_00905	GLP19_04635	GLP14_09605	GLP23_00665	GLP13_05750
	CIK00_09530	CIT27_04705	GLP21_03285	GLP24_05905	GLP09_03490	GLP22_06305	GLP17_00515	GRJ22_06295	GLP31_12755	GLP27_09320	GLP20_00750	GLP19_04790	GLP14_09450	GLP23_00820	GLP13_05595
	CIK00_13950	CIT27_13170	GLP21_16375	GLP24_00940	GLP09_07900	GLP22_08155	GLP17_04935	GRJ22_04620	GLP31_03550	GLP27_13245	GLP20_11835	GLP19_00635	GLP14_06250	GLP23_03535	GLP13_06585
Na+/H+ antiporter	CIK00_11270	CIT27_00270	GLP21_08775	GLP24_03975	GLP09_15180	GLP22_04495	GLP17_10330	GRJ22_09635	GLP31_04530	GLP27_11870	GLP20_11225	GLP19_07880	GLP14_11715	GLP23_05905	GLP13_10355
Na+/H+ antiporter NhaA	CIK00_07425	CIT27_10040	GLP21_10960	GLP24_08860	GLP09_05790	GLP22_10395	GLP17_08165	GRJ22_10390	GLP31_07500	GLP27_06835	GLP20_06280	GLP19_12300	GLP14_04350	GLP23_04390	GLP13_08470
Na+/H+ antiporter NhaC	CIK00_09510	CIT27_04685	GLP21_03305	GLP24_05925	GLP09_03470	GLP22_06285	GLP17_00495	GRJ22_06275	GLP31_12735	GLP27_09300	GLP20_00770	GLP19_04770	GLP14_09470	GLP23_00800	GLP13_05615
Na+/H+ antiporter NhaC		CIT27_05255											GLP14_07710		GLP13_12775
	CIK00_01200	CIT27_03060	GLP21_01765	GLP24_03400	GLP09_01295	GLP22_02880	GLP17_05925	GRJ22_08940	GLP31_01480		GLP20_02815	GLP19_02720	GLP14_00270	GLP23_10530	GLP13_00685
Na+/H+ antiporter	CIK00_01470	CIT27_03330	GLP21_01495	GLP24_03125	GLP09_01020	GLP22_02610	GLP17_02890	GRJ22_11900	GLP31_01210	GLP27_03595	GLP20_02540	GLP19_02450	GLP14_10300	GLP23_02590	GLP13_00415
sodium:proton exchanger															
Na+/H+ antiporter NhaC family protein	CIK00_20445	CIT27_03805	GLP21_04170	GLP24_18705	GLP09_17260	GLP22_14865	GLP17_18235	GRJ22_16410	GLP31_19765	GLP27_14945	GLP20_17915	GLP19_18405	GLP14_08375	GLP23_18290	GLP13_15505
DASS family sodium-coupled anion symporter / 2-oxoglutarate translocator	CIK00_04620	CIT27_08455	GLP21_10250	GLP24_08110	GLP09_13525	GLP22_07185	GLP17_07260	GRJ22_03265	GLP31_09795	GLP27_06195	GLP20_04535	GLP19_10375	GLP14_01570	GLP23_05305	GLP13_04775
sodium:phosphate symporter	CIK00_07430	CIT27_10035	GLP21_10955	GLP24_08855	GLP09_05795	GLP22_10390	GLP17_08170	GRJ22_10395	GLP31_07495	GLP27_06830	GLP20_06275	GLP19_12295	GLP14_04345	GLP23_04385	GLP13_08475
calcium/sodium antiporter	CIK00_08725	CIT27_11530	GLP21_06635	GLP24_11750	GLP09_07135	GLP22_09845	GLP17_13495	GRJ22_12580	GLP31_10560	GLP27_08490	GLP20_07960	GLP19_13885	GLP14_06510	GLP23_08205	GLP13_09700
DASS family sodium-coupled anion symporter	CIK00_10095	CIT27_01515	GLP21_09555	GLP24_12475	GLP09_10435	GLP22_05800	GLP17_09595	GRJ22_05365	GLP31_06185	GLP27_09880	GLP20_10015	GLP19_09355	GLP14_07230	GLP23_09480	GLP13_09125
sodium/glutamate symporter	CIK00_11165	CIT27_00150	GLP21_08880	GLP24_03875	GLP09_15065	GLP22_04380	GLP17_10220	GRJ22_09740	GLP31_04645	GLP27_11765	GLP20_11120	GLP19_07765	GLP14_11820	GLP23_05800	GLP13_10235
dicarboxylate/amino acid:cation symporter	CIK00_11450	CIT27_04965	GLP21_03030	GLP24_05650	GLP09_09625	GLP22_06565	GLP17_00770	GRJ22_06550	GLP31_04810	GLP27_10095	GLP20_00490	GLP19_05045	GLP14_07435	GLP23_01075	GLP13_12495
Na+:H+ dicarboxylate symporter	CIK00_16900	CIT27_15255	GLP21_13430	GLP24_16370	GLP09_14920	GLP22_15760	GLP17_12490	GRJ22_13675	GLP31_05585	GLP27_18135	GLP20_16470	GLP19_07415	GLP14_14225	GLP23_14000	GLP13_18220
cation:dicarboxylase symporter family transporter	CIK00_11460	CIT27_04975	GLP21_03020	GLP24_05640	GLP09_09615	GLP22_06575	GLP17_00780	GRJ22_06560	GLP31_04820	GLP27_10105	GLP20_00480	GLP19_05055	GLP14_07445	GLP23_01085	GLP13_12505
DASS family sodium-coupled anion symporter	CIK00_11685	CIT27_05205	GLP21_02790	GLP24_05400	GLP09_09385	GLP22_06810	GLP17_01020	GRJ22_06780	GLP31_05055	GLP27_10335	GLP20_00265	GLP19_05290	GLP14_07660	GLP23_01305	GLP13_12725
sodium/solute symporter	CIK00_16420	CIT27_06015	GLP21_05445	GLP24_13240	GLP09_14260	GLP22_00230	GLP17_05290	GRJ22_00945	GLP31_07950	GLP27_01835	GLP20_05390	GLP19_01735	GLP14_02705	GLP23_07420	GLP13_16965
sodium:solute symporter	CIK00_19485		GLP21_04985	GLP24_18215	GLP09_08260	GLP22_00795	GLP17_14495	GRJ22_01460	GLP31_14180	GLP27_01325	GLP20_05890	GLP19_06925	GLP14_02250	GLP23_11490	
sodium/solute symporter											GLP20_17220				GLP13_15630
sodium/solute symporter															
sodium-dependent transporter															
sodium/panthothenate symporter	CIK00_17085	CIT27_15635	GLP21_15995	GLP24_15720	GLP09_14495	GLP22_16935	GLP17_15785	GRJ22_16185	GLP31_16445	GLP27_16575	GLP20_14715	GLP19_16625	GLP14_15790	GLP23_14150	GLP13_15985
sodium/glucose cotransporter		CIT27_07930		GLP24_10205		GLP22_02175	GLP17_02560		GLP31_11320	GLP27_19535					GLP13_03310
melibiose:sodium transporter MelB			GLP21_08190												
sodium/proline symporter PutP															
sodium/proline symporter PutP															
sodium:proline symporter															
sodium:proline symporter															
sodium:proline symporter															
bile acid:sodium symporter family protein															
Motility															
chemotaxis-specific protein-glutamate methyltransferase CheB	CIK00_02045		GLP21_00860	GLP24_02550			GLP17_03465		GLP31_00635	GLP27_03005	GLP20_01965		GLP14_10055	GLP23_02015	

	P. carnosum														
	TMW 2.2021T	**TMW 2.2029**	**TMW 2.2097**	**TMW 2.2147**	**TMW 2.2149**	**TMW 2.2150**	**TMW 2.2157**	**TMW 2.2163**	**TMW 2.2169**	**TMW 2.2098**	**TMW 2.2186**	**TMW 2.2187**	**TMW 2.2188**	**TMW 2.2189**	**TMW 2.2190**
chemotaxis protein CheA	CIK00_02050		GLP21_00855	GLP24_02545			GLP17_03470		GLP31_00630	GLP27_03000	GLP20_01960		GLP14_10050	GLP23_02010	
protein phosphatase CheZ	CIK00_02055		GLP21_00850	GLP24_02540			GLP17_03475		GLP31_00625	GLP27_02995	GLP20_01955		GLP14_10045	GLP23_02005	
chemotaxis protein CheY	CIK00_02060		GLP21_00845	GLP24_02535			GLP17_03480		GLP31_00620	GLP27_02990	GLP20_01950		GLP14_10040	GLP23_02000	
RNA polymerase sigma factor FliA	CIK00_02065		GLP21_00840	GLP24_02530			GLP17_03485		GLP31_00615	GLP27_02985	GLP20_01945		GLP14_10035	GLP23_01995	
flagellar biosynthesis protein FlhF	CIK00_02075		GLP21_00830	GLP24_02520			GLP17_03495		GLP31_00605	GLP27_02975	GLP20_01935		GLP14_10025	GLP23_01985	
flagellar biosynthesis protein FlhA	CIK00_02080		GLP21_00825	GLP24_02515			GLP17_03500		GLP31_00600	GLP27_02970	GLP20_01930		GLP14_10020	GLP23_01980	
flagellar biosynthesis protein FlhB	CIK00_02085		GLP21_00820	GLP24_02510			GLP17_03505		GLP31_00595	GLP27_02965	GLP20_01925		GLP14_10015	GLP23_01975	
flagellar type III secretion system protein FliR	CIK00_02090		GLP21_00815	GLP24_02505			GLP17_03510		GLP31_00590	GLP27_02960	GLP20_01920		GLP14_10010	GLP23_01970	
flagellar biosynthetic protein FliQ	CIK00_02095		GLP21_00810	GLP24_02500			GLP17_03515		GLP31_00585	GLP27_02955	GLP20_01915		GLP14_10005	GLP23_01965	
flagellar type III secretion system pore protein FliP	CIK00_02100		GLP21_00805	GLP24_02495			GLP17_03520		GLP31_00580	GLP27_02950	GLP20_01910		GLP14_10000	GLP23_01960	
flagellar biosynthetic protein FliO	CIK00_02105		GLP21_00800	GLP24_02490			GLP17_03525		GLP31_00575	GLP27_02945	GLP20_01905		GLP14_09995	GLP23_01955	
flagellar motor switch protein FliN	CIK00_02110		GLP21_00795	GLP24_02485			GLP17_03530		GLP31_00570	GLP27_02940	GLP20_01900		GLP14_09990	GLP23_01950	
flagellar motor switch protein FliM	CIK00_02115		GLP21_00790	GLP24_02480			GLP17_03535		GLP31_00565	GLP27_02935	GLP20_01895		GLP14_09985	GLP23_01945	
flagellar basal body-associated protein FliL	CIK00_02120		GLP21_00785	GLP24_02475			GLP17_03540		GLP31_00560	GLP27_02930	GLP20_01890		GLP14_09980	GLP23_01940	
flagella biosynthesis chaperone FliJ	CIK00_02130		GLP21_00775	GLP24_02465			GLP17_03550		GLP31_00550	GLP27_02920	GLP20_01880		GLP14_09970	GLP23_01930	
flagellar protein export ATPase FliI	CIK00_02135		GLP21_00770	GLP24_02460			GLP17_03555		GLP31_00545	GLP27_02915	GLP20_01875		GLP14_09965	GLP23_01925	
flagellar assembly protein FliH	CIK00_02140		GLP21_00765	GLP24_02455			GLP17_03560		GLP31_00540	GLP27_02910	GLP20_01870		GLP14_09960	GLP23_01920	
flagellar motor switch protein FliG	CIK00_02145		GLP21_00760	GLP24_02450			GLP17_03565		GLP31_00535	GLP27_02905	GLP20_01865		GLP14_09955	GLP23_01915	
flagellar basal body M-ring protein FliF	CIK00_02150		GLP21_00755	GLP24_02445			GLP17_03570		GLP31_00530	GLP27_02900	GLP20_01860		GLP14_09950	GLP23_01910	
flagellar hook-basal body complex protein FliE	CIK00_02155		GLP21_00750	GLP24_02440			GLP17_03575		GLP31_00525	GLP27_02895	GLP20_01855		GLP14_09945	GLP23_01905	
flagellar biosynthesis protein FliS	CIK00_02180		GLP21_00725	GLP24_02415			GLP17_03600		GLP31_00500	GLP27_02870	GLP20_01830		GLP14_09920	GLP23_01880	
flagellar filament capping protein FliD	CIK00_02185		GLP21_00720	GLP24_02410			GLP17_03605		GLP31_00495	GLP27_02865	GLP20_01825		GLP14_09915	GLP23_01875	
flagellar biosynthesis protein FlaG	CIK00_02190		GLP21_00715	GLP24_02405			GLP17_03610		GLP31_00490	GLP27_02860	GLP20_01820		GLP14_09910	GLP23_01870	
flagellin	CIK00_02195		GLP21_00710	GLP24_02400			GLP17_03615		GLP31_00485	GLP27_02855	GLP20_01815		GLP14_09905	GLP23_01865	
flagellar hook-associated protein FlgL	CIK00_02200		GLP21_00705	GLP24_02395			GLP17_03620		GLP31_00480	GLP27_02850	GLP20_01810		GLP14_09900	GLP23_01860	
flagellar hook-associated protein FlgK	CIK00_02205		GLP21_00700	GLP24_02390			GLP17_03625		GLP31_00475	GLP27_02845	GLP20_01805		GLP14_09895	GLP23_01855	
flagellar hook protein	CIK00_02210		GLP21_00695	GLP24_02385			GLP17_03630		GLP31_00470	GLP27_02840	GLP20_01800		GLP14_09890	GLP23_01850	
flagellar assembly peptidoglycan hydrolase FlgJ	CIK00_02215		GLP21_00690	GLP24_02380			GLP17_03635		GLP31_00465	GLP27_02835	GLP20_01795		GLP14_09885	GLP23_01845	
flagellar basal body P-ring protein FlgI	CIK00_02220		GLP21_00685	GLP24_02375			GLP17_03640		GLP31_00460	GLP27_02830	GLP20_01790		GLP14_09880	GLP23_01840	
flagellar basal body L-ring protein	CIK00_02225		GLP21_00680	GLP24_02370			GLP17_03645		GLP31_00455	GLP27_02825	GLP20_01785		GLP14_09875	GLP23_01835	
flagellar basal-body rod protein FlgG	CIK00_02230		GLP21_00675	GLP24_02365			GLP17_03650		GLP31_00450	GLP27_02820	GLP20_01780		GLP14_09870	GLP23_01830	
flagellar basal-body rod protein FlgF	CIK00_02235		GLP21_00670	GLP24_02360			GLP17_03655		GLP31_00445	GLP27_02815	GLP20_01775		GLP14_09865	GLP23_01825	
flagellar hook protein FlgE	CIK00_02240		GLP21_00665	GLP24_02355			GLP17_03660		GLP31_00440	GLP27_02810	GLP20_01770		GLP14_09860	GLP23_01820	
flagellar biosynthesis protein FlgD	CIK00_02245		GLP21_00660	GLP24_02350			GLP17_03665		GLP31_00435	GLP27_02805	GLP20_01765		GLP14_09855	GLP23_01815	
flagellar basal body rod protein FlgC	CIK00_02250		GLP21_00655	GLP24_02345			GLP17_03670		GLP31_00430	GLP27_02800	GLP20_01760		GLP14_09850	GLP23_01810	
flagellar basal body rod protein FlgB	CIK00_02255		GLP21_00650	GLP24_02340			GLP17_03675		GLP31_00425	GLP27_02795	GLP20_01755		GLP14_09845	GLP23_01805	
chemotaxis protein CheR	CIK00_02260		GLP21_00645	GLP24_02335			GLP17_03680		GLP31_00420	GLP27_02790	GLP20_01750		GLP14_12745	GLP23_01800	
chemotaxis protein CheV	CIK00_02265		GLP21_00640	GLP24_02330			GLP17_03685		GLP31_00415	GLP27_02785	GLP20_01745		GLP14_12740	GLP23_01795	
flagellar biosynthesis protein FlhB	CIK00_02020	CIT27_12175	GLP21_00885	GLP24_02575			GLP17_03440		GLP31_00660	GLP27_03030	GLP20_01990		GLP14_10080	GLP23_02040	
chemotaxis protein CheW	CIK00_02030	CIT27_12185	GLP21_00875	GLP24_02565			GLP17_03450		GLP31_00650	GLP27_03020	GLP20_01980		GLP14_10070	GLP23_02030	
chemotaxis protein CheW/hypothetical protein	CIK00_02035	CIT27_12190	GLP21_00870	GLP24_02560	GLP09_00470	GLP22_12215	GLP17_03455	GRJ22_07835	GLP31_00645	GLP27_03015	GLP20_01975	GLP19_11235	GLP14_10065	GLP23_02025	GLP13_11465
flagellar biosynthesis anti-sigma factor FlgM	CIK00_02275	CIT27_12215	GLP21_00630	GLP24_02320	GLP09_00445	GLP22_12190	GLP17_03695	GRJ22_07810	GLP31_00405	GLP27_02775	GLP20_01735	GLP19_11260	GLP14_12730	GLP23_01785	GLP13_11490
flagellar protein FlgN	CIK00_02280	CIT27_12220	GLP21_00625	GLP24_02315	GLP09_00440	GLP22_12185	GLP17_03700	GRJ22_07805	GLP31_00400	GLP27_02770	GLP20_01730	GLP19_11265	GLP14_12725	GLP23_01780	GLP13_11495
flagellar biosynthesis protein FlgP	CIK00_02285	CIT27_12225	GLP21_00620	GLP24_02310	GLP09_00435	GLP22_12180	GLP17_03705	GRJ22_07800	GLP31_00395	GLP27_02765	GLP20_01725	GLP19_11270	GLP14_12720	GLP23_01775	GLP13_11500
flagellar basal-body protein	CIK00_02295	CIT27_12235	GLP21_00610	GLP24_02300	GLP09_00425	GLP22_12170	GLP17_03715	GRJ22_07790	GLP31_00385	GLP27_02755	GLP20_01715	GLP19_11280	GLP14_12710	GLP23_01765	GLP13_11510
flagellar export chaperone FliS	CIK00_02175		GLP21_00730	GLP24_02420			GLP17_03595		GLP31_00505	GLP27_02875	GLP20_01835		GLP14_09925	GLP23_01885	
flagella basal body P-ring formation protein FlgA	CIK00_02270	CIT27_12210	GLP21_00635	GLP24_02325	GLP09_00450	GLP22_12195	GLP17_03690	GRJ22_07815	GLP31_00410	GLP27_02780	GLP20_01740	GLP19_11255	GLP14_12735	GLP23_01790	GLP13_11485
Bioluminescence															
Phosphorelay protein LuxU	CIK00_09595	CIT27_04770	GLP21_03220	GLP24_05840	GLP09_03555	GLP22_06370	GLP17_00580	GRJ22_06360	GLP31_12820	GLP27_09385	GLP20_00685	GLP19_04855	GLP14_16125	GLP23_00885	GLP13_05530
transcriptional regulator quorum sensing regulator LuxR	CIK00_09050	CIT27_11855	GLP21_06310	GLP24_12075	GLP09_06810	GLP22_09520	GLP17_13030	GRJ22_12905	GLP31_10205	GLP27_08845	GLP20_08315	GLP19_14205	GLP14_06835	GLP23_08535	GLP13_10020
lux-rib operon															
ribB	CIK00_02620	CIT27_12560	GLP21_00280	GLP24_01940	GLP09_00055	GLP22_11805	GLP17_18835	GRJ22_07460	GLP31_00055	GLP27_18475	GLP20_01385	GLP19_11605	GLP14_12380	GLP23_01435	GLP13_11835
luxC															
Activated long-chain acyl hydrolase luxD															
luxE															
luxF															
luxG															
Beta subunit luciferase luxB															
Alpha subunit luciferase luxA															
quorum sensing regulator LuxR	CIK00_04130	CIT27_08020	GLP21_14605	GLP24_08495	GLP09_12065	GLP22_07665	GLP17_07685	GRJ22_17925	GLP31_16260	GLP27_18860	GLP20_04945	GLP19_10770	GLP14_01960	GLP23_18105	GLP13_05150
hot-dog/esterase															
esterase FrsA	CIK00_02465	CIT27_12405	GLP21_00440	GLP24_02100	GLP09_00215	GLP22_11965	GLP17_03890	GRJ22_07620	GLP31_00215	GLP27_02585	GLP20_01545	GLP19_11450	GLP14_12540	GLP23_01595	GLP13_11680
esterase YqiA	CIK00_12825	CIT27_12745	GLP21_12820	GLP24_12840	GLP09_08950	GLP22_10795	GLP17_10780	GRJ22_13335	GLP31_12420	GLP27_10915	GLP20_12305	GLP19_14615	GLP14_08775	GLP23_10015	GLP13_13050
	CIK00_17490					GLP22_16280			GLP31_19870				GLP14_09400		
Shock /stress															
cold-shock protein	CIK00_00050 + CIK00_10755 + CIK00_16320 + CIK00_05205	CIT27_06205 + CIT27_01895 + CIT27_06115 + CIT27_07170	GLP21_19210 + GLP21_05645 + GLP21_15450 + GLP21_04365 + GLP21_05580	GLP24_01835 + GLP24_18920 + GLP24_07475 + GLP24_11365	GLP09_16760 + GLP09_16690 + GLP09_13885 + GLP09_02455	GLP22_04030 + GLP22_00060 + GLP22_00130 + GLP22_01415	GLP17_01805 + GLP17_05425 + GLP17_05495 + GLP17_13145	GRJ22_00745 + GRJ22_00810 + GRJ22_02085 + GRJ22_05745 + GRJ22_09865	GLP31_02635 + GLP31_04770 + GLP31_06625 + GLP31_08050 + GLP31_08120	GLP27_02050 + GLP27_01970 + GLP27_00800 + GLP27_05065	GLP20_05255 + GLP20_02920 + GLP20_05190 + GLP20_08900 + GLP20_18320	GLP19_01565 + GLP19_01635 + GLP19_06315 + GLP19_09735 + GLP19_18120	GLP14_02840 + GLP14_02910 + GLP14_03880 + GLP14_15595	GLP23_07520 + GLP23_07590 + GLP23_14870 + GLP23_18710 + GLP23_19025 + GLP23_19670	GLP13_02035 + GLP13_02545 + GLP13_16865 + GLP13_17120
	CIK00_18345	CIT27_16095	GLP21_17115	GLP24_17505	GLP09_15545	GLP22_16690	GLP17_15140	GRJ22_17260	GLP31_16980	GLP27_15875	GLP20_15210	GLP19_16870	GLP14_16270	GLP23_15520	GLP13_16460
	CIK00_07885	CIT27_01050	GLP21_09090	GLP24_05020	GLP09_15290	GLP22_05340	GLP17_15390	GRJ22_04900	GLP31_05725	GLP27_15615	GLP20_14975	GLP19_08890	GLP14_17510	GLP23_15295	GLP13_10800
	CIK00_17920	CIT27_14310	GLP21_06000	GLP24_15245	GLP09_11065	GLP22_13305	GLP17_11520	GRJ22_15115	GLP31_14525	GLP27_11195	GLP20_13720	GLP19_16170	GLP14_11255	GLP23_14285	GLP13_12320
					GLP09_09480			GRJ22_06695		GLP27_19450	GLP20_17780	GLP19_09555	GLP14_15115	GLP23_19335 GLP23_19650	GLP13_18390

	P. carnosum														
	TMW 2.2021T	TMW 2.2029	TMW 2.2097	TMW 2.2147	TMW 2.2149	TMW 2.2150	TMW 2.2157	TMW 2.2163	TMW 2.2169	TMW 2.2098	TMW 2.2186	TMW 2.2187	TMW 2.2188	TMW 2.2189	TMW 2.2190
	CIK00_05205 + CIK00_10625 + CIK00_10755 + CIK00_16320 + CIK00_19215 + CIK00_19225	CIT27_06115 + CIT27_06205 + CIT27_06340 + CIT27_07170 + CIT27_17205 + CIT27_17215	GLP21_04365 + GLP21_05580 + GLP21_05645 + GLP21_07070 + GLP21_07080 + GLP21_19210	GLP24_01835 + GLP24_11365 + GLP24_17995 + GLP24_18005 + GLP24_18920	GLP09_11440 + GLP09_13885 + GLP09_15910 + GLP09_15920 + GLP09_16690 + GLP09_16760	GLP22_00060 + GLP22_00130 + GLP22_01415 + GLP22_12670 + GLP22_17215 + GLP22_17225	GLP17_01805 + GLP17_05425 + GLP17_05495 + GLP17_05625 + GLP17_16505 + GLP17_16515	GRJ22_00745 + GRJ22_00810 + GRJ22_02085 + GRJ22_09865 + GRJ22_17835 + GRJ22_17845	GLP31_04770 + GLP31_06625 + GLP31_08050 + GLP31_08120 + GLP31_08250 + GLP31_17960 + GLP31_17970	GLP27_00800 + GLP27_01970 + GLP27_02050 + GLP27_16885 + GLP27_16895	GLP20_05190 + GLP20_05255 + GLP20_08900 + GLP20_12930 + GLP20_16270 + GLP20_16280 + GLP20_18320	GLP19_01565 + GLP19_01635 + GLP19_06315 + GLP19_17515 + GLP19_17525 + GLP19_18120	GLP14_02840 + GLP14_02910 + GLP14_03880 + GLP14_15595 + GLP14_16915 + GLP14_16925	GLP23_07520 + GLP23_07590 + GLP23_07725 + GLP23_14870 + GLP23_16085 + GLP23_16095 + GLP23_18710 + GLP23_19025 + GLP23_19670	GLP13_02035 + GLP13_02545 + GLP13_16865 + GLP13_17120 + GLP13_17250 + GLP13_17290 + GLP13_17300
cold shock domain protein CspD	CIK00_09685	CIT27_04855	GLP21_03130	GLP24_05750	GLP09_03645	GLP22_06460	GLP17_00670	GRJ22_06450	GLP31_12910	GLP27_09475	GLP20_00595	GLP19_04945	GLP14_16035	GLP23_00975	GLP13_05440
phage shock protein C / envelope stress response membrane protein PspC	CIK00_00890	CIT27_02740	GLP21_02080	GLP24_06650	GLP09_01610	GLP22_03195	GLP17_06235	GRJ22_08620	GLP31_01795	GLP27_04235	GLP20_03770	GLP19_03035	GLP14_00585	GLP23_10220	GLP13_01005
phage shock protein B / envelope stress response membrane protein PspB	CIK00_00895	CIT27_02745	GLP21_02075	GLP24_06645	GLP09_01605	GLP22_03190	GLP17_06230	GRJ22_08625	GLP31_01790	GLP27_04230	GLP20_03775	GLP19_03030	GLP14_00580	GLP23_10225	GLP13_01000
phage shock protein PspA	CIK00_00900	CIT27_02750	GLP21_02070	GLP24_06640	GLP09_01600	GLP22_03185	GLP17_06225	GRJ22_08630	GLP31_01785	GLP27_04225	GLP20_03780	GLP19_03025	GLP14_00575	GLP23_10230	GLP13_00995
phage shock protein A	CIK00_10670	CIT27_06295	GLP21_13935	GLP24_01755	GLP09_11485	GLP22_12715	GLP17_05580	GRJ22_00655	GLP31_08205	GLP27_02135	GLP20_12975	GLP19_01475	GLP14_02995	GLP23_07680	GLP13_17205
phage shock protein operon transcriptional activator	CIK00_00905	CIT27_02755	GLP21_02065	GLP24_06635	GLP09_01595	GLP22_03180	GLP17_06220	GRJ22_08635	GLP31_01780	GLP27_04220	GLP20_03785	GLP19_03020	GLP14_00570	GLP23_10235	GLP13_00990
phage shock protein G / envelope stress response protein PspG	CIK00_18325	CIT27_16115	GLP21_17135	GLP24_17485	GLP09_15565	GLP22_16670	GLP17_15160	GRJ22_17280	GLP31_17000	GLP27_15895	GLP20_15230	GLP19_16890	GLP14_16250	GLP23_15540	GLP13_16440
heat-shock protein Hsp20	CIK00_05945	CIT27_07925	GLP21_14035	GLP24_10210	GLP09_06710	GLP22_02170	GLP17_02555	GRJ22_02845	GLP31_11315	GLP27_00075	GLP20_10885	GLP19_05565	GLP14_03145	GLP23_11420	GLP13_03305
heat-shock protein / META domain-containing protein	CIK00_13005	CIT27_03920	GLP21_04055	GLP24_17775	GLP09_02675	GLP22_14755	GLP17_14725	GRJ22_16510	GLP31_17720	GLP27_15045	GLP20_15855	GLP19_04005	GLP14_08265	GLP23_00040	GLP13_15395
heat-shock protein HslJ / META domain-containing protein	CIK00_13740 CIK00_16750	CIT27_07050 CIT27_15405	GLP21_04485 GLP21_13280	GLP24_11185 GLP24_16215	GLP09_13765 GLP09_14770	GLP22_01235 GLP22_15605	GLP17_01625 GLP17_12640	GRJ22_01905 GRJ22_13835	GLP31_06845 GLP31_05430	GLP27_00920 GLP27_18005	GLP20_08775 GLP20_16625	GLP19_06495 GLP19_07260	GLP14_14840 GLP14_14375	GLP23_14745 GLP23_13850	GLP13_02425 GLP13_17940
ribosome-associated heat shock protein Hsp15	CIK00_14610	CIT27_13695	GLP21_15025	GLP24_14235	GLP09_11805	GLP22_12840	GLP17_16625	GRJ22_14495	GLP31_14990	GLP27_12155	GLP20_13115	GLP19_14850	GLP14_10800	GLP23_12580	GLP13_13680
oxidative-stress-resistance chaperone / DJ-1 family protein	CIK00_02565	CIT27_12505	GLP21_00335	GLP24_01995	GLP09_00110	GLP22_11860	GLP17_18945	GRJ22_07515	GLP31_00110	GLP27_18530	GLP20_01440	GLP19_11550	GLP14_12435	GLP23_01490	GLP13_11780
GlsB/YeaQ/YmgE family stress response membrane protein	CIK00_05740	CIT27_07720	GLP21_14240	GLP24_10415	GLP09_06505	GLP22_01960	GLP17_02345	GRJ22_02640	GLP31_11105	GLP27_00280	GLP20_10675	GLP19_05775	GLP14_03355	GLP23_11210	GLP13_03095
peroxide stress protein YaaA	CIK00_07510	CIT27_09955	GLP21_10875	GLP24_08775	GLP09_05875	GLP22_10310	GLP17_08250	GRJ22_10475	GLP31_07415	GLP27_06750	GLP20_06195	GLP19_12215	GLP14_04265	GLP23_04305	GLP13_08555
outer membrane-stress sensor serine endopeptidase DegS	CIK00_08765	CIT27_11570	GLP21_06595	GLP24_11790	GLP09_07095	GLP22_09805	GLP17_13455	GRJ22_12620	GLP31_10520	GLP27_08530	GLP20_08000	GLP19_13925	GLP14_06550	GLP23_08245	GLP13_09740
stress response translation initiation inhibitor YciH	CIK00_12465	CIT27_09710	GLP21_11395	GLP24_00015	GLP09_09955	GLP22_11440	GLP17_04000	GRJ22_03740	GLP31_02675	GLP27_05745	GLP20_09710	GLP19_17020	GLP14_17680	GLP23_18375	GLP13_04300
stress response serine/threonine protein kinase YihE	CIK00_16035	CIT27_14965	GLP21_18985	GLP24_18745	GLP09_13220	GLP22_18270	GLP17_18280	GRJ22_15900	GLP31_20030	GLP27_14600	GLP20_13985	GLP19_15585	GLP14_13640	GLP23_13470	GLP13_14810
oxidative stress defense protein	CIK00_17895	CIT27_14285	GLP21_05975	GLP24_15270	GLP09_11040	GLP22_13330	GLP17_11495	GRJ22_15090	GLP31_14500	GLP27_11220	GLP20_13695	GLP19_16145	GLP14_11280	GLP23_14310	GLP13_12295
universal stress protein	CIK00_14320 CIK00_07125	CIT27_13990 CIT27_10340	GLP21_14735 GLP21_11260	GLP24_14530 GLP24_09160	GLP09_11515 GLP09_05490	GLP22_13130 GLP22_15110	GLP17_16315 GLP17_07865	GRJ22_14785 GRJ22_10090	GLP31_14700 GLP31_07800	GLP27_12445 GLP27_07135	GLP20_13405 GLP20_06580	GLP19_15140 GLP19_12600	GLP14_11090 GLP14_04650	GLP23_12290 GLP23_04690	GLP13_13390 GLP13_08170
universal stress protein UspE	CIK00_09800	CIT27_01210	GLP21_09255	GLP24_12170	GLP09_17015	GLP22_05500	GLP17_09290	GRJ22_05060	GLP31_05885	GLP27_09585	GLP20_10315	GLP19_09050	GLP14_06930	GLP23_09180	GLP13_09430
universal stress protein UspB	CIK00_19200	CIT27_17190	GLP21_07055	GLP24_17980	GLP09_15935	GLP22_17200	GLP17_16490	GRJ22_17820	GLP31_17945	GLP27_16910	GLP20_16295	GLP19_17540	GLP14_16940	GLP23_16070	GLP13_17315
universal stress global response regulator UspA	CIK00_19190	CIT27_17180	GLP21_07045	GLP24_17970	GLP09_15945	GLP22_17190	GLP17_16480	GRJ22_17810	GLP31_17935	GLP27_16920	GLP20_16305	GLP19_17550	GLP14_16950	GLP23_16060 GLP23_19915	GLP13_17325
envelope stress sensor histidine kinase CpxA / two-component system sensor histidine kinase	CIK00_06515	CIT27_10930	GLP21_07570	GLP24_09655	GLP09_04200	GLP22_09105	GLP17_08795	GRJ22_11155	GLP31_08895	GLP27_07760	GLP20_07230	GLP19_13290	GLP14_05260	GLP23_06810	GLP13_07800
NirD/YgiW/YdeI family stress tolerance protein / hypothetical protein	CIK00_05435 CIK00_17925	CIT27_07420 CIT27_14315	GLP21_16610 GLP21_06005	GLP24_10720 GLP24_15240	GLP09_06185 GLP09_11070	GLP22_01650 GLP22_13300	GLP17_02035 GLP17_11525	GRJ22_02325 GRJ22_15120	GLP31_06395 GLP31_14530	GLP27_00570 GLP27_11190	GLP20_10380 GLP20_13725	GLP19_06080 GLP19_16175	GLP14_03650 GLP14_11250	GLP23_16785 GLP23_14280	GLP13_02785 GLP13_12325
Iron															
ferrous iron transport protein C	CIK00_01560	CIT27_03420	GLP21_01405	GLP24_03035	GLP09_00930	GLP22_02520	GLP17_02980	GRJ22_11990	GLP31_01120	GLP27_03505	GLP20_02450	GLP19_02360	GLP14_10390	GLP23_02500	GLP13_00325
ferrous iron transport protein A	CIK00_01570	CIT27_03430	GLP21_01395	GLP24_03025	GLP09_00920	GLP22_02510	GLP17_02990	GRJ22_12000	GLP31_01110	GLP27_03495	GLP20_02440	GLP19_02350	GLP14_10400	GLP23_02490	GLP13_00315
ferrous iron transport protein B	CIK00_01565 CIK00_13430	CIT27_03425 CIT27_06735	GLP21_01400 GLP21_04890	GLP24_03030 GLP24_10870	GLP09_00925 GLP09_08355	GLP22_02515 GLP22_00890	GLP17_02985 GLP17_01315	GRJ22_11995 GRJ22_01555	GLP31_01115 GLP31_07155	GLP27_03500 GLP27_01235	GLP20_02445	GLP19_02355 GLP19_06840	GLP14_10395	GLP23_02495 GLP23_17720	GLP13_00320 GLP13_02110
ferric iron uptake transcriptional regulator	CIK00_01675	CIT27_03535	GLP21_01290	GLP24_02920	GLP09_00815	GLP22_02405	GLP17_03095	GRJ22_12105	GLP31_01005	GLP27_03390	GLP20_02335	GLP19_02245	GLP14_10505	GLP23_02385	GLP13_00210
iron chelate uptake ABC transporter family permease subunit	CIK00_05890	CIT27_07870	GLP21_14090	GLP24_10265	GLP09_06655	GLP22_02110	GLP17_02495	GRJ22_02790	GLP31_11255	GLP27_00130	GLP20_10825	GLP19_05625	GLP14_03205	GLP23_11360	GLP13_03245
iron ABC transporter substrate-binding protein	CIK00_09035	CIT27_11840	GLP21_06325	GLP24_12060	GLP09_06825	GLP22_09535	GLP17_13015	GRJ22_12890	GLP31_10220	GLP27_08830	GLP20_08300	GLP19_14190	GLP14_06820	GLP23_08520	GLP13_10005
iron chelate uptake ABC transporter family permease subunit	CIK00_11355	CIT27_00355	GLP21_08690	GLP24_04060	GLP09_04765	GLP22_04580	GLP17_10415	GRJ22_09550	GLP31_04445	GLP27_11955 GLP27_19480	GLP20_11310 GLP20_17805	GLP19_07965	GLP14_11630 GLP14_15145	GLP23_05990 GLP23_19965	GLP13_10440 GLP13_18365
	CIK00_12330	CIT27_09575	GLP21_11530	GLP24_00150	GLP09_10090	GLP22_11575	GLP17_04140	GRJ22_03875	GLP31_02810	GLP27_05610 GLP27_17550 GLP27_17555	GLP20_09575 GLP20_16120 GLP20_16115	GLP19_17155	GLP14_17990	GLP23_09095	GLP13_04165
iron ABC transporter	CIK00_16165 CIK00_16170	CIT27_15095 CIT27_15100	GLP21_16835 GLP21_16840	GLP24_16785 GLP24_16790	GLP09_13090 GLP09_13085	GLP22_15890 GLP22_15895	GLP17_14170 GLP17_14175	GRJ22_15770 GRJ22_15765	GLP31_16710 GLP31_16715	GLP27_14730 GLP27_14735	GLP20_14115 GLP20_14120	GLP19_15715 GLP19_15720	GLP14_13770 GLP14_13775	GLP23_13600 GLP23_13605	GLP13_14680 GLP13_14675
iron ABC transporter permease	CIK00_09040	CIT27_11845	GLP21_06320	GLP24_12065	GLP09_06820	GLP22_09530	GLP17_13020	GRJ22_12895	GLP31_10215	GLP27_08835	GLP20_08305	GLP19_14195	GLP14_06825	GLP23_08525	GLP13_10010
manganese/iron ABC transporter ATP-binding protein										GLP27_17560	GLP20_16110				
iron-siderophore ABC transporter substrate-binding protein														GLP23_18640	
Marine polyssacharides															
Xylose															
endoxylanase					GLP09_14220	GLP22_00295		GRJ22_01010				GLP19_01770			
xylosidase															
xylG: D-xylose ABC transporter, ATP-binding protein ABC_transporter,_permease_protein_(cluster_2,_ribose/xylose/arabinose/galactose)															
Laminarin															
laminarinase															
Chondroitin sulphate															
chondriotinase						GLP22_00270		GRJ22_00985						GLP23_17770	
chondroitin sulphate lyase															
Arabinogalactan															

	P. carnosum														
	TMW 2.2021T	**TMW 2.2029**	**TMW 2.2097**	**TMW 2.2147**	**TMW 2.2149**	**TMW 2.2150**	**TMW 2.2157**	**TMW 2.2163**	**TMW 2.2169**	**TMW 2.2098**	**TMW 2.2186**	**TMW 2.2187**	**TMW 2.2188**	**TMW 2.2189**	**TMW 2.2190**
galactanase															
beta-galactosidase			GLP21_08195												
beta-galactosidase subunit beta	CIK00_11185	CIT27_00170	GLP21_08860	GLP24_03890	GLP09_15085	GLP22_04400	GLP17_10240	GRJ22_09720	GLP31_04625	GLP27_11785	GLP20_11140	GLP19_07785	GLP14_11805	GLP23_05820	GLP13_10255
beta-galactosidase subunit alpha	CIK00_11190	CIT27_00175	GLP21_08855	GLP24_03895	GLP09_15090	GLP22_04405	GLP17_10245	GRJ22_09715	GLP31_04620	GLP27_11790	GLP20_11145	GLP19_07790	GLP14_11800	GLP23_05825	GLP13_10260
arabinofuranosidase															
arabinopyranosidase															
Pullulan															
pullulanase	CIK00_18160	CIT27_09105	GLP21_11985	GLP24_00630	GLP09_07615	GLP22_08445	GLP17_04625	GRJ22_04325	GLP31_03270	GLP27_05155	GLP20_09115	GLP19_00360	GLP14_05975	GLP23_08640	GLP13_03660
Fucoidan															
fucoidase															
L-fucose:H+ symporter permease	CIK00_13560	CIT27_06870	GLP21_04760	GLP24_11005	GLP09_08485	GLP22_01025	GLP17_01445	GRJ22_01690	GLP31_07025	GLP27_01100	GLP20_08505	GLP19_06705	GLP14_14655	GLP23_19140	GLP13_02245
L-fucose:H+ symporter permease								GRJ22_18105							
L-fucose isomerase								GRJ22_18110							
L-fuculokinase								GRJ22_18115							
L-fucose mutarotase								GRJ22_18120							
L-fuculose-phosphate aldolase								GRJ22_18125							
Chitin															
chitinase	CIK00_00180	CIT27_02025	GLP21_15320	GLP24_07345	GLP09_02325	GLP22_03900	GLP17_13275	GRJ22_05875	GLP31_02505	GLP27_04935	GLP20_03050	GLP19_03940	GLP14_17180	GLP23_15005	GLP13_01905

	P. iliopiscarium						*P. phosphoreum*									
	ATCC 51760T	ATCC 51761	NCIMB 13478	NCIMB 13481	TMW 2.2104	TMW 2.2035	TMW 2.2033	TMW 2.2034	TMW 2.2103	TMW 2.2125	TMW 2.2126	TMW 2.2130	TMW 2.2132	TMW 2.2134	TMW 2.2140	TMW 2.2142
Pentose phosphate pathway																
6-phosphogluconolactonase (dev B)	C9J51_17545	C9J52_15425	C9I87_12560	C9I88_16650	GLP10_18105	CJF27_17470	CJF25_07790	CJF26_06045	GLP34_17345	GLP32_11235	GLP35_04095	GLP37_17645	GLP38_16585	GLP25_18460	GLP44_14585	GLP29_18070
Phosphogluconate dehydrogenase (gnt Z)	C9J51_17540	C9J52_15430	C9I87_12555	C9I88_16645	GLP10_18100	CJF27_17475	CJF25_07785	CJF26_06050	GLP34_17340	GLP32_11240	GLP35_04090	GLP37_17650	GLP38_16590	GLP25_18465	GLP44_14590	GLP29_18065
ribulose-5-phosphate 3-epimerase (RibuloseP<->XyluloseP) (rp e)	C9J51_13825	C9J52_06400	C9I87_11800	C9I88_08990	GLP10_01520	CJF27_03395	CJF25_10730	CJF26_12855	GLP34_10535	GLP32_09685	GLP35_11425	GLP37_11155	GLP38_12255	GLP25_11495	GLP44_15110	GLP29_06815
Ribose 5-phosphate Isomerase (RiboseP <-> RibuloseP) (rpi A)	C9J51_16280	C9J52_15045	C9I87_15925	C9I88_14330	GLP10_11865	CJF27_09685	CJF25_18915	CJF26_18660	GLP34_18095	GLP32_16175	GLP35_18990	GLP37_18620	GLP38_18355	GLP25_15750	GLP44_19050	GLP29_17975
Transketolase (*tkt* A)	C9J51_02820	C9J52_00405	C9I87_04750	C9I88_10595	GLP10_12365	CJF27_13115	CJF25_03420	CJF26_01985	GLP34_07185	GLP32_03975	GLP35_08410	GLP37_12020	GLP38_15495	GLP25_13105	GLP44_11805	GLP29_10380
							CJF25_21305	CJF26_20330	GLP34_20415	GLP32_20265	GLP35_20655	GLP37_21380	GLP38_20685	GLP25_19930	GLP44_21510	GLP29_20585
Transaldolase (*ta l*)	C9J51_02825	C9J52_00410	C9I87_04755	C9I88_10590	GLP10_12360	CJF27_13110	CJF25_03415	CJF26_01990	GLP34_07190	GLP32_03980	GLP35_08415	GLP37_12015	GLP38_15490	GLP25_13100	GLP44_11800	GLP29_10385
Gluconeogenese																
Phoshoenolyruvate carboxylase (pyc) / PEPcase (ppc)	C9J51_13735	C9J52_06310	C9I87_11710	C9I88_08900	GLP10_01430	CJF27_03305	CJF25_10820	CJF26_12765	GLP34_10625	GLP32_09595	GLP35_11335	GLP37_11065	GLP38_12165	GLP25_11585	GLP44_15020	GLP29_06905
Pyruvate carboxylase (pyc)																
phosphoenolpyruvate carboxykinase (pckA)	C9J51_15520	C9J52_10655	C9I87_14720	C9I88_19245	GLP10_10940	CJF27_08850	CJF25_17545	CJF26_15745	GLP34_14880	GLP32_15205	GLP35_16265	GLP37_15175	GLP38_14450	GLP25_15580	GLP44_15380	GLP29_14230
PEP synthase (pps A)	C9J51_09105	C9J52_09935	C9I87_02835	C9I88_07285	GLP10_10500	CJF27_06700	CJF25_00060	CJF26_13875	GLP34_02300	GLP32_12705	GLP35_03225	GLP37_04825	GLP38_09110	GLP25_08550	GLP44_03530	GLP29_06540
phosphoenolpyruvate utilizing protein	C9J51_09105	C9J52_09935	C9I87_02835	C9I88_07285	GLP10_10500	CJF27_06700	CJF25_00235	CJF26_02940	GLP34_02145	GLP32_12865	GLP35_03035	GLP37_02820	GLP38_14610	GLP25_08315	GLP44_03360	GLP29_03040
malate dehydrogenase (oxaloacetate-decarboxylating)	C9J51_15130	C9J52_18480	C9I87_13875	C9I88_12840	GLP10_17005	CJF27_16435	CJF25_15655	CJF26_14650	GLP34_19390	GLP32_13705	GLP35_13585	GLP37_14315	GLP38_13125	GLP25_14285	GLP44_12635	GLP29_16125
Aspartate/tyrosine/aromatic aminotransferase	C9J51_12550	C9J52_13345	C9I87_18030	C9I88_18460	GLP10_00085	CJF27_00175	CJF25_04775	CJF26_20575	GLP34_05350	GLP32_07175	GLP35_06245	GLP37_19375	GLP38_05125	GLP25_09420	GLP44_17245	GLP29_17005
	C9J51_03560	C9J52_01780	C9I87_02320	C9I88_11280	GLP10_16075	CJF27_16195	CJF25_00870	CJF26_03570	GLP34_01515	GLP32_00255	GLP35_02410	GLP37_02190	GLP38_06155	GLP25_10495	GLP44_02735	GLP29_02420
Aspartate oxidase	C9J51_16200	C9J52_15125	C9I87_15845	C9I88_14410	GLP10_11785	CJF27_09605	CJF25_19000	CJF26_18575	GLP34_18010	GLP32_16260	GLP35_18905	GLP37_18705	GLP38_18440	GLP25_15835	GLP44_19135	GLP29_17890
Fructose-1,6-bisphosphatase (fdp)	C9J51_13660	C9J52_06235	C9I87_11635	C9I88_08825	GLP10_01355	CJF27_03230	CJF25_10895	CJF26_12690	GLP34_10700	GLP32_09520	GLP35_11260	GLP37_10990	GLP38_12090	GLP25_11660	GLP44_14945	GLP29_06980
	C9J51_15150	C9J52_18460	C9I87_13895	C9I88_12860	GLP10_16985	CJF27_16455							GLP38_13105			GLP29_16145
glucose-6-phosphatase (phosphatase PAP2 family) (g6pc)																
phosphatase PAP2 family	C9J51_08505	C9J52_07585	C9I87_03445	C9I88_16965	GLP10_06500	CJF27_01390	CJF25_14495	CJF26_14340	GLP34_02770	GLP32_11730	GLP35_03700	GLP37_04295	GLP38_08675	GLP25_08985	GLP44_10305	GLP29_06090
Glycolysis																
glucokinase (*glc* K) putative / sugar kinase / ROK family sugar kinase	C9J51_12710	C9J52_13510	C9I87_08555	C9I88_13680	GLP10_00245	CJF27_00325	CJF25_04610	CJF26_18835	GLP34_05515	GLP32_07375	GLP35_06425	GLP37_19205	GLP38_05325	GLP25_09620	GLP44_11490	GLP29_20070
	C9J51_01710	C9J52_16220	C9I87_07065	C9I88_15595			CJF25_06395	CJF26_00845	GLP34_03785	GLP32_04970	GLP35_09960	GLP37_09675	GLP38_01350	GLP25_02245	GLP44_05160	GLP29_08665
							CJF25_19505		GLP34_21350	GLP32_20775	GLP35_21005	GLP37_21980	GLP38_18875		GLP44_18105	GLP29_20945
										GLP32_15805		GLP37_12510				
phosphoglucomutase (pgm)	C9J51_04745	C9J52_15485	C9I87_01145	C9I88_03135	GLP10_08305	CJF27_08105	CJF25_02050	CJF26_04765	GLP34_00340	GLP32_01430	GLP35_01205	GLP37_01000	GLP38_11110	GLP25_04815	GLP44_01560	GLP29_01250
	C9J51_00725	C9J52_02615	C9I87_09265	C9I88_00845	GLP10_05100	CJF27_02570										
Glucose-6-phosphate isomerase (pgi)	C9J51_18395	C9J52_17640	C9I87_18725	C9I88_17540	GLP10_13605	CJF27_13935	CJF25_17300	CJF26_19890	GLP34_19235	GLP32_17990	GLP35_19435	GLP37_19780	GLP38_19865	GLP25_18885	GLP44_19700	GLP29_18630
mannose-6-P isomerase (man A)	C9J51_07380	C9J52_16345	C9I87_17820	C9I88_03820	GLP10_05520	CJF27_11630	CJF25_13915	CJF26_16435	GLP34_17205 + GLP34_18720	GLP32_17870	GLP35_14285	GLP37_16375	GLP38_16010	GLP25_17205	GLP44_12895 + GLP44_20055	GLP29_07825
glyceraldehyde phosphate dehydrogenase	C9J51_06880	C9J52_08740	C9I87_14140	C9I88_04330	GLP10_16670	CJF27_16265	CJF25_16240	CJF26_09850	GLP34_05895	GLP32_14640	GLP35_15030	GLP37_13560	GLP38_02665	GLP25_06275	GLP44_17820	GLP29_09395
phosphoglycerate kinase	C9J51_16305	C9J52_15020	C9I87_15950	C9I88_14305	GLP10_11890	CJF27_09710	CJF25_18890	CJF26_18685	GLP34_18120	GLP32_16150	GLP35_19015	GLP37_18595	GLP38_18330	GLP25_15725	GLP44_19025	GLP29_18000
phosphoglycerate mutase / phosphoglycerate mutase (2,3-diphosphoglycerate-independent)	C9J51_13590	C9J52_06165	C9I87_11565	C9I88_08755	GLP10_01285	CJF27_03160	CJF25_10970	CJF26_12615	GLP34_10770	GLP32_09450	GLP35_11190	GLP37_10920	GLP38_12020	GLP25_11730	GLP44_14875	GLP29_07050
2,3-diphosphoglycerate-dependent phosphoglycerate mutase							CJF25_14745	CJF26_14130	GLP34_02570	GLP32_11470	GLP35_03490	GLP37_04555	GLP38_08885	GLP25_08775	GLP44_10100	GLP29_06300
enolase	C9J51_16115	C9J52_18780	C9I87_15745	C9I88_14510	GLP10_11700	CJF27_09520	CJF25_19085	CJF26_18490	GLP34_17925	GLP32_16345	GLP35_18820	GLP37_18790	GLP38_18525	GLP25_15920	GLP44_19220	GLP29_17805
pyruvate kinase	C9J51_03925	C9J52_01415	C9I87_01955	C9I88_11645	GLP10_04765	CJF27_05915	CJF25_01235	CJF26_03935	GLP34_01150	GLP32_00625	GLP35_02035	GLP37_01825	GLP38_06515	GLP25_10855	GLP44_02370	GLP29_02060
	C9J51_14960	C9J52_10415	C9I87_13710	C9I88_12670	GLP10_08425	CJF27_09970	CJF25_15825	CJF26_14820	GLP34_15265	GLP32_13535	GLP35_13755	GLP37_14145	GLP38_13295	GLP25_14455	GLP44_12465	GLP29_15955
glucose -> pyruvate Homolactic fermentation																
6-phosphofructokinase (pfk A)	C9J51_13635	C9J52_06210	C9I87_11610	C9I88_08800	GLP10_01330	CJF27_03205	CJF25_10925	CJF26_12660	GLP34_10725	GLP32_09495	GLP35_11235	GLP37_10965	GLP38_12065	GLP25_11685	GLP44_14920	GLP29_07005
fructose-1,6-bisphosphate aldolase (fba A)	C9J51_16300	C9J52_15025	C9I87_15945	C9I88_14310	GLP10_11885	CJF27_09705	CJF25_18895	CJF26_18680	GLP34_18115	GLP32_16155	GLP35_19010	GLP37_18600	GLP38_18335	GLP25_15730	GLP44_19030	GLP29_17995
glucose -> pyruvate Heterolactic fermentation																
phosphoketolase (xpk A)																
glucose-6-phosphate dehydrogenase (zwf)	C9J51_17550	C9J52_15420	C9I87_12565	C9I88_16655	GLP10_18110	CJF27_17465	CJF25_07795	CJF26_06040	GLP34_17350	GLP32_11230	GLP35_04100	GLP37_17640	GLP38_16580	GLP25_18455	GLP44_14580	GLP29_18075
KDPG weg																
phosphogluconate dehydratase (ed d)																
KDPG aldolase (ed a)	C9J51_01705	C9J52_16215	C9I87_07060	C9I88_15600	GLP10_03835	CJF27_16955	CJF25_06390	CJF26_00840	GLP34_03790	GLP32_04975	GLP35_09965	GLP37_09670	GLP38_01345	GLP25_02250	GLP44_05155	GLP29_08660
glucose-6-phosphate dehydrogenase (1.1.1.49/1.1.1.363)	C9J51_17550	C9J52_15420	C9I87_12565	C9I88_16655	GLP10_18110	CJF27_17465	CJF25_07795	CJF26_06040	GLP34_17350	GLP32_11230	GLP35_04100	GLP37_17640	GLP38_16580	GLP25_18455	GLP44_14580	GLP29_18075
6-phosphogluconolactonase 3.1.1.31	C9J51_17545	C9J52_15425	C9I87_12560	C9I88_16650	GLP10_18105	CJF27_17470	CJF25_07790	CJF26_06045	GLP34_17345	GLP32_11235	GLP35_04095	GLP37_17645	GLP38_16585	GLP25_18460	GLP44_14585	GLP29_18070
										GLP32_15810		GLP37_12515				
Ribose																
D-ribose pyranase / Ribopyranase (*rbs* D) (ribopyranose -> ribofuranose)	C9J51_01765	C9J52_16280	C9I87_07125	C9I88_15535	GLP10_03870	CJF27_16990	CJF25_06460	CJF26_00905	GLP34_03720	GLP32_04910	GLP35_09900	GLP37_09735	GLP38_01410	GLP25_02185	GLP44_05220	GLP29_08725
Ribokinase (*rbs* K)	C9J51_01750	C9J52_16265	C9I87_07110	C9I88_15550	GLP10_03855	CJF27_16975	CJF25_06440	CJF26_00890	GLP34_03740	GLP32_04925	GLP35_09915	GLP37_09720	GLP38_01395	GLP25_02200	GLP44_05205	GLP29_08710
							CJF25_06455		GLP34_03725							
Ribose Transporter (ribose uptake protein) *rbs* U																
Putative deoxyribose-specific ABC transporter (*nup* A oder *yng* F)																
Ribose-5-phosphate isomerase (RpiA)	C9J51_16280	C9J52_15045	C9I87_15925	C9I88_14330	GLP10_11865	CJF27_09685	CJF25_18915	CJF26_18660	GLP34_18095	GLP32_16175	GLP35_18990	GLP37_18620	GLP38_18355	GLP25_15750	GLP44_19050	GLP29_17975
Ribulose-phosphate 3-epimerase (Rpe)	C9J51_13825	C9J52_06400	C9I87_11800	C9I88_08990	GLP10_01520	CJF27_03395	CJF25_10730	CJF26_12855	GLP34_10535	GLP32_09685	GLP35_11425	GLP37_11155	GLP38_12255	GLP25_11495	GLP44_15110	GLP29_06815
Xylulose-5-phosphate phosphoketolase (Xpk)																
ribose-5-phosphate pyrophosphokinase	C9J51_18800	C9J52_18670	C9I87_19325	C9I88_19705	GLP10_17970	CJF27_11975	CJF25_13560	CJF26_16800	GLP34_20380	GLP32_20390	GLP35_20770	GLP37_16005	GLP38_20565	GLP25_16845	GLP44_13255	GLP29_08190
Nucleoside																
Nucleoside-diphosphate Kinase	C9J51_16570	C9J52_12455	C9I87_15530	C9I88_18180	GLP10_12905	CJF27_10310	CJF25_17945	CJF26_08995	GLP34_15850	GLP32_16830	GLP35_17115	GLP37_15375	GLP38_04680	GLP25_16230	GLP44_00255	GLP29_15220
inosine-uridine nucleoside ribohydrolase (*iun* H)																
ribonucleoside nucleosidase (unspecific, RihC)	C9J51_12575	C9J52_13370	C9I87_18055	C9I88_18485	GLP10_00125	CJF27_00210	CJF25_04725	CJF26_20525	GLP34_05400	GLP32_07225	GLP35_06295	GLP37_19325	GLP38_05175	GLP25_09470	GLP44_17295	GLP29_17055
purine (deoxy)nucleoside phosphorylase (RibP/Pur) (deoD)	C9J51_11060	C9J52_06605	C9I87_10150	C9I88_07750	GLP10_06350	CJF27_07245	CJF25_13425	CJF26_11940	GLP34_08925	GLP32_10535	GLP35_07360	GLP37_07425	GLP38_10275	GLP25_12370	GLP44_09620	GLP29_04780
pyrimidine (deoxy)nucleoside phosphorylase (RibP/Pur) (deoA)	C9J51_11070	C9J52_06615	C9I87_10140	C9I88_07760	GLP10_06340	CJF27_07255	CJF25_13415	CJF26_11930	GLP34_08935	GLP32_10525	GLP35_07370	GLP37_07435	GLP38_10285	GLP25_12380	GLP44_09610	GLP29_04770
purine/pyrimidine nucleosidase (Rib/Pur)																
ribose 1,5-phosphopentomutase (deoB)	C9J51_11065	C9J52_06610	C9I87_10145	C9I88_07755	GLP10_06345	CJF27_07250	CJF25_13420	CJF26_11935	GLP34_08930	GLP32_10530	GLP35_07365	GLP37_07430	GLP38_10280	GLP25_12375	GLP44_09615	GLP29_04775
Nucleoside to Deoxynucleoside																
Ribonucleotide reductase alpha/assembly/beta																
nrd A	C9J51_04085	C9J52_01255	C9I87_01800	C9I88_11800	GLP10_04610	CJF27_05760	CJF25_01395	CJF26_04095	GLP34_00990	GLP32_00785	GLP35_01875	GLP37_01665	GLP38_06675	GLP25_11015	GLP44_02210	GLP29_01900

	P. iliopiscarium						*P. phosphoreum*									
	ATCC 51760T	**ATCC 51761**	**NCIMB 13478**	**NCIMB 13481**	**TMW 2.2104**	**TMW 2.2035**	**TMW 2.2033**	**TMW 2.2034**	**TMW 2.2103**	**TMW 2.2125**	**TMW 2.2126**	**TMW 2.2130**	**TMW 2.2132**	**TMW 2.2134**	**TMW 2.2140**	**TMW 2.2142**
nrdB	C9J51_04090	C9J52_01250	C9I87_01795	C9I88_11805	GLP10_04605	CJF27_05755	CJF25_01400	CJF26_04100	GLP34_00985	GLP32_00790	GLP35_01870	GLP37_01660	GLP38_06680	GLP25_11020	GLP44_02205	GLP29_01895
nrdI							CJF25_18260	CJF26_10570	GLP34_12980	GLP32_16055	GLP35_12655	GLP37_03775	GLP38_15260	GLP25_07675	GLP44_17605	GLP29_03220
DeoxyRibose from DNA																
Deoxyribose-phosphate aldolase (deoC)	C9J51_11075	C9J52_06620	C9I87_10135	C9I88_07765	GLP10_06335	CJF27_07260	CJF25_13410	CJF26_11925	GLP34_08940	GLP32_10520	GLP35_07375	GLP37_07440	GLP38_10290	GLP25_12385	GLP44_09605	GLP29_04765
Ribose from free NTP/RNA																
to PP Pathway / Hetero																
Sugar transporters																
galactose/methyl galactoside ABC transporter ATP-binding protein MglA					GLP10_16575	CJF27_05535	CJF25_08995	CJF26_07645		GLP32_02880	GLP35_13360	GLP37_06660	GLP38_09465	GLP25_01675		
galactoside ABC transporter permease MglC					GLP10_16580	CJF27_05540	CJF25_09000	CJF26_07650		GLP32_02885	GLP35_13355	GLP37_06655	GLP38_09470	GLP25_01680		
methyl-galactoside ABC transporter substrate-binding protein MglB					GLP10_16570	CJF27_05530	CJF25_08990	CJF26_07640		GLP32_02875	GLP35_13365	GLP37_06665	GLP38_09460	GLP25_01670		
maltose/maltodextrin ABC transporter substrate-binding protein MalE	C9J51_10505	C9J52_17885	C9I87_05770	C9I88_01960	GLP10_07140	CJF27_05205										
maltose ABC transporter permease MalF	C9J51_10500	C9J52_17890	C9I87_05775	C9I88_10095	GLP10_07135	CJF27_05210										
maltose ABC transporter permease MalG	C9J51_10495		C9I87_05780	C9I88_10090	GLP10_07130	CJF27_05215										
maltose/maltodextrin ABC transporter ATP-binding protein MalK	C9J51_10510	C9J52_17880	C9I87_05765	C9I88_01955	GLP10_07145	CJF27_05200										
PTS lactose/cellobiose transporter subunit IIA	C9J51_02460	C9J52_00045	C9I87_04390	C9I88_13255	GLP10_14400	CJF27_14535										
PTS cellobiose transporter subunit IIC	C9J51_02465	C9J52_00050	C9I87_04395	C9I88_13250	GLP10_14395	CJF27_14530										
PTS_system,_cellobiose-specific_IIB_component_(EC_2.7.1.205)	C9J51_02470	C9J52_00055	C9I87_04400	C9I88_13245	GLP10_14390	CJF27_14525										
PTS mannose transporter subunit IIA	C9J51_02670	C9J52_00255	C9I87_04600	C9I88_13050			CJF25_03605	CJF26_01830	GLP34_07025	GLP32_03810	GLP35_08250	GLP37_12180	GLP38_15655	GLP25_13265	GLP44_11995	GLP29_10220
PTS mannose transporter subunit IIB	C9J51_06210	C9J52_03595	C9I87_10720	C9I88_04930	GLP10_07685	CJF27_07795	CJF25_08355	CJF26_05400	GLP34_06555	GLP32_10660	GLP35_04670	GLP37_10105	GLP38_03260	GLP25_05655	GLP44_07760	GLP29_05490
Sugars																
6-phospho-beta-glucosidase	C9J51_02455	C9J52_00040	C9I87_04385	C9I88_13260	GLP10_14405	CJF27_14540										
alpha-galactosidase	C9J51_10560	C9J52_17830	C9I87_05715	C9I88_01905	GLP10_07195	CJF27_05150										
beta-galactosidase							CJF25_06620		GLP34_12725	GLP32_06255	GLP35_12435	GLP37_03545	GLP38_07745 GLP38_07750		GLP44_08925 GLP44_08930	GLP29_03445
beta-galactosidase subunit beta	C9J51_12050	C9J52_04035	C9I87_12145	C9I88_05475	GLP10_17155	CJF27_16575	CJF25_07370	CJF26_06470	GLP34_13215	GLP32_06970	GLP35_10500	GLP37_18950	GLP38_07040	GLP25_06740	GLP44_20405	GLP29_13870
beta-galactosidase subunit alpha	C9J51_12045	C9J52_04040	C9I87_12140	C9I88_05480	GLP10_17160	CJF27_16580	CJF25_07365	CJF26_06475	GLP34_13220	GLP32_06965	GLP35_10495	GLP37_18945	GLP38_07045	GLP25_06745	GLP44_20410	GLP29_13875
alpha-glucosidase	C9J51_12930	C9J52_07890	C9I87_08155	C9I88_11895	GLP10_00350	CJF27_00440	CJF25_12315	CJF26_13245	GLP34_12310	GLP32_07650	GLP35_06560	GLP37_11855	GLP38_05490	GLP25_09785	GLP44_11390	GLP29_12835
	C9J51_02595	C9J52_00180	C9I87_04525	C9I88_13125	GLP10_14335	CJF27_14475	CJF25_03675	CJF26_01755	GLP34_06955	GLP32_03735	GLP35_08175	GLP37_12255	GLP38_15730	GLP25_13340	GLP44_12065	GLP29_10145
beta-mannosidase	C9J51_14765	C9J52_10220	C9I87_13515	C9I88_12475	GLP10_08620	CJF27_10165	CJF25_16020	CJF26_15015	GLP34_15460	GLP32_13340	GLP35_13950	GLP37_13950	GLP38_13495	GLP25_14650	GLP44_12270	GLP29_19370
	C9J51_02280	C9J52_18125	C9I87_07565	C9I88_15110	GLP10_04285	CJF27_06270	CJF25_03875	CJF26_01450	GLP34_03145	GLP32_03535	GLP35_08015	GLP37_12435		GLP25_13485	GLP44_15755	GLP29_09990
alpha-mannosidase	C9J51_02060	C9J52_12120	C9I87_07440	C9I88_15235			CJF25_04035		GLP34_03300	GLP32_19005	GLP35_09430	GLP37_20930	GLP38_01810	GLP25_01785		GLP29_09125
	C9J51_02055	C9J52_12115	C9I87_07435	C9I88_15240			CJF25_04030		GLP34_03295	GLP32_19000	GLP35_09425	GLP37_20935	GLP38_01815	GLP25_01780	GLP44_15910	GLP29_09130
	C9J51_04280	C9J52_01060	C9I87_01605	C9I88_03595			CJF25_01580	CJF26_04280	GLP34_00805				GLP38_06860	GLP25_11200	GLP44_02025	GLP29_01715
	C9J51_02115	C9J52_12175	C9I87_07495	C9I88_15170	GLP10_04250	CJF27_06305	CJF25_03915	CJF26_01410	GLP34_03185	GLP32_03495	GLP35_07975	GLP37_12530	GLP38_01925	GLP25_13525	GLP44_15795	GLP29_09950
	C9J51_02110	C9J52_12170	C9I87_07490	C9I88_15175	GLP10_04245	CJF27_06310	CJF25_03955	CJF26_01370	GLP34_03225	GLP32_03455	GLP35_07935	GLP37_12570			GLP44_15835	GLP29_09910
Glycogen																
Glycogen phosphorylase (*glg* P)	C9J51_10550	C9J52_17840	C9I87_05725	C9I88_01915	GLP10_07185	CJF27_05160										
UTP-glucose-1-phosphate uridylyltransferase (gta B)	C9J51_14030	C9J52_13935	C9I87_12830	C9I88_10655	GLP10_02460	CJF27_03600 CJF27_11130	CJF25_15530	CJF26_18320 CJF26_09515	GLP34_11810 GLP34_18875	GLP32_12020 GLP32_19995	GLP35_11520	GLP37_12650	GLP38_13010	GLP25_13630	GLP44_13750 GLP44_20210	GLP29_16540
Glycogen synthase (*glg* A)																
starch synthase (GT5)																
glucoamylase (GH15)																
Glycogen biosynthesis protein (Glg D)																
1,4-alpha-glucan branching enzyme	C9J51_10540	C9J52_17850	C9I87_05735	C9I88_01925	GLP10_07175	CJF27_05170										
glycogen debranching enzyme (GH13)	C9J51_10530	C9J52_17860	C9I87_05745	C9I88_01935	GLP10_07165	CJF27_05180										
	C9J51_10515	C9J52_17875	C9I87_05760	C9I88_01950	GLP10_07150	CJF27_05195										
alpha-amylase (GH13)					GLP10_07200	CJF27_05145										
4-alpha-glucanotransferase (GH13)	C9J51_10545	C9J52_17845	C9I87_05730	C9I88_01920	GLP10_07180	CJF27_05165										
alpha-glucosidase (GH13)	C9J51_12930	C9J52_07890	C9I87_08155	C9I88_11895	GLP10_00350	CJF27_00440	CJF25_12315	CJF26_13245	GLP34_12310	GLP32_07650	GLP35_06560	GLP37_11855	GLP38_05490	GLP25_09785	GLP44_11390	GLP29_12835
	C9J51_02595	C9J52_00180	C9I87_04525	C9I88_13125	GLP10_14335	CJF27_14475	CJF25_03675	CJF26_01755	GLP34_06955	GLP32_03735	GLP35_08175	GLP37_12255	GLP38_15730	GLP25_13340	GLP44_12065	GLP29_10145
Pullulanase -type alpha-1,6-glucosidase	C9J51_10565	C9J52_17825	C9I87_05710	C9I88_01900	GLP10_07205	CJF27_05140										
Pyruvate fates **Pyruvate dehydrogenase complex (cluster)**																
Pyruvate dehydrogenase alpha E1 (acetoin-oxidoreductase) pdhA / aceE (homodimeric)	C9J51_14535	C9J52_13110	C9I87_13290	C9I88_11115	GLP10_02960	CJF27_04100	CJF25_15060	CJF26_17070	GLP34_11345	GLP32_12485	GLP35_11985	GLP37_13115	GLP38_12540	GLP25_14095	GLP44_21045	GLP29_16295
Pyruvate dehydrogenase beta E1 (oxo-isovaleriate dehydrogenase) pdhB																
Dihydrolipoamide acetyltransferase E2 pdhC	C9J51_14540	C9J52_13115	C9I87_13295	C9I88_11120	GLP10_02965	CJF27_04105	CJF25_15055	CJF26_17065	GLP34_11340	GLP32_12490	GLP35_11990	GLP37_13120	GLP38_12535	GLP25_14100	GLP44_21050	GLP29_16290
Dihydrolipoyl-Dehydrogenase E3 pdhD	C9J51_14545	C9J52_13120	C9I87_13300	C9I88_11125	GLP10_02970	CJF27_04110	CJF25_15050	CJF26_17060	GLP34_11335	GLP32_12495	GLP35_11995	GLP37_13125	GLP38_12530	GLP25_14105	GLP44_21055	GLP29_16285
Lactate++																
L-lactate dehydrogenase (ldh)																
D-lactate dehydrogenase (ldh)																
D-lactate dehydrogenase / 2-hydroxyacid dehydrogenase	C9J51_06165	C9J52_03550	C9I87_10675	C9I88_04975	GLP10_07640	CJF27_07840	CJF25_08320	CJF26_05435	GLP34_06590	GLP32_10695	GLP35_04635	GLP37_10140	GLP38_03295	GLP25_05620	GLP44_07725	GLP29_05525
lactate dehydrogenase	C9J51_02845	C9J52_00430	C9I87_04785	C9I88_10570	GLP10_12330	CJF27_13075	CJF25_03405	CJF26_02000	GLP34_07200	GLP32_03995	GLP35_08430	GLP37_12000	GLP38_15460	GLP25_13090	GLP44_11785	GLP29_10395
2-hydroxyacid dehydrogenase	C9J51_06165	C9J52_03550	C9I87_10675	C9I88_04975	GLP10_07640	CJF27_07840	CJF25_08320	CJF26_05435	GLP34_06590	GLP32_10695	GLP35_04635	GLP37_10140	GLP38_03295	GLP25_05620	GLP44_07725	GLP29_05525

	P. iliopiscarium						*P. phosphoreum*									
	ATCC 51760T	**ATCC 51761**	**NCIMB 13478**	**NCIMB 13481**	**TMW 2.2104**	**TMW 2.2035**	**TMW 2.2033**	**TMW 2.2034**	**TMW 2.2103**	**TMW 2.2125**	**TMW 2.2126**	**TMW 2.2130**	**TMW 2.2132**	**TMW 2.2134**	**TMW 2.2140**	**TMW 2.2142**
Acetate																
Phosphotransacetylase pta	C9J51_07545	C9J52_17150	C9I87_18940	C9I88_17985	GLP10_15095	CJF27_11790	CJF25_13760	CJF26_16585	GLP34_17055	GLP32_17720	GLP35_14135	GLP37_16220	GLP38_15860	GLP25_17055	GLP44_13040	GLP29_07975
Pyruvate oxidase poxB																
Acetatekinase ackA	C9J51_07540	C9J52_17155	C9I87_18935	C9I88_17990	GLP10_15100	CJF27_11785	CJF25_13765	CJF26_16580	GLP34_17060	GLP32_17725	GLP35_14140	GLP37_16225	GLP38_15865	GLP25_17060	GLP44_13035	GLP29_07970
Acylphosphatase (acyP)	C9J51_12105	C9J52_14490	C9I87_12200	C9I88_05420	GLP10_17100	CJF27_16520	CJF25_07430	CJF26_06410	GLP34_13155	GLP32_07030	GLP35_10560	GLP37_19010	GLP38_06980	GLP25_06680	GLP44_20345	GLP29_13810
Ethanol																
Acetaldehyde dehydrogenase / Alcohol dehydrogenase adhE	C9J51_04465	C9J52_11595	C9I87_01420	C9I88_03410	GLP10_08030	CJF27_08380	CJF25_01770	CJF26_04485	GLP34_00615	GLP32_01155	GLP35_01480	GLP37_01275	GLP38_11385	GLP25_05090	GLP44_01835	GLP29_01525
Ethanol/Acetate																
Pyruvate formate lyase (allerdings O2 sensitive) pflB	C9J51_07465	C9J52_17235	C9I87_18860	C9I88_18065	GLP10_15180	CJF27_11710	CJF25_13835	CJF26_16515	GLP34_17125	GLP32_17790	GLP35_14205	GLP37_16290	GLP38_15930	GLP25_17125	GLP44_12970	GLP29_07905
Formate efflux transporter / formate-nitrite transporter focA	C9J51_07460	C9J52_17240	C9I87_18855	C9I88_18070	GLP10_15185	CJF27_11705	CJF25_13840	CJF26_16510	GLP34_17130	GLP32_17795	GLP35_14210	GLP37_16295	GLP38_15935	GLP25_17130	GLP44_12965	GLP29_07900
acetaldehyde dehydrogenase			C9I87_08360				CJF25_04560		GLP34_05565	GLP32_07425						
alcohol dehydrogenase			C9I87_08350				CJF25_04550		GLP34_05575	GLP32_07435						
iron containing alcohol dehydrogenase	C9J51_03265	C9J52_00865	C9I87_05215	C9I88_10145	GLP10_10020	CJF27_12905	CJF25_02900	CJF26_02545	GLP34_07740	GLP32_04510	GLP35_05890	GLP37_05415	GLP38_08365	GLP25_00360	GLP44_10875	GLP29_20165
	C9J51_02080	C9J52_12140	C9I87_07460	C9I88_15215 + C9I88_19945	GLP10_04220	CJF27_06335	CJF25_03990	CJF26_01340 + CJF26_18705 + CJF26_20350	GLP34_03255		GLP35_20925 + GLP35_19035		GLP38_01860		GLP44_15865	
							CJF25_01180	CJF26_03875	GLP34_01210	GLP32_00565	GLP35_02090	GLP37_01880	GLP38_06460	GLP25_10800	GLP44_02430	GLP29_02115
alcohol dehydrogenase AdhP										GLP32_18960			GLP38_01855	GLP25_01740	GLP44_15870	GLP29_09175
Formate																
Formate acetyltransferase (PFL)	C9J51_07465	C9J52_17235	C9I87_18860	C9I88_18065	GLP10_15180	CJF27_11710	CJF25_13835	CJF26_16515	GLP34_17125	GLP32_17790	GLP35_14205	GLP37_16290	GLP38_15930	GLP25_17125	GLP44_12970	GLP29_07905
formate dehydrogenase (fdh)																
fdhABCE																
A	C9J51_16800	C9J52_12225	C9I87_15300	C9I88_19205	GLP10_17405	CJF27_10545	CJF25_18165	CJF26_09215	GLP34_15600	GLP32_16610	GLP35_17340	GLP37_15600	GLP38_04895	GLP25_16445	GLP44_00040	GLP29_15435
B	C9J51_16805	C9J52_12220	C9I87_15295	C9I88_19210	GLP10_17410	CJF27_10550	CJF25_18170	CJF26_09220	GLP34_15595	GLP32_16605	GLP35_17345	GLP37_15605	GLP38_04900	GLP25_16450	GLP44_00035	GLP29_15440
C	C9J51_16810	C9J52_12215	C9I87_15290	C9I88_19215	GLP10_17415	CJF27_10555	CJF25_18175	CJF26_09225	GLP34_15590	GLP32_16600	GLP35_17350	GLP37_15610	GLP38_04905	GLP25_16455	GLP44_00030	GLP29_15445
E	C9J51_16815	C9J52_12210	C9I87_15285	C9I88_19220	GLP10_17420	CJF27_10560	CJF25_18180	CJF26_09230	GLP34_15585	GLP32_16595	GLP35_17355	GLP37_15615	GLP38_04910	GLP25_16460	GLP44_00025	GLP29_15450
Acetolactate																
Acetolactate synthase (alsS)	C9J51_12365	C9J52_14235	C9I87_12485	C9I88_18780	GLP10_16120	CJF27_13490	CJF25_07690	CJF26_06140	GLP34_19890	GLP32_19505	GLP35_20420	GLP37_21090	GLP38_16710	GLP25_19400	GLP44_14675	GLP29_13540
Diacetyl																
spontaneous from acetolactate																
Acetoin																
Acetolactate decarboxylase aldC	C9J51_12370	C9J52_14230	C9I87_12490	C9I88_18775	GLP10_16115	CJF27_13495	CJF25_07695	CJF26_06135	GLP34_19885	GLP32_19500	GLP35_20415	GLP37_21095	GLP38_16705	GLP25_19395	GLP44_14670	GLP29_13535
Butane-2,3-diol																
Diacetyl reductase (Acetoin reductase) budC / butA / bdhA																
Reoxidizing NADH (O_2)																
NADH oxidase putative!	C9J51_03775	C9J52_01565	C9I87_02105	C9I88_11495	GLP10_04915	CJF27_06065	CJF25_01105	CJF26_03800	GLP34_01285	GLP32_00490	GLP35_02165	GLP37_01955	GLP38_06385	GLP25_10725	GLP44_02505	GLP29_02190
	C9J51_10740	C9J52_17405	C9I87_05570	C9I88_01740	GLP10_07360	CJF27_04990	CJF25_11575	CJF26_07070	GLP34_08135	GLP32_02300	GLP35_15980	GLP37_21355	GLP38_17810	GLP25_01070	GLP44_06910	GLP29_11360
Na+ transporting NADH:ubiquinone oxidorreductase																
nqrF: NADH:ubiquinone oxidoreductase, Na(+)-translocating, F subunit	C9J51_05670	C9J52_05540	C9I87_00175	C9I88_02150	GLP10_14875	CJF27_15125	CJF25_18730	CJF26_08740	GLP34_10215	GLP32_08245	GLP35_00180	GLP37_00180	GLP38_04425	GLP25_03755	GLP44_00515	GLP29_00180
NADH:ubiquinone reductase (Na(+)-transporting) subunit E	C9J51_05675	C9J52_05545	C9I87_00170	C9I88_02145	GLP10_14870	CJF27_15120	CJF25_18725	CJF26_08745	GLP34_10220	GLP32_08240	GLP35_00175	GLP37_00175	GLP38_04430	GLP25_03750	GLP44_00510	GLP29_00175
NADH:ubiquinone reductase (Na(+)-transporting) subunit D	C9J51_05680	C9J52_05550	C9I87_00165	C9I88_02140	GLP10_14865	CJF27_15115	CJF25_18720	CJF26_08750	GLP34_10225	GLP32_08235	GLP35_00170	GLP37_00170	GLP38_04435	GLP25_03745	GLP44_00505	GLP29_00170
Na(+)-translocating NADH-quinone reductase subunit C	C9J51_05685	C9J52_05555	C9I87_00160	C9I88_02135	GLP10_14860	CJF27_15110	CJF25_18715	CJF26_08755	GLP34_10230	GLP32_08230	GLP35_00165	GLP37_00165	GLP38_04440	GLP25_03740	GLP44_00500	GLP29_00165
Na(+)-translocating NADH-quinone reductase subunit A + nqrB: NADH:ubiquinone oxidoreductase, Na(+)-translocating, B subunit	C9J51_05690	C9J52_05560						CJF26_08760	GLP34_10235				GLP38_04445			
Na(+)-translocating NADH-quinone reductase subunit A			C9I87_00150	C9I88_02125	GLP10_14850	CJF27_15100	CJF25_18705			GLP32_08220	GLP35_00155	GLP37_00155		GLP25_03730	GLP44_00490	GLP29_00155
NADH:ubiquinone reductase (Na(+)-transporting) subunit B			C9I87_00155	C9I88_02130	GLP10_14855	CJF27_15105	CJF25_18710			GLP32_08225	GLP35_00160	GLP37_00160		GLP25_03735	GLP44_00495	GLP29_00160
NDH_I_M: proton-translocating NADH-quinone oxidoreductase, chain M	C9J51_03090	C9J52_00690	C9I87_05040	C9I88_10320	GLP10_10165	CJF27_12760	CJF25_03080	CJF26_02345	GLP34_07555	GLP32_04335	GLP35_06090	GLP37_05235	GLP38_08190	GLP25_00185	GLP44_10695	GLP29_08360
(Na+)-NQR maturation NqrM	C9J51_05660	C9J52_05530	C9I87_00185	C9I88_02160	GLP10_14885	CJF27_15135	CJF25_18740	CJF26_08730	GLP34_10205	GLP32_08255	GLP35_00190	GLP37_00190	GLP38_04415	GLP25_03765	GLP44_00525	GLP29_00190
Glycerol																
lipase	C9J51_11685	C9J52_04375	C9I87_15130	C9I88_05805	GLP10_03375	CJF27_04665	CJF25_16540	CJF26_09995	GLP34_06100	GLP32_14845	GLP35_05130	GLP37_13780	GLP38_02805	GLP25_06135	GLP44_08210	GLP29_09190
		C9J52_08605	C9I87_13980	C9I88_04465			CJF25_07010		GLP34_13560	GLP32_06635	GLP35_10140		GLP38_07380	GLP25_07080		GLP29_03935
putative esterase/lipase	C9J51_11685	C9J52_04375	C9I87_1513	C9I88_05805	GLP10_03375	CJF27_0466	CJF25_16540	CJF26_09995	GLP34_06100	GLP32_14845	GLP35_05130	GLP37_13780	GLP38_02805	GLP25_06135	GLP44_08210	GLP29_09190
		C9J52_08605	C9I87_13980	C9I88_04465			CJF25_07010		GLP34_13560	GLP32_06635	GLP35_10140		GLP38_07380	GLP25_07080		GLP29_03935
Glycerol uptake facilitator protein (glpF) putative	C9J51_13670	C9J52_06245	C9I87_11645	C9I88_08835	GLP10_01365	CJF27_03240	CJF25_10885	CJF26_12700	GLP34_10690	GLP32_09530	GLP35_11270	GLP37_11000	GLP38_12100	GLP25_11650	GLP44_14955	GLP29_06970
							CJF25_01605	CJF26_04320	GLP34_00780	GLP32_00990	GLP35_01645	GLP37_01440	GLP38_11550	GLP25_05255	GLP44_02000	GLP29_01690
Dehydrogenation pathway																
glycerol dehydrogenase	C9J51_11105	C9J52_06650	C9I87_10105	C9I88_07795	GLP10_06305	CJF27_07290	CJF25_13365	CJF26_11880	GLP34_08985	GLP32_10475	GLP35_07405	GLP37_07470	GLP38_10320	GLP25_12415	GLP44_09575	GLP29_04720
phosphoenolpyruvate-protein phosphotransferase (E/Ptsi)	C9J51_05525	C9J52_05390	C9I87_00320	C9I88_02295	GLP10_17320	CJF27_16780	CJF25_02785	CJF26_08595	GLP34_10065	GLP32_08390	GLP35_00325	GLP37_00325	GLP38_04280	GLP25_03905	GLP44_00660	GLP29_00325
phosphocarrier protein (HPr)	C9J51_05520	C9J52_05385	C9I87_00325	C9I88_02300	GLP10_17325	CJF27_16775	CJF25_02780	CJF26_08590	GLP34_10060	GLP32_08395	GLP35_00330	GLP37_00330	GLP38_04275	GLP25_03910	GLP44_00665	GLP29_00330
	C9J51_14225	C9J52_14085	C9I87_12980	C9I88_10805	GLP10_02620	CJF27_03760		CJF26_18165		GLP32_12175			GLP38_12855	GLP25_13785		GLP29_16695
Phosphorylation pathway																
glycerol kinase (glpK)	C9J51_13665	C9J52_06240	C9I87_11640	C9I88_08830	GLP10_01360	CJF27_03235	CJF25_10890	CJF26_12695	GLP34_10695	GLP32_09525	GLP35_11265	GLP37_10995	GLP38_12095	GLP25_11655	GLP44_14950	GLP29_06975
	C9J51_02475	C9J52_00060	C9I87_04405	C9I88_13240	GLP10_14385	CJF27_14520	CJF25_03700	CJF26_01730	GLP34_06930		GLP35_08150	GLP37_12280	GLP38_15755	GLP25_13365		GLP29_10120
alpha-glycerophosphate oxidase (glpO) / glycerol-3-phosphate oxidase (aerobic)																
Glycerol-3-phosphate dehydrogenase (gpsA / glpD)	C9J51_13285	C9J52_05860	C9I87_11260	C9I88_08455	GLP10_00985	CJF27_02855	CJF25_11280	CJF26_12305	GLP34_11080	GLP32_09135	GLP35_10880	GLP37_10610	GLP38_11710	GLP25_12040	GLP44_18495	GLP29_07365
NAD(P)H-dependent glycerol-3-phosphate dehydrogenase (gpsA / glpD)	C9J51_13605	C9J52_06180	C9I87_11580	C9I88_08770	GLP10_01300	CJF27_03175	CJF25_10955	CJF26_12630	GLP34_10755	GLP32_09465	GLP35_11205	GLP37_10935	GLP38_12035	GLP25_11715	GLP44_14890	GLP29_07035
anaerobic glycerol-3-phosphate dehydrogenase subunit B	C9J51_17675	C9J52_15295	C9I87_12695	C9I88_16785	GLP10_13805	CJF27_14140	CJF25_07920	CJF26_05915	GLP34_17480	GLP32_11100	GLP35_04230	GLP37_17510	GLP38_20510	GLP25_18325	GLP44_14450	GLP29_18205
anaerobic glycerol-3-phosphate dehydrogenase subunit C	C9J51_17680	C9J52_15290	C9I87_12700	C9I88_16790	GLP10_13810	CJF27_14145	CJF25_07925	CJF26_05910	GLP34_17485	GLP32_11095	GLP35_04235	GLP37_17505	GLP38_20505	GLP25_18320	GLP44_14445	GLP29_18210

	P. iliopiscarium						*P. phosphoreum*									
	ATCC 51760T	**ATCC 51761**	**NCIMB 13478**	**NCIMB 13481**	**TMW 2.2104**	**TMW 2.2035**	**TMW 2.2033**	**TMW 2.2034**	**TMW 2.2103**	**TMW 2.2125**	**TMW 2.2126**	**TMW 2.2130**	**TMW 2.2132**	**TMW 2.2134**	**TMW 2.2140**	**TMW 2.2142**
anaerobic glycerol-3-phosphate dehydrogenase subunit A	C9J51_17670	C9J52_15300	C9I87_12690	C9I88_16780	GLP10_13800	CJF27_14135	CJF25_07915	CJF26_05920	GLP34_17475	GLP32_11105	GLP35_04225	GLP37_17515	GLP38_20515	GLP25_18330	GLP44_14455	GLP29_18200
Fatty acid beta-oxidation																
Aerobic																
long-chain fatty acid transporter fadL	C9J51_11680	C9J52_04380	C9I87_15135	C9I88_05810	GLP10_03380	CJF27_04660	CJF25_07005	CJF26_11160	GLP34_13565	GLP32_06630	GLP35_10135	GLP37_03160	GLP38_07385	GLP25_07085	GLP44_08560	GLP29_03930
long-chain fatty acid CoA ligase fadD	C9J51_04595	C9J52_11725	C9I87_01290	C9I88_03280	GLP10_08160	CJF27_08250	CJF25_01900	CJF26_04615	GLP34_00485	GLP32_01285	GLP35_01350	GLP37_01145	GLP38_11255	GLP25_04960	GLP44_01705	GLP29_01395
acyl-CoA dehydrogenase fadE	C9J51_03905	C9J52_01435	C9I87_01975	C9I88_11625	GLP10_04785	CJF27_05935	CJF25_01215	CJF26_03915	GLP34_01170	GLP32_00605	GLP35_02055	GLP37_01845	GLP38_06495	GLP25_10835	GLP44_02390	GLP29_02080
	C9J51_17810	C9J52_16595	C9I87_18380	C9I88_17365	GLP10_13040	CJF27_13735	CJF25_19790	CJF26_19500	GLP34_18485	GLP32_18315	GLP35_19265	GLP37_19445	GLP38_19700	GLP25_18720	GLP44_19530	GLP29_18960
3-hydroxyacyl-CoA dehydrogenase fadB	C9J51_16850	C9J52_12550	C9I87_17195	C9I88_14985	GLP10_09485	CJF27_11605	CJF25_20075	CJF26_17670	GLP34_16605	GLP32_16925	GLP35_18125	GLP37_16745	GLP38_17285	GLP25_17230	GLP44_17000	GLP29_15835
acetyl-CoA acyltransferase fadA	C9J51 16855	C9J52 12555	C9I87 17190	C9I88 14980	GLP10 09490	CJF27 11600	CJF25 20070	CJF26 17665	GLP34 16610	GLP32 16930	GLP35 18120	GLP37 16750	GLP38 17290	GLP25 17235	GLP44 16995	GLP29 15830
Anaerobic																
long-chain fatty acid CoA ligase put. fadK	C9J51_14980	C9J52_10435	C9I87_13730	C9I88_12690	GLP10_08405	CJF27_09950	CJF25_15805	CJF26_14800	GLP34_15245	GLP32_13555	GLP35_13735	GLP37_14165	GLP38_13275	GLP25_14435	GLP44_12485	GLP29_15975
3-hydroxyacyl-CoA dehydrogenase fadJ	C9J51_05040	C9J52_04905	C9I87_00805	C9I88_02780	GLP10_15265	CJF27_15335	CJF25_02500	CJF26_05170	GLP34_09575	GLP32_08880	GLP35_00815	GLP37_00620	GLP38_03790	GLP25_04395	GLP44_01150	GLP29_00820
acetyl-CoA acyltransferase fadI	C9J51_05045	C9J52_04910	C9I87_00800	C9I88_02775	GLP10_15270	CJF27_15330	CJF25_02505	CJF26_05175	GLP34_09580	GLP32_08875	GLP35_00810	GLP37_00615	GLP38_03795	GLP25_04390	GLP44_01145	GLP29_00815
Complete Tricarboxylic acid cycle (TCA cycle)																
Citrate Synthase (citA)	C9J51_04725	C9J52_11855	C9I87_01165	C9I88_03155	GLP10_08285	CJF27_08125	CJF25_02030	CJF26_04745	GLP34_00360	GLP32_01410	GLP35_01225	GLP37_01020	GLP38_11130	GLP25_04835	GLP44_01580	GLP29_01270
Aconitate hydratase (cit B)	C9J51 14555	C9J52 13130	C9I87 13310	C9I88 11135	GLP10 02980	CJF27 04120	CJF25 15045	CJF26 17055	GLP34 11330	GLP32 12500	GLP35 12000	GLP37 13130	GLP38 12525	GLP25 14110	GLP44 21060	GLP29 16280
Isocitrate Dehydrogenase (icd A)	C9J51_06520	C9J52_03880	C9I87_10990	C9I88_04630	GLP10_14040	CJF27_12490	CJF25_16715	CJF26_10175	GLP34_06285	GLP32_15460	GLP35_04945	GLP37_09845	GLP38_02990	GLP25_05955	GLP44_08030	GLP29_05205
Oxoglutarate dehydrogenase (suc AB)	C9J51_04690	C9J52_11820	C9I87_01195	C9I88_03185	GLP10_08255	CJF27_08155	CJF25_01995	CJF26_04710	GLP34_00390	GLP32_01380	GLP35_01255	GLP37_01050	GLP38_11160	GLP25_04865	GLP44_01610	GLP29_01300
	C9J51_04695	C9J52_11825	C9I87_01190	C9I88_03180	GLP10_08260	CJF27_08150	CJF25_02000	CJF26_04715	GLP34_00385	GLP32_01385	GLP35_01250	GLP37_01045	GLP38_11155	GLP25_04860	GLP44_01605	GLP29_01295
Succinyl-CoA-Synthetase (suc CD)	C9J51 04680	C9J52 11810	C9I87 01205	C9I88 03195	GLP10 08245	CJF27 08165	CJF25 01985	CJF26 04700	GLP34 00400	GLP32 01370	GLP35 01265	GLP37 01060	GLP38 11170	GLP25 04875	GLP44 01620	GLP29 01310
	C9J51_04685	C9J52_11815	C9I87_01200	C9I88_03190	GLP10_08250	CJF27_08160	CJF25_01990	CJF26_04705	GLP34_00395	GLP32_01375	GLP35_01260 GLP35_01730	GLP37_01055 GLP37_01520	GLP38_11165	GLP25_04870	GLP44_01615	GLP29_01305
Succinate dehydrogenase (complex II) (sdh ABCD)	C9J51_04700	C9J52_11830	C9I87_01185	C9I88_03175	GLP10_08265	CJF27_08145	CJF25_02005	CJF26_04720	GLP34_00380	GLP32_01390	GLP35_01245	GLP37_01040	GLP38_11150	GLP25_04855	GLP44_01600	GLP29_01290
	C9J51_04705	C9J52_11835	C9I87_01180	C9I88_03170	GLP10_08270	CJF27_08140	CJF25_02010	CJF26_04725	GLP34_00375	GLP32_01395	GLP35_01240	GLP37_01035	GLP38_11145	GLP25_04850	GLP44_01595	GLP29_01285
	C9J51_04710	C9J52_11840	C9I87_01175	C9I88_03165	GLP10_08275	CJF27_08135	CJF25_02015	CJF26_04730	GLP34_00370	GLP32_01400	GLP35_01235	GLP37_01030	GLP38_11140	GLP25_04845	GLP44_01590	GLP29_01280
	C9J51_04715	C9J52_11845	C9I87_01170	C9I88_03160	GLP10_08280	CJF27_08130	CJF25_02020	CJF26_04735	GLP34_00365	GLP32_01405	GLP35_01230	GLP37_01025	GLP38_11135	GLP25_04840	GLP44_01585	GLP29_01275
Fumarate hydratase (Fumarase) (fum A)	C9J51 03830	C9J52 01510	C9I87 02050	C9I88 11550	GLP10 04860	CJF27 06010	CJF25 01145	CJF26 03840	GLP34 01245	GLP32 00530	GLP35 02125	GLP37 01915	GLP38 06425	GLP25 10765	GLP44 02465	GLP29 02150
Malate dehydrogenase (md h)	C9J51_15130	C9J52_18480	C9I87_13875	C9I88_12840	GLP10_17005	CJF27_16435	CJF25_15655	CJF26_14650	GLP34_19390	GLP32_13705	GLP35_13585	GLP37_14315	GLP38_13125	GLP25_14285	GLP44_12635	GLP29_16125
Phosphoenolpyruvate carboxylase	C9J51_13735	C9J52_06310	C9I87_11710	C9I88_08900	GLP10_01430	CJF27_03305	CJF25_10820	CJF26_12765	GLP34_10625	GLP32_09595	GLP35_11335	GLP37_11065	GLP38_12165	GLP25_11585	GLP44_15020	GLP29_06905
Glyoxylate cycle																
isocitrate lyase	C9J51_16665	C9J52_12360	C9I87_15435	C9I88_18275	GLP10_12810	CJF27_10405	CJF25_18040	CJF26_09090	GLP34_15755	GLP32_16735	GLP35_17210	GLP37_15470	GLP38_04775	GLP25_16325	GLP44_00160	GLP29_15315
malate synthase	C9J51 16670	C9J52 12355	C9I87 15430	C9I88 18280	GLP10 12805	CJF27 10410	CJF25 18045	CJF26 09095	GLP34 15750	GLP32 16730	GLP35 17215	GLP37 15475	GLP38 04780	GLP25 16330	GLP44 00155	GLP29 15320
AMINO ACIDS																
Arginine deiminase (arcA)	C9J51_14780	C9J52_10235	C9I87_13530	C9I88_12490	GLP10_08605 GLP10_06430	CJF27_10150 CJF27_07165	CJF25_16005	CJF26_15000	GLP34_15445	GLP32_13355	GLP35_13935	GLP37_13965	GLP38_13480	GLP25_14635	GLP44_12285	GLP29_19385
ornithine carbamoyl transferase Ornithine transcarbmoylase (arcB)	C9J51_14790	C9J52_10245	C9I87_13540	C9I88_12500	GLP10_08595 GLP10_06440	CJF27_10140 CJF27_07155	CJF25_15995	CJF26_14990	GLP34_15435	GLP32_13365	GLP35_13925	GLP37_13975	GLP38_13470	GLP25_14625	GLP44_12295	GLP29_19395
carbamate kinase (arcC)	C9J51 14785	C9J52 10240	C9I87 13535	C9I88 12495	GLP10 08600 GLP10_06435 GLP10_02920	CJF27 10145 CJF27_07160 CJF27_04060	CJF25 16000	CJF26 14995	GLP34 15440	GLP32 13360	GLP35 13930	GLP37 13970	GLP38 13475	GLP25 14630	GLP44 12290	GLP29 19390
Arginase (arg)	C9J51_01680	C9J52_16190	C9I87_07035	C9I88_15625	GLP10_03815	CJF27_16935	CJF25_06360	CJF26_00810	GLP34_02255	GLP32_05005	GLP35_09995	GLP37_09640	TMW22134_GLP25_02280	GLP25_02280	GLP44_03485	GLP29_06585
							CJF25_00105	CJF26_02790		GLP32_12750	GLP35_03180					
Malate dehydrogenase (md h)	C9J51_15130	C9J52_18480	C9I87_13875	C9I88_12840	GLP10_17005	CJF27_16435	CJF25_15655	CJF26_14650	GLP34_19390	GLP32_13705	GLP35_13585	GLP37_14315	GLP38_13125	GLP25_14285	GLP44_12635	GLP29_16125
Aminotransferasen																
Aspartate Aminofransferase (Glu/OA) aspB	C9J51_13845	C9J52_06420	C9I87_11820	C9I88_09010	GLP10_01540	CJF27_03415	CJF25_10710	CJF26_12875	GLP34_10515	GLP32_09710	GLP35_11445	GLP37_11175	GLP38_12275	GLP25_11475	GLP44_15130	GLP29_06795
Glutamate Dehydrogenase (aKG/NADH2) gdhA							CJF25_18470	CJF26_10360	GLP34_18980	GLP32_18835	GLP35_04020	GLP37_03980	GLP38_15055	GLP25_07875	GLP44_17405	GLP29_19885
Serine dehydratase (rev.) (Pyr/NH3) sdaAB	C9J51_03850	C9J52_01490	C9I87_02030	C9I88_11570	GLP10_04840	CJF27_05990	CJF25_01165	CJF26_03860	GLP34_01225	GLP32_00550	GLP35_02105	GLP37_01895	GLP38_06445	GLP25_10785	GLP44_02445	GLP29_02130
Aromatic amino acid aminotransferase (Tyr,Phe,His) (Glu) tyrB	C9J51_12550	C9J52_13345	C9I87_18030	C9I88_18460	GLP10_00085	CJF27_00175										
	C9J51_03560	C9J52_01780	C9I87_02320	C9I88_11280	GLP10_16075	CJF27_16195	CJF25_00870	CJF26_03570	GLP34_01515	GLP32_00255	GLP35_02410	GLP37_02190	GLP38_06155	GLP25_10495	GLP44_02735	GLP29_02420
Branched-chain amino acid aminotransferase (Leu,Ile,Val) (Glu) ilvE	C9J51_17085	C9J52_12785	C9I87_16960	C9I88_14750	GLP10_09720	CJF27_11370	CJF25_21020	CJF26_17435	GLP34_16840	GLP32_17160	GLP35_17890	GLP37_16980	GLP38_17520	GLP25_17465	GLP44_16765	GLP29_15600
Alanine dehydrogenase (ald)	C9J51_12135	C9J52_14460	C9I87_12230	C9I88_05390	GLP10_18170	CJF27_13260	CJF25_02275	CJF26_05030	GLP34_00075	GLP32_01655	GLP35_00980	GLP37_00775	GLP38_10885	GLP25_04550	GLP44_01335	GLP29_01025
Alanine aminotransferase																
aspartate ammonia-lyase (aspA)	C9J51_17305	C9J52_14715	C9I87_17465	C9I88_15735	GLP10_12145	CJF27_15960	CJF25_17055	CJF26_17815	GLP34_19655	GLP32_17545	GLP35_18520	GLP37_18110	GLP38_18110	GLP25_17850	GLP44_18805	GLP29_17185
aspartate oxidase (nadB)	C9J51 16200	C9J52 15125	C9I87 15845	C9I88 14410	GLP10 11785	CJF27 09605	CJF25 19000	CJF26 18575	GLP34 18010	GLP32 16260	GLP35 18905	GLP37 18705	GLP38 18440	GLP25 15835	GLP44 19135	GLP29 17890
Biogenic amines production																
histidine-histamine antiporter (aminoacid permease)							CJF25_03715	CJF26_01575			GLP35_08135	GLP37_12295				
histidine decarboxylase hdcA																
histidine decarboxylase 2 hdc2 Bjornsdottir-Butler et al.							CJF25_03720	CJF26_01570			GLP35_08130	GLP37_12300				
arginine decarboxylase speA	C9J51 04100	C9J52 01240	C9I87 01785	C9I88 11815	GLP10 04595	CJF27 05745	CJF25 01410	CJF26 04110	GLP34 00975	GLP32 00800	GLP35 01860	GLP37 01650	GLP38 06690	GLP25 11030	GLP44 02195	GLP29 01885
	C9J51_02620	C9J52_00205	C9I87_04550	C9I88_13100	GLP10_14310	CJF27_14450	CJF25_03650	CJF26_01780	GLP34_21460 + GLP34_20695	GLP32_03760	GLP35_08200	GLP37_12230	GLP38_15705	GLP25_13315	GLP44_12040	GLP29_10170
	C9J51_18275	C9J52_20640	C9I87_19605	C9I88_20325	GLP10_19210	CJF27_18300	CJF25_21660 + CJF25_21770	CJF26_20215 + CJF26_20745		GLP32_18550 + GLP32_20910		GLP37_19905	GLP38_20215 + GLP38_21490	GLP25_20370	GLP44_20025	GLP29_21055
	C9J51_19315	C9J52_20890	C9I87_19150	C9I88_20620		CJF27_18300					GLP35_21715 + GLP35_21805			GLP25_19020	GLP44_22090	GLP29_21105
	C9J51 19370		C9I87 19740	C9I88 17905 C9I88_20325								GLP37 22290 GLP37_22270			GLP44 22090 GLP44_22100	GLP29 21105
tyrosine decarboxylase tdcA							CJF25_04810	CJF26_19730	GLP34_05315	GLP32_18385	GLP35_19580	GLP37_20295	GLP38_05100	GLP25_09390	GLP44_17185	GLP29_16975
ornithine decarboxylase speF																
lysine decarboxylase ldcC	C9J51_14710	C9J52_10165	C9I87_13460	C9I88_12420			CJF25_16170	CJF26_15100	GLP34_15540	GLP32_13260	GLP35_14030	GLP37_13870	GLP38_13575	GLP25_14730	GLP44_12155	GLP29_19290
agmatinase speB	C9J51_02615	C9J52_00200	C9I87_04545	C9I88_13105	GLP10_14315	CJF27_14455	CJF25_03655	CJF26_01775	GLP34_06975	GLP32_03755	GLP35_08195	GLP37_12235	GLP38_15710	GLP25_13320	GLP44_12045	GLP29_10165
bifunctional glutathionylspermidine amidase/synthase	C9J51_11605	C9J52_04455	C9I87_15210	C9I88_05885	GLP10_03450	CJF27_04590	CJF25_06935	CJF26_11090	GLP34_12420	GLP32_06560	GLP35_10065	GLP37_03230	GLP38_07455	GLP25_07155	GLP44_08630	GLP29_03860

	P. iliopiscarium						*P. phosphoreum*									
	ATCC 51760T	**ATCC 51761**	**NCIMB 13478**	**NCIMB 13481**	**TMW 2.2104**	**TMW 2.2035**	**TMW 2.2033**	**TMW 2.2034**	**TMW 2.2103**	**TMW 2.2125**	**TMW 2.2126**	**TMW 2.2130**	**TMW 2.2132**	**TMW 2.2134**	**TMW 2.2140**	**TMW 2.2142**
glutamate decarboxylase gadB	C9J51_15660	C9J52_19595	C9I87_16110	C9I88_14155	GLP10_09150	CJF27_10595	CJF25_20690	CJF26_16415	GLP34_15935	GLP32_19465	GLP35_18150	GLP37_15645	GLP38_16150	GLP25_16490	GLP44_15995	GLP29_14790
Electron donors																
NiFe hydrogenase																
hyd ABCDE	C9J51_11805	C9J52_04275	C9I87_15040	C9I88_05715	GLP10_03280	CJF27_04760	CJF25_07125	CJF26_11260	GLP34_13465	GLP32_06725	GLP35_10245	GLP37_03050	GLP38_07290	GLP25_06985	GLP44_08450	GLP29_04035
	C9J51_11800	C9J52_04280	C9I87_15045	C9I88_05720	GLP10_03285	CJF27_04755	CJF25_07120	CJF26_11255	GLP34_13470	GLP32_06720	GLP35_10240	GLP37_03055	GLP38_07295	GLP25_06990	GLP44_08455	GLP29_04030
	C9J51_11795	C9J52_04285	C9I87_15050	C9I88_05725	GLP10_03290	CJF27_04750	CJF25_07115	CJF26_11250	GLP34_13475	GLP32_06715	GLP35_10235	GLP37_03060	GLP38_07300	GLP25_06995	GLP44_08460	GLP29_04025
	C9J51 11790	C9J52 04290	C9I87 15055	C9I88 05730	GLP10 03295	CJF27 04745	CJF25 07110	CJF26 11245	GLP34 13480	GLP32 06710	GLP35 10230	GLP37 03065	GLP38 07305	GLP25 07000	GLP44 08465	GLP29 04020
	C9J51_11785	C9J52_04295	C9I87_15060	C9I88_05735	GLP10_03300	CJF27_04740	CJF25_07105	CJF26_11240	GLP34_13485	GLP32_06705	GLP35_10225	GLP37_03070	GLP38_07310	GLP25_07005	GLP44_08470	GLP29_04015
Alternative electron receptors																
Fumarate reductase																
frdABCD	C9J51 17245	C9J52 14775	C9I87 17525	C9I88 15675	GLP10 12205	CJF27 15900	CJF25 17115	CJF26 17755	GLP34 19715	GLP32 17605	GLP35 18460	GLP37 18050	GLP38 18050	GLP25 17910	GLP44 18745	GLP29 17125
	C9J51_17250	C9J52_14770	C9I87_17520	C9I88_15680	GLP10_12200	CJF27_15905	CJF25_17110	CJF26_17760	GLP34_19710	GLP32_17600	GLP35_18465	GLP37_18055	GLP38_18055	GLP25_17905	GLP44_18750	GLP29_17130
	C9J51_17255	C9J52_14765	C9I87_17515	C9I88_15685	GLP10_12195	CJF27_15910	CJF25_17105	CJF26_17765	GLP34_19705	GLP32_17595	GLP35_18470	GLP37_18060	GLP38_18060	GLP25_17900	GLP44_18755	GLP29_17135
	C9J51_17260	C9J52_14760	C9I87_17510	C9I88_15690	GLP10_12190	CJF27_15915	CJF25_17100	CJF26_17770	GLP34_19700	GLP32_17590	GLP35_18475	GLP37_18065	GLP38_18065	GLP25_17895	GLP44_18760	GLP29_17140
TMAO reductase	C9J51_11715	C9J52_04345	C9I87_15100	C9I88_05775	GLP10_03345	CJF27_04695	CJF25_07040	CJF26_11195	GLP34_13530	GLP32_06665	GLP35_10170	GLP37_03125	GLP38_07350	GLP25_07050	GLP44_08525	GLP29_03965
tor A																
Nitrate reductase																
nap AB	C9J51_05570	C9J52_05440	C9I87_00275	C9I88_02250	GLP10_17275	CJF27_16825	CJF25_18830	CJF26_08640	GLP34_10115	GLP32_08345	GLP35_00280	GLP37_00280	GLP38_04325	GLP25_03855	GLP44_00615	GLP29_00280
	C9J51 05575		C9I87 00270	C9I88 02245	GLP10 17270	CJF27 16830	CJF25 18825	CJF26 08645	GLP34 10120	GLP32 08340	GLP35 00275	GLP37 00275	GLP38 04330	GLP25 03850	GLP44 00610	GLP29 00275
	C9J51_05580	C9J52_05450	C9I87_00265	C9I88_02240	GLP10_17265	CJF27_16835										
hydroxylamine reductase	C9J51_02910	C9J52_00495	C9I87_04850	C9I88_10505	GLP10_12270	CJF27_13015	CJF25_03280	CJF26_02125	GLP34_07325	GLP32_04120	GLP35_08550	GLP37_05030	GLP38_07940	GLP25_12970	GLP44_11660	GLP29_08575
Mannose-6-P isomerase	C9J51_07380	C9J52_16345	C9I87_17820	C9I88_03820	GLP10_05520	CJF27_11630	CJF25_13915	CJF26_16435	GLP34_17205/GLP34_18720	GLP32_17870	GLP35_14285	GLP37_16375	GLP38_16010	GLP25_17205	GLP44_20055/GLP44_12895	GLP29_07825
manA																
nitrite reductase small subunit	C9J51_12260	C9J52_14340	C9I87_12380	C9I88_18885	GLP10_16225	CJF27_13385	CJF25_07585	CJF26_06245	GLP34_21230	GLP32_19610	GLP35_20525	GLP37_20985	GLP38_16815	GLP25_19505	GLP44_14780	GLP29_13645
nitrite reductase large subunit	C9J51_12255	C9J52_14345	C9I87_12375	C9I88_18890	GLP10_16230	CJF27_13380	CJF25_07580	CJF26_06250	GLP34_21235	GLP32_19615	GLP35_20530	GLP37_20980	GLP38_16820	GLP25_19510	GLP44_14785	GLP29_13650
sulphate adenylyltransferase cysD	C9J51_18305	C9J52_19940	C9I87_18815	C9I88_17450	GLP10_13695	CJF27_14025	CJF25_17395	CJF26_19985	GLP34_21150	GLP32_17895	GLP35_19340	GLP37_19875	GLP38_19770	GLP25_18790	GLP44_19795	GLP29_18535
sulphate adenylyltransferase cysN	C9J51_18300	C9J52_19945	C9I87_18820	C9I88_17445	GLP10_13700	CJF27_14030	CJF25_17400	CJF26_19990	GLP34_21145	GLP32_17890	GLP35_19335	GLP37_19880	GLP38_19765	GLP25_18785	GLP44_19800	GLP29_18530
assimilatory sulfite reductase	C9J51 18355	C9J52 17680	C9I87 18765	C9I88 17500	GLP10 13645	CJF27 13975	CJF25 17345	CJF26 19935	GLP34 19280	GLP32 17945	GLP35 19390	GLP37 19825	GLP38 19820	GLP25 18840	GLP44 19745	GLP29 18585
dimethyl sulfoxide reductase subunit A	C9J51_10445	C9J52_09205	C9I87_05830	C9I88_10045			CJF25_00710	CJF26_03410	GLP34_01675	GLP32_00095	GLP35_02565	GLP37_02345	GLP38_06000	GLP25_10335	GLP44_02890	
dimethylsulfoxide reductase, chain B	C9J51_10450	C9J52_09200	C9I87_05825	C9I88_10050			CJF25_00715	CJF26_03415	GLP34_01670	GLP32_00100	GLP35_02560	GLP37_02340	GLP38_06005	GLP25_10340	GLP44_02885	
dimethyl sulfoxide reductase anchor subunit	C9J51_10455	C9J52_09195	C9I87_05820	C9I88_10055			CJF25_00720	CJF26_03420	GLP34_01665	GLP32_00105	GLP35_02555	GLP37_02335	GLP38_06010	GLP25_10345	GLP44_02880	GLP29_02565
Respiration																
NADH dehydrogenase (non-electrogenic)																
ndh	C9J51_12385	C9J52_14215	C9I87_12505	C9I88_18760	GLP10_16100	CJF27_13510	CJF25_07710	CJF26_06120	GLP34_19870	GLP32_19485	GLP35_20400	GLP37_21110	GLP38_16690	GLP25_19380	GLP44_14655	GLP29_13520
	C9J51 03775	C9J52 01565	C9I87 02105	C9I88 11495	GLP10 04915	CJF27 06065	CJF25 01105	CJF26 03800	GLP34 01285	GLP32 00490	GLP35 02165	GLP37 01955	GLP38 06385	GLP25 10725	GLP44 02505	GLP29 02190
NADH-quinone oxidoreductase subunit A							CJF25_05140	CJF26_15315	GLP34_04985	GLP32_13960	GLP35_15315	GLP37_14670	GLP38_00190	GLP25_03390	GLP44_03820	GLP29_12230
NADH-quinone oxidoreductase subunit B							CJF25_05135	CJF26_15310	GLP34_04990	GLP32_13955	GLP35_15310	GLP37_14675	GLP38_00185	GLP25_03395	GLP44_03815	GLP29_12235
NADH dehydrogenase (quinone) subunit D							CJF25_05130	CJF26_15305	GLP34_04995	GLP32_13950	GLP35_15305	GLP37_14680	GLP38_00180	GLP25_03400	GLP44_03810	GLP29_12240
NADH-quinone oxidoreductase subunit NuoE							CJF25_05125	CJF26_15300	GLP34_05000	GLP32_13945	GLP35_15300	GLP37_14685	GLP38_00175	GLP25_03405	GLP44_03805	GLP29_12245
NADH-quinone oxidoreductase subunit NuoF							CJF25_05120	CJF26_15295	GLP34_05005	GLP32_13940	GLP35_15295	GLP37_14690	GLP38_00170	GLP25_03410	GLP44_03800	GLP29_12250
NADH dehydrogenase (quinone) subunit G							CJF25_05115	CJF26_15290	GLP34_05010	GLP32_13935	GLP35_15290	GLP37_14695	GLP38_00165	GLP25_03415	GLP44_03795	GLP29_12255
NADH-quinone oxidoreductase subunit NuoH							CJF25_05110	CJF26_15285	GLP34_05015	GLP32_13930	GLP35_15285	GLP37_14700	GLP38_00160	GLP25_03420	GLP44_03790	GLP29_12260
NADH-quinone oxidoreductase subunit NuoI							CJF25_05105	CJF26_15280	GLP34_05020	GLP32_13925	GLP35_15280	GLP37_14705	GLP38_00155	GLP25_03425	GLP44_03785	GLP29_12265
NADH-quinone oxidoreductase subunit J							CJF25_05100	CJF26_15275	GLP34_05025	GLP32_13920	GLP35_15275	GLP37_14710	GLP38_00150	GLP25_03430	GLP44_03780	GLP29_12270
NADH-quinone oxidoreductase subunit NuoK							CJF25 05095	CJF26 15270	GLP34 05030	GLP32 13915	GLP35 15270	GLP37 14715	GLP38 00145	GLP25 03435	GLP44 03775	GLP29 12275
NADH-quinone oxidoreductase subunit L							CJF25_05090	CJF26_15265	GLP34_05035	GLP32_13910	GLP35_15265	GLP37_14720	GLP38_00140	GLP25_03440	GLP44_03770	GLP29_12280
NADH-quinone oxidoreductase subunit M							CJF25_05085	CJF26_15260	GLP34_05040	GLP32_13905	GLP35_15260	GLP37_14725	GLP38_00135	GLP25_03445	GLP44_03765	GLP29_12285
NADH-quinone oxidoreductase subunit N							CJF25_05080	CJF26_15255	GLP34_05045	GLP32_13900	GLP35_15255	GLP37_14730	GLP38_00130	GLP25_03450	GLP44_03760	GLP29_12290
NADH-quinone oxidoreductase subunit NuoB	C9J51_03110	C9J52_00710	C9I87_05060	C9I88_10300	GLP10_10145	CJF27_12780	CJF25_03060	CJF26_02365	GLP34_07575	GLP32_04355	GLP35_06070	GLP37_05255	GLP38_08210	GLP25_00205	GLP44_10715	GLP29_08340
(Na+)-NQR maturation NqrM	C9J51_05660	C9J52_05530	C9I87_00185	C9I88_02160	GLP10_14885	CJF27_15135	CJF25_18740	CJF26_08730	GLP34_10205	GLP32_08255	GLP35_00190	GLP37_00190	GLP38_04415	GLP25_03765	GLP44_00525	GLP29_00190
nqrF: NADH:ubiquinone oxidoreductase, Na(+)-translocating, F subunit	C9J51_05670	C9J52_05540	C9I87_00175	C9I88_02150	GLP10_14875	CJF27_15125	CJF25_18730	CJF26_08740	GLP34_10215	GLP32_08245	GLP35_00180	GLP37_00180	GLP38_04425	GLP25_03755	GLP44_00515	GLP29_00180
NADH:ubiquinone reductase (Na(+)-transporting) subunit E	C9J51_05675	C9J52_05545	C9I87_00170	C9I88_02145	GLP10_14870	CJF27_15120	CJF25_18725	CJF26_08745	GLP34_10220	GLP32_08240	GLP35_00175	GLP37_00175	GLP38_04430	GLP25_03750	GLP44_00510	GLP29_00175
NADH:ubiquinone reductase (Na(+)-transporting) subunit D	C9J51_05680	C9J52_05550	C9I87_00165	C9I88_02140	GLP10_14865	CJF27_15115	CJF25_18720	CJF26_08750	GLP34_10225	GLP32_08235	GLP35_00170	GLP37_00170	GLP38_04435	GLP25_03745	GLP44_00505	GLP29_00170
Na(+)-translocating NADH-quinone reductase subunit C	C9J51_05685	C9J52_05555	C9I87_00160	C9I88_02135	GLP10_14860	CJF27_15110	CJF25_18715	CJF26_08755	GLP34_10230	GLP32_08230	GLP35_00165	GLP37_00165	GLP38_04440	GLP25_03740	GLP44_00500	GLP29_00165
Na(+)-translocating NADH-quinone reductase subunit A + nqrB: NADH:ubiquinone oxidoreductase, Na(+)-translocating, B subunit	C9J51_05690	C9J52_05560						CJF26_08760	GLP34_10235				GLP38_04445			
Na(+)-translocating NADH-quinone reductase subunit A			C9I87_00150	C9I88_02125	GLP10_14850	CJF27_15100	CJF25_18705			GLP32_08220	GLP35_00155	GLP37_00155		GLP25_03730	GLP44_00490	GLP29_00155
NADH:ubiquinone reductase (Na(+)-transporting) subunit B			C9I87_00155	C9I88_02130	GLP10_14855	CJF27_15105	CJF25_18710			GLP32_08225	GLP35_00160	GLP37_00160		GLP25_03735	GLP44_00495	GLP29_00160

	P. iliopiscarium						*P. phosphoreum*									
	ATCC 51760T	ATCC 51761	NCIMB 13478	NCIMB 13481	TMW 2.2104	TMW 2.2035	TMW 2.2033	TMW 2.2034	TMW 2.2103	TMW 2.2125	TMW 2.2126	TMW 2.2130	TMW 2.2132	TMW 2.2134	TMW 2.2140	TMW 2.2142
NDH_I_M: proton-translocating NADH-quinone oxidoreductase, chain M	C9J51_03090	C9J52_00690	C9I87_05040	C9I88_10320	GLP10_10165	CJF27_12760	CJF25_03080	CJF26_02345	GLP34_07555	GLP32_04335	GLP35_06090	GLP37_05235	GLP38_08190	GLP25_00185	GLP44_10695	GLP29_08360
Menaquinone synthese (8 steps) (Vitamin K)																
1,4-dihydroxy-2-naphthoate prenyltransferase (*men* A)	C9J51_13685	C9J52_06260	C9I87_11660	C9I88_08850	GLP10_01380	CJF27_03255	CJF25_10875	CJF26_12710	GLP34_10680	GLP32_09540	GLP35_11280	GLP37_11010	GLP38_12110	GLP25_11640	GLP44_14965	GLP29_06960
Isochorismate synthase (menF)	C9J51_07000	C9J52_09045	C9I87_14260	C9I88_04210	GLP10_05930	CJF27_10960	CJF25_20235	CJF26_09715	GLP34_05770	GLP32_14510	GLP35_14685	GLP37_13430	GLP38_02535	GLP25_06405	GLP44_17690	GLP29_09745
	C9J51_07000	C9J52_09045	C9I87_14260	C9I88_04210	GLP10_05930	CJF27_10960	CJF25_20235	CJF26_09715	GLP34_05770	GLP32_14510	GLP35_14685	GLP37_13430	GLP38_02535	GLP25_06405	GLP44_17690	GLP29_09745
2-succinyl-5-enolpyruvyl-6-hydroxy-3- cyclohexene-1-carboxylic-acid synthase (menD)	C9J51_06995	C9J52_09040	C9I87_14255	C9I88_04215	GLP10_05935	CJF27_10955										
							CJF25_20240	CJF26_09720	GLP34_05775	GLP32_14515	GLP35_14690	GLP37_13435	GLP38_02540	GLP25_06400	GLP44_17695	GLP29_09740
2-succinyl-6-hydroxy-2, 4-cyclohexadiene-1-carboxylate synthase (menH)	C9J51_06990	C9J52_09035	C9I87_14250	C9I88_04220	GLP10_05940	CJF27_10950	CJF25_20245	CJF26_09725	GLP34_05780		GLP35_14695		GLP38_02545	GLP25_06395		GLP29_09735
							CJF25_11725	CJF26_06960	GLP34_08250	GLP32_02150	GLP35_16090	GLP37_05975	GLP38_17920	GLP25_00960	GLP44_07020	GLP29_11470
o-succinylbenzoate synthase (menC)	C9J51_06985	C9J52_09030	C9I87_14245	C9I88_04225	GLP10_05945	CJF27_10945	CJF25_20250	CJF26_09730	GLP34_05785	GLP32_14525	GLP35_14700	GLP37_13445	GLP38_02550	GLP25_06390	GLP44_17705	GLP29_09730
2-methoxy-6-polyprenyl-1,4-benzoquinol methylase (ubiE)	C9J51_15265	C9J52_10910	C9I87_14470	C9I88_16055	GLP10_11190	CJF27_08600	CJF25_17795	CJF26_15995	GLP34_15135	GLP32_14955	GLP35_16515	GLP37_14920	GLP38_14200	GLP25_15330	GLP44_15630	GLP29_13975
O-succinylbenzoate-CoA ligase (menE)	C9J51_06980	C9J52_09025	C9I87_14240	C9I88_04230	GLP10_05950	CJF27_10940	CJF25_20255	CJF26_09735	GLP34_05790	GLP32_14530	GLP35_14705	GLP37_13450	GLP38_02555	GLP25_06385	GLP44_17710	GLP29_09725
1,4-dihydroxy-2-naphthoyl-CoA synthase (menB)	C9J51_08655	C9J52_07695	C9I87_03335	C9I88_06840	GLP10_09090	CJF27_01280	CJF25_14650	CJF26_14230	GLP34_02665	GLP32_11570	GLP35_03590	GLP37_04450	GLP38_08785	GLP25_08875	GLP44_10200	GLP29_06200
cytochrome c oxidase																
Subunit I CoxA	C9J51_13320	C9J52_05895	C9I87_11295	C9I88_08490	GLP10_01020	CJF27_02890	CJF25_11245	CJF26_12340	GLP34_11045	GLP32_09170	GLP35_10915	GLP37_10645	GLP38_11745	GLP25_12005	GLP44_18530	GLP29_07330
Subunit II CoxB	C9J51_13315	C9J52_05890	C9I87_11290	C9I88_08485	GLP10_01015	CJF27_02885	CJF25_11250	CJF26_12335	GLP34_11050	GLP32_09165	GLP35_10910	GLP37_10640	GLP38_11740	GLP25_12010	GLP44_18525	GLP29_07335
Subunit III CoxC	C9J51_13330	C9J52_05905	C9I87_11305	C9I88_08500	GLP10_01030	CJF27_02900	CJF25_11235	CJF26_12350	GLP34_11035	GLP32_09180	GLP35_10925	GLP37_10655	GLP38_11755	GLP25_11995	GLP44_18540	GLP29_07320
cytochrome c oxidase assembly protein Cox1	C9J51_13325	C9J52_05900	C9I87_11300	C9I88_08495	GLP10_01025	CJF27_02895	CJF25_11240	CJF26_12345	GLP34_11040	GLP32_09175	GLP35_10920	GLP37_10650	GLP38_11750	GLP25_12000	GLP44_18535	GLP29_07325
cytochrome oxidase	C9J51_13345	C9J52_05920	C9I87_11320	C9I88_08515	GLP10_01045	CJF27_02915	CJF25_11220	CJF26_12365	GLP34_11020	GLP32_09195	GLP35_10940	GLP37_10670	GLP38_11770	GLP25_11980	GLP44_18555	GLP29_07305
cytochrome o ubiquinol oxidase subunit IV cyoD	C9J51_12895	C9J52_07855	C9I87_08190	C9I88_11860	GLP10_00315	CJF27_00405	CJF25_12280	CJF26_13210	GLP34_12345	GLP32_07615	GLP35_06525	GLP37_11890	GLP38_05455	GLP25_09750	GLP44_11425	GLP29_12870
cytochrome o ubiquinol oxidase subunit III cyoC	C9J51_12900	C9J52_07860	C9I87_08185	C9I88_11865	GLP10_00320	CJF27_00410	CJF25_12285	CJF26_13215	GLP34_12340	GLP32_07620	TMW22130_GLP37_11885	GLP37_11885	GLP38_05460	GLP25_09755	GLP44_11420	GLP29_12865
cytochrome o ubiquinol oxidase subunit I cyoB	C9J51_12905	C9J52_07865	C9I87_08180	C9I88_11870	GLP10_00325	CJF27_00415	CJF25_12290	CJF26_13220	GLP34_12335	GLP32_07625	GLP35_06535	GLP37_11880	GLP38_05465	GLP25_09760	GLP44_11415	GLP29_12860
CyoA: ubiquinol oxidase, subunit II	C9J51_12910	C9J52_07870	C9I87_08175	C9I88_11875	GLP10_00330	CJF27_00420	CJF25_12295	CJF26_13225	GLP34_12330	GLP32_07630	GLP35_06540	GLP37_11875	GLP38_05470	GLP25_09765	GLP44_11410	GLP29_12855
cyoE ctaB: protoheme IX farnesyltransferase	C9J51_12890	C9J52_07850	C9I87_08195	C9I88_11855	GLP10_00310	CJF27_00400	CJF25_11210	CJF26_12375	GLP34_11010	GLP32_09205	GLP35_10950	GLP37_10680	GLP38_11780	GLP25_11970	GLP44_18565	GLP29_07295
	C9J51_13355	C9J52_05930	C9I87_11330		GLP10_01055	CJF27_02925	CJF25_12275	CJF26_13205	GLP34_12350	GLP32_07610	GLP35_06520	GLP37_11895	GLP38_05450	GLP25_09745	GLP44_11430	GLP29_12875
cytochrome-c oxidase, cbb3-type subunit I ccoN	C9J51_11945	C9J52_04135	C9I87_14900	C9I88_05575	GLP10_03140	CJF27_04900	CJF25_07270	CJF26_06570	GLP34_13320	GLP32_06870	GLP35_10395	GLP37_02905	GLP38_07145	GLP25_06840	GLP44_08305	GLP29_04175
cytochrome-c oxidase, cbb3-type subunit II ccoO	C9J51_11950	C9J52_04130	C9I87_14895	C9I88_05570	GLP10_03135	CJF27_04905	CJF25_07275	CJF26_06565	GLP34_13315	GLP32_06875	GLP35_10400	GLP37_02900	GLP38_07140	GLP25_06835	GLP44_08300	GLP29_04180
cytochrome-c oxidase, cbb3-type subunit III ccoP	C9J51_11955	C9J52_04125	C9I87_14890	C9I88_05565	GLP10_03130	CJF27_04910	CJF25_07280	CJF26_06560	GLP34_13310	GLP32_06880	GLP35_10405	GLP37_02895	GLP38_07135	GLP25_06830	GLP44_08295	GLP29_04185
cbb3-type cytochrome oxidase assembly protein CcoS CcoQ							CJF25_14285	CJF26_14550	GLP34_02980	GLP32_20230	GLP35_03915	GLP37_04085	GLP38_08465	GLP25_09195	GLP44_10515	GLP29_05880
cytochrome bd oxidase																
Subunit I *cyd* A	C9J51_04400	C9J52_11530	C9I87_01485	C9I88_03475	GLP10_07965	CJF27_08445	CJF25_01705	CJF26_04420	GLP34_00680	GLP32_01090	GLP35_01545	GLP37_01340	GLP38_11450	GLP25_05155	GLP44_01900	GLP29_01590
							CJF25_02455	CJF26_05125	GLP34_09530	GLP32_08925	GLP35_00860	GLP37_00665	GLP38_03745	GLP25_04440	GLP44_01195	GLP29_00865
Subunit II *cyd* B	C9J51_04395	C9J52_11525	C9I87_01490	C9I88_03480	GLP10_07960	CJF27_08450	CJF25_02460 + CJF25_01700	CJF26_04415 + CJF26_05130	GLP34_09535 + GLP34_00685	GLP32_01085 + GLP32_08920	GLP35_01550 + GLP35_00855	GLP37_00660 + GLP37_01345	GLP38_11455 + GLP38_03750	GLP25_04435 + GLP25_05160	GLP44_01190 + GLP44_01905	GLP29_00860 + GLP29_01595
subunit cydX	C9J51_04390	C9J52_11520	C9I87_01495	C9I88_03485	GLP10_07955	CJF27_08455	CJF25_01695	CJF26_04410	GLP34_00690	GLP32_01080	GLP35_01555	GLP37_01350	GLP38_11460	GLP25_05165	GLP44_01910	GLP29_01600
							CJF25_02465	CJF26_05135	GLP34_09540	GLP32_08915	GLP35_00850	GLP37_00655	GLP38_03755	GLP25_04430	GLP44_01185	GLP29_00855
NADH:ubiquinone oxidoreductase (ndh)																
	C9J51_03775	C9J52_01565	C9I87_02105	C9I88_11495	GLP10_04915	CJF27_06065	CJF25_01105	CJF26_03800	GLP34_01285	GLP32_00490	GLP35_02165	GLP37_01955	GLP38_06385	GLP25_10725	GLP44_02505	GLP29_02190
Succinate dehydrogenase (complex II)																
sdhABCD	C9J51_04700	C9J52_11830	C9I87_01185	C9I88_03175	GLP10_08265	CJF27_08145	CJF25_02005	CJF26_04720	GLP34_00380	GLP32_01390	GLP35_01245	GLP37_01040	GLP38_11150	GLP25_04855	GLP44_01600	GLP29_01290
	C9J51_04705	C9J52_11835	C9I87_01180	C9I88_03170	GLP10_08270	CJF27_08140	CJF25_02010	CJF26_04725	GLP34_00375	GLP32_01395	GLP35_01240	GLP37_01035	GLP38_11145	GLP25_04850	GLP44_01595	GLP29_01285
	C9J51_04710	C9J52_11840	C9I87_01175	C9I88_03165	GLP10_08275	CJF27_08135	CJF25_02015	CJF26_04730	GLP34_00370	GLP32_01400	GLP35_01235	GLP37_01030	GLP38_11140	GLP25_04845	GLP44_01590	GLP29_01280
	C9J51_04715	C9J52_11845	C9I87_01170	C9I88_03160	GLP10_08280	CJF27_08130	CJF25_02020	CJF26_04735	GLP34_00365	GLP32_01405	GLP35_01230	GLP37_01025	GLP38_11135	GLP25_04840	GLP44_01585	GLP29_01275
cytochrome C																
cytochrome b	C9J51_14345	C9J52_12920	C9I87_13100	C9I88_10925	GLP10_02740	CJF27_03880	CJF25_15255	CJF26_17260	GLP34_11535	GLP32_12295	GLP35_11795	GLP37_12925	GLP38_12735	GLP25_13905	GLP44_13440	GLP29_16485
cytochrome c	C9J51_05560	C9J52_05430	C9I87_00285	C9I88_02260	GLP10_17285	CJF27_16815	CJF25_18840	CJF26_08630	GLP34_10105	GLP32_08355	GLP35_00290	GLP37_00290	GLP38_04315	GLP25_03865	GLP44_00625	GLP29_00290
Cytochrome c	C9J51_11940	C9J52_04140	C9I87_14905	C9I88_05580	GLP10_03145	CJF27_04895	CJF25_07265	CJF26_06575	GLP34_13325	GLP32_06865	GLP35_10390	GLP37_02910	GLP38_07150	GLP25_06845	GLP44_08310	GLP29_04170
cytochrome c4	C9J51_15435	C9J52_10740	C9I87_14640	C9I88_16225	GLP10_11020	CJF27_08770	CJF25_17625	CJF26_15825	GLP34_14965	GLP32_15125	GLP35_16345	GLP37_15090	GLP38_14370	GLP25_15500	GLP44_15460	GLP29_14145
cytochrome C554	C9J51_12655	C9J52_13455	C9I87_08610	C9I88_13625	GLP10_00190	CJF27_00270	CJF25_04665	CJF26_18780	GLP34_05460	GLP32_07320	GLP35_06370	GLP37_19260	GLP38_05270	GLP25_09565	GLP44_11545	GLP29_20015
cytochrome bc complex bzw. cytochrom-c-reductase(Fe-S, b, c1) qcrA/qcrb/qcrC																
	C9J51_14340	C9J52_12915	C9I87_13095	C9I88_10920	GLP10_02735	CJF27_03875	CJF25_15260	CJF26_17265	GLP34_11540	GLP32_12290	GLP35_11790	GLP37_12920	GLP38_12740	GLP25_13900	GLP44_13445	GLP29_16490
	C9J51_14345	C9J52_12920	C9I87_13100	C9I88_10925	GLP10_02740	CJF27_03880	CJF25_15255	CJF26_17260	GLP34_11535	GLP32_12295	GLP35_11795	GLP37_12925	GLP38_12735	GLP25_13905	GLP44_13440	GLP29_16485
	C9J51_14350	C9J52_12925	C9I87_13105	C9I88_10930	GLP10_02745	CJF27_03885	CJF25_15250	CJF26_17255	GLP34_11530	GLP32_12300	GLP35_11800	GLP37_12930	GLP38_12730	GLP25_13910	GLP44_13435	GLP29_16480
Fumarate reductase																
frdABCD	C9J51_17245	C9J52_14775	C9I87_17525	C9I88_15675	GLP10_12205	CJF27_15900	CJF25_17115	CJF26_17755	GLP34_19715	GLP32_17605	GLP35_18460	GLP37_18050	GLP38_18050	GLP25_17910	GLP44_18745	GLP29_17125
	C9J51_17250	C9J52_14770	C9I87_17520	C9I88_15680	GLP10_12200	CJF27_15905	CJF25_17110	CJF26_17760	GLP34_19710	GLP32_17600	GLP35_18465	GLP37_18055	GLP38_18055	GLP25_17905	GLP44_18750	GLP29_17130
	C9J51_17255	C9J52_14765	C9I87_17515	C9I88_15685	GLP10_12195	CJF27_15910	CJF25_17105	CJF26_17765	GLP34_19705	GLP32_17595	GLP35_18470	GLP37_18060	GLP38_18060	GLP25_17900	GLP44_18755	GLP29_17135
	C9J51_17260	C9J52_14760	C9I87_17510	C9I88_15690	GLP10_12190	CJF27_15915	CJF25_17100	CJF26_17770	GLP34_19700	GLP32_17590	GLP35_18475	GLP37_18065	GLP38_18065	GLP25_17895	GLP44_18760	GLP29_17140
Formate dehydrogenase fdhABCE																
A	C9J51_16800	C9J52_12225	C9I87_15300	C9I88_19205	GLP10_17405	CJF27_10545	CJF25_18165	CJF26_09215	GLP34_15600	GLP32_16610	GLP35_17340	GLP37_15600	GLP38_04895	GLP25_16445	GLP44_00040	GLP29_15435
B	C9J51_16805	C9J52_12220	C9I87_15295	C9I88_19210	GLP10_17410	CJF27_10550	CJF25_18170	CJF26_09220	GLP34_15595	GLP32_16605	GLP35_17345	GLP37_15605	GLP38_04900	GLP25_16450	GLP44_00035	GLP29_15440
C	C9J51_16810	C9J52_12215	C9I87_15290	C9I88_19215	GLP10_17415	CJF27_10555	CJF25_18175	CJF26_09225	GLP34_15590	GLP32_16600	GLP35_17350	GLP37_15610	GLP38_04905	GLP25_16455	GLP44_00030	GLP29_15445
E	C9J51_16815	C9J52_12210	C9I87_15285	C9I88_19220	GLP10_17420	CJF27_10560	CJF25_18180	CJF26_09230	GLP34_15585	GLP32_16595	GLP35_17355	GLP37_15615	GLP38_04910	GLP25_16460	GLP44_00025	GLP29_15450
Quinone Q-8 biosynthesis																
Chorismate pyruvate lyase (ubiC)	C9J51_13295	C9J52_05870	C9I87_11270	C9I88_08465	GLP10_00995	CJF27_02865	CJF25_11270	CJF26_12315	GLP34_11070	GLP32_09145	GLP35_10890	GLP37_10620	GLP38_11720	GLP25_12030	GLP44_18505	GLP29_07355

	P. iliopiscarium						*P. phosphoreum*									
	ATCC 51760T	**ATCC 51761**	**NCIMB 13478**	**NCIMB 13481**	**TMW 2.2104**	**TMW 2.2035**	**TMW 2.2033**	**TMW 2.2034**	**TMW 2.2103**	**TMW 2.2125**	**TMW 2.2126**	**TMW 2.2130**	**TMW 2.2132**	**TMW 2.2134**	**TMW 2.2140**	**TMW 2.2142**
4-hydroxybenzoate octaprenyltransferase (ubiA)	C9J51_13300	C9J52_05875	C9I87_11275	C9I88_08470	GLP10_01000	CJF27_02870	CJF25_11265	CJF26_12320	GLP34_11065	GLP32_09150	GLP35_10895	GLP37_10625	GLP38_11725	GLP25_12025	GLP44_18510	GLP29_07350
3-octaprenyl-4-hydroxybenzoate carboxy-lyase (ubiD)	C9J51_18215	C9J52_16995	C9I87_19090	C9I88_17845	GLP10_14535	CJF27_14670	CJF25_20465	CJF26_20155	GLP34_20635	GLP32_18615	GLP35_19900	GLP37_19970	GLP38_20275	GLP25_19085	GLP44_19965	GLP29_19615
2-octaprenylphenol 6-hydroxylase (ubiB)	C9J51_15275	C9J52_10900	C9I87_14480	C9I88_16065	GLP10_11180	CJF27_08610	CJF25_17785	CJF26_15985	GLP34_15125	GLP32_14965	GLP35_16505	GLP37_14930	GLP38_14210	GLP25_15340	GLP44_15620	GLP29_13985
3-demethylubiquinol 3-O-methyltransferase (ubiG)	C9J51_04080	C9J52_01260	C9I87_01805	C9I88_11795	GLP10_04615	CJF27_05765	CJF25_01390	CJF26_04090	GLP34_00995	GLP32_00780	GLP35_01880	GLP37_01670	GLP38_06670	GLP25_11010	GLP44_02215	GLP29_01905
2-octaprenyl-6-methoxyphenyl hydroxylase (ubiH)	C9J51_16255	C9J52_15070	C9I87_15900	C9I88_14355	GLP10_11840	CJF27_09660	CJF25_18940	CJF26_18635	GLP34_18070	GLP32_16200	GLP35_18965	GLP37_18645	GLP38_18380	GLP25_15775	GLP44_19075	GLP29_17950
2-methoxy-6-octaprenyl-1,4-benzoquinol methylase (ubiE)	C9J51_15265	C9J52_10910	C9I87_14470	C9I88_16055	GLP10_11190	CJF27_08600	CJF25_17795	CJF26_15995	GLP34_15135	GLP32_14955	GLP35_16515	GLP37_14920	GLP38_14200	GLP25_15330	GLP44_15630	GLP29_13975
2-octaprenyl-3-methyl-6-methoxy-1,4-benzoquinol hydroxylase (ubiF)	C9J51_15440	C9J52_10735	C9I87_14645	C9I88_16230	GLP10_11015	CJF27_08775	CJF25_17620	CJF26_15820	GLP34_14960	GLP32_15130	GLP35_16340	GLP37_15095	GLP38_14375	GLP25_15505	GLP44_15455	GLP29_14150
ubiCADBGHEF																
F0F1-ATP synthase																
F0F1 ATP synthase subunit A	C9J51_01895	C9J52_11955	C9I87_07275	C9I88_15400	GLP10_03950	CJF27_06600	CJF25_04335	CJF26_01000	GLP34_03605	GLP32_04805	GLP35_09735	GLP37_16500	GLP38_01505	GLP25_02090	GLP44_05385	GLP29_08820
ATP synthase F0 subunit B	C9J51_01885	C9J52_11945	C9I87_07265	C9I88_15410	GLP10_03940	CJF27_06610	CJF25_04345	CJF26_00990	GLP34_03615	GLP32_04815	GLP35_09745	GLP37_16490	GLP38_01495	GLP25_02100	GLP44_05375	GLP29_08810
F0F1 ATP synthase subunit C	C9J51_01890	C9J52_11950	C9I87_07270	C9I88_15405	GLP10_03945	CJF27_06605	CJF25_04340	CJF26_00995	GLP34_03610	GLP32_04810	GLP35_09740	GLP37_16495	GLP38_01500	GLP25_02095	GLP44_05380	GLP29_08815
F0F1 ATP synthase subunit alpha	C9J51_01875	C9J52_11935	C9I87_07255	C9I88_15420	GLP10_03930	CJF27_06620	CJF25_04355	CJF26_00980	GLP34_03625	GLP32_04825	GLP35_09755	GLP37_16480	GLP38_01485	GLP25_02110	GLP44_05365	GLP29_08800
F0F1 ATP synthase subunit beta	C9J51_01865	C9J52_11925	C9I87_07245	C9I88_15430	GLP10_03920	CJF27_06630	CJF25_04365	CJF26_00970	GLP34_03635	GLP32_04835	GLP35_09765	GLP37_16470	GLP38_01475	GLP25_02120	GLP44_05355	GLP29_08790
F0F1 ATP synthase subunit gamma	C9J51_01870	C9J52_11930	C9I87_07250	C9I88_15425	GLP10_03925	CJF27_06625	CJF25_04360	CJF26_00975	GLP34_03630	GLP32_04830	GLP35_09760	GLP37_16475	GLP38_01480	GLP25_02115	GLP44_05360	GLP29_08795
F0F1 ATP synthase subunit delta	C9J51_01880	C9J52_11940	C9I87_07260	C9I88_15415	GLP10_03935	CJF27_06615	CJF25_04350	CJF26_00985	GLP34_03620	GLP32_04820	GLP35_09750	GLP37_16485	GLP38_01490	GLP25_02105	GLP44_05370	GLP29_08805
F0F1 ATP synthase subunit epsilon	C9J51_01860	C9J52_11920	C9I87_07240	C9I88_15435	GLP10_03915	CJF27_06635	CJF25_04370	CJF26_00965	GLP34_03640	GLP32_04840	GLP35_09770	GLP37_16465	GLP38_01470	GLP25_02125	GLP44_05350	GLP29_08785
F0F1 ATP synthase subunit A	C9J51_17015	C9J52_12715	C9I87_17030	C9I88_14820	GLP10_09650	CJF27_11440	CJF25_19910	CJF26_17505	GLP34_16770	GLP32_17090	GLP35_17960	GLP37_16910	GLP38_17450	GLP25_17395	GLP44_16835	GLP29_15670
ATP synthase F0 subunit B	C9J51_17025	C9J52_12725	C9I87_17020	C9I88_14810	GLP10_09660	CJF27_11430	CJF25_19900	CJF26_17495	GLP34_16780	GLP32_17100	GLP35_17950	GLP37_16920	GLP38_17460	GLP25_17405	GLP44_16825	GLP29_15660
F0F1 ATP synthase subunit C	C9J51_17020	C9J52_12720	C9I87_17025	C9I88_14815	GLP10_09655	CJF27_11435	CJF25_19905	CJF26_17500	GLP34_16775	GLP32_17095	GLP35_17955	GLP37_16915	GLP38_17455	GLP25_17400	GLP44_16830	GLP29_15665
F0F1 ATP synthase subunit alpha	C9J51_17035	C9J52_12735	C9I87_17010	C9I88_14800	GLP10_09670	CJF27_11420	CJF25_19890	CJF26_17485	GLP34_16790	GLP32_17110	GLP35_17940	GLP37_16930	GLP38_17470	GLP25_17415	GLP44_16815	GLP29_15650
F0F1 ATP synthase subunit beta	C9J51_17045	C9J52_12745	C9I87_17000	C9I88_14790	GLP10_09680	CJF27_11410	CJF25_19880	CJF26_17475	GLP34_16800	GLP32_17120	GLP35_17930	GLP37_16940	GLP38_17480	GLP25_17425	GLP44_16805	GLP29_15640
F0F1 ATP synthase subunit gamma	C9J51_17040	C9J52_12740	C9I87_17005	C9I88_14795	GLP10_09675	CJF27_11415	CJF25_19885	CJF26_17480	GLP34_16795	GLP32_17115	GLP35_17935	GLP37_16935	GLP38_17475	GLP25_17420	GLP44_16810	GLP29_15645
F0F1 ATP synthase subunit delta	C9J51_17030	C9J52_12730	C9I87_17015	C9I88_14805	GLP10_09665	CJF27_11425	CJF25_19895	CJF26_17490	GLP34_16785	GLP32_17105	GLP35_17945	GLP37_16925	GLP38_17465	GLP25_17410	GLP44_16820	GLP29_15655
F0F1 ATP synthase subunit epsilon	C9J51_17050	C9J52_12750	C9I87_16995	C9I88_14785	GLP10_09685	CJF27_11405	CJF25_19875	CJF26_17470	GLP34_16805	GLP32_17125	GLP35_17925	GLP37_16945	GLP38_17485	GLP25_17430	GLP44_16800	GLP29_15635
ATP F0F1 synthase subunit I	C9J51_17010	C9J52_12710	C9I87_17035	C9I88_14825	GLP10_09645	CJF27_11445	CJF25_19915	CJF26_17510	GLP34_16765	GLP32_17085	GLP35_17965	GLP37_16905	GLP38_17445	GLP25_17390	GLP44_16840	GLP29_15675
Heme biosynthesis																
Glutamyl−tRNA reductase (hemA	C9J51_18815	C9J52_18685	C9I87_19340	C9I88_19690	GLP10_17985	CJF27_11960	CJF25_13575	CJF26_16785	GLP34_20365	GLP32_20405	GLP35_20785	GLP37_16020	GLP38_20580	GLP25_16860	GLP44_13240	GLP29_08175
glutamate-1-semialdehyde-2,1-aminomutase (hemL)	C9J51_11520	C9J52_07065	C9I87_09690	C9I88_08210	GLP10_14230	CJF27_14370	CJF25_12950	CJF26_11465	GLP34_09400	GLP32_10060	GLP35_07820	GLP37_07885	GLP38_10735	GLP25_12830	GLP44_09160	GLP29_04305
aminolevulinic acid dehydratase (hemB)					GLP10_05185	CJF27_02485	CJF25_05400	CJF26_15575	GLP34_04725	GLP32_14220	GLP35_15575	GLP37_14410	GLP38_00450	GLP25_03130	GLP44_04080	GLP29_11970
	C9J51_15300	C9J52_10875	C9I87_14505	C9I88_16090	GLP10_11155	CJF27_08635	CJF25_17760	CJF26_15960	GLP34_15100	GLP32_14990	GLP35_16480	GLP37_14955	GLP38_14235	GLP25_15365	GLP44_15595	GLP29_14010
Hydroxymethylbilane synthase (hemC)	C9J51_15335	C9J52_10840	C9I87_14540	C9I88_16125	GLP10_11120	CJF27_08670	CJF25_17725	CJF26_15925	GLP34_15065	GLP32_15025	GLP35_16445	GLP37_14990	GLP38_14270	GLP25_15400	GLP44_15560	GLP29_14045
Uroporphyrinogen-III synthase (hemD)	C9J51_15330	C9J52_10845	C9I87_14535	C9I88_16120	GLP10_11125	CJF27_08665	CJF25_17730	CJF26_15930	GLP34_15070	GLP32_15020	GLP35_16450	GLP37_14985	GLP38_14265	GLP25_15395	GLP44_15565	GLP29_14040
Uroporphyrinogen decarboxylase (hemE)	C9J51_17445	C9J52_14575	C9I87_17325	C9I88_15875	GLP10_12000	CJF27_16685	CJF25_16910	CJF26_17960	GLP34_19555	GLP32_17400	GLP35_18665	GLP37_18255	GLP38_18255	GLP25_17705	GLP44_18950	GLP29_17330
Coproporphyrinogen III oxidase (oxygen independent) (hemN)	C9J51_15450	C9J52_10725	C9I87_14655	C9I88_16240	GLP10_11005	CJF27_08785	CJF25_17610	CJF26_15810	GLP34_14950	GLP32_15140	GLP35_16330	GLP37_15105	GLP38_14385	GLP25_15515	GLP44_15445	GLP29_14160
Coproporphyrinogen III oxidase (oxygen independent) (hemN)	C9J51_15455	C9J52_10720	C9I87_14660	C9I88_16245	GLP10_11000	CJF27_08790	CJF25_17605	CJF26_15805	GLP34_14945	GLP32_15145	GLP35_16325	GLP37_15110	GLP38_14390	GLP25_15520	GLP44_15440	GLP29_14165
Coproporphyrinogen III oxidase (oxygen dependent)	C9J51_17195	C9J52_12895	C9I87_16850	C9I88_14640	GLP10_09830	CJF27_11260	CJF25_20910	CJF26_17325	GLP34_16950	GLP32_17270	GLP35_17780	GLP37_17090	GLP38_17630	GLP25_17575	GLP44_16655	GLP29_15490
menaquinone-dependent protoporphyrinogen IX dehydrogenase	C9J51_16835	C9J52_12535	C9I87_17210	C9I88_15000	GLP10_09470	CJF27_11620	CJF25_20090	CJF26_17685	GLP34_16590	GLP32_16910	GLP35_18140	GLP37_16730	GLP38_17270	GLP25_17215	GLP44_17015	GLP29_15850
Ferrochelatase (hemH)	C9J51_04810	C9J52_15550	C9I87_01080	C9I88_03070	GLP10_15605	CJF27_15555	CJF25_02125	CJF26_04840	GLP34_00265	GLP32_01505	GLP35_01130	GLP37_00925	GLP38_11035	GLP25_04740	GLP44_01485	GLP29_01175
Virulence																
VOC family virulence protein	C9J51_04945	C9J52_15685	C9I87_00910	C9I88_02895	GLP10_15470	CJF27_15425	CJF25_02305	CJF26_07515	GLP34_13665	GLP32_01685	GLP35_13495	GLP37_06790	GLP38_09330	GLP25_01535	GLP44_06420	GLP29_14445
								CJF26_05060	GLP34_00045		GLP35_00950	GLP37_00745	GLP38_10855	GLP25_04520	GLP44_01305	GLP29_00995
virulence factor BrkB family protein	C9J51_15500	C9J52_10675	C9I87_14700	C9I88_16285	GLP10_10960	CJF27_08830							GLP38_14430		GLP44_15400	
virulence protein	C9J51_02155 + C9J51_02160															
virulence associated protein																
H2O2 related enzymes																
Production																
pyruvate oxidase (Pox)																
superoxide dismutase (Sod)	C9J51_06695	C9J52_08620	C9I87_13995	C9I88_04450	GLP10_18645	CJF27_12650	CJF25_16525	CJF26_09980	GLP34_06085	GLP32_14830	GLP35_05145	GLP37_13765	GLP38_02790	GLP25_06150	GLP44_08225	GLP29_09205
	C9J51_10200	C9J52_11030	C9I87_06080	C9I88_09800	GLP10_16510	CJF27_05470	CJF25_08585	CJF26_07230	GLP34_07960	GLP32_02470	GLP35_15785	GLP37_07075	GLP38_19205	GLP25_01250	GLP44_06720	GLP29_14755
							CJF25_18375	CJF26_10455	GLP34_19075	GLP32_18930	GLP35_12765	GLP37_03885	GLP38_15150	GLP25_07780	GLP44_17500	GLP29_03110
H2O2 scavenging enzymes																
catalase			NCIMB13481_C9I88_16570				CJF25_08575	CJF26_07220	GLP34_07970	GLP32_02460	GLP35_15795	GLP37_07085	GLP38_19215	GLP25_01240	GLP44_06730	GLP29_14765
catalase/peroxidase	C9J51_02940	C9J52_00525	C9I87_04880	C9I88_10475	GLP10_12240	CJF27_12985	CJF25_03250	CJF26_02155	GLP34_07355	GLP32_04150	GLP35_08580	GLP37_05060	GLP38_07970	GLP25_12940	GLP44_11630	GLP29_08540
Pressure response																
TMAO reductase system sensor histidine kinase/response regulator TorS	C9J51_06055	C9J52_03435	C9I87_10565	C9I88_05085	GLP10_07530	CJF27_07950	CJF25_08215	CJF26_05540	GLP34_06695	GLP32_10810	GLP35_04520	GLP37_10245	GLP38_03415	GLP25_05500	GLP44_07605	GLP29_05630
Molecular chaperone Dnak	C9J51_00470	C9J52_02870	C9I87_09525	C9I88_01105	GLP10_17930	CJF27_00030	CJF25_04985	CJF26_15160	GLP34_05145	GLP32_13805	GLP35_15160	GLP37_14825	GLP38_00035	GLP25_03545	GLP44_03665	GLP29_12385
	C9J51_10910	C9J52_18010	C9I87_10320	C9I88_07600	GLP10_17675	CJF27_17215	CJF25_21070	CJF26_12125	GLP34_08740	GLP32_20605	GLP35_07170	GLP37_07135	GLP38_20820	GLP25_12215	GLP44_21700	GLP29_04995
Molecular chaperone DnaJ	C9J51_00475	C9J52_02865	C9I87_09520	C9I88_01100	GLP10_17935	CJF27_00025	CJF25_04990	CJF26_15165	GLP34_05140	GLP32_13810	GLP35_15165	GLP37_14820	GLP38_00040	GLP25_03540	GLP44_03670	GLP29_12380
	C9J51_10905	C9J52_18015	C9I87_10325	C9I88_07595	GLP10_17670	CJF27_17210	CJF25_21065	CJF26_12130	GLP34_08735	GLP32_20600	GLP35_07165	GLP37_07130	GLP38_20815	GLP25_12210	GLP44_21705	GLP29_05000
Molecular chaperone GroEL	C9J51_17285	C9J52_14735	C9I87_17485	C9I88_15715	GLP10_12165	CJF27_15940	CJF25_17075	CJF26_17795	GLP34_19675	GLP32_17565	GLP35_18500	GLP37_18090	GLP38_18090	GLP25_17870	GLP44_18785	GLP29_17165
	C9J51_17280	C9J52_14740	C9I87_17490	C9I88_15710	GLP10_12170	CJF27_15935	CJF25_17080	CJF26_17790	GLP34_19680	GLP32_17570	GLP35_18495	GLP37_18085	GLP38_18085	GLP25_17875	GLP44_18780	GLP29_17160
Co-chaperone GroES	C9J51_17290	C9J52_14730	C9I87_17480	C9I88_15720	GLP10_12160	CJF27_15945	CJF25_17070	CJF26_17800	GLP34_19670	GLP32_17560	GLP35_18505	GLP37_18095	GLP38_18095	GLP25_17865	GLP44_18790	GLP29_17170
								CJF26_21030								
Outer membrane protein OmpH	C9J51_15920	C9J52_13795	C9I87_16370	C9I88_13890	GLP10_09380	CJF27_10830	CJF25_20795	CJF26_16155	GLP34_16185	GLP32_19840	GLP35_18385	GLP37_15905	GLP38_16405	GLP25_16745	GLP44_16230	GLP29_15055
Porin-like protein OmpL					GLP10_06190	CJF27_07405		CJF26_11765	GLP34_09100	GLP32_10360	GLP35_07520	GLP37_07585		GLP25_12530	GLP44_09460	GLP29_04605
							CJF25_13250	CJF26_11765	GLP34_09100	GLP32_10360	GLP35_07520	GLP37_07585	GLP38_10435	GLP25_12530	GLP44_09460	GLP29_04605
Transcription activator system ToxR	C9J51_04825	C9J52_15565	C9I87_01065	C9I88_03055	GLP10_15590	CJF27_15540	CJF25_02140	CJF26_04895	GLP34_00210	GLP32_01520	GLP35_01115	GLP37_00910	GLP38_11020	GLP25_04685	GLP44_01470	GLP29_01160
ToxS	C9J51_04830	C9J52_15570	C9I87_01060	C9I88_03050	GLP10_15585	CJF27_15535	CJF25_02145	CJF26_04900	GLP34_00205	GLP32_01525	GLP35_01110	GLP37_00905	GLP38_11015	GLP25_04680	GLP44_01465	GLP29_01155
RNA polymerase sigma factor RpoE	C9J51_16195	C9J52_15130	C9I87_15840	C9I88_14415	GLP10_11780	CJF27_09600	CJF25_19005	CJF26_18570	GLP34_18005	GLP32_16265	GLP35_18900	GLP37_18710	GLP38_18445	GLP25_15840	GLP44_19140	GLP29_17885
Anti-sigma E factor RseA	C9J51_16190	C9J52_15135	C9I87_15835	C9I88_14420	GLP10_11775	CJF27_09595	CJF25_19010	CJF26_18565	GLP34_18000	GLP32_16270	GLP35_18895	GLP37_18715	GLP38_18450	GLP25_15845	GLP44_19145	GLP29_17880
Sigma-E factor regulatory protein RseB	C9J51_16185	C9J52_15140	C9I87_15830	C9I88_14425	GLP10_11770	CJF27_09590	CJF25_19015	CJF26_18560	GLP34_17995	GLP32_16275	GLP35_18890	GLP37_18720	GLP38_18455	GLP25_15850	GLP44_19150	GLP29_17875
Transcriptional regulator RseC	C9J51_16180	C9J52_15145	C9I87_15825	C9I88_14430	GLP10_11765	CJF27_09585	CJF25_19020	CJF26_18555	GLP34_17990	GLP32_16280	GLP35_18885	GLP37_18725	GLP38_18460	GLP25_15855	GLP44_19155	GLP29_17870
Exodeoxyribonuclease V subunit alpha, RecD	C9J51_15730	C9J52_13605	C9I87_16180	C9I88_14085	GLP10_09205	CJF27_10650	CJF25_20640	CJF26_16360	GLP34_15985	GLP32_19415	GLP35_18200	GLP37_15695	GLP38_16205	GLP25_16545	GLP44_16045	GLP29_14845

	P. iliopiscarium						*P. phosphoreum*									
	ATCC 51760T	**ATCC 51761**	**NCIMB 13478**	**NCIMB 13481**	**TMW 2.2104**	**TMW 2.2035**	**TMW 2.2033**	**TMW 2.2034**	**TMW 2.2103**	**TMW 2.2125**	**TMW 2.2126**	**TMW 2.2130**	**TMW 2.2132**	**TMW 2.2134**	**TMW 2.2140**	**TMW 2.2142**
Salt Response																
Outer membrane protein OmpW																
Major outer membrane protein OmpV																
RNA polymerase sigma factor RpoS	C9J51_01390	C9J52_15820	C9I87_06665	C9I88_00275	GLP10_11355	CJF27_02080	CJF25_05980	CJF26_00430	GLP34_04250	GLP32_05620	GLP35_08945	GLP37_09005	GLP38_00925	GLP25_02670	GLP44_04550	GLP29_10615
	C9J51_16075	C9J52_18820	C9I87_15705	C9I88_14550	GLP10_11660	CJF27_09480	CJF25_19125	CJF26_18450	GLP34_17885	GLP32_16385	GLP35_18780	GLP37_18830	GLP38_18565	GLP25_15960	GLP44_19260	GLP29_17765
	C9J51_09815	C9J52_08560	C9I87_06455	C9I88_09415	GLP10_10640	CJF27_12100	CJF25_09360	CJF26_08010	GLP34_14160	GLP32_03245	GLP35_12995	GLP37_06295	GLP38_09830	GLP25_14910	GLP44_05925	GLP29_13105
Two-component system response regulator OmpR	C9J51_13405	C9J52_05980	C9I87_11380	C9I88_08575	GLP10_01100	CJF27_02970	CJF25_11160	CJF26_12425	GLP34_10960	GLP32_09255	GLP35_11000	GLP37_10730	GLP38_11830	GLP25_11920	GLP44_18615	GLP29_07245
Two-component system sensor histidine kinase EnvZ	C9J51_13410	C9J52_05985	C9I87_11385	C9I88_08580	GLP10_01105	CJF27_02975	CJF25_11155	CJF26_12430	GLP34_10955	GLP32_09265	GLP35_11005	GLP37_10735	GLP38_11835	GLP25_11915	GLP44_18620	GLP29_07240
Porin OmpC/OmpF																
Sodium transporters																
sodium:alanine symporter family protein	C9J51_09185	C9J52_09855	C9I87_02755	C9I88_07360	GLP10_10425	CJF27_06775	CJF25_00395	CJF26_03100	GLP34_01985	GLP32_13025	GLP35_02875	GLP37_02660	GLP38_14770	GLP25_08155	GLP44_03200	GLP29_02880
	C9J51_11390	C9J52_06935	C9I87_09820	C9I88_08080	GLP10_06025	CJF27_07570	CJF25_13080	CJF26_11595	GLP34_09270	GLP32_10190	GLP35_07690	GLP37_07755	GLP38_10605	GLP25_12700	GLP44_09290	GLP29_04435
sodium:alanine (sodium:glycine) symporter family protein	C9J51_09240	C9J52_09800	C9I87_02700	C9I88_07415	GLP10_10370	CJF27_06830	CJF25_00450	CJF26_03155	GLP34_01930	GLP32_13080	GLP35_02820	GLP37_02605	GLP38_14825	GLP25_08100	GLP44_03145	GLP29_02825
sodium:proton antiporter	C9J51_02495	C9J52_00080	C9I87_04425	C9I88_13220	GLP10_14365	CJF27_14500	CJF25_03680	CJF26_01750	GLP34_06950	GLP32_03730	GLP35_08170	GLP37_12260	GLP38_15735	GLP25_13345	GLP44_12070	GLP29_10140
	C9J51_14000	C9J52_13905	C9I87_12800	C9I88_10625	GLP10_02430	CJF27_03570	CJF25_15560	CJF26_18350	GLP34_11840	GLP32_11990	GLP35_11490	GLP37_12620	GLP38_13040	GLP25_13600	GLP44_13780	GLP29_16510
	C9J51_06915	C9J52_08775	C9I87_14175	C9I88_04295	GLP10_16705	CJF27_16300	CJF25_16205	CJF26_09815	GLP34_05860	GLP32_14605	GLP35_14995	GLP37_13525	GLP38_02630	GLP25_06310	GLP44_17785	GLP29_09430
	C9J51_06685	C9J52_08610	C9I87_13985	C9I88_04460	GLP10_18635	CJF27_12640	CJF25_16535	CJF26_09990	GLP34_06095	GLP32_14840	GLP35_05135	GLP37_13775	GLP38_02800	GLP25_06140	GLP44_08215	GLP29_09195
	C9J51_00095	C9J52_18615	C9I87_16740	C9I88_01490	GLP10_16835	CJF27_09325	CJF25_11750	CJF26_06935	GLP34_08275	GLP32_02125	GLP35_16115	GLP37_05950	GLP38_17945	GLP25_00935	GLP44_07045	GLP29_11495
Na+/H+ antiporter	C9J51_11960	C9J52_04120	C9I87_14885	C9I88_05560	GLP10_03125	CJF27_04915	CJF25_07285	CJF26_06555	GLP34_13305	GLP32_06885	GLP35_10410	GLP37_02890	GLP38_07130	GLP25_06825	GLP44_08290	GLP29_04190
Na+/H+ antiporter NhaA	C9J51_11300	C9J52_06845	C9I87_09910	C9I88_07990	GLP10_06115	CJF27_07480	CJF25_13170	CJF26_11685	GLP34_09180	GLP32_10280	GLP35_07600	GLP37_07665	GLP38_10515	GLP25_12610	GLP44_09380	GLP29_04525
Na+/H+ antiporter NhaC	C9J51_06705	C9J52_08630	C9I87_14005	C9I88_04440	GLP10_18655	CJF27_12660	CJF25_16505	CJF26_09970	GLP34_06075	GLP32_14820	GLP35_05155	GLP37_13745	GLP38_02780	GLP25_06160	GLP44_08245	GLP29_09215
Na+/H+ antiporter NhaC													GLP38_03365	GLP25_05550	GLP44_07655	
		C9J52_01045														
							CJF25_05840	CJF26_00290	GLP34_04395	GLP32_05760	GLP35_09085	GLP37_17140	GLP38_00785	GLP25_02810	GLP44_04410	GLP29_18295
Na+/H+ antiporter	C9J51_04555	C9J52_11685	C9I87_01330	C9I88_03320	GLP10_08120	CJF27_08290	CJF25_01860		GLP34_00525	GLP32_01245			GLP38_11295	GLP25_05000		
sodium:proton exchanger																
Na+/H+ antiporter NhaC family protein	C9J51_18855	C9J52_18725	C9I87_19380	C9I88_19650	GLP10_18025	CJF27_11920	CJF25_13615	CJF26_16750	GLP34_20325	GLP32_20445	GLP35_20825	GLP37_16055	GLP38_20620	GLP25_16900	GLP44_13200	GLP29_08135
DASS family sodium-coupled anion symporter / 2-oxoglutarate translocator	C9J51_10145	C9J52_11085	C9I87_06135	C9I88_09740	GLP10_16565	CJF27_05525	CJF25_08985	CJF26_07635	GLP34_13790	GLP32_02870	GLP35_13370	GLP37_06670	GLP38_09455	GLP25_01665	GLP44_06295	GLP29_13475
sodium:phosphate symporter	C9J51_11305	C9J52_06850	C9I87_09905	C9I88_07995	GLP10_06110	CJF27_07485	CJF25_13165	CJF26_11680	GLP34_09185	GLP32_10275	GLP35_07605	GLP37_07670	GLP38_10520	GLP25_12615	GLP44_09375	GLP29_04520
calcium/sodium antiporter	C9J51_14270	C9J52_14130	C9I87_13025	C9I88_10850	GLP10_02665	CJF27_03805	CJF25_15330	CJF26_18120	GLP34_11610	GLP32_12220	GLP35_11720	GLP37_12850	GLP38_12810	GLP25_13830	GLP44_13515	GLP29_16740
DASS family sodium-coupled anion symporter	C9J51_08670	C9J52_07710	C9I87_03320	C9I88_06855	GLP10_09050	CJF27_01245	CJF25_14665	CJF26_14215	GLP34_02650	GLP32_11555	GLP35_03575	GLP37_04465	GLP38_08800	GLP25_08860	GLP44_10185	GLP29_06215
sodium/glutamate symporter	C9J51_12070	C9J52_04015	C9I87_12165	C9I88_05455	GLP10_17135	CJF27_16555	CJF25_07390	CJF26_06450	GLP34_13195	GLP32_06990	GLP35_10520	GLP37_18970	GLP38_07020	GLP25_06720	GLP44_20385	GLP29_13850
dicarboxylate/amino acid:cation symporter	C9J51_06395	C9J52_03780	C9I87_10880	C9I88_04735	GLP10_07850	CJF27_07630	CJF25_08515	CJF26_05230	GLP34_06395	GLP32_15565	GLP35_04835	GLP37_09945	GLP38_03100	GLP25_05845	GLP44_07930	GLP29_05320
Na+:H+ dicarboxylate symporter	C9J51_17510	C9J52_15460	C9I87_12525	C9I88_16615	GLP10_18070	CJF27_17505	CJF25_07735	CJF26_06100	GLP34_17295	GLP32_11285	GLP35_04045	GLP37_17695	GLP38_16670	GLP25_18510	GLP44_14635	GLP29_18020
cation:dicarboxylase symporter family transporter	C9J51_06385	C9J52_03770	C9I87_10870	C9I88_04745	GLP10_07840	CJF27_07640	CJF25_08505	CJF26_05240	GLP34_06405	GLP32_15575	GLP35_04825	GLP37_09955	GLP38_03110	GLP25_05835	GLP44_07920	GLP29_05330
DASS family sodium-coupled anion symporter	C9J51_06145	C9J52_03530	C9I87_10655	C9I88_04995	GLP10_07620	CJF27_07860	CJF25_08300	CJF26_05455	GLP34_06610	GLP32_10715	GLP35_04615	GLP37_10160	GLP38_03315	GLP25_05600	GLP44_07705	GLP29_05545
sodium/solute symporter	C9J51_02730	C9J52_00315	C9I87_04660	C9I88_12990	GLP10_12455	CJF27_13205	CJF25_03515	CJF26_01890	GLP34_07085	GLP32_03870	GLP35_08310	GLP37_12120	GLP38_15595	GLP25_13205	GLP44_11905	GLP29_10280
sodium:solute symporter	C9J51_02035	C9J52_12095	C9I87_07415	C9I88_15260	GLP10_04180	CJF27_06370	CJF25_04060	CJF26_01280	GLP34_03330	GLP32_19035	GLP35_09460	GLP37_20900	GLP38_01780	GLP25_01815	GLP44_15945	GLP29_09095
sodium/solute symporter																
sodium/solute symporter									GLP34_03645							
sodium-dependent transporter							CJF25_02840	CJF26_02605	GLP34_07800	GLP32_04570	GLP35_05830	GLP37_05475	GLP38_08425	GLP25_00420	GLP44_10940	GLP29_20225
sodium/panthothenate symporter	C9J51_17360	C9J52_14660	C9I87_17410	C9I88_15790	GLP10_12090	CJF27_16015	CJF25_17000	CJF26_17870	GLP34_19465	GLP32_17490	GLP35_18575	GLP37_18165	GLP38_18165	GLP25_17795	GLP44_18860	GLP29_17240
sodium/glucose cotransporter	C9J51_00460	C9J52_02880	C9I87_09535	C9I88_01115								GLP37_14835				
melibiose:sodium transporter MelB							CJF25_06615		GLP34_12730	GLP32_06250	GLP35_12440	GLP37_03550	GLP38_07755		GLP44_08935	GLP29_03440
sodium/proline symporter PutP							CJF25_03335	CJF26_02065	GLP34_07265	GLP32_04060	GLP35_08495	GLP37_04975	GLP38_07885	GLP25_13025	GLP44_11720	GLP29_10460
sodium/proline symporter PutP							CJF25_04215	CJF26_01120	GLP34_03485	GLP32_04685	GLP35_09615	GLP37_16620	GLP38_01625	GLP25_01970	GLP44_05505	GLP29_08940
sodium:proline symporter											GLP35_00920					
sodium:proline symporter																
sodium:proline symporter																
bile acid:sodium symporter family protein							CJF25_18210	CJF26_10620	GLP34_12930	GLP32_16005	GLP35_12605	GLP37_03725	GLP38_15310	GLP25_07625	GLP44_17655	GLP29_03270
Motility																
chemotaxis-specific protein-glutamate methyltransferase CheB	C9J51_05150	C9J52_05015	C9I87_00695	C9I88_02670				CJF26_08220	GLP34_09685	GLP32_08770	GLP35_00705		GLP38_03900	GLP25_04285	GLP44_01040	GLP29_00710
chemotaxis protein CheA	C9J51_05155	C9J52_05020	C9I87_00690	C9I88_02665				CJF26_08225	GLP34_09690	GLP32_08765	GLP35_00700		GLP38_03905	GLP25_04280	GLP44_01035	GLP29_00705
protein phosphatase CheZ	C9J51_05160	C9J52_05025	C9I87_00685	C9I88_02660				CJF26_08230	GLP34_09695	GLP32_08760	GLP35_00695		GLP38_03910	GLP25_04275	GLP44_01030	GLP29_00700
chemotaxis protein CheY	C9J51_05165	C9J52_05030	C9I87_00680	C9I88_02655				CJF26_08235	GLP34_09700	GLP32_08755	GLP35_00690		GLP38_03915	GLP25_04270	GLP44_01025	GLP29_00695
RNA polymerase sigma factor FliA	C9J51_05170	C9J52_05035	C9I87_00675	C9I88_02650				CJF26_08240	GLP34_09705	GLP32_08750	GLP35_00685		GLP38_03920	GLP25_04265	GLP44_01020	GLP29_00690
flagellar biosynthesis protein FlhF	C9J51_05180	C9J52_05045	C9I87_00665	C9I88_02640				CJF26_08250	GLP34_09715	GLP32_08740	GLP35_00675		GLP38_03930	GLP25_04255	GLP44_01010	GLP29_00680
flagellar biosynthesis protein FlhA	C9J51_05185	C9J52_05050	C9I87_00660	C9I88_02635				CJF26_08255	GLP34_09720	GLP32_08735	GLP35_00670		GLP38_03935	GLP25_04250	GLP44_01005	GLP29_00675
flagellar biosynthesis protein FlhB	C9J51_05190	C9J52_05055	C9I87_00655	C9I88_02630				CJF26_08260	GLP34_09725	GLP32_08730	GLP35_00665		GLP38_03940	GLP25_04245	GLP44_01000	GLP29_00670
flagellar type III secretion system protein FliR	C9J51_05195	C9J52_05060	C9I87_00650	C9I88_02625				CJF26_08265	GLP34_09730	GLP32_08725	GLP35_00660		GLP38_03945	GLP25_04240	GLP44_00995	GLP29_00665
flagellar biosynthetic protein FliQ	C9J51_05200	C9J52_05065	C9I87_00645	C9I88_02620				CJF26_08270	GLP34_09735	GLP32_08720	GLP35_00655		GLP38_03950	GLP25_04235	GLP44_00990	GLP29_00660
flagellar type III secretion system pore protein FliP	C9J51_05205	C9J52_05070	C9I87_00640	C9I88_02615				CJF26_08275	GLP34_09740	GLP32_08715	GLP35_00650		GLP38_03955	GLP25_04230	GLP44_00985	GLP29_00655
flagellar biosynthetic protein FliO	C9J51_05210	C9J52_05075	C9I87_00635	C9I88_02610				CJF26_08280	GLP34_09745	GLP32_08710	GLP35_00645		GLP38_03960	GLP25_04225	GLP44_00980	GLP29_00650
flagellar motor switch protein FliN	C9J51_05215	C9J52_05080	C9I87_00630	C9I88_02605				CJF26_08285	GLP34_09750	GLP32_08705	GLP35_00640		GLP38_03965	GLP25_04220	GLP44_00975	GLP29_00645
flagellar motor switch protein FliM	C9J51_05220	C9J52_05085	C9I87_00625	C9I88_02600				CJF26_08290	GLP34_09755	GLP32_08700	GLP35_00635		GLP38_03970	GLP25_04215	GLP44_00970	GLP29_00640
flagellar basal body-associated protein FliL	C9J51_05225	C9J52_05090	C9I87_00620	C9I88_02595				CJF26_08295	GLP34_09760	GLP32_08695	GLP35_00630		GLP38_03975	GLP25_04210	GLP44_00965	GLP29_00635
flagella biosynthesis chaperone FliJ	C9J51_05235	C9J52_05100	C9I87_00610	C9I88_02585				CJF26_08305	GLP34_09770	GLP32_08685	GLP35_00620		GLP38_03985	GLP25_04200	GLP44_00955	GLP29_00625
flagellar protein export ATPase FliI	C9J51_05240	C9J52_05105	C9I87_00605	C9I88_02580				CJF26_08310	GLP34_09775	GLP32_08680	GLP35_00615		GLP38_03990	GLP25_04195	GLP44_00950	GLP29_00620
flagellar assembly protein FliH	C9J51_05245	C9J52_05110	C9I87_00600	C9I88_02575				CJF26_08315	GLP34_09780	GLP32_08675	GLP35_00610		GLP38_03995	GLP25_04190	GLP44_00945	GLP29_00615
flagellar motor switch protein FliG	C9J51_05250	C9J52_05115	C9I87_00595	C9I88_02570				CJF26_08320	GLP34_09785	GLP32_08670	GLP35_00605		GLP38_04000	GLP25_04185	GLP44_00940	GLP29_00610
flagellar basal body M-ring protein FliF	C9J51_05255	C9J52_05120	C9I87_00590	C9I88_02565				CJF26_08325	GLP34_09790	GLP32_08665	GLP35_00600		GLP38_04005	GLP25_04180	GLP44_00935	GLP29_00605
flagellar hook-basal body complex protein FliE	C9J51_05260	C9J52_05125	C9I87_00585	C9I88_02560				CJF26_08330	GLP34_09795	GLP32_08660	GLP35_00595		GLP38_04010	GLP25_04175	GLP44_00930	GLP29_00600
flagellar biosynthesis protein FliS	C9J51_05285	C9J52_05150	C9I87_00560	C9I88_02535				CJF26_08355	GLP34_09820	GLP32_08635	GLP35_00570		GLP38_04035	GLP25_04150	GLP44_00905	GLP29_00575
flagellar filament capping protein FliD	C9J51_05290	C9J52_05155	C9I87_00555	C9I88_02530				CJF26_08360	GLP34_09825	GLP32_08630	GLP35_00565		GLP38_04040	GLP25_04145	GLP44_00900	GLP29_00570
flagellar biosynthesis protein FlaG	C9J51_05295	C9J52_05160	C9I87_00550	C9I88_02525				CJF26_08365	GLP34_09830	GLP32_08625	GLP35_00560		GLP38_04045	GLP25_04140	GLP44_00895	GLP29_00565
flagellin	C9J51_05300	C9J52_05165	C9I87_00545	C9I88_02520				CJF26_08370	GLP34_09835	GLP32	GLP35_00555		GLP38_04050	GLP25_04135	GLP44_00890	GLP29_00560
flagellar hook-associated protein FlgL	C9J51_05305	C9J52_05170	C9I87_00540	C9I88_02515				CJF26_08375	GLP34_09840	GLP32_08615	GLP35_00550		GLP38_04055	GLP25_04130	GLP44_00885	GLP29_00550
flagellar hook-associated protein FlgK	C9J51_05310	C9J52_05175	C9I87_00535	C9I88_02510				CJF26_08380	GLP34_09845	GLP32_08610	GLP35_00545		GLP38_04060	GLP25_04125	GLP44_00880	GLP29_00545
flagellar hook protein	C9J51_05315	C9J52_05180	C9I87_00530	C9I88_02505				CJF26_08385	GLP34_09850	GLP32_08605	GLP35_00540		GLP38_04065	GLP25_04120	GLP44_00875	GLP29_00540
flagellar assembly peptidoglycan hydrolase FlgJ	C9J51_05320	C9J52_05185	C9I87_00525	C9I88_02500				CJF26_08390	GLP34_09855	GLP32_08600	GLP35_00535		GLP38_04070	GLP25_04115	GLP44_00870	GLP29_00535
flagellar basal body P-ring protein FlgI	C9J51_05325	C9J52_05190	C9I87_00520	C9I88_02495				CJF26_08395	GLP34_09860	GLP32_08595	GLP35_00530		GLP38_04075	GLP25_04110	GLP44_00865	GLP29_00530
flagellar basal body L-ring protein	C9J51_05330	C9J52_05195	C9I87_00515	C9I88_02490				CJF26_08400	GLP34_09865	GLP32_08590	GLP35_00525		GLP38_04080	GLP25_04105	GLP44_00860	GLP29_00525

	P. iliopiscarium						*P. phosphoreum*									
	ATCC 51760T	**ATCC 51761**	**NCIMB 13478**	**NCIMB 13481**	**TMW 2.2104**	**TMW 2.2035**	**TMW 2.2033**	**TMW 2.2034**	**TMW 2.2103**	**TMW 2.2125**	**TMW 2.2126**	**TMW 2.2130**	**TMW 2.2132**	**TMW 2.2134**	**TMW 2.2140**	**TMW 2.2142**
flagellar basal-body rod protein FlgG	C9J51_05335	C9J52_05200	C9I87_00510	C9I88_02485				CJF26_08405	GLP34_09870	GLP32_08585	GLP35_00520		GLP38_04085	GLP25_04100	GLP44_00855	GLP29_00520
flagellar basal-body rod protein FlgF	C9J51_05340	C9J52_05205	C9I87_00505	C9I88_02480				CJF26_08410	GLP34_09875	GLP32_08580	GLP35_00515		GLP38_04090	GLP25_04095	GLP44_00850	GLP29_00515
flagellar hook protein FlgE	C9J51_05345	C9J52_05210	C9I87_00500	C9I88_02475				CJF26_08415	GLP34_09880	GLP32_08575	GLP35_00510		GLP38_04095	GLP25_04090	GLP44_00845	GLP29_00510
flagellar biosynthesis protein FlgD	C9J51_05350	C9J52_05215	C9I87_00495	C9I88_02470				CJF26_08420	GLP34_09885	GLP32_08570	GLP35_00505		GLP38_04100	GLP25_04085	GLP44_00840	GLP29_00505
flagellar basal body rod protein FlgC	C9J51_05355	C9J52_05220	C9I87_00490	C9I88_02465				CJF26_08425	GLP34_09890	GLP32_08565	GLP35_00500		GLP38_04105	GLP25_04080	GLP44_00835	GLP29_00500
flagellar basal-body rod protein FlgB	C9J51_05360	C9J52_05225	C9I87_00485	C9I88_02460				CJF26_08430	GLP34_09895	GLP32_08560	GLP35_00495		GLP38_04110	GLP25_04075	GLP44_00830	GLP29_00495
chemotaxis protein CheR	C9J51_05365	C9J52_05230	C9I87_00480	C9I88_02455				CJF26_08435	GLP34_09900	GLP32_08555	GLP35_00490		GLP38_04115	GLP25_04070	GLP44_00825	GLP29_00490
chemotaxis protein CheV	C9J51_05370	C9J52_05235	C9I87_00475	C9I88_02450				CJF26_08440	GLP34_09905	GLP32_08550	GLP35_00485		GLP38_04120	GLP25_04065	GLP44_00820	GLP29_00485
flagellar biosynthesis protein FlhB	C9J51_05125	C9J52_04990	C9I87_00720	C9I88_02695	GLP10_15350	CJF27_15250	CJF25_02585	CJF26_08195	GLP34_09660	GLP32_08795	GLP35_00730	GLP37_00535	GLP38_03875	GLP25_04310	GLP44_01065	GLP29_00735
chemotaxis protein CheW	C9J51_05135	C9J52_05000	C9I87_00710	C9I88_02685	GLP10_15360	CJF27_15240	CJF25_02595	CJF26_08205	GLP34_09670	GLP32_08785	GLP35_00720	GLP37_00525	GLP38_03885	GLP25_04300	GLP44_01055	GLP29_00725
chemotaxis protein CheW/hypothetical protein	C9J51_05140	C9J52_05005	C9I87_00705	C9I88_02680	GLP10_15365		CJF25_02600	CJF26_08210	GLP34_09675	GLP32_08780	GLP35_00715	GLP37_00520	GLP38_03890	GLP25_04295	GLP44_01050	GLP29_00720
flagellar biosynthesis anti-sigma factor FlgM	C9J51_05380	C9J52_05245	C9I87_00465	C9I88_02440	GLP10_15390	CJF27_15210	CJF25_02635	CJF26_08450	GLP34_09915	GLP32_08540	GLP35_00475	GLP37_00480	GLP38_04130	GLP25_04055	GLP44_00810	GLP29_00475
flagellar protein FlgN	C9J51_05385	C9J52_05250	C9I87_00460	C9I88_02435	GLP10_15395	CJF27_15205	CJF25_02640	CJF26_08455	GLP34_09920	GLP32_08535	GLP35_00470	GLP37_00475	GLP38_04135	GLP25_04050	GLP44_00805	GLP29_00470
flagellar biosynthesis protein FlgP	C9J51_05390	C9J52_05255	C9I87_00455	C9I88_02430	GLP10_15400	CJF27_15200	CJF25_02645	CJF26_08460	GLP34_09925	GLP32_08530	GLP35_00465	GLP37_00470	GLP38_04140	GLP25_04045	GLP44_00800	GLP29_00465
flagellar basal-body protein	C9J51_05400	C9J52_05265	C9I87_00445	C9I88_02420	GLP10_15410	CJF27_15190	CJF25_02655	CJF26_08470	GLP34_09935	GLP32_08520	GLP35_00455	GLP37_00460	GLP38_04150	GLP25_04035	GLP44_00790	GLP29_00455
flagellar export chaperone FliS	C9J51_05280	C9J52_05145	C9I87_00565	C9I88_02540			CJF25_02625	CJF26_08350	GLP34_09815	GLP32_08640	GLP35_00575	GLP37_00490	GLP38_04030	GLP25_04155	GLP44_00910	GLP29_00580
flagella basal body P-ring formation protein FlgA	C9J51_05375	C9J52_05240	C9I87_00470	C9I88_02445	GLP10_15385	CJF27_15215	CJF25_02630	CJF26_08445	GLP34_09910	GLP32_08545	GLP35_00480	GLP37_00485	GLP38_04125	GLP25_04060	GLP44_00815	GLP29_00480
Bioluminescence																
Phosphorelay protein LuxU	C9J51_06615	C9J52_03975	C9I87_11085	C9I88_04535	GLP10_14125	CJF27_12575	CJF25_16620	CJF26_10075	GLP34_06185	GLP32_15360	GLP35_05045	GLP37_21900	GLP38_02890	GLP25_06055	GLP44_08130	GLP29_05105
transcriptional regulator quorum sensing regulator LuxR	C9J51_14595	C9J52_13170	C9I87_13360	C9I88_11175	GLP10_03020	CJF27_04160	CJF25_15005	CJF26_17015	GLP34_11290	GLP32_12540	GLP35_12050	GLP37_13170	GLP38_12475	GLP25_14150	GLP44_21100	GLP29_16240
lux-rib operon																
ribB	C9J51_05790	C9J52_05660	C9I87_00050	C9I88_02025	GLP10_14750	CJF27_15000	CJF25_03290 + CJF25_18605	CJF26_02110 + CJF26_08860	GLP34_07310 + GLP34_10335	GLP32_04105 + GLP32_08120	GLP35_00055 + GLP35_08540	GLP37_00055 + GLP37_05020	GLP38_04545 + GLP38_07930	GLP25_03630 + GLP25_12980	GLP44_00390 + GLP44_11675	GLP29_00055 + GLP29_10505
luxC							CJF25_03325	CJF26_02075	GLP34_07275	GLP32_04070	GLP35_08505	GLP37_04985	GLP38_07895	GLP25_13015	GLP44_11710	GLP29_10470
Activated long-chain acyl hydrolase luxD							CJF25_03320	CJF26_02080	GLP34_07280	GLP32_04075	GLP35_08510	GLP37_04990	GLP38_07900	GLP25_13010	GLP44_11705	GLP29_10475
luxE							CJF25_03300	CJF26_02100	GLP34_07300	GLP32_04095	GLP35_08530	GLP37_05010	GLP38_07920	GLP25_12990	GLP44_11685	GLP29_10495
luxF							CJF25_03305	CJF26_02095	GLP34_07295	GLP32_04090	GLP35_08525	GLP37_05005	GLP38_07915	GLP25_12995	GLP44_11690	GLP29_10490
luxG							CJF25_03295	CJF26_02105	GLP34_07305	GLP32_04100	GLP35_08535	GLP37_05015	GLP38_07925	GLP25_12985	GLP44_11680	GLP29_10500
Beta subunit luciferase luxB							CJF25_03310	CJF26_02090	GLP34_07290	GLP32_04085	GLP35_08520	GLP37_05000	GLP38_07910	GLP25_13000	GLP44_11695	GLP29_10485
Alpha subunit luciferase luxA							CJF25_03315	CJF26_02085	GLP34_07285	GLP32_04080	GLP35_08515	GLP37_04995	GLP38_07905	GLP25_13005	GLP44_11700	GLP29_10480
quorum sensing regulator LuxR	C9J51_12690	C9J52_13490	C9I87_08575	C9I88_13660	GLP10_00225	CJF27_00305	CJF25_04630	CJF26_18815	GLP34_05495	GLP32_07355	GLP35_06405	GLP37_19225	GLP38_05305	GLP25_09600	GLP44_11510	GLP29_20050
hot-dog/esterase																
esterase FrsA	C9J51_05635	C9J52_05505	C9I87_00210	C9I88_02185	GLP10_17210	CJF27_16890	CJF25_18765	CJF26_08705	GLP34_10180	GLP32_08280	GLP35_00215	GLP37_00215	GLP38_04390	GLP25_03790	GLP44_00550	GLP29_00215
esterase YqiA	C9J51_14835	C9J52_10290	C9I87_13585	C9I88_12545	GLP10_08550	CJF27_10095	CJF25_15950	CJF26_14945	GLP34_15390	GLP32_13410	GLP35_13880	GLP37_14020	GLP38_13420	GLP25_14580	GLP44_12340	GLP29_19440
													GLP38_21315		GLP44_18185	
Shock /stress																
cold-shock protein	C9J51_01415 + C9J51_02830 + C9J51_02895 + C9J51_09100	C9J52_00415 + C9J52_00480 + C9J52_09940 + C9J52_15845	C9I87_02840 + C9I87_04760 + C9I87_04835 + C9I87_06685	C9I88_00250 + C9I88_07280 + C9I88_10520 + C9I88_10585	GLP10_10505 + GLP10_11380 + GLP10_12285 + GLP10_12355	CJF27_02060 + CJF27_06695 + CJF27_13030 + CJF27_13105	CJF25_03350 + CJF25_03410 + CJF25_06005 + CJF25_07515 + CJF25_13505 + CJF25_20520	CJF26_00455 + CJF26_01995 + CJF26_02055 + CJF26_06320 + CJF26_12020 + CJF26_20210	GLP34_04220 + GLP34_07195 + GLP34_07255 + GLP34_08845 + GLP34_13065 + GLP34_20690	GLP32_03985 + GLP32_04050 + GLP32_05590 + GLP32_07115 + GLP32_10615 + GLP32_18560	GLP35_07280 + GLP35_08420 + GLP35_08485 + GLP35_08915 + GLP35_10645	GLP37_07345 + GLP37_09035 + GLP37_11945 + GLP37_12010 + GLP37_19100 + GLP37_19915	GLP38_00955 + GLP38_06890 + GLP38_10195 + GLP38_15405 + GLP38_15485 + GLP38_20220	GLP25_02640 + GLP25_06590 + GLP25_12285 + GLP25_13035 + GLP25_13095 + GLP25_19030	GLP44_04580 + GLP44_09700 + GLP44_11730 + GLP44_11795 + GLP44_20020 + GLP44_20260	GLP29_04860 + GLP29_10390 + GLP29_10450 + GLP29_10645 + GLP29_13720
	C9J51_01415 + C9J51_02830 + C9J51_02895 + C9J51_03000 + C9J51_08130 + C9J51_18260 + C9J51_18270	C9J52_00415 + C9J52_00480 + C9J52_00600 + C9J52_07215 + C9J52_15845 + C9J52_17040 + C9J52_17050	C9I87_03820 + C9I87_04760 + C9I87_04835 + C9I87_04945 + C9I87_06685 + C9I87_19135 + C9I87_19145	C9I88_00250 + C9I88_06645 + C9I88_10415 + C9I88_10520 + C9I88_10585 + C9I88_17890 + C9I88_17900	GLP10_11380 + GLP10_12285 + GLP10_12355 + GLP10_14480 + GLP10_14490 + GLP10_14970	CJF27_02060 + CJF27_13030 + CJF27_13105 + CJF27_14615 + CJF27_14625 + CJF27_14880	CJF25_03350 + CJF25_03410 + CJF25_06005 + CJF25_06695 + CJF25_07515 + CJF25_13505 + CJF25_18400 + CJF25_20510 + CJF25_20520	CJF26_00455 + CJF26_01995 + CJF26_02055 + CJF26_06320 + CJF26_10430 + CJF26_10850 + CJF26_12020 + CJF26_20200 + CJF26_20210	GLP34_04220 + GLP34_07195 + GLP34_07255 + GLP34_08845 + GLP34_12650 + GLP34_13065 + GLP34_19050 + GLP34_20680 + GLP34_20690	GLP32_03985 + GLP32_04050 + GLP32_05590 + GLP32_06330 + GLP32_07115 + GLP32_10615 + GLP32_18560 + GLP32_18570 + GLP32_18905	GLP35_07280 + GLP35_08420 + GLP35_08485 + GLP35_08915 + GLP35_10645 + GLP35_12365 + GLP35_12790 + GLP35_19945 + GLP35_19955	GLP37_03470 + GLP37_03910 + GLP37_07345 + GLP37_09035 + GLP37_11945 + GLP37_12010 + GLP37_19100 + GLP37_19915 + GLP37_19925	GLP38_00955 + GLP38_06890 + GLP38_07685 + GLP38_10195 + GLP38_15125 + GLP38_15405 + GLP38_15485 + GLP38_20220 + GLP38_20230	GLP25_02640 + GLP25_06590 + GLP25_07385 + GLP25_07805 + GLP25_12285 + GLP25_13035 + GLP25_13095 + GLP25_19030 + GLP25_19040	GLP44_20010 + GLP44_08870 + GLP44_04580 + GLP44_11730 + GLP44_11795 + GLP44_20020 + GLP44_20260 + GLP44_17475 + GLP44_09700	GLP29_03515 + GLP29_04860 + GLP29_10390 + GLP29_10450 + GLP29_10645 + GLP29_13720 + GLP29_19660 + GLP29_19955
	C9J51_18390	C9J52_17645	C9I87_18730	C9I88_17535	GLP10_13610	CJF27_13940	CJF25_17305	CJF26_19895	GLP34_19240	GLP32_17985	GLP35_19430	GLP37_19785	GLP38_19860	GLP25_18880	GLP44_19705	GLP29_18625
	C9J51_08135	C9J52_07220	C9I87_03815	C9I88_06650	GLP10_06865	CJF27_01755	CJF25_18405	CJF26_10425	GLP34_19045	GLP32_18900	GLP35_12795	GLP37_03915	GLP38_15120	GLP25_07810	GLP44_17470	GLP29_19950
	C9J51_16315	C9J52_15010	C9I87_15960	C9I88_14295	GLP10_11900	CJF27_09720	CJF25_18875	CJF26_18700	GLP34_18135	GLP32_16135	GLP35_19030	GLP37_18580	GLP38_18315	GLP25_15710	GLP44_19010	GLP29_18015
	C9J51_12205 + C9J51_19115	C9J52_18185	C9I87_12295	C9I88_19900								GLP37_17800				
		C9J52_14395		C9I88_05325												
cold shock domain protein CspD	C9J51_06515	C9J52_03875	C9I87_10985	C9I88_04635	GLP10_14035	CJF27_12485	CJF25_16720	CJF26_10180	GLP34_06290	GLP32_15465	GLP35_04940	GLP37_09850	GLP38_02995	GLP25_05950	GLP44_08025	GLP29_05210
phage shock protein C / envelope stress response membrane protein PspC	C9J51_03955	C9J52_01385	C9I87_01925	C9I88_11675	GLP10_04735	CJF27_05885	CJF25_01265	CJF26_03965	GLP34_01120	GLP32_00655	GLP35_02005	GLP37_01795	GLP38_06545	GLP25_10885	GLP44_02340	GLP29_02030
phage shock protein B / envelope stress response membrane protein PspB	C9J51_03960	C9J52_01380	C9I87_01920	C9I88_11680	GLP10_04730	CJF27_05880	CJF25_01270	CJF26_03970	GLP34_01115	GLP32_00660	GLP35_02000	GLP37_01790	GLP38_06550	GLP25_10890	GLP44_02335	GLP29_02025
phage shock protein PspA	C9J51_03965	C9J52_01375	C9I87_01915	C9I88_11685	GLP10_04725	CJF27_05875	CJF25_01275	CJF26_03975	GLP34_01110	GLP32_00665	GLP35_01995	GLP37_01785	GLP38_06555	GLP25_10895	GLP44_02330	GLP29_02020
phage shock protein A							CJF25_03215	CJF26_02210	GLP34_07410	GLP32_04190	GLP35_06230	GLP37_05095	GLP38_08050	GLP25_00045	GLP44_10550	GLP29_08500
phage shock protein operon transcriptional activator	C9J51_03970	C9J52_01370					CJF25_01280	CJF26_03980	GLP34_01105	GLP32_00670	GLP35_01990	GLP37_01780	GLP38_06560	GLP25_10900	GLP44_02325	GLP29_02015
phage shock protein G / envelope stress response protein PspG	C9J51_18375	C9J52_17660	C9I87_18745	C9I88_17520	GLP10_13625	CJF27_13955	CJF25_17325	CJF26_19915	GLP34_19260	GLP32_17965	GLP35_19410	GLP37_19805	GLP38_19840	GLP25_18860	GLP44_19725	GLP29_18605
heat-shock protein Hsp20	C9J51_00465	C9J52_02875	C9I87_09530	C9I88_01110	GLP10_17925	CJF27_00035	CJF25_04980	CJF26_15155	GLP34_05150	GLP32_13800	GLP35_15155	GLP37_14830	GLP38_00030	GLP25_03550	GLP44_03660	GLP29_12390
heat-shock protein / META domain-containing protein	C9J51_07590	C9J52_17110	C9I87_18980	C9I88_17940	GLP10_15055	CJF27_11830	CJF25_13710	CJF26_16640	GLP34_17005	GLP32_17670	GLP35_14085	GLP37_16165	GLP38_15810	GLP25_17005	GLP44_13090	GLP29_08025
heat-shock protein HslJ / META domain-containing protein	C9J51_01535	C9J52_16050	C9I87_06885	C9I88_00130	GLP10_11560	CJF27_01880	CJF25_06215	CJF26_00665	GLP34_03965	GLP32_05340	GLP35_08700	GLP37_09290	GLP38_01170	GLP25_02425	GLP44_04790	GLP29_10900
	C9J51_17645	C9J52_15325	C9I87_12660	C9I88_16750	GLP10_13775	CJF27_14110	CJF25_07890	CJF26_05945	GLP34_17450	GLP32_11130	GLP35_04200	GLP37_17540	GLP38_20540	GLP25_18355	GLP44_14480	GLP29_18175
ribosome-associated heat shock protein Hsp15	C9J51_15530	C9J52_10645	C9I87_14730	C9I88_19255	GLP10_10930	CJF27_08860	CJF25_17535	CJF26_15735	GLP34_14870	GLP32_15215	GLP35_16255	GLP37_15185	GLP38_14460	GLP25_15590	GLP44_15370	GLP29_14240
oxidative-stress-resistance chaperone / DJ-1 family protein	C9J51_05735	C9J52_05605	C9I87_00105	C9I88_02080	GLP10_14805	CJF27_15055	CJF25_18660	CJF26_08805	GLP34_10280	GLP32_08175	GLP35_00110	GLP37_00110	GLP38_04490	GLP25_03685	GLP44_00445	GLP29_00110
GlsB/YeaQ/YmgE family stress response membrane protein	C9J51_00700	C9J52_02640	C9I87_09290	C9I88_00870	GLP10_05075	CJF27_02595										
peroxide stress protein YaaA	C9J51_11385	C9J52_06930	C9I87_09825	C9I88_08075	GLP10_06030	CJF27_07565			GLP34_09265	GLP32_10195	GLP35_07685		GLP38_10600	GLP25_12695	GLP44_09295	
outer membrane-stress sensor serine endopeptidase DegS	C9J51_14310	C9J52_14170	C9I87_13065	C9I88_10890	GLP10_02705	CJF27_03845	CJF25_15290	CJF26_17295	GLP34_11570		GLP35_11760	GLP37_12890	GLP38_12770	GLP25_13870	GLP44_13475	GLP29_16780
stress response translation initiation inhibitor YciH	C9J51_09660	C9J52_08380	C9I87_07675	C9I88_12375	GLP10_00790	CJF27_00890	CJF25_12825	CJF26_13780	GLP34_17725	GLP32_19655	GLP35_07105	GLP37_11310	GLP38_10030	GLP25_19330	GLP44_05710	GLP29_19765
stress response serine/threonine protein kinase YihE	C9J51_17110	C9J52_12810	C9I87_16935	C9I88_14725	GLP10_09745	CJF27_11345	CJF25_20995	CJF26_17410	GLP34_16865	GLP32_17185	GLP35_17865	GLP37_17005	GLP38_17545	GLP25_17490	GLP44_16740	GLP29_15575
oxidative stress defense protein	C9J51_16290	C9J52_15035	C9I87_15935	C9I88_14320	GLP10_11875	CJF27_09695										
universal stress protein	C9J51_15215	C9J52_10960	C9I87_14420	C9I88_16005	GLP10_11240	CJF27_08550	CJF25_17845	CJF26_16045	GLP34_15185	GLP32_14905	GLP35_16565	GLP37_14870	GLP38_14150	GLP25_15280	GLP44_15680	GLP29_13925
	C9J51_10990	C9J52_17910	C9I87_10220	C9I88_07680	GLP10_06415	CJF27_07180	CJF25_13495	CJF26_12010	GLP34_08855	GLP32_10605	GLP35_07290	GLP37_07355	GLP38_10205	GLP25_12300	GLP44_09690	GLP29_04850
universal stress protein UspE	C9J51_08325	C9J52_07405	C9I87_03625		GLP10_06675	CJF27_01565	CJF25_14300	CJF26_14535	GLP34_02965	GLP32_20215	GLP35_03900	GLP37_04100	GLP38_08480	GLP25_09180	GLP44_10500	GLP29_05895
universal stress protein UspB	C9J51_18245	C9J52_17025	C9I87_19120	C9I88_17875	GLP10_14505	CJF27_14640	CJF25_20495	CJF26_20185	GLP34_20665	GLP32_18585	GLP35_19930	GLP37_19940	GLP38_20245	GLP25_19055	GLP44_19995	GLP29_19645

	P. iliopiscarium						*P. phosphoreum*									
	ATCC 51760T	**ATCC 51761**	**NCIMB 13478**	**NCIMB 13481**	**TMW 2.2104**	**TMW 2.2035**	**TMW 2.2033**	**TMW 2.2034**	**TMW 2.2103**	**TMW 2.2125**	**TMW 2.2126**	**TMW 2.2130**	**TMW 2.2132**	**TMW 2.2134**	**TMW 2.2140**	**TMW 2.2142**
universal stress global response regulator UspA	C9J51_18235	C9J52_17015	C9I87_19110	C9I88_17865	GLP10_14515	CJF27_14650	CJF25_20485	CJF26_20175	GLP34_20655	GLP32_18595	GLP35_19920	GLP37_19950	GLP38_20255	GLP25_19065	GLP44_19985	GLP29_19635
envelope stress sensor histidine kinase CpxA / two-component system sensor histidine kinase	C9J51_13620	C9J52_06195	C9I87_11595	C9I88_08785	GLP10_01315	CJF27_03190	CJF25_10940	CJF26_12645	GLP34_10740	GLP32_09480	GLP35_11220	GLP37_10950	GLP38_12050	GLP25_11700	GLP44_14905	GLP29_07020
NirD/YgiW/YdeI family stress tolerance protein / hypothetical protein	C9J51_01025	C9J52_02310	C9I87_08900	C9I88_00540	GLP10_05375	CJF27_02290	CJF25_00690	CJF26_03390	GLP34_01695	GLP32_00075	GLP35_02585	GLP37_02365	GLP38_05980	GLP25_10315	GLP44_02910	GLP29_02585
	C9J51_16325	C9J52_15000	C9I87_15970	C9I88_14285	GLP10_11905	CJF27_09725	CJF25_05710	CJF26_00160	GLP34_04525	GLP32_05890	GLP35_09215	GLP37_17270	GLP38_00655	GLP25_02940	GLP44_04280	GLP29_18425
Iron																
ferrous iron transport protein C	C9J51_04645	C9J52_11775	C9I87_01240	C9I88_03230	GLP10_08210	CJF27_08200	CJF25_01950	CJF26_04665	GLP34_00435	GLP32_01335	GLP35_01300	GLP37_01095	GLP38_11205	GLP25_04910	GLP44_01655	GLP29_01345
ferrous iron transport protein A	C9J51_04655	C9J52_11785	C9I87_01230	C9I88_03220	GLP10_08220	CJF27_08190	CJF25_01960	CJF26_04675	GLP34_00425	GLP32_01345	GLP35_01290	GLP37_01085	GLP38_11195	GLP25_04900	GLP44_01645	GLP29_01335
ferrous iron transport protein B	C9J51_04650	C9J52_11780	C9I87_01235	C9I88_03225	GLP10_08215	CJF27_08195	CJF25_01955	CJF26_04670	GLP34_00430	GLP32_01340	GLP35_01295	GLP37_01090	GLP38_11200	GLP25_04905	GLP44_01650	GLP29_01340
	C9J51_01945	C9J52_12005	C9I87_07325	C9I88_15350	GLP10_04090	CJF27_06460	CJF25_04160	CJF26_01175	GLP34_03430	GLP32_04630	GLP35_09560	GLP37_16675	GLP38_01680	GLP25_01915	GLP44_05560	GLP29_08995
ferric iron uptake transcriptional regulator	C9J51_04765	C9J52_15505	C9I87_09455	C9I88_01035	GLP10_18820	CJF27_17830	CJF25_02075	CJF26_04790	GLP34_00315	GLP32_01455	GLP35_01180	GLP37_00975	GLP38_11085	GLP25_04790	GLP44_01535	GLP29_01225
iron chelate uptake ABC transporter family permease subunit	C9J51_00535	C9J52_02805	C9I87_13345	C9I88_11160	GLP10_03005	CJF27_04145	CJF25_05050	CJF26_15225	GLP34_05075	GLP32_13870	GLP35_15225	GLP37_14760	GLP38_00100	GLP25_03480	GLP44_03730	GLP29_12320
iron ABC transporter substrate-binding protein	C9J51_14580	C9J52_13155	C9I87_13350	C9I88_11165	GLP10_03010	CJF27_04150	CJF25_15020	CJF26_17030	GLP34_11305	GLP32_12525	GLP35_12035	GLP37_13155	GLP38_12490	GLP25_14135	GLP44_21085	GLP29_16255
iron chelate uptake ABC transporter family permease subunit	C9J51 11855	C9J52 04225	C9I87 07810	C9I88 12240	GLP10 00655	CJF27 00745	CJF25 07175	CJF26 11310	GLP34 11935	GLP32 07985	GLP35 10295	GLP37 03000	GLP38 05830	GLP25 10175	GLP44 11020	
	C9J51_09525	C9J52_08240	C9I87_07325	C9I88_15350	GLP10_04090	CJF27_06460	CJF25_12655	CJF26_13620			GLP35_06925	GLP37_11480				
iron ABC transporter	C9J51_16980	C9J52_12680	C9I87_17070	C9I88_14860	GLP10_09610	CJF27_11480	CJF25_05055	CJF26_15230	GLP34_16730	GLP32_13875	GLP35_15230	GLP37_14755	GLP38_00105	GLP25_03475	GLP44_03735	GLP29_12315
	C9J51_16975	C9J52_12675					CJF25_19945	CJF26_17540	GLP34_05070	GLP32_17055	GLP35_17995	GLP37_16875	GLP38_17415	GLP25_17360	GLP44_16870	GLP29_15705
iron ABC transporter permease	C9J51_14585	C9J52_13160	C9I87_14990	C9I88_05665	GLP10_03230	CJF27_04810	CJF25_15015	CJF26_17025	GLP34_16735 GLP34_11300	GLP32_12530	GLP35_12040	GLP37_13160	GLP38_12485	GLP25_14140	GLP44_21090	GLP29_16250
							CJF25_07175	CJF26_11310	GLP34_13415	GLP32_06775	GLP35_10295	GLP37_03000	GLP38_07240	GLP25_06935	GLP44_08400	GLP29_04085
							CJF25_13390	CJF26_11905	GLP34_08960	GLP32_10500						GLP29_04745
manganese/iron ABC transporter ATP-binding protein				C9I88 19870												
iron-siderophore ABC transporter substrate-binding protein							CJF25_11820	CJF26_06865	GLP34_08340	GLP32_02060			GLP38_18010	GLP25_00870		GLP29_11560
Marine polyssacharides																
Xylose																
endoxylanase	C9J51_02695	C9J52_00280	C9I87_04625	C9I88_13025			CJF25_03580	CJF26_01855	GLP34_07050	GLP32_03835	GLP35_08275	GLP37_12155	GLP38_15630	GLP25_13240	GLP44_11970	GLP29_10245
xylosidase																
xylG: D-xylose ABC transporter, ATP-binding protein							CJF25 09390	CJF26 08040	GLP34 17565	GLP32 03270	GLP35 12970	GLP37 06270	GLP38 09855	GLP25 14885	GLP44 05900	GLP29 13080
ABC_transporter,_permease_protein_(cluster_2,_ribose/xylose/arabinose/galactose)							CJF25_09385	CJF26_08035	GLP34_17560	GLP32_03265	GLP35_12975	GLP37_06275	GLP38_09850	GLP25_14890	GLP44_05905	GLP29_13085
Laminarin																
laminarinase																
Chondroitin sulphate																
chondriotinase			C9I87_07090	C9I88_15570			CJF25_03555		GLP34_03010						GLP44_11945	
chondroitin sulphate lyase																
Arabinogalactan																
galactanase																
beta-galactosidase							CJF25_06620		GLP34_12725	GLP32_06255	GLP35_12435	GLP37_03545	GLP38_07750		GLP44_08930	GLP29_03445
beta-galactosidase subunit beta	C9J51_12050	C9J52_04035	C9I87_12145	C9I88_05475	GLP10_17155	CJF27_16575	CJF25_07370	CJF26_06470	GLP34_13215	GLP32_06970	GLP35_10500	GLP37_18950	GLP38_07040	GLP25_06740	GLP44_20405	GLP29_13870
beta-galactosidase subunit alpha	C9J51_12045	C9J52_04040	C9I87_12140	C9I88_05480	GLP10_17160	CJF27_16580	CJF25_07365	CJF26_06475	GLP34_13220	GLP32_06965	GLP35_10495	GLP37_18945	GLP38_07045	GLP25_06745	GLP44_20410	GLP29_13875
arabinofuranosidase																
arabinopyranosidase																
Pullulan																
pullulanase	C9J51_10565	C9J52_17825	C9I87_05710	C9I88_01900	GLP10_07205	CJF27_05140										
Fucoidan																
fucoidase																
L-fucose:H+ symporter permease	C9J51_01760	C9J52_16275	C9I87_07120	C9I88_15540	GLP10_03865	CJF27_16985	CJF25_06450	CJF26_00900	GLP34_03730	GLP32_04915	GLP35_09905	GLP37_09730	GLP38_01405	GLP25_02190	GLP44_05215	GLP29_08720
L-fucose:H+ symporter permease																
L-fucose isomerase																
L-fuculokinase																
L-fucose mutarotase																
L-fuculose-phosphate aldolase																
Chitin																
chitinase	C9J51 09235	C9J52 09805	C9I87 02705	C9I88 07410	GLP10 10375	CJF27 06825	CJF25 05285	CJF26 15460	GLP34 04840	GLP32 14105	GLP35 15460	GLP37 14525	GLP38 00335	GLP25 03245	GLP44 03965	GLP29 12085
	C9J51_00695	C9J52_02645	C9I87_09295	C9I88_00875												

	P. phosphoreum															
	AK-3	**AK-4**	**AK-5**	**AK-8**	**ATCC 11040**	**FS-1.1**	**FS-1.2**	**FS-2.1**	**FS-2.2**	**FS-3.2**	**FS-4.1**	**FS-4.2**	**FS-5.1**	**FS-5.2**	**FS-6.1**	**GCSL-P69**
Pentose phosphate pathway																
6-phosphogluconolactonase (dev B)	CTM87_16905	C9J22_09375	C9J21_05905	CTM67_08650	CTM77_08515	CTM76_02885	CTM93_00750	CTM79_01790	C9J19_17790	DAT36_10770	CTM80_12300	CTM85_12755	CTM70_05645	CTM75_11255	C9J18_07865	AYY26_16395
Phosphogluconate dehydrogenase (gnt Z)	CTM87_16910	C9J22_09380	C9J21_05910	CTM67_08645	CTM77_08520	CTM76_02880	CTM93_00755	CTM79_01795	C9J19_17785	DAT36_10765	CTM80_12305	CTM85_12760	CTM70_05640	CTM75_11250	C9J18_07870	AYY26_16390
ribulose-5-phosphate 3-epimerase (RibuloseP<->XyluloseP) (rp e)	CTM87_08465	C9J22_11475	C9J21_09795	CTM67_03660	CTM77_11565	CTM76_12305	CTM93_04960	CTM79_02350	C9J19_07335	DAT36_07300	CTM80_01695	CTM85_05795	CTM70_01370	CTM75_05275	C9J18_10955	AYY26_12060
Ribose 5-phosphate Isomerase (RiboseP <-> RibuloseP) (rpi A)	CTM87_17185	C9J22_17765	C9J21_14570	CTM67_06330	CTM77_16420	CTM76_15995	CTM93_14800	CTM79_00940	C9J19_17095	DAT36_14420	CTM80_13165	CTM85_17295	CTM70_04695	CTM75_11330	C9J18_05505	AYY26_17170
Transketolase (*tkt* A)	CTM87_02635	C9J22_00195	C9J21_04840	CTM67_17215	CTM77_02140	CTM76_07655	CTM93_18525	CTM79_08165	C9J19_09470	DAT36_04185	CTM80_03465	CTM85_11235	CTM70_15510	CTM75_17200	C9J18_04940	AYY26_13305
	CTM87_19675	C9J22_19755	C9J21_14675	CTM67_06395	CTM77_06525	CTM76_15915	CTM93_17835	CTM79_00845	C9J19_19935	DAT36_18355	CTM80_18295	CTM85_19260	CTM70_11535	CTM75_15940	C9J18_05590	AYY26_11080
Transaldolase (*ta l*)	CTM87_02640	C9J22_00190	C9J21_04835	CTM67_17210	CTM77_02145	CTM76_07660	CTM93_18520	CTM79_08160	C9J19_09475	DAT36_04190	CTM80_03460	CTM85_11240	CTM70_15505	CTM75_17195	C9J18_04945	AYY26_13310
Gluconeogenese																
Phoshoenolyruvate carboxylase (pyc) / PEPcase (ppc)	CTM87_08555	C9J22_11565	C9J21_09705	CTM67_03750	CTM77_11475	CTM76_12395	CTM93_04870	CTM79_02440	C9J19_07245	DAT36_07210	CTM80_01605	CTM85_05705	CTM70_01280	CTM75_05185	C9J18_11045	AYY26_12150
Pyruvate carboxylase (pyc)																
phosphoenolpyruvate carboxykinase (pckA)	CTM87_15970	C9J22_15280	C9J21_10210	CTM67_04740	CTM77_14560	CTM76_15475	CTM93_08985	CTM79_08765	C9J19_14755	DAT36_09325	CTM80_08185	CTM85_12985	CTM70_05340	CTM75_14275	C9J18_16470	AYY26_14640
PEP synthase (pps A)	CTM87_06155	C9J22_10480	C9J21_17260	CTM67_14580	CTM77_03255	CTM76_00595	CTM93_10310	CTM79_19770	C9J19_11200	DAT36_17650	CTM80_14145	CTM85_17785	CTM70_16650	CTM75_15380	C9J18_12820	AYY26_08655
phosphoenolpyruvate utilizing protein	CTM87_15610	C9J22_15115	C9J21_17070	CTM67_12140	CTM77_03445	CTM76_00390	CTM93_10485	CTM79_05400	C9J19_11375	DAT36_17760	CTM80_16620	CTM85_00040	CTM70_15805	CTM75_15160	C9J18_12655	AYY26_03030
malate dehydrogenase (oxaloacetate-decarboxylating)	CTM87_14265	C9J22_19445	C9J21_18950	CTM67_15665	CTM77_09565	CTM76_15275	CTM93_16225	CTM79_16590	C9J19_13395	DAT36_04465	CTM80_14775	CTM85_10195	CTM70_07835	CTM75_14610	C9J18_15155	AYY26_13970
Aspartate/tyrosine/aromatic aminotransferase	CTM87_05415	C9J22_02860	C9J21_15925	CTM67_14720	CTM77_07870	CTM76_20115	CTM93_19060	CTM79_17350	C9J19_19415	DAT36_09530	CTM80_08700	CTM85_06670	CTM70_13995	CTM75_16420	C9J18_19050	AYY26_07695
	CTM87_10110	C9J22_05045	C9J21_09150	CTM67_06950	CTM77_01275	CTM76_14405	CTM93_16710	CTM79_04800	C9J19_05255	DAT36_16610	CTM80_19355	CTM85_00670	CTM70_17125	CTM75_15125	C9J18_02720	AYY26_03645
Aspartate oxidase	CTM87_17270	C9J22_17850	C9J21_14485	CTM67_06245	CTM77_16505	CTM76_16080	CTM93_14715	CTM79_01025	C9J19_17180	DAT36_14505	CTM80_13250	CTM85_17380	CTM70_04610	CTM75_11415	C9J18_05420	AYY26_17085
Fructose-1,6-bisphosphatase (fdp)	CTM87_08630	C9J22_11640	C9J21_09630	CTM67_03825	CTM77_11400	CTM76_12470	CTM93_04795	CTM79_02515	C9J19_07170	DAT36_07135	CTM80_01530	CTM85_05630	CTM70_01205	CTM75_05110	C9J18_11120	AYY26_12225
	CTM87_14245									DAT36_04445		CTM85_10175		CTM75_14590		
glucose-6-phosphatase (phosphatase PAP2 family) (q6pc)																
phosphatase PAP2 family	CTM87_06630	C9J22_10945	C9J21_04085	CTM67_05000	CTM77_02825	CTM76_01045	CTM93_13715	CTM79_18700	C9J19_04660	DAT36_14115	CTM80_12890	CTM85_03655	CTM70_07665	CTM75_04270	C9J18_12035	AYY26_08135
Glycolysis																
glucokinase (*glc* K) putative / sugar kinase / ROK family sugar kinase	CTM87_05790	C9J22_03035	C9J21_19570	CTM67_17780	CTM77_15600	CTM76_16920	CTM93_18365	CTM79_18325	C9J19_19150	DAT36_11820	CTM80_08875	CTM85_19870	CTM70_12370	CTM75_16700	C9J18_18865	AYY26_07525
	CTM87_15150	C9J22_01335	C9J21_20195	CTM67_14180	CTM77_12715	CTM76_06590	CTM93_02505	CTM79_19240	C9J19_14045	DAT36_14990	CTM80_15800	CTM85_02115	CTM70_10800	CTM75_10915	C9J18_03800	AYY26_09310
						CTM76 16735		CTM79 19500								
phosphoglucomutase (pgm)	CTM87_11660	C9J22_06240	C9J21_06805	CTM67_01655	CTM77_00100	CTM76_04945	CTM93_01420	CTM79_07280	C9J19_00345	DAT36_02875	CTM80_07930	CTM85_11875	CTM70_04315	CTM75_04720	C9J18_01540	AYY26_04740
Glucose-6-phosphate isomerase (pgi)	CTM87 18145	C9J22 18695	C9J21 19145	CTM67 14325	CTM77 10640	CTM76 18690	CTM93 15810	CTM79 15495	C9J19 18360	DAT36 15455	CTM80 06540	CTM85 18275	CTM70 05820	CTM75 13150	C9J18 19200	AYY26 18155
mannose-6-P isomerase (man A)	CTM87_17485	C9J22_18110	C9J21_16805	CTM67_11470	CTM77_13845	CTM76_18485	CTM93_14865	CTM79_13045	C9J19_03625	DAT36_19405	CTM80_11405	CTM85_19995	CTM70_05030	CTM75_11630	C9J18_18255	AYY26_15130
glyceraldehyde phosphate dehydrogenase	CTM87_03625	C9J22_07185	C9J21_03320	CTM67_02605	CTM77_04050	CTM76_04130	CTM93_06440	CTM79_09045	C9J19_15475	DAT36_02085	CTM80_09045	CTM85_09830	CTM70_02575	CTM75_06915	C9J18_06950	AYY26_02605
phosphoglycerate kinase	CTM87_17160	C9J22_17740	C9J21_14595	CTM67_06355	CTM77_16395	CTM76_15970	CTM93_14825	CTM79_00915	C9J19_17070	DAT36_14395	CTM80_13140	CTM85_17270	CTM70_18205	CTM75_11305	C9J18_05530	AYY26_17195
phosphoglycerate mutase / phosphoglycerate mutase (2,3-diphosphoglycerate-independent)	CTM87_08705	C9J22_11710	C9J21_09555	CTM67_03895	CTM77_11325	CTM76_12545	CTM93_04720	CTM79_02585	C9J19_07095	DAT36_07065	CTM80_01455	CTM85_05555	CTM70_01130	CTM75_05035	C9J18_11190	AYY26_12295
2,3-diphosphoglycerate-dependent phosphoglycerate mutase	CTM87_06385	C9J22_10730	C9J21_03875	CTM67_16620	CTM77_03025	CTM76_00835	CTM93_14375	CTM79_12060	C9J19_04865	DAT36_18245	CTM80_18605	CTM85_03450	CTM70_13410	CTM75_04065	C9J18_11825	AYY26_08390
enolase	CTM87 17355	C9J22 17935	C9J21 14400	CTM67 06160	CTM77 16590	CTM76 16165	CTM93 14630	CTM79 01110	C9J19 17265	DAT36 14590	CTM80 13335	CTM85 17465	CTM70 04525	CTM75 11500	C9J18 05335	AYY26 17000
pyruvate kinase	CTM87_09765	C9J22_05410	C9J21_15170	CTM67_06025	CTM77_00915	CTM76_14765	CTM93_02235	CTM79_05160	C9J19_05625	DAT36_03375	CTM80_02295	CTM85_01025	CTM70_09640	CTM75_00140	C9J18_02360	AYY26_04005
	CTM87_14435	C9J22_16370	C9J21_21260	CTM67_03070	CTM77_09395	CTM76_15105	CTM93_09450	CTM79_09610	C9J19_13225	DAT36_04635	CTM80_09340	CTM85_10365	CTM70_06835	CTM75_07870	C9J18_14985	AYY26_14140
glucose -> pyruvate Homolactic fermentation																
6-phosphofructokinase (pfk A)	CTM87_08660	C9J22_11665	C9J21_09600	CTM67_03850	CTM77_11370	CTM76_12500	CTM93_04765	CTM79_02540	C9J19_07140	DAT36_07110	CTM80_01500	CTM85_05600	CTM70_01175	CTM75_05080	C9J18_11145	AYY26_12250
fructose-1,6-bisphosphate aldolase (fba A)	CTM87 17165	C9J22 17745	C9J21 14590	CTM67 06350	CTM77 16400	CTM76 15975	CTM93 14820	CTM79 00920	C9J19 17075	DAT36 14400	CTM80 13145	CTM85 17275	CTM70 18210	CTM75 11310	C9J18 05525	AYY26 17190
glucose -> pyruvate Heterolactic fermentation																
phosphoketolase (xpk A)																
glucose-6-phosphate dehydrogenase (zwf)	CTM87_16900	C9J22_09370	C9J21_05900	CTM67_08655	CTM77_08510	CTM76_02890	CTM93_00745	CTM79_01785	C9J19_17795	DAT36_10775	CTM80_12295	CTM85_12750	CTM70_05650	CTM75_11260	C9J18_07860	AYY26_16400
KDPG weg																
phosphogluconate dehydratase (ed d)													CTM70 11210		C9J18 20810	
KDPG aldolase (ed a)	CTM87_15155	C9J22_01340	C9J21_20200	CTM67_14185	CTM77_12720	CTM76_06585	CTM93_02500	CTM79_19245	C9J19_14040	DAT36_14995	CTM80_15805	CTM85_02120	CTM70_10805	CTM75_10910	C9J18_03795	AYY26_09305
glucose-6-phosphate dehydrogenase (1.1.1.49/1.1.1.363)	CTM87_16900	C9J22_09370	C9J21_05900	CTM67_08655	CTM77_08510	CTM76_02890	CTM93_00745	CTM79_01785	C9J19_17795	DAT36_10775	CTM80_12295	CTM85_12750	CTM70_05650	CTM75_11260	C9J18_07860	AYY26_16400
6-phosphogluconolactonase 3.1.1.31	CTM87_16905	C9J22_09375	C9J21_05905	CTM67_08650	CTM77_08515	CTM76_02885	CTM93_00750	CTM79_01790	C9J19_17790	DAT36_10770	CTM80_12300	CTM85_12755	CTM70_05645	CTM75_11255	C9J18_07865	AYY26_16395
						CTM76_16730		CTM79_19505					CTM70_11205		C9J18_20805	
Ribose																
D-ribose pyranase / Ribopyranase (*rbs* D) (ribopyranose -> ribofuranose)	CTM87_15090	C9J22_01275	C9J21_20135	CTM67_14120	CTM77_12655	CTM76_06650	CTM93_02570	CTM79_19175	C9J19_14110	DAT36_14930	CTM80_15735	CTM85_02055	CTM70_10740	CTM75_10975	C9J18_03860	AYY26_09370
Ribokinase (*rbs* K)	CTM87_15105	C9J22_01290	C9J21_20150	CTM67_14135	CTM77_12670	CTM76_06635	CTM93_02550	CTM79_19195	C9J19_14090	DAT36_14945	CTM80_15755	CTM85_02070	CTM70_10755	CTM75_10960	C9J18_03845	AYY26_09355
							CTM93_02565	CTM79_19180	C9J19_14105		CTM80_15740					
Ribose Transporter (ribose uptake protein) *rbs* U																
Putative deoxyribose-specific ABC transporter (*nup* A oder *yng* F)																
Ribose-5-phosphate isomerase (RpiA)	CTM87 17185	C9J22 17765	C9J21 14570	CTM67 06330	CTM77 16420	CTM76 15995	CTM93 14800	CTM79 00940	C9J19 17095	DAT36 14420	CTM80 13165	CTM85 17295	CTM70 04695	CTM75 11330	C9J18 05505	AYY26 17170
Ribulose-phosphate 3-epimerase (Rpe)	CTM87_08465	C9J22_11475	C9J21_09795	CTM67_03660	CTM77_11565	CTM76_12305	CTM93_04960	CTM79_02350	C9J19_07335	DAT36_07300	CTM80_01695	CTM85_05795	CTM70_01370	CTM75_05275	C9J18_10955	AYY26_12060
Xylulose-5-phosphate phosphoketolase (Xpk)																
ribose-5-phosphate pyrophosphokinase	CTM87_20270	C9J22_14415	C9J21_13095	CTM67_10035	CTM77_19820	CTM76_17765	CTM93_12880	CTM79_11355	C9J19_03260	DAT36_13215	CTM80_10550	CTM85_15585	CTM70_12135	CTM75_08570	C9J18_21115	AYY26_15465
Nucleoside																
Nucleoside-diphosphate Kinase	CTM87 10525	C9J22 08645	C9J21 01690	CTM67 00465	CTM77 17335	CTM76 06225	CTM93 09560	CTM79 06050	C9J19 14970	DAT36 00155	CTM80 06320	CTM85 09065	CTM70 00685	CTM75 01815	C9J18 00285	AYY26 14855
inosine-uridine nucleoside ribohydrolase (*iun* H)																
ribonucleoside nucleosidase (unspecific, RihC)	CTM87_05465	C9J22_02895	C9J21_15875	CTM67_14770	CTM77_07920	CTM76_20065	CTM93_19110	CTM79_17290	C9J19_19465	DAT36_09470	CTM80_08750	CTM85_06720	CTM70_14045	CTM75_16370	C9J18_19000	AYY26_07645
purine (deoxy)nucleoside phosphorylase (RibP/Pur) (deoD)	CTM87 12230	C9J22 10150	C9J21 07570	CTM67 00865	CTM77 06225	CTM76 11450	CTM93 05820	CTM79 04375	C9J19 06070	DAT36 01580	CTM80 09680	CTM85 04860	CTM70 00045	CTM75 00815	C9J18 10605	AYY26 10265
pyrimidine (deoxy)nucleoside phosphorylase (RibP/Pur) (deoA)	CTM87_12240	C9J22_10140	C9J21_07560	CTM67_00875	CTM77_06215	CTM76_11460	CTM93_05810	CTM79_04365	C9J19_06080	DAT36_01570	CTM80_09690	CTM85_04850	CTM70_00055	CTM75_00825	C9J18_10595	AYY26_10255
purine/pyrimidine nucleosidase (Rib/Pur)																
ribose 1,5-phosphopentomutase (deoB)	CTM87 12235	C9J22 10145	C9J21 07565	CTM67 00870	CTM77 06220	CTM76 11455	CTM93 05815	CTM79 04370	C9J19 06075	DAT36 01575	CTM80 09685	CTM85 04855	CTM70 00050	CTM75 00820	C9J18 10600	AYY26 10260
Nucleoside to Deoxynucleoside																
Ribonucleotide reductase alpha/assembly/beta																
nrd A	CTM87_09605	C9J22_05570	C9J21_15010	CTM67_05865	CTM77_00755	CTM76_04290	CTM93_02075	CTM79_05320	C9J19_05785	DAT36_03535	CTM80_02455	CTM85_01185	CTM70_15120	CTM75_00300	C9J18_02200	AYY26_04165
nrdB	CTM87_09600	C9J22_05575	C9J21_15005	CTM67_05860	CTM77_00750	CTM76_04295	CTM93_02070	CTM79_05325	C9J19_05790	DAT36_03540	CTM80_02460	CTM85_01190	CTM70_15125	CTM75_00305	C9J18_02195	AYY26_04170

	P. phosphoreum															
	AK-3	AK-4	AK-5	AK-8	ATCC 11040	FS-1.1	FS-1.2	FS-2.1	FS-2.2	FS-3.2	FS-4.1	FS-4.2	FS-5.1	FS-5.2	FS-6.1	GCSL-P69
nrdI	CTM87_07155	C9J22_12900	C9J21_04605	CTM67_17280	CTM77_12910	CTM76_01575	CTM93_03975	CTM79_20215	C9J19_04140	DAT36_13975	CTM80_11500	CTM85_04180	CTM70_13135	CTM75_17840	C9J18_13300	AYY26_05990
DeoxyRibose from DNA																
Deoxyribose-phosphate aldolase (deoC)	CTM87_12245	C9J22_10135	C9J21_07555	CTM67_00880	CTM77_06210	CTM76_11465	CTM93_05805	CTM79_04360	C9J19_06085	DAT36_01565	CTM80_09695	CTM85_04845	CTM70_00060	CTM75_00830	C9J18_10590	AYY26_10250
Ribose from free NTP/RNA																
to PP Pathway / Hetero																
Sugar transporters																
galactose/methyl galactoside ABC transporter ATP-binding protein MglA	CTM87_00550		C9J21_16190				CTM93_18110	CTM79_13180	C9J19_18730		CTM80_14545	CTM85_12385		CTM75_19010		AYY26_00505
galactoside ABC transporter permease MglC	CTM87_00545		C9J21_16195				CTM93_18115	CTM79_13175	C9J19_18735		CTM80_14540	CTM85_12390		CTM75_19005		AYY26_00500
methyl-galactoside ABC transporter substrate-binding protein MglB	CTM87_00555		C9J21_16185				CTM93_18105	CTM79_13185	C9J19_18725		CTM80_14550	CTM85_12380		CTM75_19015		AYY26_00510
maltose/maltodextrin ABC transporter substrate-binding protein MalE																
maltose ABC transporter permease MalF																
maltose ABC transporter permease MalG																
maltose/maltodextrin ABC transporter ATP-binding protein MalK																
PTS lactose/cellobiose transporter subunit IIA																
PTS cellobiose transporter subunit IIC																
PTS_system,_cellobiose-specific_IIB_component_(EC_2.7.1.205)																
PTS mannose transporter subunit IIA	CTM87_02480	C9J22_00350	C9J21_04995	CTM67_10805	CTM77_01985	CTM76_07500	CTM93_15240	CTM79_08320	C9J19_09315	DAT36_03995	CTM80_03650	CTM85_11050	CTM70_03635	CTM75_03420	C9J18_04785	AYY26_13150
PTS mannose transporter subunit IIB	CTM87_04305	C9J22_08800	C9J21_19670	CTM67_10310	CTM77_04695	CTM76_03450	CTM93_00185	CTM79_01225	C9J19_11925	DAT36_06320	CTM80_05630	CTM85_15995	CTM70_10825	CTM75_03035	C9J18_07290	AYY26_01935
Sugars																
6-phospho-beta-glucosidase																
alpha-galactosidase																
					CTM77_08970			CTM79_09700			CTM80_00880					
beta-galactosidase	CTM87_08150				CTM77_08975			CTM79_09695	C9J19_07975		CTM80_00885	CTM85_02435		CTM75_16855		AYY26_06220
beta-galactosidase subunit beta	CTM87_07405	C9J22_19570	C9J21_11355	CTM67_05515	CTM77_15210	CTM76_02500	CTM93_07835	CTM79_16305	C9J19_12580	DAT36_05730	CTM80_00165	CTM85_03150	CTM70_08165	CTM75_11875	C9J18_16780	AYY26_17970
beta-galactosidase subunit alpha	CTM87_07410	C9J22_19565	C9J21_11360	CTM67_05510	CTM77_15215	CTM76_02495	CTM93_07840	CTM79_16310	C9J19_12575	DAT36_05735	CTM80_00170	CTM85_03145	CTM70_08160	CTM75_11880	C9J18_16785	AYY26_17975
alpha-glucosidase	CTM87_18745	C9J22_03155	C9J21_08175	CTM67_15010	CTM77_15450	CTM76_13860	CTM93_10705	CTM79_16735	C9J19_13630	DAT36_11935	CTM80_16885	CTM85_15090	CTM70_16110	CTM75_16810	C9J18_14595	AYY26_07370
	CTM87_02405	C9J22_00450	C9J21_05070	CTM67_10705	CTM77_01910	CTM76_07425	CTM93_15165	CTM79_08395	C9J19_09240	DAT36_03920	CTM80_03720	CTM85_10980	CTM70_03710	CTM75_03490	C9J18_04710	AYY26_13075
beta-mannosidase	CTM87_14630	C9J22_16565	C9J21_16335	CTM67_03265	CTM77_09200	CTM76_19835	CTM93_09255	CTM79_09415	C9J19_13030	DAT36_04830	CTM80_09535	CTM85_10560	CTM70_12920	CTM75_07675	C9J18_14785	AYY26_19385
	CTM87_02230		C9J21_05215	CTM67_13235	CTM77_01745	CTM76_07270		CTM79_16945	C9J19_09085	DAT36_09910	CTM80_03890		CTM70_07305			AYY26_12885
alpha-mannosidase	CTM87_02080	C9J22_00875	C9J21_05380	CTM67_11730	CTM77_01585	CTM76_07115	CTM93_02970		C9J19_18565	DAT36_08965	CTM80_15490	CTM85_01660	CTM70_18155	CTM75_16055	C9J18_04260	AYY26_18835
	CTM87_02085	C9J22_00870	C9J21_05375	CTM67_11735	CTM77_01590	CTM76_07120	CTM93_02975		C9J19_18570	DAT36_08970	CTM80_15495	CTM85_01655	CTM70_18150	CTM75_16060	C9J18_04265	AYY26_18840
	CTM87_09415	C9J22_05755	C9J21_06340	CTM67_05680	CTM77_00570	CTM76_04475	CTM93_01890		C9J19_19655	DAT36_03720	CTM80_02640	CTM85_01370		CTM75_00485	C9J18_02015	AYY26_04350
		C9J22_00780	C9J21_05255	CTM67_13275	CTM77_01705	CTM76_07230	CTM93_03085			DAT36_09870	CTM80_03930		CTM70_07265	CTM75_03675	C9J18_04390	AYY26_12845
	CTM87_02155	C9J22_00820	C9J21_05295	CTM67_13315	CTM77_01665					DAT36_09830	CTM80_03970		CTM70_07225	CTM75_03715	C9J18_04350	AYY26_12805
Glycogen																
Glycogen phosphorylase (*glg* P)																
UTP-glucose-1-phosphate uridylyltransferase (gta B)	CTM87_19850	C9J22_14035	C9J21_15790	CTM67_18695	CTM77_07265	CTM76_13090	CTM93_13595	CTM79_00055	C9J19_11050	DAT36_07645	CTM80_04595	CTM85_08855	CTM70_09310	CTM75_02110	C9J18_06330	AYY26_11855
	CTM87_19290						CTM93_19030					CTM85_19970			C9J18_18445	AYY26_02940
Glycogen synthase (*glg* A)																
starch synthase (GT5)																
glucoamylase (GH15)																
Glycogen biosynthesis protein (Glg D)																
1,4-alpha-glucan branching enzyme																
glycogen debranching enzyme (GH13)																
alpha-amylase (GH13)																
4-alpha-glucanotransferase (GH13)																
alpha-glucosidase (GH13)	CTM87_18745	C9J22_03155	C9J21_08175	CTM67_15010	CTM77_15450	CTM76_13860	CTM93_10705	CTM79_16735	C9J19_13630	DAT36_11935	CTM80_16885	CTM85_15090	CTM70_16110	CTM75_16810	C9J18_14595	AYY26_07370
	CTM87_02405	C9J22_00450	C9J21_05070	CTM67_10705	CTM77_01910	CTM76_07425	CTM93_15165	CTM79_08395	C9J19_09240	DAT36_03920	CTM80_03720	CTM85_10980	CTM70_03710	CTM75_03490	C9J18_04710	AYY26_13075
Pullulanase -type alpha-1,6-glucosidase																
Pyruvate fates Pyruvate dehydrogenase complex (cluster)																
Pyruvate dehydrogenase alpha E1 (acetoin-oxidoreductase) pdhA / aceE (homodimeric)	CTM87_14050	C9J22_13565	C9J21_14950	CTM67_02070	CTM77_06795	CTM76_13555	CTM93_17025	CTM79_00525	C9J19_10585	DAT36_17265	CTM80_04125	CTM85_08390	CTM70_03980	CTM75_02575	C9J18_05865	AYY26_11350
Pyruvate dehydrogenase beta E1 (oxo-isovaleriate dehydrogenase) pdhB																
Dihydrolipoamide acetyltransferase E2 pdhC	CTM87_14055	C9J22_13560	C9J21_14945	CTM67_02065	CTM77_06790	CTM76_13560	CTM93_17020	CTM79_00530	C9J19_10580	DAT36_17260	CTM80_04120	CTM85_08385	CTM70_03985	CTM75_02580	C9J18_05860	AYY26_11345
Dihydrolipoyl-Dehydrogenase E3 pdhD	CTM87_14060	C9J22_13555	C9J21_14940	CTM67_02060	CTM77_06785	CTM76_13565	CTM93_17015	CTM79_00535	C9J19_10575	DAT36_17255	CTM80_04115	CTM85_08380	CTM70_03990	CTM75_02585	C9J18_05855	AYY26_11340
Lactate++																
L-lactate dehydrogenase (ldh)																
D-lactate dehydrogenase (ldh)																
D-lactate dehydrogenase / 2-hydroxyacid dehydrogenase	CTM87_04340	C9J22_08835	C9J21_19705	CTM67_10275	CTM77_04730	CTM76_03415	CTM93_00220	CTM79_01260	C9J19_11960	DAT36_06285	CTM80_05665	CTM85_15960	CTM70_10860	CTM75_03070	C9J18_07325	AYY26_01900
lactate dehydrogenase	CTM87_02655	C9J22_00180	C9J21_04825	CTM67_17200	CTM77_02160	CTM76_07670	CTM93_18510	CTM79_08150	C9J19_09490	DAT36_04200	CTM80_03450	CTM85_11255	CTM70_15490	CTM75_17185	C9J18_04955	AYY26_13320
2-hydroxyacid dehydrogenase	CTM87_04340	C9J22_08835	C9J21_19705	CTM67_10275	CTM77_04730	CTM76_03415	CTM93_00220	CTM79_01260	C9J19_11960	DAT36_06285	CTM80_05665	CTM85_15960	CTM70_10860	CTM75_03070	C9J18_07325	AYY26_01900
Acetate																

	P. phosphoreum															
	AK-3	**AK-4**	**AK-5**	**AK-8**	**ATCC 11040**	**FS-1.1**	**FS-1.2**	**FS-2.1**	**FS-2.2**	**FS-3.2**	**FS-4.1**	**FS-4.2**	**FS-5.1**	**FS-5.2**	**FS-6.1**	**GCSL-P69**
Phosphotransacetylase pta	CTM87_17635	C9J22_14625	C9J21_16960	CTM67_11615	CTM77_13695	CTM76_18335	CTM93_15010	CTM79_12895	C9J19_03470	DAT36_15205	CTM80_11250	CTM85_18515	CTM70_05180	CTM75_11780	C9J18_20415	AYY26_15265
Pyruvate oxidase poxB																
Acetatekinase ackA	CTM87_17630	C9J22_14630	C9J21_16955	CTM67_11610	CTM77_13700	CTM76_18340	CTM93_15005	CTM79_12900	C9J19_03475	DAT36_15210	CTM80_11255	CTM85_18520	CTM70_05175	CTM75_11775	C9J18_20420	AYY26_15260
Acylphosphatase (acyP)	CTM87_07345	C9J22_19630	C9J21_11295	CTM67_05575	CTM77_15150	CTM76_02560	CTM93_07775	CTM79_16245	C9J19_12640	DAT36_05670	CTM80_00105	CTM85_03210	CTM70_15765	CTM75_18875	C9J18_16720	AYY26_17900
Ethanol																
Acetaldehyde dehydrogenase / Alcohol dehydrogenase adhE	CTM87_11940	C9J22_05955	C9J21_06525	CTM67_01375	CTM77_00380	CTM76_04665	CTM93_01700	CTM79_20320	C9J19_00065	DAT36_03155	CTM80_07650	CTM85_11595	CTM70_09145	CTM75_00675	C9J18_01815	AYY26_04460
Ethanol/Acetate																
Pyruvate formate lyase (allerdings O2 sensitive) pflB	CTM87_17565	C9J22_14695	C9J21_16890	CTM67_11545	CTM77_13770	CTM76_18405	CTM93_14940	CTM79_12970	C9J19_03545	DAT36_15275	CTM80_11325	CTM85_18585	CTM70_05110	CTM75_11710	C9J18_20490	AYY26_15190
Formate efflux transporter / formate-nitrite transporter focA	CTM87_17560	C9J22_14700	C9J21_16885	CTM67_11540	CTM77_13775	CTM76_18410	CTM93_14935	CTM79_12975	C9J19_03550	DAT36_15280	CTM80_11330	CTM85_18590	CTM70_05105	CTM75_11705	C9J18_20495	AYY26_15185
acetaldehyde dehydrogenase	CTM87_05840															
alcohol dehydrogenase	CTM87_05850															
iron containing alcohol dehydrogenase	CTM87_03190	C9J22_12240	C9J21_19375	CTM67_18255	CTM77_18690	CTM76_19315	CTM93_17120	CTM79_06625	C9J19_08855	DAT36_18050	CTM80_16135	CTM85_18845	CTM70_12400	CTM75_15495	C9J18_16075	AYY26_10545
	CTM87_02125 + CTM87_17140 + CTM87_19655	C9J22_00850 + C9J22_17720 + C9J22_19775	C9J21_05325 + C9J21_14615 + C9J21_14655	CTM67_11785 + CTM67_06375	CTM77_01635 + CTM77_06505 + CTM77_16375	CTM76_15950 + CTM76_07165 + CTM76_15935	CTM93_03020 + CTM93_14845 + CTM93_17815	CTM79_00865 + CTM79_00895 + CTM79_17715	C9J19_18610 + C9J19_17050	DAT36_14375	CTM80_19615 + CTM80_13120	CTM85_01610 + CTM85_19280	CTM70_11555	CTM75_03745 + CTM75_15960	C9J18_04320 + C9J18_05550	AYY26_21340 + AYY26_11060
	CTM87_09825	C9J22_05350	C9J21_09450	CTM67_07245	CTM77_00975	CTM76_14710	CTM93_02290	CTM79_05100	C9J19_05565	DAT36_03315	CTM80_02240	CTM85_00970	CTM70_18535	CTM75_00085	C9J18_02420	AYY26_03945
alcohol dehydrogenase AdhP			C9J21_05330	CTM67_11780	CTM77_01630	CTM76_07160	CTM93_03015			DAT36_19630	CTM80_19610	CTM85_01615	CTM70_11560	CTM75_03750	C9J18_04310	
Formate																
Formate acetyltransferase (PFL)	CTM87_17565	C9J22_14695	C9J21_16890	CTM67_11545	CTM77_13770	CTM76_18405	CTM93_14940	CTM79_12970	C9J19_03545	DAT36_15275	CTM80_11325	CTM85_18585	CTM70_05110	CTM75_11710	C9J18_20490	AYY26_15190
formate dehydrogenase (fdh)																
fdhABCE																
A	CTM87_19605	C9J22_20095	C9J21_01435	CTM67_19425	CTM77_19140	CTM76_06460	CTM93_09810	CTM79_20675	C9J19_15190	DAT36_16685	CTM80_19530	CTM85_19620	CTM70_17170	CTM75_19190	C9J18_00050	AYY26_15085
B	CTM87_19610	C9J22_20100	C9J21_01430	CTM67_19430	CTM77_19135	CTM76_06465	CTM93_09815	CTM79_20680	C9J19_15195	DAT36_16680	CTM80_19535	CTM85_19615	CTM70_17175	CTM75_19185	C9J18_00045	AYY26_15090
C	CTM87_19615	C9J22_20105	C9J21_01425	CTM67_19435	CTM77_19130	CTM76_06470	CTM93_09820	CTM79_20685	C9J19_15200	DAT36_16675	CTM80_19540	CTM85_19610	CTM70_17180	CTM75_19180	C9J18_00040	AYY26_15095
E	CTM87_19620	C9J22_20110	C9J21_01420	CTM67_19440	CTM77_19125	CTM76_06475	CTM93_09825	CTM79_20690	C9J19_15205	DAT36_16670	CTM80_19545	CTM85_19605	CTM70_17185	CTM75_19175	C9J18_00035	AYY26_15100
Acetolactate																
Acetolactate synthase (alsS)	CTM87_17000	C9J22_09465	C9J21_05995	CTM67_08560	CTM77_17875	CTM76_02795	CTM93_07540	CTM79_01885	C9J19_12880	DAT36_10680	CTM80_12395	CTM85_12850	CTM70_05550	CTM75_11160	C9J18_07955	AYY26_19010
Diacetyl																
spontaneous from acetolactate																
Acetoin																
Acetolactate decarboxylase aldC	CTM87_16995	C9J22_09460	C9J21_05990	CTM67_08565	CTM77_17880	CTM76_02800	CTM93_07535	CTM79_01880	C9J19_12885	DAT36_10685	CTM80_12390	CTM85_12845	CTM70_05555	CTM75_11165	C9J18_07950	AYY26_19015
Butane-2,3-diol																
Diacetyl reductase (Acetoin reductase) budC / butA / bdhA																
Reoxidizing NADH (O_2)																
NADH oxidase putative!	CTM87_09900	C9J22_05275	C9J21_09375	CTM67_07170	CTM77_01050	CTM76_14635	CTM93_17730	CTM79_05025	C9J19_05490	DAT36_03240	CTM80_02165	CTM85_00895	CTM70_11970	CTM75_00010	C9J18_02495	AYY26_03870
	CTM87_01560	C9J22_04785	C9J21_13460	CTM67_07415	CTM77_13475	CTM76_08670	CTM93_12335	CTM79_07810	C9J19_10185	DAT36_08325	CTM80_04860	CTM85_13565	CTM70_09720	CTM75_12590	C9J18_17185	AYY26_01075
Na+ transporting NADH:ubiquinone oxidorreductase																
nqrF: NADH:ubiquinone oxidoreductase, Na(+)-translocating, F subunit	CTM87_10785	C9J22_08390	C9J21_01950	CTM67_00210	CTM77_17700	CTM76_05970	CTM93_00985	CTM79_06310	C9J19_01335	DAT36_00415	CTM80_06065	CTM85_09345	CTM70_00945	CTM75_01560	C9J18_00545	AYY26_05535
NADH:ubiquinone reductase (Na(+)-transporting) subunit E	CTM87_10780	C9J22_08395	C9J21_01945	CTM67_00215	CTM77_17695	CTM76_05975	CTM93_00980	CTM79_06305	C9J19_01340	DAT36_00410	CTM80_06070	CTM85_09340	CTM70_00940	CTM75_01565	C9J18_00540	AYY26_05540
NADH:ubiquinone reductase (Na(+)-transporting) subunit D	CTM87_10775	C9J22_08400	C9J21_01940	CTM67_00220	CTM77_17690	CTM76_05980	CTM93_00975	CTM79_06300	C9J19_01345	DAT36_00405	CTM80_06075	CTM85_09335	CTM70_00935	CTM75_01570	C9J18_00535	AYY26_05545
Na(+)-translocating NADH-quinone reductase subunit C	CTM87_10770	C9J22_08405	C9J21_01935	CTM67_00225	CTM77_17685	CTM76_05985	CTM93_00970	CTM79_06295	C9J19_01350	DAT36_00400	CTM80_06080	CTM85_09330	CTM70_00930	CTM75_01575	C9J18_00530	AYY26_05550
Na(+)-translocating NADH-quinone reductase subunit A + nqrB: NADH:ubiquinone oxidoreductase, Na(+)-translocating, B subunit		C9J22_08410		CTM67_00230		CTM76_05990			C9J19_01355		CTM80_06085			CTM75_01580		
Na(+)-translocating NADH-quinone reductase subunit A	CTM87_10760		C9J21_01925		CTM77_17675		CTM93_00960	CTM79_06285		DAT36_00390		CTM85_09320	CTM70_00920		C9J18_00520	AYY26_05560
NADH:ubiquinone reductase (Na(+)-transporting) subunit B	CTM87_10765		C9J21_01930		CTM77_17680		CTM93_00965	CTM79_06290		DAT36_00395		CTM85_09325	CTM70_00925		C9J18_00525	AYY26_05555
NDH_I_M: proton-translocating NADH-quinone oxidoreductase, chain M	CTM87_02990	C9J22_12430	C9J21_17665	CTM67_13385	CTM77_02500	CTM76_07995	CTM93_06850	CTM79_04660	C9J19_08675	DAT36_14785	CTM80_15940	CTM85_10855	CTM70_06495	CTM75_03850	C9J18_15915	AYY26_10730
(Na+)-NQR maturation NqrM	CTM87_10795	C9J22_08380	C9J21_01960	CTM67_00200	CTM77_17710	CTM76_05960	CTM93_00995	CTM79_06320	C9J19_01325	DAT36_00425	CTM80_06055	CTM85_09355	CTM70_00955	CTM75_01550	C9J18_00555	AYY26_05525
Glycerol																
lipase	CTM87_03845	C9J22_06965	C9J21_03125	CTM67_13005	CTM77_04260	CTM76_03920	CTM93_06220	CTM79_09255	C9J19_15290	DAT36_20035	CTM80_08900	CTM85_09975	CTM70_10995	CTM75_12310	C9J18_06805	AYY26_02395
		C9J22_15890	C9J21_08350	CTM67_12330	CTM77_08610	CTM76_02145	CTM93_03455			DAT36_05005	CTM80_00515	CTM85_02810				
putative esterase/lipase	CTM87_03845	C9J22_06965	C9J21_03125	CTM67_13005	CTM77_04260	CTM76_03920	CTM93_06220	CTM79_09255	C9J19_15290	DAT36_05005	CTM80_08900	CTM85_09975	CTM70_10995	CTM75_12310	C9J18_06805	AYY26_02395
		C9J22_15890	C9J21_08350	CTM67_12330	CTM77_08610	CTM76_02145	CTM93_03455				CTM80_00515	CTM85_02810				
Glycerol uptake facilitator protein (glpF) putative	CTM87_08620		C9J21_09640	CTM67_03815	CTM77_11410	CTM76_12460	CTM93_04805	CTM79_02505	C9J19_07180		CTM80_01540	CTM85_05640	CTM70_01215	CTM75_05120		AYY26_12215
	CTM87_12105	C9J22_05790		CTM67_17580	CTM77_00545	CTM76_04500	CTM93_01865	CTM79_13465	C9J19_20100	DAT36_03760	CTM80_18595	CTM85_11430	CTM70_10425	CTM75_00510	C9J18_01980	AYY26_20745
Dehydrogenation pathway																
glycerol dehydrogenase	CTM87_12290	C9J22_10105	C9J21_07525	CTM67_00910	CTM77_06180	CTM76_11510	CTM93_05760	CTM79_04315	C9J19_06130	DAT36_01535	CTM80_09725	CTM85_04815	CTM70_00090	CTM75_00860	C9J18_10560	AYY26_10205
phosphoenolpyruvate-protein phosphotransferase (E/Ptsi)	CTM87_10930	C9J22_08245	C9J21_02095	CTM67_00060	CTM77_05555	CTM76_05825	CTM93_01130	CTM79_06455	C9J19_01190	DAT36_00560	CTM80_05920	CTM85_09490	CTM70_01090	CTM75_01415	C9J18_00695	AYY26_05395
phosphocarrier protein (HPr)	CTM87_10935	C9J22_08240	C9J21_02100	CTM67_00055	CTM77_05550	CTM76_05820	CTM93_01135	CTM79_06460	C9J19_01185	DAT36_00565	CTM80_05915	CTM85_09495	CTM70_01095	CTM75_01410	C9J18_00700	AYY26_05390
		C9J22_13880	C9J21_15635	CTM67_02380				CTM79_00210	C9J19_10895	DAT36_07800		CTM85_08700		CTM75_02265	C9J18_06175	AYY26_11660
Phosphorylation pathway																
glycerol kinase (glpK)	CTM87_08625	C9J22_11635	C9J21_09635	CTM67_03820	CTM77_11405	CTM76_12465	CTM93_04800	CTM79_02510	C9J19_07175	DAT36_07140	CTM80_01535	CTM85_05635	CTM70_01210	CTM75_05115	C9J18_11115	AYY26_12220
	CTM87_02380	C9J22_00475	C9J21_05095	CTM67_15075	CTM77_01885	CTM76_07400	CTM93_15140	CTM79_08420	C9J19_09215		CTM80_03745	CTM85_10955		CTM75_03515	C9J18_04685	
alpha-glycerophosphate oxidase (glpO) / glycerol-3-phosphate oxidase (aerobic)																
Glycerol-3-phosphate dehydrogenase (gpsA / glpD)	CTM87_09015	C9J22_12025	C9J21_14150	CTM67_06805	CTM77_12240	CTM76_12855	CTM93_04410	CTM79_02905	C9J19_06785	DAT36_12360	CTM80_01145	CTM85_05245	CTM70_04770	CTM75_06545	C9J18_11505	AYY26_12625
NAD(P)H-dependent glycerol-3-phosphate dehydrogenase (gpsA / glpD)	CTM87_08690	C9J22_11695	C9J21_09570	CTM67_03880	CTM77_11340	CTM76_12530	CTM93_04735	CTM79_02570	C9J19_07110	DAT36_07080	CTM80_01470	CTM85_05570	CTM70_01145	CTM75_05050	C9J18_11175	AYY26_12280
anaerobic glycerol-3-phosphate dehydrogenase subunit B	CTM87_18390	C9J22_09250	C9J21_05780	CTM67_10665	CTM77_08385	CTM76_03015	CTM93_00620	CTM79_01660	C9J19_17920	DAT36_10900	CTM80_12170	CTM85_12625	CTM70_02890	CTM75_09985	C9J18_07735	AYY26_16525
anaerobic glycerol-3-phosphate dehydrogenase subunit C	CTM87_18395	C9J22_09245	C9J21_05775	CTM67_10660	CTM77_08380	CTM76_03020	CTM93_00615	CTM79_01655	C9J19_17925	DAT36_10905	CTM80_12165	CTM85_12620	CTM70_02895	CTM75_09980	C9J18_07730	AYY26_16530
anaerobic glycerol-3-phosphate dehydrogenase subunit A	CTM87_18385	C9J22_09255	C9J21_05785	CTM67_10670	CTM77_08390	CTM76_03010	CTM93_00625	CTM79_01665	C9J19_17915	DAT36_10895	CTM80_12175	CTM85_12630	CTM70_02885	CTM75_09990	C9J18_07740	AYY26_16520

	P. phosphoreum															
	AK-3	AK-4	AK-5	AK-8	ATCC 11040	FS-1.1	FS-1.2	FS-2.1	FS-2.2	FS-3.2	FS-4.1	FS-4.2	FS-5.1	FS-5.2	FS-6.1	GCSL-P69
Fatty acid beta-oxidation																
Aerobic																
long-chain fatty acid transporter fadL	CTM87_07760	C9J22_15895	C9J21_08355	CTM67_12325	CTM77_08615	CTM76_02140	CTM93_03460	CTM79_15675	C9J19_08385	DAT36_05010	CTM80_00520	CTM85_02805	CTM70_08190	CTM75_10630	C9J18_13650	AYY26_06600
long-chain fatty acid CoA ligase fadD	CTM87_11810	C9J22_06090	C9J21_06655	CTM67_01505	CTM77_00250	CTM76_04795	CTM93_01570	CTM79_07430	C9J19_00195	DAT36_03025	CTM80_07780	CTM85_11725	CTM70_04165	CTM75_04570	C9J18_01685	AYY26_04590
acyl-CoA dehydrogenase fadE	CTM87_09785	C9J22_05390	C9J21_15190	CTM67_07280	CTM77_00935	CTM76_14745	CTM93_02255	CTM79_05140	C9J19_05605	DAT36_03355	CTM80_02275	CTM85_01005	CTM70_17210	CTM75_00120	C9J18_02380	AYY26_03985
	CTM87_17795	C9J22_14145	C9J21_12830	CTM67_09795	CTM77_18020	CTM76_17500	CTM93_12615	CTM79_11105	C9J19_02995	DAT36_12950	CTM80_10830	CTM85_15305	CTM70_06145	CTM75_08290	C9J18_19395	AYY26_18490
3-hydroxyacyl-CoA dehydrogenase fadB	CTM87_16120	C9J22_16685	C9J21_12400	CTM67_08400	CTM77_13975	CTM76_17425	CTM93_10995	CTM79_10375	C9J19_16345	DAT36_12540	CTM80_09980	CTM85_14470	CTM70_02490	CTM75_07210	C9J18_17840	AYY26_16310
acetyl-CoA acyltransferase fadA	CTM87_16125	C9J22_16690	C9J21_12395	CTM67_08395	CTM77_13980	CTM76_17420	CTM93_11000	CTM79_10380	C9J19_16350	DAT36_12545	CTM80_09985	CTM85_14465	CTM70_02485	CTM75_07215	C9J18_17845	AYY26_16305
Anaerobic																
long-chain fatty acid CoA ligase put. fadK	CTM87_14415	C9J22_16350	C9J21_21240	CTM67_03050	CTM77_09415	CTM76_15125	CTM93_09470	CTM79_09630	C9J19_13245	DAT36_04615	CTM80_09320	CTM85_10345	CTM70_06815	CTM75_07890	C9J18_15005	AYY26_14120
3-hydroxyacyl-CoA dehydrogenase fadJ	CTM87_11215	C9J22_07755	C9J21_02580	CTM67_04325	CTM77_05070	CTM76_05340	CTM93_13130	CTM79_19365	C9J19_00705	DAT36_19090	CTM80_03055	CTM85_07940	CTM70_01750	CTM75_09515	C9J18_01180	AYY26_05110
acetyl-CoA acyltransferase fadI	CTM87_11210	C9J22_07760	C9J21_02575	CTM67_04320	CTM77_05075	CTM76_05345	CTM93_13135	CTM79_19370	C9J19_00710	DAT36_19085	CTM80_03050	CTM85_07935	CTM70_01755	CTM75_09520	C9J18_01175	AYY26_05115
Complete Tricarboxylic acid cycle (TCA cycle)																
Citrate Synthase (citA)	CTM87_11680	C9J22_06220	C9J21_06785	CTM67_01635	CTM77_00120	CTM76_04925	CTM93_01440	CTM79_07300	C9J19_00325	DAT36_02895	CTM80_07910	CTM85_11855	CTM70_04295	CTM75_04700	C9J18_01560	AYY26_04720
Aconitate hydratase (cit B)	CTM87_14075	C9J22_13550	C9J21_14935	CTM67_02055	CTM77_06780	CTM76_13570	CTM93_17000	CTM79_00540	C9J19_10570	DAT36_17250	CTM80_04110	CTM85_08375	CTM70_03995	CTM75_02590	C9J18_05850	AYY26_11335
Isocitrate Dehydrogenase (icd A)	CTM87_04025	C9J22_06780	C9J21_02940	CTM67_09705	CTM77_04435	CTM76_03735	CTM93_06040	CTM79_10775	C9J19_18085	DAT36_02470	CTM80_05365	CTM85_16615	CTM70_10140	CTM75_02750	C9J18_06625	AYY26_02220
Oxoglutarate dehydrogenase (suc AB)	CTM87_11715	C9J22_06185	C9J21_06750	CTM67_01600	CTM77_00155	CTM76_04890	CTM93_01475	CTM79_07335	C9J19_00290	DAT36_02930	CTM80_07875	CTM85_11820	CTM70_04260	CTM75_04665	C9J18_01590	AYY26_04685
	CTM87_11710	C9J22_06190	C9J21_06755	CTM67_01605	CTM77_00150	CTM76_04895	CTM93_01470	CTM79_07330	C9J19_00295	DAT36_02925	CTM80_07880	CTM85_11825	CTM70_04265	CTM75_04670	C9J18_01585	AYY26_04690
Succinyl-CoA-Synthetase (suc CD)	CTM87_11720	C9J22_06175	C9J21_06740	CTM67_01590	CTM77_00165	CTM76_04880	CTM93_01485	CTM79_07345	C9J19_00280	DAT36_02940	CTM80_07865	CTM85_11810	CTM70_04250	CTM75_04655	C9J18_01600	AYY26_04675
	CTM87_09460	C9J22_06180	C9J21_06745	CTM67_01595	CTM77_00160	CTM76_04885	CTM93_01480	CTM79_07340	C9J19_00285	DAT36_02935	CTM80_07870	CTM85_11815	CTM70_04255	CTM75_04660	C9J18_01595	AYY26_04680
Succinate dehydrogenase (complex II) (sdh ABCD)	CTM87_11705	C9J22_06195	C9J21_06760	CTM67_01610	CTM77_00145	CTM76_04900	CTM93_01465	CTM79_07325	C9J19_00300	DAT36_02920	CTM80_07885	CTM85_11830	CTM70_04270	CTM75_04675	C9J18_01580	AYY26_04695
	CTM87_11700	C9J22_06200	C9J21_06765	CTM67_01615	CTM77_00140	CTM76_04905	CTM93_01460	CTM79_07320	C9J19_00305	DAT36_02915	CTM80_07890	CTM85_11835	CTM70_04275	CTM75_04680	C9J18_01575	AYY26_04700
	CTM87_11695	C9J22_06205	C9J21_06770	CTM67_01620	CTM77_00135	CTM76_04910	CTM93_01455	CTM79_07315	C9J19_00310	DAT36_02910	CTM80_07895	CTM85_11840	CTM70_04280	CTM75_04685	C9J18_01570	AYY26_04705
	CTM87_11690	C9J22_06210	C9J21_06775	CTM67_01625	CTM77_00130	CTM76_04915	CTM93_01450	CTM79_07310	C9J19_00315	DAT36_02905	CTM80_07900	CTM85_11845	CTM70_04285	CTM75_04690	C9J18_01565	AYY26_04710
Fumarate hydratase (Fumarase) (fum A)	CTM87_09860	C9J22_05315	C9J21_09415	CTM67_07210	CTM77_01010	CTM76_14675	CTM93_17770	CTM79_05065	C9J19_05530	DAT36_03280	CTM80_02205	CTM85_00935	CTM70_12010	CTM75_00050	C9J18_02455	AYY26_03910
Malate dehydrogenase (md h)	CTM87_14265	C9J22_19445	C9J21_18950	CTM67_15665	CTM77_09565	CTM76_15275	CTM93_16225	CTM79_16590	C9J19_13395	DAT36_04465	CTM80_14775	CTM85_10195	CTM70_07835	CTM75_14610	C9J18_15155	AYY26_13970
Phosphoenolpyruvate carboxylase	CTM87_08555	C9J22_11565	C9J21_09705	CTM67_03750	CTM77_11475	CTM76_12395	CTM93_04870	CTM79_02440	C9J19_07245	DAT36_07210	CTM80_01605	CTM85_05705	CTM70_01280	CTM75_05185	C9J18_11045	AYY26_12150
Glyoxylate cycle																
isocitrate lyase	CTM87_10430	C9J22_08740	C9J21_01595	CTM67_00560	CTM77_17430	CTM76_06320	CTM93_09655	CTM79_19845	C9J19_15065	DAT36_00060	CTM80_06415	CTM85_08970	CTM70_00590	CTM75_01910	C9J18_00190	AYY26_14950
malate synthase	CTM87_10425	C9J22_08745	C9J21_01590	CTM67_00565	CTM77_17435	CTM76_06325	CTM93_09660	CTM79_19840	C9J19_15070	DAT36_00055	CTM80_06420	CTM85_08965	CTM70_00585	CTM75_01915	C9J18_00185	AYY26_14955
AMINO ACIDS																
Arginine deiminase (arcA)	CTM87_14615	C9J22_16550	C9J21_16350	CTM67_03250	CTM77_09215	CTM76_14920	CTM93_09270	CTM79_09430	C9J19_13045	DAT36_04815	CTM80_09520	CTM85_10545	CTM70_18710	CTM75_07690	C9J18_14805	AYY26_14325
ornithine carbamoyl transferase Ornithine transcarbmoylase (arcB)	CTM87_14605	C9J22_16540	C9J21_16360	CTM67_03240	CTM77_09225	CTM76_14930	CTM93_09280	CTM79_09440	C9J19_13055	DAT36_04805	CTM80_09510	CTM85_10535	CTM70_18720	CTM75_07700	C9J18_14815	AYY26_14315
carbamate kinase (arcC)	CTM87_14610	C9J22_16545	C9J21_16355	CTM67_03245	CTM77_09220	CTM76_14925	CTM93_09275	CTM79_09435	C9J19_13050	DAT36_04810	CTM80_09515	CTM85_10540	CTM70_18715	CTM75_07695	C9J18_14810	AYY26_14320
Arginase (arg)	CTM87_15185	C9J22_01370	C9J21_21655	CTM67_14215	CTM77_12750	CTM76_00550	CTM93_02470	CTM79_19725	C9J19_14010	DAT36_15025	CTM80_15835	CTM85_02150	CTM70_16480	CTM75_10880	C9J18_03770	AYY26_09275
	CTM87_06110		C9J21_17210											CTM75_15335	C9J18_12775	
Malate dehydrogenase (md h)	CTM87_14265	C9J22_19445	C9J21_18950	CTM67_15665	CTM77_09565	CTM76_15275	CTM93_16225	CTM79_16590	C9J19_13395	DAT36_04465	CTM80_14775	CTM85_10195	CTM70_07835	CTM75_14610	C9J18_15155	AYY26_13970
Aminotransferasen																
Aspartate Aminofransferase (Glu/OA) aspB	CTM87_08445	C9J22_11455	C9J21_09815	CTM67_03640	CTM77_11585	CTM76_12285	CTM93_04980	CTM79_02330	C9J19_07355	DAT36_07320	CTM80_01715	CTM85_05815	CTM70_01390	CTM75_05295	C9J18_10935	AYY26_12040
Glutamate Dehydrogenase (aKG/NADH2) gdhA	CTM87_06945	C9J22_12700	C9J21_04400	CTM67_13570	CTM77_13120	CTM76_01360	CTM93_04190	CTM79_15910	C9J19_04350	DAT36_13775	CTM80_11710	CTM85_03965	CTM70_11315	CTM75_13545	C9J18_13500	AYY26_05790
Serine dehydratase (rev.) (Pvr/NH3) sdaAB	CTM87_09840	C9J22_05335	C9J21_09435	CTM67_07230	CTM77_00990	CTM76_14695	CTM93_17790	CTM79_05085	C9J19_05550	DAT36_03300	CTM80_02225	CTM85_00955	CTM70_12030	CTM75_00070	C9J18_02435	AYY26_03930
Aromatic amino acid aminotransferase (Tyr,Phe,His) (Glu) tyrB	CTM87_10110	C9J22_05045	C9J21_09150	CTM67_06950	CTM77_01275	CTM76_14405	CTM93_16710	CTM79_04800	C9J19_05255	DAT36_16610	CTM80_19355	CTM85_00670	CTM70_17125	CTM75_15125	C9J18_02720	AYY26_03645
Branched-chain amino acid aminotransferase (Leu,Ile,Val) (Glu) ilvE	CTM87_16355	C9J22_16920	C9J21_12165	CTM67_08165	CTM77_14210	CTM76_17190	CTM93_11230	CTM79_10610	C9J19_16580	DAT36_12770	CTM80_10215	CTM85_14235	CTM70_02255	CTM75_07445	C9J18_18075	AYY26_16080
Alanine dehydrogenase (ald)	CTM87_11435	C9J22_06475	C9J21_20710	CTM67_01880	CTM77_04925	CTM76_05170	CTM93_18235	CTM79_20645	C9J19_00570	DAT36_02645	CTM80_03220	CTM85_08090	CTM70_16065	CTM75_04950	C9J18_01315	AYY26_04960
Alanine aminotransferase																
aspartate ammonia-lyase (aspA)	CTM87_18550	C9J22_17145	C9J21_13670	CTM67_09005	CTM77_10400	CTM76_18155	CTM93_12010	CTM79_12755	C9J19_19770	DAT36_13605	CTM80_06785	CTM85_16100	CTM70_03215	CTM75_09200	C9J18_18705	AYY26_16790
aspartate oxidase (nadB)	CTM87_17270	C9J22_17850	C9J21_14485	CTM67_06245	CTM77_16505	CTM76_16080	CTM93_14715	CTM79_01025	C9J19_17180	DAT36_14505	CTM80_13250	CTM85_17380	CTM70_04610	CTM75_11415	C9J18_05420	AYY26_17085
Biogenic amines production																
histidine-histamine antiporter (aminoacid permease)	CTM87_02365			CTM67_11660		CTM76_07390	CTM93_15130	CTM79_08435				CTM85_10945				AYY26_20330
histidine decarboxylase hdcA																
histidine decarboxylase 2 hdc2 Bjornsdottir-Butler et al.	CTM87_02360			CTM67_19985		CTM76_07385	CTM93_19920	CTM79_08440				CTM85_01380				AYY26_20325
arginine decarboxylase speA	CTM87_09590	C9J22_05585	C9J21_14995	CTM67_05850	CTM77_00740	CTM76_04305	CTM93_02060	CTM79_05335	C9J19_05800	DAT36_03550	CTM80_02470	CTM85_01200	CTM70_15135	CTM75_00315	C9J18_02185	AYY26_04180
	CTM87_02430	C9J22_00400	C9J21_05045	CTM67_10755	CTM77_01935	CTM76_07450	CTM93_15190	CTM79_08370	C9J19_09265	DAT36_03945	CTM80_03695	CTM85_11005	CTM70_03685	CTM75_03465	C9J18_04735	AYY26_13100
	CTM87_09180 + CTM87_09170 + CTM87_09160	C9J22_18855	C9J21_16535 + C9J21_16525	CTM67_20235 + CTM67_19900	CTM77_12095 + CTM77_12085	CTM76_13000 + CTM76_13010 + CTM76_13020	CTM93_19670	CTM79_15130 + CTM79_15120	C9J19_19255	DAT36_16395	CTM80_01000 + CTM80_19925	CTM85_17930	CTM70_20130	CTM75_20275	C9J18_20120	AYY26_21285 + AYY26_21275
		C9J22_20600	C9J21_22570	CTM67_20745			CTM93_19680		C9J19_19245	DAT36_12505	CTM80_20460	CTM85_17920	CTM70_17765 + CTM70_17775	CTM75_19435 + CTM75_19425	C9J18_20110	
		C9J22_18845 C9J22_20725					CTM93_20315			DAT36_12515 DAT36_19950			CTM70_17765 CTM70_20100		C9J18_21800 C9J18_20120 C9J18_21880	
tyrosine decarboxylase tdcA	CTM87_05370	C9J22_02825	C9J21_15975	CTM67_14675	CTM77_07840	CTM76_09890	CTM93_06955	CTM79_17380	C9J19_01535	DAT36_09565	CTM80_08670	CTM85_06645	CTM70_14330	CTM75_16445	C9J18_20145	AYY26_07730
ornithine decarboxylase speF																
lysine decarboxylase lcdC	CTM87_14715	C9J22_16645	C9J21_20780	CTM67_03345	CTM77_09120	CTM76_19750	CTM93_09140	CTM79_09330	C9J19_12945	DAT36_04895	CTM80_09615	CTM85_10645	CTM70_18280	CTM75_07590	C9J18_14720	AYY26_19465
agmatinase speB	CTM87_02425	C9J22_00405	C9J21_05050	CTM67_10750	CTM77_01930	CTM76_07445	CTM93_15185	CTM79_08375	C9J19_09260	DAT36_03940	CTM80_03700	CTM85_11000	CTM70_03690	CTM75_03470	C9J18_04730	AYY26_13095
bifunctional glutathionylspermidine amidase/synthase	CTM87_07830	C9J22_15965	C9J21_08425	CTM67_12255	CTM77_08690	CTM76_02070	CTM93_03535	CTM79_09990	C9J19_08315	DAT36_05080	CTM80_00590	CTM85_02735	CTM70_12865	CTM75_10560	C9J18_13720	AYY26_06530
glutamate decarboxylase gadB	CTM87_19045	C9J22_16320	C9J21_10930	CTM67_09425	CTM77_14700	CTM76_16640	CTM93_09875	CTM79_10025	C9J19_15995	DAT36_10965	CTM80_12035	CTM85_14085	CTM70_09375	CTM75_06385	C9J18_17800	AYY26_20255
Electron donors																

	P. phosphoreum															
	AK-3	**AK-4**	**AK-5**	**AK-8**	**ATCC 11040**	**FS-1.1**	**FS-1.2**	**FS-2.1**	**FS-2.2**	**FS-3.2**	**FS-4.1**	**FS-4.2**	**FS-5.1**	**FS-5.2**	**FS-6.1**	**GCSL-P69**
NiFe hydrogenase																
hyd ABCDE	CTM87_07665	C9J22_15800	C9J21_11600	CTM67_05270	CTM77_20025	CTM76_02245	CTM93_08080	CTM79_15770	C9J19_12335	DAT36_05980	CTM80_00415	CTM85_02900	CTM70_08285	CTM75_12125	C9J18_17020	AYY26_06720
	CTM87 07670	C9J22 15805	C9J21 11605	CTM67 05265	CTM77 20020	CTM76 02240	CTM93 08085	CTM79 15765	C9J19 12330	DAT36 05985	CTM80 00420	CTM85 02895	CTM70 08280	CTM75 12130	C9J18 17025	AYY26 06715
	CTM87_07675	C9J22_15810	C9J21_11610	CTM67_05260	CTM77_20015	CTM76_02235	CTM93_08090	CTM79_15760	C9J19_12325	DAT36_05990	CTM80_00425	CTM85_02890	CTM70_08275	CTM75_12135	C9J18_17030	AYY26_06710
	CTM87 07680	C9J22 15815	C9J21 11615	CTM67 05255	CTM77 20010	CTM76 02230	CTM93 08095	CTM79 15755	C9J19 12320	DAT36 05995	CTM80 00430	CTM85 02885	CTM70 08270	CTM75 12140	C9J18 17035	AYY26 06705
	CTM87_07685	C9J22_15820	C9J21_11620	CTM67_05250	CTM77_20005	CTM76_02225	CTM93_08100	CTM79_15750	C9J19_12315	DAT36_06000	CTM80_00435	CTM85_02880	CTM70_08265	CTM75_12145	C9J18_17040	AYY26_06700
Alternative electron receptors																
Fumarate reductase																
frdABCD	CTM87_18490	C9J22_17085	C9J21_13610	CTM67_09065	CTM77_10465	CTM76_18215	CTM93_12075	CTM79_20855	C9J19_19705	DAT36_13665	CTM80_06725	CTM85_16035	CTM70_03150	CTM75_09135	C9J18_18765	AYY26_16850
	CTM87_18495	C9J22_17090	C9J21_13615	CTM67_09060	CTM77_10460	CTM76_18210	CTM93_12070	CTM79_20850	C9J19_19710	DAT36_13660	CTM80_06730	CTM85_16040	CTM70_03155	CTM75_09140	C9J18_18760	AYY26_16845
	CTM87_18500	C9J22_17095	C9J21_13620	CTM67_09055	CTM77_10455	CTM76_18205	CTM93_12065	CTM79_20845	C9J19_19715	DAT36_13655	CTM80_06735	CTM85_16045	CTM70_03160	CTM75_09145	C9J18_18755	AYY26_16840
	CTM87 18505	C9J22 17100	C9J21 13625	CTM67 09050	CTM77 10450	CTM76 18200	CTM93 12060	CTM79 20840	C9J19 19720	DAT36 13650	CTM80 06740	CTM85 16050	CTM70 03165	CTM75 09150	C9J18 18750	AYY26 16835
TMAO reductase	CTM87_07725	C9J22_15860	C9J21_08320	CTM67_12360	CTM77_08580	CTM76_02175	CTM93_03425	CTM79_15710	C9J19_08420	DAT36_04970	CTM80_00485	CTM85_02840	CTM70_08225	CTM75_10665	C9J18_13615	AYY26_06635
tor A																
Nitrate reductase																
nap AB	CTM87_10885	C9J22_08290	C9J21_02050	CTM67_00110	CTM77_05600	CTM76_05870	CTM93_01085	CTM79_06410	C9J19_01235	DAT36_00515	CTM80_05965	CTM85_09445	CTM70_01045	CTM75_01460	C9J18_00645	AYY26_05440
	CTM87 10880	C9J22 08295	C9J21 02045	CTM67 00115	CTM77 05605	CTM76 05875	CTM93 01080	CTM79 06405	C9J19 01240	DAT36 00510	CTM80 05970	CTM85 09440	CTM70 01040	CTM75 01465	C9J18 00640	AYY26 05445
hydroxylamine reductase	CTM87 02780	C9J22 00050	C9J21 04700	CTM67 18715	CTM77 02285	CTM76 07795	CTM93 06640	CTM79 04445	C9J19 09615	DAT36 04330	CTM80 18355	CTM85 11375	CTM70 13895	CTM75 18370	C9J18 05085	AYY26 10945
Mannose-6-P isomerase	CTM87_17485	C9J22_18110	C9J21_16805	CTM67_11470	CTM77_13845	CTM76_18485	CTM93_14865	CTM79_13045	C9J19_03625	DAT36_19405	CTM80_11405	CTM85_19995	CTM70_05030	CTM75_11630	C9J18_18255	AYY26_15130
manA																
nitrite reductase small subunit	CTM87_17110	C9J22_09570	C9J21_06105	CTM67_08455	CTM77_17770	CTM76_02690	CTM93_07645	CTM79_01990	C9J19_12770	DAT36_05530	CTM80_12500	CTM85_19365	CTM70_16315	CTM75_11050	C9J18_08060	AYY26_18900
nitrite reductase large subunit	CTM87_17115	C9J22_09575	C9J21_06110	CTM67_08450	CTM77_17765	CTM76_02685	CTM93_07650	CTM79_01995	C9J19_12765	DAT36_05535	CTM80_12505	CTM85_19360	CTM70_16310	CTM75_11045	C9J18_08065	AYY26_18895
sulphate adenylyltransferase cysD	CTM87_18050	C9J22_18600	C9J21_20090	CTM67_14420	CTM77_10735	CTM76_18785	CTM93_15905	CTM79_15590	C9J19_18465	DAT36_15360	CTM80_06445	CTM85_18180	CTM70_05915	CTM75_13055	C9J18_19300	AYY26_18250
sulphate adenylyltransferase cysN	CTM87_18045	C9J22_18595	C9J21_20095	CTM67_14425	CTM77_10740	CTM76_18790	CTM93_15910	CTM79_15595	C9J19_18470	DAT36_15355	CTM80_06440	CTM85_18175	CTM70_05920	CTM75_13050	C9J18_19305	AYY26_18255
assimilatory sulfite reductase	CTM87_18100	C9J22_18650	C9J21_20040	CTM67_14370	CTM77_10685	CTM76_18735	CTM93_15855	CTM79_15540	C9J19_18415	DAT36_15410	CTM80_06495	CTM85_18230	CTM70_05865	CTM75_13105	C9J18_19250	AYY26_18200
dimethyl sulfoxide reductase subunit A	CTM87_10270	C9J22_18475	C9J21_08995	CTM67_17410			CTM93_14010	CTM79_05880	C9J19_05100	DAT36_10470		CTM85_00515				AYY26_03490
dimethylsulfoxide reductase, chain B	CTM87_10265	C9J22_18470	C9J21_09000	CTM67_17415			CTM93_14005	CTM79_05885	C9J19_05105	DAT36_10475		CTM85_00520				AYY26_03495
dimethyl sulfoxide reductase anchor subunit	CTM87_10260	C9J22_18465	C9J21_09005	CTM67_17420	CTM77_01420	CTM76_19900	CTM93_14000	CTM79_05890	C9J19_05110	DAT36_10480	CTM80_07450	CTM85_00525	CTM70_15950	CTM75_18110	C9J18_02865	AYY26_03500
Respiration																
NADH dehydrogenase (non-electrogenic)																
ndh	CTM87_16980	C9J22_09445	C9J21_05975	CTM67_08580	CTM77_17895	CTM76_02815	CTM93_07520	CTM79_01865	C9J19_12900	DAT36_10700	CTM80_12375	CTM85_12830	CTM70_05570	CTM75_11180	C9J18_07935	AYY26_19030
	CTM87_09900	C9J22_05275	C9J21_09375	CTM67_07170	CTM77_01050	CTM76_14635	CTM93_17730	CTM79_05025	C9J19_05490	DAT36_03240	CTM80_02165	CTM85_00895	CTM70_11970	CTM75_00010	C9J18_02495	AYY26_03870
NADH-quinone oxidoreductase subunit A	CTM87_05025	C9J22_02500	C9J21_01155		CTM77_07500	CTM76_10215	CTM93_07295	CTM79_18105	C9J19_01865		CTM80_15500	CTM85_06295	CTM70_07425	CTM75_05915		AYY26_13575
NADH-quinone oxidoreductase subunit B	CTM87_05030	C9J22_02505	C9J21_01160		CTM77_07505	CTM76_10210	CTM93_07290	CTM79_18110	C9J19_01860		CTM80_15505	CTM85_06300	CTM70_07430	CTM75_05920		AYY26_13570
NADH dehydrogenase (quinone) subunit D	CTM87_05035	C9J22_02510	C9J21_01165		CTM77_07510	CTM76_10205	CTM93_07285	CTM79_18115	C9J19_01855		CTM80_15510	CTM85_06305	CTM70_07435	CTM75_05925		AYY26_13565
NADH-quinone oxidoreductase subunit NuoE	CTM87_05040	C9J22_02515	C9J21_01170		CTM77_07515	CTM76_10200	CTM93_07280	CTM79_18120	C9J19_01850		CTM80_15515	CTM85_06310	CTM70_07440	CTM75_05930		AYY26_13560
NADH-quinone oxidoreductase subunit NuoF	CTM87_05045	C9J22_02520	C9J21_01175		CTM77_07520	CTM76_10195	CTM93_07275	CTM79_18125	C9J19_01845		CTM80_15520	CTM85_06315	CTM70_07445	CTM75_05935		AYY26_13555
NADH dehydrogenase (quinone) subunit G	CTM87_05050	C9J22_02525	C9J21_01180		CTM77_07525	CTM76_10190	CTM93_07270	CTM79_18130	C9J19_01840		CTM80_15525	CTM85_06320	CTM70_07450	CTM75_05940		AYY26_13550
NADH-quinone oxidoreductase subunit NuoH	CTM87 05055	C9J22 02530	C9J21 01185		CTM77 07530	CTM76 10185	CTM93 07265	CTM79 18135	C9J19 01835		CTM80 15530	CTM85 06325	CTM70 07455	CTM75 05945		AYY26 13545
NADH-quinone oxidoreductase subunit NuoI	CTM87_05060	C9J22_02535	C9J21_01190		CTM77_07535	CTM76_10180	CTM93_07260	CTM79_18140	C9J19_01830		CTM80_15535	CTM85_06330	CTM70_07460	CTM75_05950		AYY26_13540
NADH-quinone oxidoreductase subunit J	CTM87_05065	C9J22_02540	C9J21_01195		CTM77_07540	CTM76_10175	CTM93_07255	CTM79_18145	C9J19_01825		CTM80_15540	CTM85_06335	CTM70_07465	CTM75_05955		AYY26_13535
NADH-quinone oxidoreductase subunit NuoK	CTM87_05070	C9J22_02545	C9J21_01200		CTM77_07545	CTM76_10170	CTM93_07250	CTM79_18150	C9J19_01820		CTM80_15545	CTM85_06340	CTM70_07470	CTM75_05960		AYY26_13530
NADH-quinone oxidoreductase subunit L	CTM87 05075	C9J22 02550	C9J21 01205		CTM77 07550	CTM76 10165	CTM93 07245	CTM79 18155	C9J19 01815		CTM80 15550	CTM85 06345	CTM70 07475	CTM75 05965		AYY26 13525
NADH-quinone oxidoreductase subunit M	CTM87_05080	C9J22_02555	C9J21_01210		CTM77_07555	CTM76_10160	CTM93_07240	CTM79_18160	C9J19_01810		CTM80_15555	CTM85_06350	CTM70_07480	CTM75_05970		AYY26_13520
NADH-quinone oxidoreductase subunit N	CTM87_05085	C9J22_02560	C9J21_01215		CTM77_07560	CTM76_10155	CTM93_07235	CTM79_18165	C9J19_01805		CTM80_15560	CTM85_06355	CTM70_07485	CTM75_05975		AYY26_13515
NADH-quinone oxidoreductase subunit NuoB	CTM87_03010	C9J22_12410	C9J21_17685	CTM67_13405	CTM77_02520	CTM76_08015	CTM93_06870	CTM79_04680	C9J19_08695	DAT36_14805	CTM80_15960	CTM85_10875	CTM70_06515	CTM75_03830	C9J18_15935	AYY26_10710
(Na+)-NQR maturation NqrM	CTM87_10795	C9J22_08380	C9J21_01960	CTM67_00200	CTM77_17710	CTM76_05960	CTM93_00995	CTM79_06320	C9J19_01325	DAT36_00425	CTM80_06055	CTM85_09355	CTM70_00955	CTM75_01550	C9J18_00555	AYY26_05525
nqrF: NADH:ubiquinone oxidoreductase, Na(+)-translocating, F subunit	CTM87_10785	C9J22_08390	C9J21_01950	CTM67_00210	CTM77_17700	CTM76_05970	CTM93_00985	CTM79_06310	C9J19_01335	DAT36_00415	CTM80_06065	CTM85_09345	CTM70_00945	CTM75_01560	C9J18_00545	AYY26_05535
NADH:ubiquinone reductase (Na(+)-transporting) subunit E	CTM87_10780	C9J22_08395	C9J21_01945	CTM67_00215	CTM77_17695	CTM76_05975	CTM93_00980	CTM79_06305	C9J19_01340	DAT36_00410	CTM80_06070	CTM85_09340	CTM70_00940	CTM75_01565	C9J18_00540	AYY26_05540
NADH:ubiquinone reductase (Na(+)-transporting) subunit D	CTM87_10775	C9J22_08400	C9J21_01940	CTM67_00220	CTM77_17690	CTM76_05980	CTM93_00975	CTM79_06300	C9J19_01345	DAT36_00405	CTM80_06075	CTM85_09335	CTM70_00935	CTM75_01570	C9J18_00535	AYY26_05545
Na(+)-translocating NADH-quinone reductase subunit C	CTM87_10770	C9J22_08405	C9J21_01935	CTM67_00225	CTM77_17685	CTM76_05985	CTM93_00970	CTM79_06295	C9J19_01350	DAT36_00400	CTM80_06080	CTM85_09330	CTM70_00930	CTM75_01575	C9J18_00530	AYY26_05550
Na(+)-translocating NADH-quinone reductase subunit A + nqrB: NADH:ubiquinone oxidoreductase, Na(+)-translocating, B subunit		C9J22_08410		CTM67_00230		CTM76_05990			C9J19_01355		CTM80_06085			CTM75_01580		
Na(+)-translocating NADH-quinone reductase subunit A	CTM87_10760		C9J21_01925		CTM77_17675		CTM93_00960	CTM79_06285		DAT36_00390		CTM85_09320	CTM70_00920		C9J18_00520	AYY26_05560
NADH:ubiquinone reductase (Na(+)-transporting) subunit B	CTM87_10765		C9J21_01930		CTM77_17680		CTM93_00965	CTM79_06290		DAT36_00395		CTM85_09325	CTM70_00925		C9J18_00525	AYY26_05555
NDH_I_M: proton-translocating NADH-quinone oxidoreductase, chain M	CTM87_02990	C9J22_12430	C9J21_17665	CTM67_13385	CTM77_02500	CTM76_07995	CTM93_06850	CTM79_04660	C9J19_08675	DAT36_14785	CTM80_15940	CTM85_10855	CTM70_06495	CTM75_03850	C9J18_15915	AYY26_10730
Menaquinone synthese (8 steps) (Vitamin K)																
1,4-dihydroxy-2-naphthoate prenyltransferase (*men* A)	CTM87_08610	C9J22_11620	C9J21_09650	CTM67_03805	CTM77_11420	CTM76_12450	CTM93_04815	CTM79_02495	C9J19_07190	DAT36_07155	CTM80_01550	CTM85_05650	CTM70_01225	CTM75_05130	C9J18_11100	AYY26_12205

	P. phosphoreum															
	AK-3	**AK-4**	**AK-5**	**AK-8**	**ATCC 11040**	**FS-1.1**	**FS-1.2**	**FS-2.1**	**FS-2.2**	**FS-3.2**	**FS-4.1**	**FS-4.2**	**FS-5.1**	**FS-5.2**	**FS-6.1**	**GCSL-P69**
Isochorismate synthase (menF)	CTM87_03490	C9J22_07320	C9J21_03455	CTM67_02740	CTM77_03915	CTM76_04265	CTM93_06575	CTM79_08910	C9J19_15605	DAT36_01950	CTM80_09180	CTM85_09695	CTM70_02710	CTM75_07050	C9J18_07085	AYY26_02740
	CTM87 03490	C9J22 07320	C9J21 03455	CTM67 02740	CTM77 03915	CTM76 04265	CTM93 06575	CTM79 08910	C9J19 15605	DAT36 01950	CTM80 09180	CTM85 09695	CTM70 02710	CTM75 07050	C9J18 07085	AYY26 02740
2-succinyl-5-enolpyruvyl-6-hydroxy-3- cyclohexene-1-carboxylic-acid synthase (menD)	CTM87_03495	C9J22_07315	C9J21_03450	CTM67_02735	CTM77_03920	CTM76_04260	CTM93_06570	CTM79_08915	C9J19_15600	DAT36_01955	CTM80_09175	CTM85_09700	CTM70_02705	CTM75_07045	C9J18_07080	AYY26_02735
2-succinyl-6-hydroxy-2, 4-cyclohexadiene-1-carboxylate synthase (menH)	CTM87_03500				CTM77_03925			CTM79_08920			CTM80_09170	CTM85_09705	CTM70_02700	CTM75_07040		AYY26_02730
	CTM87_01665	C9J22_04890	C9J21_13345	CTM67_07530	CTM77_13365	CTM76_08565	CTM93_12230	CTM79_07915	C9J19_10295	DAT36_08215	CTM80_04965	CTM85_13460	CTM70_08595	CTM75_12695	C9J18_17295	AYY26_01220
o-succinylbenzoate synthase (menC)	CTM87 03505	C9J22 07305	C9J21 03440	CTM67 02725	CTM77 03930	CTM76 04250	CTM93 06560	CTM79 08925	C9J19 15590	DAT36 01965	CTM80 09165	CTM85 09710	CTM70 02695	CTM75 07035	C9J18 07070	AYY26 02725
2-methoxy-6-polyprenyl-1,4-benzoquinol methylase (ubiE)	CTM87_15720	C9J22_15530	C9J21_10460	CTM67_04485	CTM77_19970	CTM76_15725	CTM93_08735	CTM79_08515	C9J19_14505	DAT36_09075	CTM80_08435	CTM85_13235	CTM70_08395	CTM75_13780	C9J18_16215	AYY26_14395
O-succinylbenzoate-CoA ligase (menE)	CTM87_03510	C9J22_07300	C9J21_03435	CTM67_02720	CTM77_03935	CTM76_04245	CTM93_06555	CTM79_08930	C9J19_15585	DAT36_01970	CTM80_09160	CTM85_09715	CTM70_02690	CTM75_07030	C9J18_07065	AYY26_02720
1,4-dihydroxy-2-naphthoyl-CoA synthase (menB)	CTM87_06480	C9J22_10830	C9J21_03975	CTM67_04890	CTM77_02930	CTM76_00935	CTM93_14470	CTM79_18810	C9J19_04765	DAT36_17375	CTM80_18135	CTM85_03545	CTM70_07770	CTM75_04160	C9J18_11925	AYY26_08295
cytochrome c oxidase																
Subunit I CoxA	CTM87_08980	C9J22_11990	C9J21_14115	CTM67_06770	CTM77_12275	CTM76_12820	CTM93_04445	CTM79_02870	C9J19_06820	DAT36_12325	CTM80_01180	CTM85_05280	CTM70_04805	CTM75_06580	C9J18_11470	AYY26_12590
Subunit II CoxB	CTM87_08985	C9J22_11995	C9J21_14120	CTM67_06775	CTM77_12270	CTM76_12825	CTM93_04440	CTM79_02875	C9J19_06815	DAT36_12330	CTM80_01175	CTM85_05275	CTM70_04800	CTM75_06575	C9J18_11475	AYY26_12595
Subunit III CoxC	CTM87_08970	C9J22_11980	C9J21_14105	CTM67_06760	CTM77_12285	CTM76_12810	CTM93_04455	CTM79_02860	C9J19_06830	DAT36_12315	CTM80_01190	CTM85_05290	CTM70_04815	CTM75_06590	C9J18_11460	AYY26_12580
cytochrome c oxidase assembly protein Cox1	CTM87_08975	C9J22_11985	C9J21_14110	CTM67_06765	CTM77_12280	CTM76_12815	CTM93_04450	CTM79_02865	C9J19_06825	DAT36_12320	CTM80_01185	CTM85_05285	CTM70_04810	CTM75_06585	C9J18_11465	AYY26_12585
cytochrome oxidase	CTM87_08955	C9J22_11965	C9J21_14090	CTM67_06745	CTM77_12300	CTM76_12795	CTM93_04470	CTM79_02845	C9J19_06845	DAT36_12300	CTM80_01205	CTM85_05305	CTM70_04830	CTM75_06605	C9J18_11445	AYY26_12565
cytochrome o ubiquinol oxidase subunit IV cyoD	CTM87_18710	C9J22_03120	C9J21_08210	CTM67_14975	CTM77_15485	CTM76_13825	CTM93_10670	CTM79_16770	C9J19_13595	DAT36_11900	CTM80_16850	CTM85_15125	CTM70_14505	CTM75_19525	C9J18_14625	AYY26_07405
cytochrome o ubiquinol oxidase subunit III cyoC	CTM87_18715	C9J22_03125	C9J21_08205	CTM67_14980	CTM77_15480	CTM76_13830	CTM93_10675	CTM79_16765	C9J19_13600	DAT36_11905	CTM80_16855	CTM85_15120	CTM70_14510	CTM75_19520	C9J18_14620	AYY26_07400
cytochrome o ubiquinol oxidase subunit I cyoB	CTM87_18720	C9J22_03130	C9J21_08200	CTM67_14985	CTM77_15475	CTM76_13835	CTM93_10680	CTM79_16760	C9J19_13605	DAT36_11910	CTM80_16860	CTM85_15115	CTM70_14515	CTM75_19515	C9J18_14615	AYY26_07395
CyoA: ubiquinol oxidase, subunit II	CTM87_18725	C9J22_03135	C9J21_08195	CTM67_14990	CTM77_15470	CTM76_13840	CTM93_10685	CTM79_16755	C9J19_13610	DAT36_11915	CTM80_16865	CTM85_15110	CTM70_14520	CTM75_19510	C9J18_14610	AYY26_07390
cyoE_ctaB: protoheme IX farnesyltransferase	CTM87_08945	C9J22_11955	C9J21_14080	CTM67_06735	CTM77_12310	CTM76_12785	CTM93_04480	CTM79_02835	C9J19_06855	DAT36_12290	CTM80_01215	CTM85_05315	CTM70_04840	CTM75_06615	C9J18_11435	AYY26_12555
	CTM87_18705	C9J22_03115	C9J21_08215	CTM67_14970	CTM77_15490	CTM76_13820	CTM93_10665	CTM79_16775	C9J19_13590	DAT36_11895	CTM80_16845	CTM85_15130	CTM70_14500	CTM75_19530	C9J18_14630	AYY26_07410
cytochrome-c oxidase, cbb3-type subunit I ccoN	CTM87_07520	C9J22_15655	C9J21_11455	CTM67_05415	CTM77_15310	CTM76_02390	CTM93_07935	CTM79_16410	C9J19_12480	DAT36_05825	CTM80_00270	CTM85_03045	CTM70_08060	CTM75_11980	C9J18_16875	AYY26_06865
cytochrome-c oxidase, cbb3-type subunit II ccoO	CTM87_07515	C9J22_15650	C9J21_11450	CTM67_05420	CTM77_15305	CTM76_02395	CTM93_07930	CTM79_16405	C9J19_12485	DAT36_05820	CTM80_00265	CTM85_03050	CTM70_08065	CTM75_11975	C9J18_16870	AYY26_06870
cytochrome-c oxidase, cbb3-type subunit III ccoP	CTM87_07510	C9J22_15645	C9J21_11445	CTM67_05425	CTM77_15300	CTM76_02400	CTM93_07925	CTM79_16400	C9J19_12490	DAT36_05815	CTM80_00260	CTM85_03055	CTM70_08070	CTM75_11970	C9J18_16865	AYY26_06875
cbb3-type cytochrome oxidase assembly protein CcoS CcoQ	CTM87_06840	C9J22_11155	C9J21_04295	CTM67_05210	CTM77_02615	CTM76_01255	CTM93_13925	CTM79_20040	C9J19_04450	DAT36_14325	CTM80_13105	CTM85_03865	CTM70_08705	CTM75_04480	C9J18_12245	AYY26_07925
cytochrome bd oxidase																
Subunit I *cyd* A	CTM87_12005	C9J22_05890	C9J21_06460	CTM67_17480	CTM77_00445	CTM76_04600	CTM93_01765	CTM79_13365	C9J19_20200	DAT36_03860	CTM80_18495	CTM85_11530	CTM70_15530	CTM75_00610	C9J18_01880	AYY26_04395
	CTM87_11255	C9J22_07710	C9J21_02620	CTM67_04365	CTM77_05030	CTM76_05295	CTM93_13090	CTM79_19320	C9J19_00660	DAT36_19135	CTM80_03100	CTM85_07980	CTM70_01705	CTM75_09470	C9J18_01225	AYY26_05065
Subunit II *cyd* B	CTM87_11250 + CTM87_12010	C9J22_05885 + C9J22_07715	C9J21_02615 + C9J21_06455	CTM67_04360 + CTM67_17485	CTM77_05035 + CTM77_00450	CTM76_04595 + CTM76_05300	CTM93_13095 + CTM93_01770	CTM79_13370 + CTM79_19325	C9J19_20195 + C9J19_00665	DAT36_19130 + DAT36_03855	CTM80_03095 + CTM80_18500	CTM85_11525 + CTM85_07975	CTM70_01710 + CTM70_15535	CTM75_09475 + CTM75_00605	C9J18_01885	AYY26_05070 + AYY26_04390
subunit cydX	CTM87_12015	C9J22_05880	C9J21_06450	CTM67_17490	CTM77_00455	CTM76_04590	CTM93_01775	CTM79_13375	C9J19_20190	DAT36_03850	CTM80_18505	CTM85_11520	CTM70_15540	CTM75_00600	C9J18_01890	AYY26_04385
	CTM87 11245	C9J22 07720	C9J21 02610	CTM67 04355	CTM77 05040	CTM76 05305	CTM93 13100	CTM79 19330	C9J19 00670	DAT36 19125	CTM80 03090	CTM85 07970	CTM70 01715	CTM75 09480	C9J18 01215	AYY26 05075
NADH:ubiquinone oxidoreductase (ndh)																
	CTM87 09900	C9J22 05275	C9J21 09375	CTM67 07170	CTM77 01050	CTM76 14635	CTM93 17730	CTM79 05025	C9J19 05490	DAT36 03240	CTM80 02165	CTM85 00895	CTM70 11970	CTM75 00010	C9J18 02495	AYY26 03870
Succinate dehydrogenase (complex II) sdhABCD	CTM87_11705	C9J22_06195	C9J21_06760	CTM67_01610	CTM77_00145	CTM76_04900	CTM93_01465	CTM79_07325	C9J19_00300	DAT36_02920	CTM80_07885	CTM85_11830	CTM70_04270	CTM75_04675	C9J18_01580	AYY26_04695
	CTM87 11700	C9J22 06200	C9J21 06765	CTM67 01615	CTM77 00140	CTM76 04905	CTM93 01460	CTM79 07320	C9J19 00305	DAT36 02915	CTM80 07890	CTM85 11835	CTM70 04275	CTM75 04680	C9J18 01575	AYY26 04700
	CTM87_11695	C9J22_06205	C9J21_06770	CTM67_01620	CTM77_00135	CTM76_04910	CTM93_01455	CTM79_07315	C9J19_00310	DAT36_02910	CTM80_07895	CTM85_11840	CTM70_04280	CTM75_04685	C9J18_01570	AYY26_04705
	CTM87_11690	C9J22_06210	C9J21_06775	CTM67_01625	CTM77_00130	CTM76_04915	CTM93_01450	CTM79_07310	C9J19_00315	DAT36_02905	CTM80_07900	CTM85_11845	CTM70_04285	CTM75_04690	C9J18_01565	AYY26_04710
cytochrome C																
cytochrome b	CTM87_13855	C9J22_13760	C9J21_18140	CTM67_02260	CTM77_06985	CTM76_13365	CTM93_17230	CTM79_00330	C9J19_10775	DAT36_07920	CTM80_04320	CTM85_08580	CTM70_03785	CTM75_02385	C9J18_06055	AYY26_11540
cytochrome c	CTM87_10895	C9J22_08280	C9J21_02060	CTM67_00100	CTM77_05590	CTM76_05860	CTM93_01095	CTM79_06420	C9J19_01225	DAT36_00525	CTM80_05955	CTM85_09455	CTM70_01055	CTM75_01450	C9J18_00655	AYY26_05430
Cytochrome c	CTM87_07525	C9J22_15660	C9J21_11460	CTM67_05410	CTM77_15315	CTM76_02385	CTM93_07940	CTM79_16415	C9J19_12475	DAT36_05830	CTM80_00275	CTM85_03040	CTM70_08055	CTM75_11985	C9J18_16880	AYY26_06860
cytochrome c4	CTM87_15890	C9J22_15360	C9J21_10290	CTM67_04655	CTM77_14480	CTM76_15555	CTM93_08905	CTM79_08685	C9J19_14675	DAT36_09245	CTM80_08265	CTM85_13065	CTM70_05260	CTM75_14355	C9J18_16390	AYY26_14560
cytochrome C554	CTM87_05735	C9J22_02980	C9J21_19625	CTM67_17835	CTM77_15655	CTM76_16975	CTM93_18420	CTM79_18270	C9J19_19095	DAT36_11765	CTM80_08820	CTM85_19815	CTM70_12315	CTM75_16645	C9J18_18920	AYY26_07580
cytochrome bc complex bzw. cytochrom-c-reductase(Fe-S, b, c1) qcrA/qcrb/qcrC	CTM87_13850	C9J22_13765	C9J21_18145	CTM67_02265	CTM77_06990	CTM76_13360	CTM93_17225	CTM79_00325	C9J19_10780	DAT36_07915	CTM80_04325	CTM85_08585	CTM70_03780	CTM75_02380	C9J18_06060	AYY26_11545
	CTM87_13855	C9J22_13760	C9J21_18140	CTM67_02260	CTM77_06985	CTM76_13365	CTM93_17230	CTM79_00330	C9J19_10775	DAT36_07920	CTM80_04320	CTM85_08580	CTM70_03785	CTM75_02385	C9J18_06055	AYY26_11540
	CTM87_13860	C9J22_13755	C9J21_18135	CTM67_02255	CTM77_06980	CTM76_13370	CTM93_17235	CTM79_00335	C9J19_10770	DAT36_07925	CTM80_04315	CTM85_08575	CTM70_03790	CTM75_02390	C9J18_06050	AYY26_11535
Fumarate reductase frdABCD	CTM87_18490	C9J22_17085	C9J21_13610	CTM67_09065	CTM77_10465	CTM76_18215	CTM93_12075	CTM79_20855	C9J19_19705	DAT36_13665	CTM80_06725	CTM85_16035	CTM70_03150	CTM75_09135	C9J18_18765	AYY26_16850
	CTM87_18495	C9J22_17090	C9J21_13615	CTM67_09060	CTM77_10460	CTM76_18210	CTM93_12070	CTM79_20850	C9J19_19710	DAT36_13660	CTM80_06730	CTM85_16040	CTM70_03155	CTM75_09140	C9J18_18760	AYY26_16845
	CTM87_18500	C9J22_17095	C9J21_13620	CTM67_09055	CTM77_10455	CTM76_18205	CTM93_12065	CTM79_20845	C9J19_19715	DAT36_13655	CTM80_06735	CTM85_16045	CTM70_03160	CTM75_09145	C9J18_18755	AYY26_16840
	CTM87 18505	C9J22 17100	C9J21 13625	CTM67 09050	CTM77 10450	CTM76 18200	CTM93 12060	CTM79 20840	C9J19 19720	DAT36 13650	CTM80 06740	CTM85 16050	CTM70 03165	CTM75 09150	C9J18 18750	AYY26 16835
Formate dehydrogenase fdhABCE																
A	CTM87_19605	C9J22_20095	C9J21_01435	CTM67_19425	CTM77_19140	CTM76_06460	CTM93_09810	CTM79_20675	C9J19_15190	DAT36_16685	CTM80_19530	CTM85_19620	CTM70_17170	CTM75_19190	C9J18_00050	AYY26_15085
B	CTM87_19610	C9J22_20100	C9J21_01430	CTM67_19430	CTM77_19135	CTM76_06465	CTM93_09815	CTM79_20680	C9J19_15195	DAT36_16680	CTM80_19535	CTM85_19615	CTM70_17175	CTM75_19185	C9J18_00045	AYY26_15090
C	CTM87_19615	C9J22_20105	C9J21_01425	CTM67_19435	CTM77_19130	CTM76_06470	CTM93_09820	CTM79_20685	C9J19_15200	DAT36_16675	CTM80_19540	CTM85_19610	CTM70_17180	CTM75_19180	C9J18_00040	AYY26_15095
E	CTM87_19620	C9J22_20110	C9J21_01420	CTM67_19440	CTM77_19125	CTM76_06475	CTM93_09825	CTM79_20690	C9J19_15205	DAT36_16670	CTM80_19545	CTM85_19605	CTM70_17185	CTM75_19175	C9J18_00035	AYY26_15100
Quinone Q-8 biosynthesis																
Chorismate pyruvate lyase (ubiC)	CTM87_09005	C9J22_12015	C9J21_14140	CTM67_06795	CTM77_12250	CTM76_12845	CTM93_04420	CTM79_02895	C9J19_06795	DAT36_12350	CTM80_01155	CTM85_05255	CTM70_04780	CTM75_06555	C9J18_11495	AYY26_12615
4-hydroxybenzoate octaprenyltransferase (ubiA)	CTM87_09000	C9J22_12010	C9J21_14135	CTM67_06790	CTM77_12255	CTM76_12840	CTM93_04425	CTM79_02890	C9J19_06800	DAT36_12345	CTM80_01160	CTM85_05260	CTM70_04785	CTM75_06560	C9J18_11490	AYY26_12610
3-octaprenyl-4-hydroxybenzoate carboxy-lyase (ubiD)	CTM87_09240	C9J22_18920	C9J21_16600	CTM67_11850	CTM77_12020	CTM76_18865	CTM93_16100	CTM79_15195	C9J19_19320	DAT36_16330	CTM80_14965	CTM85_17995	CTM70_07050	CTM75_13990	C9J18_20040	AYY26_18600
2-octaprenylphenol 6-hydroxylase (ubiB)	CTM87_15730	C9J22_15520	C9J21_10450	CTM67_04495	CTM77_19980	CTM76_15715	CTM93_08745	CTM79_08525	C9J19_14515	DAT36_09085	CTM80_08425	CTM85_13225	CTM70_08405	CTM75_13790	C9J18_16225	AYY26_14405
3-demethylubiquinol 3-O-methyltransferase (ubiG)	CTM87 09610	C9J22 05565	C9J21 15015	CTM67 05870	CTM77 00760	CTM76 04285	CTM93 02080	CTM79 05315	C9J19 05780	DAT36 03530	CTM80 02450	CTM85 01180	CTM70 15115	CTM75 00295	C9J18 02205	AYY26 04160
2-octaprenyl-6-methoxyphenyl hydroxylase (ubiH)	CTM87_17210	C9J22_17790	C9J21_14545	CTM67_06305	CTM77_16445	CTM76_16020	CTM93_14775	CTM79_00965	C9J19_17120	DAT36_14445	CTM80_13190	CTM85_17320	CTM70_04670	CTM75_11355	C9J18_05480	AYY26_17145
2-methoxy-6-octaprenyl-1,4-benzoquinol methylase (ubiE)	CTM87_15720	C9J22_15530	C9J21_10460	CTM67_04485	CTM77_19970	CTM76_15725	CTM93_08735	CTM79_08515	C9J19_14505	DAT36_09075	CTM80_08435	CTM85_13235	CTM70_08395	CTM75_13780	C9J18_16215	AYY26_14395

	P. phosphoreum															
	AK-3	AK-4	AK-5	AK-8	ATCC 11040	FS-1.1	FS-1.2	FS-2.1	FS-2.2	FS-3.2	FS-4.1	FS-4.2	FS-5.1	FS-5.2	FS-6.1	GCSL-P69
2-octaprenyl-3-methyl-6-methoxy-1,4-benzoquinol hydroxylase (ubiF)	CTM87_15895	C9J22_15355	C9J21_10285	CTM67_04660	CTM77_14485	CTM76_15550	CTM93_08910	CTM79_08690	C9J19_14680	DAT36_09250	CTM80_08260	CTM85_13060	CTM70_05265	CTM75_14350	C9J18_16395	AYY26_14565
ubiCADBGHEF																
F0F1-ATP synthase																
F0F1 ATP synthase subunit A	CTM87_14975	C9J22_01180	C9J21_10655	CTM67_12810	CTM77_12560	CTM76_06810	CTM93_02665	CTM79_14255	C9J19_14205	DAT36_08665	CTM80_16345	CTM85_01960	CTM70_17280	CTM75_14530	C9J18_03955	AYY26_09475
ATP synthase F0 subunit B	CTM87_14985	C9J22_01190	C9J21_10645	CTM67_12820	CTM77_12570	CTM76_06800	CTM93_02655	CTM79_14265	C9J19_14195	DAT36_08655	CTM80_16355	CTM85_01970	CTM70_17270	CTM75_14540	C9J18_03945	AYY26_09465
F0F1 ATP synthase subunit C	CTM87_14980	C9J22_01185	C9J21_10650	CTM67_12815	CTM77_12565	CTM76_06805	CTM93_02660	CTM79_14260	C9J19_14200	DAT36_08660	CTM80_16350	CTM85_01965	CTM70_17275	CTM75_14535	C9J18_03950	AYY26_09470
F0F1 ATP synthase subunit alpha	CTM87_14995	C9J22_01200	C9J21_10635	CTM67_12830	CTM77_12580	CTM76_06790	CTM93_02645	CTM79_14275	C9J19_14185	DAT36_08645	CTM80_16365	CTM85_01980	CTM70_17260	CTM75_14550	C9J18_03935	AYY26_09455
F0F1 ATP synthase subunit beta	CTM87_15005	C9J22_01210	C9J21_10625	CTM67_12840	CTM77_12590	CTM76_06780	CTM93_02635	CTM79_14285	C9J19_14175	DAT36_08635	CTM80_16375	CTM85_01990	CTM70_17250	CTM75_14560	C9J18_03925	AYY26_09445
F0F1 ATP synthase subunit gamma	CTM87_15000	C9J22_01205	C9J21_10630	CTM67_12835	CTM77_12585	CTM76_06785	CTM93_02640	CTM79_14280	C9J19_14180	DAT36_08640	CTM80_16370	CTM85_01985	CTM70_17255	CTM75_14555	C9J18_03930	AYY26_09450
F0F1 ATP synthase subunit delta	CTM87_14990	C9J22_01195	C9J21_10640	CTM67_12825	CTM77_12575	CTM76_06795	CTM93_02650	CTM79_14270	C9J19_14190	DAT36_08650	CTM80_16360	CTM85_01975	CTM70_17265	CTM75_14545	C9J18_03940	AYY26_09460
F0F1 ATP synthase subunit epsilon	CTM87_15010	C9J22_01215	C9J21_10620	CTM67_12845	CTM77_12595	CTM76_06775	CTM93_02630	CTM79_14290	C9J19_14170	DAT36_08630	CTM80_16380	CTM85_01995	CTM70_17245	CTM75_14565	C9J18_03920	AYY26_09440
F0F1 ATP synthase subunit A	CTM87_16285	C9J22_16850	C9J21_12235	CTM67_08235	CTM77_14140	CTM76_17260	CTM93_11160	CTM79_10540	C9J19_16510	DAT36_12700	CTM80_10145	CTM85_14305	CTM70_02325	CTM75_07375	C9J18_18005	AYY26_16150
ATP synthase F0 subunit B	CTM87_16295	C9J22_16860	C9J21_12225	CTM67_08225	CTM77_14150	CTM76_17250	CTM93_11170	CTM79_10550	C9J19_16520	DAT36_12710	CTM80_10155	CTM85_14295	CTM70_02315	CTM75_07385	C9J18_18015	AYY26_16140
F0F1 ATP synthase subunit C	CTM87_16290	C9J22_16855	C9J21_12230	CTM67_08230	CTM77_14145	CTM76_17255	CTM93_11165	CTM79_10545	C9J19_16515	DAT36_12705	CTM80_10150	CTM85_14300	CTM70_02320	CTM75_07380	C9J18_18010	AYY26_16145
F0F1 ATP synthase subunit alpha	CTM87_16305	C9J22_16870	C9J21_12215	CTM67_08215	CTM77_14160	CTM76_17240	CTM93_11180	CTM79_10560	C9J19_16530	DAT36_12720	CTM80_10165	CTM85_14285	CTM70_02305	CTM75_07395	C9J18_18025	AYY26_16130
F0F1 ATP synthase subunit beta	CTM87_16315	C9J22_16880	C9J21_12205	CTM67_08205	CTM77_14170	CTM76_17230	CTM93_11190	CTM79_10570	C9J19_16540	DAT36_12730	CTM80_10175	CTM85_14275	CTM70_02295	CTM75_07405	C9J18_18035	AYY26_16120
F0F1 ATP synthase subunit gamma	CTM87_16310	C9J22_16875	C9J21_12210	CTM67_08210	CTM77_14165	CTM76_17235	CTM93_11185	CTM79_10565	C9J19_16535	DAT36_12725	CTM80_10170	CTM85_14280	CTM70_02300	CTM75_07400	C9J18_18030	AYY26_16125
F0F1 ATP synthase subunit delta	CTM87_16300	C9J22_16865	C9J21_12220	CTM67_08220	CTM77_14155	CTM76_17245	CTM93_11175	CTM79_10555	C9J19_16525	DAT36_12715	CTM80_10160	CTM85_14290	CTM70_02310	CTM75_07390	C9J18_18020	AYY26_16135
F0F1 ATP synthase subunit epsilon	CTM87_16320	C9J22_16885	C9J21_12200	CTM67_08200	CTM77_14175	CTM76_17225	CTM93_11195	CTM79_10575	C9J19_16545	DAT36_12735	CTM80_10180	CTM85_14270	CTM70_02290	CTM75_07410	C9J18_18040	AYY26_16115
ATP F0F1 synthase subunit I	CTM87_16280	C9J22_16845	C9J21_12240	CTM67_08240	CTM77_14135	CTM76_17265	CTM93_11155	CTM79_10535	C9J19_16505	DAT36_12695	CTM80_10140	CTM85_14310	CTM70_02330	CTM75_07370	C9J18_18000	AYY26_16155
Heme biosynthesis																
Glutamyl−tRNA reductase (hemA	CTM87_20285	C9J22_14430	C9J21_13110	CTM67_10050	CTM77_19835	CTM76_17780	CTM93_12895	CTM79_11370	C9J19_03275	DAT36_13230	CTM80_10535	CTM85_15600	CTM70_12120	CTM75_08585	C9J18_21130	AYY26_15450
glutamate-1-semialdehyde-2,1-aminomutase (hemL)	CTM87_12705	C9J22_09690	C9J21_07110	CTM67_15955	CTM77_05765	CTM76_11925	CTM93_05345	CTM79_03900	C9J19_06545	DAT36_01120	CTM80_11075	CTM85_04400	CTM70_00505	CTM75_01275	C9J18_10145	AYY26_09790
aminolevulinic acid dehydratase (hemB)	CTM87_04765	C9J22_02240	C9J21_00895	CTM67_12465	CTM77_19735	CTM76_10475	CTM93_17520	CTM79_18650	C9J19_02125	DAT36_06795	CTM80_13490	CTM85_07470	CTM70_15435	CTM75_05655	C9J18_15810	AYY26_13835
	CTM87_15755	C9J22_15495	C9J21_10425	CTM67_04520	CTM77_14345	CTM76_15690	CTM93_08770	CTM79_08550	C9J19_14540	DAT36_09110	CTM80_08400	CTM85_13200	CTM70_08430	CTM75_13815	C9J18_16250	AYY26_14430
Hydroxymethylbilane synthase (hemC)	CTM87_15790	C9J22_15460	C9J21_10390	CTM67_04555	CTM77_14380	CTM76_15655	CTM93_08805	CTM79_08585	C9J19_14575	DAT36_09145	CTM80_08365	CTM85_13165	CTM70_08465	CTM75_13850	C9J18_16285	AYY26_14465
Uroporphyrinogen-III synthase (hemD)	CTM87_15785	C9J22_15465	C9J21_10395	CTM67_04550	CTM77_14375	CTM76_15660	CTM93_08800	CTM79_08580	C9J19_14570	DAT36_09140	CTM80_08370	CTM85_13170	CTM70_08460	CTM75_13845	C9J18_16280	AYY26_14460
Uroporphyrinogen decarboxylase (hemE)	CTM87_19450	C9J22_17290	C9J21_13815	CTM67_08860	CTM77_19415	CTM76_18010	CTM93_11865	CTM79_12610	C9J19_18960	DAT36_13460	CTM80_06930	CTM85_16245	CTM70_03360	CTM75_09345	C9J18_18560	AYY26_16645
Coproporphyrinogen III oxidase (oxygen independent) (hemN)	CTM87_15905	C9J22_15345	C9J21_10275	CTM67_04670	CTM77_14495	CTM76_15540	CTM93_08920	CTM79_08700	C9J19_14690	DAT36_09260	CTM80_08250	CTM85_13050	CTM70_05275	CTM75_14340	C9J18_16405	AYY26_14575
Coproporphyrinogen III oxidase (oxygen independent) (hemN)	CTM87_15910	C9J22_15340	C9J21_10270	CTM67_04675	CTM77_14500	CTM76_15535	CTM93_08925	CTM79_08705	C9J19_14695	DAT36_09265	CTM80_08245	CTM85_13045	CTM70_05280	CTM75_14335	C9J18_16410	AYY26_14580
Coproporphyrinogen III oxidase (oxygen dependent)	CTM87_16495	C9J22_17030	C9J21_12055	CTM67_08055	CTM77_14320	CTM76_17080	CTM93_11340	CTM79_10720	C9J19_16690	DAT36_12885	CTM80_10325	CTM85_14125	CTM70_02145	CTM75_07555	C9J18_18185	AYY26_15970
menaquinone-dependent protoporphyrinogen IX dehydrogenase	CTM87_16105	C9J22_16670	C9J21_12415	CTM67_08415	CTM77_13960	CTM76_17440	CTM93_10980	CTM79_10360	C9J19_16330	DAT36_12525	CTM80_09965	CTM85_14485	CTM70_02505	CTM75_07195	C9J18_17825	AYY26_16325
Ferrochelatase (hemH)	CTM87_11585	C9J22_06320	C9J21_06885	CTM67_01730	CTM77_00025	CTM76_05020	CTM93_01345	CTM79_07205	C9J19_00420	DAT36_02800	CTM80_08005	CTM85_11950	CTM70_04390	CTM75_04795	C9J18_01465	AYY26_04815
Virulence																
VOC family virulence protein	CTM87_00760	C9J22_06500	C9J21_20735	CTM67_01905	CTM77_17030	CTM76_09175	CTM93_18705	CTM79_13310	C9J19_09745	DAT36_02615	CTM80_14675	CTM85_12255	CTM70_12755	CTM75_14830	C9J18_08420	AYY26_04990
	CTM87_11405				CTM77_04955	CTM76_05200	CTM93_18265	CTM79_20615	C9J19_00600		CTM80_03190	CTM85_08060	CTM70_18035	CTM75_04980	C9J18_01290	
virulence factor BrkB family protein	CTM87_15950										CTM80_08205	CTM85_13005				
virulence protein																
virulence associated protein													CTM70_19700			
H2O2 related enzymes																
Production																
pyruvate oxidase (Pox)																
superoxide dismutase (Sod)	CTM87_03830	C9J22_06980	C9J21_03140	CTM67_12990	CTM77_04245	CTM76_03935	CTM93_06235	CTM79_09240	C9J19_15305	DAT36_02280	CTM80_08915	CTM85_09960	CTM70_11010	CTM75_12325	C9J18_06820	AYY26_02410
	CTM87_01045	C9J22_04610	C9J21_20945	CTM67_15765	CTM77_16740	CTM76_08875	CTM93_15625	CTM79_15095	C9J19_10020	DAT36_13870	CTM80_04690	CTM85_20135	CTM70_19075	CTM75_20085	C9J18_08190 / C9J18 20760	AYY26_00895
	CTM87_07040	C9J22_12795	C9J21_04500	CTM67_13475	CTM77_13025	CTM76_01460	CTM93_04090	CTM79_16010	C9J19_04255		CTM80_11615	CTM85_04065	CTM70_11410	CTM75_13645	C9J18_13405	AYY26_05880
H2O2 scavenging enzymes																
catalase	CTM87_01055	C9J22_04620	C9J21_20935	CTM67_15755	CTM77_16730	CTM76_08865	CTM93_15635	CTM79_15105	C9J19_10030		CTM80_04700	CTM85_20145	CTM70_19720	CTM75_19745	C9J18_08180	AYY26_00905
catalase/peroxidase	CTM87_02810	C9J22_00020	C9J21_04670	CTM67_20140	CTM77_02315	CTM76_07830	CTM93_06675	CTM79_04475	C9J19_09645	DAT36_04365	CTM80_19455	CTM85_11405	CTM70_13925	CTM75_05570	C9J18_05115	AYY26_10915
Pressure response																
TMAO reductase system sensor histidine kinase/response regulator TorS	CTM87_04445	C9J22_08960	C9J21_05490	CTM67_10160	CTM77_08085	CTM76_03310	CTM93_00325	CTM79_01365	C9J19_12065	DAT36_06180	CTM80_05770	CTM85_15840	CTM70_11860	CTM75_03175	C9J18_07445	AYY26_01795
Molecular chaperone Dnak	CTM87_05180	C9J22_02660	C9J21_01310	CTM67_07735	CTM77_07655	CTM76_10060	CTM93_07140	CTM79_17200	C9J19_01710	DAT36_09720	CTM80_15655	CTM85_06450	CTM70_07580	CTM75_13455	C9J18_15260	AYY26_13420
	CTM87_20480	C9J22_10310	C9J21_18760	CTM67_16190	CTM77_06435	CTM76_11230	CTM93_18765	CTM79_17905	C9J19_05880	DAT36_01760	CTM80_15325	CTM85_05070	CTM70_14745	CTM75_17700	C9J18_10770	AYY26_10440
				CTM67_13930	CTM77_16095							CTM85_17145		CTM75_12980		
Molecular chaperone DnaJ	CTM87_05175	C9J22_02655	C9J21_01305	CTM67_07740	CTM77_07650	CTM76_10065	CTM93_07145	CTM79_17205	C9J19_01715	DAT36_09725	CTM80_15650	CTM85_06445	CTM70_07575	CTM75_13460	C9J18_15265	AYY26_13425
	CTM87_20475	C9J22_10315	C9J21_18755	CTM67_16195	CTM77_06440	CTM76_11225	CTM93_18760	CTM79_17900	C9J19_05875	DAT36_01765	CTM80_15330	CTM85_05075	CTM70_14750	CTM75_17695	C9J18_10775	AYY26_10445
Molecular chaperone GroEL	CTM87_18530	C9J22_17125	C9J21_13650	CTM67_09025	CTM77_10420	CTM76_18175	CTM93_12030	CTM79_12775	C9J19_19750	DAT36_13625	CTM80_06765	CTM85_16080	CTM70_03195	CTM75_09180	C9J18_18725	AYY26_16810
	CTM87_18525	C9J22_17120	C9J21_13645	CTM67_09030	CTM77_10430	CTM76_18180	CTM93_12040	CTM79_12780	C9J19_19740	DAT36_13630	CTM80_06760	CTM85_16070	CTM70_03185	CTM75_09170	C9J18_18730	AYY26_16815
Co-chaperone GroES	CTM87_18535	C9J22_17130	C9J21_13655	CTM67_09020	CTM77_10415	CTM76_18170	CTM93_12025	CTM79_12770	C9J19_19755	DAT36_13620	CTM80_06770	CTM85_16085	CTM70_03200	CTM75_09185	C9J18_18720	AYY26_16805
Outer membrane protein OmpH	CTM87_19155	C9J22_16065	C9J21_11165	CTM67_09175	CTM77_14955	CTM76_16365	CTM93_10135	CTM79_10265	C9J19_16235	DAT36_11220	CTM80_11790	CTM85_13825	CTM70_06665	CTM75_06120	C9J18_17560	AYY26_19580
Porin-like protein OmpL		C9J22_09990						CTM79_04200	C9J19_06245	DAT36_01420	CTM80_09840			CTM75_00975	C9J18_10445	
	CTM87_12405	C9J22_09990			CTM77_06065	CTM76_11625	CTM93_05645	CTM79_04200	C9J19_06245		CTM80_09840	CTM85_04700	CTM70_00205	CTM75_00975	C9J18_10445	AYY26_10090
Transcription activator system ToxR	CTM87_11570	C9J22_06335	C9J21_06900	CTM67_01745	CTM77_04790	CTM76_05035	CTM93_01330	CTM79_07190	C9J19_00435	DAT36_02785	CTM80_03355	CTM85_08225	CTM70_10005	CTM75_04810	C9J18_01450	AYY26_04830
ToxS	CTM87_11565	C9J22_06340	C9J21_06905	CTM67_01750	CTM77_04795	CTM76_05040	CTM93_01325	CTM79_07185	C9J19_00440	DAT36_02780	CTM80_03350	CTM85_08220	CTM70_10010	CTM75_04815	C9J18_01445	AYY26_04835
RNA polymerase sigma factor RpoE	CTM87_17275	C9J22_17855	C9J21_14480	CTM67_06240	CTM77_16510	CTM76_16085	CTM93_14710	CTM79_01030	C9J19_17185	DAT36_14510	CTM80_13255	CTM85_17385	CTM70_04605	CTM75_11420	C9J18_05415	AYY26_17080
Anti-sigma E factor RseA	CTM87_17280	C9J22_17860	C9J21_14475	CTM67_06235	CTM77_16515	CTM76_16090	CTM93_14705	CTM79_01035	C9J19_17190	DAT36_14515	CTM80_13260	CTM85_17390	CTM70_04600	CTM75_11425	C9J18_05410	AYY26_17075
Sigma-E factor regulatory protein RseB	CTM87_17285	C9J22_17865	C9J21_14470	CTM67_06230	CTM77_16520	CTM76_16095	CTM93_14700	CTM79_01040	C9J19_17195	DAT36_14520	CTM80_13265	CTM85_17395	CTM70_04595	CTM75_11430	C9J18_05405	AYY26_17070
Transcriptional regulator RseC	CTM87_17290	C9J22_17870	C9J21_14465	CTM67_06225	CTM77_16525	CTM76_16100	CTM93_14695	CTM79_01045	C9J19_17200	DAT36_14525	CTM80_13270	CTM85_17400	CTM70_04590	CTM75_11435	C9J18_05400	AYY26_17065
Exodeoxyribonuclease V subunit alpha, RecD	CTM87_18995	C9J22_16265	C9J21_10985	CTM67_09370	CTM77_14755	CTM76_16585	CTM93_09930	CTM79_10075	C9J19_16045	DAT36_11020	CTM80_11980	CTM85_14030	CTM70_09430	CTM75_06330	C9J18_17745	AYY26_20205
Salt Response																
Outer membrane protein OmpW																
Major outer membrane protein OmpV																
RNA polymerase sigma factor RpoS	CTM87_13125	C9J22_01750	C9J21_00365	CTM67_19835	CTM77_11035	CTM76_10990	CTM93_08315	CTM79_03445	C9J19_02625	DAT36_11680	CTM80_19020	CTM85_07000	CTM70_13655	CTM75_18260	C9J18_03395	AYY26_08900
	CTM87_17395	C9J22_17975	C9J21_14360	CTM67_06120	CTM77_16630	CTM76_16205	CTM93_14590	CTM79_01150	C9J19_17305	DAT36_14630	CTM80_13375	CTM85_17505	CTM70_04485	CTM75_11540	C9J18_05295	AYY26_16960
	CTM87_00185	C9J22_03860	C9J21_11780	CTM67_16075	CTM77_09900	CTM76_09665	CTM93_11485	CTM79_12370	C9J19_17650	DAT36_16125	CTM80_13740	CTM85_14630	CTM70_12280	CTM75_08940	C9J18_08910	AYY26_00145

	P. phosphoreum															
	AK-3	**AK-4**	**AK-5**	**AK-8**	**ATCC 11040**	**FS-1.1**	**FS-1.2**	**FS-2.1**	**FS-2.2**	**FS-3.2**	**FS-4.1**	**FS-4.2**	**FS-5.1**	**FS-5.2**	**FS-6.1**	**GCSL-P69**
Two-component system response regulator OmpR	CTM87_08895	C9J22_11905	C9J21_14030	CTM67_06685	CTM77_18465	CTM76_12735	CTM93_04530	CTM79_02785	C9J19_06905	DAT36_12240	CTM80_01265	CTM85_05365	CTM70_04890	CTM75_06665	C9J18_11385	AYY26_12505
Two-component system sensor histidine kinase EnvZ	CTM87_08890	C9J22_11900	C9J21_14025	CTM67_06680	CTM77_18470	CTM76_12730	CTM93_04535	CTM79_02780	C9J19_06910	DAT36_12235	CTM80_01270	CTM85_05370	CTM70_04895	CTM75_06670	C9J18_11380	AYY26_12500
Porin OmpC/OmpF																
Sodium transporters																
sodium:alanine symporter family protein	CTM87_15450	C9J22_14950	C9J21_17275	CTM67_12225	CTM77_03605	CTM76_00230	CTM93_19215	CTM79_05560	C9J19_11535	DAT36_19015	CTM80_07130	CTM85_00200	CTM70_13335	CTM75_10315	C9J18_12490	AYY26_03190
	CTM87_12575	C9J22_09820	C9J21_07240	CTM67_01195	CTM77_05895	CTM76_11795	CTM93_05475	CTM79_04030	C9J19_06415	DAT36_01250	CTM80_10945	CTM85_04530	CTM70_00375	CTM75_01145	C9J18_10275	AYY26_09920
sodium:alanine (sodium:glycine) symporter family protein	CTM87_15395	C9J22_14895	C9J21_17330	CTM67_19060	CTM77_03660	CTM76_00175	CTM93_14270	CTM79_05615	C9J19_11590	DAT36_10215	CTM80_07185	CTM85_00255	CTM70_13280	CTM75_10260	C9J18_12435	AYY26_03250
sodium:proton antiporter	CTM87_02400	C9J22_00455	C9J21_05075	CTM67_15055	CTM77_01905	CTM76_07420	CTM93_15160	CTM79_08400	C9J19_09235	DAT36_03915	CTM80_03725	CTM85_10975	CTM70_03715	CTM75_03495	C9J18_04705	AYY26_13070
	CTM87_19820	C9J22_14065	C9J21_21420	CTM67_18665	CTM77_07295	CTM76_13060	CTM93_13625	CTM79_00025	C9J19_11080	DAT36_07615	CTM80_04625	CTM85_08885	CTM70_09340	CTM75_02080	C9J18_06360	AYY26_11885
	CTM87_03590	C9J22_07220	C9J21_03355	CTM67_02640	CTM77_04015	CTM76_04165	CTM93_06475	CTM79_09010	C9J19_15510	DAT36_02050	CTM80_09080	CTM85_09795	CTM70_02610	CTM75_06950	C9J18_06985	AYY26_02640
	CTM87_03840	C9J22_06970	C9J21_03130	CTM67_13000	CTM77_04255	CTM76_03925	CTM93_06225	CTM79_09250	C9J19_15295	DAT36_02290	CTM80_08905	CTM85_09970	CTM70_11000	CTM75_12315	C9J18_06810	AYY26_02400
	CTM87_01690	C9J22_04915	C9J21_13320	CTM67_07555	CTM77_13340	CTM76_08540	CTM93_12205	CTM79_07940	C9J19_10320	DAT36_08190	CTM80_04990	CTM85_13435	CTM70_08620	CTM75_12720	C9J18_17320	AYY26_01245
Na+/H+ antiporter	CTM87_07505	C9J22_15640	C9J21_11440	CTM67_05430	CTM77_15295	CTM76_02405	CTM93_07920	CTM79_16395	C9J19_12495	DAT36_05810	CTM80_00255	CTM85_03060	CTM70_08075	CTM75_11965	C9J18_16860	AYY26_06880
Na+/H+ antiporter NhaA	CTM87_12485	C9J22_09910	C9J21_07330	CTM67_01105	CTM77_05985	CTM76_11705	CTM93_05565	CTM79_04120	C9J19_06325	DAT36_01340	CTM80_09920	CTM85_04620	CTM70_00285	CTM75_01055	C9J18_10365	AYY26_10010
Na+/H+ antiporter NhaC	CTM87_03810	C9J22_07000	C9J21_03150	CTM67_12980	CTM77_04235	CTM76_03945	CTM93_06255	CTM79_09230	C9J19_15315	DAT36_02270	CTM80_08925	CTM85_09950	CTM70_11020	CTM75_12335	C9J18_06840	AYY26_02420
Na+/H+ antiporter NhaC		C9J22_08910			CTM77_08035							CTM85_15890				
	CTM87_13265	C9J22_01890	C9J21_00505	CTM67_11415	CTM77_11175	CTM76_10845	CTM93_08455	CTM79_03585	C9J19_02465	DAT36_15890	CTM80_16435	CTM85_07140	CTM70_13005	CTM75_08115	C9J18_03260	AYY26_17255
Na+/H+ antiporter	CTM87_11850	C9J22_06050	C9J21_06615	CTM67_01465	CTM77_00290		CTM93_01610		C9J19_00155	DAT36_03065	CTM80_07740	CTM85_11685		CTM75_00765	C9J18_01725	AYY26_04550
sodium:proton exchanger		C9J22_01850	C9J21_00465	CTM67_11455												
Na+/H+ antiporter NhaC family protein	CTM87_20320	C9J22_14470	C9J21_13150	CTM67_10090	CTM77_19875	CTM76_17820	CTM93_12930	CTM79_11410	C9J19_03315	DAT36_13270	CTM80_10495	CTM85_15640	CTM70_12080	CTM75_08625	C9J18_21170	AYY26_15415
DASS family sodium-coupled anion symporter / 2-oxoglutarate translocator	CTM87_00560	C9J22_04230	C9J21_16180	CTM67_17985	CTM77_17155	CTM76_09295	CTM93_19380	CTM79_13190	C9J19_18720	DAT36_16910	CTM80_14555	CTM85_12375	CTM70_14920	CTM75_14950	C9J18_08545	AYY26_00515
sodium:phosphate symporter	CTM87_12490	C9J22_09905	C9J21_07325	CTM67_01110	CTM77_05980	CTM76_11710	CTM93_05560	CTM79_04115	C9J19_06330	DAT36_01335	CTM80_09925	CTM85_04615	CTM70_00290	CTM75_01060	C9J18_10360	AYY26_10005
calcium/sodium antiporter	CTM87_13780	C9J22_13835	C9J21_15590	CTM67_02335	CTM77_07060	CTM76_13290	CTM93_13395	CTM79_00255	C9J19_10850	DAT36_07845	CTM80_04395	CTM85_08655	CTM70_08935	CTM75_02310	C9J18_06130	AYY26_11615
DASS family sodium-coupled anion symporter	CTM87_06465	C9J22_10815	C9J21_03960	CTM67_04875	CTM77_02945	CTM76_00920	CTM93_14455	CTM79_18825	C9J19_04780	DAT36_17360	CTM80_18120	CTM85_03530	CTM70_07785	CTM75_04145	C9J18_11910	AYY26_08310
sodium/glutamate symporter	CTM87_07385	C9J22_19590	C9J21_11335	CTM67_05535	CTM77_15190	CTM76_02520	CTM93_07815	CTM79_16285	C9J19_12600	DAT36_05710	CTM80_00145	CTM85_03170	CTM70_15725	CTM75_18915	C9J18_16760	AYY26_17940
dicarboxylate/amino acid:cation symporter	CTM87_04140	C9J22_06685	C9J21_02820	CTM67_09585		CTM76_03615	CTM93_00025	CTM79_10885	C9J19_11765	DAT36_06505	CTM80_05470	CTM85_16510	CTM70_13980	CTM75_02865	C9J18_06530	AYY26_02095
Na+:H+ dicarboxylate symporter	CTM87_16960	C9J22_09425	C9J21_05955	CTM67_08600	CTM77_17915	CTM76_02835	CTM93_00800	CTM79_01845	C9J19_17735	DAT36_10720	CTM80_12355	CTM85_12810	CTM70_05590	CTM75_11200	C9J18_07915	AYY26_16340
cation:dicarboxylase symporter family transporter	CTM87_04150	C9J22_06675	C9J21_02810	CTM67_09575	CTM77_04550	CTM76_03605	CTM93_00035	CTM79_10895	C9J19_11775	DAT36_06495	CTM80_05480	CTM85_16500	CTM70_13970	CTM75_02875	C9J18_06520	AYY26_02085
DASS family sodium-coupled anion symporter	CTM87_04360	C9J22_08855	C9J21_19725	CTM67_10255	CTM77_07985	CTM76_03395	CTM93_00240	CTM79_01280	C9J19_11980	DAT36_06265	CTM80_05685	CTM85_15940	CTM70_10880	CTM75_03090	C9J18_07345	AYY26_01880
sodium/solute symporter	CTM87_02540	C9J22_00290	C9J21_04935	CTM67_10865	CTM77_02045	CTM76_07560	CTM93_15300	CTM79_08260	C9J19_09375	DAT36_04055	CTM80_03560	CTM85_11140	CTM70_03575	CTM75_03330	C9J18_04845	AYY26_13210
sodium:solute symporter	CTM87_02055			CTM67_11705	CTM77_19260	CTM76_07090	CTM93_02945	CTM79_17655	C9J19_18530		CTM80_15465	CTM85_01685	CTM70_14300	CTM75_16030	C9J18_04235	AYY26_18810
sodium/solute symporter																
sodium/solute symporter																
sodium-dependent transporter	CTM87_03250	C9J22_12180	C9J21_21825	CTM67_18320	CTM77_20325	CTM76_19255	CTM93_17055	CTM79_06685	C9J19_08915	DAT36_17990	CTM80_16195	CTM85_18785	CTM70_06385	CTM75_15555	C9J18_16140	AYY26_10485
sodium/panthothenate symporter	CTM87_18605	C9J22_17200	C9J21_13725	CTM67_08950	CTM77_10345	CTM76_18100	CTM93_11955	CTM79_12700	C9J19_19050	DAT36_13550	CTM80_06840	CTM85_16155	CTM70_03270	CTM75_09255	C9J18_18650	AYY26_16735
sodium/glucose cotransporter				CTM67_07725												
melibiose:sodium transporter MelB	CTM87_08155				CTM77_08980			CTM79_09690	C9J19_07970		CTM80_00890	CTM85_02430		CTM75_16860		AYY26_06215
sodium/proline symporter PutP	CTM87_02725	C9J22_00110	C9J21_04760	CTM67_17135	CTM77_02225	CTM76_07740	CTM93_18445		C9J19_09555	DAT36_04265	CTM80_03385	CTM85_11320	CTM70_16600	CTM75_17115	C9J18_05025	AYY26_11005
sodium/proline symporter PutP	CTM87_14855	C9J22_01060	C9J21_10775	CTM67_12690	CTM77_12440	CTM76_06930	CTM93_02785	CTM79_14135	C9J19_14325	DAT36_08785	CTM80_16225	CTM85_01840	CTM70_11080	CTM75_14410	C9J18_04075	AYY26_09595
sodium:proline symporter		C9J22_07615					CTM93_18295									
sodium:proline symporter								CTM79_08080								
sodium:proline symporter								CTM79_21310								
bile acid:sodium symporter family protein	CTM87_07205		C9J21_08885		CTM77_12860	CTM76_01625	CTM93_03925	CTM79_20165	C9J19_04090		CTM80_19940	CTM85_04230	CTM70_13085	CTM75_17790	C9J18_13245	AYY26_06040
Motility																
chemotaxis-specific protein-glutamate methyltransferase CheB		C9J22_07875	C9J21_02460	CTM67_04205	CTM77_05180	CTM76_05450		CTM79_13935	C9J19_00815	DAT36_00935	CTM80_02945	CTM85_07830	CTM70_01860	CTM75_09625	C9J18_01070	
chemotaxis protein CheA		C9J22_07870	C9J21_02465	CTM67_04210	CTM77_05185	CTM76_05455		CTM79_13930	C9J19_00820	DAT36_00930	CTM80_02940	CTM85_07825	CTM70_01865	CTM75_09630	C9J18_01065	
protein phosphatase CheZ		C9J22_07875	C9J21_02460	CTM67_04205	CTM77_05190	CTM76_05460		CTM79_13925	C9J19_00825	DAT36_00925	CTM80_02935	CTM85_07820	CTM70_01870	CTM75_09635	C9J18_01060	
chemotaxis protein CheY		C9J22_07880	C9J21_02455	CTM67_04200	CTM77_05195	CTM76_05465		CTM79_13920	C9J19_00830	DAT36_00920	CTM80_02930	CTM85_07815	CTM70_01875	CTM75_09640	C9J18_01055	
RNA polymerase sigma factor FliA		C9J22_07885	C9J21_02450	CTM67_04195	CTM77_05200	CTM76_05470		CTM79_13915	C9J19_00835	DAT36_00915	CTM80_02925	CTM85_07810	CTM70_01880	CTM75_09645	C9J18_01050	
flagellar biosynthesis protein FlhF		C9J22_07895	C9J21_02440	CTM67_04185	CTM77_05210	CTM76_05480		CTM79_13905	C9J19_00845	DAT36_00905	CTM80_02915	CTM85_07800	CTM70_01890	CTM75_09655	C9J18_01040	
flagellar biosynthesis protein FlhA		C9J22_07900	C9J21_02435	CTM67_04180	CTM77_05215	CTM76_05485		CTM79_13900	C9J19_00850	DAT36_00900	CTM80_02910	CTM85_07795	CTM70_01895	CTM75_09660	C9J18_01035	
flagellar biosynthesis protein FlhB		C9J22_07905	C9J21_02430	CTM67_04175	CTM77_05220	CTM76_05490		CTM79_13895	C9J19_00855	DAT36_00895	CTM80_02905	CTM85_07790	CTM70_01900	CTM75_09665	C9J18_01030	
flagellar type III secretion system protein FliR		C9J22_07910	C9J21_02425	CTM67_04170	CTM77_05225	CTM76_05495		CTM79_13890	C9J19_00860	DAT36_00890	CTM80_02900	CTM85_07785	CTM70_01905	CTM75_09670	C9J18_01025	
flagellar biosynthetic protein FliQ		C9J22_07915	C9J21_02420	CTM67_04165	CTM77_05230	CTM76_05500		CTM79_13885	C9J19_00865	DAT36_00885	CTM80_02895	CTM85_07780	CTM70_01910	CTM75_09675	C9J18_01020	
flagellar type III secretion system pore protein FliP		C9J22_07920	C9J21_02415	CTM67_04160	CTM77_05235	CTM76_05505		CTM79_13880	C9J19_00870	DAT36_00880	CTM80_02890	CTM85_07775	CTM70_01915	CTM75_09680	C9J18_01015	
flagellar biosynthetic protein FliO		C9J22_07925	C9J21_02410	CTM67_04155	CTM77_05240	CTM76_05510		CTM79_13875	C9J19_00875	DAT36_00875	CTM80_02885	CTM85_07770	CTM70_01920	CTM75_09685	C9J18_01010	
flagellar motor switch protein FliN		C9J22_07930	C9J21_02405	CTM67_04150	CTM77_05245	CTM76_05515		CTM79_13870	C9J19_00880	DAT36_00870	CTM80_02880	CTM85_07765	CTM70_01925	CTM75_09690	C9J18_01005	
flagellar motor switch protein FliM		C9J22_07935	C9J21_02400	CTM67_04145	CTM77_05250	CTM76_05520		CTM79_13865	C9J19_00885	DAT36_00865	CTM80_02875	CTM85_07760	CTM70_01930	CTM75_09695	C9J18_01000	
flagellar basal body-associated protein FliL		C9J22_07940	C9J21_02395	CTM67_04140	CTM77_05255	CTM76_05525		CTM79_13860	C9J19_00890	DAT36_00860	CTM80_02870	CTM85_07755	CTM70_01935	CTM75_09700	C9J18_00995	
flagella biosynthesis chaperone FliJ		C9J22_07950	C9J21_02385	CTM67_04130	CTM77_05265	CTM76_05535		CTM79_13850	C9J19_00900	DAT36_00850	CTM80_02860	CTM85_07745	CTM70_01945	CTM75_09710	C9J18_00985	
flagellar protein export ATPase FliI		C9J22_07955	C9J21_02380	CTM67_04125	CTM77_05270	CTM76_05540		CTM79_13845	C9J19_00905	DAT36_00845	CTM80_02855	CTM85_07740	CTM70_01950	CTM75_09715	C9J18_00980	
flagellar assembly protein FliH		C9J22_07960	C9J21_02375	CTM67_04120	CTM77_05275	CTM76_05545		CTM79_13840	C9J19_00910	DAT36_00840	CTM80_02850	CTM85_07735	CTM70_01955	CTM75_09720	C9J18_00975	
flagellar motor switch protein FliG		C9J22_07965	C9J21_02370	CTM67_04115	CTM77_05280	CTM76_05550		CTM79_13835	C9J19_00915	DAT36_00835	CTM80_02845	CTM85_07730	CTM70_01960	CTM75_09725	C9J18_00970	
flagellar basal body M-ring protein FliF		C9J22_07970	C9J21_02365	CTM67_04110	CTM77_05285	CTM76_05555		CTM79_13830	C9J19_00920	DAT36_00830	CTM80_02840	CTM85_07725	CTM70_01965	CTM75_09730	C9J18_00965	
flagellar hook-basal body complex protein FliE		C9J22_07975	C9J21_02360	CTM67_04105	CTM77_05290	CTM76_05560		CTM79_13825	C9J19_00925	DAT36_00825	CTM80_02835	CTM85_07720	CTM70_01970	CTM75_09735	C9J18_00960	
flagellar biosynthesis protein FliS		C9J22_08000	C9J21_02335	CTM67_04080	CTM77_05315	CTM76_05585		CTM79_13800	C9J19_00950	DAT36_00800	CTM80_02810	CTM85_07695	CTM70_01995	CTM75_09760	C9J18_00935	
flagellar filament capping protein FliD		C9J22_08005	C9J21_02330	CTM67_04075	CTM77_05320	CTM76_05590		CTM79_13795	C9J19_00955	DAT36_00795	CTM80_02805	CTM85_07690	CTM70_02000	CTM75_09765	C9J18_00930	
flagellar biosynthesis protein FlaG		C9J22_08010	C9J21_02325	CTM67_04070	CTM77_05325	CTM76_05595		CTM79_13790	C9J19_00960	DAT36_00790	CTM80_02800	CTM85_07685	CTM70_02005	CTM75_09770	C9J18_00925	
flagellin		C9J22_08015	C9J21_02320	CTM67_04065	CTM77_05330	CTM76_05600		CTM79_13785	C9J19_00965	DAT36_00785	CTM80_02795	CTM85_07680	CTM70_02010	CTM75_09775	C9J18_00920	
flagellar hook-associated protein FlgL		C9J22_08020	C9J21_02315	CTM67_04060	CTM77_05335	CTM76_05605		CTM79_13780	C9J19_00970	DAT36_00780	CTM80_02790	CTM85_07675	CTM70_02015	CTM75_09780	C9J18_00915	
flagellar hook-associated protein FlgK		C9J22_08025	C9J21_02310	CTM67_04055	CTM77_05340	CTM76_05610		CTM79_13775	C9J19_00975	DAT36_00775	CTM80_02785	CTM85_07670	CTM70_02020	CTM75_09785	C9J18_00910	
flagellar hook protein		C9J22_08030	C9J21_02305	CTM67_04050	CTM77_05345	CTM76_05615		CTM79_13770	C9J19_00980	DAT36_00770	CTM80_02780	CTM85_07665	CTM70_02025	CTM75_09790	C9J18_00905	
flagellar assembly peptidoglycan hydrolase FlgJ		C9J22_08035	C9J21_02295	CTM67_04045	CTM77_05350	CTM76_05620		CTM79_13760	C9J19_00985	DAT36_00765	CTM80_02775	CTM85_07660	CTM70_02030	CTM75_09795	C9J18_00900	
flagellar basal body P-ring protein FlgI		C9J22_08040	C9J21_02295	CTM67_04040	CTM77_05355	CTM76_05625		CTM79_13760	C9J19_00990	DAT36_00760	CTM80_02770	CTM85_07655	CTM70_02035	CTM75_09800	C9J18_00895	
flagellar basal body L-ring protein		C9J22_08045	C9J21_02290	CTM67_04035	CTM77_05360	CTM76_05630		CTM79_13755	C9J19_00995	DAT36_00755	CTM80_02765	CTM85_07650	CTM70_02040	CTM75_09805	C9J18_00890	
flagellar basal-body rod protein FlgG		C9J22_08050	C9J21_02285	CTM67_04030	CTM77_05365	CTM76_05635		CTM79_13750	C9J19_01000	DAT36_00750	CTM80_02760	CTM85_07645	CTM70_02045	CTM75_09810	C9J18_00885	
flagellar basal-body rod protein FlgF		C9J22_08055	C9J21_02280	CTM67_04025	CTM77_05370	CTM76_05640		CTM79_13745	C9J19_01005	DAT36_00745	CTM80_02755	CTM85_07640	CTM70_02050	CTM75_09815	C9J18_00880	
flagellar hook protein FlgE		C9J22_08060	C9J21_02275	CTM67_04020	CTM77_05375	CTM76_05645		CTM79_13740	C9J19_01010	DAT36_00740	CTM80_02750	CTM85_07635	CTM70_02055	CTM75_09820	C9J18_00875	
flagellar biosynthesis protein FlgD		C9J22_08065	C9J21_02270	CTM67_04015	CTM77_05380	CTM76_05650		CTM79_13735	C9J19_01015	DAT36_00735	CTM80_02745	CTM85_07630	CTM70_02060	CTM75_09825	C9J18_00870	
flagellar basal body rod protein FlgC		C9J22_08070	C9J21_02265	CTM67_04010	CTM77_05385	CTM76_05655		CTM79_13730	C9J19_01020	DAT36_00730	CTM80_02740	CTM85_07625	CTM70_02065	CTM75_09830	C9J18_00865	
flagellar basal body rod protein FlgB		C9J22_08075	C9J21_02260	CTM67_04005	CTM77_05390	CTM76_05660		CTM79_13725	C9J19_01025	DAT36_00725	CTM80_02735	CTM85_07620	CTM70_02070	CTM75_09835	C9J18_00860	

	P. phosphoreum														
	AK-3	AK-4	AK-5	AK-8	ATCC 11040	FS-1.1	FS-1.2	FS-2.1	FS-2.2	FS-3.2	FS-4.1	FS-4.2	FS-5.1	FS-5.2	FS-6.1	GCSL-P69
chemotaxis protein CheR		C9J22_08085	C9J21_02255	CTM67_04000	CTM77_05395	CTM76_05665		CTM79_13715	C9J19_01030	DAT36_00720	CTM80_02730	CTM85_07615	CTM70_02075	CTM75_18165	C9J18_00855	
chemotaxis protein CheV		C9J22_08090	C9J21_02250	CTM67_03995	CTM77_05400	CTM76_05670		CTM79_13710	C9J19_01035	DAT36_00715	CTM80_02725	CTM85_07610	CTM70_02080	CTM75_18170	C9J18_00850	
flagellar biosynthesis protein FlhB	CTM87_11130	C9J22_07840	C9J21_02495	CTM67_04240	CTM77_05155	CTM76_05425	CTM93_13220	CTM79_13960	C9J19_00790	DAT36_00960	CTM80_02970	CTM85_07855	CTM70_01835	CTM75_09600	C9J18_01095	AYY26_05195
chemotaxis protein CheW	CTM87_11120	C9J22_07850	C9J21_02485	CTM67_04230	CTM77_05165	CTM76_05435	CTM93_13230	CTM79_13950	C9J19_00800	DAT36_00950	CTM80_02960	CTM85_07845	CTM70_01845	CTM75_09610	C9J18_01085	AYY26_05205
chemotaxis protein CheW/hypothetical protein	CTM87_11115	C9J22_07855	C9J21_02480	CTM67_04225	CTM77_05170	CTM76_05440	CTM93_13235	CTM79_13945	C9J19_00805	DAT36_00945	CTM80_02955	CTM85_07840	CTM70_01850	CTM75_09615	C9J18_01080	AYY26_05210
flagellar biosynthesis anti-sigma factor FlgM	CTM87_11080	C9J22_08100	C9J21_02240	CTM67_03985	CTM77_05410	CTM76_05680	CTM93_13270	CTM79_13700	C9J19_01045	DAT36_00705	CTM80_02715	CTM85_07600	CTM70_02090	CTM75_18180	C9J18_00840	AYY26_05245
flagellar protein FlgN	CTM87_11075	C9J22_08105	C9J21_02235	CTM67_03980	CTM77_05415	CTM76_05685	CTM93_13275	CTM79_13695	C9J19_01050	DAT36_00700	CTM80_02710	CTM85_07595	CTM70_02095	CTM75_18185	C9J18_00835	AYY26_05250
flagellar biosynthesis protein FlgP	CTM87_11070	C9J22_08110	C9J21_02230	CTM67_03975	CTM77_05420	CTM76_05690	CTM93_13280	CTM79_13690	C9J19_01055	DAT36_00695	CTM80_02705	CTM85_07590	CTM70_02100	CTM75_18190	C9J18_00830	AYY26_05255
flagellar basal-body protein	CTM87_11065	C9J22_08120	C9J21_02220	CTM67_03965	CTM77_05430	CTM76_05700	CTM93_13290	CTM79_13680	C9J19_01065	DAT36_00685	FS32_DAT36_00685	CTM85_07580	CTM70_02110	CTM75_18200	C9J18_00820	AYY26_05260
flagellar export chaperone FliS	CTM87_11090	C9J22_07995	C9J21_02340	CTM67_04085	CTM77_05310	CTM76_05580	CTM93_13260	CTM79_13805	C9J19_00945	DAT36_00805	CTM80_02815	CTM85_07700	CTM70_01990	CTM75_09755	C9J18_00940	AYY26_05235
flagella basal body P-ring formation protein FlgA	CTM87_11085	C9J22_08095	C9J21_02245	CTM67_03990	CTM77_05405	CTM76_05675	CTM93_13265	CTM79_13705	C9J19_01040	DAT36_00710	CTM80_02720	CTM85_07605	CTM70_02085	CTM75_18175	C9J18_00845	AYY26_05240
Bioluminescence																
Phosphorelay protein LuxU	CTM87_03925	C9J22_06880	C9J21_03040	CTM67_13090	CTM77_04340	CTM76_03835	CTM93_06135	CTM79_19910	C9J19_18180	DAT36_02370	CTM80_17025	CTM85_10055	CTM70_16895	CTM75_12230	C9J18_06725	AYY26_02315
transcriptional regulator quorum sensing regulator LuxR	CTM87_14115	C9J22_13510	C9J21_14885	CTM67_02015	CTM77_06740	CTM76_13610	CTM93_16960	CTM79_00590	C9J19_10520	DAT36_17200	CTM80_04070	CTM85_08325	CTM70_04035	CTM75_02630	C9J18_05800	AYY26_11295
lux-rib operon																
ribB	CTM87_02770 + CTM87_10660	C9J22_00065 + C9J22_08510	C9J21_01825 + C9J21_04715	CTM67_00330 + CTM67_18700	CTM77_02270 + CTM77_17575	CTM76_06090 + CTM76_07785	CTM93_00860 + CTM93_06630	CTM79_04430 + CTM79_06185	C9J19_01455 + C9J19_09600	DAT36_00290 + DAT36_04315	CTM80_06185 + CTM80_18345	CTM85_09220 + CTM85_11365	CTM70_00820 + CTM70_13880	CTM75_01680 + CTM75_18380	C9J18_00420 + C9J18_05070	AYY26_05660 + AYY26_10960
luxC	CTM87_02735	C9J22_00100	C9J21_04750	CTM67_19575	CTM77_02235	CTM76_07750	CTM93_06595	CTM79_21090	C9J19_09565	DAT36_04280	CTM80_18310	CTM85_11330	CTM70_17380	CTM75_19355	C9J18_05035	AYY26_10995
Activated long-chain acyl hydrolase luxD	CTM87_02740	C9J22_00095	C9J21_04745	CTM67_19580	CTM77_02240	CTM76_07755	CTM93_06600	CTM79_21095	C9J19_09570	DAT36_04285	CTM80_18315	CTM85_11335	CTM70_17385	CTM75_19360	C9J18_05040	AYY26_10990
luxE	CTM87_02760	C9J22_00075	C9J21_04725	CTM67_19600	CTM77_02260	CTM76_07775	CTM93_06620	CTM79_04420	C9J19_09590	DAT36_04305	CTM80_18335	CTM85_11355	CTM70_17405	CTM75_19380	C9J18_05060	AYY26_10970
luxF	CTM87_02755	C9J22_00080	C9J21_04730	CTM67_19595	CTM77_02255	CTM76_07770	CTM93_06615	CTM79_21110	C9J19_09585	DAT36_04300	CTM80_18330	CTM85_11350	CTM70_17400	CTM75_19375	C9J18_05055	AYY26_10975
luxG	CTM87_02765	C9J22_00070	C9J21_04720	CTM67_19605	CTM77_02265	CTM76_07780	CTM93_06625	CTM79_04425	C9J19_09595	DAT36_04310	CTM80_18340	CTM85_11360	CTM70_17410-partial	CTM75_19385	C9J18_05065	AYY26_10965
Beta subunit luciferase luxB	CTM87_02750	C9J22_00085	C9J21_04735	CTM67_19590	CTM77_02250	CTM76_07765	CTM93_06610	CTM79_21105	C9J19_09580	DAT36_04295	CTM80_18325	CTM85_11345	CTM70_17395	CTM75_19370	C9J18_05050	AYY26_10980
Alpha subunit luciferase luxA	CTM87_02745	C9J22_00090	C9J21_04740	CTM67_19585	CTM77_02245	CTM76_07760	CTM93_06605	CTM79_21100	C9J19_09575	DAT36_04290	CTM80_18320	CTM85_11340	CTM70_17390	CTM75_19365	C9J18_05045	AYY26_10985
quorum sensing regulator LuxR	CTM87_05770	C9J22_03015	C9J21_19590	CTM67_17800	CTM77_15620	CTM76_16940	CTM93_18385	CTM79_18305	C9J19_19130	DAT36_11800	CTM80_08855	CTM85_19850	CTM70_12350	CTM75_16680	C9J18_18885	AYY26_07545
hot-dog/esterase																
esterase FrsA	CTM87_10820	C9J22_08355	C9J21_01985	CTM67_00175	CTM77_17735	CTM76_05935	CTM93_01020	CTM79_06345	C9J19_01300	DAT36_00450	CTM80_06030	CTM85_09380	CTM70_00980	CTM75_01525	C9J18_00580	AYY26_05500
esterase YqiA	CTM87_14560	C9J22_16495	C9J21_16405	CTM67_03195	CTM77_09270	CTM76_14975	CTM93_09325	CTM79_09485	C9J19_13100	DAT36_04760	CTM80_09465	CTM85_10490	CTM70_06960	CTM75_07745	C9J18_14860	AYY26_14270
						CTM76_08800	CTM93_15665					CTM85_13700		CTM75_12460		
Shock /stress																
cold-shock protein	CTM87_02645 + CTM87_02710 + CTM87_07250 + CTM87_09185 + CTM87_12150 + CTM87_13100	C9J22_00125 + C9J22_00185 + C9J22_01725 + C9J22_10230 + C9J22_18860 + C9J22_20155	C9J21_00340 + C9J21_04770 + C9J21_04830 + C9J21_06160 + C9J21_16540 + C9J21_21515	CTM67_00780 + CTM67_05665 + CTM67_17145 + CTM67_17205 + CTM67_18420 + CTM67_20455	CTM77_02150 + CTM77_02215 + CTM77_06310 + CTM77_11010 + CTM77_12080 + CTM77_15060	CTM76_02650 + CTM76_07665 + CTM76_07725 + CTM76_11015 + CTM76_11365 + CTM76_13030 + CTM76_13035	CTM93_07685 + CTM93_08290 + CTM93_16155 + CTM93_16160 + CTM93_18455 + CTM93_18515	CTM79_03420 + CTM79_08095 + CTM79_08155 + CTM79_15140 + CTM79_18005 + CTM79_20410	C9J19_02650 + C9J19_05985 + C9J19_09480 + C9J19_09545 + C9J19_12730 + C9J19_19265	DAT36_01660 + DAT36_04195 + DAT36_04255 + DAT36_05590 + DAT36_11655 + DAT36_16390	CTM80_00015 + CTM80_03395 + CTM80_03455 + CTM80_15175 + CTM80_18995 + CTM80_19930	CTM85_03300 + CTM85_04940 + CTM85_06975 + CTM85_11245 + CTM85_11310 + CTM85_17940	CTM70_13680 + CTM70_15500 + CTM70_16610 + CTM70_17785 + CTM70_17790 + CTM70_18605	CTM75_17130 + CTM75_17190 + CTM75_18285 + CTM75_19440 + CTM75_19445 + CTM75_19955	C9J18_03420 + C9J18_04950 + C9J18_05010 + C9J18_10685 + C9J18_16625 + C9J18_20100	AYY26_08925 + AYY26_10345 + AYY26_13315 + AYY26_13375 + AYY26_17810 + AYY26_18545
	CTM87_02645 + CTM87_02710 + CTM87_07015 + CTM87_07250 + CTM87_08075 + CTM87_09185 + CTM87_09195 + CTM87_12150 + CTM87_13100	C9J22_00125 + C9J22_00185 + C9J22_01725 + C9J22_10230 + C9J22_12770 + C9J22_18860 + C9J22_18865 + C9J22_18875 + C9J22_19300 + C9J22_20155	C9J21_00340 + C9J21_04470 + C9J21_04770 + C9J21_04830 + C9J21_06160 + C9J21_08655 + C9J21_16540 + C9J21_16545 + C9J21_16555 + C9J21_21515	CTM67_00780 + CTM67_05665 + CTM67_11045 + CTM67_11805 + CTM67_13500 + CTM67_17145 + CTM67_17205 + CTM67_20455 + CTM67_20460	CTM77_02150 + CTM77_02215 + CTM77_06310 + CTM77_08915 + CTM77_11010 + CTM77_12065 + CTM77_12075 + CTM77_12080 + CTM77_13050 + CTM77_15060	CTM76_01435 + CTM76_01825 + CTM76_02650 + CTM76_07665 + CTM76_07725 + CTM76_11015 + CTM76_11365 + CTM76_13030 + CTM76_13035 + CTM76_18820	CTM93_03770 + CTM93_04115 + CTM93_07685 + CTM93_08290 + CTM93_16145 + CTM93_16155 + CTM93_16160 + CTM93_18455 + CTM93_18515	CTM79_03420 + CTM79_08095 + CTM79_08155 + CTM79_09760 + CTM79_15140 + CTM79_15150 + CTM79_15985 + CTM79_18005 + CTM79_20410	C9J19_02650 + C9J19_04280 + C9J19_05985 + C9J19_08050 + C9J19_09480 + C9J19_09545 + C9J19_12730 + C9J19_19265 + C9J19_19275	DAT36_01660 + DAT36_04195 + DAT36_04255 + DAT36_05310 + DAT36_05590 + DAT36_11655 + DAT36_13845 + DAT36_16375 + DAT36_16385 + DAT36_16390	CTM80_00015 + CTM80_00825 + CTM80_03395 + CTM80_03455 + CTM80_11640 + CTM80_14920 + CTM80_15175 + CTM80_18995 + CTM80_19930	CTM85_02510 + CTM85_03300 + CTM85_04040 + CTM85_04940 + CTM85_06975 + CTM85_11245 + CTM85_11310 + CTM85_17940 + CTM85_17950	CTM70_11385 + CTM70_13680 + CTM70_15500 + CTM70_16610 + CTM70_17785 + CTM70_17790 + CTM70_18245 + CTM70_18605	CTM75_13620 + CTM75_16320 + CTM75_17130 + CTM75_18285 + CTM75_19440 + CTM75_19445 + CTM75_19955	C9J18_03420 + C9J18_04950 + C9J18_05010 + C9J18_10685 + C9J18_13430 + C9J18_13960 + C9J18_16625 + C9J18_20085 + C9J18_20095 + C9J18_20100	AYY26_05860 + AYY26_06285 + AYY26_08925 + AYY26_10345 + AYY26_13315 + AYY26_13375 + AYY26_17810 + AYY26_18545 + AYY26_18555
	CTM87_18140	C9J22_18690	C9J21_19150	CTM67_14330	CTM77_10645	CTM76_18695	CTM93_15815	CTM79_15500	C9J19_18365	DAT36_15450	CTM80_06535	CTM85_18270	CTM70_05825	CTM75_13145	C9J18_19205	AYY26_18160
	CTM87_07010	C9J22_12765	C9J21_04465	CTM67_13505	CTM77_13055	CTM76_01430	CTM93_04120	CTM79_15980	C9J19_04285	DAT36_13840	CTM80_11645	CTM85_04035	CTM70_11380	CTM75_13615	C9J18_13435	AYY26_05855
	CTM87_17145	C9J22_17725	C9J21_14610	CTM67_06370	CTM77_16380	CTM76_15955	CTM93_14840	CTM79_00900	C9J19_17055	DAT36_14380	CTM80_13125	CTM85_17255	CTM70_18190	CTM75_11290	C9J18_05545	AYY26_17210
			C9J21_03230			CTM76_18810	CTM93_19665						CTM70_07005			
							CTM93_05900									
cold shock domain protein CspD	CTM87_04030	C9J22_06775	C9J21_02935	CTM67_09700	CTM77_04440	CTM76_03730	CTM93_06035	CTM79_10780	C9J19_18080	DAT36_02475	CTM80_05370	CTM85_16610	CTM70_10145	CTM75_02755	C9J18_06620	AYY26_02215
phage shock protein C / envelope stress response membrane protein PspC	CTM87_09735	C9J22_05440	C9J21_15140	CTM67_05995	CTM77_00885	CTM76_14795	CTM93_02205	CTM79_05190	C9J19_05655	DAT36_03405	CTM80_02325	CTM85_01055	CTM70_09610	CTM75_00170	C9J18_02330	AYY26_04035
phage shock protein B / envelope stress response membrane protein PspB	CTM87_09730	C9J22_05445	C9J21_15135	CTM67_05990	CTM77_00880	CTM76_14800	CTM93_02200	CTM79_05195	C9J19_05660	DAT36_03410	CTM80_02330	CTM85_01060	CTM70_09605	CTM75_00175	C9J18_02325	AYY26_04040
phage shock protein PspA	CTM87_09725	C9J22_05450	C9J21_15130	CTM67_05985	CTM77_00875	CTM76_14805	CTM93_02195	CTM79_05200	C9J19_05665	DAT36_03415	CTM80_02335	CTM85_01065	CTM70_09600	CTM75_00180	C9J18_02320	AYY26_04045
phage shock protein A	CTM87_02855	C9J22_12565	C9J21_17570	CTM67_12885	CTM77_02365	CTM76_07860	CTM93_06715	CTM79_04525	C9J19_08540	DAT36_15670	CTM80_10370	CTM85_10720	CTM70_17845	CTM75_03985	C9J18_05150	AYY26_10870
phage shock protein operon transcriptional activator	CTM87_09720	C9J22_05455	C9J21_15125	CTM67_05980	CTM77_00870	CTM76_14810	CTM93_02190	CTM79_05205		DAT36_03420	CTM80_02340	CTM85_01070	CTM70_09595	CTM75_00185	C9J18_02315	AYY26_04050
phage shock protein G / envelope stress response protein PspG	CTM87_18120	C9J22_18670	C9J21_20020	CTM67_14350	CTM77_10665	CTM76_18715	CTM93_15835	CTM79_15520	C9J19_18395	DAT36_15430	CTM80_06515	CTM85_18250	CTM70_05845	CTM75_13125	C9J18_19230	AYY26_18180
heat-shock protein Hsp20	CTM87_05185	C9J22_02665	C9J21_01315	CTM67_07730	CTM77_07660	CTM76_10055	CTM93_07135	CTM79_17195	C9J19_01705	DAT36_09715	CTM80_15660	CTM85_06455	CTM70_07585	CTM75_13450	C9J18_15255	AYY26_13415
heat-shock protein / META domain-containing protein	CTM87_17685	C9J22_14575	C9J21_20520	CTM67_16550	CTM77_13645	CTM76_18285	CTM93_15060	CTM79_12840	C9J19_03420	DAT36_15155	CTM80_11200	CTM85_18465	CTM70_17610	CTM75_11830	C9J18_20360	AYY26_15325
heat-shock protein HslJ / META domain-containing protein	CTM87_12895	C9J22_01515	C9J21_00135	CTM67_17050	CTM77_10800	CTM76_20150	CTM93_02320	CTM79_03210	C9J19_02860	DAT36_11450	CTM80_17370	CTM85_02295	CTM70_12670	CTM75_10735	C9J18_03625	AYY26_09130
	CTM87_18360	C9J22_09275		CTM67_10695	CTM77_08415	CTM76_02985	CTM93_00650	CTM79_01690	C9J19_17890	DAT36_10870		CTM85_12655	CTM70_02860	CTM75_10015		AYY26_16495
ribosome-associated heat shock protein Hsp15	CTM87_15980	C9J22_15270	C9J21_10200	CTM67_04750	CTM77_14570	CTM76_15465	CTM93_08995	CTM79_08775	C9J19_14765	DAT36_09335	CTM80_08175	CTM85_12975	CTM70_05350	CTM75_14265	C9J18_16480	AYY26_14650
oxidative-stress-resistance chaperone / DJ-1 family protein	CTM87_10715	C9J22_08455	C9J21_01880	CTM67_00275	CTM77_17630	CTM76_06035	CTM93_00915	CTM79_06240	C9J19_01400	DAT36_00345	CTM80_06130	CTM85_09275	CTM70_00875	CTM75_01625	C9J18_00475	AYY26_05605
GlsB/YeaQ/YmgE family stress response membrane protein																
peroxide stress protein YaaA	CTM87_12570	C9J22_09825	C9J21_07245	CTM67_01190	CTM77_05900		CTM93_05480	CTM79_04035	C9J19_06410	DAT36_01255	CTM80_10940	CTM85_04535	CTM70_00370		C9J18_10280	AYY26_09925
outer membrane-stress sensor serine endopeptidase DegS	CTM87_13820	C9J22_13795	C9J21_21555		CTM77_07020	CTM76_13330	CTM93_13355	CTM79_00295	C9J19_10810	DAT36_07885	CTM80_04355	CTM85_08615	CTM70_08895	CTM75_02350	C9J18_06090	AYY26_11575
stress response translation initiation inhibitor YciH	CTM87_16845	C9J22_03655	C9J21_07700	CTM67_10430	CTM77_10105	CTM76_19135	CTM93_16470	CTM79_16180	C9J19_15760	DAT36_17445	CTM80_12730	CTM85_16800	CTM70_16945	CTM75_16475	C9J18_20550	AYY26_19075
stress response serine/threonine protein kinase YihE	CTM87_16410	C9J22_16945	C9J21_12140	CTM67_08140	CTM77_14235	CTM76_17165	CTM93_11255	CTM79_10635	C9J19_16605	DAT36_12795	CTM80_10240	CTM85_14210	CTM70_02230	CTM75_07470	C9J18_18100	AYY26_16055
oxidative stress defense protein																
universal stress protein	CTM87_15670	C9J22_15580	C9J21_10510	CTM67_04435	CTM77_19920	CTM76_15775	CTM93_08685	CTM79_08465	C9J19_14455	DAT36_09025	CTM80_08485	CTM85_13285	CTM70_19760	CTM75_13730	C9J18_16165	AYY26_14345
	CTM87_12160	C9J22_10220	C9J21_21525	CTM67_00790	CTM77_06295	CTM76_11380	CTM93_05890	CTM79_18020	C9J19_06000	DAT36_01650	CTM80_15160	CTM85_04930	CTM70_18590	CTM75_16330	C9J18_10675	AYY26_10335
universal stress protein UspE	CTM87_06825	C9J22_11140	C9J21_04280	CTM67_05195	CTM77_02630	CTM76_01240	CTM93_13910	CTM79_20025	C9J19_04465	DAT36_14310	CTM80_13090	CTM85_03850	CTM70_08720	CTM75_04465	C9J18_12230	AYY26_07940
universal stress protein UspB	CTM87_09210	C9J22_18890	C9J21_16570	CTM67_11820	CTM77_12050	CTM76_18835	CTM93_16130	CTM79_15165	C9J19_19290	DAT36_16360	CTM80_14935	CTM85_17965	CTM70_07020	CTM75_13960	C9J18_20070	AYY26_18570
universal stress global response regulator UspA	CTM87_09220	C9J22_18900	C9J21_16580	CTM67_11830	CTM77_12040	CTM76_18845	CTM93_16120	CTM79_15175	C9J19_19300	DAT36_16350	CTM80_14945	CTM85_17975	CTM70_07030	CTM75_13970	C9J18_20060	AYY26_18580

	P. phosphoreum															
	AK-3	**AK-4**	**AK-5**	**AK-8**	**ATCC 11040**	**FS-1.1**	**FS-1.2**	**FS-2.1**	**FS-2.2**	**FS-3.2**	**FS-4.1**	**FS-4.2**	**FS-5.1**	**FS-5.2**	**FS-6.1**	**GCSL-P69**
envelope stress sensor histidine kinase CpxA / two-component system sensor histidine kinase	CTM87_08675	C9J22_11680	C9J21_09585	CTM67_03865	CTM77_11355	CTM76_12515	CTM93_04750	CTM79_02555	C9J19_07125	DAT36_07095	CTM80_01485	CTM85_05585	CTM70_01160	CTM75_05065	C9J18_11160	AYY26_12265
NirD/YgiW/YdeI family stress tolerance protein / hypothetical protein	CTM87_10290	C9J22_18495	C9J21_08975	CTM67_17390	CTM77_01440	CTM76_19920	CTM93_14030	CTM79_05860	C9J19_05080	DAT36_10450	CTM80_07430	CTM85_00495	CTM70_15930	CTM75_18090	C9J18_02885	AYY26_03470
	CTM87_13395	C9J22_02020	C9J21_00635	CTM67_11285	CTM77_18280	CTM76_10715	CTM93_08585	CTM79_03715	C9J19_02335	DAT36_15760	CTM80_13705	CTM85_07270	CTM70_15300	CTM75_07985	C9J18_03130	AYY26_17410
Iron																
ferrous iron transport protein C	CTM87_11760	C9J22_06140	C9J21_06705	CTM67_01555	CTM77_00200	CTM76_04845	CTM93_01520	CTM79_07380	C9J19_00245	DAT36_02975	CTM80_07830	CTM85_11775	CTM70_04215	CTM75_04620	C9J18_01635	AYY26_04640
ferrous iron transport protein A	CTM87_11750	C9J22_06150	C9J21_06715	CTM67_01565	CTM77_00190	CTM76_04855	CTM93_01510	CTM79_07370	C9J19_00255	DAT36_02965	CTM80_07840	CTM85_11785	CTM70_04225	CTM75_04630	C9J18_01625	AYY26_04650
ferrous iron transport protein B	CTM87_11755	C9J22_06145	C9J21_06710	CTM67_01560	CTM77_00195	CTM76_04850	CTM93_01515	CTM79_07375	C9J19_00250	DAT36_02970	CTM80_07835	CTM85_11780	CTM70_04220	CTM75_04625	C9J18_01630	AYY26_04645
	CTM87_14800	C9J22_01000	C9J21_10835	CTM67_19275	CTM77_12385	CTM76_06985	CTM93_02840	CTM79_14080	C9J19_14380	DAT36_08840	CTM80_15360	CTM85_01785	CTM70_17720	CTM75_19600	C9J18_04135	AYY26_09650
ferric iron uptake transcriptional regulator	CTM87_05115	C9J22_02590	C9J21_01245	CTM67_07800	CTM77_07590	CTM76_10125	CTM93_07205	CTM79_18195	C9J19_01775	DAT36_09780	CTM80_15590	CTM85_06385	CTM70_07515	CTM75_06005	C9J18_15325	AYY26_04765
iron chelate uptake ABC transporter family permease subunit	CTM87_14100	C9J22_13525	C9J21_14900	CTM67_02030	CTM77_06755	CTM76_13595	CTM93_16975	CTM79_00575	C9J19_10535	DAT36_17215	CTM80_04085	CTM85_08340	CTM70_04020	CTM75_02615	C9J18_05815	AYY26_13485
iron ABC transporter substrate-binding protein	CTM87_14105	C9J22_13520	C9J21_14895	CTM67_02025	CTM77_06750	CTM76_13600	CTM93_16970	CTM79_00580	C9J19_10530	DAT36_17210	CTM80_04080	CTM85_08335	CTM70_04025	CTM75_02620	C9J18_05810	AYY26_11310
iron chelate uptake ABC transporter family permease subunit	CTM87_16705	C9J22_04985	C9J21_13250	CTM67_18980	CTM77_15740	CTM76_14235	CTM93_19280	CTM79_20915	C9J19_15900		CTM80_19500	CTM85_19075	CTM70_16575	CTM75_15625	C9J18_14220	AYY26_06990
	CTM87_01760			CTM67_07625	CTM77_13270	CTM76_08470		CTM79_08010	C9J19_10390		CTM80_05060	CTM85_13365	CTM70_08690			
iron ABC transporter	CTM87_07615	C9J22_16810	C9J21_12275	CTM67_05320	CTM77_20075	CTM76_02295	CTM93_08030	CTM79_15820	C9J19_12385	DAT36_12660	CTM80_00365	CTM85_02950	CTM70_08335	CTM75_12075	C9J18_16970	AYY26_13490
		C9J22_15750	C9J21_11550						FS21_CTM79_17515	DAT36_05925						AYY26_16185
		C9J22_13000														
iron ABC transporter permease	CTM87_11760	C9J22_06140	C9J21_06705	CTM67_01555	CTM77_00200	CTM76_04845	CTM93_08030	CTM79_07380	C9J19_00245	DAT36_02975	CTM80_07830	CTM85_11775	CTM70_04215	CTM75_12075	C9J18_16970	AYY26_11305
	CTM87_14800	C9J22_01000	C9J21_10835	CTM67_19275	CTM77_12385	CTM76_06985	CTM93_01520	CTM79_14080	C9J19_14380	DAT36_08840	CTM80_15360	CTM85_01785	CTM70_17720	CTM75_04620	C9J18_01635	AYY26_06770
							CTM93_02840							CTM75_19600	C9J18_04135	AYY26_10230
manganese/iron ABC transporter ATP-binding protein																
iron-siderophore ABC transporter substrate-binding protein	CTM87_05110	C9J22_02585	C9J21_01240	CTM67_07805	CTM77_07585	CTM76_10130	CTM93_07210	CTM79_18190	C9J19_01780	DAT36_09785	CTM80_15585	CTM85_06380	CTM70_07510	CTM75_06000	C9J18_15330	AYY26_01315
Marine polyssacharides																
Xylose																
endoxylanase	CTM87_02505	C9J22_00325	C9J21_04970	CTM67_10830	CTM77_02010	CTM76_07525	CTM93_15265	CTM79_08295	C9J19_09340	DAT36_04020	CTM80_03625	CTM85_11075	CTM70_03610	CTM75_03395	C9J18_04810	AYY26_13175
xylosidase																
xylG: D-xylose ABC transporter, ATP-binding protein	CTM87_00155	C9J22_03830	C9J21_11750	CTM67_18630	CTM77_09930	CTM76_09695	CTM93_11460	CTM79_12400	C9J19_17680	DAT36_16155	CTM80_12560	CTM85_14600	CTM70_19030	CTM75_08970	C9J18_08940	AYY26_00115
ABC_transporter,_permease_protein_(cluster_2,_ribose/xylose/arabinose/galactose)	CTM87_00160	C9J22_03835	C9J21_11755	CTM67_18635	CTM77_09925	CTM76_09690	CTM93_11465	CTM79_12395	C9J19_17675	DAT36_16150	CTM80_12555	CTM85_14605	CTM70_19025	CTM75_08965	C9J18_08935	AYY26_00120
Laminarin																
laminarinase																
Chondroitin sulphate																
chondriotinase	CTM87_15125					CTM76_06615	CTM93_02530				CTM80_03600	CTM85_11100		CTM75_03370		
chondroitin sulphate lyase																
Arabinogalactan																
galactanase																
beta-galactosidase	CTM87_08150				CTM77_08975			CTM79_09695	C9J19_07975		CTM80_00885	CTM85_02435		CTM75_16855		AYY26_06220
beta-galactosidase subunit beta	CTM87_07405	C9J22_19570	C9J21_11355	CTM67_05515	CTM77_15210	CTM76_02500	CTM93_07835	CTM79_16305	C9J19_12580	DAT36_05730	CTM80_00165	CTM85_03150	CTM70_08165	CTM75_11875	C9J18_16780	AYY26_17970
beta-galactosidase subunit alpha	CTM87_07410	C9J22_19565	C9J21_11360	CTM67_05510	CTM77_15215	CTM76_02495	CTM93_07840	CTM79_16310	C9J19_12575	DAT36_05735	CTM80_00170	CTM85_03145	CTM70_08160	CTM75_11880	C9J18_16785	AYY26_17975
arabinofuranosidase																
arabinopyranosidase																
Pullulan																
pullulanase																
Fucoidan																
fucoidase																
L-fucose:H+ symporter permease	CTM87_15095	C9J22_01280	C9J21_20140	CTM67_14125	CTM77_12660	CTM76_06645	CTM93_02560	CTM79_19185	C9J19_14100	DAT36_14935	CTM80_15745	CTM85_02060	CTM70_10745	CTM75_10970	C9J18_03855	AYY26_09365
L-fucose:H+ symporter permease																
L-fucose isomerase																
L-fuculokinase																
L-fucose mutarotase																
L-fuculose-phosphate aldolase																
Chitin																
chitinase	CTM87_04880	C9J22_02355	C9J21_01010	CTM67_07970	CTM77_07355	CTM76_10360	CTM93_07440	CTM79_11730	C9J19_02010	DAT36_06680	CTM80_14410	CTM85_06150	CTM70_17665	CTM75_05770	C9J18_15490	AYY26_13720

Table S3. Strains used in the study and the accession numbers of all housekeeping genes used to perfom the MLSA-based phylogenetic tree, and the *fur* gene-based phylogenetic tree. Type strains of each species are marked in bold letters and with a ^{T}.

	*gyr*B	*rpo*D	*rpo*A	*rec*A	*mre*B	*fts*Z	*fur*
***P. carnosum* DSM 105454T**	CIK00 16240	CIK00 12710	CIK00 06040	CIK00 17665	CIK00 08625	CIK00 08915	CIK00 01675
P. carnosum TMW 2.2029	CIT27 15170	CIT27 12860	CIT27 17980	CIT27 14055	CIT27 11430	CIT27 11720	CIT27 03535
P. carnosum TMW 2.2097	GLP21 16910	GLP21 12935	GLP21 08050	GLP21 05745	GLP21 06735	GLP21 06445	GLP21 01290
P. carnosum TMW 2.2098	GLP27 14805	GLP27 10800	GLP27 08235	GLP27 11450	GLP27 08390	GLP27 08680	GLP27 03390
P. carnosum TMW 2.2147	GLP24 16860	GLP24 12955	GLP24 19300	GLP24 15500	GLP24 11650	GLP24 11940	GLP24 02920
P. carnosum TMW 2.2149	GLP09 13015	GLP09 08835	GLP09 04675	GLP09 10810	GLP09 07235	GLP09 06945	GLP09 00815
P. carnosum TMW 2.2150	GLP22 15965	GLP22 10910	GLP22 18430	GLP22 13560	GLP22 09945	GLP22 09655	GLP22 02405
P. carnosum TMW 2.2157	GLP17 14245	GLP17 10895	GLP17 18705	GLP17 11265	GLP17 13595	GLP17 12895	GLP17 03095
P. carnosum TMW 2.2163	GRJ22 15695	GRJ22 13220	GRJ22 11630	GRJ22 14860	GRJ22 12480	GRJ22 12770	GRJ22 12105
P. carnosum TMW 2.2169	GLP31 16785	GLP31 12305	GLP31 20330	GLP31 14270	GLP31 10660	GLP31 10370	GLP31 01005
P. carnosum TMW 2.2186	GLP20 14190	GLP20 12420	GLP20 07705	GLP20 13465	GLP20 07860	GLP20 08150	GLP20 02335
P. carnosum TMW 2.2187	GLP19 15790	GLP19 14495	GLP19 18745	GLP19 15915	GLP19 13785	GLP19 14075	GLP19 02245
P. carnosum TMW 2.2188	GLP14 13845	GLP14 08660	GLP14 18180	GLP14 11510	GLP14 06410	GLP14 06700	GLP14 10505
P. carnosum TMW 2.2189	GLP23 13675	GLP23 09900	GLP23 18965	GLP23 14540	GLP23 08105	GLP23 08395	GLP23 02385
P. carnosum TMW 2.2190	GLP13 14605	GLP13 13165	GLP13 18760	GLP13 12065	GLP13 09600	GLP13 09890	GLP13 00210
***P. iliopiscarium* DSM 9896T**	C9J51 16905	C9J51 14950	C9J51 19040	C9J51 16060	C9J51 14170	C9J51 14460	C9J51 04765
P. iliopiscarium ATCC 51761	C9J52 12605	C9J52 10405	C9J52 19320	C9J52 18835	C9J52 14030	C9J52 13035	C9J52 15505
P. iliopiscarium NCIMB 13478	C9I87 17140	C9I87 13700	C9I87 12080	C9I87 15690	C9I87 12925	C9I87 13215	C9I87 01125
P. iliopiscarium NCIMB 13481	C9I88 14930	C9I88 12660	C9I88 09270	C9I88 14565	C9I88 10750	C9I88 11040	C9I88 03115
P. iliopiscarium TMW 2.2035	CJF27 11550	CJF27 09980	CJF27 17650	CJF27 09465	CJF27 03705	CJF27 03995	CJF27 08085
P. iliopiscarium TMW 2.2104	GLP10 09540	GLP10 08435	GLP10 18595	GLP10 11645	GLP10 02565	GLP10 02855	GLP10 08325
***P. phosphoreum* DSM 15556T**	CTM77 14030	CTM77 09385	CTM77 11845	CTM77 16645	CTM77 07160	CTM77 06870	CTM77 00075
P. phosphoreum AK-3	CTM87 16175	CTM87 14445	CTM87 20545	CTM87 17410	CTM87 13680	CTM87 13970	CTM87 11635
P. phosphoreum AK-4	C9J22 16740	C9J22 16380	C9J22 11195	C9J22 17990	C9J22 13935	C9J22 13645	C9J22 06265
P. phosphoreum AK-5	C9J21 12345	C9J21 16520	C9J21 10075	C9J21 14345	C9J21 15690	C9J21 18025	C9J21 06830
P. phosphoreum AK-8	CTM67 08345	CTM67 03080	CTM67 03380	CTM67 06105	CTM67 02435	CTM67 02145	CTM67 01680
P. phosphoreum FS-1.1	CTM76 17370	CTM76 15090	CTM76 12025	CTM76 16220	CTM76 13190	CTM76 13480	CTM76 04970
P. phosphoreum FS-1.2	CTM93 11050	CTM93 09440	CTM93 05240	CTM93 14575	CTM93 13495	CTM93 17345	CTM93 01395
P. phosphoreum FS-2.1	CTM79 10430	CTM79 09600	CTM79 02070	CTM79 01165	CTM79 00155	CTM79 00445	CTM79 07255
P. phosphoreum FS-2.2	C9J19 16400	C9J19 13215	C9J19 07615	C9J19 17320	C9J19 10950	C9J19 10660	C9J19 00370
P. phosphoreum FS-3.2	DAT36 12590	DAT36 04645	DAT36 07580	DAT36 14645	DAT36 07745	DAT36 08035	DAT36 02850
P. phosphoreum FS-4.1	CTM80 10035	CTM80 09350	CTM80 01975	CTM80 13390	CTM80 04495	CTM80 04205	CTM80 07955
P. phosphoreum FS-4.2	CTM85 14415	CTM85 10375	CTM85 06075	CTM85 17520	CTM85 08755	CTM85 08465	CTM85 11900

	***gyr*B**	***rpo*D**	***rpo*A**	***rec*A**	***mre*B**	***fts*Z**	***fur***
P. phosphoreum FS-5.1	CTM70 02435	CTM70 06845	CTM70 01650	CTM70 04470	CTM70 09035	CTM70 03900	CTM70 04340
P. phosphoreum FS-5.2	CTM75 07265	CTM75 07860	CTM75 05555	CTM75 11555	CTM75 02210	CTM75 02500	CTM75 04745
P. phosphoreum FS-6.1	C9J18 17895	C9J18 14975	C9J18 21360	C9J18 05280	C9J18 06230	C9J18 05940	C9J18 01515
P. phosphoreum GCSL-P69	AYY26 16255	AYY26 14150	AYY26 20665	AYY26 16945	AYY26 11715	AYY26 11425	AYY26 04765
P. phosphoreum TMW 2.2033	CJF25 20020	CJF25 15835	CJF25 10450	CJF25 19140	CJF25 15430	CJF25 15140	CJF25 02075
P. phosphoreum TMW 2.2034	CJF26 17615	CJF26 14830	CJF26 13135	CJF26 18435	CJF26 18220	CJF26 17145	CJF26 04790
P. phosphoreum TMW 2.2103	GLP34 16660	GLP34 15275	GLP34 20895	GLP34 17870	GLP34 11710	GLP34 11420	GLP34 00315
P. phosphoreum TMW 2.2125	GLP32 16980	GLP32 13525	GLP32 09970	GLP32 16400	GLP32 12120	GLP32 12410	GLP32 01455
P. phosphoreum TMW 2.2126	GLP35 18070	GLP35 13765	GLP35 21235	GLP35 18765	GLP35 11620	GLP35 11910	GLP35 01180
P. phosphoreum TMW 2.2130	GLP37 16800	GLP37 14135	GLP37 21715	GLP37 18845	GLP37 12750	GLP37 13040	GLP37 00975
P. phosphoreum TMW 2.2132	GLP38 17340	GLP38 13305	GLP38 21155	GLP38 18580	GLP38 12910	GLP38 12620	GLP38 11085
P. phosphoreum TMW 2.2134	GLP25 17285	GLP25 14465	GLP25 11215	GLP25 15975	GLP25 13730	GLP25 14020	GLP25 04790
P. phosphoreum TMW 2.2140	GLP44 16945	GLP44 12455	GLP44 21865	GLP44 19275	GLP44 13615	GLP44 13325	GLP44 01535
P. phosphoreum TMW 2.2142	GLP29 15780	GLP29 15945	GLP29 20780	GLP29 17750	GLP29 16640	GLP29 16370	GLP29 01225
P. kishitanii ATCC BAA-1194T	AY455877.1	EF415606.1	EF415588.1	EF415552.2	AB453696.1	AB453688.1	>JZSP01000001.1:183520-183966_ Photobacterium_kishitanii_ strain_ATCC_BAA-1194_ CFSAN029432_ contig0000_ whole_genome_shotgun_ sequence

Table S4. ANI values of all strains included in the study from species *P. carnosum*, *P. phosphoreum* and *P. iliopiscarium*, and the type strain of *P. kishitanii*. The colors over the strain designation mark the source of isolation: red for meat, blue for fish/sea-related source. Colors on the ANI values mark in green those above the species delineation threshold (<95% identity), in yellow those values between 90 and 95% identity, and in red those values below the 85% identity.

		Photobacterium carnosum														
		DSM 105454T / TMW 2.2021T	TMW 2.2029	TMW 2.2097	TMW 2.2147	TMW 2.2149	TMW 2.2150	TMW 2.2157	TMW 2.2163	TMW 2.2169	TMW 2.2098	TMW 2.2186	TMW 2.2187	TMW 2.2188	TMW 2.2189	TMW 2.2190
Photobacterium carnosum	**DSM 105454T / TMW 2.2021T**	---	98.78	98.76	98.75	98.75	98.9	98.74	98.57	98.83	98.53	98.73	98.57	98.76	98.63	98.71
Photobacterium carnosum	TMW 2.2029	98.69	---	98.71	98.56	98.76	98.82	98.64	98.66	98.69	98.47	98.72	98.66	98.67	98.71	99
Photobacterium carnosum	TMW 2.2097	98.79	98.78	---	98.5	98.71	98.85	98.67	98.54	98.8	98.42	98.73	98.53	98.62	98.67	98.73
Photobacterium carnosum	TMW 2.2147	98.73	98.65	98.52	---	98.66	98.82	98.77	98.68	98.72	98.27	98.57	98.63	98.62	98.49	98.67
Photobacterium carnosum	TMW 2.2149	98.78	98.81	98.7	98.69	---	98.87	98.71	98.66	98.67	98.44	98.68	98.62	98.68	98.65	98.77
Photobacterium carnosum	TMW 2.215	98.85	98.87	98.84	98.8	98.83	---	98.84	98.7	98.85	98.5	98.74	98.7	98.72	98.77	98.83
Photobacterium carnosum	TMW 2.2157	98.76	98.71	98.73	98.79	98.67	98.9	---	98.62	98.75	98.35	98.66	98.57	98.68	98.65	98.71
Photobacterium carnosum	TMW 2.2163	98.65	98.69	98.54	98.61	98.61	98.72	98.53	---	98.62	98.35	98.55	98.67	98.6	98.57	98.7
Photobacterium carnosum	TMW 2.2169	98.83	98.74	98.77	98.7	98.69	98.83	98.71	98.62	---	98.43	98.7	98.52	98.68	98.71	98.7
Photobacterium carnosum	TMW 2.2098	98.51	98.5	98.42	98.21	98.41	98.46	98.27	98.32	98.43	---	98.48	98.29	98.37	98.31	98.24
Photobacterium carnosum	TMW 2.2186	98.7	98.69	98.64	98.49	98.63	98.68	98.6	98.56	98.64	98.4	---	98.52	98.72	98.66	98.62
Photobacterium carnosum	TMW 2.2187	98.53	98.7	98.49	98.61	98.62	98.68	98.5	98.68	98.5	98.32	98.55	---	98.51	98.47	98.61
Photobacterium carnosum	TMW 2.2188	98.85	98.78	98.65	98.66	98.74	98.8	98.69	98.66	98.77	98.44	98.9	98.61	---	98.65	98.79
Photobacterium carnosum	TMW 2.2189	98.59	98.69	98.64	98.42	98.58	98.7	98.64	98.46	98.62	98.29	98.72	98.45	98.49	---	98.52
Photobacterium carnosum	TMW 2.219	98.65	99.04	98.66	98.57	98.75	98.75	98.63	98.68	98.7	98.19	98.71	98.59	98.67	98.52	---
Photobacterium iliopiscarium	**DSM 9896T**	91.4	91.59	91.47	91.54	91.58	91.54	91.34	91.68	91.35	91.52	91.45	91.73	91.38	91.51	91.55
Photobacterium iliopiscarium	ATCC 51761	91.31	91.54	91.52	91.35	91.56	91.37	91.28	91.6	91.25	91.42	91.45	91.54	91.25	91.42	91.43
Photobacterium iliopiscarium	NCIMB 13478	91.34	91.51	91.51	91.43	91.54	91.42	91.29	91.6	91.31	91.52	91.44	91.62	91.32	91.47	91.51
Photobacterium iliopiscarium	NCIMB 13481	91.5	91.55	91.47	91.51	91.59	91.64	91.4	91.66	91.53	91.63	91.52	91.77	91.58	91.62	91.61
Photobacterium iliopiscarium	TMW 2.2035	91.84	91.85	91.87	91.91	91.88	91.8	91.84	91.97	91.92	91.91	91.92	91.97	91.79	91.85	91.84
Photobacterium iliopiscarium	TMW 2.2104	92.37	91.9	92.4	92.49	91.98	92.4	92.44	92	92.43	91.9	91.93	91.95	91.84	91.84	91.87
Photobacterium phosphoreum	**DSM 15556T**	85.82	85.88	85.81	85.74	86	85.88	85.8	85.81	85.87	85.87	85.87	85.91	85.84	86	85.94
Photobacterium phosphoreum	AK-3	85.91	85.95	85.97	85.78	85.99	85.94	85.8	85.91	85.87	85.69	85.82	85.89	85.83	85.86	86.06
Photobacterium phosphoreum	AK-4	85.83	85.87	85.86	85.77	85.89	85.85	85.76	85.88	85.77	85.69	85.72	85.91	85.74	85.85	86.02
Photobacterium phosphoreum	AK-5	85.66	85.98	85.94	85.93	86	85.79	85.87	85.96	85.69	85.71	85.76	86.04	85.84	86.09	85.85
Photobacterium phosphoreum	AK-8	85.84	85.88	85.79	85.88	85.95	85.83	85.8	85.98	85.79	85.81	85.81	85.95	85.77	85.96	85.8
Photobacterium phosphoreum	FS-1.1	85.83	85.86	85.76	85.71	85.95	85.85	85.74	85.76	85.86	85.8	85.74	85.79	85.82	85.97	85.93
Photobacterium phosphoreum	FS-1.2	85.87	85.92	85.9	85.71	85.99	85.86	85.77	85.81	85.9	85.79	85.78	85.85	85.82	85.88	85.97
Photobacterium phosphoreum	FS-2.1	85.82	85.91	85.84	85.67	86.02	85.84	85.77	85.78	85.85	85.63	85.78	85.81	85.82	85.76	86.18
Photobacterium phosphoreum	FS-2.2	85.87	85.93	85.95	85.82	86.01	85.9	85.85	85.92	85.93	85.94	85.79	85.96	85.95	86.01	85.97
Photobacterium phosphoreum	FS-3.2	85.69	85.76	85.78	85.46	85.81	85.68	85.54	85.58	85.65	85.64	85.7	85.58	85.65	85.72	85.8
Photobacterium phosphoreum	FS-4.1	85.73	85.82	85.65	85.63	85.88	85.82	85.67	85.79	85.75	85.71	85.64	85.8	85.73	85.84	85.86
Photobacterium phosphoreum	FS-4.2	85.89	85.97	85.84	85.8	86.04	85.98	85.8	85.93	85.93	85.9	85.76	85.89	85.94	85.93	86.02
Photobacterium phosphoreum	FS-5.1	85.84	85.93	85.81	85.72	85.99	85.91	85.71	85.82	85.87	85.8	85.76	85.9	85.85	85.99	85.93
Photobacterium phosphoreum	FS-5.2	85.81	85.91	85.82	85.71	85.95	85.89	85.77	85.89	85.85	85.83	85.83	85.88	85.85	85.88	85.98
Photobacterium phosphoreum	FS-6.1	86.11	85.86	85.76	85.66	85.85	85.77	85.64	85.78	86.1	85.89	85.7	85.79	85.72	85.66	85.97
Photobacterium phosphoreum	GCSL-P69	86.79	86.12	85.97	86.02	86.17	85.92	85.89	86.04	86.49	86.78	85.84	85.89	85.94	85.91	85.98
Photobacterium phosphoreum	TMW 2.2033	86.82	86.08	85.88	85.99	86.1	86	85.85	86.21	86.39	86.68	85.85	85.92	85.91	85.99	85.96
Photobacterium phosphoreum	TMW 2.2034	85.89	85.95	85.84	85.89	86.01	85.9	85.73	86.08	85.98	85.85	85.75	85.86	85.8	85.92	85.96
Photobacterium phosphoreum	TMW 2.2103	86.84	86.01	86.79	86.93	86.12	86.86	86.81	86.1	86.88	85.86	85.85	85.87	85.89	85.92	85.93
Photobacterium phosphoreum	TMW 2.2125	85.88	85.98	85.76	85.9	86.05	85.91	85.79	86.06	85.87	85.71	85.77	85.86	85.9	85.82	86.1
Photobacterium phosphoreum	TMW 2.2126	86.76	86.12	85.93	85.95	86.18	86	85.8	86.06	86.57	86.75	85.82	85.95	85.86	85.89	85.96
Photobacterium phosphoreum	TMW 2.213	86.58	86.03	85.9	86.03	86.08	85.98	85.79	86.12	86.44	86.55	85.89	86.01	85.95	85.92	85.85
Photobacterium phosphoreum	TMW 2.2132	86.66	86.13	85.92	85.94	86.17	85.93	85.81	86.15	86.55	86.67	85.79	85.88	85.87	85.97	85.95
Photobacterium phosphoreum	TMW 2.2134	85.98	86.04	85.86	85.94	86.11	85.89	85.8	85.99	85.95	85.93	85.81	85.81	85.79	85.95	85.9
Photobacterium phosphoreum	TMW 2.214	86.8	85.96	86.76	86.82	86.05	86.97	86.85	86.04	86.84	85.94	85.79	85.95	85.97	85.98	86
Photobacterium phosphoreum	TMW 2.2142	85.99	85.97	85.87	85.98	86.04	85.99	85.9	86.12	85.92	85.88	85.76	85.95	85.82	85.95	86.01
Photobacterium kishitanii	**DSM 19954T**	84.47	84.42	84.47	84.37	84.49	84.46	84.48	84.33	84.5	84.54	84.38	84.4	84.49	84.54	84.49

		Photobacterium iliopiscarium					
		DSM 9896T	ATCC 51761	NCIMB 13478	NCIMB 13481	TMW 2.2035	TMW 2.2104
Photobacterium carnosum	**DSM 105454T / TMW 2.2021T**	91.46	91.38	91.37	91.54	91.79	92.28
Photobacterium carnosum	TMW 2.2029	91.6	91.6	91.57	91.61	91.76	91.72
Photobacterium carnosum	TMW 2.2097	91.47	91.52	91.49	91.57	91.91	92.39
Photobacterium carnosum	TMW 2.2147	91.62	91.49	91.53	91.64	91.9	92.39
Photobacterium carnosum	TMW 2.2149	91.66	91.62	91.62	91.65	91.88	91.92
Photobacterium carnosum	TMW 2.215	91.59	91.48	91.53	91.71	91.8	92.35
Photobacterium carnosum	TMW 2.2157	91.42	91.38	91.39	91.52	91.82	92.37
Photobacterium carnosum	TMW 2.2163	91.78	91.69	91.68	91.79	92.01	91.97
Photobacterium carnosum	TMW 2.2169	91.46	91.36	91.41	91.57	91.85	92.34
Photobacterium carnosum	TMW 2.2098	91.53	91.49	91.53	91.72	91.86	91.85
Photobacterium carnosum	TMW 2.2186	91.44	91.42	91.45	91.56	91.84	91.81
Photobacterium carnosum	TMW 2.2187	91.67	91.55	91.59	91.83	91.91	91.87
Photobacterium carnosum	TMW 2.2188	91.46	91.41	91.4	91.67	91.75	91.74
Photobacterium carnosum	TMW 2.2189	91.48	91.45	91.49	91.66	91.74	91.73
Photobacterium carnosum	TMW 2.219	91.55	91.47	91.55	91.63	91.78	91.74
Photobacterium iliopiscarium	**DSM 9896T**	---	98.99	98.98	98.96	97.83	97.78
Photobacterium iliopiscarium	ATCC 51761	98.91	---	98.96	98.7	97.56	97.57
Photobacterium iliopiscarium	NCIMB 13478	98.96	98.99	---	98.99	97.66	97.61
Photobacterium iliopiscarium	NCIMB 13481	98.91	98.76	98.92	---	97.69	97.67
Photobacterium iliopiscarium	TMW 2.2035	97.91	97.84	97.82	97.88	---	99.81
Photobacterium iliopiscarium	TMW 2.2104	97.94	97.82	97.83	97.93	99.82	---
Photobacterium phosphoreum	**DSM 15556T**	85.55	85.43	85.49	85.58	85.64	85.54
Photobacterium phosphoreum	AK-3	85.58	85.51	85.68	85.7	85.63	85.56
Photobacterium phosphoreum	AK-4	85.57	85.5	85.53	85.64	85.53	85.49
Photobacterium phosphoreum	AK-5	85.75	85.64	85.76	85.8	85.72	85.66
Photobacterium phosphoreum	AK-8	85.67	85.59	85.68	85.68	85.68	85.64
Photobacterium phosphoreum	FS-1.1	85.58	85.41	85.49	85.57	85.59	85.55
Photobacterium phosphoreum	FS-1.2	85.57	85.46	85.53	85.59	85.58	85.54
Photobacterium phosphoreum	FS-2.1	85.58	85.46	85.56	85.61	85.71	85.64
Photobacterium phosphoreum	FS-2.2	85.63	85.51	85.58	85.68	85.72	85.66
Photobacterium phosphoreum	FS-3.2	85.32	85.28	85.33	85.38	85.45	85.39
Photobacterium phosphoreum	FS-4.1	85.47	85.41	85.42	85.47	85.62	85.55
Photobacterium phosphoreum	FS-4.2	85.51	85.47	85.47	85.5	85.66	85.62
Photobacterium phosphoreum	FS-5.1	85.54	85.49	85.51	85.61	85.68	85.62
Photobacterium phosphoreum	FS-5.2	85.62	85.48	85.53	85.59	85.66	85.61
Photobacterium phosphoreum	FS-6.1	85.44	85.42	85.47	85.49	85.49	85.44
Photobacterium phosphoreum	GCSL-P69	85.56	85.38	85.46	85.57	85.61	85.57
Photobacterium phosphoreum	TMW 2.2033	85.64	85.49	85.65	85.61	85.6	85.58
Photobacterium phosphoreum	TMW 2.2034	85.49	85.4	85.48	85.49	85.62	85.57
Photobacterium phosphoreum	TMW 2.2103	85.4	85.37	85.47	85.44	85.63	86.52
Photobacterium phosphoreum	TMW 2.2125	85.46	85.28	85.48	85.43	85.55	85.54
Photobacterium phosphoreum	TMW 2.2126	85.56	85.43	85.46	85.57	85.71	85.69
Photobacterium phosphoreum	TMW 2.213	85.6	85.4	85.54	85.62	85.65	85.64
Photobacterium phosphoreum	TMW 2.2132	85.45	85.33	85.44	85.52	85.58	85.53
Photobacterium phosphoreum	TMW 2.2134	85.49	85.39	85.5	85.54	85.61	85.58
Photobacterium phosphoreum	TMW 2.214	85.47	85.34	85.44	85.73	85.65	86.61
Photobacterium phosphoreum	TMW 2.2142	85.5	85.39	85.43	85.53	85.58	85.58
Photobacterium kishitanii	**DSM 19954T**	84.06	83.99	84.02	84.15	84.11	84.11

		Photobacterium phosphoreum															
		DSM 15556T	AK-3	AK-4	AK-5	AK-8	FS-1.1	FS-1.2	FS-2.1	FS-2.2	FS-3.2	FS-4.1	FS-4.2	FS-5.1	FS-5.2	FS-6.1	GCSL-P69
Photobacterium carnosum	**DSM 105454T / TMW 2.2021T**	86.04	86.15	85.99	85.84	86.06	86.03	86.12	86.06	86.02	85.9	86.07	86.06	86.2	86.05	86.23	87.04
Photobacterium carnosum	TMW 2.2029	86.11	86.12	86.02	86.09	86.12	86.06	86.14	86.09	86.13	85.92	86.13	86.1	86.24	86.13	85.96	86.37
Photobacterium carnosum	TMW 2.2097	85.99	86.13	86	86.08	86.02	85.93	86.1	86.03	86.18	85.94	85.98	85.96	86.15	86.01	85.89	86.24
Photobacterium carnosum	TMW 2.2147	85.93	86.04	85.96	86.13	86.14	85.96	86.04	85.97	86.06	85.74	85.97	85.97	86.04	85.98	85.84	86.26
Photobacterium carnosum	TMW 2.2149	86.15	86.22	86.08	86.17	86.21	86.12	86.22	86.21	86.2	86	86.18	86.16	86.31	86.19	86.03	86.41
Photobacterium carnosum	TMW 2.215	86.04	86.14	86.01	85.94	86.04	86.01	86.1	86.03	86.09	85.88	86.07	86.06	86.18	86.12	85.91	86.15
Photobacterium carnosum	TMW 2.2157	86.08	86.12	86.01	86.1	86.12	86.02	86.12	86.09	86.08	85.81	86.06	86.06	86.09	86.07	85.88	86.19
Photobacterium carnosum	TMW 2.2163	86.02	86.1	86.11	86.24	86.25	85.98	86.11	86	86.07	85.85	86.07	86.08	86.12	86.11	85.97	86.28
Photobacterium carnosum	TMW 2.2169	86.06	86.18	85.98	85.83	86.04	86.05	86.2	86.09	86.11	85.92	86.06	86.07	86.2	86.09	86.28	86.79
Photobacterium carnosum	TMW 2.2098	86.02	85.92	85.83	85.82	86.01	85.9	86.07	85.84	86.1	85.91	85.99	85.97	86.08	86.01	86.15	86.97
Photobacterium carnosum	TMW 2.2186	85.87	86	85.83	85.85	85.97	85.89	85.99	85.88	85.95	85.79	85.87	85.89	85.99	85.95	85.77	86.01
Photobacterium carnosum	TMW 2.2187	86.03	86.1	86.04	86.06	86.15	85.96	86.1	86	86.12	85.82	86.06	86.06	86.21	86.07	85.97	86.18
Photobacterium carnosum	TMW 2.2188	85.99	86.09	85.94	86.01	86.02	86	86.13	86.04	86.11	85.84	86.04	86.04	86.14	86.08	85.88	86.13
Photobacterium carnosum	TMW 2.2189	86.1	86.09	85.98	86.16	86.15	86.08	86.07	85.99	86.19	85.88	86.1	86.09	86.27	86.08	85.85	86.2
Photobacterium carnosum	TMW 2.219	86.07	86.26	86.12	85.9	86.02	86.09	86.13	86.27	86.08	85.96	86.13	86.13	86.22	86.14	86.06	86.18
Photobacterium iliopiscarium	**DSM 9896T**	85.69	85.72	85.7	85.85	85.84	85.69	85.72	85.72	85.71	85.5	85.71	85.63	85.79	85.77	85.57	85.73
Photobacterium iliopiscarium	ATCC 51761	85.62	85.61	85.63	85.68	85.74	85.53	85.61	85.56	85.64	85.42	85.67	85.65	85.77	85.59	85.57	85.61
Photobacterium iliopiscarium	NCIMB 13478	85.59	85.76	85.68	85.79	85.78	85.6	85.62	85.69	85.65	85.47	85.66	85.57	85.75	85.63	85.57	85.63
Photobacterium iliopiscarium	NCIMB 13481	85.65	85.83	85.71	85.81	85.85	85.65	85.72	85.63	85.74	85.5	85.7	85.62	85.83	85.73	85.61	85.69
Photobacterium iliopiscarium	TMW 2.2035	85.87	85.88	85.81	85.96	85.95	85.82	85.85	85.83	85.91	85.73	85.86	85.8	85.96	85.86	85.68	85.84
Photobacterium iliopiscarium	TMW 2.2104	85.81	85.83	85.74	85.9	85.94	85.76	85.83	85.83	85.88	85.67	85.8	85.79	85.94	85.83	85.67	85.84
Photobacterium phosphoreum	**DSM 15556T**	---	98.64	96.73	96.47	96.56	98.83	98.81	98.79	98.73	95.87	98.93	98.79	99.06	98.83	96.53	98.76
Photobacterium phosphoreum	AK-3	98.69	---	96.8	96.5	96.6	98.73	99.05	98.76	98.82	95.89	98.83	98.69	98.74	98.7	96.47	98.88
Photobacterium phosphoreum	AK-4	96.74	96.83	---	97.96	97.8	96.74	96.85	96.65	96.74	97.16	96.73	96.83	96.73	96.82	97.56	96.76
Photobacterium phosphoreum	AK-5	96.52	96.54	97.95	---	98.62	96.52	96.59	96.56	96.5	97.1	96.6	96.57	96.59	96.61	97.14	96.36
Photobacterium phosphoreum	AK-8	96.51	96.53	97.76	98.6	---	96.42	96.6	96.52	96.53	96.89	96.5	96.56	96.58	96.58	97.28	96.58
Photobacterium phosphoreum	FS-1.1	98.85	98.75	96.75	96.46	96.5	---	98.89	98.79	98.75	95.85	98.94	98.92	98.84	99.01	96.47	98.89
Photobacterium phosphoreum	FS-1.2	98.85	99	96.84	96.56	96.65	98.88	---	98.83	98.83	95.93	98.86	98.82	98.86	98.84	96.55	98.88
Photobacterium phosphoreum	FS-2.1	98.86	98.76	96.67	96.55	96.6	98.81	98.9	---	98.99	95.98	98.87	98.78	98.87	98.85	96.37	98.9
Photobacterium phosphoreum	FS-2.2	98.75	98.87	96.69	96.47	96.56	98.78	98.88	98.94	---	95.83	98.75	98.65	98.77	98.77	96.49	98.83
Photobacterium phosphoreum	FS-3.2	95.88	95.9	97.18	97.07	96.92	95.82	95.99	95.91	95.85	---	95.83	95.86	95.87	95.87	96.98	95.89
Photobacterium phosphoreum	FS-4.1	98.93	98.8	96.75	96.54	96.55	98.94	98.86	98.84	98.71	95.85	---	99.01	98.86	98.98	96.48	98.97
Photobacterium phosphoreum	FS-4.2	98.82	98.67	96.84	96.56	96.59	98.95	98.84	98.77	98.69	95.95	99.02	---	98.78	98.9	96.54	98.91
Photobacterium phosphoreum	FS-5.1	99.09	98.69	96.73	96.47	96.55	98.88	98.86	98.83	98.74	95.87	98.93	98.78	---	98.9	96.46	98.83
Photobacterium phosphoreum	FS-5.2	98.85	98.74	96.77	96.56	96.62	99.03	98.86	98.82	98.78	95.95	99.01	98.9	98.85	---	96.58	98.92
Photobacterium phosphoreum	FS-6.1	96.56	96.41	97.48	97.06	97.27	96.5	96.55	96.36	96.48	96.86	96.51	96.52	96.53	96.56	---	96.49
Photobacterium phosphoreum	GCSL-P69	98.71	98.82	96.65	96.2	96.58	98.81	98.82	98.76	98.69	95.83	98.89	98.81	98.71	98.82	96.41	---
Photobacterium phosphoreum	TMW 2.2033	98.72	98.89	96.75	96.31	96.6	98.92	98.9	98.79	98.79	95.87	98.88	98.84	98.74	98.87	96.43	98.99
Photobacterium phosphoreum	TMW 2.2034	98.71	98.73	96.56	96.29	96.47	98.75	98.72	98.85	98.87	95.79	98.75	98.72	98.7	98.79	96.43	98.87
Photobacterium phosphoreum	TMW 2.2103	98.75	98.68	96.61	96.41	96.5	98.76	98.77	98.89	98.84	95.86	98.8	98.77	98.79	98.81	96.42	98.9
Photobacterium phosphoreum	TMW 2.2125	98.82	98.78	96.61	96.5	96.57	98.89	98.88	98.82	98.94	95.92	98.97	98.86	98.88	98.88	96.36	99.03
Photobacterium phosphoreum	TMW 2.2126	98.75	98.65	96.79	96.27	96.48	98.92	98.79	98.79	98.75	95.86	98.9	98.81	98.8	98.91	96.43	99.01
Photobacterium phosphoreum	TMW 2.213	98.79	98.68	96.61	96.27	96.6	98.84	98.86	98.46	98.74	95.85	98.91	98.87	98.83	98.89	96.31	99.06
Photobacterium phosphoreum	TMW 2.2132	98.89	98.79	96.81	96.27	96.6	99.04	98.88	98.76	98.77	95.87	99.13	99.52	98.86	99	96.53	99.01
Photobacterium phosphoreum	TMW 2.2134	98.84	98.79	96.83	96.54	96.65	98.95	98.88	98.68	98.71	95.95	99.09	99.34	98.85	98.95	96.55	98.97
Photobacterium phosphoreum	TMW 2.214	98.68	98.75	96.62	96.26	96.38	98.83	98.72	98.54	98.62	95.64	98.85	98.79	98.71	98.86	96.43	98.8
Photobacterium phosphoreum	TMW 2.2142	98.8	98.74	96.82	96.56	96.57	99.04	98.89	98.72	98.73	95.87	99.01	98.92	98.85	98.96	96.55	98.93
Photobacterium kishitanii	**DSM 19954T**	85.6	85.6	85.68	85.68	85.67	85.59	85.63	85.64	85.74	85.7	85.64	85.54	85.71	85.68	85.76	85.58

		Photobacterium phosphoreum									
		TMW 2.2033	TMW 2.2034	TMW 2.2103	TMW 2.2125	TMW 2.2126	TMW 2.2130	TMW 2.2132	TMW 2.2134	TMW 2.2140	TMW 2.2142
Photobacterium carnosum	**DSM 105454T / TMW 2.2021T**	86.97	86.15	87.02	86.07	86.99	86.79	86.85	86.22	87.19	86.12
Photobacterium carnosum	TMW 2.2029	86.23	86.25	86.17	86.09	86.32	86.23	86.3	86.25	86.19	86.14
Photobacterium carnosum	TMW 2.2097	85.99	86.01	86.94	85.9	86.11	86.03	86.09	86.05	87.04	86.01
Photobacterium carnosum	TMW 2.2147	86.22	86.24	87.2	86.15	86.16	86.27	86.2	86.2	87.16	86.18
Photobacterium carnosum	TMW 2.2149	86.27	86.29	86.32	86.24	86.41	86.24	86.35	86.32	86.37	86.16
Photobacterium carnosum	TMW 2.215	86.2	86.13	87.04	86.06	86.14	86.14	86.07	86.07	87.3	86.07
Photobacterium carnosum	TMW 2.2157	86.11	86.1	87.12	86.03	86.1	86.11	86.12	86.13	87.18	86.12
Photobacterium carnosum	TMW 2.2163	86.4	86.33	86.26	86.23	86.28	86.27	86.34	86.19	86.27	86.3
Photobacterium carnosum	TMW 2.2169	86.62	86.23	87.07	86.08	86.77	86.72	86.76	86.22	87.23	86.13
Photobacterium carnosum	TMW 2.2098	86.85	86.1	85.98	85.89	86.94	86.76	86.77	86.11	86.33	85.99
Photobacterium carnosum	TMW 2.2186	85.95	85.95	85.94	85.88	85.93	86.01	85.89	85.89	86.06	85.87
Photobacterium carnosum	TMW 2.2187	86.11	86.1	86.03	86.08	86.12	86.2	86.06	85.98	86.33	86.12
Photobacterium carnosum	TMW 2.2188	86.12	86.09	86.08	86.06	86.1	86.17	86.02	86.01	86.33	86.02
Photobacterium carnosum	TMW 2.2189	86.2	86.09	86.1	85.9	86.03	86.1	86.11	86.05	86.31	86.07
Photobacterium carnosum	TMW 2.219	86.09	86.13	86.09	86.29	86.11	86.06	86.09	86.12	86.3	86.17
Photobacterium iliopiscarium	**DSM 9896T**	85.72	85.69	85.61	85.59	85.6	85.7	85.64	85.64	85.68	85.67
Photobacterium iliopiscarium	ATCC 51761	85.55	85.6	85.48	85.42	85.55	85.47	85.55	85.56	85.58	85.6
Photobacterium iliopiscarium	NCIMB 13478	85.77	85.68	85.61	85.59	85.55	85.59	85.58	85.57	85.58	85.62
Photobacterium iliopiscarium	NCIMB 13481	85.71	85.64	85.51	85.45	85.63	85.62	85.6	85.55	85.96	85.62
Photobacterium iliopiscarium	TMW 2.2035	85.82	85.85	85.81	85.7	85.81	85.82	85.74	85.74	85.86	85.78
Photobacterium iliopiscarium	TMW 2.2104	85.83	85.86	86.8	85.74	85.8	85.82	85.76	85.77	86.87	85.82
Photobacterium phosphoreum	**DSM 15556T**	98.75	98.78	98.76	98.78	98.74	98.76	98.87	98.78	98.75	98.77
Photobacterium phosphoreum	AK-3	98.92	98.77	98.78	98.72	98.67	98.73	98.78	98.76	98.84	98.71
Photobacterium phosphoreum	AK-4	96.83	96.61	96.67	96.56	96.71	96.67	96.79	96.77	96.78	96.83
Photobacterium phosphoreum	AK-5	96.37	96.41	96.46	96.45	96.27	96.31	96.34	96.49	96.44	96.59
Photobacterium phosphoreum	AK-8	96.58	96.49	96.49	96.43	96.38	96.49	96.53	96.52	96.5	96.55
Photobacterium phosphoreum	FS-1.1	98.9	98.83	98.81	98.8	98.88	98.87	99	98.89	98.91	99.04
Photobacterium phosphoreum	FS-1.2	98.88	98.8	98.73	98.83	98.75	98.88	98.87	98.82	98.83	98.88
Photobacterium phosphoreum	FS-2.1	98.89	98.96	98.98	98.85	98.82	98.38	98.79	98.72	98.73	98.72
Photobacterium phosphoreum	FS-2.2	98.82	98.96	98.93	98.92	98.73	98.82	98.75	98.68	98.74	98.73
Photobacterium phosphoreum	FS-3.2	95.89	95.83	95.9	95.85	95.78	95.81	95.88	95.86	95.74	95.87
Photobacterium phosphoreum	FS-4.1	98.94	98.84	98.89	98.87	98.86	98.89	99.11	99	98.95	99.02
Photobacterium phosphoreum	FS-4.2	98.89	98.82	98.85	98.8	98.83	98.88	99.49	99.32	98.87	98.92
Photobacterium phosphoreum	FS-5.1	98.77	98.77	98.8	98.76	98.78	98.79	98.85	98.8	98.78	98.83
Photobacterium phosphoreum	FS-5.2	98.94	98.92	98.85	98.82	98.92	98.91	98.98	98.91	99.01	98.96
Photobacterium phosphoreum	FS-6.1	96.48	96.52	96.43	96.31	96.41	96.25	96.53	96.5	96.56	96.51
Photobacterium phosphoreum	GCSL-P69	99.02	98.87	98.84	98.92	98.98	99.01	98.92	98.87	98.85	98.86
Photobacterium phosphoreum	TMW 2.2033	---	98.94	98.88	98.9	98.99	99.04	98.95	98.83	98.99	98.87
Photobacterium phosphoreum	TMW 2.2034	98.96	---	98.94	98.91	98.88	98.94	98.84	98.76	98.81	98.84
Photobacterium phosphoreum	TMW 2.2103	98.92	99	---	98.99	98.78	98.88	98.88	98.79	98.93	98.89
Photobacterium phosphoreum	TMW 2.2125	99.02	99.07	99.06	---	98.89	98.69	98.96	98.94	98.81	98.87
Photobacterium phosphoreum	TMW 2.2126	99.05	98.97	98.8	98.86	---	99.01	99	98.9	98.99	98.85
Photobacterium phosphoreum	TMW 2.213	99.07	98.99	98.88	98.67	98.97	---	98.95	98.87	99.02	98.91
Photobacterium phosphoreum	TMW 2.2132	98.95	98.93	98.93	98.9	98.96	98.97	---	99.4	98.93	99.05
Photobacterium phosphoreum	TMW 2.2134	98.9	98.87	98.86	98.89	98.94	98.94	99.42	---	98.89	98.99
Photobacterium phosphoreum	TMW 2.214	98.91	98.76	98.85	98.69	98.84	98.87	98.83	98.72	---	98.83
Photobacterium phosphoreum	TMW 2.2142	98.92	98.95	98.88	98.86	98.89	98.92	99.06	98.97	98.93	---
Photobacterium kishitanii	**DSM 19954T**	85.59	85.57	85.61	85.55	85.53	85.57	85.54	85.51	85.64	85.54

Table S5. Table including all the genome statistics for each genome included in the study. Marked in red, strains isolated from meat and meat products, while in blue strains isolated from fish or sea-related environment. The type strain of each species is marked in bold letters and with a ^{T}.

Strain	Genome Size (Mbp):	Per. GC	ContigCount:	Per.LargestSeq	N25	N50	N75	Total genes	Transposases
***Photobacterium carnosum* DSM 105454T**	4.559543	38.48	75	12.678	203718	124814	78723	4059	34
Photobacterium carnosum TMW2.2029	3.968401	38.72	47	21.233	403986	191817	93646	3483	22
Photobacterium carnosum TMW2.2097	4.332675	38.6	65	12.804	339080	186153	87362	3860	33
Photobacterium carnosum TMW2.2098	4.351095	38.71	82	12.91	561191	119868	59621	3943	45
Photobacterium carnosum TMW2.2147	4.322931	38.56	65	9.867	333569	162753	77486	3836	29
Photobacterium carnosum TMW2.2149	3.971074	38.66	57	14.359	177429	124125	76609	3501	21
Photobacterium carnosum TMW2.2150	4.188414	38.65	59	11.852	376361	160689	77516	3721	30
Photobacterium carnosum TMW2.2157	4.257654	38.61	72	7.021	225737	152244	56371	3792	29
Photobacterium carnosum TMW2.2163	4.044991	38.7	44	16.763	383311	200408	109897	3549	37
Photobacterium carnosum TMW2.2169	4.503077	38.55	66	12.78	186849	152827	78709	4050	37
Photobacterium carnosum TMW2.2186	4.178468	38.62	101	7.493	234795	144569	77041	3724	46
Photobacterium carnosum TMW2.2187	4.205183	38.72	55	11.068	371225	278022	142903	3738	46
Photobacterium carnosum TMW2.2188	4.14065	38.76	70	6.215	182526	111843	70104	3678	29
Photobacterium carnosum TMW2.2189	4.362186	38.75	94	7.631	180787	106191	58974	3938	28
Photobacterium carnosum TMW2.2190	4.177036	38.67	68	10.985	224484	143292	77830	3755	51
***Photobacterium iliopiscarium* DSM 9896T**	4.308695	38.99	43	19.036	541550	388872	156611	3713	34
Photobacterium iliopiscarium ATCC 51761	4.543322	39.08	151	5.792	180026	99138	62614	4053	52
Photobacterium iliopiscarium NCIMB 13478	4.387987	38.99	57	12.628	287370	182293	93823	3794	32
Photobacterium iliopiscarium NCIMB 13481	4.574576	39.05	122	9.688	363347	160820	76922	4003	51
Photobacterium iliopiscarium TMW2.2104	4.199153	38.89	86	4.304	125601	78174	48035	3755	34
Photobacterium iliospiscarium TMW2.2035	3.961514	39.03	77	5.096	148933	88352	52267	3526	34
***Photobacterium phosphoreum* DSM 15556T**	4.50825	39.61	81	7.747	220960	124777	73751	3956	46
Photobacterium phosphoreum AK-3	4.612148	39.46	60	8.821	280147	222168	94157	4030	33
Photobacterium phosphoreum AK-4	4.54851	39.64	58	24.793	337909	183923	93716	3970	24
Photobacterium phosphoreum AK-5	4.823203	39.32	180	6.159	194909	85146	53498	4366	83
Photobacterium phosphoreum AK-8	4.483978	39.59	190	3.476	89425	68620	32806	3996	68
Photobacterium phosphoreum FS-1.1	4.596818	39.52	49	20.955	490361	296712	98282	4001	32
Photobacterium phosphoreum FS-1.2	4.458778	39.5	124	6.555	181270	84183	61494	3928	30
Photobacterium phosphoreum FS-2.1	4.701582	39.58	117	5.05	140254	77411	49339	4134	33
Photobacterium phosphoreum FS-2.2	4.553203	39.52	76	7.174	193306	154715	84032	3998	24
Photobacterium phosphoreum FS-3.2	4.397289	39.54	117	4.834	125935	89017	53990	3845	40
Photobacterium phosphoreum FS-4.1	4.526515	39.58	138	4.886	141973	77617	45713	3941	29
Photobacterium phosphoreum FS-4.2	4.545936	39.52	83	6.958	193948	128030	75820	3963	27

Strain	Genome Size (Mbp):	Per. GC	ContigCount:	Per.LargestSeq	N25	N50	N75	Total genes	Transposases
Photobacterium phosphoreum FS-5.1	4.392675	39.82	329	3.464	54440	31728	14632	3892	43
Photobacterium phosphoreum FS-5.2	4.475701	39.67	176	3.892	113459	72622	39918	3953	39
Photobacterium phosphoreum FS-6.1	4.771574	39.36	71	13.513	234987	182801	95507	4224	28
Photobacterium phosphoreum GCSL-P69	4.882271	39.19	121	7.029	289750	188701	77574	4254	57
Photobacterium phosphoreum TMW2.2033	4.832374	39.24	61	12.743	438986	180599	140819	4230	38
Photobacterium phosphoreum TMW2.2034	4.724905	39.74	147	14.338	542159	233926	94158	4179	26
Photobacterium phosphoreum TMW2.2103	4.82342	39.29	66	14.326	607310	164949	81515	4235	38
Photobacterium phosphoreum TMW2.2125	4.705559	39.4	56	8.249	293320	172370	92749	4115	28
Photobacterium phosphoreum TMW2.2126	4.839609	39.3	61	18.591	261751	156540	98491	4271	30
Photobacterium phosphoreum TMW2.2130	4.939823	39.23	64	12.634	295499	163788	78188	4356	29
Photobacterium phosphoreum TMW2.2132	4.810084	39.23	64	9.727	229379	174799	83029	4241	27
Photobacterium phosphoreum TMW2.2134	4.55596	39.4	51	9.215	361444	243247	101350	3977	26
Photobacterium phosphoreum TMW2.2140	4.980977	39.33	63	16.208	380631	152456	78113	4358	39
Photobacterium phosphoreum TMW2.2142	4.689415	39.34	62	14.487	196386	141291	77013	4120	26

Table S6. Summary of presence/absence of several metabolic pathways and gene loci by species (Pc = *P. carnosum*; Pi = *P. iliopiscarium*; Pp = *P. phosphoreum*). Symbols refer to specified gene/metabolic pathway as follows: + = all strains of a species have it; - = no strain of the species have it; (+) = all strains except one of a species have it; +/- = some (undefined number) of strains of a species have it; (-) = only one strain of the species has it. The color of the symbol indicates if the strains that have that feature are all isolated from meat (red), from fish/marine environment (blue), or mixed (black). An asterisk (*) next to the symbol indicates that the feature is present in only one of the distinct phylogenetic clades of the species.

			Pc	Pi	Pp
Carbohydrate metabolism	Gluconeogenese/glycolysis		+	+	+
		2,3-diphosphoglycerate-dependent phosphoglycerate mutase (*gpm*A)	-	-	+
	Pentose phosphate pathway		+	+	+
	Homolactic fermentation		+	+	+
	Heterolactic fermentation	xylulose-5-phosphate phosphoketolase *xpk*A	-	-	-
	Entner-Doudoroff	KDPG aldolase (*ed*A)	+	+	+
		phosphogluconate dehydratase (*ed*D)	(-)	-	+/-
	Fructose		+	+	+
	Ribose		+	+	+
		Ribose Transporter (ribose uptake protein) *rbs*U	-	-	-
		Putative deoxyribose-specific ABC transporter (*nup*A)	-	-	-
	Nucleosides and deoxynucleosides		+	+	+
		Ribonucleotide reductase *nrd*AB	+	+	+
		Ribonucleotide reductase *nrd*I (assembly)	+/-	-	+
	Sugar transporters	galactose/methyl galactoside ABC transporter ATP-binding protein *mgl*ABC	+/-	+/-*	+/-
		maltose/maltodextrin ABC transporter *mal*FGK	+	+	-
		maltose/maltodextrin ABC transporter *malE*	+	+/-*	-
		PTS lactose/cellobiose transporter subunit ABC	+/-	+	-
		PTS mannose transporter	+/-	+/-*	+
	Other sugars	alpha-galactosidase	+	+	+/-
		alpha-mannosidase	+/-	+	(+)
		6-phospho-beta-glucosidase	+/-	+	-
	Glycogen/starch degradation		+	+	-
		alpha-amylase	+	+/-*	-
		glycogen/starch synthase	-	-	-
	Xylose	endoxylanase	+/-	+/-*	+
		xylG: D-xylose ABC transporter, ATP-binding protein	-	-	+
		ABC_transporter ribose/xylose/arabinose/galactose	-	-	+
	Chondroitin sulphate	chondriotinase	+/-	+/-	+/-
	Arabinogalactan	beta-galactosidase	+	+	+
	Pullulan	Pullulanase	+	+	-
	Fucoidan	L-fucose:H+ symporter permease	+	+	+
		L-fucose isomerase	(-)	-	-
		L-fuculokinase	(-)	-	-
		L-fucose mutarotase	(-)	-	-

			Pc	Pi	Pp
		L-fuculose-phosphate aldolase	(-)	-	-
Pyruvate metabolism	Pyruvate dehydrogenase complex		+	+	+
	Pyruvate to lactate		+	+	+
	Pyruvate to acetate	Pyruvate oxidase (*pox*B)	+	-	-
		Acylphosphatase (*acy*P)	-	+	+
	Pyruvate to ethanol	acetaldehyde dehydrogenase/alcohol dehydrogenase (*adh*E)	+	+	+
	Pyruvate to formate		+	+	+
	Pyruvate to acetolactate (diacetyl)		+	+	+
	Pyruvate to acetoin		+	+	+
	Pyruvate to butane-2,3-diol		-	-	-
Citrate	TCA cycle		+	+	+
	Glyoxylate cycle		+	+	+
Triacylglyceride metabolism	Glycerol utilization		+	+	+
	Fatty acid beta-oxidation aerobic		+	+	+
	Fatty acid beta-oxidation anaerobic		+	+	+
Amino acids		histidine-histamine antiporter (aminoacid permease)	(-)	-	+/-
		histidine decarboxylase 2 (*hdc*2)	(-)	-	+/-
		histidine decarboxylase (*hdc*)	-	-	-
		arginine decarboxylase (*spe*A)	+	+	+
		tyrosine decarboxylase (*tdc*A)	+/-	-	+
		ornithine decarboxylase (*spe*F)	+/-	-	-
		lysine decarboxylase (*lcd*C)	-	+/-*	+
		agmatinase (*spe*B)	(+)*	+	+
		glutamate decarboxylase (*gad*B)	+	+	+
	Aminotransferases				
		Aspartate Aminofransferase	+	+	-
		Alanine aminotransferase	-	-	-
		Glutamate Dehydrogenase (aKG/NADH2) *gdh*A	-	-	+
Respiration	Menaquinone syntheses		+	+	+
	Quinone Q-8 biosynthesis		+	+	+
	Heme biosynthesis		+	+	+
	NADH dehydrogenase		+	+	+
	Complex I: proton transporting NADH dehydrogenase (*nuo*)		-	-	+/-
		subunit nuoB	+	+	+
	Na+ transporting NADH:ubiquinone reductase complex (*nqr*)		+	+	+
	Complex II: Succinate dehydrogenase		+	+	+
	Complex III: cytochrome bc complex		+	+	+
	Complex IV: cytochrome c oxidase		+	+	+
	cytochrome bd oxidase		+	+	+
	cytochrome o ubiquinol oxidase		+	+	+
	cytochrome-c oxidase, cbb3-type		-	+	+
	Electron donors	NiFe hydrogenase	+	+	+

			Pc	Pi	Pp
	Alternative electron acceptors	Fumarate reductase	+	+	+
		TMAO reductase	+	+	+
		Nitrate reductase	+	+	+
		Nitrite reductase	+	+	+
		sulfate adenylyltransferase + assimilatory sulfite reductase	+	+	+
		DMSO reductase	-	+/-*	+/-
Environmental adaptation and stress response	H2O2 production	pyruvate oxidase (*Pox*)	+	-	-
		superoxide dismutase (*Sod*)	+	+	+
	H2O2 scavenging enzymes	catalase	-	(-)	(+)
		catalase/peroxidase	+	+	+
	Pressure response		+	+	+
		Porin-like protein OmpL	+/-	+/-*	+/-
	Salt Response		+	+	+
		Outer membrane protein OmpW	-	-	-
		Major outer membrane protein OmpV	-	-	-
		Porin OmpC/OmpF	-	-	-
	Unspecific stress response		+	+	+
	Sodium transporters		26.6	25.8	30.7
	Motility	Flagellar cluster	+/-	+/-*	+/-
	Bioluminescence		-	-	+
	Iron uptake		+	+	+

15.4 Supplementary files to publication 4

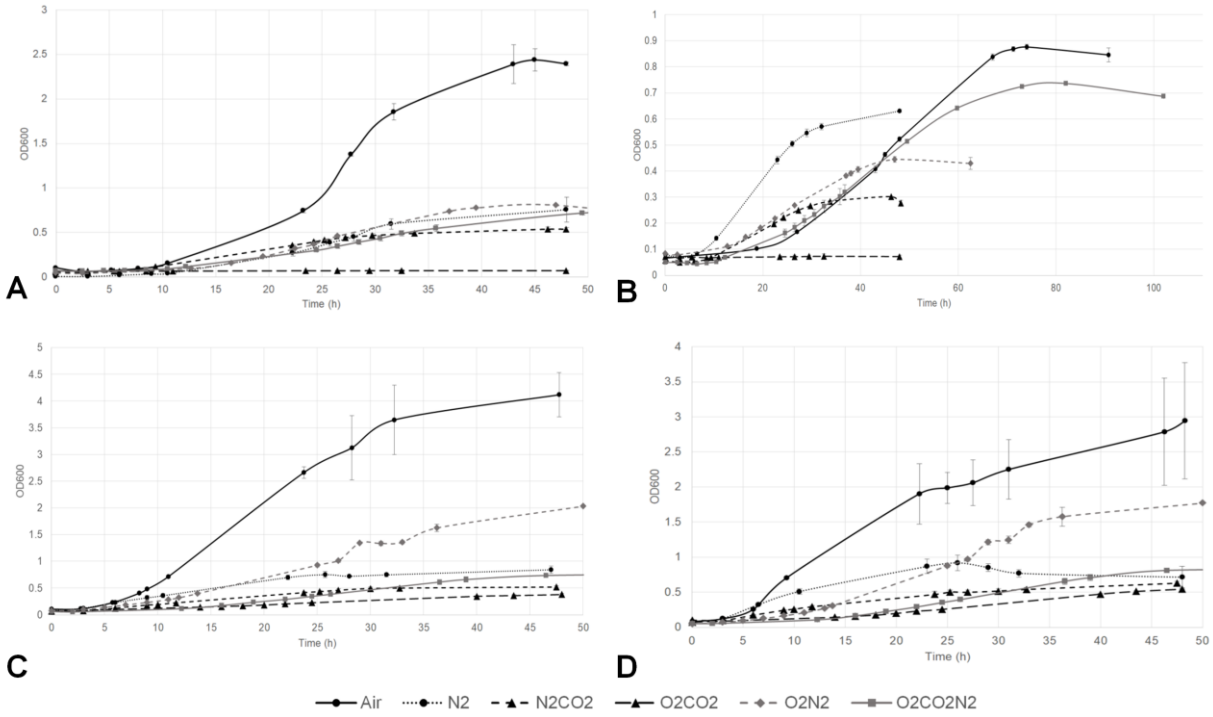

Figure S1. Growth curves of *P. carnosum* A. TMW 2.2021T, B. TMW 2.2149 and *P. phosphoreum* C. TMW 2.2103, D. TMW 2.2134 under different gas mixtures: air, N2 (100 %), N2/CO2 (70/30 %), O2/CO2 (70/30 %), O2/N2 (70/30 %), O2/CO2/N2 (21/30/49 %) measured as increase in OD600 over time (h).

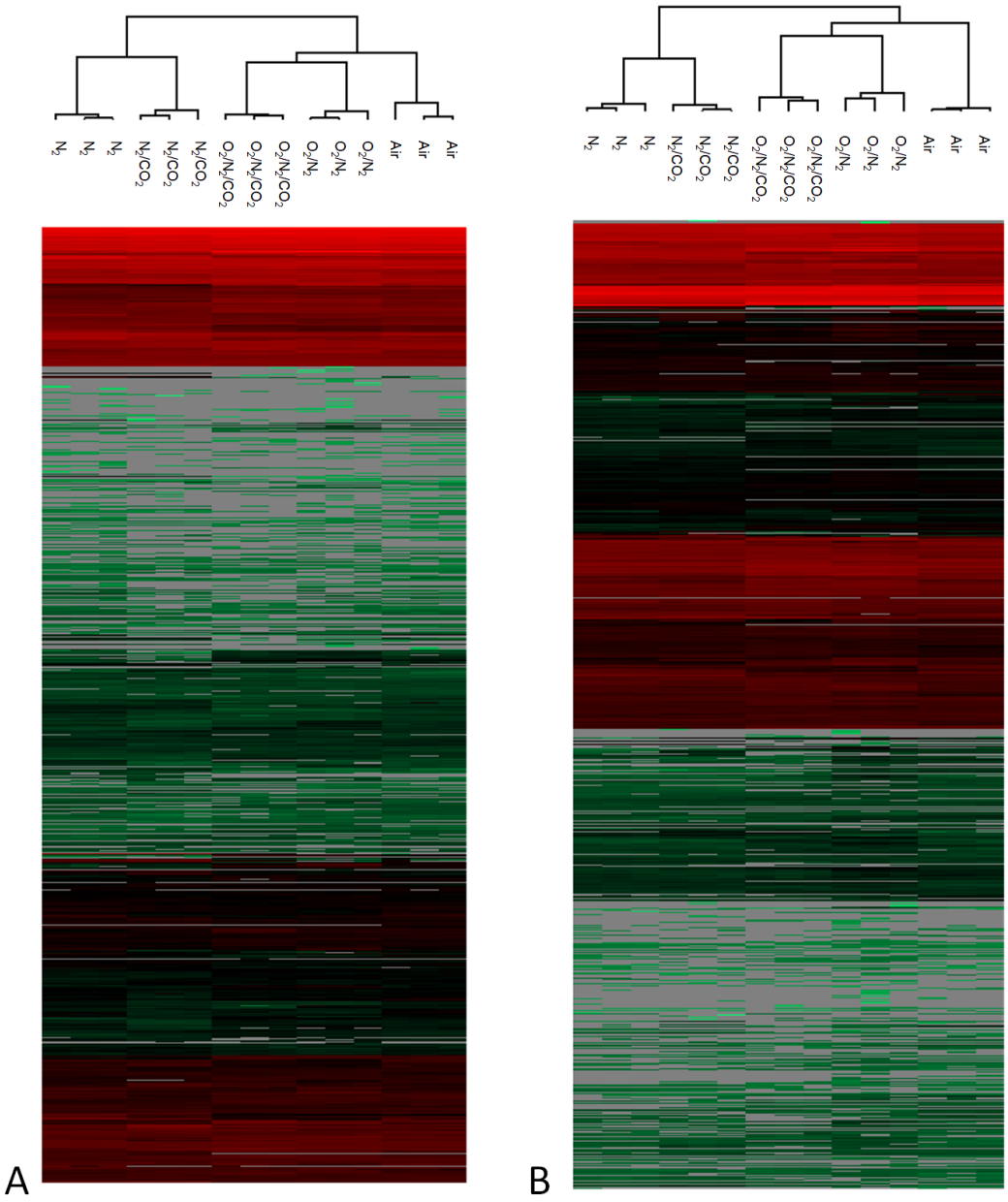

Figure S2. Unsupervised hierarchical clustering analysis of proteomics samples (LFQ data) from *P. carnosum* strains A. TMW 2.2021^T, B. TMW 2.2149.

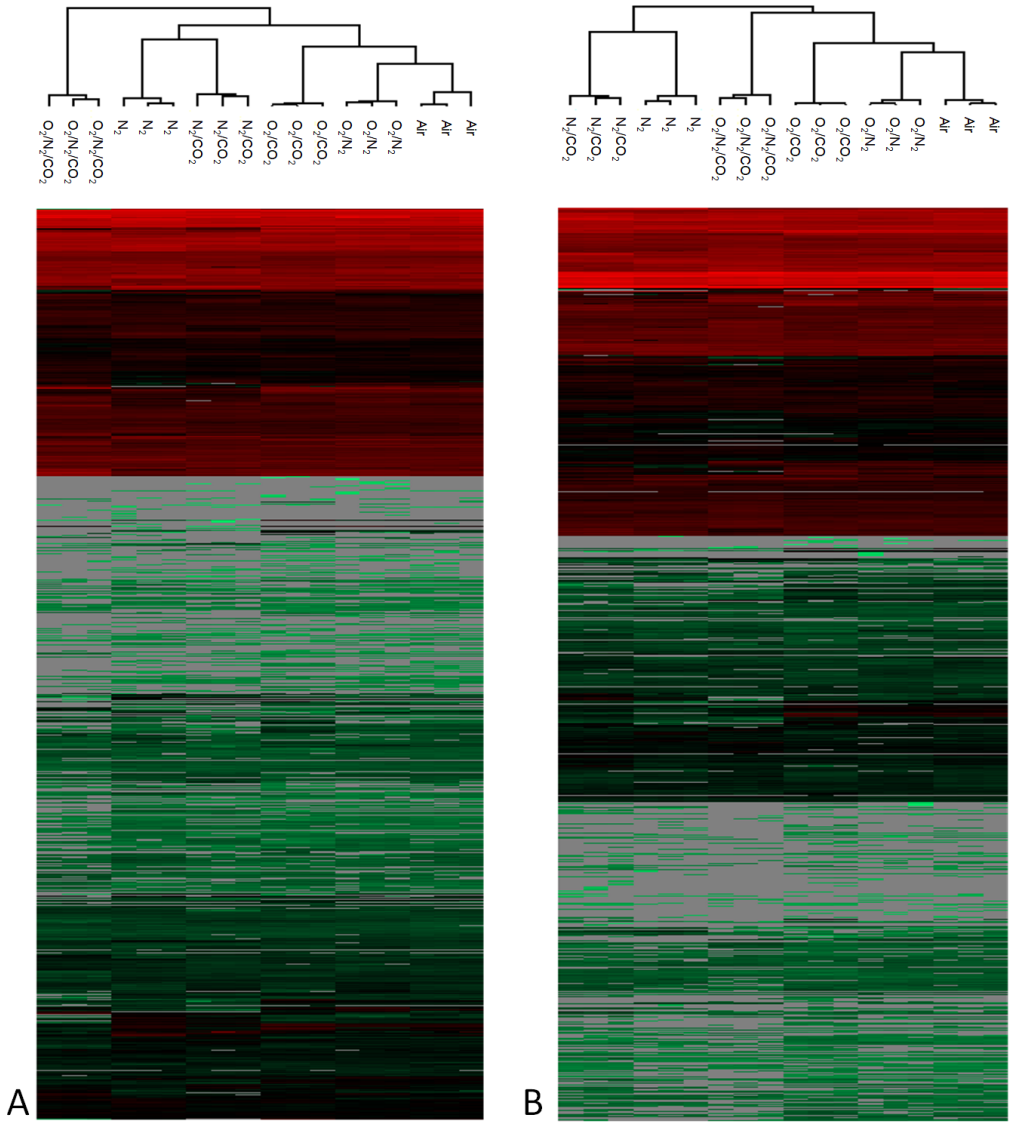

Figure S3. Unsupervised hierarchical clustering analysis of proteomics samples (LFQ data) from *P. phosphoreum* strains A. TMW 2.2103, B. TMW 2.2134.

Table S1. Growth parameters of all strains under different gas atmospheres on meat simulation media.

	Lag-phase (h)	SE (h)	OD_{max}	SE	μ_{max} (division/h)	SE (division/h)
P. carnosum TMW 2.2021^T						
Air	$14.83^{b,c,d}$	0.74	$2.42^{b,c,d,e}$	0.05	$0.0994^{b,c,d,e}$	0.0084
N_2	$12.02^{a,d,e}$	0.51	$0.76^{a,d}$	0.14	$0.0281^{a,d}$	0.0029
O_2/N_2	$13.36^{a,d,e}$	0.03	$0.8^{a,d}$	0.01	$0.0308^{a,d,e}$	0.0003
N_2/CO_2	$6.08^{a,b,c,e}$	1.09	$0.54^{a,b,c,e}$	0.02	$0.0191^{a,b,c}$	0.0012
$O_2/CO_2/N_2$	$13.9^{b,c,d}$	0.25	$0.75^{a,d}$	0.01	$0.0225^{a,c}$	0.0016
O_2/CO_2	N.A.	N.A.	N.A.	N.A.	N.A.	N.A.
P. carnosum TMW 2.2149						
Air	$21.57^{b,c,d,e}$	0.38	$0.85^{b,c,d,e}$	0.02	$0.0171^{b,c,d,e}$	0.0002
N_2	$4.64^{a,c,d,e}$	0.39	$0.63^{a,c,d,e}$	0.01	$0.0198^{a,c,d,e}$	0.0002
O_2/N_2	$11.12^{a,b,d,e}$	0.05	$0.44^{a,b,d,e}$	0.01	$0.0121^{a,b,d,e}$	0.0004
N_2/CO_2	$6.96^{a,b,c,e}$	0.50	$0.29^{a,b,c,e}$	0.01	$0.0098^{a,b,c,e}$	0.0001
$O_2/CO_2/N_2$	$17.73^{a,b,c,d}$	0.33	$0.74^{a,b,c,d}$	0.04	$0.0147^{a,b,c,d}$	0.0013
O_2/CO_2	N.A.	N.A.	N.A.	N.A.	N.A.	N.A.
P. phosphoreum TMW 2.2103						
Air	$6.35^{b,c,d,e}$	2.73	$4.12^{b,c,d,e}$	0.42	$0.143^{b,c,d,e,f}$	0.0408
N_2	$1.17^{a,c,e,f}$	0.73	$0.84^{a,c,d,f}$	0.07	$0.0309^{a,c,f}$	0.0005
O_2/N_2	$11.71^{a,b,d,f}$	1.30	$2.03^{a,b,d,e,f}$	0.02	$0.0662^{a,b,d,e,f}$	0.0048
N_2/CO_2	$2.87^{a,c,e,f}$	0.27	$0.52^{a,b,c,f}$	0.03	$0.0169^{a,c,f}$	0.0014
$O_2/CO_2/N_2$	$11.62^{a,b,d,f}$	0.17	$0.76^{a,c,f}$	0.03	$0.0226^{a,c,f}$	0.0018
O_2/CO_2	$6.54^{b,c,d,e}$	0.98	$0.38^{b,c,d,e}$	0.02	$0.0086^{a,b,c,d,e}$	0.0009
P. phosphoreum TMW 2.2134						
Air	$2.41^{b,c,d,e,f}$	0.39	$2.94^{b,c,d,e,f}$	0.83	$0.0884^{b,c,d,e,f}$	0.0130
N_2	$0.45^{a,c,d,e,f}$	0.21	$0.89^{a,c,f}$	0.01	$0.0424^{a,f}$	0.0048
O_2/N_2	$13.02^{a,b,d,f}$	0.44	$1.77^{a,b,d,e,f}$	0.04	$0.0694^{a,f}$	0.0037
N_2/CO_2	$1.89^{a,b,c,e,f}$	0.25	$0.63^{a,c,f}$	0.02	$0.0194^{a,f}$	0.0016
$O_2/CO_2/N_2$	$12.67^{a,b,d,f}$	0.35	$0.83^{a,c,f}$	0.02	$0.0253^{a,f}$	0.0015
O_2/CO_2	$10.74^{a,b,c,d,e}$	0.60	$0.54^{a,b,c,d,e}$	0.00	$0.0134^{a,b,c,d,e}$	0.0008

Displayed numbers represent average values and standard errors obtained from the three independent replicates. The superscript letters indicate significant differences between conditions according to a confidence interval of 95% (p-value 0.05): **a**. Air; **b**. N_2; **c.** O_2/N_2; **d.** N_2/CO_2; **e.** $O_2/CO_2/N_2$; **f.** O_2/CO_2.

Table S2_A. Differentially expressed proteins for every pair of conditions analyzed for *P. carnosum* TMW 2.2021^T, and the log_2 values representing the difference in expression intensity between the two conditions.

Annotation	Air_vs_N_2	O_2/N_2_vs_N_2	Air_vs_O_2/N_2	N_2_vs_N_2/CO_2	N_2/CO_2_vs_O_2/CO_2/N_2
Respiratory chain					
succinate dehydrogenase flavoprotein subunit	2.03675245	2.95422808			
F0F1 ATP synthase subunit gamma	-2.12672958				
F0F1 ATP synthase subunit delta		-2.06955274			
F0F1 ATP synthase subunit B		2.15079371			
ferredoxin--NADP(+) reductase		2.01862335			
cytochrome C napC/nirT	-3.31686236	-3.38516744			
NADH-quinone oxidoreductase subunit B family protein	-4.47828089	-4.99625015			4.85541153
ubiquinone-binding protein					-2.36826833
Oxidoreductases					
FAD-dependent oxidoreductase	2.82208138	3.23345439			-3.90547244
NADPH-dependent FMN reductase	2.56902199	4.56747818			-3.71414884
FAD-dependent oxidoreductase	2.22273674	3.11725426			-2.23666827
Riboflavin metabolism					
NAD(P)H-flavin reductase	2.25124957	2.40128454			-2.13847415
acid phosphatase AphA					2.90841103
Heme transport					
heme ABC transporter ATP-binding protein		-3.14669164			
Alternative electron acceptors					
succinate dehydrogenase/fumarate reductase iron-sulfur subunit	-2.02690188	-2.02392832			
trimethylamine-N-oxide reductase TorA	-2.42258148	-3.06104724			
nitrite reductase (NAD(P)H) small subunit	-3.07063929				
nitrite reductase (NAD(P)H)	-5.49995893	-6.45068932			
hydroxylamine reductase	-5.59822006	-6.46073914			2.98407364
trimethylamine-N-oxide reductase TorA			-2.86401736		
assimilatory sulfite reductase (NADPH) flavoprotein subunit					-3.73450279
Alternative electron donors					
formate dehydrogenase subunit beta	-3.69546356	-5.41568947			2.91572444
formate dehydrogenase-N subunit alpha	-4.20034638	-3.60467084			2.63794772
formate dehydrogenase subunit alpha	-7.98754234	-8.42516009			4.00570297
formate dehydrogenase accessory sulfurtransferase FdhD		-2.14332581			
hydrogenase 3 large subunit	-6.55800298	-6.45906766			5.70970917
Peroxisome/oxidative stress					
alkyl hydroperoxide reductase subunit F	2.45765851	3.00489108			
peroxidase		2.44456482			
peroxiredoxin		2.36879857			
Cellular stress					
carbonic anhydrase	-2.28527044	-2.62579028			3.7512811
DNA starvation/stationary phase protection protein		4.36663818			
DNA starvation/stationary phase protection protein				-2.28397242	
carbon storage regulator				-2.68703206	2.9934775
aerotolerance protein BatD				-2.17352486	
Glutathione metabolism					
bifunctional glutathionylspermidine amidase/synthase		-5.02694384			3.63384883
S-(hydroxymethyl)glutathione synthase		2.25283686			
S-(hydroxymethyl)glutathione synthase					-3.52431679
Metal/ion transport					
cobalamin ABC transporter substrate-binding protein	3.45549583	4.88201332			-4.0879186
cobalamin ABC transporter substrate-binding protein	3.45549583	4.88201332			-4.0879186
iron ABC transporter substrate-binding protein	2.97795855	5.45831808	-2.15743586		-4.48572477
iron ABC transporter		2.87248166			-2.02904383
ferrous iron transport protein A		3.10910352			-2.24730937
ferrous iron transport protein B		3.18835068			
zinc transporter ZntB			3.73171298		
copper-translocating P-type ATPase		2.15643756	-2.19367167		
tungsten ABC transporter substrate-binding protein				2.41277568	
sulfate ABC transporter substrate-binding protein	-3.78207754	-3.26552391			2.28418541
Amino acids transport					
methionine ABC transporter substrate-binding protein MetQ		3.37468338			
Unspecific transporters					
ABC transporter ATP-binding protein	-2.31052144	-2.12972132			
hydrophobe/amphiphile efflux-1 family RND transporter		3.23577309	-2.43548317		
ABC transporter substrate-binding protein				2.53551038	
C4-dicarboxylic acid transporter DauA				-2.71136093	
Fe-S cluster					
4Fe-4S ferredoxin		-2.74708557			
iron-sulfur cluster assembly protein IscA		2.22010295			
co-chaperone HscB		2.19984309			
Pyruvate metabolism					
pyruvate dehydrogenase (acetyl-transferring), homodimeric type	2.33110835	2.65776952			-2.19974391
pyruvate dehydrogenase complex dihydrolipoyllysine-residue acetyltransferase	2.04436391	2.47890091			
dihydrolipoyl dehydrogenase		2.14010366			
acetaldehyde dehydrogenase (acetylating)				2.04137103	
Fermentation					
2-hydroxyacid dehydrogenase		2.17403094			
Lipoic acid					
octanoyltransferase	3.1474116	3.69477209			
lipoyl synthase	2.81906929	2.72124163			-2.88401731
TCA cycle					
citrate (Si)-synthase	2.22530022	3.97172229			-4.40748215
succinate dehydrogenase flavoprotein subunit	2.03675245	2.95422808			
isocitrate dehydrogenase (NADP(+))		2.23494848			
succinate dehydrogenase/fumarate reductase iron-sulfur subunit	-2.02690188	-2.02392832			
Sugar metabolism					
phosphoglucomutase	2.12935346	2.98178291			-3.11365128
phosphonomutase	4.58050118		6.04030062		
Starch/glycogen and maltose metabolism					
4-alpha-glucanotransferase	-2.47666969	-6.69684537	4.22017568		
glucohydrolase	-2.84724744	-4.73424657			3.93209521
1,4-alpha-glucan branching enzyme	-3.22029597	-2.41024208			
maltose ABC transporter substrate-binding protein MalE	-4.82829043	-5.87985929			5.40335337
maltoporin		-4.77688281			
amidase		-3.92935435	3.85077972		
glycogen phosphorylase		-7.40986697	5.51473134		4.21661313
glucohydrolase		-2.1075395			2.41777484
Fatty acid degradation					
acyl-CoA dehydrogenase	-2.17652639		-4.06368332		-3.08644994
acyl-CoA dehydrogenase	-2.17652639		-4.06368332		-3.08644994
acetyl-CoA acetyltransferase		3.34254901			
Glycerophospholipid metabolism					
anaerobic glycerol-3-phosphate dehydrogenase subunit B	-2.36210391				-3.4567407
glycerol-3-phosphate dehydrogenase					-2.79728381
anaerobic glycerol-3-phosphate dehydrogenase subunit A					-2.60456785
glycerol kinase					-2.08439128
Motility and chemotaxis					
chemotaxis response regulator protein-glutamate methylesterase	-2.19360695				
flagellin		2.4062856	-2.09180552	-2.91569583	
Choline degradation (anaerobic)					
choline trimethylamine-lyase	-2.92621028	-5.57253075	2.64632047	2.78990428	
Production of H2					
formate hydrogenlyase maturation protein HycH	-3.60402896				
formate hydrogenlyase complex iron-sulfur subunit	-4.31250598	-4.89668274			3.58283615
Nucleosides and Nucleotides					
anaerobic ribonucleoside-triphosphate reductase		-2.50713666			
anaerobic ribonucleotide reductase-activating protein	-2.04688911				2.84955279
bifunctional phosphoribosylaminoimidazolecarboxamide formyltransferase/IMP cyclohydrolase		2.09840202			-4.33696938
5-(carboxyamino)imidazole ribonucleotide mutase		2.58708064			
phosphoribosylformylglycinamidine synthase					-2.68480492
bifunctional UDP-sugar hydrolase/5'-nucleotidase					-2.37224833

Annotation	Air_vs_N_2	O_2/N_2_vs_N_2	Air_vs_O_2/N_2	N_2_vs_N_2/CO_2	N_2/CO_2_vs_$O_2/CO_2/N_2$
Cell envelope/membrane					
pilus (MSHA type) biogenesis protein MshL		-2.506347	2.21088982		
LPS assembly protein LptD			2.18866768		
LPS biosynthesis protein WavE				2.56176122	-2.10939153
Sulfur metabolism					
arylsulfatase		5.44567363	-2.6147123		-2.38480123
assimilatory sulfite reductase (NADPH) flavoprotein subunit					-3.73450279
Nitrogen metabolism					
glutamate synthase large subunit					-2.13734309
Peptidases/proteases					
U32 family peptidase	2.39090106	2.30774117			-2.21570079
dipeptidase	-2.3079732				
ATP-dependent protease	-2.3809116		-2.5824622		
U32 family peptidase	-3.449476				
protease	-4.0933149	-4.1917483			3.51857122
peptidase T	-4.375333	-4.4446411			4.19722366
peptidase M20	-5.0866314	-6.6018155			4.64240837
peptidase M23		-3.4089788	2.42296461	2.81875038	
peptidase					-2.90222677
peptidase M16				2.71534284	
signal peptide peptidase SppA		2.58117549			
collagenase-like protease		3.77277056			-4.42655436
protease SohB			-2.3148974		
Amino acids metabolism					
acetyl-CoA acetyltransferase		3.34254901			
bifunctional aspartate kinase/homoserine dehydrogenase I		3.71010971			
D-3-phosphoglycerate dehydrogenase				2.98532041	-2.99926885
Valine, leucine and isoleucine biosynthesis					
branched chain amino acid aminotransferase ilvE		3.4017175			
acetolactate synthase 3 large subunit ilvB	3.06371829	3.34875488			-3.00204976
2-isopropylmalate synthase leuA	2.89523977	3.35174878			
3-isopropylmalate dehydrogenase leuB	2.42012914	2.34142685			
ketol-acid reductoisomerase ilvC	2.52752304	3.57726542			-3.41165733
dihydroxy-acid dehydratase ilvD		4.61912791			
Valine, leucine and isoleucine degradation					
acetolactate synthase 3 large subunit	3.06371829	3.34875488			-3.00204976
acyl-CoA dehydrogenase	-2.1765264		-4.0636833		-3.08644994
acyl-CoA dehydrogenase	-2.1765264		-4.0636833		-3.08644994
Methionine degradation					
S-ribosylhomocysteine lyase				2.43812752	
Aspartate metabolism					
aspartate carbamoyltransferase					-5.01541901
L-aspartate oxidase					-3.37252871
aspartate carbamoyltransferase regulatory subunit					-2.74953588
Glycine metabolism					
glycine dehydrogenase (aminomethyl-transferring)					-2.46964773
Methionine biosynthesis					
Met repressor		2.0567131			
Arginine degradation, urea cycle					
aspartate aminotransferase family protein		2.09666506			
Alanine, aspartate and glutamate metabolism					
L-asparaginase 2	-2.1784382		-2.9584405		
aspartate ammonia-lyase	-2.429347	-2.5556895			
Glycine, serine and threonine metabolism					
L-threonine dehydrogenase	-4.6353053	-6.7256012			4.14291763
Selenocysteine metabolism					
L-seryl-tRNA(Sec) selenium transferase	-5.3052256	-6.1447824			
selenocysteine-specific translation elongation factor	-2.8756255	-4.5255343			2.86610349
Ribosomal proteins					
30S ribosomal protein S6--L-glutamate ligase	2.00688795				
30S ribosomal protein S17					6.72583771
RNA/DNA					
RNA polymerase factor sigma-54		-2.2497444	3.58484586		
recombinase RecQ		6.53371493			
DNA repair protein RecN				2.00343514	
exodeoxyribonuclease III					-2.07860565
exodeoxyribonuclease III					2.33213361
DEAD/DEAH box helicase					2.40653356
DNA topoisomerase				-2.2436835	
exodeoxyribonuclease V subunit beta		-3.3588123		3.70138168	
Resistance					
fluoroquinolone resistance protein		-2.4776471			
Proteins not assigned to pathway					
hypothetical protein	2.12160556				
STAS/SEC14 domain-containing protein	2.04861094			-3.4259237	
hypothetical protein					2.11871592
hypothetical protein					2.13992945
hypothetical protein					-2.22685115
hypothetical protein				5.23647245	
hypothetical protein				5.23647245	
IS3 family transposase				5.23647245	
transposase				5.23647245	
hypothetical protein				-2.2171714	
YecA family protein					-4.19887606
type I-F CRISPR-associated endoribonuclease Cas6/Csy4					4.35440509
hypothetical protein			-2.0571829		
SpoVR family protein		3.81497065	-3.3326389		
transcriptional regulator		3.39097595	-2.0896875		-2.53638331
hypothetical protein		2.94845899			-2.60835457
hypothetical protein		2.60816892			-2.21567599
hypothetical protein		2.76498731	-2.9166372		-2.65417862
hypothetical protein		-2.6125043			
transcriptional regulator		-2.5807234		2.02975273	
hypothetical protein		-2.5569935			
effector protein	-7.1027246	-6.242513			6.09148789
TIGR02099 family protein	-6.185583	-6.4877116		6.36753337	
hypothetical protein	-5.0219289	-5.8931936			5.98380852
hypothetical protein	-2.0346694				
SCP2 domain-containing protein	-2.3164413	-4.6300831			
BMC domain-containing protein	-2.8812205			3.05797831	
BMC domain-containing protein	-3.130699	-2.5058244			
hypothetical protein	-3.2103549	-3.0480029			2.09477488
BMC domain-containing protein	-3.3114765	-2.8540688			
transcriptional regulator	-3.5589453	-2.4889399			2.68600019
hypothetical protein	-3.6518981	-4.0430794			3.74488195
conjugal transfer protein TraR	-3.8293634	-4.557888			3.7572422
hypothetical protein	2.68315862	2.1088829			
phasin family protein	2.70352821	2.44306564			
YjjI family glycine radical enzyme	-2.0578028	-2.6803335			
Accessory colonization factor AcfD		-5.8520629	4.55494537	2.50613912	2.81653404
AraC family transcriptional regulator		-3.031388			
molybdenum-dependent transcriptional regulator		-2.8246606			
hypothetical protein			-2.8662123		
PrkA family serine protein kinase		3.40198771			
hcalcium-binding protein		3.71296438			-3.6910038
sigma factor-binding protein Crl			-2.000415		
BolA family transcriptional regulator				4.80360603	-4.02987607
DNA-binding transcriptional regulator FruR					3.5953687
4Fe-4S dicluster domain-containing protein	-4.851151	-3.8885021			
(Fe-S)-binding protein		-3.2221578			

Table S2_B. Differentially expressed proteins for every pair of conditions analyzed for *P. carnosum* TMW 2.2149, and the $\log_2$ values representing the difference in expression intensity between the two conditions.

Annotation	Air_ vs_ N_2	O_2/N_2_ vs_ N_2	Air_ vs_ O_2/N_2	N_2_ vs_ N_2/CO_2	N_2/CO_2_ vs_ O_2/CO_2/N_2
Respiratory chain					
F0F1 ATP synthase subunit epsilon	3.34724859				
F0F1 ATP synthase subunit gamma		2.15599569			
F0F1 ATP synthase subunit B		2.15640767			
F0F1 ATP synthase subunit delta		2.02696673			
cytochrome ubiquinol oxidase subunit I	2.68765895	2.37731361			
succinate dehydrogenase assembly factor 2 family protein					2.223127365
ubiquinone biosynthesis regulatory protein kinase UbiB		2.7792956			
(2E,6E)-farnesyl diphosphate synthase	2.94506302	2.79394213			
ferredoxin--NADP(+) reductase		2.1728967			
Oxidoreductases					
FAD-dependent oxidoreductase					-2.01143201
SDR family NAD(P)-dependent oxidoreductase			-3.18992386		
molybdopterin-dependent oxidoreductase	-2.2561381				
Re/Si-specific NAD(P)(+) transhydrogenase subunit beta	2.50628154	2.4765288			
NAD(P)/FAD-dependent oxidoreductase		2.59505908			-2.03422991
NADPH-dependent FMN reductase		4.17739741	-3.82647146		
Riboflavin metabolism					
flavodoxin FldB					-2.09895515
Alternative electron acceptors					
hydroxylamine reductase	-7.61107038	-7.45142937		2.14481545	4.963281631
nitrite reductase large subunit	-6.18237228	-4.97351583			7.54024442
nitrite reductase small subunit NirD	-4.392143	-4.34418424			4.394297282
assimilatory sulfite reductase (NADPH) flavoprotein subunit	3.77490629	3.013141			
trimethylamine-N-oxide reductase TorA				-2.04828135	3.253094355
trimethylamine-N-oxide reductase TorA		2.88620567	-2.74085147		
sulfate adenylyltransferase subunit CysN		2.77225558			
Alternative electron donors					
formate dehydrogenase subunit alpha	-4.32056872	-4.75888888			4.052124023
Re/Si-specific NAD(P)(+) transhydrogenase subunit alpha	3.68050029				
Peroxisome/oxidative stress					
carbonic anhydrase	-2.61093458				
alkyl hydroperoxide reductase subunit C		2.1767362			-2.19544983
alkyl hydroperoxide reductase subunit F		2.3837293			-2.95615578
Cellular stress					
DNA starvation/stationary phase protection protein	-2.38231138		-2.65730527		
DNA starvation/stationary phase protection protein		3.24323209	-2.31146278		-3.61266009
phage shock protein PspA	2.54193827		3.53120181		
cold-shock protein		-5.30160968			
carbon storage regulator CsrA		-4.42728297	3.19437574		
envelope stress response membrane protein PspB	2.32817663		2.86402779		
periplasmic heavy metal sensor	3.93718948		3.06068776		
co-chaperone GroES	4.05085297				
molecular chaperone TorD		-3.60070547			
ribosome-associated heat shock protein Hsp15		2.31083616			
molecular chaperone					2.490166982
N-ethylmaleimide reductase					-2.61444346
Glutathione metabolism					
glutathione S-transferase					2.806126277
Metal/ion transport					
magnesium/cobalt transporter CorA					2.423933665
ferrous iron transport protein A		2.61386744			-3.23895963
Fe(3+) ABC transporter substrate-binding protein		5.31332016			-4.28248596
Amino acids transport					
preprotein translocase subunit SecY		2.02726301			
Unspecific transporters					
ABC transporter substrate-binding protein	3.74504547	5.03389359	-2.20236511		-3.32872963
ABC transporter substrate-binding protein		2.54903666	-2.55228996		
porin	2.06875445				
transporter		2.30893707	-2.34483299		
efflux RND transporter periplasmic adaptor subunit		2.67434184			
multidrug DMT transporter permease					-4.5312074
secretion protein			3.07306824		
porin			-3.14606997		
Pyruvate metabolism					
pyruvate dehydrogenase (acetyl-transferring), homodimeric type		2.42471314			-2.25130844
pyruvate dehydrogenase complex dihydrolipoyllysine-residue acetyltransferase		2.01430512			
acetoacetyl-CoA reductase	2.84837036				
efflux RND transporter permease subunit		2.02282016			
iron-containing alcohol dehydrogenase			-2.25904617		
Lipoic acid					
lipoyl synthase	2.37488594				-2.69402377
lipoyl(octanoyl) transferase LipB	3.726946	3.70363553			
TCA cycle					
bifunctional aconitate hydratase 2/2-methylisocitrate dehydratase	2.08131091				
bifunctional isocitrate dehydrogenase kinase/phosphatase					3.528494517
Sugar metabolism					
ribokinase	-5.35759583				
D-ribose pyranase	-3.84528643	-4.21536636			
glucohydrolase	-3.099823	-4.44436836			2.647504171
phospho-sugar mutase	2.19214986	2.44861221			
glycosyl hydrolase		-2.27716255			
Starch/glycogen and maltose metabolism					
maltose/maltodextrin ABC transporter substrate-binding protein MalE	-4.67056325	-6.18965594			5.102377574
maltoporin	-2.00043297	-2.16551145		2.38735708	
glycogen/starch/alpha-glucan family phosphorylase	-3.11019516	-2.97234408			2.406649907
maltose/maltodextrin ABC transporter ATP-binding protein MalK		-2.607481			
1,4-alpha-glucan branching protein GlgB	-2.31158587				
4-alpha-glucanotransferase	-2.48285624	-3.01181857			2.455808004
alpha,alpha-phosphotrehalase					2.420810699
Amino sugar and nucleotide sugar metabolism					
N-acetylneuraminate lyase		-3.02736219	2.86899961		
N-acetylmannosamine kinase			2.01400464		
putative N-acetylmannosamine-6-phosphate 2-epimerase			2.95721486		
1,6-anhydro-N-acetylmuramyl-L-alanine amidase AmpD			2.42178154		
Fatty acid degradation					
fatty acid oxidation complex subunit alpha FadJ	3.62185071	3.84629377		-2.07175891	
acetyl-CoA C-acyltransferase	4.06277123	3.18461673		-4.3524971	
fatty acid oxidation complex subunit alpha FadB	4.25915718	4.96462631			
acyl-CoA dehydrogenase					5.86356163
Glycerophospholipid metabolism					
glycerol kinase GlpK		2.51066335			
glycerol-3-phosphate dehydrogenase subunit GlpB		2.4348081	-2.48860118		
anaerobic glycerol-3-phosphate dehydrogenase subunit A		4.67093531			
glycerol-3-phosphate dehydrogenase		2.76076253			
glycerol-3-phosphate transporter		2.70016925			
Motility and chemotaxis					
flagellar biosynthesis anti-sigma factor FlgM		2.0455176			
Nucleosides and nucleotides					
adenylosuccinate synthase	-2.1750178		-2.00095952		
anaerobic ribonucleoside-triphosphate reductase	-2.14036102	-2.38017082			2.49396197
phosphoribosylformylglycinamidine synthase	2.25449041	3.46268972		-2.74996885	3.12652715
bifunctional metallophosphatase/5'-nucleotidase			-2.44139175		
phosphoribulokinase		2.45971108			
Cell envelope/membrane					
LPS biosynthesis protein WavE		3.12413915			
LysM peptidoglycan-binding domain-containing protein			-2.36013018		-4.11533356
1,6-anhydro-N-acetylmuramyl-L-alanine amidase AmpD			2.42178154		
D-alanyl-D-alanine endopeptidase		2.45797984			-2.44648234
Sulfur metabolism					
sulfatase-like hydrolase/transferase	3.27295405		2.54180056		
Nitrogen metabolism					
bifunctional uridylyltransferase/uridylyl-removing protein GlnD	3.17422562	2.5609417			
glutamate synthase small subunit	3.29310519	2.23435084			
Peptidase/protease					
U32 family peptidase	-5.13213755	-4.47962952			4.909673691
U32 family peptidase	-4.19312566	-4.55903244			4.373228709
peptidase T	-3.84822324	-4.18742625			3.760497411

Annotation	Air_vs_N_2	O_2/N_2_vs_N_2	Air_vs_O_2/N_2	N_2_vs_N_2/CO_2	N_2/CO_2_vs_$O_2/CO_2/N_2$
C69 family dipeptidase					4.08900197
U32 family peptidase		2.28168233			
signal peptidase I	3.01391284				
signal peptide peptidase SppA	3.35789757				
Amino acid metabolism					
bifunctional aspartate kinase/homoserine dehydrogenase I	2.16606178				
fatty acid oxidation complex subunit alpha FadJ	3.62185071	3.84629377		-2.07175891	
fatty acid oxidation complex subunit alpha FadB	4.25915718	4.96462631			
Valine, leucine and isoleucine biosynthesis					
threonine ammonia-lyase, biosynthetic tdcB	2.06836319				
3-isopropylmalate dehydratase small subunit leuB	2.14458631				
3-isopropylmalate dehydratase large subunit leuB	2.16804199				
acetolactate synthase small subunit ilvB	2.70243543				
acetolactate synthase 3 large subunit ilvB	3.8732933	2.65504392		-2.61400731	
dihydroxy-acid dehydratase ilvD	2.82596842	2.4071312			
ketol-acid reductoisomerase ilvC	3.20931676	2.28923162			-2.03999837
acetyl-CoA C-acyltransferase	4.06277123	3.18461673		-4.3524971	
Valine, leucine and isoleucine degradation					
acyl-CoA dehydrogenase					5.86356163
Cysteine and methionine metabolism					
phosphoglycerate dehydrogenase	2.15708885				
methionine synthase	3.29150035				
Arginine biosynthesis					
argininosuccinate synthase	2.81959559	2.98683929		-3.15801748	
Arginine degradation and urea cycle					
acetylornithine/succinylornithine family transaminase	2.00833893				
Alanine, aspartate and glutamate metabolism					
adenylosuccinate synthase	-2.1750178		-2.00095952		
glutamate synthase small subunit	3.29310519	2.23435084			
aspartate carbamoyltransferase regulatory subunit		2.43513235		-2.81840642	2.77749125
aspartate carbamoyltransferase		2.58528582		-2.69677289	2.61531131
Glycine, serine and threonine metabolism					
L-threonine dehydrogenase	-5.68856697	-5.0455176			5.68676694
aminomethyl-transferring glycine dehydrogenase	3.95917384	4.19964409		-3.73149173	
threonine ammonia-lyase, biosynthetic	2.06836319				
phosphoglycerate dehydrogenase	2.15708885				
Phenylalanine, tyrosine and tryptophan biosynthesis					
tryptophan synthase subunit beta	2.5950798	2.1363074			
Lysine biosynthesis					
lysine-sensitive aspartokinase 3	3.62416623				
lysine-sensitive aspartokinase 3	3.62416623				
Tyrosine metabolism					
5-carboxymethyl-2-hydroxymuconate isomerase					2.05195872
Selenocysteine metabolism					
L-seryl-tRNA(Sec) selenium transferase	-5.39461568	-5.53185972			4.16072337
selenocysteine-specific translation elongation factor	-2.72338104	-3.33370972			
Biosynthesis of cofactors					
GTP 3',8-cyclase MoaA		3.23566183	-2.2251592		-2.90855789
alkaline phosphatase family protein			-2.66494255	-4.40109825	3.08941205
bifunctional phosphoribosylaminoimidazolecarboxamide formyltransferase/IMP cyclohydrolase		2.2974542			
2-C-methyl-D-erythritol 2,4-cyclodiphosphate synthase		-3.19133504			
Ribosomal proteins					
ribosome assembly RNA-binding protein YhbY	-4.6339934	-5.09935951			
30S ribosomal protein S15					2.10591761
30S ribosomal protein S20		2.00472895			
50S ribosomal protein L34		2.28455099			
30S ribosomal protein S14		2.40648842			
ribosome maturation factor RimP		-4.66926257	3.57125855		
ribosome hibernation promoting factor					2.16011683
50S ribosomal protein L2		2.71610006			
rRNA maturation RNase YbeY		-2.33028221			
RNA/DNA					
exodeoxyribonuclease III					-2.46035576
DNA (cytosine-5-)-methyltransferase					-2.11010742
DNA topoisomerase		3.27204323			
30S ribosomal protein S17		-8.34147453	6.59942919		7.70869891
site-specific tyrosine recombinase XerD		2.0046285			
ExeM/NucH family extracellular endonuclease		3.54380989	-4.70415662		
ribonuclease P protein component			-2.01066144		
Proteins not assigned to pathways					
SCP2 domain-containing protein	-3.55805448				3.30504354
hypothetical protein	-2.68112297				3.79906273
hypothetical protein					4.53510157
transcriptional regulator	-3.18674342	-2.1305968			3.63897959
hypothetical protein					2.21698189
hypothetical protein				2.20873324	
hypothetical protein			4.85265872		
DUF1338 family protein				-2.87778791	
DUF444 family protein		2.82463137			
DTW domain-containing protein			-2.46717885		
DUF305 domain-containing protein			-2.39326808		
hypothetical protein		2.628884			
hypothetical protein		2.33219592	-2.66216011		
hypothetical protein		-4.95920881	3.85147247		
HTH domain-containing protein		2.01170095			
DUF3389 family protein		2.24612236			
hypothetical protein	2.26380552	2.79483859			
helix-turn-helix domain-containing protein	-2.49898186				
YcgN family cysteine cluster protein	-2.62252795				
hypothetical protein	-2.00260951				
DUF2492 family protein	-2.27174085				
hypothetical protein	4.46401113	6.88740667			
hypothetical protein		-2.12127813			
TIGR02099 family protein		-7.04233042			
SpoVR family protein					3.36059634
hypothetical protein			3.05725136		
AAA domain-containing protein			-2.01318347		
M20/M25/M40 family metallo-hydrolase	-6.54538714	-6.01443281			7.09279887
ClpXP protease specificity-enhancing factor	-4.19926389	-4.28243001			4.43055916
conjugal transfer protein TraR	-3.95753644	-4.41797002			3.25753593
TetR family transcriptional regulator	-2.83598379				
patatin family protein	-2.65171	-2.04678218			3.56281535
YciI family protein	-2.22823703				
GNAT family N-acetyltransferase	2.35461871				
co-chaperone DjlA	2.38692042				
response regulator	2.97754784		3.39854736		
ATP-binding cassette domain-containing protein	3.04934794	3.07939339			
YdcF family protein		-2.63311068			3.39257368
XdhC family protein		2.34827932			
phasin family protein	3.5366923			-3.15800794	
metalloregulator ArsR/SmtB family transcription factor		-3.34635862			3.1894563
phosphotransferase					5.44373703
4Fe-4S dicluster domain-containing protein					2.44966443
PrkA family serine protein kinase					2.11290868
sigma D regulator					2.04525439
tRNA 5-hydroxyuridine modification protein YegQ					-2.0588239
ABC-F family ATPase				4.35143089	-6.37283007
GNAT family N-acetyltransferase				-3.03220876	
YhcH/YjgK/YiaL family protein			2.03876343		
PHP domain-containing protein			-2.47349052		
sigma factor-binding protein CrI		3.04647001			
AAA family ATPase		3.79974111	-2.69925893		
helix-turn-helix domain-containing protein			2.08401642		
Slp/YeaY family lipoprotein			2.29109179		
alpha-hydroxy-acid oxidizing protein	2.19479599				

Table S2_C. Differentially expressed proteins for every pair of conditions analyzed for *P. phosphoreum* TMW 2.2103, and the $\log_2$ values representing the difference in expression intensity between the two conditions.

Annotation	Air_vs_N_2	O_2/N_2_vs_N_2	Air_vs_O_2/N_2	N_2_vs_N_2/CO_2	N_2/CO_2_vs_$O_2/CO_2/N_2$	$O_2/CO_2/N_2$_vs_O_2/CO_2
Respiratory chain						
F0F1 ATP synthase subunit alpha	-2.08319473	-2.23509216				
F0F1 ATP synthase subunit gamma	-2.0248305					
F0F1 ATP synthase subunit delta		-2.12591616				
F0F1 ATP synthase subunit beta		-2.03980128				
NADH-quinone oxidoreductase subunit NuoB		-2.03028552			5.69806671	-3.23965645
succinate dehydrogenase iron-sulfur subunit						-2.33334351
succinate dehydrogenase/fumarate reductase iron-sulfur subunit					2.93652789	-2.39979808
pentaheme c-type cytochrome TorC					3.29258792	
pentaheme c-type cytochrome TorC					3.37563705	
c-type cytochrome						-3.89786593
Oxidoreductases						
SDR family NAD(P)-dependent oxidoreductase		3.77101453			-3.27436066	
SDR family NAD(P)-dependent oxidoreductase				-2.85622533		2.33835093
SDR family NAD(P)-dependent oxidoreductase					3.17419815	
SDR family oxidoreductase		6.51982053	-6.39385732		-6.15047582	-2.11684736
LLM class flavin-dependent oxidoreductase						-3.31096904
LLM class flavin-dependent oxidoreductase						-3.26119487
LLM class flavin-dependent oxidoreductase						-2.81307348
FAD-binding protein		-5.6765391		4.60256767		
NAD(P)H-flavin reductase						-4.10164706
NADH:flavin oxidoreductase		-2.41773669				
NAD(P)H nitroreductase		2.47125244				
molybdopterin-dependent oxidoreductase	2.12507757	2.20033773				
FAD-dependent oxidoreductase				3.45142937	-2.6721096	
ferredoxin--NADP(+) reductase		2.25251261			-2.06568845	
Riboflavin metabolism						
bifunctional 3,4-dihydroxy-2-butanone-4-phosphate synthase/GTP cyclohydrolase II	2.19326146	2.2029953				-4.24214681
6,7-dimethyl-8-ribityllumazine synthase						-3.96848933
Nicotinate and nicotinamide metabolism						
Si-specific NAD(P)(+) transhydrogenase						-2.24534289
Heme tansport and utilization						
heme utilization cystosolic carrier protein HutX		2.33462588				
heme utilization protein HutZ		2.82012685			-3.3206323	3.79895401
TonB-dependent hemoglobin/transferrin/lactoferrin family receptor					-4.26095772	4.18651327
Alternative electron acceptors						
sulfate adenylyltransferase subunit CysD						-2.31216812
sulfate adenylyltransferase subunit CysN				4.77531242		-2.80108325
assimilatory sulfite reductase (NADPH) flavoprotein subunit				4.20892588		-2.76438141
assimilatory sulfite reductase (NADPH) hemoprotein subunit				3.01705424		
phosphoadenylyl-sulfate reductase				3.08625094		-2.3305378
nitrite reductase large subunit		-3.75598653			6.43651072	
nitrite reductase small subunit NirD					4.04755656	
periplasmic nitrate reductase electron transfer subunit					2.60718791	
periplasmic nitrate reductase subunit alpha					4.83764839	-4.29280663
hydroxylamine reductase		-2.71084849				
fumarate reductase (quinol) flavoprotein subunit					2.79011854	
trimethylamine-N-oxide reductase TorA					2.52521388	
Alternative electron donors						
hydrogenase 2 large subunit					2.28412883	
hydrogenase large subunit					6.15278753	
hydrogenase maturation peptidase HycI	-3.33758354	-2.63052432			2.67110062	
hydrogenase small subunit		-2.33911769				
hydrogenase nickel incorporation protein HypB					3.75152524	-2.12788709
formate C-acetyltransferase		-2.10133489				
formate dehydrogenase accessory sulfurtransferase FdhD	3.09673055	2.54584122				
formate dehydrogenase		-2.14383761				
formate dehydrogenase subunit alpha					8.7217528	-6.67812284
formate dehydrogenase subunit beta					2.37545967	
formate hydrogenlyase maturation protein HycH		-2.14110947			3.28448677	
Peroxisome/oxidative stress						
superoxide dismutase		2.58945274				
catabolite repressor/activator		2.23608017				
catalase		2.52395376				
alkyl hydroperoxide reductase subunit C					-3.08191299	
alkyl hydroperoxide reductase subunit F					-2.48656337	
thiol peroxidase		2.04965274			-2.57913335	
thioredoxin TrxC		2.06217384				
Cellular stress						
cold shock domain-containing protein CspD		3.87947973				
cold-shock protein;cold-shock protein	6.78553454	8.22868919				
cold-shock protein;cold-shock protein				2.29658699	-2.2118206	
copper resistance protein NlpE	-2.64452807			2.0498956	-2.06959407	
universal stress global response regulator UspA					-2.04279455	
universal stress protein				-2.35285123		
DNA starvation/stationary phase protection protein	-2.14216042					
DNA starvation/stationary phase protection protein		2.5649236	-2.04858907		-3.71934954	
periplasmic heavy metal sensor					-2.19585546	2.02141953
Glutathione metabolism						
S-(hydroxymethyl)glutathione synthase					-2.55487696	
glutathione S-transferase				-2.0469265		
Metal/ion transport						
ferrous iron transport protein A					-2.31436602	
zinc chelation protein SecC		-3.93919627		4.85417811		
tungsten ABC transporter substrate-binding protein	3.46779823	2.8892231			-3.37003136	
Amino acids transport						
urea ABC transporter substrate-binding protein		4.73918343	-2.24792735			
preprotein translocase subunit SecG				2.68295352		
Unspecific transports						
ABC transporter substrate-binding protein	3.20328649	5.56452179			-6.05404027	
ABC transporter substrate-binding protein				5.24497604		-5.65473366
ABC transporter substrate-binding protein					-5.26341566	4.98778661
ABC transporter substrate-binding protein						-3.79263496
Fe-S clusters						
Fe-S cluster assembly ATPase SufC		3.24732463			-3.87929599	3.60097313
Fe-S cluster assembly protein SufB		2.95068804			-4.08231354	2.91449801
Fe-S cluster assembly transcriptional regulator IscR		3.47437859			-2.48807526	
iron-sulfur cluster assembly accessory protein		2.39023145			-4.85633024	2.89497693
Pyruvate metabolism						
pyruvate dehydrogenase complex transcriptional repressor PdhR					-2.60612551	
phosphoenolpyruvate carboxykinase (ATP)					2.01284663	
phosphoenolpyruvate synthase						-3.60361735
phosphoenolpyruvate-utilizing protein						-2.09939194
oxaloacetate-decarboxylating malate dehydrogenase					5.44424502	-6.02987099
bifunctional acetaldehyde-CoA/alcohol dehydrogenase		-2.11329778				
aldehyde dehydrogenase family protein				3.00728798		-4.2853686
aldehyde dehydrogenase family protein						-5.07323265
acetate--CoA ligase						-2.83768018
TCA cycle						
succinate dehydrogenase iron-sulfur subunit						-2.33334351
succinate dehydrogenase/fumarate reductase iron-sulfur subunit					2.93652789	-2.39979808
citrate synthase						-3.10043399
bifunctional aconitate hydratase 2/2-methylisocitrate dehydratase						-2.96870359
ADP-forming succinate--CoA ligase subunit beta						-2.06746229
Glyoxylate cycle						
malate synthase A						-4.82547951
isocitrate lyase				3.05011368		-5.5401001
bifunctional 4-hydroxy-2-oxoglutarate aldolase/2-dehydro-3-deoxy-phosphogluconate aldolase		-3.71741994				-5.13958804

Annotation	Air_vs_N_2	O_2/N_2_vs_N_2	Air_vs_O_2/N_2	N_2_vs_N_2/CO_2	N_2/CO_2_vs_ O_2/CO_2/N_2	O_2/CO_2/N_2 _vs_O_2/CO_2
Glycolysis/gluconeogenesis						
class 1 fructose-bisphosphatase						-2.10698636
2,3-diphosphoglycerate-dependent phosphoglycerate mutase					-2.53103383	
Sugar metabolism						
1-phosphofructokinase				-2.07249196		
ribokinase	-2.62524414	-2.31178157			2.93273481	
PTS fructose transporter subunit IIBC				-2.03504117		
phospho-sugar mutase	2.41197904	3.84199079			-3.69937197	
phosphoglucomutase/phosphomannomutase family protein						-5.85773913
D-ribose pyranase	-2.50285975				3.71969668	
bifunctional 4-hydroxy-2-oxoglutarate aldolase/2-dehydro-3-deoxy-phosphogluconate aldolase		-3.71741994				-5.13958804
Starch/glycogen and maltose metabolism						
amidohydrolase family protein						-3.94403331
Amino sugar and nucleotide sugar metabolism						
N-acetylmannosamine kinase		-3.62301763				
putative N-acetylmannosamine-6-phosphate 2-epimerase	-2.36644681				2.06928444	
Fatty acid biosynthesis						
long-chain fatty acid--CoA ligase						-3.3040301
cyclopropane fatty acyl phospholipid synthase					2.06164678	
acyl-CoA thioester hydrolase YciA					2.06568273	
Fatty acid degradation						
fatty acid oxidation complex subunit alpha FadB						-3.66452853
fatty acid oxidation complex subunit alpha FadJ				2.99911881		-6.98925273
acetyl-CoA C-acyltransferase FadI	2.29364077	2.16452471		2.01083247		-5.3185571
long-chain fatty acid--CoA ligase						-3.3040301
Glycerophospholipid metabolism						
anaerobic glycerol-3-phosphate dehydrogenase subunit A					2.78455353	
anaerobic glycerol-3-phosphate dehydrogenase subunit C		-2.27379863			5.18243027	-3.48082161
NAD(P)H-dependent glycerol-3-phosphate dehydrogenase					-2.31662814	
glycerol-3-phosphate dehydrogenase subunit GlpB					2.38243866	
glycerophosphodiester phosphodiesterase						-2.0082976
Choline degradation (anaerobic)						
choline trimethylamine-lyase						-3.96252823
Nucleosides and nucleotides						
phosphoribosylformylglycinamidine synthase						-3.06486003
nucleotide sugar dehydrogenase					2.01304944	
nucleotide sugar dehydrogenase					2.01304944	
IMP dehydrogenase					-2.27607091	
glutamine-hydrolyzing GMP synthase					-2.36316045	
bifunctional UDP-sugar hydrolase/5'-nucleotidase						-2.72797457
bifunctional phosphoribosylaminoimidazolecarboxamide formyltransferase/IMP cyclohydrolase						-2.07329241
Cell envelope/membrane						
outer membrane protein assembly factor BamE						3.5360438
MetQ/NlpA family lipoprotein	-2.09064229	-2.21936735				
Sulfur metabolism						
sulfate adenylyltransferase subunit CysD						-2.31216812
sulfate adenylyltransferase subunit CysN				4.77531242		-2.80108325
assimilatory sulfite reductase (NADPH) flavoprotein subunit				4.20892588		-2.76438141
assimilatory sulfite reductase (NADPH) hemoprotein subunit				3.01705424		
rhodanese-related sulfurtransferase	5.71616364	6.52637037			-6.22744433	
phosphoadenylyl-sulfate reductase				3.08625094		-2.3305378
Nitrogen metabolism						
P-II family nitrogen regulator		3.48181152				
periplasmic nitrate reductase electron transfer subunit					2.60718791	
periplasmic nitrate reductase subunit alpha					4.83764839	-4.29280663
Peptidases/proteases						
U32 family peptidase	-2.27299945	-2.77338537				
U32 family peptidase	2.36005783	2.10645739			-2.8000056	
U32 family peptidase					3.58213234	
C69 family dipeptidase					2.00269318	
peptidase C45				-2.45214017		
peptidoglycan DD-metalloendopeptidase family protein					-3.55716705	
Valine, leucine and isoleucine biosynthesis						
acetolactate synthase 2 catalytic subunit						-2.03017044
acetolactate synthase 3 large subunit						-2.10780271
Glycine metabolism						
glycine cleavage system aminomethyltransferase GcvT						-2.86357307
glycine cleavage system transcriptional repressor		2.08299891				
Cysteine and methionine metabolism						
S-ribosylhomocysteine lyase						-2.31953812
methionine synthase						-4.1491197
Arginine and proline mtabolism						
bifunctional proline dehydrogenase/L-glutamate gamma-semialdehyde dehydrogenase PutA	2.25946871	2.19946098				-4.0231603
Alanine, aspartate and glutamate metabolism						
glutamate decarboxylase					2.14340591	
glutamate synthase large subunit				5.41088931		-5.87466431
glutamate synthase large subunit						-2.50090154
glutamine--fructose-6-phosphate transaminase (isomerizing)					-2.22562536	
bifunctional proline dehydrogenase/L-glutamate gamma-semialdehyde dehydrogenase PutA	2.25946871	2.19946098				-4.0231603
aspartate carbamoyltransferase					2.17536036	-2.25336965
aspartate carbamoyltransferase regulatory subunit					2.53518422	-2.79797808
aspartate-semialdehyde dehydrogenase						-2.85338974
asparagine synthase B						-2.56058757
adenylosuccinate synthase						2.39288457
Glycine, serine and threonine metabolism						
threonine ammonia-lyase, biosynthetic						-3.87432226
threonine synthase						-2.33558337
phosphoserine phosphatase						-2.63784917
L-threonine dehydrogenase	-2.23951467	-3.25997098			5.20816167	-3.92567825
homoserine kinase						-2.09475581
2,3-diphosphoglycerate-dependent phosphoglycerate mutase					-2.53103383	
aminomethyl-transferring glycine dehydrogenase						-2.31962458
Arginine biosynthesis						
N-acetyl-gamma-glutamyl-phosphate reductase		-3.28381729		2.23290634		-4.35378456
arginine deiminase					2.57813517	
argininosuccinate lyase						-3.76805687
argininosuccinate synthase		-2.03036753		2.46232414		-2.70723407
arginine ABC transporter ATP-binding protein ArtP	-2.43139585					
acetylglutamate kinase		-2.22606214		2.02692286		-3.62618637
Arginine degradation and urea cycle						
arginine decarboxylase						-2.18598747
Histidine metabolism						
1-(5-phosphoribosyl)-5-[(5- phosphoribosylamino)methylideneamino]imidazole-4- carboxamide isomerase hisA		2.00946299				
histidinol dehydrogenase hisD		2.05845769				
histidinol-phosphate transaminase hisC		2.1837527				
ATP phosphoribosyltransferase hisG		2.56162008				
Phenylalanine, tyrosine and tryptophan biosynthesis						
tryptophan synthase subunit alpha						-2.25039101
tryptophan synthase subunit beta						-2.91418966
3-deoxy-7-phosphoheptulonate synthase AroG						-2.05150159
Selenocysteine metabolism						
selenocysteine-specific translation elongation factor		-2.37912623			3.80344391	-4.21988996
L-seryl-tRNA(Sec) selenium transferase					4.25695165	
Lysine biosynthesis						
lysine--tRNA ligase	-2.35516739	-3.05378596			2.58203252	
Lysine degradation						
lysine decarboxylase					3.0500857	

Annotation	Air_vs_N_2	O_2/N_2_vs_N_2	Air_vs_O_2/N_2	N_2/CO_2_vs_N_2/CO_2	N_2/CO_2_vs_O_2/CO_2/N_2	O_2/CO_2/N_2_vs_O_2/CO_2
Biosynthesis of cofactors						
dihydroorotase				2.26678022	-2.28344091	
bifunctional phosphopantothenoylcysteine decarboxylase/phosphopantothenate--cysteine ligase CoaBC		-2.43288549				
bifunctional 3,4-dihydroxy-2-butanone-4-phosphate synthase/GTP cyclohydrolase II	2.19326146	2.2029953				-4.24214681
4-hydroxy-3-polyprenylbenzoate decarboxylase					-2.16005198	
6,7-dimethyl-8-ribityllumazine synthase						-3.96848933
7-cyano-7-deazaguanine synthase QueC					-2.07725143	
Quorum sensing/two-component system						
activated long-chain acyl hydrolase LuxD						-3.93044853
acyl-CoA reductase						-3.46412023
Ribosomal proteins						
30S ribosomal protein S12		-2.84197362		2.68806839		
30S ribosomal protein S19				-2.01831118		
30S ribosomal protein S3		-2.01286316				
50S ribosomal protein L2	-2.1367391	-2.19356918				
50S ribosomal protein L35		-2.86078835		2.13208834		
ribosome hibernation promoting factor						-2.42566363
ribosome maturation factor RimP	3.44008573	3.37516085		-2.56484985		
ribosome modulation factor			-2.28894297			
RNA/DNA						
excinuclease ABC subunit UvrB					2.46057193	
excinuclease ABC subunit UvrB					4.30967013	
exodeoxyribonuclease V subunit beta				2.48182297		
deoxyribodipyrimidine photo-lyase						2.33321571
deoxyribonuclease IV					2.19240061	
DNA mismatch repair endonuclease MutL					3.64022891	-2.30568568
Resistance						
penicillin-binding protein activator LpoB		2.80068461		-3.16745186		
penicillin-insensitive murein endopeptidase						-3.19545428
Proteins not assigned to pathway						
DUF1045 domain-containing protein					2.90640195	-2.2579511
DUF1255 family protein		2.13296191				
DUF1311 domain-containing protein	-4.16236115	-3.92288399		3.82911809		
DUF1501 domain-containing protein					3.00780296	
DUF1904 family protein						-4.28218651
DUF1971 domain-containing protein	-2.06693776			2.61061223		
DUF2999 family protein				-3.49533971		
DUF3412 domain-containing protein						-2.19108772
DUF4432 family protein	-2.51153437	-2.08129184			2.0443395	
DUF465 domain-containing protein					2.0899264	-2.77071826
DUF494 family protein					-2.26145172	
hypothetical protein		-2.21530914			3.71120262	
hypothetical protein		2.0657959			-5.00461133	
hypothetical protein		2.59151395				
hypothetical protein			-2.37844785	-2.31298637		
hypothetical protein				2.11548551		
hypothetical protein				3.73217646		
hypothetical protein				3.85941569		
hypothetical protein					-3.60983276	
hypothetical protein					-2.44600232	2.630071
hypothetical protein					-2.18495687	2.09479205
hypothetical protein					-2.09215037	
hypothetical protein					2.07480621	-3.41582235
hypothetical protein					2.19326909	
hypothetical protein					3.06579463	
hypothetical protein					4.9301637	
hypothetical protein						-4.59579976
hypothetical protein						-4.08827464
hypothetical protein						-3.63194911
hypothetical protein						-2.91288885
hypothetical protein						-2.6208388
hypothetical protein						2.70621618
hypothetical protein						4.11558088
hypothetical protein;hypothetical protein					-2.05270513	
XdhC family protein					2.65930303	
YcgN family cysteine cluster protein		-2.87740644			2.31596184	
YfcL family protein		-2.51684443				
YfcL family protein		-2.51684443				
YjhT family mutarotase						2.84799767
YjjI family glycine radical enzyme					4.25953865	-2.88779831
YwbE family protein;YwbE family protein						-2.83656629
(Fe-S)-binding protein	3.75286484	3.44053523				
(Fe-S)-binding protein					2.18654569	
4Fe-4S dicluster domain-containing protein	-2.31574249	-3.41993586			5.63698451	
4Fe-4S dicluster domain-containing protein	-2.25576909	-2.84962082			5.79762205	
4Fe-4S dicluster domain-containing protein	2.01524289	2.05965742				
4Fe-4S dicluster domain-containing protein		-2.9477857			7.36498578	-3.356287
BMC domain-containing protein	2.0983181		2.67585627			-4.64511935
BMC domain-containing protein						-3.15398661
BON domain-containing protein						2.53664843
Trm112 family protein				4.47245344	-4.58289464	
ATP-binding cassette domain-containing protein		3.02024651	-3.31958962		-4.171573	4.72199376
ATP-binding cassette domain-containing protein					-2.25033887	
CBS domain-containing protein		-2.49952189			4.48603249	-4.70961316
GGGtGRT protein					3.17676671	
HTH domain-containing protein	2.1425012				-3.08386803	
Ig-like domain-containing protein					2.85936546	
SCP2 domain-containing protein		-4.53419304			2.35866674	2.60170428
SsrA-binding protein SmpB	-4.43332291	-3.859876				
Tat pathway signal protein				2.2391688	-2.87890371	
TetR family transcriptional regulator			-2.70679792			
Rsd/AlgQ family anti-sigma factor						-4.4308637
RNA-binding protein					2.61259524	-2.09511185
PrkA family serine protein kinase					5.43331464	-5.91794459
phosphotransferase					4.14520645	-3.81308428
phasin family protein				-2.43938446		
nuclear transport factor 2 family protein						-2.52032089
NAD-dependent protein deacylase		2.74927902		-3.55078252		
NAD(P)H-binding protein			4.58601189		5.01866531	
methylated-DNA--[protein]-cysteine S-methyltransferase						-3.09141922
metallophosphoesterase					2.04913839	
LysM peptidoglycan-binding domain-containing protein		-2.01508077				
M20/M25/M40 family metallo-hydrolase		-2.23078092			4.68929354	
insulinase family protein						-2.67399534
iron-sulfur cluster-binding protein					2.06193097	
L,D-transpeptidase family protein					2.39710363	
glycosyltransferase				-2.55578105	3.73211479	
GNAT family N-acetyltransferase				-2.13382912		
extracellular solute-binding protein					-5.38888931	
DeoR family transcriptional regulator					-2.14832497	2.36779849
cystatin						-3.55505498
DEAD/DEAH box helicase		-2.99255053		2.54315313		
agglutination protein						-5.08083026
AAA family ATPase					2.98665746	-3.8256073
ABC-F family ATPase				2.34038607		
AAA domain-containing protein	-2.26902072	-2.23633067				
ATP-dependent Clp protease adapter ClpS		2.90989304				
autonomous glycyl radical cofactor GrcA		-2.03403854			4.05828158	
ArsC family reductase						-2.65590922
alpha-L-glutamate ligase-like protein				-2.13419342		2.68394089

Table S2_D. Differentially expressed proteins for every pair of conditions analyzed for *P. phosphoreum* TMW 2.2134, and the $\log_2$ values representing the difference in expression intensity between the two conditions.

Annotation	Air_vs_N_2	O_2/N_2_vs_N_2	Air_vs_O_2/N_2	N_2_vs_N_2/CO_2	N_2/CO_2_vs_$O_2/CO_2/N_2$	$O_2/CO_2/N_2$_vs_O_2/CO_2
Respiratory chain						
NADH dehydrogenase (quinone) subunit D				3.00530752		-2.81188011
NADH-quinone oxidoreductase subunit NuoB		-2.03372256			4.44463221	-3.29691887
NADH-quinone oxidoreductase subunit NuoF						-3.14215279
F0F1 ATP synthase subunit B	-2.27527618	-2.35512352				
F0F1 ATP synthase subunit delta		-2.01103083				
c-type cytochrome						-2.90026347
c-type cytochrome biogenesis protein CcmI						-2.33098602
pentaheme c-type cytochrome TorC	-2.52044169	-3.6161925			3.11641185	-2.2632122
pentaheme c-type cytochrome TorC		-2.27692159				
Oxidoreductases						
LLM class flavin-dependent oxidoreductase	2.97928429	2.43629265				-3.56124814
LLM class flavin-dependent oxidoreductase	4.14828364	4.4147892			-4.44412231	-2.86301422
LLM class flavin-dependent oxidoreductase					-3.52987099	-2.82487742
NAD(P)H nitroreductase		2.12389755				
NAD(P)H-flavin reductase					-2.00518545	
NADPH-dependent FMN reductase						-2.40341695
nitroreductase family protein				4.27601242		
oxidoreductase				-2.37573369		
SDR family NAD(P)-dependent oxidoreductase		2.67813047			-4.13266627	
SDR family oxidoreductase		5.55595525	-5.06352615		-4.60091972	
FAD-dependent oxidoreductase					-2.80114428	
ferredoxin--NADP(+) reductase		2.26033783				
Riboflavin metabolism						
acid phosphatase AphA						-2.30307897
FAD:protein FMN transferase		-2.40305265				
Heme tansport						
radical SAM family heme chaperone HemW						4.47312228
heme utilization protein HutZ		2.99826177				
Alternative electron acceptors						
assimilatory sulfite reductase (NADPH) flavoprotein subunit				3.06668663	-2.660326	
assimilatory sulfite reductase (NADPH) hemoprotein subunit						-7.30181313
sulfate adenylyltransferase subunit CysD				2.90417099		-2.14726575
sulfate adenylyltransferase subunit CysN				3.46194013	-2.80455589	
sulfurtransferase TusE					-6.11870893	7.06656392
hydroxylamine reductase	-5.63805262	-5.00228818		4.78441938		
nitrite reductase large subunit					5.7868913	-3.09844971
nitrite reductase small subunit NirD				-2.75282033		
periplasmic nitrate reductase electron transfer subunit					3.82890701	-2.2323157
periplasmic nitrate reductase subunit alpha					3.28150749	
TMAO reductase system periplasmic protein TorT	-2.15555445					
Alternative electron donors						
formate C-acetyltransferase	-2.2133344	-2.12271627				
formate dehydrogenase accessory sulfurtransferase FdhD					-2.8438104	
formate dehydrogenase subunit alpha					5.6266791	-3.77162361
formate dehydrogenase subunit beta		-2.34466744			2.07757505	
formate dehydrogenase-N subunit alpha					2.04255168	
formate hydrogenlyase maturation protein HycH		-2.04013379				
hydrogenase 2 large subunit					2.08428574	
hydrogenase large subunit		-2.21994336			5.75547791	-3.67615891
hydrogenase maturation peptidase HycI					3.77541987	
hydrogenase nickel incorporation protein HypB					4.29761759	-3.70449003
hydrogenase small subunit		-2.71962484				
Peroxisome/oxidative stress						
alkyl hydroperoxide reductase subunit C					-2.59933599	
alkyl hydroperoxide reductase subunit F					-2.5770944	
thiol peroxidase		2.48910968			-3.7325484	
NO-inducible flavohemoprotein	-3.39711889		-2.26275126	2.28876813		
Cellular stress						
DNA starvation/stationary phase protection protein		2.2898744	-2.31846555		-3.13388189	
DNA starvation/stationary phase protection protein			-2.30972099			
cold shock domain-containing protein CspD		2.98970795				
cold-shock protein	2.49586614					
copper resistance protein NlpE	-2.90257708			3.49679311	-3.37104861	
carbonic anhydrase					-4.52829107	
periplasmic heavy metal sensor					-2.82769521	2.42746989
TerB family tellurite resistance protein					-2.13925107	
Glutathione metabolism						
bifunctional glutathionylspermidine amidase/synthase	4.01257769	3.79239082		-5.83550771		
Metal/ion transport						
tungsten ABC transporter substrate-binding protein	4.06262779	2.99828148		2.67017365	-5.31238874	
zinc chelation protein SecC						-4.74890328
Amino acids transport						
dipeptide ABC transporter ATP-binding protein	2.0820605					
Unspecific transports						
ABC transporter substrate-binding protein	4.95333799	5.16379674			-5.54311307	
ABC transporter substrate-binding protein						-3.5105203
ABC transporter substrate-binding protein;ABC transporter substrate-binding protein	3.64969826	3.56771151		2.84186999	-3.10126686	-3.80639585
translocation/assembly module TamB					2.12230873	-2.52645747
transporter substrate-binding domain-containing protein					-2.026076	
extracellular solute-binding protein	6.49063937	6.1261851			-6.84299469	
extracellular solute-binding protein				-2.37703069		
extracellular solute-binding protein					-2.11381785	
sodium/solute symporter				2.60740407		
Fe-S clusters						
Fe-S cluster assembly ATPase SufC			-2.25135295		-2.91129303	
Fe-S cluster assembly protein SufB			-2.16244062		-2.85338656	2.31692569
Fe-S cluster assembly transcriptional regulator IscR	2.06149864	3.23438962			-2.3619353	
iron-sulfur cluster assembly accessory protein			-3.08689435		-3.02657191	
Pyruvate metabolism						
iron-containing alcohol dehydrogenase			-3.58984884			
iron-containing alcohol dehydrogenase					3.26744461	
alcohol dehydrogenase AdhP	-2.89766185		-3.00646782		-3.02296193	2.71423022
aldehyde dehydrogenase family protein	3.38860385	2.43734741				-2.29199664
phosphoenolpyruvate synthase						-2.2200915
oxaloacetate-decarboxylating malate dehydrogenase						-4.70036062
bifunctional acetaldehyde-CoA/alcohol dehydrogenase					2.17153549	
alpha-keto acid decarboxylase family protein					-2.06290881	
Fermentation						
2-hydroxyacid dehydrogenase		2.17655627				
Lipoic acid						
lipoyl(octanoyl) transferase LipB			-2.31133652			
TCA cycle						
citrate synthase						-2.31410408
bifunctional isocitrate dehydrogenase kinase/phosphatase						-2.3429877
bifunctional aconitate hydratase 2/2-methylisocitrate dehydratase						-2.17567062
Glyoxylate cycle						
isocitrate lyase	2.37484423					-3.16015943
malate synthase A		3.12301127				-3.86571439
bifunctional 4-hydroxy-2-oxoglutarate aldolase/2-dehydro-3-deoxy-phosphogluconate aldolase				3.49019369		-5.39876429
Glycolysis/gluconeogenesis						
2,3-diphosphoglycerate-dependent phosphoglycerate mutase	2.089866	2.77771632			-2.45532608	

Annotation	Air_vs_N_2	O_2/N_2_vs_N_2	Air_vs_O_2/N_2	N_2_vs_N_2/CO_2	N_2/CO_2_vs_$O_2/CO_2/N_2$	$O_2/CO_2/N_2$_vs_O_2/CO_2
Sugar metabolism						
D-ribose pyranase	-3.6799984	-2.87565994				
ribokinase	-2.00558154					
phospho-sugar mutase	2.26237996	3.38349025			-3.13121605	
sugar transferase	-2.13669459	-2.68079376				
beta-galactosidase subunit alpha						-2.97454198
galactose/glucose ABC transporter substrate-binding protein MglB	3.0654335	4.59089597				
phosphoglucomutase/phosphomannomutase family protein				5.27805646	-5.34194311	
Starch/glycogen and maltose metabolism						
amidohydrolase family protein		-3.895497		4.28980382		
amidohydrolase family protein		2.23826472				-3.31011772
amidohydrolase family protein						-2.51803716
Fatty acid biosynthesis						
acetyl-CoA carboxylase biotin carboxyl carrier protein	-2.90961838		-2.45213763			
Fatty acid degradation						
fatty acid oxidation complex subunit alpha FadJ						-5.65536817
acetyl-CoA C-acyltransferase FadI	4.64217567	3.93946521				-5.9207414
Glycerophospholipid metabolism						
glycerol kinase						-2.0678552
glycerol-3-phosphate dehydrogenase					-2.45607821	
glycerol-3-phosphate transporter		-2.93019613				
glycerophosphoryl diester phosphodiesterase					-2.06980197	
anaerobic glycerol-3-phosphate dehydrogenase subunit C		-2.21263377				-2.91416931
1-acylglycerol-3-phosphate O-acyltransferase	-2.12186305	-2.56438573				
Amino sugar and nucleotide sugar metabolism						
N-acetylmannosamine kinase	-4.65641403	-4.50657145				
putative N-acetylmannosamine-6-phosphate 2-epimerase	-2.23550161	-2.00899824				2.47615178
Nucleosides and nucleotides						
phosphoribosylformylglycinamidine synthase						-2.72574361
bifunctional UDP-sugar hydrolase/5'-nucleotidase						-2.23131816
anaerobic ribonucleoside-triphosphate reductase					3.03405571	
Cell envelope/membrane						
LPS assembly protein LptD					2.02705638	
TolC family outer membrane protein		-2.86331876				
peptidoglycan DD-metalloendopeptidase family protein					-2.25444285	
peptidoglycan-binding protein LysM						-2.32078997
polysaccharide biosynthesis protein		-2.30233002				
lipopolysaccharide assembly protein LapB		-3.36136055		3.78420321		
Sulfur metabolism						
assimilatory sulfite reductase (NADPH) flavoprotein subunit				3.06668663	-2.660326	
assimilatory sulfite reductase (NADPH) hemoprotein subunit						-7.30181313
sulfate adenylyltransferase subunit CysD				2.90417099		-2.14726575
sulfate adenylyltransferase subunit CysN				3.46194013	-2.80455589	
sulfurtransferase TusE					-6.11870893	7.06656392
rhodanese-related sulfurtransferase	6.12106959	5.60321999			-4.70757103	
Nitrogen metabolism						
nitrite reductase large subunit					5.7868913	-3.09844971
nitrite reductase small subunit NirD				-2.75282033		
periplasmic nitrate reductase electron transfer subunit					3.82890701	-2.2323157
periplasmic nitrate reductase subunit alpha					3.28150749	
P-II family nitrogen regulator	2.50547091	4.39530691				
Peptidases/proteases						
U32 family peptidase	-3.44338036				3.12743123	
U32 family peptidase		-4.25580533	2.22984759		3.27456029	
U32 family peptidase		-4.07471911			4.19678688	
Valine, leucine and isoleucine biosynthesis						
acetolactate synthase 2 catalytic subunit						-2.64706167
Valine, leucine and isoleucine degradation						
acetyl-CoA C-acyltransferase FadI	4.64217567	3.93946521				-5.9207414
Glycine metabolism						
glycine cleavage system aminomethyltransferase GcvT						-2.19274585
glycine cleavage system protein GcvH						-2.32016627
Methionine biosynthesis						
methionine synthase						-2.39579392
Cysteine and methionine metabolism						
S-ribosylhomocysteine lyase						-2.14671453
Arginine biosynthesis						
N-acetyl-gamma-glutamyl-phosphate reductase	2.54437192		2.70053736			-4.09193675
acetylglutamate kinase			2.02417692			-3.04711978
argininosuccinate lyase						-2.58819453
argininosuccinate synthase						-2.67800395
Arginine degradation and urea cycle						
biosynthetic arginine decarboxylase				2.9439621		
Arginine and proline metabolism						
bifunctional proline dehydrogenase/L-glutamate gamma-semialdehyde dehydrogenase PutA						-3.11439769
arginine N-succinyltransferase		-2.57068571				
Alanine, aspartate and glutamate metabolism						
aspartate carbamoyltransferase						-2.15622711
aspartate carbamoyltransferase regulatory subunit						-2.48662694
aspartate-semialdehyde dehydrogenase						-2.51120758
glutamate synthase large subunit	3.35646947	3.173268		2.15169271		
bifunctional proline dehydrogenase/L-glutamate gamma-semialdehyde dehydrogenase PutA						-3.11439769
Glycine, serine and threonine metabolism						
2,3-diphosphoglycerate-dependent phosphoglycerate mutase	2.089866	2.77771632			-2.45532608	
threonine ammonia-lyase, biosynthetic						-2.34613673
threonine synthase						-2.0454464
phosphoserine phosphatase						-3.20234553
L-threonine dehydrogenase		-2.28712908			4.04479154	-3.21518389
aminomethyl-transferring glycine dehydrogenase						-2.08790271
Tyrosine metabolism						
5-carboxymethyl-2-hydroxymuconate isomerase		2.58991941				
Lysine degradation						
lysine decarboxylase					2.51223882	
Selenocysteine metabolism						
L-seryl-tRNA(Sec) selenium transferase					4.57089869	-3.42035294
Phenylalanine, tyrosine and tryptophan biosynthesis						
tryptophan synthase subunit alpha						-2.6862812
tryptophan synthase subunit beta						-2.34469795
bifunctional indole-3-glycerol-phosphate synthase TrpC/phosphoribosylanthranilate isomerase TrpF						-2.57642746
Biosynthesis of cofactors						
thiazole synthase				2.29305712		-3.23656464
chorismate lyase					-2.69232559	
molybdenum cofactor guanylyltransferase MobA					-3.04327647	
4-hydroxy-3-polyprenylbenzoate decarboxylase		2.10871697			-2.44459534	2.00277901
Quorum sensing/two-component systems						
preprotein translocase subunit SecG				2.76443799		
bifunctional uridylyltransferase/uridylyl-removing protein GlnD					2.21914482	-2.73911031
activated long-chain acyl hydrolase LuxD	3.80729993	2.35922241				
acyl-CoA reductase	3.26184336	3.65377045				-2.52342669

Annotation	Air_vs_N_2	O_2/N_2_vs_N_2	Air_vs_O_2/N_2	N_2_vs_N_2/CO_2	N_2/CO_2_vs_$O_2/CO_2/N_2$	$O_2/CO_2/N_2$_vs_O_2/CO_2
Ribosomal proteins						
50S ribosomal protein L32		5.08826319	-3.21724002			
50S ribosomal protein L35		-2.63550949	2.0149854			
ribosome hibernation promoting factor						-2.32194901
30S ribosomal protein S12		-2.65927506		2.23828507		
HPF/RaiA family ribosome-associated protein					-2.12707583	
RNA/DNA						
DNA mismatch repair endonuclease MutL					3.19527499	-2.26773961
DNA topoisomerase III				2.2561156	-4.59221776	3.66175397
DNA topoisomerase III					2.41354497	
DNA-binding transcriptional regulator Fis					-2.24865341	
excinuclease ABC subunit UvrB						-2.02909215
exodeoxyribonuclease III		-2.18678347				
restriction endonuclease						-2.42709414
restriction endonuclease subunit S					2.2476902	
molecular chaperone GroEL		-3.49189186		3.33799744		
Proteins not assigned to pathway						
(Fe-S)-binding protein	2.12769445			2.91298612	-3.7822628	
4Fe-4S dicluster domain-containing protein	-2.99902471	-4.10898654			4.46191597	
4Fe-4S dicluster domain-containing protein	-2.4651432	-3.42670631			7.85358556	-3.27224859
4Fe-4S dicluster domain-containing protein	-2.34927623	-2.97816594			4.82776833	
4Fe-4S dicluster domain-containing protein				4.31453451	-2.5546697	
ATP-binding cassette domain-containing protein	2.19959323				-2.76954206	
ATP-binding cassette domain-containing protein		3.86703173				
ATP-binding cassette domain-containing protein					-2.29976273	
DUF1043 family protein	-2.37690989	-2.26560338			2.22266642	
DUF1045 domain-containing protein						-2.75492986
DUF1800 family protein		-3.76505915			2.96071307	
DUF2999 family protein			-2.0419337	-2.65967051		
DUF3108 domain-containing protein				2.0890789		
DUF4209 domain-containing protein					2.51071421	
DUF4432 family protein	-3.65424856	-3.40576108				
DUF465 domain-containing protein						-2.49592908
hypothetical protein	-4.82890765			2.68200556		
hypothetical protein	-2.24587504					
hypothetical protein	-2.11201159					
hypothetical protein	2.09121768					-2.3441728
hypothetical protein		-3.32045682				
hypothetical protein		-2.21820068			3.09414291	
hypothetical protein		-2.09754944				
hypothetical protein		2.1099987		-3.15828578		
hypothetical protein		2.57682037		-2.16230138		
hypothetical protein		3.15635554				
hypothetical protein			-2.76550102			
hypothetical protein			3.60439491			
hypothetical protein				-2.28391139		
hypothetical protein				2.45089785		-4.67233022
hypothetical protein				2.5282383		
hypothetical protein					-6.79315758	7.52396774
hypothetical protein					-5.05518786	3.58577156
hypothetical protein					3.46222623	
hypothetical protein						-3.12555122
hypothetical protein						-2.59651756
hypothetical protein						-2.57091077
hypothetical protein						-2.52173233
hypothetical protein						-2.41174189
hypothetical protein						-2.34365654
hypothetical protein						-2.14717929
hypothetical protein						2.15179253
type I-F CRISPR-associated endoribonuclease Cas6/Csy4	2.14087741					
YcgN family cysteine cluster protein		-2.6938928				
YhcH/YjgK/YiaL family protein	-2.02603404					
YjbQ family protein		2.24040922				
YjhT family mutarotase				2.10477257		4.0680968
YjjI family glycine radical enzyme						-3.37941488
YoaH family protein		2.47508049		-2.45588684		-2.55502701
YwbE family protein;YwbE family protein		-2.79865583	4.06522115			
GGGtGRT protein					2.56997299	
helix-turn-helix domain-containing protein	-2.05077553					
helix-turn-helix domain-containing protein		-2.81092835				
helix-turn-helix domain-containing protein					3.34016037	
DEAD/DEAH box helicase		-2.31459491				
DeoR family transcriptional regulator					-3.03142738	
NUDIX domain-containing protein					-2.63534037	
DJ-1 family protein						-2.61779277
M20/M25/M40 family metallo-hydrolase					6.14095179	-4.11764526
MarR family transcriptional regulator		-3.4354159				
NAD(P)-binding protein		-2.82105255	2.00564321			
NAD(P)-binding protein						-5.40911738
NAD(P)H-binding protein					3.57882245	
SsrA-binding protein SmpB		-4.40138435				
StbB					-2.37132327	3.56131744
AsmA family protein						-2.71481387
PHP domain-containing protein				-3.52548281		
autotransporter domain-containing protein						2.16309929
AMP-binding protein					2.42116801	-2.34819857
agglutination protein						-4.63818105
addiction module toxin RelE		-2.37756411				
co-chaperone DjlA		-2.21481641				
FAD-binding protein		-4.49526151	5.19114558	3.11316109		-4.01780637
family 20 glycosylhydrolase		2.08706474		-2.76718839		
catabolite repressor/activator	2.52229691					
DUF1722 domain-containing protein					2.52521261	
CBS domain-containing protein						-2.20685069
thioredoxin domain-containing protein	-2.06453451					
thermolabile hemolysin	3.62878164					
Rsd/AlgQ family anti-sigma factor						-2.81943003
response regulator		2.85145187				
rRNA maturation RNase YbeY					-3.50644302	
tRNA (pseudouridine(54)-N(1))-methyltransferase TrmY					4.13601812	-3.35135078
PilT/PilU family type 4a pilus ATPase					2.49175835	
PrkA family serine protein kinase					2.09868558	-2.73994319
phosphotransferase					2.24987666	-3.01217079
nucleotidyltransferase				-2.21814219		
NAD-dependent protein deacylase				-3.14910571		
conjugal transfer protein TraR					2.65312322	
GNAT family N-acetyltransferase					-4.11226018	
insulinase family protein						-2.72758548
elongation factor P						2.00633621
FKBP-type peptidyl-prolyl cis-trans isomerase	-2.57701937					
2Fe-2S iron-sulfur cluster binding domain-containing protein					3.49946658	-3.22422981
haloacid dehalogenase type II					2.87367566	-2.23567518
lysine--tRNA ligase		-2.09604009				
alpha-L-glutamate ligase-like protein					2.25164414	
autonomous glycyl radical cofactor GrcA					2.55081177	